

Xiao-Su Yi
Shanyi Du
Litong Zhang *Editors*

Composite Materials Engineering, Volume 1

Fundamentals of Composite Materials



Chemical Industry Press



Springer

Composite Materials Engineering, Volume 1

Xiao-Su Yi · Shanyi Du · Litong Zhang
Editors

Composite Materials Engineering, Volume 1

Fundamentals of Composite Materials



Chemical Industry Press



Springer

Editors

Xiao-Su Yi
Beijing Institute of Aeronautical Materials
(BIAM)
Beijing, Hebei
China

Litong Zhang
Northwestern Polytechnical University
Xi'an, Shaanxi
China

Shanyi Du
Center for Composite Materials
Harbin Institute of Technology
Harbin, Heilongjiang
China

ISBN 978-981-10-5695-6 ISBN 978-981-10-5696-3 (eBook)
<https://doi.org/10.1007/978-981-10-5696-3>

Jointly published with Chemical Industry Press, Beijing

ISBN of the China Mainland edition: 978-7-122-06373-1

The print edition is not for sale in China Mainland. Customers from China Mainland please order the print book from: Chemical Industry Press, Beijing.

Library of Congress Control Number: 2017947741

Translation from the Chinese language edition: 中国材料工程大典 第10卷 复合材料工程. © Chemical Industry Press 2006. All Rights Reserved.

© Chemical Industry Press, Beijing and Springer Nature Singapore Pte Ltd. 2018

This work is subject to copyright. All rights are reserved by the Publishers, whether the whole or part of the material is concerned, specifically the rights of translation, reprinting, reuse of illustrations, recitation, broadcasting, reproduction on microfilms or in any other physical way, and transmission or information storage and retrieval, electronic adaptation, computer software, or by similar or dissimilar methodology now known or hereafter developed.

The use of general descriptive names, registered names, trademarks, service marks, etc. in this publication does not imply, even in the absence of a specific statement, that such names are exempt from the relevant protective laws and regulations and therefore free for general use.

The publishers, the authors and the editors are safe to assume that the advice and information in this book are believed to be true and accurate at the date of publication. Neither the publishers nor the authors or the editors give a warranty, express or implied, with respect to the material contained herein or for any errors or omissions that may have been made. The publishers remains neutral with regard to jurisdictional claims in published maps and institutional affiliations.

Printed on acid-free paper

This Springer imprint is published by Springer Nature

The registered company is Springer Nature Singapore Pte Ltd.

The registered company address is: 152 Beach Road, #21-01/04 Gateway East, Singapore 189721, Singapore

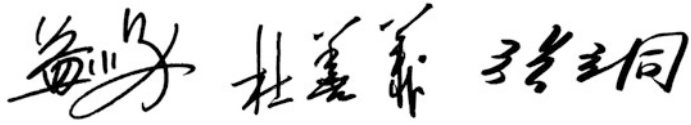
Preface

The concept of composites is well illustrated by biological materials such as wood, bone, teeth, and hides; these are all composites with complex internal structures that provide mechanical properties well suited to the performance requirements. In general, heterogeneous materials combining the best aspects of dissimilar constituents have been used by nature for millions of years. These could be considered the first composite materials. In modern materials engineering, the term ‘composite’ has become a broad and important class of engineering materials, typically referring to a matrix material that is reinforced with fibers. For instance, GFRP is a thermosetting polyester matrix containing glass fibers, and this particular composite has the lion’s share of today’s commercial composite market.

Nowadays, composite materials are found in a wide variety of situations, and they play important supporting roles in economic development and defense applications. Many composites used today are at the cutting edge of materials technology, with performance and costs appropriate to ultra-demanding applications such as spacecraft. Composite materials are undoubtedly a pillar of the materials family, parallel to metallic, polymeric, and nonmetallic inorganic materials, in terms of the worldwide demand and production. Composite materials are so fundamental and so critical that their importance is hard to overemphasize.

The main objective of the book is to provide a comprehensive overview of current composite materials that have considerable influence on technical and economic development in China. Many achievements presented in this book result from individual research groups and research and development projects financially supported by Chinese government. Hence, one aim of this book is to bring state-of-the-art knowledge and accomplishments on composite materials together in a single book of two volumes. Of course, this book also provides an understanding of the physical structure–properties relationship of composites for postgraduate students and researchers, scientists, and engineers alike. This understanding forms a basis for the application and improvement of the properties, manufacturing processes, characterization and testing, selection methods, and design of products made from composites. This knowledge has evolved from many disciplines and is common to all composite materials.

This book is a part of a large-scale publishing project, *China Materials Engineering Canon*, initiated and supported by the Chinese Mechanical Engineering Society and the Chinese Materials Research Society, co-sponsored by many governmental ministries and national institutions, including the Chinese Academy of Sciences and the Chinese Academy of Engineering. We would like to acknowledge the support and contribution of many colleagues in different universities, institutes, and national research establishments, many of whom are well known in the composite materials community in China. They were kindly agreed to provide their particular expertise for individual chapters. We are also grateful to many other scientists who made their contribution by taking part in the extensive reviewing process, particularly in the translation process from Chinese to English. Finally, we would like to thank the organizer of this book, Chemical Industry Press, for its management.



Beijing, China
Harbin, China
Xi'an, China

Xiao-Su Yi
Shanyi Du
Litong Zhang

Contents

1 An Introduction to Composite Materials	1
Xiao-Su Yi	
2 Fiber Reinforcement	63
Chunxiang Feng and Zengyong Chu	
3 Polymer Matrix Materials	151
Xiangbao Chen, Jianwen Bao, Chao Shen, Baoyan Zhang, Yahong Xu and Zhen Shen	
4 Composite Structure Design and Analysis	353
Zhen Shen, Xianxin Tong, Naibin Yang, Mingjiu Xie, Ye Li and Puhui Chen	
5 Composite Property Testing, Characterization, and Quality Control	589
Zuoguang Zhang, Zilong Zhang, Zhen Shen, Shuangqi He, Yubin Li and Ming Chao	

Editors and Contributors

About the Editors



Prof. Xiao-Su Yi is the director of the National Key Laboratory of Advanced Composites at Beijing Institution of Aeronautical Materials. His major research fields include high-performance structural composite materials, functional composite materials, materials process and engineering, and polymeric materials. Prof. Yi is the author or editor of more than 10 academic books and over 300 academic papers. He is a member of the ACCM Council; IOC member of WRCAP; standing member of the Chinese Material Research Society and Chinese Society for Composite Materials; chief editor of *Acta Materiae Compositae Sinica*, *Aviation Journal*, and the *Journal of Aeronautical Materials*, among others.



Prof. Shanyi Du is a member of the Chinese Academy of Engineering and works at the Center for Composite Materials and Structures of Harbin Institution of Technology (HIT), where he is involved in education and research courses in mechanics and composite materials. His achievements include theories and methods for performance characterization and safety evaluation of composite materials. Prof. Du has authored or co-authored over 260 academic papers, as well as 10 monographs on mechanics and composite materials. Prof. Du is president of the Chinese Society for Composite Materials and executive councilor of the International Committee on Composite Materials (ICCM), member of the editorial committees of several international

journals, such as *Composite Science and Technology*, *ACTA MACHANICA SOLIDA SINICA*, and the *International Journal of Computational Methods*.



Prof. Litong Zhang is a member of the Chinese Academy of Engineering and works in Northwestern Polytechnical University. She was engaged in research on aerospace ceramic and composites in the last 20 years and completed a series of innovative research projects. She and her research group innovated manufacturing techniques in the field of continuous fiber-reinforced silicon carbide ceramic matrix composites and established equipment systems with independent intellectual property rights. She received 26 national invention patents and the First Class Award for Technological Inventions of People's Republic of China in 2004. Prof. Zhang has published more than 260 scientific papers and several books. She is the director of academic board at the National Key Laboratory of Thermostructure Composite Materials and vice president of Chinese Society for Composite Materials.

Contributors

Jianwen Bao Beijing Institute of Aeronautical Materials, Beijing, China

Ming Chao Beihang University, Beijing, China

Puhui Chen Nanjing University of Aeronautics and Astronautics, Nanjing, Jiangsu, China

Xiangbao Chen Beijing Institute of Aeronautical Materials, Beijing, China

Zengyong Chu National University of Defense Technology, Changsha, Hunan, China

Chunxiang Feng National University of Defense Technology, Changsha, Hunan, China

Shuangqi He Beijing Research Institute of Aerospace Materials & Technology, Beijing, China

Ye Li Aircraft Strength Research Institute of China, Xi'an, Shaanxi, China

Yubin Li Beihang University, Beijing, China

Chao Shen Beijing Institute of Aeronautical Materials, Beijing, China

Zhen Shen China Institute of Aircraft Strength, Xi'an, Shaanxi, China; Aircraft Strength Research Institute of China, Xi'an, Shaanxi, China

Xianxin Tong Aircraft Strength Research Institute of China, Xi'an, Shaanxi, China

Mingjiu Xie Aircraft Strength Research Institute of China, Xi'an, Shaanxi, China

Yahong Xu Beijing Institute of Aeronautical Materials, Beijing, China

Naibin Yang Beihang University, Beijing, China

Xiao-Su Yi Beijing Institute of Aeronautical Materials, Beijing, China

Baoyan Zhang Beijing Institute of Aeronautical Materials, Beijing, China

Zilong Zhang Beijing Institute of Aeronautical Materials, Beijing, China

Zuoguang Zhang Beihang University, Beijing, China

Abbreviations

2D	Two-dimensional
2E4MZ	2-phenyl-4-methylimidazole
3D	Three-dimensional
6FDE	Hexafluoro-trimethylene di-o-phenyl dimethyl ester
ABS resins	Polyacrylonitrile-butadiene-styrene resins
AC	Dielectric
ACEE	Aircraft energy efficiency
ACE-MRL	Advanced Civil Engineering Materials Research Laboratory
ACI	American Concrete Institute
ACM	Advanced composite materials
ACT	Advanced composite technology
ACT plan	A NASA's plan to improve textile composites in civil aircraft
AE	Allyl phenol-oxidant resin
AEC	French Atomic Energy Commission
AFM	Atomic force microscopy
AFML	Air Force Material Laboratory
AFP	Automated fiber placement
AGA	Agile combat aircraft
AIN	Aluminum nitride
AMC	Aerospace Metal Matrix Composites Company
ANN	Artificial neural networks
ANOVA	Analysis of variance
APA	1,3-di-(3-amine phenoxy) phenyl
APB	3-acetylene phenol amine
AR coating	Anti-reflection coating
ARALL	Aramid fiber-reinforced Al laminate
ARPA	Advanced Research Projects Agency
AS	Average stress criterion
ASTM	American Society for Testing and Materials
ATF	Advanced fighter plane

ATL	Automated tape-laying
ATP	Automated tow placement; automated tape placing
ATS	Applications Technology Satellite
BA	Butyl acrylate
BAS	BaO–Al ₂ O ₃ –SiO ₂
BBA	Building block approach
BDAF	Bietherdisphenylamine-6F-bisphenyl-A
BDAO	Bietherdiphenylamine oxide
BDAP	Bietherdisphenylaminebisphenyl-A
BDAS	Bietherdisphenylaminesulfone
BEM	Boundary element method
BG	2,4-biamine-6-phenol-1,3,5 triazine
BIAM	Beijing Institute of Aeronautical Materials
BM	Bridging model
BMAS	BaO–MgO–Al ₂ O ₃ –SiO ₂
BMC	Bulk molding compounds
BMI	Bismaleimide
BN	Boron nitride
BPACy	Cyanate ester
BPTA	Benaophenonel-tetra-dianhydride
BSAS	BaO–SrO–Al ₂ O ₃ –SiO ₂
BSU	Basic structural unit
BTDE	Bisphenyl ketone tetraanhydride dimethyl ester
BUE	Build-up edge
BVID	Barely visible impact damage, low-energy impact damage
C/C	Carbon/Carbon
CAA	Chromic acid anodization
CAD	Computer-aided design
CAE	Computer assisted engineering
CAI	Composite affordability initiative; compression after impacting
CAM	Computer-aided manufacturing
CAS	Calcium aluminosilicate, CaO–Al ₂ O ₃ –SiO ₂
CB	Carbon black
CBCC	CB-filled cement-based composites
CBT™	Cyclobutanone terephthalate
CDF	Cumulative density function
CE	Cyanate ester
CEC	Cation exchange capacity
CF	Carbon fiber
CFA	Composite factor of American
CFCC	Continuous fiber-reinforced ceramic matrix composite
CFRC	Carbon fiber-reinforced concrete
CFRCMC	Continuous fiber-reinforced ceramic matrix composite
CFRP	Carbon fiber-reinforced plastic
CIMS	Computer-integrated manufacturing system

CIRTM	Co-injection RTM
CL	Central line
CLT	Classical laminate theory
CLVI	Chemical liquid-vaporized infiltration
CM	Crimp model
CMC	Ceramic matrix composites
CME	Coefficient of moisture expansion
CMR	Creep mismatch ratio
CNT	Carbon nanotube
CPCy	Single functional degree cyanate ester model compound
CRADA	Cooperation research and developing agreement
CRC	Compact-reinforced concrete
CRTM	Continuous RTM
CTA	Cold temperature ambient
CTBN	Carboxylic-terminal butadiene-nitride
CTE	Coefficient of thermal expansion
CTNN	Carboxyl NBR
CVD	Chemical vapor deposition
CVI	Chemical vapor infiltration
D/MI	Design/manufacturing integration
DABDT	2,5-diamino- 1,4-benzenedithiol salt
DABPA	O,O'-diallyl-bisphenol A
DABPS	Diallyl bisphenol S
DBDPO	Decabromodiphenyl oxide
DCC	Dicyclohexylcarbodiimide
DCP	Peroxidate diisopropyl phenol
DDA	Dynamic dielectric analysis
DDAC	Dimethyl di-dodecyl ammonium salt
DDS	Data damage structure; diaminedipheylsulfone
DETA	Dielectric thermal analysis
DFM	Design for manufacture
DGEBA	Diglycidyl ether bisphenyl-A, bisphenol A epoxy
DGEBF	Fluorine epoxy; 9,9-bi (4-hydroxyl-benzol)-p-fluorine-diglycidyl ether
DGEBS	Bisphenyl-S diglycidyl ether
DGEIB	Bi-(4-hydroxyl-benzol)-p-diisopropyl benzene-diglycidyl ether
DGEPP	Phenolphthalein epoxy resins
DI	Damage influence criterion XX
DMA	Dynamic mechanical analysis
DMC	Dough molding compounds
DMP	Dimethyl polyamide
DMTA	Dynamic mechanical thermal analysis
DOS	Directionally oriented structures
DSC	Differential scanning calorimetry
DSP	Densified system with ultra-fine particles

DTA	Differential thermal analysis
DTMA	Dynamic thermal mechanical analysis
DUL	Design ultimate loads
EAR	Earth antenna reflector
EB	Electronic beam
EBED	Electron beam evaporation deposition
ECC	Engineered cementitious composite
EELS	Electronic energy loss spectroscopy
EFG	Edge-defined film-fed growth
EL	Electroluminescent
EMC	Electromagnetic compatibility
EMI	Electromagnet interference
EP	Thermosetting epoxy resin
EPDM	Ethylene propylene diene rubber
EPMA	Electron probe microscope analysis
EP-PUR	An epoxy modified by hygrothermally decomposed polyurethane
ER	Electrorheological
ETW	Elevated temperature wet
EVA	Ethylene-vinyl acetate
EVID	Evident visible impact damage
EW	Explosive welding
F/I	Fiber/interphase interface
FBG	Fiber Bragg gratings
FCC	Face-centered cubic
FCVI	Forced chemical vapor infiltration, forced convection CVI; forced-flow CVI
FD	Fiber breakage damage failure criterion
FDN	A water-reducing agent
FEA	Finite element analysis
FEM	Finite element method
FGM	Functionally gradient materials
FHC	Filled hole compression
FHT	Filled hole tensile
FIM	Fiber inclination model
FIT	Fluid impact technology
FML	Fiber-metal laminates
FMS	Flexible manufacturing system
FPF	First ply failure
FPI	Fast probability integrator; fiber optic interferometer
FPL	Forest Products Laboratory
FPZ	Fracture process zone
FRDSP	DSP mortar + steel fiber, $V_f = 6\%$
FRP	Fiber-reinforced plastic
FRS	Fine Rahmen surface
FRTM	Flexible RTM

FT-IR	Infrared spectroscopy
FT-IR	Fourier transform infrared spectrometry
FW	Filament winding
GC	Chromatography
GEM	General effective medium equation
GFRP	Glass fiber-thermosetting matrix composites; glass fiber-reinforced polymer
GLARE	Glass fiber-reinforced Al
GM	General Motors Corporation
GP	Graphite
GP zone	Guinier-Preston
GPC	Gel penetration chromatography
GRC	Glass fiber-reinforced cement-based composites
GrF	Graphite fibers
HCL	Hard contact lens
HCVI	Heaterless chemical vapor infiltration
HDPE	High-density polyethylene
HDT	Heat distortion temperature; heat deflection temperature; heat deformation temperature
HEMA	Hydroxyethyl methacrylate
HIP	Hot isostatic pressing
HIPN	Half-interpenetrating networks
HIT	Harbin Institution of Technology
HM	High modulus type
HMDS	Chlorosilane and hexamethyldisilazane
HMEPE	High molecular weight polyethylene
HMW	High molecular weight
HOLZ	High-order Laue zone
HPC60	High-performance concrete
HPLC	High-pressure liquid chromatograph
HRR	Heat release rate
HSRS	High-strain-rate superplasticity
HT	High tenacity type
H.T.	High temperature
H/W	Hot/Wet
ICCAS	Institute of Chemistry of Chinese Academy of Sciences
ICCM	International Committee on Composite Materials
ICVI	Isothermal CVI; isobaric CVI
IF	Infrared light
IHPTET	Integrated high-performance turbine engine technology
ILSS	Inter-laminar shear strength
IMU	Inertial measurement unit
IPACS	Integrated probabilistic assessment of composite structures
IR	Infrared spectrometer
ISC	Inter-system conversion

ISO	Isotropic
LACVD	Laser-assisted CVD
LAS	$\text{Li}_2\text{O}-\text{Al}_2\text{O}_3-\text{SiO}_2$; lithium aluminosilicate
LC	Superduralumin alloy
LCL	Low control limit
LCM	Liquid composite molding
LCMC	Laminated ceramic matrix composite
LCP	Liquid crystal polymers
LD	Forged aluminum alloy
LDPE	Low-density polyethylene
LEC	Linear expansion coefficient
LED	Light-emitting diodes
LMO	Local molecular orientation
LMW	Low molecular weight
LOI	Limit oxygen index
LROM	Linear rule of mixtures
LSS	Lamianting stacking sequency
LTCVI	Limited temperature forced-flow CVI
LTM	Low-temperature molding
LVDT	Linear voltage differential transducer
LWA	Lower boundary predictions
LWC	Upper boundary predictions
LY	Duralumin alloy
MI	Matrix/interphase interface
M5	Polypyridobisimidazole
MA	Mechanical alloying; maleic anhydride; methyl acrylate
MAO	Methylaluminumoxane
MAS	$\text{MgO}-\text{Al}_2\text{O}_3-\text{SiO}_2$
MBMI	Bi-phenyl methyl bismaleimide
MC	Methyl cellulose
MCM	Plasma spray coating method
MD	Machine direction
MDA	Bimethyl diphenyl amine
MDF	Macro-defect-free
MDI	4,4'-Diphenylmethane diisocyanate
MEL	Magnesium Elektron Ltd.
MM	Mosaic model
MMA	Methyl methacrylate
MMC	Metal matrix composite
MMW	Medium molecular weight
MNR	Maximum normed residual
MOL	Material Operation Limit
MOR	Modulus of rupture
MS	Magnetron sputtering
MTS	Material testing system; methyltrichlorosilane

MTT	Montmorillonite
MWCNT	Multiwalled carbon nanotube
MWK	Multiaxial warp-knitted
nano-TPO	Thermoplastic polypropylene nanocomposites
NASA	The National Aeronautics and Space Administration
NASP	National Aeronautics and Space Shuttle
NBR	Nitrile-butadiene rubber
NC30	Normal concrete
NCF	Non-crimp fabric
NCH	Nylon-clay hybrids
NDI	Non-destructive inspection
NE	Nadic acid methyl ester
NEC	Nano-engineered concrete
NEMC	Nano-enabled multifunctional concrete
NGC	Northrop Grumman Corp.
NGCAD	Northrop Grumman Commercial Aircraft Division
NMP	N-methyl ketopyrrolidine
NMR	Nuclear magnetic resonance
NOL	Noel ring, ring specimen firstly used by Naval Ordnance Laboratory of American
N-PNMI	N-phenyl maleimide
NPU	Northwestern Polytechnical University
NSF	American National Science Foundation
NTC	Negative temperature coefficient of resistance
OC	Owens Corning
OCF	Owens Corning Fiberglass
ODA	Diamine phenylate
OHC	Open hole compression
OHT	Open hole tensile
OMMT	Organic modified montmorillonite
O-phase	Orthorhombic structure phase
ORNL	Oak Ridge National Laboratory
P3AT	Poly(3-alkylthiophene)
PA	Polyamide
PAA	Polyarylacetylene; phosphoric acid anodization
PAAM	Polyacrylamide
PAE	Polyacrylic ester
PAI	Polyamide-imide
PAN	Polyacrylonitrile; polyphenylamine
PANI	Polyaniline
PAR	Polyarylate
PAVCD	Plasma-assisted CVD
PBI	Poly(p-phenylene benzimidazole); polybenzimidazole
PBO	Poly(p-phenylene benzobisoxazole); polybenzoxazole; poly-p-phenylene benzo-bis; polybutadiene

PBOX	Phenylene bioxazoline
PBS	4-tert-butylstyrene-SBR
PBT	Poly(p-phenylene benzobisthiazole); polybenzothiazoles; polybutylene terephthalate
PC	Phenolic resin polymer matrix composites; polycarbonate
PCC	Polymer cement concrete
PCL	Polycaprolactone
PCN	Polymer/clay nanocomposites
PCP	Propinyl-substituted cyclopentadiene
PCS	Polycarbosilane
PCT	Polyethylenecyclodimethyl terephthalate
PCVI	Pulsed CVI
PDA	Phenyl diamine
PDF	Probability density function
PDFCE	Polydifluorochloroethylene
PE	Polyethylene
PECVD	Plasma-enhanced chemical vapor deposition
PEEK	Polyether ether ketone
PEG	Polyethylene glycol
PEI	Polyether imide
PEK	Polyetherketone
PEK-C	Modified polyetherketone
PEO	Polyoxyethylene
PES	Polyethersulfone
PES-C	Modified polyethersulfone
PET	Polyester; polyethylene glycol terephthalate
PFE	Polyfluoroethylene
PGLA	Polyglycolide-co-L-lactide
PH	Polyhydantoin
PI	Thermosetting polyimide; polyimide
PIC	Polymer-impregnated concrete
PIP	Polymer impregnation and pyrolysis
PIPD	Polypyridobisimidazole
PL	Photoluminescent
PLA	Polylactic acid
PLC	Polymer matrix nanocomposite
PM	Powder metallurgy
PMC	Resin matrix composites
PMMA	Polymethyl methacrylamide-acrylic; polymethyl methacrylate
PMR	Polyimide resin
POF	Plastic optic fiber
POM	Polyoxymethylene
PP	Polypropylene
PPD	p-phenylenediamine; pre-ceramic polymer-derived
PPE	Polyphenylether

PPP	Poly-p-phenylene
PPS	Polyphenylsulfureter; polyphenylene sulfide
PPTA	Poly p-phenylene p-phenylenediamine terephthalamide; p-phenylene terephthalamide
PPV	Polyphenylene vinylene
PS	Parallel-series; polysulfone; point stress criterion; polystyrene
PSU	Polysulfone
PSZ	Partially stabilized zirconia; polysilazane
PT	Phenol-triazine
PTBPCN	Tert-butyl phenyl cyanate ester
PTC	Positive temperature coefficient
PTFCE	Polytrifluorinechloroethylene
PTFE	Polytetrafluoroethylene
PTMC	Particle-reinforced titanium matrix composite
PU	Polyurethane
PVA	Polyvinyl alcohol; polyvinyl acetate
PVC	Polyvinyl chloride
PVD	Physical vapor deposition
PVDF	Polyvinylidene fluoride
PVK	Polyvinyl karbazol
PyC	Pyrolytic carbon
QA	Quiacrodone
QI	α components
RA	Rheological analysis
RAM	Resonate energy absorption
RARTM	Rubber-aided RTM
RBSN	Reactive-sintered Si ₃ N
RC	Enhanced layer
RCS	Cross section
RE	Rare earth
RFI	Resin film infusion
RICRTM	Resin injection circulating RTM
RIM	Reaction injection molding
RIMP	Variable infusion molding process
RIRM	Resin injection re-circulating molding
RL	Rough laminar
RMI	Reactive melt infiltration
RPC	Reactive powder concrete
RPMP	Glass fiber-reinforced plastic mortar
RQL	Rich-Quench-Lean
RRIM	Reinforced reaction injection molding
RT	Room temperature
RTA	Room temperature ambient
RTL	Ratios of transverse strain to the longitudinal strain
RTM	Resin transfer mold; resin transfer molding

RVE	Radius of a composite volume element; representative volume element
SAN	Styrene-acrylonitrile copolymer
SARTM	Solution-aided RTM
SAW	Surface acoustic wave
SAXS	Small angle X-ray scattering
SBR	Styrene-butadiene rubber
SBS	Short beam shear
SCF	Short carbon fiber
SCL	Soft contact lens
SCRIMP	Seaman's composite resin infusion molding process
SCS-6	CVD SiC fibers on carbon cores
SEA	Specific extinction area
SEM	Scanning electron microscopy
SFRP	Short fiber-reinforced polymer
SGL Carbon	A transnational corporation situated in Germany
SHS	Self-propagating high-temperature synthesis
SIFCON	A fiber-reinforced cement-based composite
SL	Smooth laminar
SM	Surface of mat
SMA	Styrene-malei anhydride; shape memory alloy
SMC	Sheet molding compounds
SOC	Spiro ortho carbonates
SP	Series-parallel
SPC	Statistical processing control
SPM	Scanning probe microscopy
SRIM	Structure reaction injection molding
SRM	Short-range missiles
SS	Stainless steel
SThM	Scanning thermal microscopy
STM	Scanning tunneling microscope
SVF	Silicone vacuum fluid
SWCNT	Single-walled carbon nanotube
TA	Terephthalic acid; thermal analysis; α titanium alloys
TANGO	Technology application to the near-term business goals and objectives
TB	β titanium alloys
TBA	Thermal braiding analysis; torsion braid analysis
TC	α + β titanium alloys
TCRDL	Toyota Central Research and Development Laboratories, Inc.
TEC	Thermal expansion coefficient
TEM	Transmission electron microscope; transverse electromagnetic waves
TEMPEST	Transient electromagnetic pulse emanation standards
TEOS	Tetraethoxysilane

TERTM	Thermal expansion RTM
TFAA	Trifluoroacetic anhydride
TG	Thermogravimetry
TGA	Thermal gravimetric analysis
TGAP	Tri-glycidyl p-aminophenol amines
TGBAP	Bi-(4-hydroxyl-benzol)-p-diisopropyl benzene-N,N, N' N'-tetra-glycidyl ether
TGDDM	4,4-tetraglycidyl-amine-diaminodiphenylmethane; Cured 4-functional epoxy resins
TGIL	Tri-glycidyl ether
TGMBAP	Bi-(3,5-dimethyl-4-amine-l-benzol)-p-diisopropyl benzene-N,N,N', N'-tetraglycidyl ether
THF	Tetrahydrofuran
TLC	Thermotropic liquid crystal
TLCP	Thermal liquid crystal polymer
TLP	Tension leg platform
TMA	Thermal mechanical analysis
TMC	Titanium matrix composites
TNK	Toa Nenryo Kogyo K. K.
TOS	Thermal oxidative stability
TP	Thermoplastics
TPU	Thermoplastic polyurethane
TS	Triode sputtering
TsAGI	The Central Aero-Hydrodynamic Institute
TTA	Thenoyl trichloroacetone
TZP	Tetragonal zirconia polycrystals
UCL	Up control limit
UD	Unidirectional
UHM	Ultra-high modulus type
UHMWPE	Ultra-high molecular weight polyethylene
UHT	Ultra-high tenacity type
UP	Unsaturated polyester resin
UV	Ultraviolet
UVRTM	Ultraviolet (cure) RTM
VA/VeoVa	Poly vinyl acetate-vinyl versatate
VAATE	Versatile affordable advanced turbine engines
VAFI	Vacuum-assisted resin infusion
VARI	Vacuum-aided resin injection
VARTM	Vacuum-assisted resin transfer molding; vacuum-assisted RTM
VB	Vacuum bag
VE	Virtual enterprise
VGCF	Vapor-grown carbon fiber
VHP	Vacuum hot pressing
VID	Visible impact damage
VIP	Vacuum injection process; vacuum infusion process

VLS	Vapor–Liquid–Solid
VLSI	Very-large-scale integration
VM	Virtual manufacturing
VR	Virtual reality
VRTM	Vacuum RTM
VS	Vapor–Solid
VTP	Virtual-type project
WAXD	Wide angle X-ray diffraction
WBL	Weak boundary layer
WCMC	Whisker-reinforced ceramic matrix composite
WFM	Woven meso-mechanical analysis program
W/C ratio	Water/Cement ratio
XD	Exothermic dispersion; a trademark of the Martin Marietta Corporation
XRD	X-ray diffraction
ZL	Cast aluminum alloy
ZTA	Zirconia-toughened alumina
ZTC	Zirconia-toughened ceramics

Chapter 1

An Introduction to Composite Materials

Xiao-Su Yi

A composite is a material with two or more distinct constituents or phases that have different physical or chemical properties, which are constructed into a complex architecture at micro-, meso- or macro-scale levels. The development and application of single materials like metals, ceramics and polymers has led to the combination of such materials to form synthetic composites. The development of composite materials has enriched modern material systems, contributed to sustainable advances in materials science and engineering and improved human life.

Advanced composites are a class of materials that can provide improved performance compared with that of their constituent materials. Generally, advanced composites can be regarded as the results of structural design and optimization at different dimensions and levels, often combining the latest developments of different individual materials. Improved performance or a new function that a single constituent material cannot provide can be realized in composites through compositing, interface or dimensional effects at different levels. These factors form the basis of composite science.

In the 1950s and 1960s, the exacting requirements of the aerospace and defense industries triggered the design of advanced composite materials. Today, advanced composites are still target structural materials, with the rich potential in these fields promoted by the advancement of industrial technology. As knowledge of composite science and technology grows, a large number of new materials and technologies are being developed, such as composites with structure–function integration, functional and multifunctional composites, intelligent composites and nanocomposites. Advanced structural composites and functional composites combined with developments in computing, processing, characterization and composite applications are ushering in a new era of composite materials in the twenty-first century.

X.-S. Yi (✉)
Beijing Institute of Aeronautical Materials, Beijing 100095, China
e-mail: Xiaosu.yi@biam.ac.cn

Structural composites are an important member of the composite family because of their value in technology, economics and society. The development and application of polymer (resin) matrix composites has been the main focus of composite development globally [1]. Therefore, this introduction chapter focuses on polymer matrix composites, related fundamental theories and their latest developments.

1.1 Introduction to Composite Science and Engineering

The objective of composite science and engineering is to answer the following questions with respect to purpose, methods and results. First, why we combine two or more components with different physical and chemical properties together? Second, how do we combine these components together? Thirdly, what kind of interface will be formed after the combination of the components? Fourthly, what is the performance of the resulting composites? Finally, how do we measure the composite structures and their performance? In particular, researchers need to determine the exact relationship between the designed structure and its performance. Answering these questions requires characterization and evaluation of the composites, as well as verification of their performance and functions, using both experimental and simulation techniques.

Generally, the science and engineering of metals, ceramics and polymers are the most important factors affecting composites. The unique features of composites, including their surfaces and interfaces, processing, characterization, performance and functional principles, also affect their structure and properties. For example, structural composites are designed to possess improved mechanical properties, while functional composites are prepared with the goal of obtaining intermediate or totally new physical/chemical functions from those of the parent materials. To date, great progress has been made in both structural and functional composites.

The typical features that define composites in relation to other engineering materials are their wealth of multi-scale, multi-level structures, together with the enriched correlation between each structural dimension and level with their micro-, meso- and macro-scale performance and functions. The microscopic structural and morphological performance or functions of a material can be expressed as its figure of merit, which is generally the specific integration of the physical properties and structural parameters of a material (tensor). A composite can have changeable structural parameters that a single material cannot display. By changing structural parameters such as composition, connectivity, symmetry, scale and periodicity, the physical property tensors of a material can be tailored over a wide range. This kind of strong intercorrelation between structure and function endows composites with large changeability potential, which makes it possible to design and manufacture composites with high combined performance based on specific performance or functional requirements and to fulfill the integration of structure and function. Controlling the intrinsic structure and performance of matrix-phase and filling-phase materials is included in the category of research and development of

single materials, such as polymer matrixes and filling materials like fibers or inorganic particles. In terms of composite systems, their important dimensions are within the range from nanometers to microns. Therefore, it is possible to produce composites with high combined performance based on specific performance or functional requirements and to integrate structure and function. The most influential structural levels of composites are the phase interfaces of multiple-phase polymers, the interface of heterogeneous structures (such as fibers and resins) and interlaminar structures (including interfacial phases, fiber interlaminates and low-dimensional flake interlaminates), as well as their texture and morphology. Importantly, these structures never exist in individual materials.

It is impossible to fully describe the science and engineering of composites in such a brief introduction. Therefore, here we use typical examples to highlight important issues in composite science and engineering. Based on this, polymer matrix composites were chosen to exemplify the surface and interface issues facing advanced composite materials. The multi-dimensional and multi-level constructions and innovative processing techniques for current aerospace structural composites are considered. The development of advanced composites is also highlighted, and current research trends are explored, including low-dimensional composites, and the integration of composite structures and functions. The performance of nanocomposites is predicted, and the function principles of 0–3 filling composites and their mathematical/physical expressions are also discussed.

The examples considered in this chapter describe work carried out by the author and his research team, quoting original data and results to explain the principles of composite science and engineering.

1.2 Surfaces and the Reinforcement–Matrix Interface

Generally, composites consist of different heterogeneous components, and thus, interfaces are inevitable. The interface in a composite, also called the interface or interfacial layer, is a layer of material that exists between two components with distinct structure from both adjacent sides. Obviously, this layer of material must have a thickness. The thickness and structure of an interface are correlated with the properties of the contacting states on both adjacent sides as well as the thermodynamic, kinetic and processing conditions. In some cases, surface treatment of one or both adjacent sides can also affect interface structure and thickness and determine the ultimate performance and functions of a bulk composite. At the same time, the structure of an interface is not necessarily symmetrical and may be inhomogeneous, asymmetric or disordered. Thus, from a general point of view, a distinct surface could be generated by the unique structure in the subsurface of a composite because of its surface contact with molds or other media during long-term use, which normally can be ignored in practice.

There are two methods to form an interface layer. One is chemical reaction under certain conditions, or diffusion/dissolution of the elements from both phases of

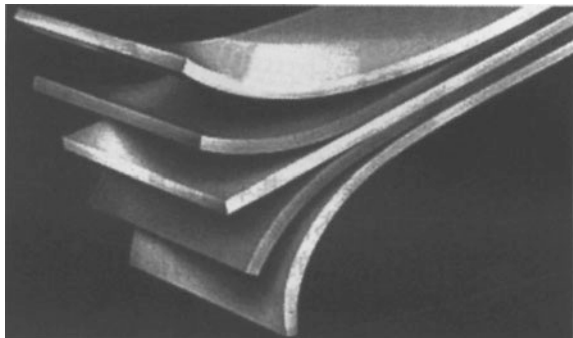
heterogeneous materials. The other is the internal stresses generated during curing, or the interaction between two-phase structures, which can make the structures located close to a reinforcement surface differ from the matrix itself, generating an interface. Moreover, the various coating layers pre-applied to reinforce a surface, or the structural changes caused by surface treatment can also be referred to as an interface. Interface structures influence the integral performance of composites, e.g., stresses have to be transferred through the interface in structural composites, and the residual stresses on an interface can also affect the integral mechanical properties of composites. In particular, the functions of functional composites need to coordinate through interfaces. As a result, the interfaces of composites need to be well designed and controlled.

The compositing of heterogeneous materials involves formulating many materials, making it difficult to describe the whole process thoroughly. In the following sections, a standard compositing of heterogeneous materials called fiber–metal laminates (FMLs) is used as an example to discuss the material surface and its treatment, the interface and the correlation between interface structures and their related interface properties.

1.2.1 Fiber–Metal Laminates and Their Interface Structures

In the late 1970s and early 1980s, a novel type of composite, FML, was developed at Delft University, the Netherlands [3–10], where metal plies (Al and Ti alloys) were alternately bonded with resin prepregs composed of glass fiber, aramid and carbon fiber with the epoxy bismaleimide (BMI) to form a 2–2 laminate with five layers (Fig. 1.1). The first product developed was aramid fiber-reinforced Al laminate (ARALL), and the second was glass fiber-reinforced Al laminate (GLARE). FMLs combine the advantages of both metals and resin matrixes to exhibit excellent fatigue performance. FMLs have been widely certified and are used in fuselage structures in commercial airplanes such as the Airbus A380. To date, this may be the only advanced composite originally developed by a university to find successful commercial applications in the aerospace industry.

Fig. 1.1 A fiber–metal laminate

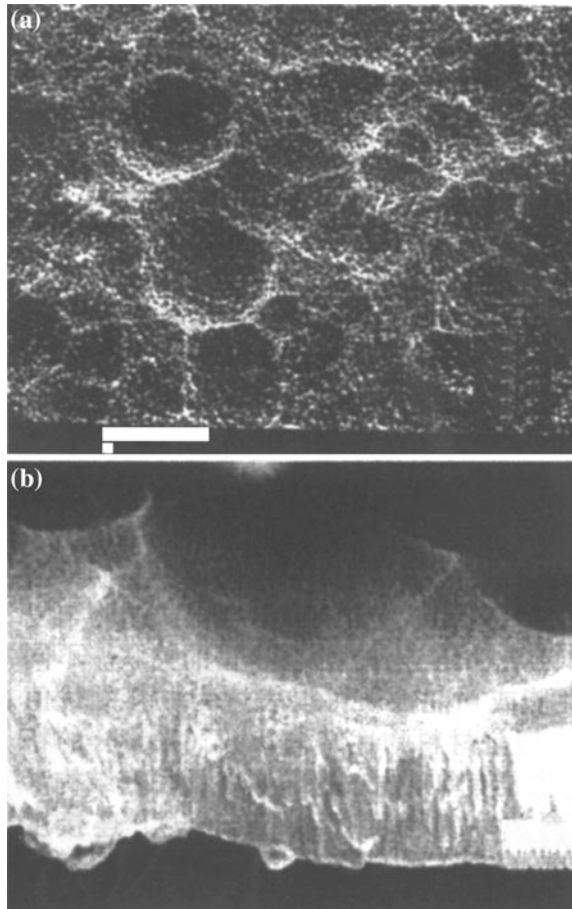


For FMLs consisting of Al alloy, epoxy resin and fibers, the interface between the Al alloy and epoxy is the dominant factor controlling their properties. This multi-level interface structure results in very complicated mechanical performance and aging problems.

In the following experiments, Al alloy panels were treated with different chemicals to change their surface morphology. Uneven morphological characteristics of oxidized Al surface were observed under low magnification after chromic acid immersion or chromic acid anodization (CAA) (Fig. 1.2).

Transmission electron microscopy (TEM) revealed the irregular closed cavity structure of the oxidized layer of a certain thickness between two cavities [3]. Observing a cross section of the oxide layer formed by CAA revealed that the depth of these cavities was 3–4 μm , while their diameter was only 20–30 nm, less than 1% of the cavity depth (Fig. 1.3). This nanoscale oxidized-layer cavity structure gives the Al alloy surface a very large specific surface area.

Fig. 1.2 **a** Morphology of an oxidized Al surface and **b** its cubic image after peel off



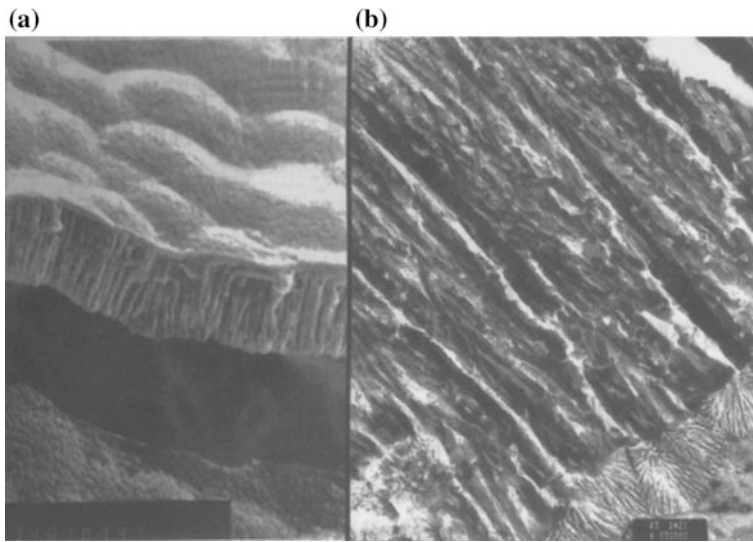


Fig. 1.3 **a** Cross-sectional image and **b** cubic morphology of an oxide layer after peel off

Table 1.1 Comparison of oxidized Al surface structures produced by four typical processes

Process	FPL	Pickling	CAA	PAA
Layer thickness/nm	40	10–20	$3.5\text{--}4.0 \times 10^8$	$0.25\text{--}0.4 \times 10^8$
Cavity diameter/nm	~40	10–30	~25	~40
Cavity depth/nm	40	8–9	$0.1\text{--}1.0 \times 10^8$	–
Cavity wall thickness/nm	5	6–7	12–14	10
Block layer thickness/nm	5	1–2	20–50	5
Structure	–	Non-crystal	Non-crystal	Non-crystal
Chemical composition	Al ₂ O ₃	Al ₂ O ₃	Al ₂ O ₃	Al ₂ O ₃
OH:O ratio	–	0.038	0.052	0.14
Unknown ion	–	$S < 1 \text{ At.}\%$	$S < 1 \text{ At.}\%$	P, F

The Al alloy substrate lies under the oxide layer formed by CAA. After the Al alloy substrate was removed by chemical etching, only the CAA oxide layer remained, as illustrated in Figs. 1.2 and 1.3. The closed bottom of the cavity structure means the interface between the oxide layer and Al alloy substrate has a camber (Fig. 1.4).

The formation process of FMLs depends on the generation of an oxide layer, which is controlled by surface treatment. As a result, it is important to study the influence of the oxidized layer on the metal–polymer interface. Apart from pickling and CAA, the Forest Products Laboratory (FPL) process and phosphoric acid anodization (PAA) have also been widely used and standardized as surface treatment methods by the aerospace industry. Table 1.1 shows the structural characteristics of oxidized Al surfaces prepared by these four methods.

Fig. 1.4 Cross-sectional image of the arc cubic interface on the bottom of an Al oxide layer



For an oxide layer with large specific surface area and high reactivity, the first step of compositing is the impregnation of low-viscosity liquid resin, and the reaction of the resin with the oxidized layer. Microzone analysis of the oxidized Al surface by electronic energy loss spectroscopy showed that carbon atoms at the bottom of the cavity were transported through the cavity structures. This indicates that low-viscosity polymers, e.g., primer, coupling agent or adhesives, are capable of deeply impregnating the microstructures of the oxidized layer, which guarantees the success of the first step of the compositing process. The product is a unique three-dimensional composite structure, where the interface structure between the Al oxide and polymer is formed in the nanocavities in the oxide layer.

In this interface structure, the top layer is polymer. Because Al oxide structures with large specific surface area have different ratios of reactive thermosetting polymer in localized zones, the cured resin in the oxide layer as well as its adjacent zones might be different from that of zones in other locations. Thus, a new polymer interface structure appears. The type of polymer interface structure formed with common epoxy resins will have the same morphology as that shown in Fig. 1.5.

The typical morphology shown in Fig. 1.5 is a fiber-like structure with one end adhered to the interface structure between the Al oxide and polymer, and the other end penetrating deeply into the epoxy resin matrix. Because this matrix is removed from the influence of the oxidized Al layer, its structure and properties will be identical to those of conventional bulk epoxy materials. Unlike the interface, this bulk-type material with particles and cross-linked structure can be referred to as the

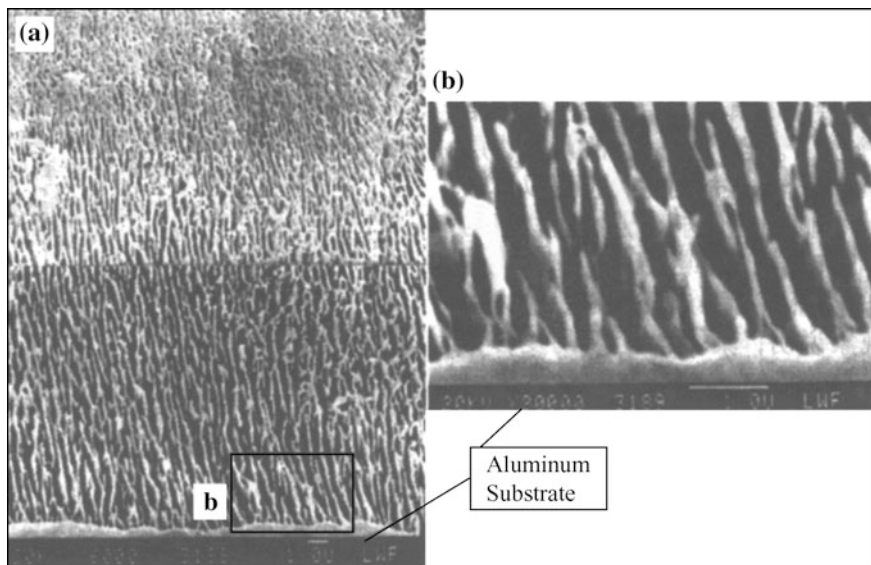


Fig. 1.5 **a** Epoxy resin interface structure formed on an oxidized Al surface layer and **b** enlarged image of area *B*

base phase of epoxy. This fiber-like structure demonstrates that the polymer is inhomogeneous, the density of the material is non-uniform, and the density of the materials present between the fiber structures is low.

At least two different interface structures, nanoscale oxide–polymer and fiber-like epoxy resin, can exist between the bulk Al alloy and bulk epoxy resin (or at their interface), and their source, formation and growth can be considered as a three-dimensional structure. Thus, some traditional theories, such as impregnation, diffusion, static electric and rheological theories, are not suitable to fully describe typical Al–epoxy adhering behavior, because their interfaces are simply considered planar in these theories. Even some modern and more complicated models, including micromechanical adhesion and physical–mechanical engaging models, cannot comprehensively explain the chemical and physical adsorption processes occurring in such three-dimensional interface zones. Based on the understanding of this typical interfacial adhesion of Al and epoxy resin, the following three conditions should be satisfied for the metal side:

- (1) Absorption specific surface area should be as large as possible;
- (2) Molecules and even atoms on both adsorption sides should stay as close as possible to achieve deep impregnation on the microscale;
- (3) Chemical and physical structures on each interface-adsorbing side should be as stable as possible to form strong interfacial bonds.

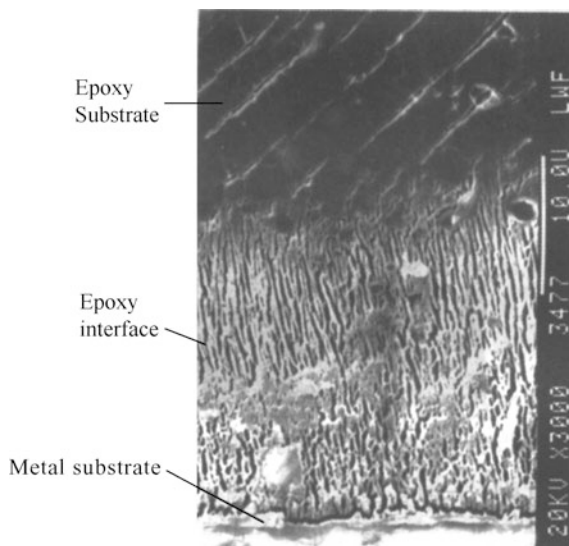
Composite interface engineering hopes to achieve the above structures through surface treatment and metal processing.

As for the polymer in composites, especially for thermosetting resins with high reactivity, the specialized heterogeneous material (Al oxide layer) should have some short-distance influence on the polymer cross-linking reaction to form an oriented fiber-like structure vertical to the surface of the oxidized metal layer. The distance of this influence depends on reaction conditions. Interface structures composed of heterogeneous materials can be controlled by using a metal surface coating and the related application process, designing and preparing compatible coating materials, or by matching polymer materials with suitable design and preparation conditions. All of these approaches are important in composite interface engineering.

1.2.2 Mechanical Characteristics and Aging Behavior of the Interface Structures of FMLs

It was realized early that thin-layer materials might perform differently from that of bulk materials and may be subject to short-range reactions with attached heterogeneous materials. Behind these observations lies the interface issue. Interface materials can have different structures and performances from those of the adjacent materials on both sides, as shown in Fig. 1.6. When an epoxy resin layer is subjected to average shear stresses, shear cracks with 45° orientation form at the plane of symmetry and are only located in the base phase of the polymer layer. Meanwhile, tensile cracks form close to the Al oxide layer or at the bottom of the fiber-like structure, indicating that a weak interfacial layer exists close to the metal side in the interface structure.

Fig. 1.6 Shear cracks generated in epoxy resin base phase and normal stress fracture in the interface



The simplest way to study the relationship between interface structure and performance in FMLs is to construct a metal–polymer–metal laminate and then gradually decrease the polymer layer thickness to an equivalent interfacial layer thickness to examine the mechanical response. Here, the first issue is to find a suitable measurement technology to determine the mechanical response of such a polymer layer. A metal–polymer–metal laminate is equivalent to a metal-adhered joint. Tensile–shear testing is the main method used to measure the mechanical properties of such joints and has some international and domestic standards. However, all such mechanical measurement methods encounter a common problem; that is, the multi-axis stress condition. Because of this stress condition, the measured joint strength cannot reflect the mechanical response behavior of adhesive layer materials and cannot be used to study the performance of thin-layer materials. The book “An Introduction to Laminated Adhering Composites” [2] proposes many testing configurations to determine characteristic single-axis shear stress–strain response curves. Generally, these configurations can provide the characteristic shear response curves of adhesive layers.

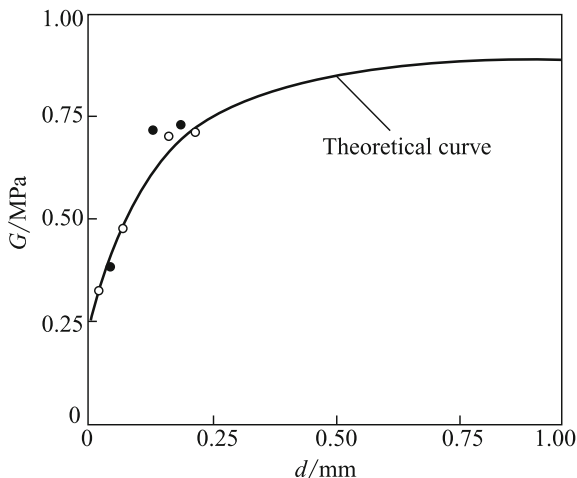
The pure shear response of epoxy resin layers strongly depends on adhesive layer thickness. When the adhesive layer is thinner, the shear strain is larger and the initial shear mold is smaller and vice versa. From the aspect of materials science, the reason for this is that two different polymer layers form a sandwich structure configuration of “interface layer–base phase layer/intermediate phase layer–interface layer.” For a given set of materials, the layer thickness of the polymer interface is essentially constant, although it can be affected by the Al oxide layer. As a result, changing the total adhesive layer thickness can only affect the layer thickness of the intermediate polymer phase. However, if this joint is twice the thickness of the interface layer, the measured adhesive layer shear curve will be the shear curve of the interface layer. When the adhesive layer is very thick, the thinner interface layer can be neglected. At this point, the shear curve is almost equivalent to that of the intermediate polymer layer. As illustrated in Fig. 1.6, the interface layer thickness is about 20 μm , so the curve of the 0.03- μm layer is basically the shear performance curve of the interface layer, which shows a small initial shear modulus and large shear deformation.

As understood from the oriented fiber-like structure layer, especially compared with the intermediate layer phase with an aggregated structure, the response of the interface layer under external shear action can be used to quantitatively study the relationship between adhesive layer total modulus, G , and total thickness, d :

$$G = \frac{d}{\frac{d-2d_{\text{inter}}}{G_m} + 2\frac{d_{\text{inter}}}{G_{\text{inter}}}}$$

where d_{inter} is the polymer interface layer thickness, and G_m and G_{inter} are the polymer shear modulus in intermediate and interface layers, respectively. The calculated G – d relation curve based on this equation is displayed in Fig. 1.7. This curve indicates that the shear modulus of the adhering layer will increase with layer

Fig. 1.7 Correlation between polymer-adhering layer shear modulus and thickness (G - d correlation), and comparison of the theoretical curve with experimental values



thickness until a maximum point is reached. The calculated values fit the test results well, which verifies the theoretical model; that is, the initial shear modulus is lower than the average modulus of the adhesive layer.

Because a certain ratio of low-density materials is present in the interface layer, its moisture absorption behavior will differ from that of the adhesive intermediate interface layer with an aggregated structure. Taking adhesive layer thickness as a variable to measure the moisture absorption content, the test results indicate that the thicker the layer, the higher the absolute absorbed moisture content will be. Furthermore, the moisture content absorbed in a specific volume of the interface layer increases with layer thickness. In other words, the interface layer can absorb much more water than the bulk layer in the same time interval, resulting in a higher moisture concentration. Moisture in the interface layer can lower hot/wet stability, which should be carefully considered in aero-based metal-adhering structures.

Leaving aside the acidic or alkali hot/wet aging on the Al side of the oxide interfacial layer, stronger shear creep and lower residual shear fracture strength have been observed in the epoxy resin interface layer compared with those in the intermediate interface layer [11]. As time passes, this decrease in shear strength as well as increase in shear creep becomes more obvious until the adhesive layer fails. From a microscopic viewpoint, microscale creep damage formed during the aging process has been found in fiber-like interface layers. When the apparent shear deformation in whole adhesive layer reached 22%, the real shear strain in the interface layer increased to 31%. The fiber-like interface layer structure could not sustain such a high shear strain, so shear failure occurred in the layer adjacent to the metal surface.

Studies on FMLs have proved that their material surfaces and interfaces as well as their construction and properties are complicated. In fact, an interface forms at any area where a material structure is subjected to change. From this point of view, it is difficult to generalize the interfacial behavior of composites.

1.2.3 Interfaces of Fiber-Reinforced Resin Matrixes

FMLs make up only a small part of the advanced composites family; the largest member is fiber-reinforced polymer composites. In fact, the Al plate surfaces and interfaces generated in the compositing of metal and resin described above did not include the fiber surface or the interface between fiber and resin. The main reason for this is because surface treatment of fibers is normally carried out to match the resin matrix in the fiber suppliers before composite manufacture, and usually the compatibility between fiber and resin can meet the service requirements for composites. In other words, commercial fibers have already been coated, so they can be defined according to the resin coating rather than the fiber surface itself.

The sizing and finishing of commercial fibers are diverse and can be organic- or water-based, including diluted resin, curing agent, surface lubricant, antistatic agent, pH-adjusting agent and emulsions. Fibers are usually coated with multiple layers to obtain combined performance. The main functions of sizing and finishing are to protect the structure and surface conditions of the fresh fibers to obtain good interface adhesion between the fiber and resin (coupling effect) and to increase their anti-friction and antistatic properties. Fiber surface-treating agents and their applications are core techniques in fiber production. Because the suppliers must satisfy various customers, the surface coatings for commercial fibers must be general purpose. Therefore, fibers from various suppliers may have different coatings with different chemical properties, among which there will not be a type of coating specially produced for a specific epoxy resin. Using a de-coating method to study these fibers, or applying a new coating after the old is removed, generally hinders compositing. The reason for this may be that the original surface treatment processes might provide a much higher surface activity than the subsequent treatment. The exception is small-scale, innovative fibers or matrixes, which is a new direction of fundamental study.

The interface between a fiber and resin is not two-dimensional, but a three-dimensional interface structure, and its performance differs from that of bulk materials such as polymers or coatings, as shown in Fig. 1.8. Like an Al alloy surface, a fiber surface also has a particular topology, which depends on fiber type.

Fig. 1.8 Schematic diagram of the interface between a fiber and matrix

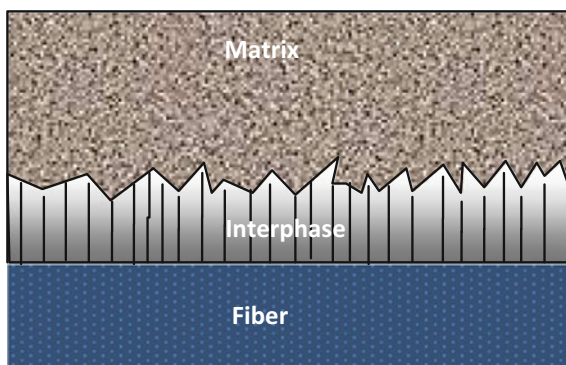
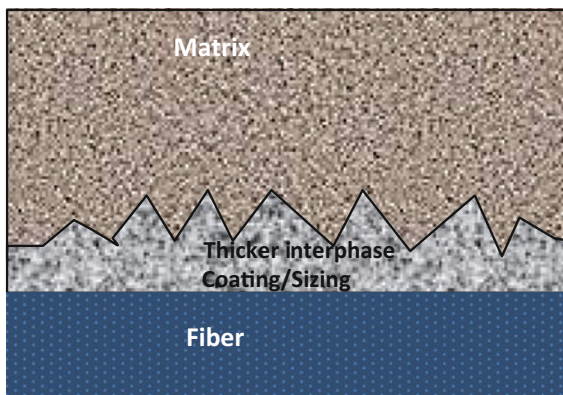


Fig. 1.9 Schematic diagram of time-dependent formation of an interface between a fiber and its sizing and a liquid matrix



Interface formation in a fiber and resin matrix is an equilibrium process. During resin transfer molding (RTM) processing, for example, the freshly injected resin will swell or dissolve the fiber coating, and react with it to form an interface until the equilibrium state is reached. This process requires time, as shown in Fig. 1.9. For a multi-injection system, newly and previously generated interfaces may coexist. An inter-reaction phase may also form between these interfaces, depending on the sequence of fiber wetting with fresh resin and the time needed for equilibration. It is clear that interface formation is a multi-dimensional, multi-level, and time/location-dependent process.

Fiber–resin interface construction requires surface reactions and occurs as a result of the time-dependent balanced inter-reactions taking place at the interface between the solid fiber surface and liquid resin. Nevertheless, composite engineers can use processing conditions and windows to control interface construction. To fully understand interface construction and its influence on composite performance is a long-term goal of materials scientists.

Fibers in advanced composites are used in bundles rather than individually. The surface treatment of a bundle of fibers differs from that of a single fiber. This influences the interface impregnation process, such as RTM processing.

1.3 Multi-scale, Multi-level Construction and Optimization of Composites

The multi-dimensional, multi-level construction and optimization of composites are important fundamental research issues in composite science and engineering that cannot be limited to only interfaces [12].

According to the concept of connectivity, composites with fillers are defined as 0–3 construction, while laminated composites are 2–2 construction and bicontinuous composites are 3–3 construction. Starting from a homogeneous phase, the reaction induces phase splitting. And the coarsening process of thermoplastic–

thermosetting complex-phase polymer materials is equivalent to a continuous phase-change process with 0–0, 0–3 and 3–3 constructions according to the connectivity concept, which means each time domain contains numerous changes in the structure and morphology of the material.

When this continuous phase change is put in a 2–2-type confined zone (such as carbon fiber laminates), 3–3 double-continuous structures in a dimensional gradient distribution will be formed, which can produce materials with excellent integrated toughness, stiffness and strength. This combination is impossible to obtain under uncontrolled conditions. According to the above classification, generally 3–3-type thermoplastic–thermosetting complex-phase polymer materials do not belong to the class of composites, but are multi-phase polymer materials. In terms of finite-element, highly integrated mechanical performance, it is possible to realize the design and controlled manufacture of multi-scale, multi-level constructions with morphologies like 0–3, 1–3, 2–2 and 3–3 series. It is predicted that 0–3, 3–3 series and periodic 2–2 series will be possible breakthroughs in coming years. It is also worth pointing out that real composite constructions are much more complex than these X – X series expressions.

In this section, we focus on aerospace structural carbon fiber-reinforced advanced composites. We examine their development trends and national demand and discuss their multi-dimensional, multi-level construction and optimization.

1.3.1 Composite Development and Controlled Conditions

In early 1996, five organizations in the United States of America (USA)—the Committee on New Materials for Advanced Civil Aircraft, the National Materials Advisory Board, the Aeronautics and Space Engineering Board, the Commission on Engineering and Technical Systems and the National Research Council—published a joint research report called “New Materials for Next-Generation Commercial Transport” [13], which stated “The current, turbulent economic climate affecting the airline, manufacturer, and materials industries has significantly changed the application criteria for advanced materials. As a result, material performances will not be the first standard for materials selection; aircraft manufacturers are responding to airline concerns about reducing overall costs including the costs of acquisition and maintenance. The result is incremental, evolutionary—rather than revolutionary—changes in materials.” According to this report, the main obstacles to the commercialization of high-performance materials included:

- (1) The high expense of new materials compared with conventional ones, including acquisition, manufacture, certification and life-cycle costs;
- (2) Limited understanding of failure mechanisms and their interactions in high-performance composites and their structures;

- (3) Considering technical and safety risks, industries have little enthusiasm to understand advanced materials, no experience in their application, and are impatient for advanced materials to mature;
- (4) Serious competition in global commerce makes it difficult for materials administration to provide long-term financial support for middle- and long-term plans. It is also difficult to establish a capable, effective hub for materials research, development and supply.

Because of these impediments, the applications of advanced aerospace composites in the 1990s were actually much lower than the optimistic expectations of the late 1980s. To overcome this, a succession of research projects on aerospace composites were proposed in the USA, with targets of 50% weight reduction, 80% part reduction, 25% overall cost reduction and 80% fastening reduction. At the same time, a number of large research programs, such as Design Manufacturing of Low-Cost Composites, Advanced Fuselage Structure, Low-Cost Composites Processing, Advanced Composite Technology, Advanced Technology Composite Aircraft Structure and Composites Affordability Initiative, have been started. In the twenty-first century, applications of aerospace composites have increased sharply with a remarkable representation in Airbus A380 and Boeing 7E7. This suggests that considerable progress has been made in aerospace composites, particularly with regard to performance and cost.

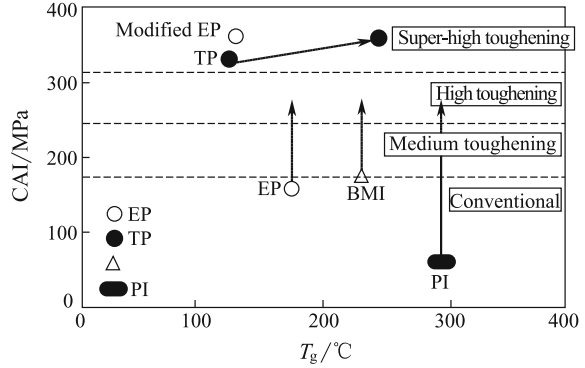
This progress also improved our understanding of the multi-dimensional, multi-level structure of advanced carbon fiber-reinforced composites. There remains great opportunity for aerospace composite development in areas such as cost reduction, high damage tolerance, microstructure-optimized design, and manufacture and application of generalized composites, as well as further development of low-cost, effective, toughening liquid molding processes, for example, RTM and resin film infusion (RFI).

1.3.2 The “Ex Situ” Toughening Technique and Its Origins

As airplane fuselage materials, two critical characteristics of carbon fiber laminates, their impact damage resistance (tolerance) and glass transition temperature (T_g , or thermal-wet service temperature), are determined by the resin matrix. In the aerospace industry, the impact damage resistance is expressed as compression strength after impact (CAI) and is usually used to classify resin toughness and generation (Fig. 1.10).

The first generation of aerospace composites ($C^{\text{composites}}$) was simply laminates (2–2 composition) composed of resin ($A_{0-3}^{\text{resin phase}}$) and fibers ($B_{2-2}^{\text{reinforcement}}$), which can be expressed as $A_{0-3}^{\text{resin phase}} + B_{2-2}^{\text{reinforcement}} = C_{2-3}^{\text{reinforcement}}$. The matrix resins used in the first generation of aerospace composites were mainly common thermosetting resins like epoxy, BMI and polyimide (PI). Because of their inherent brittleness (the corresponding points of CAI in Fig. 1.10), matrix resin toughening occurred.

Fig. 1.10 Correlation between the compression strength after impact (CAI) and glass transition temperature (T_g) of aerospace composites (arrows show direction of improvement)



Toughening thermosetting resins can be produced by addition of high-performance thermoplastic resin to induce thermal reaction destabilization and phase splitting, which results in particulates, especially in double-continuous 3–3 constructions. That is, the mixture $(A_1 + A_2)_{3-3}^{\text{reinf phase}}$, where A_1 is a thermosetting resin and A_2 is a thermoplastic resin, can form a medium resin. This process can be simply expressed as $(A_1 + A_2)_{3-3}^{\text{reinf phase}} + B_{2-2}^{\text{reinforcement}} = C_{3-2}^{\text{reinforcement}}$. On this basis, in the late 1980s and 1990s, the so-called second generation of toughened resin composites was developed with CAI higher than 200 MPa (refer to the toughening materials in Fig. 1.10).

Thermoplastics are usually hard and tacky-free at room temperature, so this toughening technique often degrades the good handling of original thermosetting resins and the drapability of prepregs, causing some processing performance to be lost. Furthermore, the CAI of such toughened resins is usually below 300 MPa, which does not meet NASA or Boeing’s requirements for commercial aerospace composite damage tolerance. Consequently, the second-generation techniques are limited.

Simultaneously, thermoplastic composites like polyetheretherketone (PEEK) came onto the horizon because of their inherent high toughness, which can easily reach CAI of up to 300 MPa. PEEK is a representative of the third generation of high-toughness composites (see Fig. 1.10). However, thermoplastic composites generally have poor processability, and their high cost has limited their use. Moreover, the understanding of these composites is much poorer than that of thermosetting materials. To date, the application of high-performance thermoplastic composites is still limited. In terms of compositing, thermoplastic composites possess the simple $(A_{0-3}^{\text{resin}} + B_{2-2}^{\text{reincres}} = C_{2-3}^{\text{composite}})$ structure, where only the matrix resins are varied.

To achieve considerable development of traditional composites, including both high damage tolerance ($\text{CAI} \geq 300$ MPa) and good prepreg processability, an “ex situ” toughening technology has been developed in China [14]. In terms of the principle of compositing, “ex situ” means that the toughening phase is extracted from the matrix and composited independently with a reinforcing phase,

Table 1.2 Comparison of CAI values of epoxy resin laminates and polyetheretherketone (PEEK) composites

Sample	CAI/MPa
Typical first-generation epoxy composite laminate (baseline)	150
Typical second-generation high-toughness composite laminate 5288 (baseline)	267
PEEK composite (APC-2) (baseline)	331
PEEK/AS4 composite (baseline)	285
“Ex situ” toughening composite laminate (ES-1)	345 ^a
“Ex situ” toughening composite laminate (ES-2)	345 ^a
“Ex situ” toughening composite laminate (B)	298
“Ex situ” toughening composite laminate (ES-3)	308

^aThese two values are occasionally the same

and thus, the equation $(A_1 + A_2)_{3-3}^{\text{resin}} + B_{2-2}^{\text{reinforce}} = C_{3-2}^{\text{composite}}$ can be changed to $(A_1)_{3-3}^{\text{resin}} + (A_2 + B_{2-2})_{2-2}^{\text{reinforce}} = C_{2-2}^{\text{composite}}$ [15]. Using this method, the impact tolerance resistance of the resulting composites was enhanced remarkably with CAI values of higher than 300 MPa achieved while keeping cost low, and without degrading the advantages of thermosetting prepregs and in-plane mechanical performance [16]. Some successful examples of epoxy resin (EP) composites are presented in Table 1.2.

Because the “ex situ” method is not affected by the chemical properties of matrix resins, this toughening approach is suitable for epoxy, BMI [17] and PI resins. Many studies have been conducted on this method to date. An important advantage of the “ex situ” method is that materials with high damage tolerance can be achieved at low cost without changing the resin structure and preparation processes of current traditional composites [18].

1.3.3 “Ex Situ” Liquid Molding

Non-autoclave low-cost manufacturing techniques have become the main approach in composite development. A typical liquid molding process is RTM, which includes variations such as vacuum-aided RTM (VARTM), vacuum RTM (VRTM), vacuum-aided resin injection (VARI), vacuum infusion process (VIP), thermal expansion RTM (TERTM), continuous RTM (CRTM), ultraviolet-curing RTM (UVRTM), solution-aided RTM (SARTM), RFI, resin injection circulating RTM (RICRTM), rubber-aided RTM (RARTM) and Seeman resin immersion RTM (SCRIRTM). Among these processes, the five most important are RTM, VARTM, RFI, SCRIRTM and VIP. The major advantage of RTM and RFI is their ability to produce large, complex components with high fiber volume content and high structure design efficiency. For example, more than 400 load-bearing structures, which had around 45% the weight of non-skin composite structures, were made by RTM for an F-22 jet [19]. RTM can control the tolerance of structural

parts within 0.5%, has a rejection rate of less than 5% and provides parts weight and cost reduction of 40 and 10%, respectively, when compared with metal counterparts.

Liquid molding techniques all involve the following process: Closed molds are filled with low-viscosity liquid resin to immerse and impregnate dry fiber structures. Entrapped gas is removed by pressure injection or vacuum, and then, the molds are cured to obtain the part. In terms of flow distance, RTM can withstand a long flow distance, while RFI can only tolerate a short one. Therefore, different resin systems with different viscosities are used in various RTM and RFI techniques.

In all liquid molding processes, two sub-processes coexist simultaneously: physical processes such as resin flow, immersion, impregnation and filling, and chemical processes in which low-viscosity resins became solid materials. Because these two sub-processes coexist, the resin viscosity will increase with flow time and distance, resulting in a series of technical defects:

- (1) Flow over a long distance will become increasingly difficult, especially for large RTM parts;
- (2) Toughening will cause immersion difficulties and dry spots;
- (3) The viscosity of resins will increase over time, which can degrade mechanical properties;
- (4) The traditional toughening method of adding thermoplastic polymers will increase system viscosity, which is undesirable.

In response to these challenges, a study on chemical rheology was carried out with the aim of quantitatively calculating the relationships between viscosity, temperature and time in a resin system to optimize process design. Chemical rheology has now become the theoretical foundation of liquid molding processes, and many types of simulation software have recently been developed [20]. However, the liquid molding theory represented by chemical rheology is limited by the inherent shortcomings in this molding technique. Additionally, such a problem in itself will contain many incorrectly measured parameters and processing parameter inconsistencies, which are very difficult to deal with using chemical rheology.

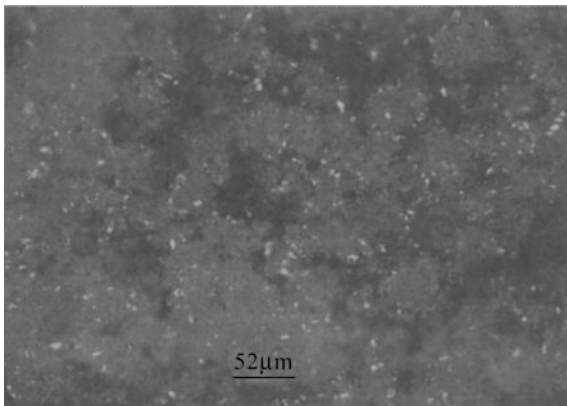
The “ex situ” liquid molding concept was developed in 2001 by Chinese scientists [14, 21, 22]. The philosophy of this concept is to separate liquid molding processes into the physical process characterized by resin flow and the chemical process involving resin reaction. That is, these two parallel sub-processes were divided into two linked sub-processes of before and after, so that the self-inherent contradiction of the interaction of these two sub-processes can be ultimately settled.

The main issue in “ex situ” liquid molding is to separate the constituents in chemical reactions. The concept is similar to that of “ex situ” toughening, $(A_1)_{3-3}^{\text{resin}} + (A_2 + B_{2-2})_{2-2}^{\text{reinforce}} = C_{2-2}^{\text{composite}}$; the only difference is that A_1 and A_2 are referred to as the reactive constituents. For example, in high-temperature BMI composites, the carbon composites prepared using PDM (a meta-substituted BMI monomer with a benzene ring) as the BMI system monomer and an “ex situ” RTM

Table 1.3 Comparison of the interlayer mechanical properties of BMI composites prepared by RTM [23]

	G827/BMI-ES (“ex situ”)	G827/BMI (conventional)
Bending strength/MPa	1740	1730
Bending modulus/GPa	115	125
Shear strength/MPa	98	92
Fiber content/vol.%	55	55

Fig. 1.11 Microscope image of an “ex situ” composite showing BMI monomer particles embedded in a carbon textile



process will give equivalent mechanical performance to that of composites prepared by common RTM (Table 1.3). This gives laminates with a uniform distribution of physical properties, revealing the advantage of “ex situ” molding processes that the viscosity will not increase during resin flow. As a result, long-distance flow in low-pressure injection RTM can be realized, and the open period of the resin system becomes much longer. This widens the injection window, which is convenient for storage and application.

Based on $(A_1)_{3-3}^{resin} + (A_2 + B_{2-2})_{2-2}^{reinforce} = C_{2-2}^{composite}$, Fig. 1.11 shows an optical microscope image of the combined product prepared from the second reactive constituent (A_2) and carbon fiber fabric (B_{2-2}). The first reactive constituent (A_1) with low viscosity was added by injection at low temperature until fibers were fully immersed and impregnated and then heated to achieve further chemical reaction. During the chemical reaction, resin parts A_2 and A_1 adhered to fiber fabric B_{2-2} were dissolved and infused to form a uniform phase, increasing the immersing effect. The final dried fabric was fully impregnated with resin.

Another challenge in liquid molding is how to toughen a composite without losing processability. In Table 1.4, epoxy composites prepared by liquid molding (RTM) are used as an example to compare the mechanical properties of composites prepared by “ex situ” and traditional processes. It should be pointed out that the “ex situ” RTM composites possess CAI almost twice those of composites prepared conventionally.

Table 1.4 Comparison of the mechanical properties of epoxy composites prepared by RTM

	G827/EP (conventional)	G827/EP-ES (“ex situ”)
Fiber content/vol.%	55	55
Bending strength/MPa	1580	1540
Bending modulus/GPa	103	105
Interlayer shear strength/MPa	85	86
CAI/MPa	193	294
Toughening phase content/%	0	15

Table 1.5 Multi-scale and multi-level optimization of composites: natural and artificial materials

Natural materials	Artificial materials
Perfect distribution of reinforcement phase in the composite structure	Limited control of distribution and orientation
Perfectly optimized micro- and macrostructures	Fairly optimized micro- and macrostructures
Proper response and control of the structure to loading	Little control over the response of the structure to loading

1.3.4 Multi-Scale and Multi-Level Optimization

The most attractive feature of advanced composites is the design freedom in their multi-dimensional and multi-level construction. The most successful example of advanced composites is natural materials (Table 1.5). Compared with the perfect macro- and microstructures in natural materials, the challenges we face in terms of composite cost and performance are how to use various constituent materials with medium performance (low cost) to achieve high- or ultrahigh-toughness composites (high performance) with the aid of construction techniques (multi-dimensional and multi-level optimization).

At the microscale, the foundation of conventional toughening methodology is the thermal reaction that induces phase splitting and its coarsening process, where grain and double-continuous 3–3 constructions are formed above the percolation threshold [24] (see Fig. 1.12). After “ex situ” treatment, this highly effective toughened microstructure was evenly distributed between the carbon fiber layers (Fig. 1.13), which markedly increased the interlaminar shear strength, G_{IC} and G_{IIC} , as well as impact damage resistance. Inside the layer, the impregnation of single-phase resin into the fibers was not changed by either pre-impregnation or liquid molding. Thus, the inherent advantages of conventional thermosetting resin matrix composites, such as high stiffness, high strength and strong interfacial bonding, as well as tackiness and drapability that are vital to processing, can be preserved [25]. The resulting material has a typical 2–2 laminated composite structure.

The unique structure of “ex situ” compounds includes a transition zone between the intra- and interlaminar layers, where the diffusion of the shallow surface layer of intralaminar 3–3 grain structure gives interlaminar 2–2 structure (Fig. 1.13).

Fig. 1.12 Grain and double-continuous 3-3 construction formed by thermal reaction phase splitting and its coarsening process

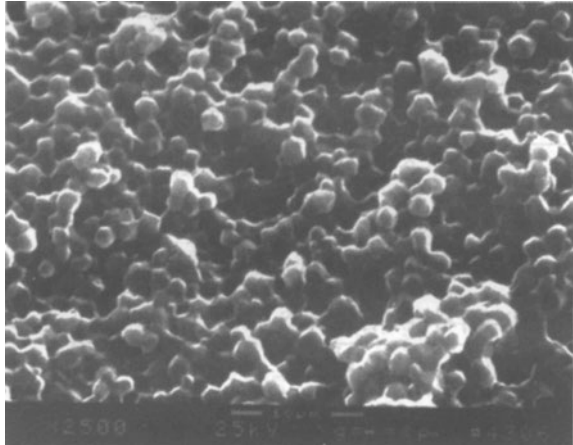


Fig. 1.13 Grain and double-continuous 3-3 construction of carbon fiber layers and infusion inside layers, showing the interface between the carbon fibers and the resin impregnating layer

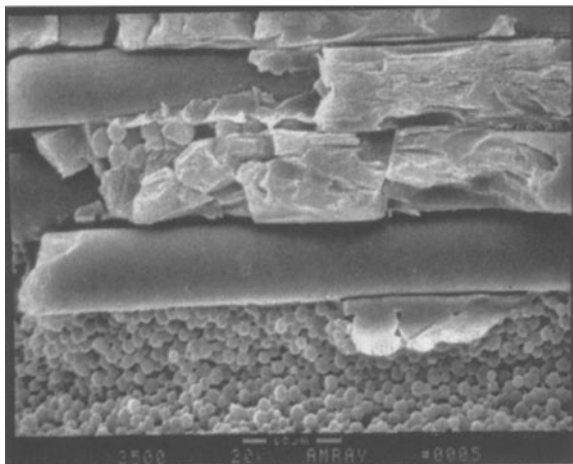
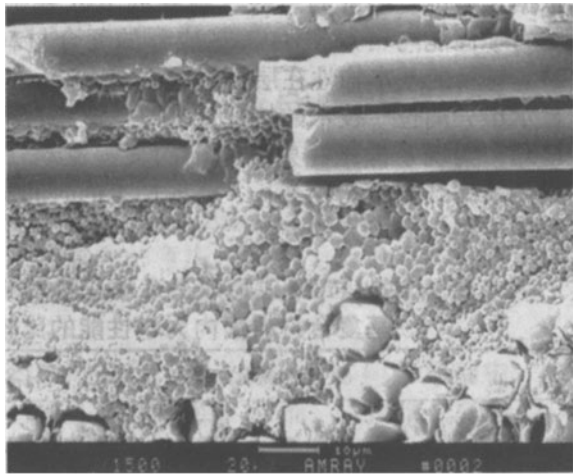


Fig. 1.14 Mechanical interlock generated by superficial layer infusion of 3–3 grain construction, resulting in a large number of fibers pulling out and fracturing

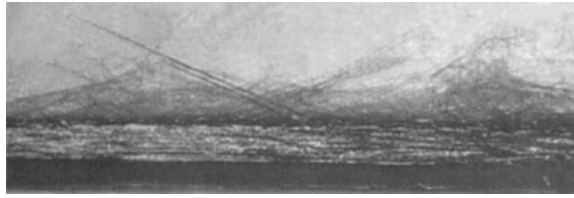


Table 1.6 Comparison of composite interlayer toughening configurations and their corresponding impact damage and CAI

Sample	1	2	3
Construction of intralayer toughness			
C-scanning result			
CAI/MPa	229	244	285

As a result, mechanical interlock appears together with the “plow” effect generated during impact delamination. The latter effect causes a great number of fibers to be pulled out and fractured (Fig. 1.14) and results in an exponential increase in delamination resistance.

Integrated laminate structures should also be included in microstructure design and space optimization. For example, selectively establishing non-symmetric and non-periodic interlaminar toughened structures (Table 1.6) can tune the anti-impact performance of laminates [26].

The periodically or non-periodically adjusted 3–3 double-continuous grain interlaminar toughened construction in 2–2 carbon fiber-laminated composites, and its infusion toward the surface layer of the textures, are typical microstructural features of structures produced by the “ex situ” approach. This microstructural foundation is affected by the combined performances of its base materials. Using low-dimensional constructions of matrix materials, such as molecules, chains and

cross-linked structures, integrated performances have been markedly enhanced by optimizing the microstructure of composites based on existing chemical structures. This is a recent international research trend to maximize the performance of traditional materials. The essence of the “ex situ” process is to optimize the composite’s microstructure and take full advantage of the potential of constructions at different levels to produce a coordinated action. In terms of toughening, the objective is to control the contribution of the layers inside the construction to in-plane mechanical properties and interlayer structure to damage resistance, and organize them periodically or non-periodically to maximize combined efficiency.

1.3.5 Advanced Liquid Molding Resin Systems

To cope with the challenges of producing low-cost and high-performance traditional composites, the Beijing Institute of Aeronautical Materials (BIAM) developed a series of material systems using the “ex situ” technique specifically targeting

Table 1.7 Liquid molding resin matrix composite backbone systems proposed by BIAM

Material	Main features
3266 epoxy resin composites (RTM) Service temperature ≤ 75 °C, 3266ES CAI ≥ 300 MPa Performance equivalent to or higher than that of CYCOM 823 RTM	Injection at room temperature with a pot life of at least 24 h, high fatigue performance and toughness. Can be used in helicopter bodies and propeller blades, engine short carbines and secondary structures in civil planes
5268 epoxy resin composites (RTM) Service temperature ≤ 130 °C 5268ES CAI ≥ 300 MPa Performance equivalent to CYCOM 875 RTM	Injection below 75°C with a pot life of at least 12 h. Can be used in primary and secondary structures in civil planes and helicopters
5288 epoxy resin composites (prepreg, RTM and RFI general type) Service temperature ≤ 130 °C 5288ES CAI ≥ 300 MPa Combined performance equivalent to 977-2 or 977-3	Good processability for both prepreg and RFI. Can be used in primary and secondary structures in airplanes and helicopters
6421 BMI composites (prepreg, RFI general type) Service temperature 180 °C 6421ES CAI ≥ 300 MPa Performance near to that of CYCOM5250-4 RTM	General use for prepreg, RTM and RFI, can be used in primary structures, engine parts and missile bodies
High-temperature PI resin composites Service temperature ≤ 280 °C, two options (1) LP 15 PI composites, prepreg hot press molding, CAI ≥ 300 MPa (2) PI resin composites for RTM liquid molding, including RTM and RFI, in development stage	Prepreg hot press molding, good processability, can be used in engine parts PI resins for RTM and RFI are basically synchronous with those produced by NASA

liquid molding (RTM and RFI) applications. As listed in Table 1.7, the heat resistance based on the different resin performances covers from ambient to medium and high temperatures (up to 280 °C), and the CAI can exceed 300 MPa, producing a straight line parallel to the horizontal axis in Fig. 1.10.

1.3.6 Unity and the Struggle of Opposites of “Ex Situ” and “In Situ” Approaches

Logically, the idea of the “ex situ” approach is simply to split the composite structures into independent substructures, or the preparation processes into independent sub-processes without any interactions; that is, to solve problems by the “divide-and-rule” method. Based on present understanding, we can approximately divide in-plane strength, stiffness, interlaminar toughness and delaminating resistance and can also separate flow processes from chemical reactions. This separation may take place in space and/or time. Extending this concept, the core of “in situ” methods is to provide suitable conditions to make the sub-processes that can occur in different spaces and times combine in the same time and space, that is, a one-step process. In composites research, “in situ” processes can be used to produce not only polymer matrix composites, but also metal matrix and ceramic matrix composites.

For example, the traditional method to prepare thermoplastic composites modified by thermally crystallized polymers “in situ” is to place the solid reinforcing phase (particles or fibers) into a resin matrix and to carry out compositing under the melting conditions of the thermoplastic polymer to yield composites with 0–3 construction. Under such conditions, the fillers do not melt or dissolve, so their shapes are retained. In “in situ” compounding, two components are also mixed together, and these two parts are melted simultaneously in an appropriate temperature window.

Because of a unique rheological discrepancy, the behaviors of melting and flow processes change the low-viscosity phase into a fibroid structure, resulting in a dispersed phase with oriented fibers at certain length/diameter ratios. During this process, a fine fiber-like structure is generated, and consequently, a 1–3 dispersion and orientated construction is formed. This is the origin of the “in situ” concept.

The advantages of “in situ” approaches are simplicity, convenience and efficiency, while their shortcomings are complicated process control and poor reproducibility of microstructures, making them difficult to adapt for practical applications. For example, in the above-mentioned “in situ” processing, fiber formation strongly depends on the flow conditions. As a result, the effect on rheology is beyond that tolerated by industrial applications. Therefore, “ex situ” processes were developed to overcome the drawbacks of “in situ” ones.

1.3.7 *Summary and Prospects*

The inspiration for technical innovation comes from experience, especially from technical practice with strong applicability. In other words, requirements drive research, and applications promote innovations in core technology.

Currently, the main trend in aerospace composite development is to produce materials that are low in cost with high damage tolerance and are general-purpose, multi-functional and integrate structure and function without depending on chemical methods. Obviously, “ex situ” techniques align with this trend, because “ex situ” toughening is suitable for many resin matrixes, including general and inexpensive options. The biggest challenge facing low-cost techniques is to directly achieve high performance using traditional materials. Research of traditional impregnated composite laminates is quite mature [27, 28], and great effort has expended to optimize their performance and enlarge their application ranges. At present, the materials used in the most advanced airplanes, e.g. Airbus A 380 and Boeing 7E7, are still traditional materials [29], so it is necessary to pay attention to maximizing material performance. In fact, “ex situ” processes originated from the desire to optimize the performance of traditional materials.

The scientific foundation of “ex situ” processes is based on fully understanding and utilizing the rich effects at the micro- and meso-dimensional and multi-level scales. The purpose of these processes is to develop new materials that combine performance and functions and to optimize the performance of low-cost traditional materials. However, the best way to optimize performance and functions using the coordination and coupling effects between different phases, dimensions and levels is still unknown.

1.4 **Advanced Manufacturing Techniques**

In Sect. 1.3, an important processing technology of advanced composites, liquid molding (e.g., RTM), was introduced. In addition to their importance in manufacturing polymer matrix composites, liquid molding processes can also be used to fabricate metal and ceramic matrix composites. A typical example is the melt impregnation technique suitable for metal or ceramic matrix composites, where metals, intermetallic compounds, or glass are impregnated into metal or ceramic backbones with high melting points.

The traditional approach to introduce composite processing technologies is based on classification, which we use in this book. However, one important developing trend is that research on advanced composites focuses on integration much more than that of other material systems. As a result, it is necessary to develop integrated manufacture technologies, as well as integrating design, materials, manufacture and certification. This trend mirrors that of “unit operation toward integrated processes” in the chemical industry. In the following section, aerospace composites are used as an example to introduce the current integration technology.

1.4.1 Definition and Development of Integrated Manufacturing Technology

Facing challenges from economic globalization, the performance/price ratio of aerospace materials and processing has become increasingly important. According to statistics from the International Committee of Composite Materials, materials are 15%, laminating is 25%, assembling is 45%, curing is 10%, and fasteners are 5% of the total cost of aerospace composite components. Subsequently, lowering assembling and laminating expenses can probably have the largest effects on total cost. However, changing laminating and assembling methods will change the micro- and macrostructures of the composites. Simultaneously, the cost of fasteners and fastening steps can be decreased, which can substantially increase structural compactness (saving weight), load-bearing ratio, performance and price benefits. The integration of aerospace structures is driven by this reasoning.

A good example of aerospace structure integration is the fourth-generation jet fighter F-22 developed in the USA. By structural integration, 11,000 metal parts were lowered to 450,600 composite parts to 200 and 135,000 fasteners to 600. The direct benefits are weight reduction and increased manufacture efficiency; in particular, the assembling cost dropped considerably [30].

For composites, the premise of integration technology is design. From the aspects of materials and manufacturing, one breakthrough should be to automate traditional hand-based processing. There are two possible ways to do this. One is the automated tape-laying (ATL) technique or automated fiber placement (AFP), where fibers, filaments or prepregs with various widths can be laminated as required. The final components can then be manufactured by autoclaves, advanced liquid molding methods, or “in situ” beam curing technology. ATL has advantages such as low-cost cycle time, manufacture of flat or curved assemblies, manufacture of large structures in one step, automation, and improved accuracy, repeatability and quality. This technology is usually realized in manufacturing factories.

The second method is to choose a material/fabric medium, which may be woven, knit, braided, stitched, nonwoven or warped, and form and then place on molds after proper tailoring. This method is especially suited to thick fabrics used for dry placing or two- or three-dimensional construction. The integrated structure is then obtained using advanced liquid molding technology. This procedure normally involves cooperation between weavers and composite structure workers. ATL has high manufacturing flexibility, high capital investment and high professional requirements. In contrast, the textile composite technology has strong industrial commonality and lower investment, but still needs further time to obtain certification because of its difference from traditional processes used to fabricate laminate structures. At present, these two methods are both popular worldwide.

The integration of composite structures also covers two aspects: the integration of structures (e.g., F-22 fighter) and that of structure and function. The latter has attracted considerable attention globally and is regarded as the next stage of integration technology.

1.4.2 Integration Technology of Textile Composites

In aerospace structural integration technology, textile composites may have the biggest development opportunity. In the USA, NASA conducted a combined review and evaluation of the textile technologies applicable to advanced composites; the results are presented in Table 1.8.

In addition to the above review, the integrated composites suitable for typical civil aircraft fuselage and wing structures were also summarized by NASA

Table 1.8 Textile techniques suitable for advanced composites

Textile technique	Advantages	Disadvantages
Low-crimp nonwoven cloth	Excellent in-plane performance Good tailorability Highly mechanized fabrication	Poor transverse and out-of-plane performances Low stability of fabric construction Hand layup
Two-dimensional mechanical weaving fabrics	Excellent in-plane performance Good tailorability Highly mechanized fabrication Possibility of integrated mechanical weaving Suit large-area placing Rich data available	Limited off-axis tailorability Low out-of-plane performance
Three-dimensional mechanical weaving fabrics	Medium in-plane and out-of-plane performances Highly mechanized fabrication Limited possibility of mechanized weaving	Limited off-axis tailorability Low placing ability
Two-dimensional braiding preform	Balanced off-axis performances Highly mechanized fabrication Suitable for complex curved surfaces Superior placing ability	Limited preform dimensions because of equipment restrictions Low out-of-plane performance
Three-dimensional braiding preform	Excellent in-plane and out-of-plane performance Suitable for complex curved surfaces	Low-efficiency preform manufacture Limited preform dimension because of equipment restrictions
Multi-NCFs	Can tailor and obtain balanced in-plane performance Highly mechanized fabrication Scale production in multi-layer fabrics Suits large-area placing	Low out-of-plane performance
Knitted	Excellent in-plane performance Highly mechanized fabrication Very high damage tolerance and out-of-plane performance Superior auxiliary assembling	Substantial loss of in-plane performance Low complex curved surface-forming ability

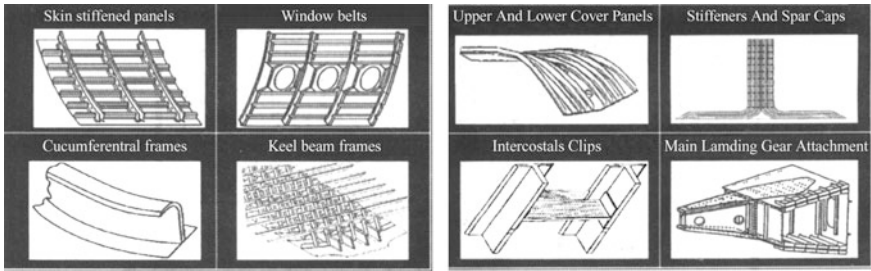


Fig. 1.15 Schematic diagrams of integrated fuselages (*top*) and wings (*bottom*) approved by NASA. The standard techniques used to form these materials are textile composite integrated liquid molding techniques

(Fig. 1.15). These conclusions on textile composite and aerospace structure integration have been widely accepted by Airbus. For example, wing skin structures generally use multi-warp woven fabrics such as non-crimp fabric (NCF) manufactured by vacuum-aided liquid molding. NCF used can be used to prepare spars, ribs and beams which can either be preformed by placing or knitting in molds, or 2.5-D/3-D braiding or machine weaving preforms. Then, knitting, pre-adhering and co-RTM techniques are used to integrate the materials. In Airbus A380 manufacture, these structure integration technologies have been certified and are used in scale production.

Here, several issues need to be pointed out. Firstly, textile technology can only provide structure preforms, and only after combination with liquid molding are they suitable for use. Secondly, the integration degree of composite structures depends on that of the textile preforms as well as the degree of mold integration in liquid molding processes. Thirdly, aerospace structure integration or structure–function integration needs to surpass traditional manufacture limits to move toward the new “design–materials–structure” integrated methodology. In terms of manufacture techniques, flexible textile preforms are the main issue in “materials–structure” and liquid molding processes.

1.4.3 Automated Tape-Laying (ATL) Technology

The ATL technique is an integrated manufacturing technique that was developed in parallel with textile composite integration and is certified by the aerospace industry. The ATL technique originated from the hand layup process. The drawbacks of hand layup are the high professional requirement of technicians, the unique skill needed and the time-consuming, together with low efficiency and high cost (25% of the total cost of composite production). As a result, automated tape placement (ATP) was developed in the early 1960s, a few years after hand layup started. ATP was widely used in the US defense industry from 1980 to 1988. In the 1990s, the interest of aerospace manufacturers turned to AFP and automated tow placement techniques.

Now, both of these processes have been transferred from military to civil purposes; for example, the horizontal and vertical stabilizers in Boeing 777 and wing skin in A330/A340 airplanes are fabricated by automated placement techniques.

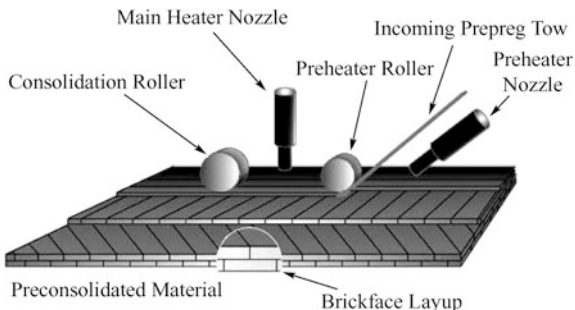
In terms of materials, the tapes to be placed in ATL are the impregnating tapes of various widths, while the fiber in AFP is dry carbon fiber bundles, or thermoplastic commingled yarn. Table 1.9 lists the specifications of typical thermosetting prepregs used in fiber placement techniques.

The principle of the ATL technique is very simple (Fig. 1.16), which is to use mechanized or automated placement to replace hand layup. In terms of discipline, ATL should belong to manufacturing, because its main topics are the design, manufacture and engineering application of automated equipment. ATL involves two main techniques: control and placement. The control technique is a multi-degree, precisely positioned space trace where location control is achieved by a robot or multi-axis placing system. The other is the placing head technique, which is used in automated placing because it integrates many functional processes such as preheating, heating the under layer, precise positioning and placement as well as pre-compacting and compacting, and can also suit prepreg tapes and fiber tows with

Table 1.9 Specifications of typical thermoset prepregs used in fiber placement techniques

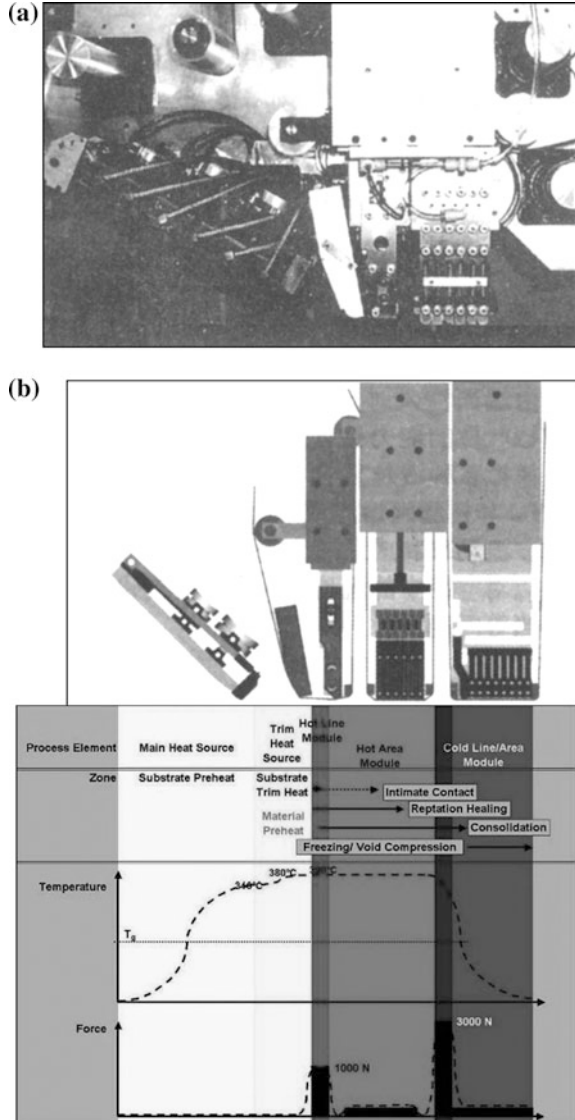
Property	Specification
Width	0.635 ± 0.0254 cm (narrow tape) 7.62 ± 0.0254 cm (wide tape)
Nominal thickness	0.015 cm
Thickness accuracy	25%
Resin content	35 ± 5%
Void volume	<3%
Tensile strength	To be tested and reported (only for narrow tape)
Product shape	Rectangular cross section
Tow splitting	<0.076 cm in width <7.62 cm in length
Tow concentricity	<0.76 cm error (any line)
Residual solvent	<0.01%

Fig. 1.16 Schematic diagram of thermoplastic composite preparation by automated tow placement



different width, mass and resin loading. Heated gas, infrared light or an in situ electron beam can be used for heating. During the placement of components with variable curvature or section thickness, large dimensions and complex profiles, important processing requirements are to apply necessary uniform compacting pressure, temperature and compression time. A placing head of typical placing equipment is depicted in Fig. 1.17. This placing head contains various pressure and temperature distribution zones so that pressure and temperature distribution can be transferred a very short distance. This allows the fiber or tow to be precisely placed,

Fig. 1.17 a Structure of an automated placing head and b temperature and pressure distributions related to placing head position



positioned and profiled to form specific composite structures. This is a new direction of research to advance composite manufacturing equipment.

Thermosetting prepregs are easy to place because the impregnating resin can freeze the fiber tape. However, it is necessary to moor dried fiber tows in automated placing heads. One alternative method is to knit during placing; that is, the placing head is attached to a single-side knitting head. Obviously, the resulting placing head is very complicated. Generally, the same placing machine can use different placing heads to suit different fiber placing requirements.

Besides placing heads, typical placing machines are often equipped with a robot controlling system to realize complex space positioning, including negative curvature profile placing. In terms of manufacturing, the core technique is the computer-controlled space trace design, as illustrated in Fig. 1.18. An intake placing trace design is also depicted in this figure. Figure 1.19 shows several typical placing machines. Automated placing is an impressive example of digital technology that allows precise manufacture as well as materials–structure integration in composite manufacturing.

The top and bottom wing skins of F-22 fighter wings have been successfully laminated by the ATL technique. The outer dimensions of the wing skin are about 6.0×5.7 m with a certain curvature, its thickness changes from 3.8 mm at the wing tip to 14.2 mm at the root, and the mass of a single wing is about 113 kg. The equipment places carbon fiber prepreg tapes with a width range of 76.2–152.4 mm (0.2 mm thick), and the moving speed could reach 30 m/min with an accuracy of ± 1.27 mm to give precise laminating. Compared with hand layup, advanced ATL could lower production costs by 30–50%. The wings of F-35 aircraft are manufactured by seven-axis AFP machines. The skin is connected to a wing load-bearing structure that is 3.66×4.27 m in size and 162.7 kg in weight.

The main difference between ATL and AFP is that the former is used for laminating parts with a large area and low curvature radius, such as wing skin structures, while the latter is mainly suitable for laminating structures with large

Fig. 1.18 Trace design of intake placing

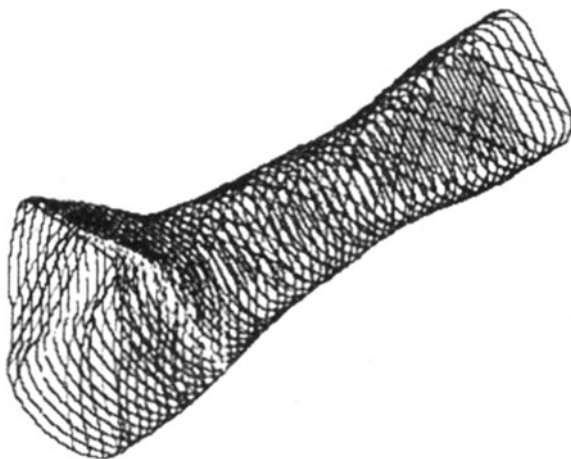
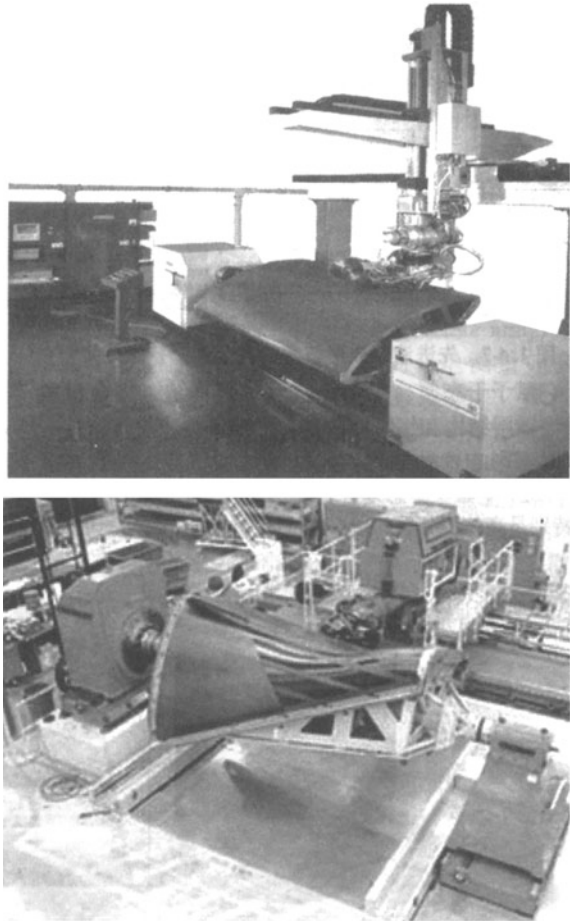


Fig. 1.19 Example showing AFP manufacturing [31] (reprinted with permission)

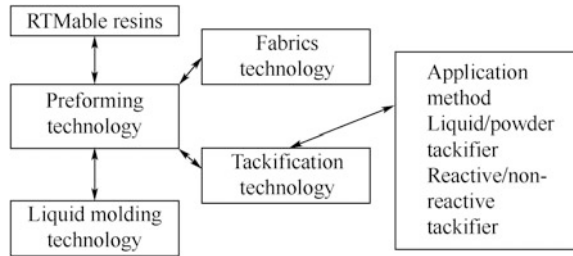


curvature and rotating parts; for example, air intake structures. Because AFP is a laminating process between automated winding and tape placing, it is suitable for complex structure fabrication. Consequently, most functions of ATL can be covered by AFP.

1.4.4 Preforming Technology of Integrated Structures

Whether textile composite or automated placing preforming, the objective output is near net-shape preforms. The near net-shape fabrication of composite components with accurate shape and dimensions is the goal of modern manufacture. In resin composites, this near net-shape processing is regarded as preforming technology. This is because fabric and its preforms or the half-forms normally show a loosened

Fig. 1.20 Relationship of advanced liquid molding technology with several important elements like preforming and tackification technology



state during the placement processes and have a nonlinear deformability under pressure together with a deformation limitation. Thus, it is necessary to study the correlation between this deformation ability and near net-shape fabrication to allow the preformed state to be finally fixed with the help of a shape-fixing material. This particular technology is also called tackification technology, and the material used for preforming is called a tackifier. Preform and tackification technologies have the follow features (Fig. 1.20).

- (1) They impart necessary free-standing ability to dried composite structures, especially textile composites (including fabric laminated and braided structures), without affecting their loosening conditions. This ensures that the liquid resin can readily immerse or impregnate structure preforms during liquid molding.
- (2) They leave the dried composite structure near net-shape (near final dimensions), especially those with a high fiber volume fraction (fiber volume fraction higher than 58%). In fact, the closer the dried composite preform is to its final dimensions, the easier it is to place and fix in RTM molds, and the higher the liquid molding quality.
- (3) Considering that complex composite structures may encounter many cycles of tackification and assembly in molds, it is required that the preforms after tackification can be re-deformed by suitable thermal treatment without any large influence on free-standing ability and near net-shape formation.
- (4) The preforms after treatment with liquid tackifier should have good tackiness and drapability to meet the requirements of complex curvature tackification and positioning in molds.

If RTM is selected as the principal process for composite structure manufacturing, the tackifier must be compatible with the RTM resins without affecting the porosity of the preforms. Research has shown that the tackification materials, processing technology and method and subsequent liquid molding control are all important. There are many innovative examples of multi-functional tackification materials and technologies based on the “ex situ” concept, including the two functions of tackification/location and “ex situ” toughening, bifunctional tackification/location and “ex situ” liquid molding, bifunctional “ex situ” liquid molding/“ex situ” toughening and other combinations of these functions.

1.4.5 Virtual and Intelligent Manufacturing Technologies

As the manufacture of composites and their structural components heads toward mechanized and automated direction, digital manufacture has become attractive. Early digital analogy or simulation was used in highly mechanized filament winding, while current applications have been widely adapted for liquid molding processes (such as RTM-Worx, PAM-RTM) and automated placing trace calculation (Acraplace), which were first combined with composite laminating design and structure design software like FiberSim, TEXCAD and CATIA, and then combined with CAM software, processing control software (such as COBRA) and equipment to generate a composite engineering system with integrated design, materials, manufacture and certification. For example, in the simulation of RTM liquid molding, for a given resin and its rheological expression, and a given textile preform and its immersion data, RTM software can accurately calculate processing parameters, predict the processing effect on liquid molding and evaluate possible defects. As a result, the processing can be optimized by this virtual method, and the processing quality can be guaranteed.

Figure 1.21 shows an example of a cone cap using RTM software to pre-evaluate the correlation between mouth position and injection time. When resin is injected from the cone tip, 3600 s is needed to complete the whole injection, which is decreased to 800 s for injection from the cone bottom. In current liquid molding simulation software, the capability has exceeded this simple structural range, and these programs can model various liquid molding processes, including common RTM, VARTM and RFI. Existing software can also optimize parameters such as injection pressure, flow rate and processing temperature, calculate mold closing force and perform visible monitoring of resin flow profiles in mold cavities to prevent incorrect reinforcement filling.

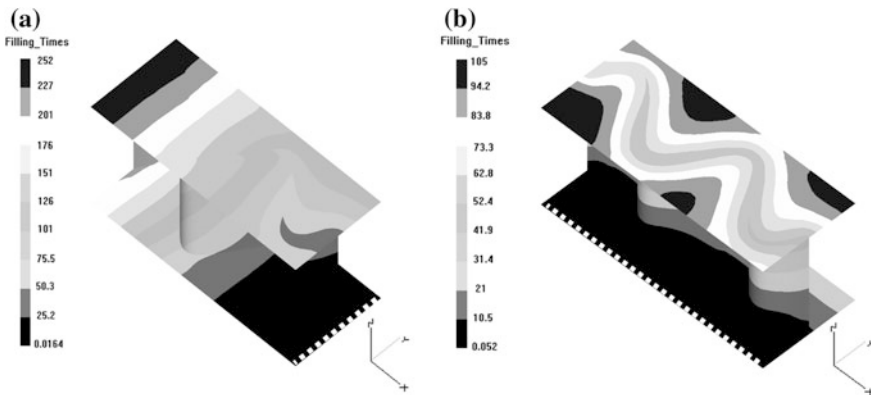


Fig. 1.21 Computer simulation of different RTM resin injection modes for injection times of (a) 270 s and (b) 100 s

The curing process after resin injection can also be simulated. For example, COBRA software is mainly used to model and optimize autoclave curing processes. In F-22 structure manufacture, one traditional cure test will cost \$3000 and take 2 days. Using COBRA software to simulate the same curing process only takes about 20 min and costs \$20. Based on these simulations, the first set of composite parts of F-22 was obtained with 98% quality rate.

Looking to the future, advanced composite intelligent processing technology will be a general and important technical breakthrough. One smart manufacturing system covers five essential factors, which are advanced sensors and their application, material and processing models (virtual technology), correlation models between processing and structural parameters, computer artificial intelligence (or intelligent system) and equipment for real-time monitoring during materials preparation, such as an autoclave, filament winding machine, automated placing machine or liquid molding system. A flow chart outlining the intelligent manufacture concept of composites is illustrated in Fig. 1.22.

Advanced intelligent manufacturing systems based on advanced sensor technology use sensing and monitoring techniques to determine processing or material parameters, such as temperature, pressure, resin flow and curing conditions by “in situ”, online, real-time and non-destructive methods. Typical examples of these methods are summarized in Table 1.10.

Usually, wave spectra are measured using transition optical fibers. For example, fluorescence conductive cure sensors are based on fiber-optic fluorescence measurement principles and determine the change of fluorescence during the resin cross-linking process. Quartz fibers with a diameter of 1 mm are used as sensors to measure the change of wavelength and fluorescence intensity during resin curing, indicating the correlation between viscosity and curing degree. Infrared transition fiber-optic sensors are mainly used to monitor the intensity of specific peaks and quantitatively monitor chemical processes. Spectral information is used to detect types and density of functional groups at any time point, which can be used to study reaction kinetics and mechanism. Thermocouples are used to monitor temperature and are usually inserted in molds or inside the composites to track reaction progress. In electromagnetic methods, dielectric sensors are typically used to measure the changes in electric capacity, conductivity or resistance as a curing reaction proceeds. DC dielectric sensors are most commonly used to detect the resin curing process before gelling, and distribution sensors called “SMART weave” are

Fig. 1.22 Flow chart showing an intelligent system to manufacture composites

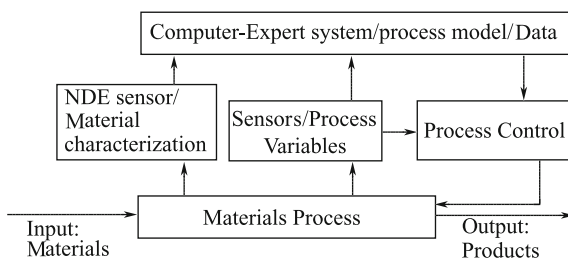


Table 1.10 Sensor techniques used in composite processing

Sensor method	Measured variables	Sensor/Monitor	Examples
Wave spectrum	Chemical conditions	Flow and curing	Infrared, Raman, ultraviolet and fluorescence emission
Electromagnetic	Electrical performance (capacity, conductivity)	Temperature, flow, curing	Dielectric (AC) gel time measurement, DC dielectric medium distribution network (SMART weave)
Visible	Visible changes in processing conditions	Resin flow	Optical photographs and accessory software
Thermal	Temperature	Temperature (heating onset)	Infrared images, thermocouple
Acoustic wave	Mechanical response	Resin flow and cure	Direct measurement, surface wave, reflecting wave, waveguide acoustic emission
Mechanical	Compression and viscosity (stiffness)	Pressure (release curing)	

commercially available. Acoustic emission can be used to measure the changes in acoustic information during curing processing and to determine resin flow and cure characteristics. In general, dielectric, acoustic, ultraviolet and visible light sensing is applicable, but can only provide limited curing information. A new promising method is to use far-infrared measurement principles to collect a large quantity of information on curing processes near the fiber-optic transition. Such information can usually be obtained in the infrared region of the electromagnetic spectrum.

Thermocouples, pressure sensors and viscometers are the basic sensor devices typically used to monitor reaction processes. For large, thick components, the temperature is increased by reaction heat, resulting in much higher temperature inside the components than outside. The temperature difference between inside and outside the composites strongly depends on the resin system. Pressure sensors are usually inserted into the internal surface of molds and used to monitor the local pressure change in them. Viscosity measurements are mainly used to monitor the change of resin viscosity during curing processes, but it is difficult to eliminate the influences of fibers and interfaces.

To precisely obtain two- or three-dimensional measurements or sensing, advanced sensors are used to construct a sensor array. Typical examples include infrared imaging for temperature measurement, distribution dielectric measurement like SMART weave, as well as systems with fiber optics embedded at specific positions.

The processing and materials information collected by a sensing system become the input variables, and by using a computer analog system, artificial intelligence or expert system, the proper processing parameters will be output to allow processing and equipment control and realize controllable composite fabrication. Obviously,

the returns from the investment in intelligent manufacturing systems should be higher production rate and product quality, and reject-free fabrication. Computer-aided composite microstructure design combined with large-structure design achieved through structure–function integration will enhance modern composite design and manufacture, and eventually lower their cost.

1.5 Development Trends of Advanced Composites

Composites are an important topic in materials science and engineering. In this field, a few developing tendencies that show promise for the future have been observed: (1) composite materials with low-dimensional construction (also referred to as fine compositing), such as nanocomposites; (2) composite materials with multi-function and property–function or structure–function integration; (3) supported by computer science, much attention is being paid to developing performance and function analogs using the “trial-and-error” method to realize controllable structures and designable performances and functions; (4) composite materials for intelligent and bionic simulation. In the following sections, the first three points will be discussed using examples.

1.5.1 Development Trends of Low-dimensional Composites

In recent decades, low-dimensional technology and materials have attracted considerable attention and nanocomposites have been a hot topic. In polymer matrix composites, nanoclay-modified composites were studied first, among which an important breakthrough was the nylon 6/nanoclay composites developed by Toyota in 1989. These composites exhibit very good mechanical properties and heat resistance, and are fire retardant and of low density. This fundamental achievement was quickly transferred to industrialization, bringing great hope for the potential of nanoscale materials. Developed countries then invested heavily in fundamental research and applications of nanocomposites, focusing on the study of nanocomposites composed of thermoplastic polymers, such as nylon 6, nylon 66, polyolefin, polyester (PET), polymethylmethacrylate (PMMA) and polycarbonate, and thermoplastic elastomers (polyurethanes, silicon rubbers). The emphasis was on how to disperse the nanoscale inorganic materials in the resin matrix and improve the interfacial compatibility between fillers and resin matrix, as well as processability. However, clay-modified nanocomposites are not universally suitable, and the efficiency problem of nanocomposite formation needs to be considered.

In this section, two relatively novel topics will be discussed: the self-assembly behavior of nanocomposites, and nanostructure preform technology and the resulting composites.

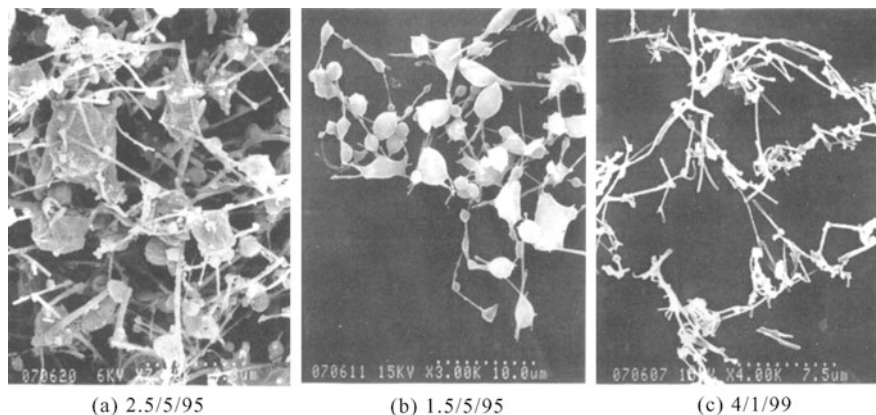
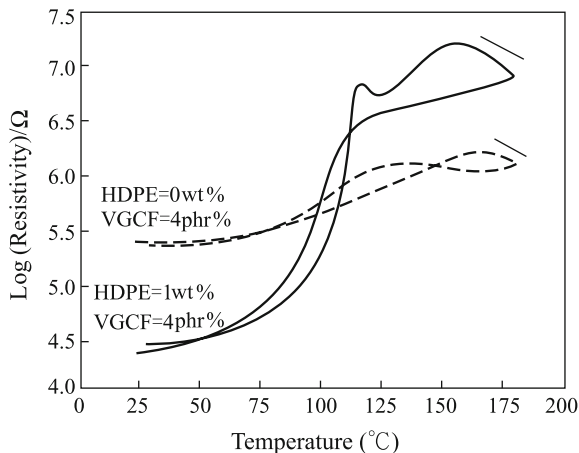


Fig. 1.24 SEM images of VGCF/PMMA/HDPE three-phase composites after PMMA was extracted (values in **a**, **b** and **c** are the VGCF/PMMA/HDPE mass ratios)

Fig. 1.25 Resistance–temperature curves of VGCF/PMMA/HDPE three-phase composites (samples prepared by hot pressing at 190 °C for 15 min and then at 220 °C for 30 min)



Consequently, if this kind of HDPE “clamp” dramatically expanded near its melting point, the connected VGCF ends would separate and result in a large positive temperature coefficient (PTC). This assumption was proved by an experiment (Fig. 1.25). In comparison, the two-phase VGCF/PMMA composites without HDPE exhibited a small PTC.

From the viewpoint of materials science, the reason for the formation of this self-assembly is the geometric structural changes of the VGCF ends against the fiber segment surface. Because of the particular conditions in chemical vapor deposition (CVD), a quantity of crystalline carbon grains will be exposed on both ends of each VGCF filament. Their physical and chemical surface structures as well as surface roughness of the order of 10 nm are similar to those of carbon black clusters. The surface of the VGCF is smooth and its microstructures are different from those of isolated carbon black clusters [36–38]. Therefore, just like carbon

black clusters that always aggregate on the HDPE phase in HDPE/PMMA two-phase polymer–polymer systems, the HDPE phase in an HDPE/PMMA two-phase matrix will first be adsorbed on the ends of VGCF. Nonpolar HDPE selectively adsorbs on the VGCF ends, while polar PMMA selectively adsorbs on the VGCF surfaces. Such thermodynamic phase splitting of HDPE and PMMA will drive VGCF to form a conductive microstructure with the lowest filtration threshold in melted polymer matrixes.

1.5.3 *Oriented Carbon Nanotube (CNT) Array/Polymer Matrix Composites*

Large oriented CNT arrays can be prepared by CVD. The length of CNTs depends on growing time and can reach up to a few micrometers. Accordingly, CNT arrays can act as natural preforms. Figure 1.26 displays SEM images of an oriented CNT mat. Figure 1.26a shows the high orientation and straightness of the CNT clusters. Figure 1.26b indicates that the CNTs have a diameter distribution of 50–70 nm and clear surfaces with few impurities such as catalyst particles. Figure 1.26c, d shows the size of the CNTs and top surface of the oriented CNT mat, respectively. In the latter image, the CNT tips are visible, as is the void and open structure existing between the tubes, which can facilitate resin penetration. As a consequence, the preparation of oriented CNT array/resin matrix composites involves penetrating

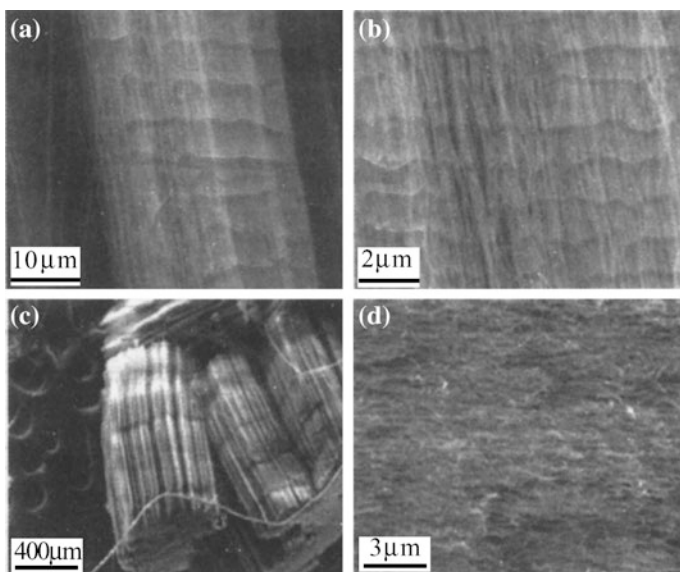


Fig. 1.26 SEM images of an oriented CNT mat at different magnifications

liquid resin into oriented CNT arrays. Nanocomposites with oriented CNTs distributed in a matrix are obtained after resin curing [39].

Figure 1.27 presents SEM images of the inside and top surface of a prepared composite. Figure 1.27a, b depicts cross-sectional views of the structures and indicates that the resin in the CNT mat did not destroy the orientation of CNTs. Figure 1.27c, d reveals the morphology of the composites viewed from the top.

Figure 1.28a shows the change in friction coefficient of oriented CNT array/epoxy resin composites over time. The friction plate was made of steel 45 with a rotational speed of 200 rpm and load of 50 kg. Epoxy resin has a high friction coefficient (>0.45). When the maximum shear stress generated from surface friction is higher than the strength of the cured epoxy resin, cracks form on the surface areas with maximum stress, and damaged block particles will fall off as alternating stress is applied. When a block is formed through a plow action on a surface, the friction coefficient will increase. The friction coefficient on the upper surface of the composite is slightly lower than that of epoxy resin, but is still quite large (about 0.42). The friction coefficient on the side surfaces of the composite is much lower than that of epoxy resin (about 0.17). Figure 1.5.6b contains a bar chart comparing composite abrading damage with a friction time of 70 min. The wear-out rates of composites decreased when CNTs were added. The side wear rate is lower than that of the top surface.

Figure 1.29 shows the change in friction coefficient of compacted (the filling-phase volume fraction was increased) and oriented CNT array/epoxy resin composites over time. The curves were obtained under the same testing conditions. After compaction, the friction coefficients on both top and side surfaces decreased

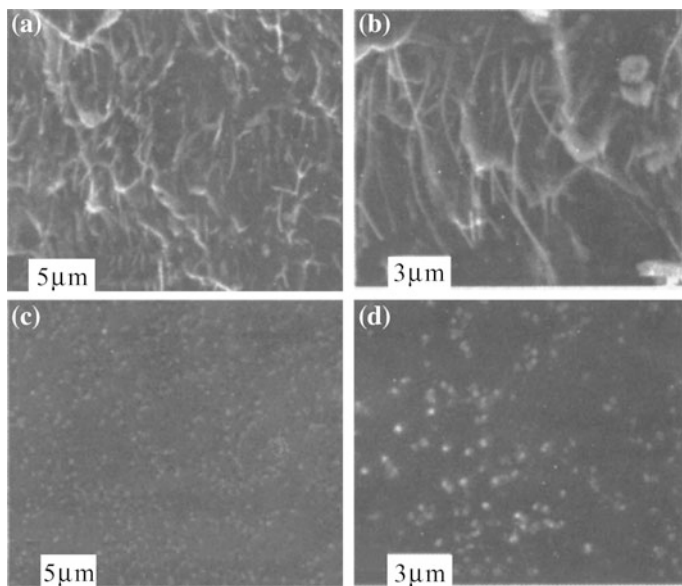


Fig. 1.27 SEM images of a CNT-resin composite. a, b cross-sectional and c, d top views

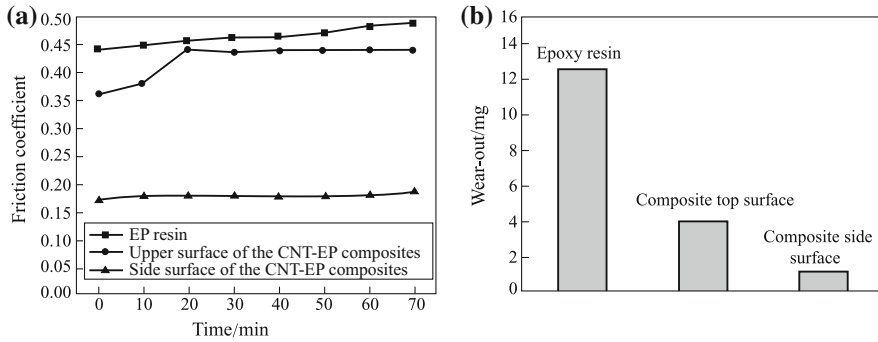


Fig. 1.28 Friction performance of oriented CNT array/epoxy composites

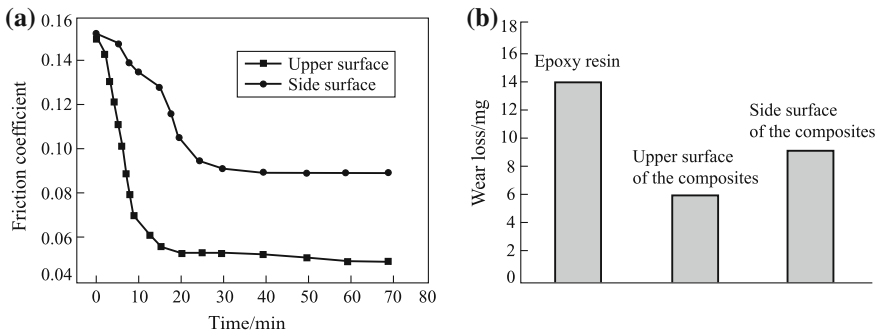


Fig. 1.29 Friction performance of compacted and oriented CNT array/epoxy composites

to 0.05 and 0.09, respectively. A bar chart showing compacted composite abrading damage is presented in Fig. 1.29b. The wear-out rate increased after compaction, and the wear-out rate of the side is higher than that of the top surface.

To further study the friction wear mechanism in these composites, SEM was used to observe the composites after the friction experiments, as illustrated in Fig. 1.30. The surface contains numerous voids, indicating that many CNTs were pulled out under friction, so the friction coefficient of the composites is equivalent to that of epoxy resin (Fig. 1.30a). Figure 1.30b displays the side of the non-compacted composite after friction; many circular grain structures were found on the abraded surface. Numerous CNTs could be clearly observed on the top surface of the compacted composite after friction (Fig. 1.30c). Figure 1.30d depicts the side of the compacted composite after friction. A series of wear features were observed on this surface.

The above investigations proved that the oriented CNT array/epoxy resin composites could achieve good friction performance. When the loading of CNTs was 7.1 vol.%, the friction coefficient of the top surface was as low as 0.05,

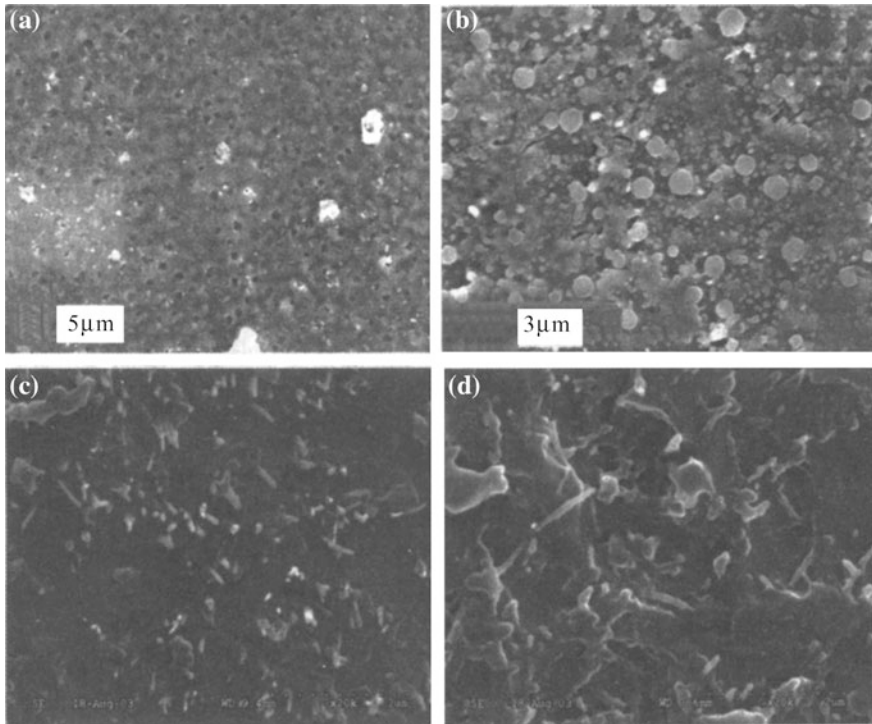


Fig. 1.30 SEM images of composite surfaces after friction experiments

which makes it an excellent solid lubricant. Further studies demonstrated that CNTs have self-lubricating properties and can form a continuous solid lubricant film on the friction surface, resulting in composites with a low friction coefficient.

1.5.4 Function-Integrated Technology of Composite Structures

In the advancement of composite engineering, especially in the field of aerospace composites, structure–function integration has become an important trend, an example of which is energy-absorbing structures. As a load-bearing structure, energy-absorbing composite structures must provide adequate basic mechanical performance such as strength and stiffness. As an energy-absorbing functional structure, it should rapidly fail under certain conditions to absorb a large quantity of energy. Simultaneously providing both structural and functional properties in the same structure is the underlying feature of composites with structure–function integration. In this section, two facets of energy-absorbing structure–function-integrated composites will be discussed: (1) the pipe structure used as a basic

energy-absorbing element; (2) the fabrication and energy absorption of sine-wave beams as aerospace structures.

(1) **Crashworthiness as Important Technology in Integrated Structures [40]**

The operation costs of traffic and transportation tools (highway, rail and airplane) are proportional to their weight, so using light, strong composites will lower operation costs. However, as the traffic speed increases, the chance of crashing also increases, so traffic safety becomes an important concern. As a result, the term crashworthiness was coined to describe the ability of materials in trains, automobiles and commercial airplanes to withstand accidents.

Unlike metals, advanced composites cannot absorb impact energy by large deformation, which results in conflict between structural performance and the functional property of energy absorption. Here, light weight and high mechanical strength are the structural properties of the advanced composites, while crashworthiness is the functional property.

Therefore, the manufacture of crash worthy composites is actually typical structural–functional integration. The functional indication of anti-crash composite structures is their specific energy consumption, e.g., the maximum failure energy divided by structure weight. The larger the specific energy consumption is, the higher the crashworthiness of the structure. The anti-crash specific energy consumption mainly depends on the unit design and material selection of crashworthy structures, which is also related to the resin matrix. Generally, the resin will need to have high CAI, G_{IC} and G_{IIC} (interlaminar fracture toughness); reinforcements are also required to have a certain toughness.

Anti-crash protection is particularly critical for helicopters. During the Vietnam War, the US army was aware that the death rate of helicopter pilots was higher than those of ordinary aircrafts, and studied helicopter anti-crash and survival design. Many details were considered in these studies, from anti-crash components to assemblies to entire helicopter crashworthiness testing. The developed technology was applied in helicopters such as AH-64 and RAH-66. According to some reports, at present all international fighting helicopters except for K-50 contain anti-crash structures and composites, including PAH-2, AH-64, RAH-66 and NH-90. In China, supported by the Defense Research-in-Advance Plans, National High-Tech Research and Development Programs and National Key Fundamental Research Plans, corresponding research has also been carried out with the objectives of product serialization and producing self-owned intelligence and patented technology that can eventually be extended to land-based vehicles such as trains and automobiles.

The anti-crash structures of a helicopter can be divided into the following several structural sublevels, as outlined in Fig. 1.31, where the ultimate structures are the energy-absorbing floor structures composed of various beams. The beams can also be divided into surface panels (beam flange) and web plates, where the web plate is typically a sine-wave structure. The sine-wave structures are equivalent to thin-walled pipe structures (circular pipes), which is the principle structure in energy-absorbing studies of composites.

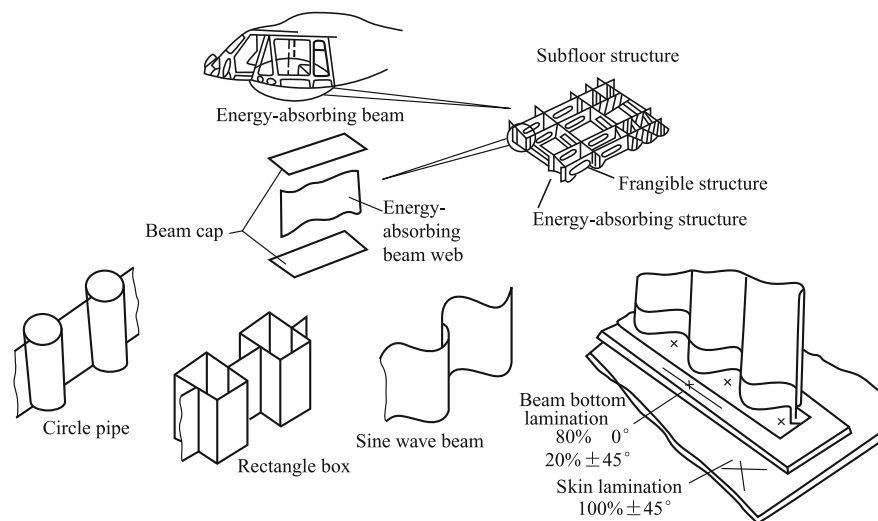


Fig. 1.31 Schematic representation of a crashworthy floor in a helicopter [41] (with permission)

(2) Composite Elements in Basic Energy-Absorption Research

There is no direct connection between high CAI and crashworthy; in fact, they have a relation of unity of opposites. High toughness and high CAI reflect the bear-impact ability, while anti-crash represents the plastic failure delamination under a given yield stress, as well as the consequent local disassembly and breakage until crashing absorbs energy on a large scale. In this process, there are a large number of structural levels, including the physical properties of basic constituents (polymer and fibers), interfaces and interfaces, heterocomposite interfaces, inter-laminar structures, fiber textures, as well as the coordinated effects of these structures in space and time. Because the total energy consumption in a crash is far beyond the linear range, current studies on this topic are still at the empirical stage.

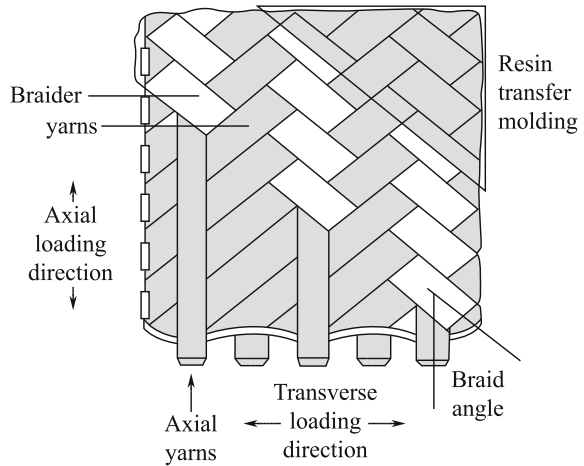
The basic structural units for energy-absorbing study are thin-walled pipes. The geometric parameters that can influence the energy-absorbing ability of pipe elements include diameter and wall thickness. Two types of composite thin-walled pipes are used as examples, two-dimensional, triaxial braided preforms formed by liquid molding (plus knitting if necessary) and unidirectional prepreps prepared by autoclave processing. The dimensions of the selected elements are a wall thickness of 1.5 mm, outer diameter of 60 mm, pipe length of 100 mm and end chamfer angle of 45°. In these examples, three resin matrixes were used: medium-toughness epoxy resin 5224, high-toughness epoxy resin 5288 and liquid molding epoxy resin 5268. The processing routes used considering the compatibility of resins and processing techniques are given in Table 1.11.

Comparison of these results allows the effects of different materials (liquid molding and prepreg resins), different braided preform structures (two-dimensional, triaxial braided and unidirectional fiber-laminated structures) as well as different

Table 1.11 Materials and corresponding manufacturing methods used to investigate energy-absorbing ability

Prepreg + autoclave	Medium-toughness epoxy 5224
	High-toughness epoxy 5288
Braiding preform + liquid molding	Liquid molding epoxy 5268

Fig. 1.32 Typical cell structure of two-dimensional triaxial braided materials



processing methods (RTM and autoclave) on the structure of energy-absorbing abilities to be studied.

A typical two-dimensional, triaxial braided element structure is shown in Fig. 1.32. In this structure, when the braiding direction uses 6K fiber, and the axis direction uses 0K, 3K, 6K, 9K, 12K, 15K and 18K, the highest energy absorption is achieved by the 12K fiber in the axis direction [42]. As the axial fiber is increased from 1K to 12K, the specific energy-absorbing rate increases. In contrast, as the axial fiber is further increased from 12K to 18K, the specific energy-absorbing rate decreases.

Besides the axial fibers, when the braid angle in the two-dimensional triaxial preform is between 20° and 50° , the specific energy-absorbing rate decreases as the angle increases. The specific energy-absorbing rate is the highest when the angle is 20° , indicating that the braid angle of all fibers to the loading direction should be as small as possible.

Thin-walled pipe preforms with a braid angle of $\pm 45^\circ$ and axial reinforcement were made using carbon fiber (12K) and then injected with low-viscosity RTM-5268 resin. Quasi-static collapse testing (0.1 mm/s) was then carried out on the pipes; typical load–displacement curves are given in Fig. 1.33. In this figure, the two lower curves were obtained from braided + knitted pipes, where Kevlar fibers were used in knitting. The curves reveal that knitting decreased pipe energy-absorbing capability. A possible reason for this is that the pipes were too thin, so knitting did not improve the anti-crash property of the composites and decrease their crushability.

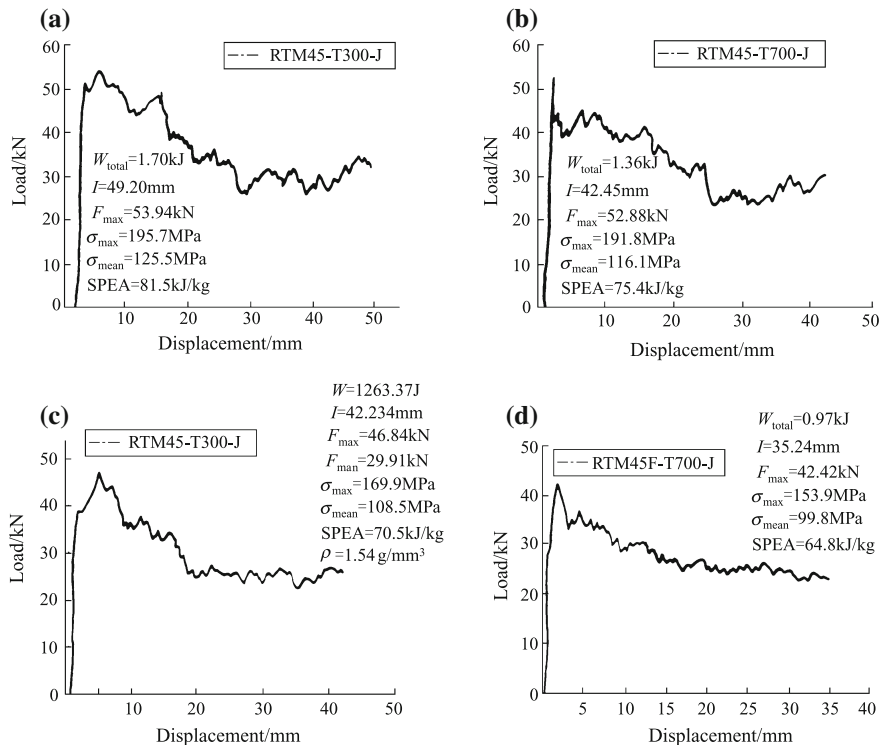


Fig. 1.33 Representative load–displacement curves of different braided + liquid molded tubes in crush tests. **a** 5268T300; **b** 5268T700; **c** 5268T300+stitching; **d** 5268T700+stitching

In another experiment, two kinds of carbon fiber prepgs, which were infused with epoxy resins 5224 and 5288, were laminated in $[+45^\circ/-45^\circ/0^\circ/90^\circ/0^\circ]$ directions. The final pipes were prepared by autoclave processing before performing quasi-static crush testing. Typical load–displacement curves are presented in Fig. 1.34. The compressing/crushing energy-absorption ability, including maximum compressing/crushing stress (σ_{max}), average compressing/crushing stress (σ_{mean}) and specific energy absorption, of the high-toughness 5288 composite is much higher than that of the composite containing medium-toughness 5224 resin. In general, for carbon fiber/epoxy basic elements, $0^\circ-90^\circ$ laminating can provide larger energy-absorption effects than $\pm 45^\circ$ laminating [43]. For $0^\circ \pm \theta$ -laminated structures, the specific energy absorption will decrease very quickly as θ increases when θ is $15^\circ-45^\circ$ and decrease slowly or remain unchanged when θ is $45^\circ-90^\circ$ [44].

The main failure modes of high-performance composite pipe components are splaying and fragmentation, and their micro-failure mechanisms are fiber breakage and delamination. The typical fragmentation and splaying failure modes are illustrated in Fig. 1.35a, b, respectively. In many cases, there will be a mixture of failure modes. Epoxy resins 5224 and 5288 with different toughness exhibit similar static

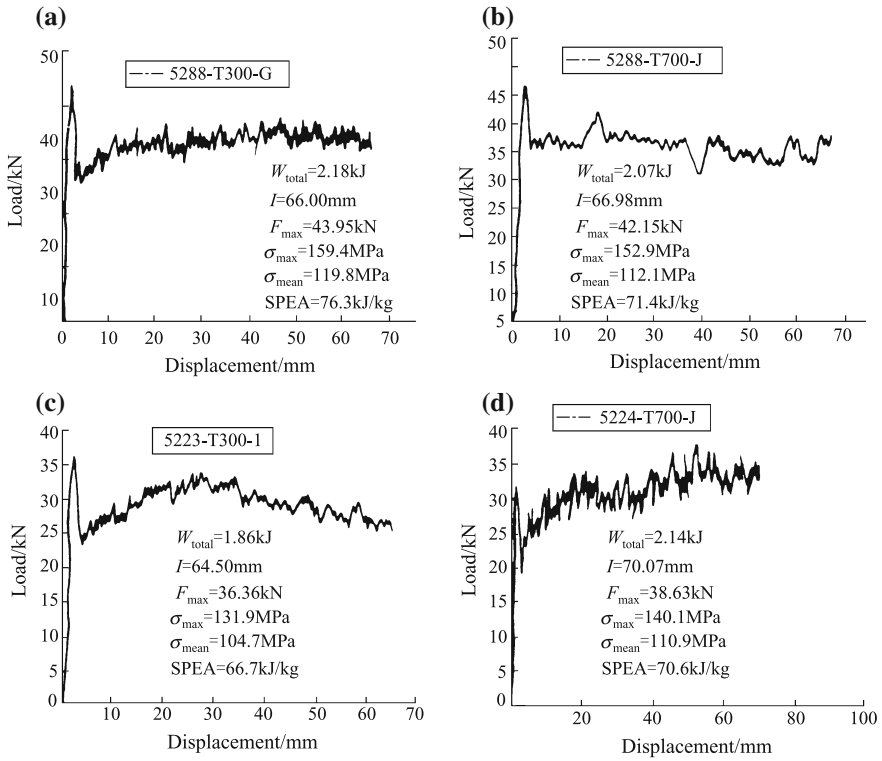
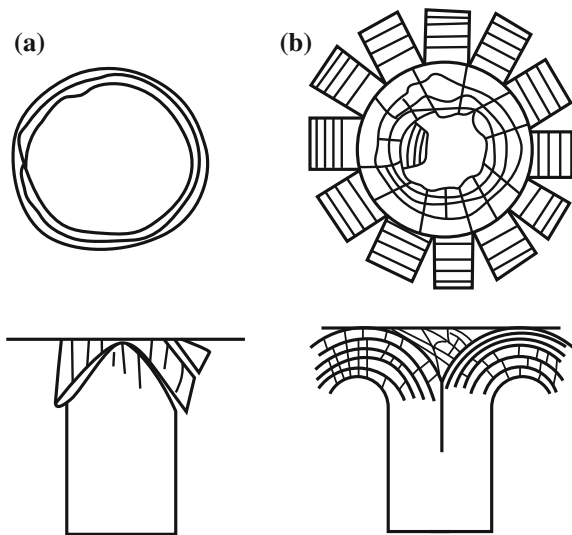


Fig. 1.34 Representative load–displacement curves of tubes made of different prepregs in crush tests. **a** 5288T300; **b** 5288T700; **c** 5224T300; **d** 5224T700

Fig. 1.35 Comparison of **(a)** fragmentation and **(b)** splaying failure modes



collapse performance, especially when T700 fiber is used as reinforcement. In this case, the main failure mode is splaying, so splaying failure is the main static collapse mode for brittle fiber composites, together with fragmentation failure. When the fiber was changed to T300, the 5288 matrix composite exhibited obviously higher static collapse performance than the 5224 matrix composite, and the main failure mode changed to fragmentation. The samples were surrounded with composite fragments, indicating that there were many simultaneous micro-failure mechanisms, including fracture and delamination of fibers, brittle failure and shear of resins.

Unexpectedly, the composite pipe samples prepared by RTM liquid molding with non-toughening resin 3268 and braided preform exhibited very high anti-compression and crashing capabilities. The crashing stress (maximum and average values) and specific impact energy consumption are higher than those of composites using 5224 and 5288 prepreg technology. This reveals the extraordinary anti-crash performance of these low-cost braided composites. Their profiles after crashing are also different from those of the prepreg composites. The main failure mode of T300/3268 is splaying, whereas T700/3268 exhibits a mixed fragmentation failure mode, unlike the 5224 and 5288 prepreg composites.

It can be concluded that increasing the axial and thin-wall interlaminar performances is a suitable approach to increase the anti-collapse abilities of thin-walled pipes. The simplest way to increase axial performance is to increase the number of axial fiber yarns in braided composites, or adjust the ply angles as close as possible to parallel to the axial direction in prepreg composites. The most effective method to increase the interlaminar performance of thin-walled pipes is to increase interlaminar toughness (e.g., CAI value).

(3) Sine-Wave Composite Beams as Energy-Absorbing Structures

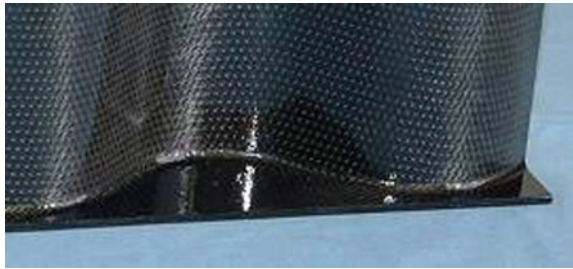
The sine-wave beam is a critical structural component in aircraft wings. It is the lightest anti-buckling structure and has become the symbol of modern fighter wings. However, it is difficult to manufacture sine-wave beams; the most common technique is to bond the bottom plates together with sine-wave webs using glue joints. F-22 was the first to use sine-wave beams made by the RTM process, which lowered the production cost by up to 20%, the number of stiffeners and fasteners by 50%, and gave a precision of up to ± 0.13 mm. Similarly, Lockheed used RTM to make a full-scale vertical tail where the support structure was a braided composite without any fasteners in the whole box structure.

Using their experience in fabricating the load-bearing sine-wave wing beams of F-22s by integrated RTM processing, energy-absorbing sine-wave beams with structure–function integration were manufactured from braiding composites by BIAM, as shown in Fig. 1.36. To study different materials and processing techniques, a selection of materials including high-toughness 5288 epoxy composites (unidirectional carbon fiber) and liquid molding 5268 epoxy resin (carbon fiber fabric) were used. The processing techniques investigated were autoclave and RTM. The results indicated that both material systems and corresponding processes

Fig. 1.36 Representative sine-wave beam formed by liquid molding at BIAM



Fig. 1.37 Photograph of a flange edge in a fabric preform formed by RTM



can meet the design requirements, but their technical problems are different. It was difficult to place the unidirectional carbon fiber prepreg (resin 5288) in a half-mold, especially at the right-angled edge reverse.

In contrast, preform manufacture (including tackification) showed problems during dried fabric RTM processing (resin 5268). In terms of fabric RTM processes, important steps included planar fabric with 90° curvature at the edge reverse, which is achieved much more easily than in preregs, but tackification is required. Figure 1.37 shows the local enlarged edge reverse of a sine-wave beam fabricated by BIAM, illustrating its good quality.

The main reason for shifting from pipe elements to real structure is to control the function transfer mechanism from structural load-bearing to crash energy absorption. This is because there is no direct relationship between the failure mechanism induced in a pipe end chamfer and that in a stable sine-wave beam. For a pipe sample with end chamfers, effective crash energy absorption can usually be triggered. Conversely, for real sine-wave beam structures, it is difficult to observe similar failure modes to those of effective crash energy absorption in pipe samples with end chamfers in either impact testing or simulations (Fig. 1.38). Generally, structural collapse and localized crushing occur in a real sine-wave beam. However, further work is required to trigger highly effective crash energy absorption in beam

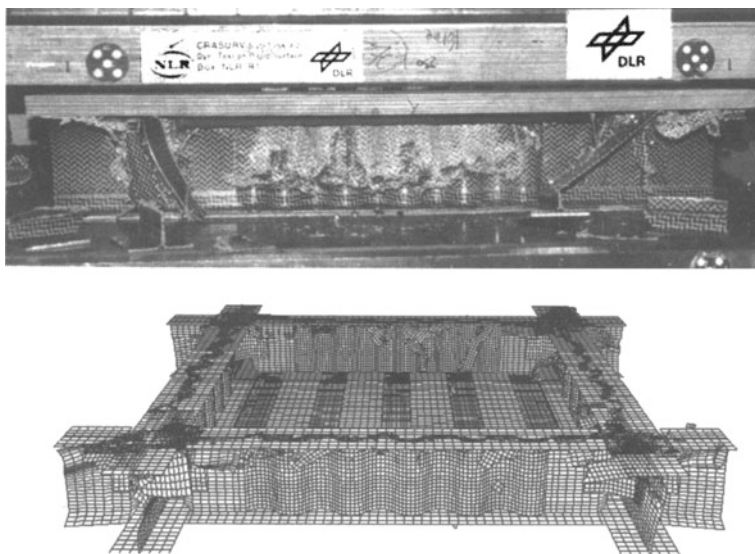


Fig. 1.38 Comparison of final states of a full model and test sample [45] (with permission)

structures while keeping good structural performance. In particular, computer simulations on composite structures are currently popular in Europe and America, which may provide advances in this research direction.

1.5.5 Modeling and Simulation Technology

In the above section, we mentioned computer modeling and simulation of composites with anti-crash structures. We will further discuss the modeling and simulation of composite material performance in this section.

Many mechanical and physical design tools have been established for structural composites, including the mechanical properties of non-uniform materials represented by mesomechanics and numerical simulations. Considering mechanics methodology, a wealth of research has been accumulated on the stiffness (modulus) of inclusion-matrix composites, and their shapes, dimensions, distributions, orientations and interactions can be effectively calculated. Chinese scientists have also made great contributions to the developments in this field. An alternative approach is to use a high-performance computer or microcomputer to carry out numerical simulation and parallel calculations. Numerical simulations of plastics, strengthening and failure behavior have been carried out based on the microstructure, displacement and slide in polycrystalline materials containing millions of grains. The progress of theoretical models and simulations means they can now be used for quantitative studies of composites with multi-dimensional, multi-level microstructures and to establish frameworks for theoretical prediction and material designs.

Simulation of materials encompasses the fields of mechanics, materials science and computer science and covers much more than the description provided in this chapter. In the following sections, two examples are used to give a brief introduction to related work and developments in this field.

(1) Microstructure Models and Modulus Prediction of Low-dimensional Composites

To help develop composites further, their calculation, which is based on mechanical simulation, should be examined further. Using material simulation, it can be expected that structure and performance predictions could serve as guides for material design and manufacture to give specific structures and performance. Here, we use common nanoclay/polymer nanocomposites as an example. Simulation can help us to answer questions such as how much clay can be effectively inserted into a polymer matrix and how a clay with low elastic modulus can stiffen flexible high molecular weight polymers.

It is well known that there are three dispersion levels in 0–3-type clay–polymer composites, which are clay clusters, polymer macromolecules inserted in clay interlayers and clay peel off (see Fig. 1.39a–c, respectively), which may all coexist. Normally, macromolecules either insert entirely into clay layers, or are not inserted at all; there will not be a medium state.

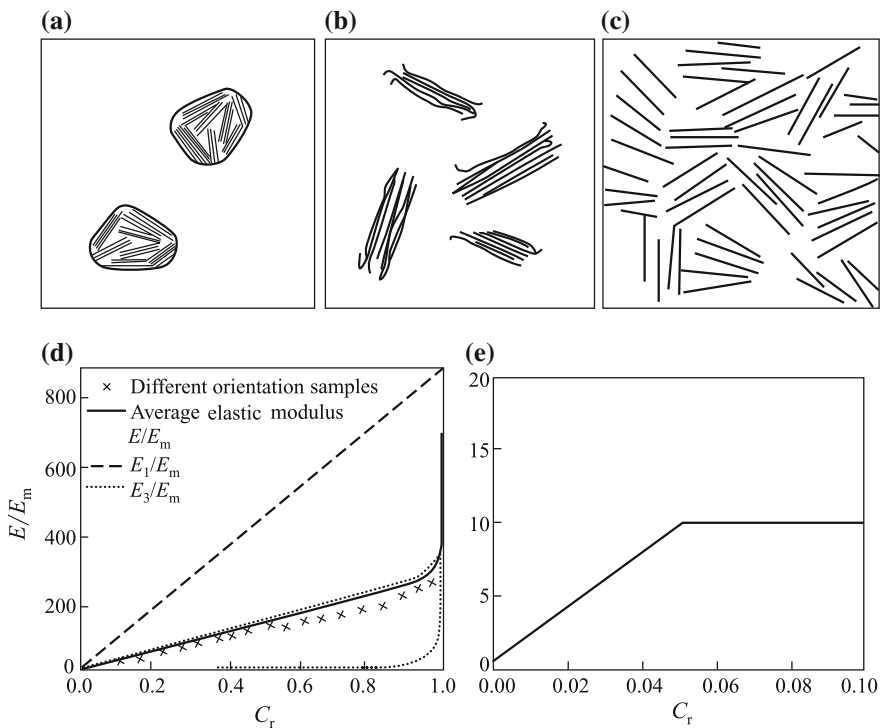


Fig. 1.39 Correlations between modulus ratio and volume fraction (C_r) of clay composites [46] (with permission)

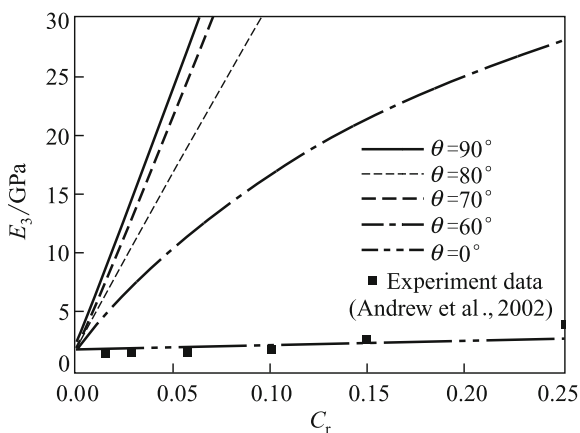
In the case of inserted layers, interface structures with a certain thickness will be generated at the interface between clay flakes and polymer. The large specific surface area of nanoclays and the sizeable volume fraction of the corresponding interface structures result in a limited volume fraction of additives, and thus, the upper limit of nanoclay effectively filled in a polymer matrix can be defined.

The mechanical simulation of nanoclay composites was carried out by using flakes to simulate clay layers (Fig. 1.39e). It was found that the composite modulus had an upper limit depending on clay volume fraction when considering the effective inserted quantity (Fig. 1.39e). In contrast, no upper limit existed without considering effective inserted quantity (Fig. 1.39d), which obviously cannot match experimental results. The results in Fig. 1.39d also indicated that the oriented clay layer state (E1) had a different modulus–volume fraction response from that of the transverse state (E2). In this manner, the modulus of clay–polymer composites can be estimated. Obviously, it is not expected to realize the high modulus of this nanocomposite experimentally, even if a uniform distribution or well-orientated nanoclay could be produced.

Another example is numerical simulation of the modulus of CNT-reinforced resin matrix composites. CNTs have a range of unique properties. For example, if taking common steel as the reference, the theoretical modulus of CNTs is more than five times higher, and their tensile strength is more than 100 times higher, while their density is only one-sixth that of steel. Although the length of CNTs is currently limited, their critical length/diameter ratio can still reach up to around 1000 because their diameter is only about 1 millionth that of a single hair. As a consequence, CNTs are a promising reinforcement material. At BIAM, CNTs were used to reinforce epoxy resin, but the improvement was not large. The reasons for this problem could be very complicated and include the CNT morphology, clustering and the interface bonding between CNTs and the matrix.

To solve this problem, Feng and his research group studied the effects of these three factors on the modulus of CNT composites using numerical micromechanics [47]. The morphology of the CNTs studied is shown in Fig. 1.40. CNTs are

Fig. 1.40 CNT model and correlation between CNT modulus and volume fraction/orientation (C_r) for calculation and experimental data



basically curled and tangled and can be defined at any state between a straight line and circle in modeling. In Feng's study, CNTs were abstracted into a spring model, where θ is the spring lift angle; $\theta = 0$ means a planar circle and $\theta = \pi/2$ means a stretched line. The calculated results given in Fig. 1.40 were obtained, where E_3 is the composite modulus in the spring axial direction, and Cr is the CNT volume fraction. This figure shows that a planar circular CNT has little influence on the modulus of the polymer composite. Only CNTs with a large lift angle can stiffen the matrix.

Low-dimensional composites are currently an important subject in materials science and engineering. Although we do not have conclusive results yet, both calculations and supporting experimental methods are promising to extend this direction of materials research. The research efficiency will increase considerably with further work, which is not discussed here.

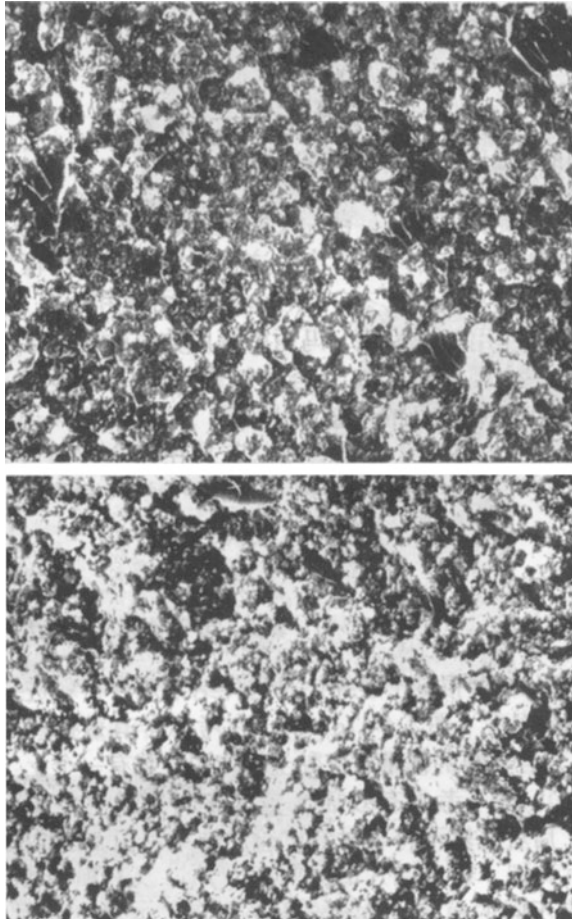
(2) Functional Mechanism of 0–3-Type Polymer Matrix Composites

It may be possible to use the interactions between different materials to form composites with a new combination of performance and function. For instance, by using a special connectivity design, or different phase-to-phase functions (mechanical, electric, magnetic) and information transfer, or phase-to-phase coupling and multiplication, it may be possible to induce a functional change. As a result, multiplicity and complexity have become important topics in composite science, but their understanding is still limited.

Regarding composite structures, ferrous composites with fine structure (such as nanoferrous composites) could be expected to exhibit new reinforcing effectiveness after nanocrystallization because of nanodimensional and interfacial effects, which can change performance, although the mechanism of this is still unclear. Structure–function-integrated composites rely on their compositing effectiveness to advance toward high combined performances, intensive coupling and multi-function integration. However, a commonly encountered problem is the current shortage of related fundamental studies. As for the processing and preparing techniques of these composites, how to render specific performance or function and produce a material system by compositing at different micro-, meso- and macro-scales and levels of two or more materials with different chemical and physical properties is still difficult. In the following section, 0–3-type filler/polymer matrix composites will be used as an example to discuss the principle of this kind of functional composite [48], i.e., thermally conductive composites.

A two-phase composite consisting of A and B constituents is a typical unit, and the two constituents in 0–3 construction are the largest category. The performance of this kind of composite will depend not only on the properties of A and B constituents, but also on the interaction between them. Explaining the relationship between constituent properties and composite performance, especially additive functions, has always been a basic goal in composite science research. Regarding the thermal conductivity of 0–3-type two-phase composites, when thermally conductive grains (zero-dimensional) are added to a polymer matrix (phase 3) (for example, when aluminum nitride (AlN) grains with high thermal conductivity are

Fig. 1.41 SEM images of PI/AlN composite microstructures (*top* 50 wt% AlN; *bottom* 80 wt% AlN, $\times 1000$)



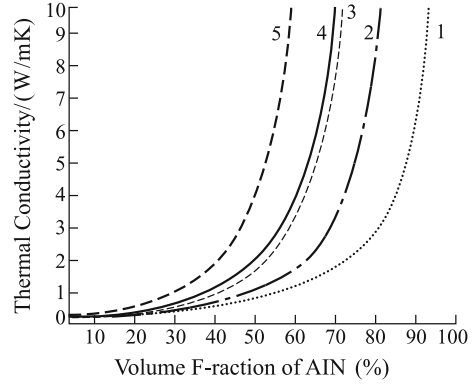
added to a high-temperature PI matrix (Fig. 1.41)), the inherently low transport properties of polymer materials will be improved to show higher thermal conductivity. If the thermally conductive grains are spherical, the correlation between thermal conductivity coefficient and grain concentration is nonlinear, as shown in Fig. 1.42.

By considering grain shape, a functional model of positive summation, which can be traced back to the generalized model developed by Hamilton and Crosser, can be derived. The summation equation of thermal conductivity of the composite constituents can be given as [49–52]:

$$\lambda_c = \lambda_1 \left[\frac{\lambda_2 + (n-1)\lambda_1 + (n-1)V_2(\lambda_2 - \lambda_1)}{\lambda_2 + (n-1)\lambda_1 - V_2(\lambda_2 - \lambda_1)} \right],$$

where λ is the thermal conductivity and n is the grain shape.

Fig. 1.42 Thermal conductivity coefficient–particle content curves of 0–3 PI/AlN composites



If the grain is spherical, $\Psi = 1$, e.g., $n = 3$. In this case, the Hamilton–Crosser equation will return to the Maxwell equation (curve 1 in Fig. 1.42) [53].

Commonly, adding grains with high thermal conductivity can substantially increase the thermal conductivity of polymer matrix composites. However, sometimes when such grains are added, the thermal conductivity of the resulting composite increases little or even decreases. This is because adding grains to a polymer matrix can introduce voids or defects. The reason for this problem is related to the interfacial thermal resistance between matrixes and grains [51, 54–58]. When considering the effect of interfacial thermal resistance on the thermal conductivity of a composite, it can be hypothesized that spherical grains are randomly dispersed in a continuous matrix with a large grain-to-grain distance. Subsequently, the summation equation of the thermal conductivity coefficient of such a composite can be given as [59]:

$$\lambda_c = \lambda_1 \frac{[\lambda_2(1 + (n-1)\alpha) + (n-1)\lambda_1] + (n-1)V_2[\lambda_2(1-\alpha) - \lambda_1]}{[\lambda_2(1 + (n-1)\alpha) + (n-1)\lambda_1] - V_2[\lambda_2(1-\alpha) - \lambda_1]}$$

where λ is the thermal conductivity, n is the grain shape, and α is the interfacial thermal resistance.

If the grain is spherical, no interfacial thermal resistance is present, $n = 3$ and $\alpha = 0$, and the above equation will return to the Maxwell equation (curve 1 in Fig. 1.42).

Figure 1.42 illustrates the thermal conductivity models of PI/AlN composites and compares them with experimental results [60]. Obviously, the Maxwell equation (curve 1) cannot fit the curve with high AlN content, as expected. In fact, both grain shape and interfacial thermal resistance have a considerable effect on the thermal conductivity of these composites, so considering the effect of interfacial thermal resistance only (curve 2) can give a more precise prediction than the Maxwell equation (curve 1), but is still not ideal. Conversely, considering the effect of grain shape only (curve 5) gives predicted results that are too low. However, when the effects of both grain shape and interfacial thermal resistance on the

thermal conductivity of a composite with high grain content are considered, the resulting modified Bruggeman equation [59] (curve 4) fitted the experimental results very well. The reason for this is that grain shape and interfacial thermal resistance have similar effects on the thermal conductivity of the composite, and thus, the interaction between them can be eliminated.

Based on the above derivation, the summation relationship in 0–3-type thermally conductive composites can be used for parameter adjustment. From curve 4 in Fig. 1.42, the effects of n on the thermal conductivity of the composite (given that $\alpha = 0$) were derived; the corresponding theoretical prediction is presented in Fig. 1.43. These results show that a spherical grain ($n = 3$) will give the smallest improvement of thermal conductivity. As n increases (grain sphericity decreases), much larger improvement of thermal conductivity can be achieved. Additionally, grain shape is more effective than grain content at improving composite thermal conductivity. For example, if the thermal conductivity of a composite is required to be 10 times higher than that of the matrix, 53.6 vol.% of AlN grains will be needed. Using $n = 6$ grains to achieve the same effectiveness requires 31.9 vol.% of spherical AlN grains. However, 31.9 vol.% of spherical AlN grains can only increase thermal conductivity by about three times. Therefore, changing grain shape is an effective approach to increase the thermal conductivity of composites.

Figure 1.44 shows the effects of predicted α on the thermal conductivity of PI/AlN composites based on curve 4 in Fig. 1.42 (assuming spherical grain shape). The interfacial thermal resistance can provide a very large barrier to the enhancement of the thermal conductivity of a composite. For example, for grains with $\alpha = 1$, regardless of their thermal conductivity or the amount added, no effective improvement of thermal conductivity can be expected. If the interfacial thermal resistance of the additives is higher than 1, the added grains can decrease the thermal conductivity of the composite. Therefore, decreasing or eliminating interfacial thermal resistance is important to prepare composites with high thermal conductivity. According to the theoretical prediction in Fig. 1.44 obtained from curve 4 in Fig. 1.42, the effect of interfacial thermal resistance is greater than that observed experimentally.

Fig. 1.43 Predicted effect of grain shape, n , on composite thermal conductivity based on curve 4 in Fig. 1.42

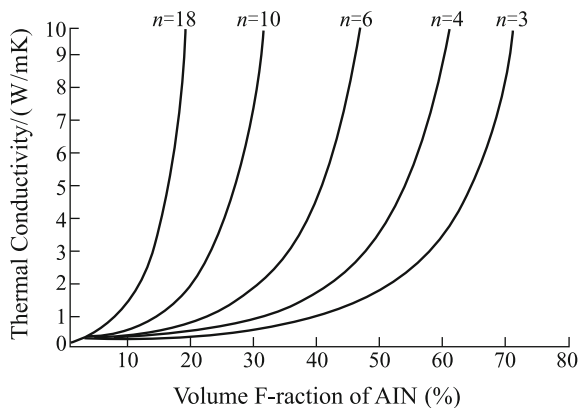
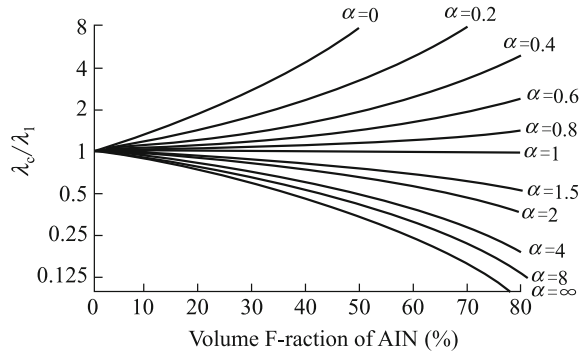


Fig. 1.44 Effect of predicted interfacial thermal resistance on composite thermal conductivity based on curve 4 in Fig. 1.42



The thermal conductivity of 0–3-structure two-phase composites is determined by the volume fraction, size and shape of conductive fillers, as well as the interfacial thermal resistance between grains and matrix. The dependence of thermal conductivity on grain concentration is typically nonlinear, similar to the positive summation of filtration curves. Theoretical models are convenient to measure the effects of grain shape and interfacial thermal resistance in varied grain contents, and to predict some material parameters that are difficult to measure experimentally, such as the AlN grain sphericity, ψ (0.70), the Kapitza radius α_k of a PI/AlN interface (73 nm), as well as the interfacial thermal resistance R_{bd} ($0.332 \times 10^{-6} \text{ m}^2\text{K/W}$).

1.6 Advanced Composites in National Economics and Defense

Advanced composites were originally developed by high-tech fields represented by the aerospace and electronics industries and have become important materials in these areas. Advanced composites are a core technology in advanced countries and are also a key development field in China. In particular, advanced composites can be used for both civil and military purposes and have become some of the most important fundamental structural materials in aerospace, marine and ground weapon structures.

Aerospace composites pioneered the development of structural materials for transportation. Especially in China, high-speed light rail and subway trains, high-speed electric lifts, as well as various cars and ships are being developed rapidly. Thus, advanced structural composites, including light composites as well as those with structure–function integration, will hopefully be adopted *en masse*. This is why we chose to present the features of aerospace composites in this introduction. Other applications of advanced composites include infrastructural constructions (bridges and highway facilities), marine engineering (marine oil platforms and

engineering facilities), energy resources (wind energy), sporting goods and biomedical devices.

The applications of composite materials in national economics and safety will be presented in detail in subsequent chapters.

Acknowledgements The content and examples in this chapter are important for engineering applications and are currently issues in composite research and development. All of these projects were kindly supported by the Fundamental Research Program (National 973 Program), High-Tech Plan (National 863 Plan), National Natural Science Foundation, as well as other pre-research programs and National Tackle Key plans. The author thanks these organizations for their aid.

(Translated by Jianmao Tang and Wenming Zhao; reviewed by Zhen Shen.)

References

1. Zou ZW (1999) Structure and properties of composite materials (trans: Wu R-J). The Science Press, Beijing (in Chinese)
2. Yi XS (1991) An introduction to laminated adhering composites. Jilin Science and Technology Press (in Chinese)
3. Schijve J, van Lipzig H, van Gestel G, Hoeymakers A (1979) Fatigue properties of adhesive bonded laminated sheet material of aluminum alloys. *Eng Fract Mech* 12:561–579
4. Schijve J (1994) Fatigue of aircraft materials and structure. *Fatigue* 16:21–32
5. Marissen R (1980) Fatigue properties of aramid reinforced aluminum laminates. Thesis, Delft University of Technology, Netherlands
6. Marissen R (1988) Fatigue crack growth in ARALL (Aramid reinforced aluminum laminates)—A hybrid aluminum-aramid composite material: Crack growth mechanisms and quantitative predictions of the crack growth rates. Report DFVLR-FB-88-56, Dissertation (Dr.-Ing), DFVLR, Cologne, Germany
7. Roebroeks GHJJ, Intvelt JC (1986) Mechanistic aspects of fatigue crack growth in ARALL. Report VTH-LR-502. Department of Aerospace Engineering, Delft University of Technology, Netherlands
8. Roebroeks GHJJ (1987) Constant amplitude fatigue of ARALL-2 laminates. Report LR-539. Dept. of Aerospace Engineering, Delft University of Technology, Netherlands
9. Roebroeks GHJJ (1986) Observation of cyclic delamination in ARALL under fatigue loading. Report VTH-LR-496, Department of Aerospace Engineering, Delft University of Technology, Netherlands
10. Chen D (1987) Some aspects of test frequency influence on the fatigue behavior of ARALL. Report LR-549. Department of Aerospace Engineering, Delft University of Technology, Netherlands
11. Yi XS (1991) An introduction to laminated adhering composites. Jilin Press of Science and Technology, Changchun (in Chinese)
12. Yi XS (2004) Challenges and innovations of advanced composite materials. *Aeronaut Manuf Technol* 7:24–30 (in Chinese)
13. Anon (1996) New materials for next-generation commercial transport. Committee on New Materials for Advanced Civil Aircraft, National Materials Advisory Board, Aeronautical Materials Advisory Board, Aeronautical and Space Engineering Board, Commission on Engineering and Technical Systems, National Research Council, NMAB-476, The National Academic Press of America, Washington DC
14. Yi XS (2003) The general ex-situ technique to prepare the toughness phase and high toughness composite. National Defense Patent, 200310102017.0 (in Chinese)

15. An X, Ji S, Tang B et al (2002) Toughness improvement of carbon laminates by periodic interleaving thin thermoplastic films. *J Mater Sci Lett* 21:1763–1765 (in Chinese)
16. Yi XS, An X, Tang B et al (2002) Ex-situ formation of periodic interlayer structure to significantly improve the impact damage resistance of carbon laminates. *Adv Eng Mater* 83(14):3117–3122
17. Xu YH (2003) The study of RTM resin and ex-situ RTM technology. Thesis, Beijing Institute of Aeronautical Materials (in Chinese)
18. Tang BM, Yi XS (2003) A general technique for preparation of toughness phase and high toughening composite material by ex-situ processing. 200310102017.0 (in Chinese)
19. F-22 Raptor Materials and Processes (2004) www.globalsecurity.org/military/systems/aircraft/f-22-mp.html
20. RTM-Worx (2004) (Simulation of resin transfer molding and vacuum infusion). www.polyworx.com
21. Yi XS (2003) The infusion processing method by ex-situ resin film, 03105536.2 (in Chinese)
22. Yi XS (2001) The method to improve the toughness of composite laminate. Defense Patent, 01 100981.0 (in Chinese)
23. Yi XS (2001) One method to improve the toughness of intra-layer laminates. Patent No. 01 100981.0, China (in Chinese)
24. Li Y, Yi X, Tang B (2004) Experimental study on PEK-C modified epoxies and the carbon fiber composites for aerospace application. *Chin J Aeronaut* 13(4):242–250 (in Chinese)
25. An XF (2004) The study on the laminated-toughened polymeric matrix laminates. Thesis, Zhejiang University (in Chinese)
26. Yi XS, An X (2004) Effect of interleaf sequence on impact damage and residual strength in a graphite/epoxy laminate. *J Mater Sci Lett* 39:3253–3255
27. Anon (1999) Prepreg remains strong. *High Performance Composites*, Jan/Feb
28. Anon (1999) Pragmatism prevails in aerospace industry. *Reinforced Plastics*, Jan
29. Anon (2004) Composite aircraft structures, International Symposium on Manufacturing Technology for Composite Aircraft Structures. In: Proceedings of ISCM 2004. Braunschweig
30. <http://www.lockheedmartin.com/us/products/f22.html> (2008)
31. http://blog.frpnl.com.cn/dutingting/article_1925.html (2008)
32. Wu GZ, Asai S, Sumita M (1999) A self-assembled electric conductive network in short carbon fiber filled poly(methyl methacrylate) composites with selective adsorption of polyethylene. *Macromolecules* 32:3534/3536
33. Wu GZ, Miura T, Asai S, Sumita M (1999) A supramolecular organization in vapor-grown carbon fiber polymer blends. *Polym Preprints, Japan*, 48(11):2905–2906
34. Wu GZ, Miura T, Asai S, Sumita M (1999) A self-assembly electric conductive network in short carbon fiber filled poly(methyl methacrylate) Composite with selective adsorption of polyethylene. *Macromolecules* (32):3534–3536
35. Yi XS (2004) Function principle of filled conductive polymer composites. National Defense Industry Press, p 161 (in Chinese)
36. Oberlin A, Endo M, Koyama T (1976) *Cryst J Growth*, (32):335
37. Endo M, Takeuchi K, Kobori K, Takahashi K, Kroto HW, Sarkar A (1995) *Carbon* 33:873
38. Wu GZ, Miura T, Asai S, Sumita M (2001) Carbon black-loading induced phase fluctuations in PVDF/PMMA miscible blends: dynamic percolation measurements. *Polymer* 42:3271–3279
39. Li D (2003) The Research on the directionally grown carbon nanotubes composites. Thesis, Tsinghua University (in Chinese)
40. Yi XS (2004) Study on energy absorption behavior of composite tubes and integrated manufacturing of composite structure. *J Mater Eng* 9:3–6 (in Chinese)
41. Farley GL (1993) Relationship between mechanical-property and energy absorption trends for composite tube [R]. NASA TP-3284
42. Chiu CH et al (1993) Effects of braiding parameters on energy absorption capability of triaxially braided composite tubes. *J Compos Mater* 32(2):1964–1983

43. Thornton PH, Edwards PJ (1982) Energy absorption in composite tubes. *J Compos Mater* 16:521–545
44. Farley Gary L (1983) Energy absorption of composite materials. *J Compos Mater* 17:267–279
45. McCarthy MA, Wiggensraad JFM (2001) Numerical investigation of a crash test of a composite helicopter subfloor structure. *Compos Struct* 51:345–359
46. Feng XQ (2001) Effective elastic moduli of polymer-layered silicate nanocomposites. *Chin Sci Bull* 46(13):1130–1133 (in Chinese)
47. Feng XQ (2004) The research on the multi-level structure and property of advanced polymeric composites. The First Report. Beijing, April (in Chinese)
48. Wang JJ (2001) The preparation and characterization of PMR PI/AlN composites. Zhejiang University, Hangzhou Shi (in Chinese)
49. Hamilton RL et al (1962) *Ind Eng Chem Fund* 1:187
50. Garrent KW et al (1974) *J Phys D: Appl Phys* 7:1247
51. Benvensite Y (1987) *Appl J Phys* 61:2840
52. Hasselman DHP et al (1987) *J Comp Mater* 21:508
53. Powell BP et al (1980) *J Am Ceram Soc* 63:581
54. Every AG et al (1992) *Acta Metall Mater* 40:123
55. Hasselman DHP et al (1992) *J Am Ceram Soc* 75:3137
56. Davis LC et al (1995) *J Appl Phys* 77(10):4954
57. Lipton R (1996) *Appl J Phys* 80:5583
58. Lipton R (1998) *Comp J Mater* 32(14):1322
59. Yi XS (2004) Function principle of filled conductive polymer composites. National Defense Industry Press, Beijing, pp 229–231 (in Chinese)
60. Wang J, Yi XS (2003) Preparing and the properties of PMR-type polyimide composites with aluminum nitride. *J Appl Polym Sci* 41:1287–1312

Chapter 2

Fiber Reinforcement

Chunxiang Feng and Zengyong Chu

Composite materials mainly consist of matrixes (polymers, metals and ceramics) and reinforcements (continuous fibers, whiskers and particles) [1]. Reinforcements are the important component of composites because they contribute the main strength to the composites [2]. According to the definitions of the Air Force Materials Laboratory (AFML) and the National Aeronautics and Space Administration (NASA), high-performance fibers are fiber reinforcements with specific strengths (tensile strength/density) and specific moduli (elastic modulus/density) higher than 6.5×10^6 and 6.5×10^8 cm, respectively. Additionally, advanced composite materials are composites made from these fibers [3].

The variety of fiber reinforcements range from widely used glass fibers and plant fibers to new fibrous reinforcement varieties such as organic fibers like aramid, polyester, polybenzoxazole (PBO) and ultra-high molecular weight polyethylene (UHMWPE) fibers. Inorganic fibers like alumina, carbon, silicon carbide and specialty glass fibers are also of note [2, 3].

In the 1990s, a variety of new technologies and new equipment was developed to prepare advanced composite materials, and this promoted the development of high-performance fibers. Development is currently advancing well with regard to research, production and marketing. As a result, a new generation of high-performance fibers such as ultra-high-temperature silicon carbide fibers and carbon nanotubes are receiving much attention.

The development of high-performance fibers will accelerate the development of advanced composite materials. This chapter will briefly introduce the main types of high-performance fiber reinforcements, including their preparation, characteristics and applications. Major developments in China over the last two decades are also highlighted.

C. Feng · Z. Chu (✉)
National University of Defense Technology, Changsha, Hunan 410073, China
e-mail: z.y.chu@163.net

2.1 Glass Fibers

Glass fibers are usually drawn from a molten mixture of quartz sand, limestone, dolomite and paraffin, as well as a certain fraction of soda and boric acid [4]. To facilitate the process or to achieve the desired performance, an appropriate fraction of TiO_2 , ZrO_2 or Al_2O_3 is also incorporated. The components and the drawing process greatly affect the performance of the final fibers.

Glass fibers are non-combustible and do not decompose, and they are characterized by good chemical stability, good heat resistance, high tensile strength, high electrical insulation, low tensile strain, low insulation and a low coefficient of thermal expansion. They were the first fibers to be used for the preparation of polymer matrix composites. They are commonly known to be low-cost reinforcements for fiberglass-reinforced plastics (FRP) [5]. The diameters of the glass fibers vary from 5 to 20 μm , and a finer fiber diameter generally results in better performance.

The types and specifications of commercially available glass fibers are mainly as follows:

- A-glass fiber, containing high alkali metal oxides;
- C-glass fiber, resistant to chemical attack;
- D-glass fiber, with a high dielectric property;
- E-glass fiber, with high electric insulation;
- M-glass fiber, with a high Young's modulus;
- S-glass fiber, with a high tensile strength;
- AR-glass fiber, alkaline resistant and suitable for reinforcing cement matrix composites.

As reinforcements, glass fibers can be processed into yarns, cloths, belts, as well as three-dimensional fabrics, such as carpets. Table 2.1 lists the types and compositions of commercial glass fibers, and their typical properties are listed in Table 2.2. The glass fiber varieties and grades produced in China have different

Table 2.1 Types and compositions of commercial glass fibers

Type	Composition/%						
	SiO_2	Al_2O_3	B_2O_3	CaO	Na_2O	MgO	Others
A	72	0.6–1.5	–	10	14.2	2.5	0.7% SO_3
C	65	4	6	14	8	3	
D	74	0.3	22	0.5	1.0	–	0.5% LiO_2
E	52–56	12–16	5–13	16–25	0–2	0.6	0–1.5% TiO_2
E-CR	58–63	10–13	1.0–2.5	21–23	0–1.2	–	1–2.5% TiO_2 , 0–3.5% ZnO
M	53.7	–	–	12.9	–	9.0	2.0% ZrO_2 , 8% BeO_2 , 8% TiO_2 , 3% CeO_2
S	65	25	–	–	–	10	–
Z or AR	71	–	–	–	11	–	16% ZrO_2 , 2% TiO_2

Table 2.2 Properties of commercial glass fibers

Type	Diameter/ μm	Density/ (g/cm^3)	Coefficient of thermal expansion/ $(\times 10^{-6} \text{ K})$	Young's modulus/GPa	Tensile strength/GPa	Tensile strain/%	Poisson's ratio	Softening temperature/ $^{\circ}\text{C}$
E	12	2.54	-5.0	72.4-76	3.6	-2.0	0.21	845
AR	12	2.68	7.5	70-80	3.6	-2.0	0.22	-
M	12	2.89	5.7	110	3.5	-	-	-
S	12	-2.48	2.9-5.0	-86	4.6	-	-	968

Table 2.3 Properties of the glass fiber varieties produced in China

Property	Non-alkali	Medium alkali 5 [#]	Medium alkali 5-2 [#]	High alkali	High strength 2 [#]	High modulus M ₂	Alkali resistant R ₁₃
Tensile strength/GPa	3.12	2.68	—	—	4.10	—	—
Young's modulus/GPa	73	—	—	—	85	95	—
Density/g·cm ⁻³	2.57	2.53	2.54	2.51	2.54	2.77	2.73
Permittivity at 10 ⁶ Hz	6.6	—	—	—	—	—	—
Loss tangent angle at 10 ⁶ Hz	1.1×10^{-3}	—	—	—	—	—	—
Volume resistivity/Ω·cm	1.2×10^{15}	—	—	—	—	—	—
Surface resistivity/Ω·cm	2.2×10^{14}	—	—	—	—	—	—

—2[#] is equivalent to No.2; 5-2[#] is equivalent to No.5-2.

Table 2.4 Properties of the high-strength glass fiber varieties produced in China

Type	Density/g·cm ⁻³	Tensile strength/GPa	Specific tensile strength/ $\times 10^7$ cm	Young's modulus/GPa	Specific modulus/ $\times 10^8$ cm
S ₁	2.55	2.8–3.10	1.10–1.20	80–83	3.14–3.25
S ₂	2.54	3.00–4.10	1.18–1.61	85–87	3.35–3.43
S ₃	2.64	3.72	1.41	89	3.38
No alkali	2.54	2.0	0.79	73	2.83

Table 2.5 Effect of heat treatment temperature on high-strength glass fibers

Type	Tensile strength/GPa					
	Room temperature	300 °C	400 °C	500 °C	600 °C	700 °C
S ₁	3.39	2.31	1.90	1.40	1.70	—
S ₂	3.40	3.35	—	2.30	2.20	1.50
S ₃	3.75	3.08	3.10	3.32	2.26	1.70

specifications, and these are listed in Table 2.3. Among these fibers, the high-strength type can be subclassified as in Table 2.4, and their tensile strength variations are listed in Table 2.5 as a function of heat treatment temperature.

2.1.1 E-Glass Fibers

E-glass fibers, also referred to as non-alkali glass fibers, were the first fiber species used for electronic insulation belts. They are a kind of Ca–Al–B–Si glass fiber with a total alkali content less than 0.8 wt%, which ensures their excellent corrosion resistance and high conductivity resistance. As a favored insulation material, they have been processed into electromagnetic wires, impregnation materials, mica products, laminated products and polymer matrix composite products. The insulation grade of these products varies from B, F and H to C, which enables their widespread use in the electric and electronic fields.

They are also the most common fiber reinforcements for polymer matrix composites. They are regarded as ideal polymer strengthening glass fibers with a high strength, high Young's modulus, low density and good water resistance. As an example, they have accounted for 90% of the glass fiber market. They can be used both structurally and functionally. For example, E-glass fiber-reinforced rubber products or filter products can be used in the cement, power, metallurgy and carbon black industries where processing temperatures reach up to 150–300 °C. However, a significant disadvantage of E-glass fibers is their limited chemical corrosion resistance to acid or alkali media, thus restricting their application in a cement matrix.

2.1.2 AR-Glass Fibers

AR-glass fibers, namely alkali-resistant glass fibers, contain about 16 wt% ZrO₂. They are used as reinforcements for cement matrix composites with an anti-alkaline property better than that of ordinary glass fibers. Compared with unreinforced cement, AR-glass fiber-reinforced cement has a 2–3 times higher tensile strength, a 3–4 times higher bending strength and a 15–20 times higher toughness. The reinforced composite can be used for manufacturing large panels, roof slabs, corrugated tiles, balcony slabs, all kinds of pipes and permanent templates.

2.1.3 S-Glass Fibers

S-glass fibers are referred to as high-strength glass fibers with a tensile strength about 35% higher than that of E-glass fibers. Their main components are SiO₂, Al₂O₃ and MgO. A representative S-glass fiber is “S-994” with a tensile strength of 4.3–4.9 GPa, a Young's modulus of 85 GPa, a density of 2.49 g/cm³ and a softening point of 970 °C. Typical S-glass fibers produced in China are high-strength type I and type II with a tensile strength of 4.1 GPa and a Young's modulus of 85 GPa. Based on different purposes, the fiber diameters vary from 7 to 12 μm.

S-glass fibers can be made into a variety of twistless rovings, twist yarns, cloths and other products. If the coupling agent KH-550 is applied, they can be impregnated directly into epoxy, phenolic resins and nylon, and they act as reinforcements of polymer matrix composites that require high strength. The reinforced composites can be fabricated as weapon components such as rocket engine shells and launcher shells, plane spiral lamina and landing gear, radomes, artillery covers and fuses, deep water mine shells, bulletproof vests, and ammunition boxes. They have played an important role in improving arms performance. In civilian fields, they have been used in high-pressure containers such as air cylinders, health cylinders, lifeboats, refrigerated vessels and spiral laminas.

2.1.4 M-Glass Fibers

M-glass fibers, also referred to as high-modulus glass fibers, generally have a higher modulus than common glass fibers. Their specific modulus is much higher than that of steel because their density is about two-thirds lower. Improving the modulus of glass fibers allows their use in structural composites, which results in better performance.

For $\text{SiO}_2\text{-Al}_2\text{O}_3\text{-MgO}$ glass fibers, oxides such as BeO , Y_2O_3 , ZrO_2 , TiO_2 and CeO_2 are usually incorporated to increase their Young's modulus. However, highly toxic BeO and expensive Y_2O_3 have not been industrially used even though they are particularly effective in increasing moduli.

Chinese type "M₂" glass fibers with a Young's modulus of about 95 GPa have been produced, and they contain CeO_2 , TiO_2 and ZrO_2 [5]. Table 2.6 shows the mechanical properties of several typical high-modulus glass fibers.

M-glass fibers have a high modulus and also a high tensile strength. Additionally, their insulation properties are good and they can be used to reinforce epoxy, phenolic resins and nylon for the production of high-performance composite materials that are widely used in the space industry as structural materials. At the same time, they have found important use in civil products such as EHV-operation

Table 2.6 Mechanical properties of several typical high-modulus glass fibers

Type	Production country	Density/g·cm ⁻³	Young's modulus/GPa	Specific modulus/ $\times 10^7$ cm	Tensile strength/GPa
M ₁	China	2.80	93–95	3.32–3.39	3.10–3.40
M ₂	China	2.77	94–95	3.39–3.43	3.20–3.81
Non-alkali	China	2.54	73	2.83	3.10
YM _{31A}	US	2.89	110–120	3.81–4.15	3.70
BM-1	Russia	–	93	–	3.80
BM-100	Russia	–	105	–	3.50
M-11	Russia	–	112	–	4.30
M-12	Russia	–	120	–	4.50

poles with resistance to 5,00,000 V, high jump poles and diving boards. Product forms include yarn, cloth and twistless rovings.

2.1.5 High Silica Glass Fibers

High silica glass fibers contain about 96–99 wt% SiO_2 as well as small amounts of B_2O_3 , Na_2O and Al_2O_3 . For the preparation of SiO_2 – B_2O_3 – Na_2O system glass fibers, raw materials were molten and drawn into fiber products, phase separated at 500–600 °C and then soaked in hydrochloric acid at a certain temperature. B_2O_3 and Na_2O were leached, and a porous SiO_2 skeleton was left; the skeleton was then sintered at 700–900 °C with the SiO_2 content increasing to more than 96 wt%. The high silica glass fibers have fiber diameters of 4–10 μm , a density of 2.20 g/cm^3 , a tensile strength of 1.50 GPa and a Young's modulus of 73 GPa.

The main characteristics of these products are high-temperature stability, shape stability, thermal shock resistance and chemical stability, which enable their use as a high-temperature ablation reinforcement.

For example, high silica glass fiber-reinforced phenolic resins, in various composite forms, have been used as ablation-resistant parts of missiles and rockets such as missile headgear, end skirts, shell and rocket large nozzles. High silica glass fiber carpets, fabrics and other products are superior insulation materials and can function as a thermal protection layer for missiles and rockets or as impurity filters in steel materials. In addition, because of their porous structure they can be used as catalyst supports and can be fabricated into reverse osmosis membranes for use in desalination and gas separation.

2.1.6 Specialty Glass Fibers

Characterized by high strength, superior integrated performance and low cost, glass fibers are currently the most widely used and most produced reinforcements. Special glass fibers have been developed to meet some special performance requirements:

(1) Hollow Glass Fibers

As a new type of glass fiber, hollow glass fibers have features such as lightness, high stiffness, low dielectric constants and low thermal conductivity. Their main technical indexes are hollow percentage and hollow degree. The hollow percentage refers to the ratio of the number of hollow filaments versus the total number of filaments and is expressed as a percentage; the hollow degree refers to the ratio of the inner diameter versus the outer diameter of the hollow fibers, often expressed as a K value.

Table 2.7 Properties of hollow glass fiber-reinforced epoxy phenolic laminate

Fiber type	Density/g·cm ⁻³	Thermal conductivity/ kJ·(m·h·°C) ⁻¹	Dielectric constant/ $\times 10^{10}$ Hz	Dielectric loss tan σ
Hollow fiber	1.38	2.97	2.80	0.01
Dense fiber	1.98	5.94	4.65	0.02

Hollow fibers are generally prepared from E-glass. Their tensile strength increases when the K value increases from zero to 0.8 and decreases when the K value increases more than this. For general industrially produced hollow glass fibers, $K = 0.5\text{--}0.7$.

They are characterized by low thermal conductivity and low dielectric constant, as listed in Table 2.7. Composites made from hollow glass fibers can be used in the aviation industry and in underwater facilities such as radomes, deep water containers and high pressure containers.

Additionally, hollow glass fibers with metal coatings of zinc or aluminum can be used as electronic-interference materials. Because of their excellent lightness, reliability, capacity and response time, they can float in air over long periods and proliferate over a large area while having good interference effects. These antistatic and electromagnetic shielding fields allow hollow glass fibers to be widely applied.

(2) Radiation-Resistant Insulating Fibers

These fibers are composed of SiO₂, Al₂O₃, CaO and MgO and characterized by a small thermal neutron capture area, high insulation resistance, excellent mechanical properties and better water resistance than E-glass fibers.

Their insulation resistance is highly stable under high doses of γ -rays or strong neutron irradiation. The fibers can thus be used at high temperatures and under strong irradiation environments. For example, they can be used as main insulation materials in high-temperature cables or radiation-resistant cables in nuclear reactors. They are also insulation materials that can be used for high-temperature wires and are important reinforcements for polymer matrix composites. They can also be applied as low dielectric loss and low-density materials for electronic components or radomes.

2.2 Carbon Fibers

Fibrous carbons include continuous carbon (graphite) fibers, carbon whiskers and the recently developed carbon nanotubes, and these are new types of nonmetallic materials [3]. Among them, carbon fibers are a kind of polycrystalline fiber with incompletely crystallized graphite arranged along the fiber axial [6].

Table 2.8 Categories and mechanical properties of carbon fibers

Property	UHM	HM	UHT	HT
Young's modulus/GPa	>400	300–400	200–350	200–250
Tensile strength/GPa	>1.70	>1.70	>2.76	2.0–2.75
Carbon content/%	99.8	99.0	96.5	94.5

All the commercial continuous carbon fibers are manufactured from carbon precursors followed by spinning into fiber form (spinning step), cross-linking using proper agents (stabilization step), and heating up to 1200–3000 °C under inert gas to remove non-carbon elements (carbonation step) [6–21].

As the most successful commercialized carbon products in the last 40 years, carbon fibers have developed into one of the most important modern industrial materials. They are mainly used as reinforcements for polymer matrixes, ceramic matrixes and carbon matrix composites. At present, most countries regard high-performance carbon fibers as important engineering materials for the twenty-first century [6, 7].

Based on their mechanical properties, carbon fibers can be classified into the following categories: high-tenacity type (HT), ultra-high-tenacity type (UHT), high-modulus type (HM) and ultra-high-modulus type (UHM). Their corresponding mechanical property ranges are listed in Table 2.8.

Based on the type of carbon precursor, carbon fibers can be classified as polyacrylonitrile (PAN)-based carbon fibers, pitch-based carbon fibers and rayon (viscose filament)-based carbon fibers, whose typical species and major mechanical properties are listed in Tables 2.9, 2.10 and 2.11.

From the above tables, the most representative manufacturer is the Toray Company, whose high-performance carbon fibers are second to none in terms of production and performance. Additionally, their fiber varieties tend to be serialized [8–12].

As functional reinforcements, in addition to high specific strength and high specific modulus [10], carbon fibers also have excellent properties like high-temperature stability, chemical corrosion resistance, heat impact resistance, electrical conductivity, thermal conductivity, anti-friction properties, anti-radiation properties, damping, shock absorption, noise reduction and weavability.

Carbon fiber-reinforced composites have been widely used in the aerospace, defense and other military fields, as well as in advanced sporting goods, medical equipment, the auto industry and in other civilian areas. Their fields of application and their characteristics are listed in Table 2.12.

There are a variety of carbon fiber precursors, but those that are industrially applied mainly include polyacrylonitrile (PAN), pitch or phenolic, and rayon. Comparative mechanical properties of different precursor-based carbon fibers are listed in Table 2.13.

Table 2.9 Manufacturers, brand names and characteristics of some typical carbon fibers

Type	Manufacturer	Brand name	Diameter/ μm	Density/ $\text{g}\cdot\text{cm}^{-3}$	Tensile strength/GPa	Young's modulus/GPa	Tensile strain/%	Compressive strength/GPa	Note
PAN-CF	Amoco	T-50	6.5	1.81	2.90	300	0.7	1.61-4.09	C
		T-40	5.1	1.81	5.65	290	1.8	1.88-2.7	C
		T-650/35	6.8	1.77	4.55	241	1.8	≤ 0.8	C
		T-300	7	1.76	3.45	231	1.4	2.8-2.88	C
	BASF	CelionGy-70	8.4	1.90	1.86	517	0.30	1.38-2.2	M
								1.05	C
								0.413	M
	Grafil Inc.	CelionG30-500	7	1.78	3.79	234	1.62	6.2-8.3	C
		Grafil34-700	6.9	1.80	4.5	234	1.9	2.76	C
		Grafil43-750	5.0	-	5.5	305	-	1.66-2.2	C
		GrafilHM-ST	6.9	-	3.2	390	-	0.8	M
								>2.0	C
		GrafilXA	7.0	-	3.5	230	-	1.39-2.0	C

(continued)

Table 2.9 (continued)

Type	Manufacturer	Brand name	Diameter/ μm	Density/ $\text{g}\cdot\text{cm}^{-3}$	Tensile strength/GPa	Young's modulus/GPa	Tensile strain/%	Compressive strength/GPa	Note	
PAN-CF	Hercules	MagnamiteHMS4	7	1.80	2.34	345	0.8	1.66	C	
		MagnamiteIM6	5.4	1.74	5.1	303	1.7	2.8-7.1	C	
		MagnamiteIM7	5	1.80	5.3	303	1.8	6.39-8.8	C	
		MagnamiteIM8	5	1.80	5.3	303	1.6	3.22	C	
		MagnamiteAS1	8	1.80	3.1	228	1.3	5.9	C	
		MagnamiteAS4	8	1.79	4.0	221	1.6	1.44	M	
		Toho Rayon	Besfight-HTA	7	1.77	3.72	235	1.6	2.8	C
									1.9	M
	Toray	Torayca-M30	6.5	1.81	1.74	392	0.6	1.6	C	
		Torayca-M40						1.2	M	
		Torayca-M40J	6	1.77	4.41	377	1.2	2.33	C	
								3.41	C	
		Torayca-M46	6.5	1.88	2.55	451	0.6	1.4	C	
							1.2	M		
		Torayca-M50J	5	1.8	3.92	465	0.8	4.0	C	
		Torayca-M60J	4.7	1.94	3.92	588	0.7	1.67	C	
		Torayca-T300	7	1.75	3.53	230	1.5	2.8-3.7	C	
							2.55	M		
		Torayca-T300S	7	1.82	4.8	230	2.1	6.1	C	
		Torayca-T800H	5	1.81	5.49	294	1.9	2.74-7.86	C	
		Torayca-T1000	5	-	4.8	294	2.4	2.2	M	

(continued)

Table 2.9 (continued)

Type	Manufacturer	Brand name	Diameter/ μm	Density/ $\text{g}\cdot\text{cm}^{-3}$	Tensile strength/GPa	Young's modulus/GPa	Tensile strain/%	Compressive strength/GPa	Note
Pitch-CF	Amoco	Thormel P-120	10	2.18	2.37	827	0.3	0.45 0.30-0.40	C M
		Thormel P-100	10	2.15	2.37	758	0.3	0.48 0.20-0.50	C M
		Thormel P-75S	10	2.0	1.9	520	0.4	0.69	C
		Thormel P-55S	10	2.0	1.9	380	0.5	0.5 0.85	M C
		Thormel P-25	11	1.9	1.4	160	0.9	0.5 1.15 0.5-1.4	M C M
		FiberG-E120	9.2	2.14	3.3	827	0.48	0.7	M
		FiberG-E105	9.3	2.14	3.1	717	0.5	0.74 0.80	C M
		FiberG-E75	9.3	2.14	3.1	524	0.57	0.81	C
		FiberG-E55	9.35	2.10	3.2	393	0.75	1.1	M
		FiberG-E35	9.4	2.04	2.9	262	1.0	1.26 1.60	C M
Pitch-CF	Mitsubishi Nippon Steel	Dialead-K135	10.0	-	2.08	201	-	1.2	C
		NT-20							
		NT-40	9.5	-	3.5	400	-	1.1-2.0 1.9	C M
		NT-60	9.4	-	3.0	595	-	0.8-1.8 0.7	C M

Note M—measured; C—calculated

Table 2.10 Other properties of typical carbon fibers

Type	Manufacturer	Brand name	Horizontal compressive strength/MPa	Horizontal fracture strain/%	Shear modulus/GPa	Damping factor	Horizontal compressive modulus/GPa	
PAN-CF	Hercules	Magnamite-AS4	—	—	17.0	1.10	—	
		Torayca M30	—	—	1.42	—	3.2	
	Toray	Torayca T40	—	—	14.0	2.00	—	
		Torayca T40J	—	—	17.0	1.96	—	
	Pitch-CF	Amoco	Torayca T50	—	—	3.52	—	4.0
			Torayca T300	556	26	17.5	1.98	—
			Thornel P-25	600	—	14.0	1.50	—
			Thornel P-55S	300	—	15.0	1.36	—
			Thornel P-75S	200	—	15.0	1.30	3.21
			Thornel P-100	130	—	—	—	—
PAN-CF	DuPont de Nemours	FiberG-E35	80	—	6.6	0.85	—	
		FiberG-E75	—	—	7.0	0.81	—	
		FiberG-E105	—	—	8.0	0.85	—	
		FiberG-E105	—	—	9.0	0.88	—	
		FiberG-E105	—	—	4.7	1.00	—	
		FiberG-E105	—	—	5.0	1.04	—	
Pitch-CF	Mitsubishi Nippon Steel	NT-20	160	8	8.0	0.70	—	
		NT-40	94.3	10	8.5	0.73	—	
		NT-60	54.9	5	5.7	1.00	—	

Table 2.11 Mechanical properties of carbon yarns

Type	Production country	Density/g·cm ⁻³	Tensile strength/GPa	Young's modulus/GPa	Tensile strain/%
MT	China	1.73	2.06	188	1.0
HT-I	China	1.75	2.56	225	1.1
T300	Japan	1.76	3.34	235	1.3
Graphite	China	1.78	1.96	310	0.9
M40	Japan	1.83	2.36	387	0.6

Table 2.12 Fields of application and characteristics of carbon fiber composites

Applications	Characteristics
Aerospace, roads, transport and sporting goods	High strength, toughness and lightness
Missiles, aircraft brakes, air and spacecraft antennas	High-dimensional stability and low thermal expansion coefficient
Audio equipment, hi-fi equipment capsules and robot arms	Excellent vibration damping, strength and toughness
Covered vehicles, electrical equipment, casts and bases, brushes	Electrical conductivity
Surgery and X-ray equipment and transplantation	Biologically inert and X-ray penetrating property
Textile machinery and general engineering	Anti-fatigue, self-lubricating and high damping
Chemical industry, nuclear field, valves and sealing materials	Chemically inert and corrosion resistance
Fixed circles of large generators and radiation equipment	Electromagnetic property

Table 2.13 Mechanical properties of different precursor-based carbon fibers

Precursor	Tensile strength/GPa	Young's modulus/GPa	Tensile strain/%
PAN	3.5–8.0	230–600	0.6–2.0
Rayon	0.7–1.8	40	1.8
Homogeneous pitch	0.8–1.2	40	2.0
Mesopitch	2.0–4.0	200–850	0.3–0.7

2.2.1 Polyacrylonitrile (PAN)-Based Carbon Fibers

PAN-based carbon fibers are the main type of carbon fibers accounting for 80% of the world's total output. Seventy percentage of these fibers were produced by Japanese companies like Toray, Toho and Mitsubishi, and the rest were shared by the US companies Hexcel, BP Amoco and also China's Formosa Plastics [8, 11–13].

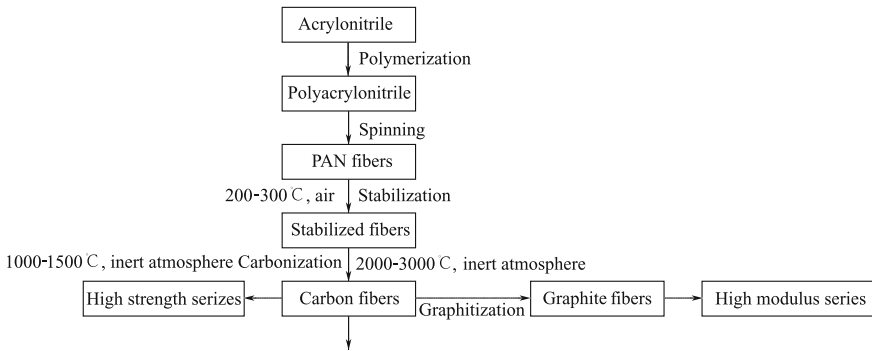


Fig. 2.1 Flowchart for PAN-based carbon fibers

PAN-based carbon fibers were invented in 1959 and were significantly improved in 1963 when the British Royal Air Research Center introduced tension into the stabilization process. They underwent rapid development in the 1990s and steady development occurred in the early twenty-first century. Currently, development is focused on high-performance PAN-based carbon fibers with higher strength, higher modulus and larger filament counts [12].

A flowchart showing PAN-based carbon fibers is shown in Fig. 2.1.

PAN-based carbon fibers are characterized by the following features: ① good weaving capability; ② low density, $1.7\text{--}2.1\text{ g/cm}^3$; ③ high modulus, $200\text{--}700\text{ GPa}$; ④ high strength, $2\text{--}7\text{ GPa}$; ⑤ fatigue resistant; ⑥ self-lubricating and wear resistant; ⑦ energy absorbing and impact resistant; ⑧ low coefficient of thermal expansion, $0\text{--}1.1 \times 10^{-6}\text{ K}^{-1}$; ⑨ good thermal conductivity without heat accumulation; ⑩ good electrical conductivity, $15\text{--}5\ \mu\Omega\cdot\text{m}$, and non-magnetic; good X-ray penetration and good biological compatibility.

Toray is the most comprehensive company in terms of PAN-based carbon fiber production, and their fiber specifications and performances are listed in Table 2.14 [8].

The performance of carbon fibers increases from T300 to T1000G and from M30S to M60 J. The company's goal is to further increase the tensile strength to 8.56 GPa . Even though their current laboratory data indicate a value of 8.05 GPa , the tensile strength can still be improved significantly because the current strength is only 4.76% that of the theoretical value. The theoretical strength of a graphite crystal is 180 GPa [13].

High-modulus carbon fibers are also referred to as graphite fibers (GrF), and they have a carbon content of $92\text{--}96\%$. The carbon content of ultra-high-modulus (UHM) graphite fibers is more than 99% , and the available brands and their performance are listed in Table 2.15.

Research in China on PAN-based carbon fibers started in the 1960s [12, 13]. In the mid-1970s, the tensile strength and Young's modulus reached 2.00 and 180 GPa , respectively, while in the early 1980s they reached 2.5 and $180\text{--}200\text{ GPa}$, respectively, and were named HT-I. In the late 1980s, they reached $3.0\text{--}3.6$ and 220

Table 2.14 Brand names and properties of Japanese company Toray's carbon fibers

Brand name	Filament count	Tensile strength/GPa	Young's modulus/GPa	Tensile strain/%	Size/tex	Density/(g/cm ³)
T300	1k	3.53	230	1.5	66	1.76
	3k				198	
	6k				396	
	12k				800	
T300J	3k	4.21	230	1.8	198	1.78
	6k				396	
	12k				800	
T400H	3k	4.41	250	1.8	198	1.8
	6k				396	
T600S	24k	4.12	230	1.9	1700	1.79
T700S	6k	4.9	230	2.1	400	1.8
	12k				800	
	24k				1650	
T700G	12	4.90	240	2.0	800	1.78
	24				1650	
T800H	6k	5.49	294	1.9	223	1.81
	12k				445	
T1000G	12	6.37	294	2.2	485	1.80
M35J	6k	4.70	343	1.4	225	1.75
	12k				450	
M40J	6k	4.41	377	1.2	225	1.77
	12k				445	
M46J	6k	4.21	436	1.0	223	1.84
	12k				445	
M50J	6k	4.12	475	0.8	216	1.88
M60J	3k	3.92	588	0.7	100	1.94
	6k				200	
M30S	18	5.49	294	1.9	760	1.73
M30G	18k	5.10	294	1.7	760	1.73
M40	1k	2.74	392	0.7	61	1.81
	3k				182	
	6k				364	
	12k				728	

GPa, respectively, with small quantities approaching 2.0 GPa and 280 GPa, respectively. With a graphitization temperature of 2500 °C, the Young's modulus reached 300 GPa, but the tensile strength was only 0.8–1.2 GPa [14]. By the end of the last century, continuous fibers were produced with tensile strength higher than 2.45 GPa and a Young's modulus higher than 392 GPa, and this is listed in Table 2.16.

Table 2.15 Brand names and properties of ultra-high-modulus (uhm) carbon fibers

Brand name	Young's modulus/GPa	Tensile strength/GPa	Tensile strain/%	Coefficient of thermal expansion/ $\times 10^{-6} \text{ K}^{-1}$	Thermal conductivity/W·(m·K) $^{-1}$	Electrical conductivity/ $\mu\Omega\cdot\text{cm}$	Density/g·cm $^{-3}$
P100S ^a	724	2.20	0.31	-1.45	520	2.5	2.15
P120S ^a	827	2.20	0.27	-1.45	640	2.2	2.18
M60J	588	3.92	0.70	-0.90	75	8.0	1.94
M70J	690	—	—	—	—	—	—
Gy-70	517	1.86	0.36	-1.10	142	6.5	1.90
Gy-80	527	1.96	0.32	—	—	6.0	1.92

^aPitch-based carbon fibers

Table 2.16 Brand names and properties of Chinese PAN-based carbon fibers

Brand name	Manufacturer	Tensile strength/GPa	Young's modulus/GPa	Tensile strain/%	Density/g·cm ⁻³	Diameter/ μ m	Electrical conductivity/ $\times 10^{-6}$ Ω ·cm
J9107	Jilin Carbon Co. Ltd.	3.49	227.6	1.63	1.68	6.3	19.6
S9206	Shanghai Carbon Co. Ltd. ^a	3.10	217.3	1.45	1.71	6.3	19.8
L8506	Lanzhou Carbon Co. Ltd. ^a	2.90	203.3	1.48	1.71	6.5	24.8

^a At a standstill

With the continuous improvement in carbon fibers as well as developments in processing and equipment, more people have come to realize that the key to high-strength carbon fibers is to control the polymer composition, to make fiber diameter finer, to produce a homogenous fiber bulk and to produce a fiber surface with few defects. With the support of national key projects, China can produce 3K or 12K T300-type carbon fibers at 100 t/a. These fibers have a tensile strength of 3.84 GPa, a Young's modulus of 235.6 GPa and a tensile strain of 1.6%.

The theoretical modulus of graphite fibers is about 1020 GPa, as listed in Table 2.15. Pitch-based carbon fibers such as P120S have reached 81.1% of the theoretical value, while PAN-based carbon fibers such as M70 J have reached 67.7%. By the end of the last century, with proper graphitization, China had produced high-modulus PAN-based carbon fibers with a tensile strength of 2.85 GPa and a Young's modulus of 382 GPa [15]. With the introduction of boron and graphitization at 2400–2900 °C, the tensile strength and the Young's modulus reached 2.53–2.89 and 400–520 GPa, respectively [16, 17].

2.2.2 Pitch-Based Carbon Fibers

As raw materials; bituminous coal, petroleum bitumen and asphalt or polyoxyethylene asphalt should be appropriately treated so that their rheological property, chemical composition and structure will meet the requirements for carbonization and graphitization.

Asphalt can be isotropic or anisotropic (such as mesopitch or LCD). Carbon fibers derived from the isotropic system generally have poor performance; for example, their tensile strength is about 950 MPa, Young's modulus is 40–45 GPa and the tensile strain is 2.0–2.2%. These fibers are referred to as common-class products and are mainly used in composites that do not require high performance. Alternatively, high-performance carbon fibers, particularly the ultra-high-modulus carbon fibers, can be manufactured from mesopitch [18–20].

Since the original carbon content of pitch is higher than that of PAN, its carbon yield is higher after carbonation. In addition to a high Young's modulus, pitch-based carbon fibers also have good thermal conductivity, electrical conductivity and a negative coefficient of thermal expansion. However, their processing properties and compressive strength are not as good as those of PAN-based carbon fibers.

High-performance pitch-based carbon fibers have unique applications in aerospace and space satellites, etc. The mechanical properties of some typical commercial pitch-based carbon fibers are listed in Table 2.17. The mechanical properties of the pitch-based carbon fibers produced by Nippon Graphite Fiber Corporation are listed in Table 2.18.

Table 2.17 Mechanical properties of some typical commercial pitch-based carbon fibers

Manufacturer	Brand name	Tensile strength/GPa	Young's modulus/GPa	Tensile strain/%
Amoco Corp.	Thornel P25	1.40	140	1.0
	Thornel P55	2.10	380	0.5
	Thornel P75	2.00	500	0.44
	Thornel P100	2.20	690	0.30
	Thornel P120	2.20	820	0.20
Osaka Gas	DannCarl F140	1.80	140	1.3
	DannCarl F60	3.00	600	0.5
Kureca	Kureca KCF100	0.90	38	2.4
	Kureca KCF200	0.85	42	2.1

The Granoc XN series are a kind of low modulus, low strength carbon fiber with a fiber diameter of about 10 μm , a Young's modulus of 55–155 GPa and a tensile strength of 1.10–2.40 GPa. However, their density is low at 1.65–2.80 g/cm^3 and their tensile strain is relatively high at 1.5–2.0%. They are mainly used for civil engineering and infrastructure in the form of sealing materials, reinforcing sheets for repairing concrete, tunnel walls and poles.

The Granoc CN series are a kind of carbon fiber mainly used for recreational sport supplies and general industrial applications. Compared with T300-type PAN-based carbon fibers, their Young's modulus is much higher and applicable to materials requiring stiffness. They can be used in electronic equipment, precision optical instruments, acoustics and audio equipment, robot arms and various rollers.

The Granoc YSH series of carbon fibers are mainly used in the manufacture of satellite antennas, satellite structure components, solar panels, joysticks, stings, missile components and rocket components.

In China, researchers mainly focus on common pitch-based carbon fibers using an isotropic pitch as the precursor as well as high-performance pitch-based carbon fibers using mesopitch as the precursor [18, 19]. The common carbon fibers have been continuously prepared with a tensile strength of 0.80–0.95 GPa, a Young's modulus of 40–45 GPa and a tensile strain of 2.0–2.5%, but these have not yet been industrialized. Because of their poor mechanical properties, they are mainly used for functional or cement matrix composites.

High-performance pitch-based carbon fibers are prepared from mesopitch by melt spinning, pre-oxidation, carbonation and graphitization [19]. Their performance depends largely on the structure and composition of the precursor. Mesopitch has been studied in-depth, and at the end of the last century, graphite fibers were produced by the modification and modulation of oil residue and coal. Spinnable pitch has a softening point of 264–278 $^{\circ}\text{C}$ and a mesopitch content above 95%. Typical mechanical properties of final continuous carbon fibers are listed in Table 2.19.

Table 2.18 Brand names and properties of carbon fibers from Nippon Graphite Fiber Corporation

Brand name	Tensile strength/GPa	Young's modulus/GPa	Tensile strain/%	Density/g·cm ⁻³	Diameter/ μ m	Coefficient of thermal expansion/ $\times 10^{-6}$ K ⁻¹	Thermal conductivity/W·(m·K) ⁻¹	Electrical conductivity/ $(\times 10^{-4}$ Ω ·cm)
XN-05	1.10	54	2.0	1.65	10	+3.4	47	28
XN-10	1.70	110	1.6	1.70	10	-0.1	-	100
XN-15	2.40	155	1.5	1.85	10	-0.8	6.3	20
CN-05	3.43	620	0.6	2.12	10	-	-	-
CN-15	3.43	780	0.5	2.17	10	-	-	-
YSH-50A10H	3.83	520	0.7	2.10	6	-1.4	140	7
YSH-50A15S	3.83	520	0.7	2.10	7	-1.4	140	7
YSH-60A	3.83	630	0.6	2.12	7	-1.4	200	6
YSH-70A	3.83	720	0.5	2.15	7	-1.5	260	5
YS-80A	3.63	785	0.5	2.15	7	-1.5	320	5
YS-90A	3.53	880	0.3	2.18	7	-1.5	500	3
YS-95A	3.53	920	0.3	2.19	7	-1.5	660	2.2

Table 2.19 Typical mechanical properties of Chinese high-modulus carbon fibers

No.	Diameter		Tensile strength		Young's modulus		Tensile strain	
	μm	C.V. %	GPa	C.V. %	GPa	C.V. %	%	C.V. %
1	13.25	12.38	2.31	20.72	525.6	17.0	0.44	18.6
2	13.68	12.33	2.18	22.70	483.2	9.95	0.46	22.5

Table 2.20 Mechanical properties of Y-shaped and circular carbon fibers

Cross section	Equivalent diameter/ μm	Oxidation gas	Temperature/ $^{\circ}\text{C}$	Oxidation time/h	Tensile strength/GPa
Y-shaped	35.5	Air	300	2.0	0.882
Circular	34.9	Oxygen + air	240	10.0	0.607
Y-shaped	27.5	Air	300	0.5	0.976
Circular	29.6	Air	240	24.0	0.603

The preparation of mesopitch by the modulation of coal tar has been reported. Green filaments with a diameter of 10.3 μm and a length of 29 km were obtained after spinning, and graphite fibers with a tensile strength of 2.5 GPa and a Young's modulus of 973 GPa were obtained after pre-oxidation, carbonation and 3000 $^{\circ}\text{C}$ graphitization [18]. Additionally, Y-shaped carbon fibers have also been reported, as listed in Table 2.20 [20]. Their mechanical properties are much better than those of the circular cross-sectional fibers, but these fibers have not yet been industrialized.

2.2.3 Rayon-Based Carbon Fibers

α -Cellulose can be extracted from cellulose raw materials such as wood, cotton seed cashmere and bagasse. When they are purified with soda or carbon disulfide, dissolved in dilute NaOH, wet-spun and post-processed, viscose fibers are obtained. Carbon fibers can be obtained after oxidation in air below 300 $^{\circ}\text{C}$ and carbonization in inert atmosphere above 800 $^{\circ}\text{C}$. If graphitized in argon above 2500 $^{\circ}\text{C}$, their crystallinity, thermal conductivity, anti-oxidation, lubrication and heat capacity increase greatly and graphite fibers are obtained with a carbon content of more than 99% [21]. The USA and Russia are the two major producers of rayon-based carbon fibers.

Rayon-based carbon fiber products come in various forms such as short fibers, continuous fibers, yarns, fabrics, belts and clothes. They can also be divided into rayon-based carbon fibers and rayon-based graphite fibers. In addition to their high specific strength, high specific modulus, good corrosion resistance and good lubrication properties, the fibers are also characterized by low density, low thermal conductivity, high purity, high tensile strain, good flexibility, large surface area and easy activation, etc.

These fibers play an irreplaceable role in thermal insulation-resistant and ablative materials, in reinforcement materials as well as in promising biological engineering materials because of their excellent biocompatibility. Brand names and properties of rayon-based carbon fiber products are listed in Tables 2.21, 2.22 and 2.23.

Rayon-based carbon fibers are mainly used as large area ablation shielding materials for aircraft brakes, car brakes, radioisotope boxes, solid-fuel engine nozzles, reentry vehicles, rocket and missile noses or heads. They can also be used to reinforce polymer composites with applications in corrosion-resistant pumps, laminas, pipes, containers and conductive wires, heating bodies, sealing materials, catalyst supports and medical absorption materials, and colloidal materials in addition to medical bandages and anti-chemical clothes.

In China, research on rayon-based carbon fibers started in the 1980s but still lags far behind the USA and Russia. Some achievements have been made in that a production line with an annual output of 300 kg was built in 2002. In addition, there are reports on the improvement of the mechanical properties of rayon-based carbon fibers wherein SiC-coated carbon fibers were prepared after surface treatment with multi-amine fire retardant and polycarbosilane with subsequent heat treatment at 1000 °C [22]. Their tensile strength, Young's modulus, electrical resistance, diameter and density, respectively, are 1.3–2.0 GPa, 70–130 GPa, 10^{-2} – 10^{-3} Ω-cm, 4–6 μm and 1.55–1.60 g/cm³.

2.3 Ceramic Fibers

As one of the outstanding Chinese achievements, traditional ceramic material is a class of clay material that can be cast into various shapes that hardens upon high-temperature treatment. They are polycrystalline materials with a specific strength. With the scientific and technological development of ceramic manufacturing including purification and related fields, ceramics have progressed from traditional ceramics to advanced ceramics [23–27].

Advanced ceramics mainly refer to nonmetallic oxides, quasi-metal oxides, carbides, nitrides, alumina, aluminum nitride and carbon, etc. Their raw materials are generally high purity, ultra-fine synthetic inorganic compounds. Their common characteristics are high-temperature stability, oxidation resistance, erosion resistance, corrosion resistance, wear resistance, high hardness and a low creep rate as well as coupling features related to their light, electrical, magnetic, acoustic and thermal properties. They are mainly used in high-tech and military technical areas that require high-temperature stability, corrosion resistance and wear resistance, etc. Examples might be mechanical seals, ceramic bearings, ball valves, ceramic cylinders and cutting tools.

With the development of materials science and engineering, advanced ceramic materials have developed from polycrystalline bulk materials to low-dimensional materials such as fibers or whiskers. They not only retain the original characteristics

Table 2.21 Mechanical properties of Chinese rayon-based carbon fibers

Type	Diameter/ μm	Tensile strength/GPa	Young's modulus/GPa	Tensile strain/%	Density/ $\text{g}\cdot\text{cm}^{-3}$	Electrical conductivity/ $\times 10^{-2} \Omega\cdot\text{cm}$	Carbon content/%
Carbon fibers	5-7	0.40-0.60	25-35	1.5-2.0	1.4	4	91-95
Graphite fibers	5-7	0.60-0.80	60-80	1.0-1.5	1.5-1.8	4	99.6

Table 2.22 Mechanical properties of US high-performance rayon-based carbon fibers

Manufacturer	Brand name	Tensile strength/GPa	Young's modulus/GPa	Density/g·cm ⁻³
Union Carbide Corporation (UCC)	Thornel-25	1.260	175	1.40–1.45
	Thornel-40	1.750	280	1.56
	Thornel-50	1.995	350	1.60
	Thornel-100	3.500	700	1.79
HITCO Carbon Composites (HITCO)	HMG-20	1.120–2.100	154–210	1.5
	HMG-40	1.400–1.645	245–350	1.7
	HMG-50	2.100–2.205	350–427	1.8

Table 2.23 Mechanical properties of Russian rayon-based carbon fibers

Brand name	Form	Carbon content/%	Fracture load (5-cm-wide fabric strength)/GPa		Tensile strength/GPa
			Radial	Latitudinal	
YPaIT-22	Cloth or belt	≥ 99.5	1.4	0.5	1.30
YPaITp3/2-15	Fabric	≥ 95.0	1.5	–	1.00
YPaITp3/2-20	Fabric	≥ 99.5	1.5	–	1.00
YPaITM/4-22	Multilayer fabric	≥ 99.5	3.0	2.0	1.30
YPaIII0-22	One-directional belt	≥ 99.5	–	–	2.00
YPaIII0-15	One-directional belt	≥ 95.0	–	–	2.00
YPaIC	Mesh	≥ 99.5	–	–	1.80
YPaIH	Textile	≥ 99.5	–	–	1.60
YPaIIII	Sewing yarn	≥ 99.5	–	–	1.60
YPaITp3/2-152	Surface-modified fabric	≥ 96.0	1.59	–	–
YVT-2	Fabric	≥ 94.0	1.40	0.8	0.80
YTM-8	Fabric	≥ 70.0	0.60	0.2	0.60
YTIeH	Yarn	≥ 94.0	–	–	0.50

of ceramics but also have new features that greatly extend the possible applications of ceramic materials and lead to a new variety of products.

However, high-tech fields such as space, energy and chemicals demand materials with excellent mechanical properties and also require them to withstand extreme environmental conditions such as aerodynamic heating and the resultant high temperatures, high heat flux densities, high-speed particle erosion and salt spray corrosion. These materials should have excellent chemical and thermal mechanical stabilities at 1500 °C.

Much research has been devoted to the development of ceramic matrix composites and intermetallic compound matrix composites. However, because of the

inherent brittleness and poor reliability of ceramics, it is the only effective method to produce excellent ceramic matrix composites using reinforcing ceramics with high-performance fibers or whiskers. Ceramic fiber-reinforced ceramic matrix composites are currently used in the manufacture of space shuttle components, thermal protection materials, high-performance engines, high-temperature heat exchangers, and other high-temperature structure materials.

Some oxide ceramics like quartz and Al_2O_3 can be melt-spun into ceramic fibers using high purity or controlled purity and composition ceramic materials, but most ceramics cannot be directly spun into ceramic fibers because of their high melting points. The general approach is to synthesize pre-ceramic precursors, which could be either inorganic precursors or organic polymer precursors. The precursors can be easily spun into green fibers and then be transformed into ceramic fibers after firing and sintering at high temperatures.

Like organic fibers, ceramic fibers have high strength, high modulus, fine diameters and good weaving performance; however, ceramic fibers also have high-temperature stability, oxidation resistance and high hardness. Therefore, ceramic fibers are believed to be important reinforcements for advanced polymers, metals and ceramic matrix composites [23–27].

2.3.1 Alumina Fibers

The main phase of alumina fibers is $\alpha\text{-Al}_2\text{O}_3$, and small amounts of SiO_2 , B_2O_3 , Zr_2O_3 , MgO , etc. are also present. These fibers have excellent high-temperature oxidation resistance and high-temperature stability as high as 1400°C . They have been given much attention recently. As a typical example, the 3M Company in the USA produced a new Al_2O_3 fiber using iron oxide for grain refinement. The tensile strength and elasticity modulus of this fiber are as high as 3.2 and 370 GPa, respectively (Nextel610). In addition, Nextel610 has a low thermal conductivity, unique electrochemical properties and corrosion resistance properties [24].

Compared with other ceramic fibers, alumina fibers have simple processing procedures, minimal equipment requirement and no need for inert gas protection. Therefore, it is cost-effective and has great commercial value. It is an important strengthening fiber that can be widely used in the military and civilian composite materials industries. The preparation methods and compositions of alumina fibers are various, and their characteristics are different from product to product. Alumina fibers can be continuous or non-continuous and common brands, and their properties are listed in Table 2.24.

From the above table, the fiber properties are shown to differ greatly upon a variation in method and composition. Alumina fibers are mainly classified as two kinds of fibers, namely composite reinforcements or high-temperature insulation materials. Continuous fibers can be woven into sheets, braids, ropes and other special forms. They are mainly used to strengthen Al, Ti, SiC and oxide matrixes to manufacture flexible insulation composites. Because the fibers and these matrixes

Table 2.24 Properties of typical alumina fibers

Brand name	Manufacturer	Diameter/ μm	Composition/ %(wt)	Tensile strength/GPa	Young's modulus/GPa	Tensile strain/%	Density/ g cm^{-3}	Working temperature/ $^{\circ}\text{C}$
FP	Du Pont	15–20	$\alpha\text{-Al}_2\text{O}_3$ 99	1.4–2.1	350–390	0.29	3.95	1000–1100
PRO	Du Pont	15–25	$\alpha\text{-Al}_2\text{O}_3$ 80 Zr_2O_3 20	2.2–2.4	385–420	0.40	–	1400
Altel	Sumitomo	9–17	$\alpha\text{-Al}_2\text{O}_3$ 75 SiO_2 25	1.8–2.6	210–250	0.80	3.2–3.3	1250
Safil	ICI	3	$\alpha\text{-Al}_2\text{O}_3$ 95 SiO_2 5	1.03	100	0.67	2.8	1000
Nextel1312	3M	11	$\alpha\text{-Al}_2\text{O}_3$ 62 SiO_2 24 B_2O_3 14	2.0	300	–	3.3	1000
ACO ₂	3M	10	$\alpha\text{-Al}_2\text{O}_3$ 70 SiO_2 29 Cr_2O_3 1	1.38	159	–	2.8	1400
Nextel1440	3M	–	$\alpha\text{-Al}_2\text{O}_3$ 70 SiO_2 28 B_2O_3 2	1.72	207–240	1.72	3.1	1430
Nextel1480	3M	10–12	$\alpha\text{-Al}_2\text{O}_3$ 60 SiO_2 40	1.90	220	0.86	3.05	–
Nextel1550	3M	10–12	$\alpha\text{-Al}_2\text{O}_3$ 73 SiO_2 27	2.2	220	0.98	3.75	–
Nextel1720	3M	10	$\alpha\text{-Al}_2\text{O}_3$ 85 SiO_2 15	2.1	260	0.81	3.4	–
Nextel1610	3M	10–12	$\alpha\text{-Al}_2\text{O}_3$ 99 SiO_2 0.25	3.2	370	0.5	3.75	–

are well matched, their composites have been used in supersonic aircraft, rocket engine nozzles and gaskets. Alumina short fibers are mainly used as insulation refractory materials in metallurgical furnaces, ceramic sintering furnaces or other high-temperature furnaces.

In addition to their abilities to enhance mechanical properties and to improve the hardness and wear resistance of the matrixes, alumina fibers have low density, good insulation, low thermal capacity, are effective energy savers, and have a low coefficient of thermal expansion. Therefore, alumina fiber-reinforced aluminum matrix composites have been applied to the production of car pistons, connecting rods, brake parts, gas compressor rotating blades and helicopter transmission devices. Furthermore, the Young's modulus of alumina fibers is higher than that of glass fibers and their compressive strength is higher than that of carbon fibers. Importantly, the fibers are white and alumina fiber-reinforced polymers can thus be fabricated into colored fishing rods, golf pars, skis, tennis rackets and other items that require high intensity and high rigidity properties.

Alumina fibers are still in the laboratory stage of development in China, but aluminum silicate and aluminum borate short insulation fibers have been produced on large scale. China lags behind in high-performance continuous alumina fibers.

2.3.2 Silicon Carbide Fibers

This fiber series consists of silicon carbide (SiC) fibers, silicon nitride (Si₃N₄) fibers and new silicon-based ceramic fibers in which silicon is the main element containing small amounts of B, Ti, Zr and C [23–35].

SiC fibers are a new kind of ceramic fiber with excellent strength, modulus, high-temperature stability, oxidation resistance, corrosion resistance, antineutron radiation properties and electromagnetic transmission and absorption properties. SiC fibers are an important species that are ideal reinforcements for structural composites and have undergone rapid development for use in ceramic fibers in the 1980s.

The preparation of continuous SiC fibers is mainly carried out by chemical vapor deposition (CVD) and by the pre-ceramic polymer-derived (PPD) method. Both methods can be used to produce continuous SiC fibers [25–29]. The properties of several typical commercial and developmental SiC fibers are listed in Table 2.25, and their high-temperature resistances are listed in Table 2.26.

2.3.2.1 Chemical Vapor-Deposited (CVD) SiC Fibers

CVD was the first approach used for the production of SiC fiber core-shell composite filaments. In 1961, Gareis and coworkers applied for a patent using ultra-fine W silk as the deposition support to produce SiC (W core) fibers [28]. In 1972, US company AVCO Corporation produced large-diameter C-wire, and as a result, SiC

Table 2.25 Properties of several typical SiC fibers

Brand name	Manufacturer	Composition/ %(wt)	Density/g·cm ⁻³	Diameter/ μ m	Tensile strength/GPa	Young's modulus/GPa	Status
NL202	Nippon Carbon	Si57C31O12	2.55	14	3.0	220	C
Hi-Nicalon	Nippon Carbon	Si62C32O0.5	2.74	14	2.8	270	C
Hi-Nicalon-S	Nippon Carbon	Si68.9C30.9O0.2	3.10	12	2.6	420	C
Tyranno LoxM	Ube Industries	Si55.4C32.4 O10.2Ti2.0	2.48	11	3.3	187	C
Tyranno ZM	Ube Industries	Si55.3C33.9 O9.8Zr1.0	2.48	11	3.3	192	C
Tyranno SA	Ube Industries	Si67C31 O < 1.0Al < 2.0	3.10	10	2.8	380	C
SiBNC	Bayer	Si-B-N-C	1.8-1.9	8-14	3.0	358	C
UF SiC	3 M	SiC(98.9)O1.1	2.70	10-12	2.8	210-240	D
SCS-6	Textron	SiC(C)	3.00	140	4.0	390	C
Sylramic	Dow Corning	SiC(95) TiB ₂ (3)B ₄ C(1.3)	3.00	10	3.4	386	C
KD-I	NUDT, China	Si-C-O	2.42	12-15	2.4-3.0	150-190	D
SiC(W)	CAS, China	SiC(W)	3.4	100 \pm 3	3.7	426	D

Note C—commercialized; D—developmental

Table 2.26 High-temperature resistances of typical SiC fibers

Brand name	Composition	Highest working temperature/°C	Working temperature/°C	Application field	Price/\$·kg ⁻¹
NL202	Si-C-O	1300	1100	PMC, MMC, CMC	1295
Hi-Nicalon	Si-C	1400	1200	PMC, MMC, CMC	6900
Tyranno LoxM	Si-C-O-Ti	1400	1100	MMC	–
Sylramic	SiC, TiB ₂	1400	1200	CMC	10000
SCS-6	SiC	1400	1300	PMC, MMC	8800

Note PMC—polymer matrix composites; MMC—metal matrix composites; CMC—ceramic matrix composites

(C core) fibers were produced with better performance and lower cost. Subsequently, from 1981 to 1984, SiC (C core) fibers were successfully commercialized by AVCO. Recently, the US company Textron (formerly AVCO Corporation) was allowed to produce a series of SCS-2, SCS-6 and SCS-8 SiC (C core) fibers.

British company BP bought the original German technology for the production of SiC (W core) fibers. It produced a series of fibers referred to as SM1040, SM1140 and SM1240 with different surface coatings. These fibers were applied, respectively, to reinforce polymers, aluminum, titanium, intermetallic compounds and ceramic matrixes.

Research has been carried out in China on mercury electrode-heated CVD SiC (W core) fibers as early as 1975 [29]. The tensile strength of the fibers was 2.6 GPa, and the continuous length reached 900 m. The radio-frequency heating method was then successfully applied to produce CVD SiC (W core) fibers. Meanwhile, detailed studies on the reaction mechanism revealed characteristics such as microstructure and optimal parameters. Continuous SiC (W core) fibers with surface protection coatings were successfully manufactured with properties close to the similar US and UK products in the 1990s (see Table 2.27). The production capacity reached an annual output of 12 kg. The dispersion coefficient of the tensile strength was less than 10%, and the continuous length was longer than 1000 m.

2.3.2.2 Pre-ceramic Polymer-Derived (PPD) SiC Fibers

The precursor approach of transferring organic materials into inorganic materials by high-temperature treatment under oxygen-free atmospheres has been used since ancient times. Similar to the method to obtain carbon fibers wherein PAN or other organic fibers are carbonized in an inert atmosphere at high temperatures, this kind of precursor method has been applied to the commercial production of ceramic fibers [23].

Table 2.27 Properties of CVD SiC (W core) fibers

Location	Brand name	Diameter/ μm	Tensile strength/GPa	Young's modulus/GPa	Density/ $\text{g}\cdot\text{cm}^{-3}$	Surface coating
USA	SCS series	≈ 140	3.50	400	3.0	Si/C
UK	SM1040	100	3.50	400	3.4	N/A
UK	SM1140	107 ± 3	3.00–3.30	–	–	C
UK	SM1240	101 ± 4	3.00–3.50	–	–	C + TiB_x
CN	–	100 ± 3	3.70	>426	3.4	C

The process includes four steps: ① synthesis of pre-ceramic polymers (pre-cursors); ② melt spinning of polymers into green fibers; ③ curing of green fibers by oxidation or EB radiation, and ④ pyrolysis of the cured fibers under an inert atmosphere at high temperatures. Fine-diameter continuous SiC fibers are finally obtained from polycarbosilane precursors. Nippon Carbon Co. first realized the industrial production of a series of continuous SiC fibers under the trademark Nicalon.

Compared with CVD SiC fibers, the biggest advantage of PPD SiC fibers is their much smaller diameter, which allows easy weaving into a variety of fabrics. It can then be easily used as reinforcements in complicated composites. In addition, PPD SiC fibers are very good heat-resistant materials and can be used as insulation materials, high-temperature conveying belts, melt filters, etc. The properties of Nicalon serial fibers are listed in Table 2.28.

The successful development of SiC fibers by the PPD method resulted in a large amount of interest from material scientists. Recently, plenty of research has been carried out on Nicalon fibers and their composites resulting in an understanding of their advantages and disadvantages. This lay the foundation for further enhancements of fiber performance and a reduction in production costs. Newer silicon-based ceramic fibers have also produced such as *M*-containing SiC fibers ($M = \text{Ti}, \text{Zr}, \text{Al}, \text{etc.}$), near-stoichiometric SiC fibers, silicon nitride (Si_3N_4) and Si–B–C–N fibers [23, 25, 30–41]. China entered this field in the early 1980s, and a variety of SiC fibers have been studied including carbon-rich SiC fibers, magnetic particle-containing SiC fibers and non-circular SiC fibers.

(1) Continuous SiC fibers

In the 1970s, Professor Yajima first obtained SiC fibers from a silicon-based polymer, polycarbosilane. This is the first ceramic fiber obtained using polymer techniques. Subsequently, Nippon Carbon procured the patent and started scale-up production. A series of fibers were then commercialized and trademarked as Nicalon, as listed in Table 2.28.

Table 2.28 Properties of the Nicalon serial fibers

Property	NL-200	HVR NL-400	LVR NL-500	NL-607	Hi-Nicalon	Hi-Nicalon-S
Diameter/ μm	14/12	14	14	14	14	12
Filament count	250/500	250/500	500	500	500	500
Denier/(g/1000 m)	105/210	110/220	210	210	200	180
Tensile strength/GPa	3.00	2.80	3.00	3.00	2.80	2.60
Young's modulus/GPa	220	180	220	220	270	420
Tensile strain/%	1.4	1.6	1.4	1.4	1.0	0.6
Density/(g/cm^{-3})	2.55	2.30	2.50	2.55	2.74	3.10
Electric conductivity/ $\Omega\cdot\text{m}$	$10^3\text{--}10^4$	$10^6\text{--}10^7$	0.5–5.0	0.8	1.4	0.1
Coefficient of thermal expansion/($\times 10^{-6}/\text{K}$)	3	–	–	3.1	–	–
Specific heat/[J/(kg·K)]	1140	–	–	1140	–	–
Dielectric constant	9	6.5	20–30	12	–	–

Polycarbosilane-derived Nicalon fibers (NL-200, for example) are not pure SiC fibers as they contain oxygen (14.0 wt%) and a trace of hydrogen (0.15 wt%) in addition to silicon (55.5 wt%) and carbon (28.4 wt%). These elements are in the β -SiC (1–5 nm), SiC_xO_y and free carbon forms, respectively. In addition, the fiber surface is oxygen-rich in the form of SiO_2 .

The high-temperature mechanical properties of Nicalon fibers are limited because of the unstable SiC_xO_y phase, which will undergo decomposition upon an increase in the grain size of β -SiC at temperatures higher than 1200 °C. Therefore, Nicalon fibers are not good enough to be used as heat-resistant materials or as advanced composite reinforcements.

One effective method is to reduce oxygen incorporation using oxygen-free approaches such as electron beam curing [31, 32]. Based on this modification, oxygen-free Hi-Nicalon and Hi-Nicalon type S fibers have been produced by Nippon Carbon, and these fibers can withstand temperatures up to 1500–2000 °C.

China started to synthesize polycarbosilane from polysilane according to a modified Yajiam route at normal pressure using domestic raw materials. However, this precursor is unstable in air, and the SiC fibers obtained had low tensile strength. After several years of research, important progress was made such as the synthesis of polycarbosilane at normal pressure, multi-spinneret melt spinning, continuous curing and continuous pyrolysis. The tensile strength of the continuous fibers ranged from 2.6 to 3.0 GPa with Young's moduli of 150–190 GPa and diameters of 12–15 μm , which are close to those of the Nicalon fibers.

(2) *M*-Containing SiC Fibers (*M* = Ti, Zr, Al, B)

Another effective method to improve Nicalon fibers is the introduction of metal or other nonmetallic elements such as Ti, Zr, Al and B [32–39]. Ti-, Zr- and

Al-containing SiC fibers have been developed by Ube Industries in Japan. These SiC fibers have been commercialized and have the trade name Tyranno. Compared with the Nicalon fibers, the obvious advantages of Tyranno fibers are their higher thermal stability and good compatibility with aluminum and aluminum alloys. They are thus more suitable for reinforcing aluminum matrixes.

Ti and Zr only increase the thermal stability of SiC fibers to a limited extent, and more stable fibers are obtained upon the incorporation of Al and B. These elements act as sintering agents at higher temperatures. The Tyranno SA fibers by Ube Industries and the Sylramic fibers by Dow Corning have been produced by the sintering effect of Al and B near-stoichiometric SiC fibers, as listed in Table 2.25. They can withstand temperatures up to 2000 °C just like the Hi-Nicalon type S fibers.

China also developed Ti-containing SiC fibers and obtained continuous fibers longer than 300 m with a filament count of 400–600 [33]. The fiber diameter range is 14–16 μm, the tensile strength range is 2.20–2.80 GPa and the Young's moduli range is 160–180 GPa. The improvement in mechanical properties upon titanium introduction is due to a generation of TiC microcrystals preventing the growth of β-SiC crystals. However, more oxygen was also introduced, which has negative influence on their thermal stabilities.

China has also developed Al- and B-doped SiC fibers from polyaluminocarbosilane or a hybrid precursor of polyborazine and polycarbosilane [34, 35]. Their tensile strengths are 2.8 and 2.2 GPa, respectively, with diameters of 12 μm and 13 μm, respectively. Upon heating to 1400 °C for 1 h under argon, their retained tensile strengths are both over 95% of the original value, confirming that their thermal stabilities are better than that of the Nicalon NL201 fibers. In addition, the creep resistance of the Al-containing SiC fibers is better than that of the Nicalon fibers. Additionally, B-containing SiC fibers with improved mechanical properties can also be obtained by mixing a polycarbosilane precursor with polyborosilazane or polyborazine, or by curing polycarbosilane fibers in a B-containing atmosphere, such as BCl₃.

(3) Silicon Nitride (Si₃N₄) and Si–B–C–N Fibers

As another type of important Si-based ceramic fibers, silicon nitride (Si₃N₄) fibers also have excellent mechanical properties [25]. Furthermore, they have a low coefficient of thermal expansion, low thermal conductivity, good thermal shock resistance, good oxidation resistance and good insulation. They are mainly used in metal matrix composites (MMC), ceramic matrix composites (CMC) and heatproof composite materials.

The processing of Si₃N₄ fibers is similar to that of SiC fibers in terms of synthesis, spinning, curing and pyrolysis. Their pre-ceramic polymers are polysilazanes or polycarbosilazanes, which can be synthesized in various strategies. The composition, microstructure and properties of the Si₃N₄ fibers differ greatly depending on the polymers. There are thus two strategies for the preparation of target Si₃N₄ fibers, pure Si₃N₄ fibers and Si₃N₄–SiC fibers.

Three typical Si_3N_4 fibers are available from the Dow Corning Corporation in the USA, Toa Nenryo Kogyo K. K. (TNK) in Japan and Domaine University in France, and these represent three different preparation technologies.

In 1987, Si_3N_4 fibers were prepared by Dow Corning by the synthesis of polymers from chlorosilane and hexamethyldisilazane (HMDS), melt spinning, curing in a chlorosilane atmosphere and pyrolysis at up to 1200 °C under an inert atmosphere. The ultimate fibers are stoichiometric Si_3N_4 . Their diameter is 10–15 μm , their tensile strength is 3.1 GPa and their Young's modulus is 260 GPa.

TNK began research into Si_3N_4 fibers slightly later than Dow Corning. They synthesized a hydropolysilazane precursor via ammonolysis of dichlorosilane. The precursor only contains Si, N and H, resulting in plenty of Si–H bonds and N–H bonds and thus a very reactive material. The precursor can be cross-linked by heating giving an infusible but still soluble fiber, and therefore, it is suitable for the preparation of high-purity Si_3N_4 fibers without other elements. These Si_3N_4 fibers are good reinforcing candidates for CMCs and MMCs because of their high thermal stabilities and oxidation resistance. Their properties are listed in Table 2.29.

Domaine University used polycarbosilazane as the precursor for Si_3N_4 –SiC fibers, and this was synthesized from chlorosilanes by ammonolysis and polymerization. Because Si_3N_4 and SiC coexist in the Si–C–N–O fibers, they are expected to have new features. Their diameter, tensile strength and Young's modulus are 20 μm , 1.85 and 186 GPa, respectively. If their green fibers are cured by γ -ray irradiation, oxygen-free Si–C–N fibers can be obtained with a tensile strength and Young's modulus of 2.4 and 214 GPa, respectively. After 1600 °C treatment, their tensile strength and Young's modulus are still as high at 2.1 and 220 GPa, respectively.

Because of the limited thermal stability of Si–C–N fibers, B was introduced and an amorphous Si–B–N–C fiber, SiBN_3C , is currently being developed by Bayer HG in Germany. This fiber has high room-temperature strength and stiffness and is reported to have remarkable strength retention and creep resistance at elevated temperatures.

China has also carried out a series of similar studies and obtained Si–C–N–O fibers from chlorosilane. Low oxygen content Si_3N_4 fibers were also obtained by electron beam irradiation, but their mechanical properties need to be improved. Recently, a kind of carbon-free Si–B–N fiber has been developed in China [36].

(4) Functional SiC Fibers

Based on their high strength, high modulus, low coefficient of thermal expansion and adjustable electrical resistivity, SiC fibers are not only good reinforcements for structural composites but are also good high-temperature radar-absorbing reinforcements for functional composites.

For use as good radar absorbents, their electrical resistance should be in the range of 10^1 – 10^3 $\Omega\cdot\text{cm}$. Pure SiC is a semiconducting material with an electrical resistance lies in the range of 10^4 – 10^6 $\Omega\cdot\text{cm}$. Therefore, measures are required to adjust their electrical resistance.

Table 2.29 Typical properties of the Si_3N_4 fibers

Manufacture	Fiber	Composition/%(wt)				Density/ $\text{g}\cdot\text{cm}^{-3}$	Diameter/ μm	Tensile strength/GPa	Young's modulus/GPa	Status
		Si	N	C	O					
TNK	Si_3N_4	59.8	37.1	0.4	2.7	2.39	10	2.5	300	D
Dow Corning	HPZ	59	28	10	3	2.32	8–15	1.75–1.85	140–175	C
Dow Corning	HPZ	60	27	9	3.4	2.48	10–12	2.06	165–220	C
Rhone-Poulenc	FDBE-Ramil	56	22	15	8	2.40	15	1.80	220	C
NUDT	Si-C-N-O						15	1.5–1.8	140–165	D

Note C—commercialized; D—development

Fortunately, precursor varieties, processing parameters and ultimate microstructures (cross section of the fibers) can all be used to achieve this target, and radar-absorbing fibers with the best absorption capacities in the range of 10–12 GHz can be obtained [39–42].

For example, the electrical resistance of Nicalon fibers of low-volume-resistivity (LVR) type, NL-500, is 0.5–5.0 Ω·cm. They have good radar-absorbing properties. Another type of Nicalon fiber is the high-volume-resistivity (HVR) type such as NL-400, which has an electrical resistance of 10⁶–10⁷ Ω·cm, and can be used as an excellent radar transmission fiber. They are all reinforcements with functional properties, as listed in Table 2.28.

① Non-circular SiC fibers

A reason to change the cross section of SiC fibers from circular to non-circular can be explained using carbon fibers, which are radar reflection fibers with an electric resistance of about 10⁻² Ω·cm. They can also absorb microwaves if the shape and size of the cross section are changed.

Systematic studies were carried out on non-circular fibers by changing the shapes of the spinnerets upon melt-spinning polycarbosilanes [38]. The results showed that at the same equivalent diameters, the tensile strength of the fibers with a trilobal cross section is about 30% higher than that with a circular cross section, and the rate of tensile strength reduction upon increasing the diameter is also lower.

The electromagnetic parameters of trilobal SiC fibers measured using a rectangular waveguide approach in the X-band are listed in Table 2.30. The electromagnetic parameters of the trilobal SiC fibers are similar to those of the circular fibers (NL202) at lower pyrolysis temperatures. However, when the pyrolysis temperature was increased to 1100 °C or 1250 °C, the imaginary part of the permittivity (ϵ'') of the trilobal SiC fibers is about 30–60 times that of circular fibers. A higher ϵ'' is beneficial because it implies a better ability to transfer microwave energy to heat. The reflection curve of a composite with two-orthogonal-layered trilobal SiC fibers is shown in Fig. 2.2 [38]. The size of the composite is 80 mm × 180 mm × 4 mm.

The reflection is lower than -10 dB in the range of 11.6–18.0 GHz or lower than -15 dB in the range of 13.9–18.0 GHz. The lowest reflection of -19.8 dB is achieved at 17.2 GHz.

Table 2.30 Electromagnetic parameters of trilobal SiC fibers ($f = 10$ GHz)

Pyrolysis temperature/°C	ϵ'	ϵ''	μ'	μ''
800	3.06	0.17	1.03	0.05
900	3.47	0.11	1.04	0.01
1000	4.02	1.78	0.94	0.09
1100	4.87	8.96	1.03	0.00
1250	5.04	4.69	0.87	0.04
Comparison: NL202	3–5	0–0.15	0.98–1.03	0–0.5

Fig. 2.2 Reflection curve of a trilobal SiC fiber composite

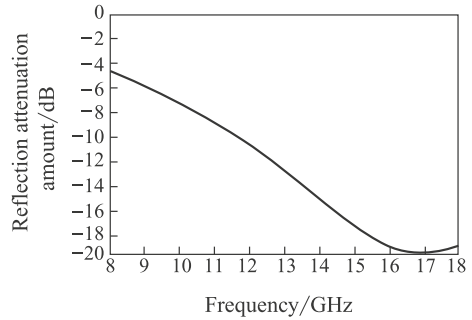
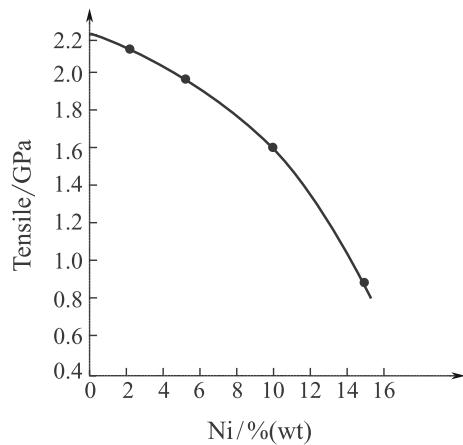


Fig. 2.3 Tensile strength of metal-containing SiC fibers as a function of Ni content



- ② **Metal particle-containing SiC fibers** A kind of metal particle-containing SiC fiber was produced by simply mixing metal particles with precursors followed by subsequent melt spinning, curing and pyrolysis [39–41]. Changing the metal content can change the electrical resistance and the electromagnetic parameters of the target SiC fibers. The metal particles studied were ultra-fine metal powders of Fe, Co, Ni and Ti with 30–50 nm diameters. The electrical resistance of the SiC fibers can be adjusted continuously over a wide range, as shown in Figs. 2.3 and 2.4 and Table 2.31. The electrical resistance decreases with increasing metal content, but the tensile strength decreases too.

When nano-ferrous powder was added to polycarbosilane, the electrical resistivity of the obtained SiC fibers decreased sharply. For example, 1–5% (wt) of the nano-ferrous powder effectively reduced the electrical resistance to 10^0 – 10^3 Ω -cm. The fibers still retained a relatively high tensile strength, as listed in Table 2.31. Figure 2.5 shows the reflection curve of an epoxy matrix composite reinforced with Fe-containing SiC fibers with a thickness of 6 mm.

Fig. 2.4 Electrical resistance of metal-containing SiC fibers

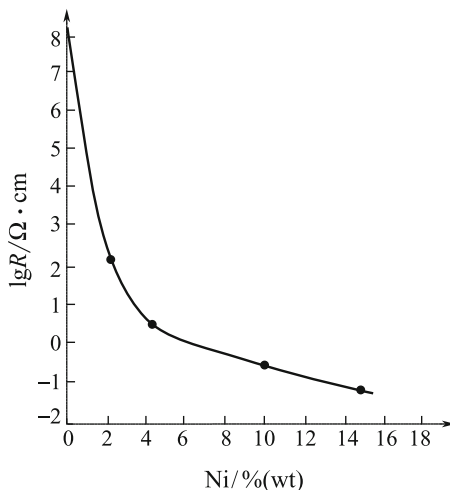
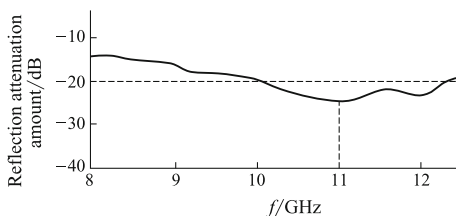


Table 2.31 Effect of addition of nano Fe, Co, Ni and Ti on the properties of SiC fibers

Amount of addition	Fe / %wt						Ni / %wt		
	0	1.0	2.0	3.0	5.0	10.0	2.0	5.0	10.0
Tensile strength/GPa	2.26	1.92	1.82	1.80	1.65	1.08	2.16	1.95	1.65
Electrical resistance/Ω·cm	7106	730	82.7	10.44	0.84	0.29	1.1		
Amount of addition	Co / %wt						Ti / %wt		
	1.0	2.0	3.0	5.0	10.0	10.0	20.0	30.0	50.0
Tensile strength/GPa	1.92	1.76	1.72	1.55	1.18	1.92	1.75	1.55	1.32
Electrical resistance/Ω·cm	5220	516.5	107.4	15.4	1.58	13500	2407	214.6	26.4

Fig. 2.5 Reflection curve of an Fe-containing SiC fiber composite



The reflections are all less than -14 dB in the range of 8–12.4 GHz with the lowest achieved being -25.1 dB. Additionally, the reflection bandwidth at less than -20 dB is about 2.2 GHz, indicating a much improved microwave-absorbing property with the addition of magnetic ferrous powder.

Other than Fe, Ti and Zr can also be introduced to the body of SiC fibers to lower their electrical resistance while retaining their high tensile strength. Ube

Table 2.32 Properties of the Tyranno fibers

Brand name	Diameter/ μm	Tensile strength/GPa	Young's modulus/GPa	Density/ (g/cm^3)	Electrical resistance/ $\Omega\cdot\text{cm}$	Coefficient of thermal expansion/ $(\times 10^{-6}/\text{K})$
Tyranno	8–10	3.0–3.3	180–200	2.3–2.4	$10^5\text{--}10^4$	3.1
A	8–7	3.0	170	2.29	10^6	3.1
D(s)	8–10	3.3	180	2.35	10^3	3.1
E	8–10	3.3	180	2.35	10^2	3.1
F	8–10	3.3	180	2.40	10^1	3.1
G	8–10	3.3	180	2.40	10^0	3.1
LoxM	8–10	3.3	187–180	2.48	30	3.1
LoxE	8–10	3.4	206	2.55	0.8	3.1
ZE ^a	8–10	3.5	233	2.55	0.3	–

^aZr-containing SiC fibers

Table 2.33 Effect of Ti content on the properties of SiC fibers

Samples	Ti content/ $\%(\text{wt})$	Electrical resistance/ $\Omega\cdot\text{m}$	Tensile strength/GPa
SiC	0	1.0×10^6	1.97
Si–Ti–C–O-1	1.35	1.96×10^5	1.83
Si–Ti–C–O-2	3.5	4.35×10^3	1.84
Si–Ti–C–O-3	4.0	2.98×10^3	1.79

Industries has developed and commercialized a series of Tyranno fibers for different applications, and their properties are listed in Table 2.32.

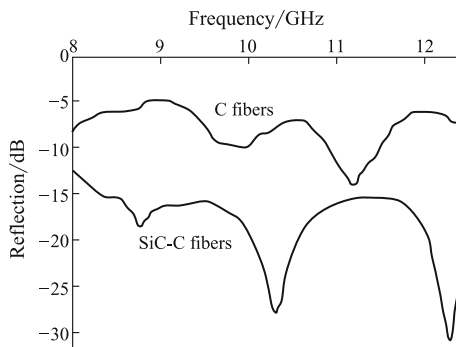
Titanium can be introduced by reacting polycarbosilane with titanium alkoxide, and the properties of the thus-obtained SiC fibers are listed in Table 2.33. It was found that the elemental composition and microstructure are closely related to the electrical resistance. With an increase in the titanium content, the resistance decreased and a relatively high strength was retained.

Carbon is conductive and can be introduced to the SiC fibers to change their electrical resistance. A kind of SiC–C fiber was prepared from a blended precursor consisting of polycarbosilane and pitch. Because of an easy phase detachment, the blended precursor is spun with difficulty into fine fibers. Therefore, even the electrical resistance is adjustable in the range of $10^0\text{--}10^4 \Omega\cdot\text{cm}$, and the tensile strength is relatively low at about 1.0–1.2 GPa. They cannot be used as reinforcements for structural radar-absorbing composites.

An improved method consists of the synthesis of carbon-rich polycarbosilane by the co-thermolysis of polysilane and polyvinylchloride (PVC). When PVC is pyrolyzed, plenty of double bonds are created, which can be grafted onto the main chain of Si–C bonds by a hydrosilation reaction. Therefore, carbon was dispersed into the precursor at the molecular level and the spinning property improved greatly. The properties of the SiC–C fibers are listed in Table 2.34.

Table 2.34 Properties of the SiC–C fibers

Sample	Composition/%(wt)			Tensile strength/GPa	Electrical resistance/ Ω -cm
	Si	C	O		
SiC	40	31.6	28.3	1.50	10^6
SiC–P5	46.2	40.8	12.9	1.71	35.2
SiC–P10	45.1	43.3	11.6	1.45	31.8
SiC–P30	42.9	42.1	11.8	0.87	25.8

Fig. 2.6 Reflection curve of a rayon-based SiC–C composite fiber and comparison of rayon-based carbon fibers

A substantial reduction in the electrical resistance is apparent. At a PVC content of 5 wt% the electrical resistance is low enough to meet application requirements. Additionally, the tensile strength is also slightly higher than for those without PVC addition.

A different method exists for SiC–C fiber production and comprises increasing the silicon content of the C fibers by the infiltration of carbon precursor fibers with polycarbosilane. For example, rayon filament or natural cellulose fiber was infiltrated with polycarbosilane solution, pre-oxidized and heat-treated at high temperature, and a kind of SiC–C composite fiber was obtained [22]. The carbon yield of the composite fiber was improved by up to 35–38%(wt) by the promotion of pyrolysis with flame retardants consisting of multi-amines and surfactants. Furthermore, the electrical resistance of the fibers can be adjusted by the concentration of polycarbosilane solution. The tensile strength of the fiber was as high as 1.8 GPa. Figure 2.6 shows the reflection curve of this composite fiber, indicating wideband microwave-absorbing properties.

2.3.3 Boron Nitride (BN) Fibers

As a variety of inorganic heat-resistant fiber, BN fibers are white, flexible polycrystalline fibers. According to the manufacturing method and their microstructure, they are usually divided into composite fibers and pure fibers [43, 44].

The former is prepared by CVD using borane, ammonia and boron trichloride as gas vapors, and a hot W wire as the deposition support and the core of the composite fiber. The latter usually comes from melt-spun B_2O_3 fibers after treatment with NH_3 to give unstable boron amine at low temperatures and heat resistance polycrystalline BN at 1800 °C.

BN fibers have superior thermal insulation and high-temperature stability, excellent electrical insulation and good dielectric properties; in addition, they have good resistance to radiation, infrared rays and chemical corrosion. When used as reinforcements for ceramic matrix composites, they can increase the toughness and thermal shock resistance. They have been used to fabricate microwave window components, separation rings in continuous casting technology and cell membranes in communication satellites.

For example, BN fiber-reinforced quartz has been used as a missile antenna window component and meets all the requirements of the space environment. BN fiber-reinforced Si_3N_4 can survive the erosion of carbon steel and stainless steel at 1600 °C, indicating that the composite can withstand the thermal shock generated by a tremendous temperature difference.

BN fibers can withstand long-term erosion by a 40 wt% KOH solution and as cell membranes of alkaline batteries and high-energy batteries, they are corrosion resistant, Ag_2O migration resistant and stable at high temperatures with the ability to retain the electrolyte. Therefore, BN fibers are a good cell membrane material.

Furthermore, BN fibers are ideal lubrication materials because of their good high-temperature lubrication property, which comes from their structure similarity with graphite. BN fibers can be used as protective clothing materials because they have the capacity to absorb neutrons with resistance toward ultraviolet and cosmic rays. Based on their excellent chemical stabilities, BN fibers can also be used in the form of paper and carpets as chemical filters and gas filters.

The USA was the first country to produce BN fibers. The former Soviet Union and Japan also carried out systematic studies into BN fibers. The properties of typical BN fibers are listed in Table 2.35.

In 1966, the Emery Co. in the USA was the first to produce BN fibers and they produced high-strength, high-modulus BN fibers in 1978. At the same time, various BN fiber products such as paper, felts and boards were developed. In 1976, research was carried out in China into reacting B_2O_3 with ammonia, and the relationship between microstructure and performance was systematically studied. In 1993, BN fibers with similar performance were obtained, as listed in Table 2.35.

Because of the complexity of the solid-gas reaction, the obtained BN fibers were hardly homogenous [43]. In the 1990s, research focused on the manufacture of BN fibers from polymer precursors to overcome the shortcomings of the nitridation process [44]. Currently, the tensile strength of polymer-derived BN fibers is up to 1.5 GPa.

Table 2.35 Properties of typical BN fibers

Property	USA			China short fiber
	Short fiber	Continuous fiber	High strength and high modulus	
Diameter/ μm	4–6	5.19	6	4–6
Tensile strength/MPa	350–870	302	830–1400	350–800
Young's modulus/GPa	28–84	35.7	210	18–120
Density/(g/cm^3)	1.4–1.9	1.8	1.8–1.9	1.4–1.8
Tensile strain/%	2–3	1	–	2–3

2.3.4 Boron Fibers

Boron fibers are important reinforcements for advanced composites. They are produced by CVD by depositing B on W or C fibers in the form of a continuous monofilament with an outer diameter of 100–200 μm .

The commonly used W wire has a diameter of 3.5–50 μm . At reaction temperatures of 1120–1200 $^{\circ}\text{C}$, more infiltration of B into W is found. Therefore, the composition of the core changes from W to a variety of tungsten diborides such as WB, W_2B_5 and WB_4 . As a result, only a small amount of boron is deposited into the core. However, when the temperature is increased to 1200–1300 $^{\circ}\text{C}$, the deposition rate of B increases and the target B fibers can be obtained.

During the course of deposition, the core has a pressing stress and the initial deposition layer has a drawing stress, and therefore, radial cracks form in the B fibers. To avoid the propagation of cracks and any unexpected interface reactions, a coating process is usually carried out in addition to the CVD process. Therefore, a coating of boron carbide (B_4C) is applied using a mixed gas consisting of BCl_3 , CH_4 and H_2 . The thickness of the coating is generally 3 μm . A commercialized B fiber with the trademark BoSiC is obtained when the coating is SiC.

The most promising advantages of boron fibers are their mechanical properties (tensile strength and Young's modulus are 3.5 and 400 GPa, respectively) and low density ($2.5 \text{ g}/\text{cm}^3$). The processing maturity and reasonable price are essential reasons for their development. In addition, B fibers have good bending strength, and their corresponding compressive strength is very high at 6.9 GPa, which is twice their tensile strength. Boron fibers can survive at 500 $^{\circ}\text{C}$ in air for 1 h with no obvious change in tensile strength. However, at temperatures exceeding 500 $^{\circ}\text{C}$, their tensile strength decreases significantly.

Boron fibers are mainly used in the aviation and aerospace industries with special applications in MMC and PMC composites that have specific demands regarding weight and stiffness. Boron fiber-reinforced aluminum composites are one successful example. Boron fiber-reinforced epoxy composites have also been used to repair airplane metal bodies and to fabricate sports and entertainment items such as golf clubs and skis.

Table 2.36 Properties of typical boron fibers

Property	B						BorSiC			
	B/W			B/C			BorSiC/W		BorSiC/C	
Diameter/ μm	102	142	203	102	142	203	107	147	107	147
Density/ (g/cm^3)	2.31	2.31	2.30	2.29	2.29	2.29	2.32	2.32	2.31	2.31
Tensile strength/GPa	3.24– 3.51	3.24– 3.51	3.30– 3.50	3.10	3.10	3.17	3.24	3.24	3.17	3.17
Young's modulus/GPa	378– 400	378– 400	378– 400	345– 358	345– 358	345– 365	378– 400	378– 400	351– 365	351– 365

The USA was the earliest and most important country regarding the research and development of boron fibers. In the mid-1960s, AVCO produced W core and C core boron fibers using hydrogen and boron trichloride. The diameters of the continuous fibers were 100–200 μm . Textron Inc. then produced a high-strength, high-modulus and low-density boron fiber. In July 1985, the Japanese vacuum metallurgy company developed the world's highest tensile strength boron fiber at 5.2 GPa and established a pilot plant.

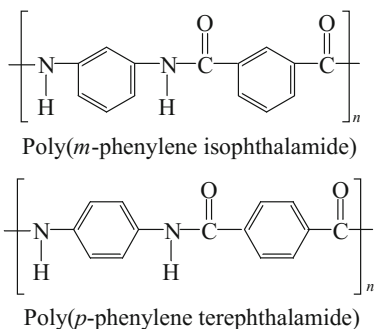
The former Soviet Union and France also carried out research and made extensive progress. China began these studies in the early 1970s, and five pilot lines have been completed. The performances of the fibers are close to those of other countries. The properties of typical boron fibers are listed in Table 2.36. Their performance is closely related to their diameters.

2.4 Aromatic Polyamide Fibers

Aromatic polyamide fibers are also referred to as aramid fibers. Aramid fibers are a class of heat-resistant and strong synthetic polymer fibers in which the fiber-forming substance is a long-chain synthetic polyamide with at least 85% amide linkages ($-\text{CO}-\text{NH}-$) attached directly to two aromatic rings. Aramids are generally prepared by the reaction between an amine group and a carboxylic acid halide group.

Polyamides in dimethyl acetamide solution can be directly spun into fibers using dry-spinning, wet-spinning or dry-wet spinning methods. After washing and drying, the fibers are heat-treated at 500–600 $^{\circ}\text{C}$ under tension to obtain the target aramid fibers [45, 56].

Aromatic polyamides were first used commercially as meta-aramid fibers in the early 1960s, and para-aramid fibers were subsequently developed in the 1960s and 1970s. Their structures are as follows:



Apart from production in the USA by DuPont, meta-aramid was also produced in the Netherlands and in Japan by Teijin under the trade name TeijinConex and in China by Yantai under the trade name New Star, and a variant of meta-aramid was produced in France by Kermel under the trade name Kermel. The most representative para-aramid fibers are *p*-phenylene terephthalamide (PPTA) fibers and their trade names are Kevlar (DuPont), Twaron (previously Akzo and currently owned by Teijin) and Technora (Teijin). After the industrialization of PPTA fibers by DuPont in the 1970s, a series of products with improved performance and higher production efficiency were made.

PPTA aramid fibers are classified as two types: one is a high-strength type with a tensile strength of up to 3.0–5.5 GPa and a Young's modulus of 60–90 GPa. This is mainly used in high-strength, middle-hardness textile materials and in flexible composite materials such as tires and industrial rubber products; the other is a high-modulus type with a Young's modulus of up to 100–170 GPa, and it is mainly used in high-strength, high-hardness textile materials and in hard composite materials [47, 48]. The world's major producers of PPTA fibers are listed in Table 2.37.

PPTA is characterized by its ultra-fine molecular structure, its high degree of orientation and the regular arrangement of long chains so that each molecule can contribute when tensile loaded. This is the reason for their excellent mechanical properties. Table 2.38 shows the main structures of the PPTA from different producers. Their statistical chain length is about 20–50 nm, bearing a large number of polar groups. The fibers have high intra-chain atomic combination energy and high inter-chain interface energy as well as many polar groups and many rigid blocks in

Table 2.37 Major producers and brand names of PPTA fibers

Manufacture	Brand name	Type
DuPont, USA	Kevlar	High strength, high modulus
Teijin, Japan	Twaron	High strength, high modulus
Institute of Synthetic fibers, Russia	Terlon	High strength, high modulus
Institute of Synthetic fibers, Russia	SVM	High modulus
Institute of Synthetic fibers, Russia	Armos	High modulus
Teijin, Japan	Technora	High strength

Table 2.38 Structural characteristics of PPTA fibers

Brand name	Molecular level	Super-molecular level	Microscopic level
Kevlar Twaron Terlon	PPTA; statistical chain length is 30–50 nm; polar group is CONH	Three-dimensional crystal structure, highly oriented, chain ratio with load is 0.5–0.7	Cross section: homogeneous, circular-shaped
SVM	Heterocyclic aromatic polyamide; statistical chain length is 20–40 nm; polar groups are CONH and –N–	One-dimensional crystal structure, highly oriented, chain ratio with load is 0.5–0.7	Cross section: homogeneous, circular-shaped
Armos	Heterocyclic aromatic polyamide copolymer; statistical chain length is 20–40 nm; Polar groups are CONH and –N–	Three-dimensional crystal structure, highly oriented, chain ratio with load is 0.5–0.7	Cross section: homogeneous, circular-shaped

Table 2.39 Representative mechanical properties of PPTA fibers

Brand name	Density/g·cm ⁻³	Tensile strength/GPa	Young's modulus/GPa	Tensile strain/%	Standard moisture regain/%
High-modulus type: Kevlar, Twaron, Terlon	1.44	3.0–3.5	120–170	2.5–3.0	2.0–3.0
High-strength type: Kevlar, Twaron, Terlon, Technora	1.44	3.0–3.5	60–90	3.0–4.5	3.0–3.0
High-modulus type: SVM	1.43	4.2–4.5	125–150	3.0–3.5	3.5–4.0
High-modulus type: Armos	1.43	4.5–5.5	130–160	3.5–4.0	3.0–3.5

the molecular chains. This gives the fiber a high glass transition temperature and high thermal stability. In addition, the high homogeneity of the structure and the low amount of structural defects are also one of the reasons for their good mechanical properties.

Tables 2.39 and 2.40 show the mechanical properties of world's most important PPTA fibers. Armos yarn has been regarded as one of the best types.

The first generation of Kevlar series products produced by DuPont are Kevlar RI, Kevlar29 and Kevlar49, and the second generation are Kevlar HX, which includes the high-adhesive type (Ha), high-strength type (Ht, 129), solution-colored type (Hc, 100), middle-modulus type (Hp68), high-modulus type (Hm, 149) and high-tensile-strain type (He, 119). Their typical physical properties are listed in Table 2.41.

Table 2.40 Thermal properties of PPTA fibers

Brand name	Glass transition temperature/ $^{\circ}\text{C}$	Processing extreme temperature/ $^{\circ}\text{C}$	Pyrolysis temperature/ $^{\circ}\text{C}$	Combustion temperature/ $^{\circ}\text{C}$	Spontaneous combustion temperature/ $^{\circ}\text{C}$	Limiting oxygen index ($\text{CO} \pm 7\%$)
Terlon, Kevlar, Twaron	345–360	250–270	450–550	450–500	500–600	27–30
SVM, Armos	270–280	300–330	550–600	500–600	550–650	37–43

Table 2.41 Typical physical properties Kevlar fibers

Property	Kevlar RI Kevlar29	Kevlar Ht (129)	Kevlar He (119)	Kevlar Hp (68)	Kevlar 49	Kevlar Hm (149)
Toughness/cN·Tex ⁻¹	205	235	205	205	205	170
Tensile strength/GPa	2.90	3.32	2.90	2.90	2.90	2.40
Young's modulus/GPa	60	75	45	90	120	160
Tensile strain/%	3.6	3.6	4.5	3.1	1.9	1.5
Moisture regain/%	7	7	7	4.2	3.5	1.2
Density/(g/cm ³)	1.44	1.44	1.44	1.44	1.45	1.47
Pyrolysis temperature/°C	≈500	≈500	≈500	≈500	≈500	≈500

Research into aramid fibers started in China in the early 1970s and the performance of the products are close to that of Kevlar49, with a production capacity of 200 t/a. There are two types of aramid fibers in China, Aramid I and Aramid II. Aramid II consists of four types.

Their performances are listed in Table 2.42. Although the tensile strength of Aramid II is higher than that of Aramid I, its Young's modulus is lower. Aramid I maintains its strength better at high temperatures, i.e., a better aging property, and therefore, it is a better candidate for high-temperature composites.

In addition to the p-aramid fibers, aramid copolymer fibers also exist. The introduction of a new diamine or a third monomer during the synthesis of a new aramid is an important approach to improving performance. Examples include Technora, SVM and Armos. Typical properties of Russian aramid fibers are listed in Table 2.43.

In addition to the above-mentioned continuous aramid yarns, other forms like staple fibers, short fibers, pulps, fabrics and laminates also exist. For example, KevlarT970, Twaron1070, Twaron1072, Twaron1075 and Twaron1077 are short fibers, while KevlarT979, KevlarT982, KevlarT953 and Twaron 1095 are pulps.

Aramid fibers are a kind of light, high strength, widely used high-performance organic fiber [45, 46]. They are mainly used to reinforce polymer matrix composites, rubbers, cements and metals, resulting in significant improvements in toughening aspects, and therefore, they are mainly used in the fields of space, aviation, petroleum, building materials, traffic, transportation and public security departments. They are especially used in the shells of solid rocket motors, bullet-proof vests, tires, cables and in asbestos substitutes.

Because of their superior specific strength and specific modulus compared with S-994 high-strength glass fibers, the characteristic factor, PV/W (P , blast pressure, V , vessel volume and W , vessel weight), of a Kevlar-reinforced epoxy engine shell was increased up to 30%. Kevlar-reinforced epoxy composites have also been widely used in the manufacture of advanced aircraft in the form of engine shells, central engine cowlings, wings and fuselage cowlings. In addition, aramid fibers are

Table 2.42 Typical properties of the aramid fibers produced in China

Property	Aramid I		Aramid II ^a					
	Green fiber	Heat-treated fiber	Green fiber	Heat-treated fiber	II-1	II-2	II-3	II-4
Density/g·cm ⁻³	1.42	1.46	1.44	1.45	—	—	—	—
Tensile strength/cN·dtex ⁻¹	8.8–10.1	16.0–17.7	19.5–21.2	19.5–21.2	17.7–19.4	≥ 15.9	17.7–19.4	19.4–21.1
Young's modulus/cN·dtex ⁻¹	340–400	903–1062	354–400	624–703	423	—	618–706	618–706
Tensile strain/%	5.5–6.5	1.5–2.0	3.5–5.5	2.5–3.5	3.5–3.6	≥ 6	2.5–3.5	2.5–3.5

^a Aramid II has four types: II-1, common; II-2, high tensile strain; II-3, middle-strength, high modulus; II-4, high strength, high modulus

Table 2.43 Typical properties of Russian aramid fibers

Brand name	Filament count	Young's modulus/GPa	Tensile strength/GPa	Tensile strain/%	Density/g·cm ⁻³	Mass per unit/g·km ⁻¹	Glass transition temperature/°C	Coefficient of thermal conductivity/W·(m·K) ⁻¹	Moisture regain/%
Terlon	40k	98-147	2.94-3.5	2-4	1.45	6	345-400	0.04-0.65	2.0-3.5
SVM	70k	122-132	3.72-4.12	3.5-4.5	1.42	14.3	230-250	0.045	4-7
Armos	50k	142-147	4.5-5.2	3-3.5	1.45	14.3	160-520	-	3.5-5.0

also widely used in aircraft high-pressure oil pipes. Therefore, they are very important in aviation materials.

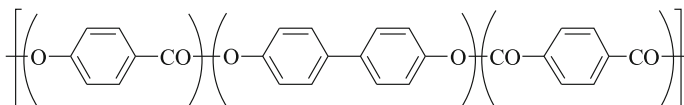
They are also applied as armored protection for warships and aircraft carriers, as well as sonar diversion covers. Aramid fibers can also be used to manufacture soft bulletproof vests, train brakes and sealing fillers.

The application of Kevlar in reinforcing cement to substitute steel bars or to reduce application of steel bars is known to be more suitable in extreme ocean conditions. When used as wall materials, their tensile strength is 5–10 times that of ordinary cement.

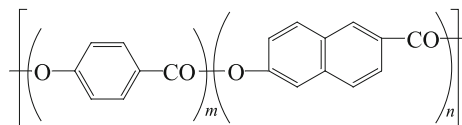
2.5 Aromatic Polyester Fibers

Aromatic polyester fibers are also referred to as polyarylate (PAR) fibers and are actually a kind of aromatic polyester copolymer fiber derived from aromatic dicarboxylic acids and diphenols. The spinnability of aromatic polyesters from one type of monomer is not good enough to obtain high-performance fibers. The copolymerizing component should be of relative low cost, low melting point and be a good spinning copolymer, which is able to maintain high strength and high modulus.

The trade names of current aromatic polyester products are Ekonol and Vectron. They were both spun from all-aromatic polyester copolymers. Ekonol fibers were commercialized jointly by the Carborundum and Sumitomo companies, and their chemical structure is as follows:



They have high strength and high modulus but also a high manufacturing cost, which restricts their further development. Vectron fibers were prepared by Kuraray exclusively in 1990, and its structure is as follows:



With the same level of strength and modulus as PPTA fibers, the most outstanding feature of aromatic polyester fibers is that their retained strength after dry-heat or wet-heat treatment is superior to that of PPTA fibers. This is because they are not hygroscopic and do not shrink after creeping or aging under dry or wet conditions. Additionally, their resistance to wear, cutting, solvents, acid and impact,

Table 2.44 Performance comparison between aromatic polyesters and PPTA monofilaments

Brand name	Density/g·cm ⁻³	Pyrolysis temperature/°C	Moisture regain/%	COI/%	Tensile strength/GPa	Tensile strain/%	Young's modulus/GPa
Vectron HT	1.41	>400	0	37	3.61	3.8	833
Vectron HM	1.42	>400	0	—	—	3.5	—
PPTA common	1.44	>400	4.9	42	3.72	3.6	788
PPTA HM	1.45	>400	44.3	39	3.20	3.0	1228
Ekonol	1.40	—	—	—	3.83	2.6	968

Table 2.45 Performance comparison between Vectron and PPTA yarns

Brand name	Denier/ (dtex/filament count)	Tensile strength/GPa	Tensile strain/%	Young's modulus/GPa	Sintering strength/N·dtex ⁻¹
Vectron HT	1667/300	3.23	3.8	746	6.0
Vectron HM	1667/300	2.90	3.5	1043	–
PPTA Common	1667/300	2.67	3.9	709	6.2
PPTA HM	1578/1000	2.69	2.7	1121	5.7

Table 2.46 Types and applications of Vectron fibers

Type	Code	Structure	Application
Filament Yarn HT	T-101	8333/1667/1111/556/278-28 (dtex)	General industrial supplies
Filament Yarn HM	T-117	1667(dtex)	Ropes, cords, tension components
Filament Yarn HM	T-150	1667/556/278-28(dtex)	Harnesses, fishing lines, sutures
Filament Yarn NT	T-155	1111(dtex)	Tension components
Original spun yarn	AP	10/20(S)	Protective clothing, gloves, aprons
Core–sheath yarn	CY	3.7/7.4(S)	Fishing lines
Short fiber	CF	1/3/6(mm)	Advanced composite materials
Puple	HP	1–3(mm)	Asbestos substitutes
Puple	NP	1–3(mm)	Synthetic paper, speaker cones
Fabric	–	–	Advanced composite materials, general industrial supplies
Laminate	–	UD fabric	Advanced composite materials

as well as vibration absorption, is also better than that of PPTA fibers. Their spontaneous combustion stability, non-melting ability upon combustion and weather resistance are similar to those of PPTA fibers. Performance comparisons of aromatic polyester and PPTA fibers, in monofilaments and yarns, are listed in Tables 2.44 and 2.45, respectively.

Aromatic polyester fibers hardly absorb water and have good dimensional stability, but their interface bonding and fatigue resistance are relatively poor when used to reinforce rubbers and polymers. Aromatic polyester fibers are used in speaker cones, tennis rackets, table tennis bats, safety helmets and pipes, as these items take advantage of their high modulus, high shock absorbance and vibration attenuation properties.

Table 2.46 shows the types and applications of Vectron fibers. To date, no related fiber development has taken place in China. These fibers should be developed further because they are high-performance reinforcements for composite materials, and generally their performance is better than that of PPTA fibers. More importantly, their cost is also lower.

2.6 Heterocyclic Polymer Fibers

Although aramid fibers have been used as aerospace structural materials, bullet-proof materials, automotive structural materials, tire cords, etc., they have a clear weakness in that they possess poor environmental stability, which limits their application. This comes from the amide bonds in the main chain of the molecule, which tends toward oxidation and hydrolysis.

Modern theory and practice show that, surprisingly, rod-like heterocyclic polymer fibers spun from a liquid crystal phase solution have superior mechanical properties compared with aromatic polyamide fibers, and also have much improved thermal stability, which is close to the theoretical limit of organic polymer crystals [48, 49].

As representatives of the heterocyclic polymer fiber family, poly(*p*-phenylene benzobisoxazole) (PBO), poly(*p*-phenylene benzobisthiazole) (PBT) and poly(*p*-phenylene benzimidazole) (PBI) are considered to be a new generation of polymer fiber, which have high strength, high modulus and high-temperature stability. Their main chains contain rigid-rod-like units of benzene and heterocyclic structures like oxazole, thiazole and imidazole [49]. A new PBO-like heterocyclic polymer fiber, polypyridobisimidazole (PIPD or M5), is believed to have more promising applications than general PBO fibers. These fiber products will be fully commercialized in the twenty-first century, and more applications will be targeted. Table 2.47 shows some typical characteristics of heterocyclic polymer fibers.

2.6.1 Polybenzoxazole (PBO) Fibers

PBO is poly(*p*-phenylene-2,6-benzobisoxazole), and its *cis* and *trans* structures are shown below:

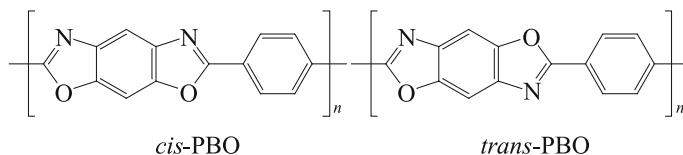


Table 2.47 Typical characteristics of heterocyclic polymer fibers

Type	Molecular cross-sectional area/($\times 10^{-2}$ nm ²)	Theoretical Young's modulus/GPa	Measured Young's modulus/GPa
<i>cis</i> -PBO	19.17	730	350
<i>trans</i> -PBO	19.21	707	–
<i>cis</i> -PBT	20.68	580	–
<i>trans</i> -PBT	20.60	605	300
<i>cis</i> -PBI	20.89	630	–
<i>trans</i> -PBI	20.90	640	–
PPTA	20.20	182	125
UHMPE	18.20	362	160

There is a high degree of orientation of molecular chains because they are spun in the liquid crystal state, which gives them a high tensile strength of 4.8–6.2 GPa and a high Young's modulus of 280–380 GPa. Their moisture uptake is less than 1%, and their decomposition temperature is as high as 670 °C. They do not melt. In addition, they are abrasion resistant and have a low creep rate.

The fibers are very thin and feel good and can be prepared in various forms such as yarns, worsted yarns, cloths, fabrics, chopped fibers and pulps. Similar to other rigid polymers, the fibers are also processed from anisotropic solutions. The solvent is polyphosphoric acid. Because of their much higher rigidity than aramids as well as the lack of amide bonds, their thermal properties and mechanical properties are much improved. However, because of expensive ingredients and the highly aggressive solvent combined with extremely high solution viscosities of 30 dl/g, they cost much more than aramid fibers. Typical properties of PBO fibers compared with other fibers are listed in Table 2.48.

The series of PBO fibers include the PBO-AS fibers by Dow Chemical Company, Zylon and the PBO-HM fibers by Toyobo, and others by DuPont. Their most striking characteristics are their high strength and high modulus, which is nearly two times that of PPTA fibers. Their LOI is also much higher.

The applications of PBO fibers are mainly in the following areas [50]:

- ① High-strength ropes, as well as high-performance canvases;
- ② High-strength composite materials. PBO fibers are a new generation of high-performance fibers because they meet the requirements of light weight, high strength, high modulus and high humidity resistance. They are prospective materials for use in pressure vessel structural materials and advanced sports goods;
- ③ Bulletproof anti-shock materials. PBO fiber composites have excellent performance in terms of impact resistance, as shown in Figs. 2.7 and 2.8. Therefore, they have been used in impact energy absorption devices such as aircraft fuselages, bulletproof vests and helmets;

Table 2.48 Property comparison between PBO fibers and other fibers

Property	PBO	PBO-AS	PBO-HM	M5	PBT	PBI	Kevlar49	Kevlar129
Density/(g/cm ³)	1.57	1.54	1.56	1.70	1.57	1.40	1.47	1.45
Young's modulus/GPa	406	180	280	330	373	5–6	143	99
Tensile strength/GPa	3.4	5.8	5.8	–	3.5	0.40	2.3	2.4
Tensile strain/%	–	3.5	2.5	1.2	1.3	30	1.5	3.3
LOI	–	68	68	75	–	41	26	26
Decomposition temperature/°C	650	650	650	–	600	550	555	555
Highest usage temperature/°C	350	350	350	–	350	–	250	250

Fig. 2.7 Mechanical properties of PBO/epoxy composites

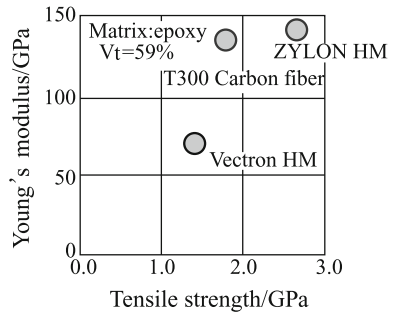
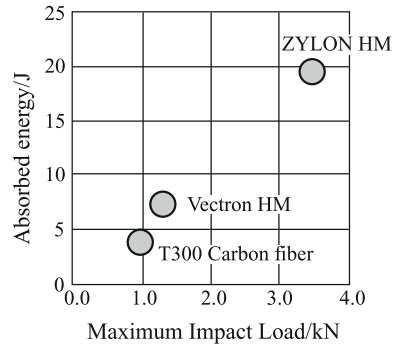
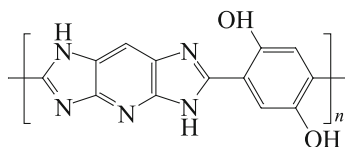


Fig. 2.8 Impact property of PBO/epoxy composites



- ④ Other special protective materials. Because of their superior heat resistance, flame-retardant properties, cut resistance, wear resistance, etc., they can be used to create light, soft products such as optical cable protection materials, safety gloves, thermal blankets, special conveyors, fireproof clothes and footwear.

PBO fibers have excellent performance, but they also have some shortcomings such as poor compressive performance, which is mainly caused by the tangling of the microfiber structures under compressive stress. This leads to fibrillation. Improvements are focused on eliminating the severe temperature changes in the preparation process and to use different monomers for copolymerization. The most successfully strategy so far is to create polymers that are rigid-rod-like as in PBO, but with strong intermolecular hydrogen bonds. This has been done for the recently developed PIPD or M5 fibers with a structure as follows:



Polypyridobisimidazole(PIPID)

PIPID is a polypyridobisimidazole made from 2,3,5,6-tetraamino pyridine and 2,6-dihydroxy-terephthalic acid. It was developed by Akzo-Nobel upon correcting the above-mentioned problem by maintaining the rigid-rod structure while adding extra hydrogen bonding sites. The restructuring of Akzo-Nobel led to this project being abandoned, and Magellan Systems International was formed to commercialize this product using A-N equipment. Composites made from this fiber show much improved impact resistance, damage tolerance and wear resistance.

Another reason for the poor performance of PBO fibers, and polymer matrixes are generally lower than that of aramid, which limits their application in high-performance composite materials.

Therefore, surface treatment is usually applied to improve the interface bonding strength, mainly including plasma treatment, the formation of microfibers on surfaces, chemical grafting and blending. One method reported in China is to modify the surface structures by applying both reactive monomers and high-energy radiation technologies. It is a promising surface modification method because it can deal with large-scale fibers resulting in good improvements.

Modified PBO fibers still have high rigidity and high strength, excellent resistance to oxidation, ultraviolet and moisture. They are particularly suitable for high-performance composite materials such as the insulation components of rockets and engines. They can also be used to reinforce cement. Because of their low creep rate and good abrasion resistance, they can be used to reinforce rubbers and heat-resistant equipment. Composite materials reinforced by modified PBO fibers are especially suitable for aircraft, transport machinery, electrical machinery, etc.

In short, modified PBO fibers are superior to polyester, nylon and high-strength polyolefin fibers in terms of heat resistance and mechanical properties. They are a new type of advanced synthetic fiber. It is thought that PBO fibers have started a revolution in new organic fibers. An increasing number of researchers in China are involved in the development of PBO fibers, but no pilot production has been

Table 2.49 Property comparison between Zylon fabrics and aramid fabrics

Name	Type	Yarn count, Warp/s	Yarn count, Weft/s	Yarn count, Warp/cm	Yarn count, Weft/cm	Thickness/mm	Density/(g/m ³)
Zylon	Plain weave	20	20	33.9	19.7	0.35	170.1
Meta-aramid	Plain weave	20	20	34.3	19.3	0.39	171.4
Para-aramid	Plain weave	20	20	34.3	20.1	0.40	176.7

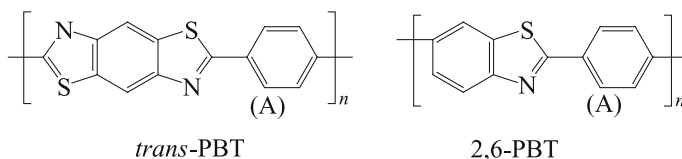
Table 2.50 Mechanical properties of Zylon fabrics and aramid fabrics

Name	Tear strength/kN		Tensile strength/(N/cm ²)		Tensile strain/%		Rupture strength/MPa	Abrasion resistance/cycles
	Warp	Weft	Warp	Weft	Warp	Weft		
Zylon	≥ 125.4	≥ 125.4	2.283	1.497	17.0	6.6	≥ 4.1	441
Meta-aramid	83.3	83.3	1.412	0.998	17.7	5.3	2.4	236
Para-aramid	68.6	39.2	0.807	0.481	46	29.8	2.1	193

reported to date. A property comparison between Zylon fabrics and aramid fabrics is listed in Tables 2.49 and 2.50.

2.6.2 Polybenzothiazoles (PBT) Fibers

Polybenzothiazole (PBT) is a high-temperature, high-modulus heterocyclic polymer whose main chain contains benzothiazole repeat units. It is obtained by reacting mixed toluides, sulfur and 4-aminophthalimide. PBT has two types of structures: *trans*-PBT and 2,6-PBT, as shown below:



For these structures, “A” stands for aromatic or aliphatic hydrocarbons. In the former case, PBT is not soluble in common organic solvents but only soluble in polyphosphate acid, mesylate acid, chlorosulfonic acid and concentrated sulfuric acid; in the latter case, PBT can be soluble in *m*-cresol and methanoic acid. PBT is a

Table 2.51 Typical properties of PBT fibers compared with other fibers

Type	Young's modulus/GPa	Tensile strength/GPa	Tensile strain/%	Density/(g/cm ³)
PET	5–12	1	10–16	1.38
Nylon	5	1	18	1.14
Glass	55	3.5	4	2.55
Steel	180–200	2–3	2–3	7.9
Kevlar29	60	3.7	3–4	1.44
Kevlar49	120	4.1	2.5	1.44
PBT	250	2.4	1.5	1.50

kind of incombustible lyotropic liquid crystal polymer with a density of 1.42–1.60 g/cm³.

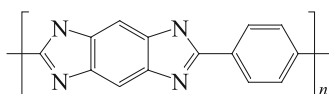
Air Force Wright Aeronautical Laboratories, referred as AFWAL, carried out an industrialization assessment of PBT fibers. The synthesis process starts from *p*-phenylenediamine (PPD), and an intermediate product of 2,5-diamino-1,4-benzenedithiol salt (DABDT) is obtained after four steps. DABDT needs to be refined by recrystallization and then polycondensation with terephthalic acid (TA) in a solution of polyphosphate acid. After PBT synthesis, its fiber can also be obtained after dry-wet spinning and heat treatment. Typical properties of PBT fibers are listed in Table 2.51.

In addition to the necessary heterocyclic aromatic chemical structures, another reason for the high performance of PBT fibers is their degree of orientation along the axial direction of molecular chains. This orientation is the result of spinning in the lyotropic liquid crystal state, which enables the obtained fiber structure to be close to the ideal structure of the fibers.

PBT fibers are a new type of high-performance composite reinforcement and can be used to substitute asbestos and cables. Their fabrics can be used to prepare bulletproof suits, space rocket engines, solar arrays, pressure valves and space frame structures. They are, therefore, prospective aerospace materials. However, their complicated synthesis procedure and the high cost of the solvent limit their development and application, especially in China.

2.6.3 Polybenzimidazole (PBI) Fibers

Polybenzimidazole fibers are stable at high temperature and comprise a variety of flame-retardant synthetic fibers. They are known as PBI with the trade name Togyon. Their main chain contains heterocyclic units, as shown below:



The polymer is usually synthesized by solid-phase polymerization in vacuum or by a two-step polycondensation method. The PBI fibers are gold in color. Two types of these fibers are available, yarns and staple fibers, and their deniers are 11–200 tex and 0.12–0.44 tex, tensile strength is 300–500 and 250–400 MPa, tensile strain is 15–20% and 20–30%, respectively. Additionally, their Young's modulus, density, boiling water shrinkage, LOI and moisture uptake are, respectively, 18 GPa, 1.43 g/cm³, 46.2 and 13–14%. These fibers are neither combustible nor melt in a flame, and they do not give off-gases even at 560 °C. They have good chemical resistance and a good fire-retardant property. They remain soft and retain their insulation property even after carbonation.

They are mainly used as suits or uniforms for fire services, steel-making, welding, aerospace and military applications as well as protective gloves, aprons, flame-retardant decorations, high-temperature tracks, fire-retardant composite reinforcements, high-performance threads, asbestos substitutes and deceleration cables.

In addition, these fibers have been used as moon-landing suits and expansion structures for spacecraft reentry into earth. As hollow forms, these fibers are pressure resistant, semi-permeable and heat resistant and can thus be used as a reverse osmosis desalination film for boiling water.

2.7 Ultra-High Molecular Weight Polyethylene (UHMWPE) Fibers

Ultra-high molecular weight polyethylene (UHMWPE) fibers are gel-spun from UHMWPE and have a molecular weight of more than 10⁶ D, and this is followed by a stretching technique [51]. Gel spinning includes both melt spinning and dry spinning, which forces the entangled molecules of the gel polymers to fully unwrap and thus affords fibers with high strength and high modulus.

UHMWPE fibers have been developed since the 1980s and were commercialized quickly because of the low cost of the raw materials as well as their prospective application in the development of high-strength, high-modulus light composites. Their strength and modulus are around 4 and 120 GPa, respectively. However, their density is less than 1.0 g/cm³.

Table 2.52 shows trade names and production companies of commercial UHMWPE fibers, and their properties are compared in Table 2.53.

The densities of the commercialized UHMWPE fibers are all less than 0.97 g/cm³, which is two-thirds those of aramid fibers and half that of high-modulus carbon fibers, as shown in these tables. Their densities are the lowest among all the developed high-performance fibers. For example, the specific tensile strength of Spectra1000 is higher than that of all other high-performance fibers as it is nearly 135% that of Kevlar fibers and 150% that of carbon fibers; in addition, their specific Young's modulus is 2.5 times that of Kevlar fibers.

Table 2.52 Manufacturers and trade names of commercial UHMWPE fibers

Manufacturer	Brand name	Type/ (dtex/f)	Tensile strength/ (cN/dtex)	Young's modulus/ (cN/dtex)	Tensile strain/%
Togobo	DyneemaSK60	36–154	26.5	882.3–1650	3.0–6.0
DSM	DyneemaSK76	1760	37.0	1200.0	3.8
Allied	Spectra900	1333/98	26.5	1235.2	–
	Spectra1000	722/120	30.9	1764.6	–
Mitoui	Tekmilon I	111/200	29.1	997.0	3.0
	Tekmilon II	555/60	25.0	897.3	–

Table 2.53 Properties of UHMWPE fibers compared with other selected fibers

Property	Spectra900	Spectra1000	Kevlar LM	Kevlar HM	HS carbon fiber	HM carbon fiber	S-glass fiber
Diameter/ μm	38	27	12	12	7	7	7
Density/(g/cm^3)	0.97	0.97	1.44	1.44	1.81	1.81	2.50
Tensile strength/GPa	2.50	3.0	2.8	2.8	3.0–4.5	2.4	4.6
Young's modulus/GPa	117	172	62	124	228	379	90
Tensile strain/%	3.5	2.7	3.6	2.8	1.2	0.8	5.4
Specific tensile strength/ ($\times 10^8$ cm)	2.67	3.09	1.94	1.94	1.76	1.32	1.84
Specific Young's modulus/ ($\times 10^8$ cm)	120.6	117.8	43.05	36.11	125.9	209.3	36.0

UHMWPE fibers were invented by DSM, patented in 1979 and were piloted in 1990. The fibers have the trade name Dyneema. Subsequently, Mitsui Oil Company built its own pilot line of 300 t/a in 1999 and started to produce Tekmilon fibers. The Allied company bought the patent from DSM and built an improved pilot line producing Spectra900 and Spectra1000 fibers. DSM also undertook a joint enterprise with Toyobo and produced DyneemaSK-60 fibers. China also built a production line in 2000 and produced high-modulus fibers with the trade name Qianglun. Additionally, a new pilot line of 100 t/a was also built to produce high-strength fibers with a tensile strength of 36.83 cN/dtex, a Young's modulus of 1309.6 cN/dtex and a tensile strain of 3.7%.

UHMWPE fibers have excellent mechanical properties and dielectric properties, as listed in Table 2.54. Their dielectric constant and dielectric loss are very low, and therefore, the electromagnetic wave transmission of their composites of close to 100% is higher than that of glass fiber composites. They are the best reinforcement

Table 2.54 Dielectric properties of high-performance fibers

Type	Dielectric constant (ϵ)	Dielectric loss tangent/ $\times 10^{-4}$
UHMWPE	2.3	4
Kevlar	2.8	–
<i>E</i> -glass	6.0	60
PA66	3.0	23
PET	3.0	90

Table 2.55 Impact properties of selected composites

Property	Spectra900	<i>E</i> -glass	Kevlar	Graphite
Total absorption energy/J	45.2584	46.7758	21.8287	21.6981
Specific absorption energy/J	16.4	8.9	6.3	5.4

candidates for the preparation of radar radomes and for fiber optic cable cores. Among all the high-performance fibers, UHMWPE has the highest impact strength, as listed in Table 2.55.

The specific absorption energy of the UHMWPE fiber composite is twice that of the *E*-glass fiber composite and three times those of Kevlar and carbon fiber composites [45–47, 51]. Therefore, they are important fibers for bulletproof vests, cut-resistant clothing, police shields and bulletproof helmets, bulletproof vehicles, tanks and other armors.

Other advantages are their good solvent resistance and lower price, which gives them great potential for development. For example, Spectra fibers had an original price of 49–61 \$/kg and this will be further lowered as a result of their recent major breakthrough in gel spinning, which enabled a thousand times increase in productivity. The potential application fields of UHMWPE fibers are listed in Table 2.56.

The interface bonding performance of UHMWPE fibers and fabrics in polymer matrixes can be improved by surface treatment. The biggest advantages of UHMWPE fiber composites are their significantly lower weight and their significantly higher impact strength. Therefore, they can be used to manufacture many excellent protection products such as protective shields, bulletproof vests, protective helmets, aircraft structural components and tank anti-debris linings. Table 2.57 illustrates the comparative impact strengths of UHMWPE fiber and Kevlar fiber-reinforced composites.

Additionally, because they are chemically inert, they can be used in medical equipment such as sutures and artificial muscles. Other than the above-mentioned attractive features, UHMWPE fibers also have shortcomings such as their poor thermal stability, high creep rate and bad interface bonding property.

The melting point of polyethylene fibers is around 134 °C, and a higher melting point of 144–154 °C can be observed in highly oriented UHMWPE fibers. Because of these low melting points, their strength and modulus vary according to changes in temperature. At temperatures lower than 100 °C, their strength is higher than that

Table 2.56 Potential applications of UHMWPE fibers

Application fields	Fabrics	Knitwear	Non-woven fabrics	Ropes	Composites
Protective supplies		Protective gloves, cut-resistant clothing			Motor covers
Maritime supplies	Sails			Departure ropes, mooring cables, trawls	Hulls
Transportation	Tapes, balloons			Lift cable, cables	Lightweight armor, ships
Bulletproof products	Shelter, protection products		Bulletproof, anti-riot vests		Helmets, board materials, armor
Sports goods	Sails	Fencing clothes, skating clothes		Speedboat ropes, fishing lines	Skiing board, hockey sticks, fishing rod

Table 2.57 Comparative impact strength of UHMWPE fiber and Kevlar fiber-reinforced composites

Type	Number of layers	Impact rate/ (m/s)	Maximum load/N	Absorbed energy/J
UHMWPE	1	4.2	3500	1040
Spectera900	3	4.3	4370	540
Kevlar	1	4.3	830	40
	3	4.5	1650	120

of the aramid fibers; however, at temperatures higher than 100 °C it is lower than that of the aramid fiber. Resistance to a constant tensile load also drops rapidly at temperatures close to 100 °C. Therefore, UHMWPE fibers are not suitable for extended tensile load at 90–100 °C. Studies have shown that their thermal stability and creep resistance can be improved by physical or chemical cross-linking such as high radiation modification.

Additionally, even though shrinkage between UHMWPE fibers and the epoxy resin composite matches well, the interface property of the composite is worse than that of aramid fibers. Surface modifications are necessary to improve this performance. Methods include washing, drying, chemical erosion treatment, flame treatment and low-temperature plasma processing. Improved UHMWPE fibers can undoubtedly be used in a wide variety of applications. They are very promising new generation of high-performance fibers, particularly because they are cost-effective.

2.8 Characterization Methods for Long Fibers

Because fiber characterization methods are very specific, it is necessary to discuss these in a separate section. As reinforcements of composite materials, mechanical properties such as tensile strength, the Young's modulus and tensile strain are of interest; additionally, for specific composite performance their density, coefficient of thermal expansion, thermal conductivity, resistivity, etc. are of concern. This section briefly introduces the main characterization methods for long-fiber reinforcements such as monofilaments and yarns. Short fibers such as whiskers are not considered because of different testing approaches.

2.8.1 Mechanical Characterization Methods

2.8.1.1 Monofilaments

The mechanical property of monofilaments is generally measured by placing a monofilament of specific length in a paper frame followed by tensioning until fracture under a specific tensile strain rate using a constant pulling machine. Tensile strength and Young's modulus can be calculated from the recorded fracture load and the tensile strain curve. Adhesions or coatings on the surface of the fibers, if any, are removed by washing with suitable solvents, and the fibers are dried before measurement.

Specifically, fibers 4–5 cm long are cut randomly from fiber yarns, and monofilament samples are separated undamaged and then stuck onto the center line of the paper frame, as shown in Fig. 2.9. The space and thickness of the paper frame are 25 ± 0.5 mm and 0.07–0.3 mm, respectively. The outer side width and length should be in accordance with the clip size of the testing machine. According to the standard, the laboratory temperature and the relative humidity should be 23 ± 5 °C and 50–70%, respectively. The paper frame is then fixed using a clip and cut using a small pair of scissors. The monofilament is subjected to tensile pulling at a constant speed of 5 mm/min, and the extension curve is recorded until fracturing occurs.

Fig. 2.9 Illustration of a paper frame with a monofilament (A sticking position, B fixed position)

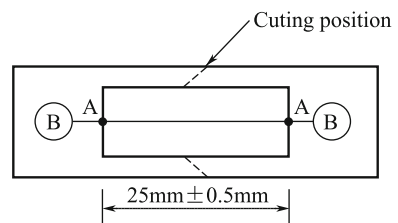
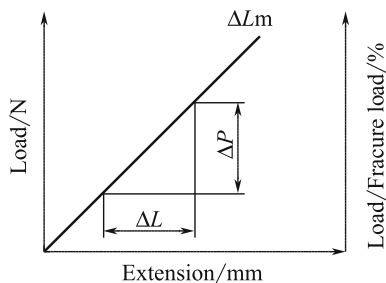


Fig. 2.10 Load–extension curve from a monofilament tensile test



A typical tensile load–extension curve for a monofilament is shown in Fig. 2.10. For a confidence level of 90% and a precision of 4%, no less than 25 samples should be collected.

The cross-sectional area of a monofilament is measured in accordance with Chinese standard GB/T3364, using a transmission microscope or a projector to investigate the diameters of fibers scattered on a slide. If the number of monofilaments is known for a given yarn, the cross-sectional area can also be obtained according to Appendix C, GB/T3362, in which the monofilament cross-sectional area is derived from the yarn cross-sectional area. The tensile strength of a monofilament can be calculated as follows:

$$\sigma = \frac{P}{A} \quad (2.1)$$

Here, σ is the tensile strength in MPa; P is the fracture load in N; A is the monofilament average cross-sectional area in mm^2 .

When the apparent Young's modulus is required, the middle part of the load–extension curve, which is 20–90% of the fracture load, is selected and tangent, as shown in Fig. 2.10. Then, ΔP and ΔL can be calculated, and Young's modulus is obtained using Eq. (2.2).

$$E_a = \frac{\Delta P}{A} \times \frac{L}{\Delta L} \quad (2.2)$$

Here, E_a is the apparent Young's modulus in MPa; ΔP is the intercept of the load increment in N; L is the length of the sample in mm; ΔL is net extension corresponding to the load increment ΔP in mm.

The tensile strain, ε , is related to the fiber length and the maximum extension (ΔL_m in Fig. 2.10), namely:

$$\varepsilon = \frac{\Delta L_m}{L} \times 100 \quad (2.3)$$

According to standard GB8170, the arithmetic mean value of the results should be reported to three significant digits, the standard deviation and the coefficient of variation to two digits.

2.8.1.2 Yarns

The tensile strength, Young's modulus and tensile strain of reinforcements can also be obtained through yarn tensile measurements. The samples are prepared with epoxy resin-impregnated yarns, as shown in Fig. 2.11. Both ends are stuck onto 0.2- to 0.4-mm-thick paper frames and fixed using any room-temperature curing adhesive.

The samples should be smooth, straight, uniform and without defects. The amount of epoxy resin should be in a control of 35–50%. If an inertia-free tensile machine is used the relative error should be less than $\pm 1\%$; if an automatic load record machine is used, the error in paper recording rate should be no more than $\pm 1\%$. Standard environmental conditions for the measurement are as follows: temperature of $(23 \pm 2)^\circ\text{C}$ and an air relative humidity of $50 \pm 5\%$. Ten samples are included in each test, and if a fracture occurs at the fixed position, the sample result is invalid. The tensile strength can be calculated as follows:

$$\sigma_t = \frac{P}{A} \quad (2.4)$$

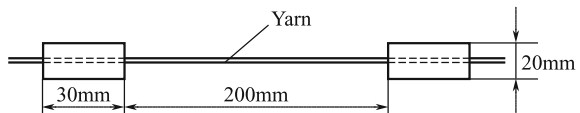
where σ_t is the tensile strength in MPa; P is the load in N; A is the yarn cross-sectional area in mm^2 (or m^2). A is obtained from the yarn axial density divided by the yarn volume density.

The apparent Young's modulus can be obtained as follows:

$$E_a = \frac{\Delta P}{A} \times \frac{L}{\Delta i} \quad (2.5)$$

where E_a is the apparent Young's modulus in MPa (or GPa); ΔP is the intercept of the selected load from the load–extension curve in N; L is the length of the specimens in mm; Δi is the incremental extension within the gauge corresponding to ΔP in mm.

Fig. 2.11 Illustration of a yarn sample



The tensile strain is calculated by Eq. (2.6):

$$\varepsilon = \frac{\Delta L}{L} \times 100 \quad (2.6)$$

where ε is the tensile strain %, and ΔL is the apparent tensile extension in mm.

2.8.2 Physical Characterization Methods

2.8.2.1 Density

The linear density of yarns can be measured with a balance of 0.1 mg accuracy. The samples should be three 1-m-long yarns, accurate to ± 0.5 mm. As for volumetric density, the floating method or the density gradient method can be used.

(1) Floating Method

Surface adhesives are removed with appropriate solvents, and the samples are dried for measurement. A mixed solution is prepared using a high-density solvent, e.g., dibromoethane, and a low-density solvent, e.g., *n*-heptane. The density should be close to the assumed density of the samples. The solution is put into a plugged graduated cylinder. Fiber samples are cut 0.5–1.0 mm long and put into the above-mentioned cylinder and stirred using a glass rod until fully dispersed in the solution. The cylinder is then put into a water bath at (25 ± 1) °C.

If the fibers float upward (or sinking downward) in the mixture, more *n*-heptane (or dibromoethane) is required to decrease (or increase) the density of the mixture until the fibers are evenly distributed. After 4 h in the water bath, the solution density will be regarded to be the same as the fiber density if they are still dispersed uniformly.

A densitometer is then used to measure the solution density. This will be the fiber density value.

(2) Density Gradient Method

A density gradient tube is prepared using a high-density solvent and a low-density solvent. Both the solvents can be pure solvents or mixture solvents. Their volumes are calculated as follows:

$$d \cdot V = A \cdot a + B(V - a) \quad (2.7)$$

where d is density of the mixture in g/cm^3 ; V is the volume of the mixture in cm^3 ; A is the density of the heavy solvent in g/cm^3 ; B is the density of the light solvent in g/cm^3 ; a is the volume of the heavy solvent in cm^3 ; $(V - a)$ is the volume of the light solvent in cm^3 .

Different mixtures with different densities are checked with a densitometer of 0.001 g accuracy, and densities are adjusted by the addition of a heavy solvent or a light solvent until they reach the required accurate density.

From the lower-density to the higher-density solvents, the mixtures are transferred to a scaled gradient tube through a funnel and a long capillary of 0.8–1.0 mm in diameter. After the last mixture, i.e., the heaviest mixture is added, the capillary is removed from the gradient tube. The gradient tube is covered with a lid and placed in the water bath at $(25 \pm 0.5)^\circ\text{C}$ and held still for 24 h.

The density gradient tube is checked as follows: four to five small balls with standard densities are put into the tube in turn, from higher to lower densities. After 4 h, the relative heights of the balls are measured using an altimeter, and then, a curve of height versus density can be obtained based on the known densities of the small balls. The linear part of the curve should be no less than 5 cm, and the density difference between each 1-cm height graduation should be lower than 0.002 g/cm^3 .

The tube is then ready for sample preparation and measurement. The fibers are organized into small-fiber yarns and then bent into four circular rings of about 0.5 cm in diameter. No broken fibers are permitted to guarantee the smoothness of the rings. The rings are then immersed in an appropriate solvent such as acetone for 4 h to become unglued. The rings are then dried for 2 h at 60°C and cooled to room temperature in a dryer. The dried fibers are submerged in a solution with a density similar to the fiber and placed into the centrifuge tube and degassed for 15 min at 2000 r/min. The degassed samples are then ready for the test. They are quickly placed in the gradient tube and left for 4 h. The height of the fiber samples, as well as the heights of the standard balls, is obtained using an altimeter.

The fiber density can be obtained using the interpolation method as follows:

$$d_x = \frac{x-b}{a-b}(d_a - d_b) + d_b \quad (2.8)$$

Here, d_x is the fiber sample density in g/cm^3 ; x is the height of the fiber sample in mm; a is the height of the heavy ball in mm; b is the height of the light ball in mm; d_a is the density of the heavy ball in g/cm^3 ; d_b is the density of the light ball in g/cm^3 .

2.8.2.2 Electrical Resistivity

Electrical resistance can be determined using a resistance instrument, which requires that the fibers be pressed into a measurement box. Resistance is an intrinsic property of a conductor. According to the resistance law, the resistance of a conductor, R , is proportional to its length, L , and inversely proportional to the cross-sectional area, S , as shown below:

$$R = \rho_v \frac{L}{S} \quad (2.9)$$

Here, ρ_v is the resistivity, also known as the volume resistivity, and its unit is $\Omega\cdot\text{cm}$.

$$\rho_v = R \frac{S}{L} \quad (2.10)$$

Because air is present in the fibers in the measurement box, the real area of the plate is not S , but SF , where F is the filling factor and can be calculated as below:

$$F = \frac{v_f}{V_r} = \frac{\frac{m}{d}}{SL} = \frac{m}{SLd} \quad (2.11)$$

Here, v_f is the real volume of the fiber; V_r is the volume of the measurement box; m is the mass of the fiber sample; d is the density of the fiber sample.

The volume resistivity is calculated as follows:

$$\rho_v = R \frac{SF}{L} = R \frac{m}{L^2 d} \quad (2.12)$$

The volume resistivity is the resistance when the current transfers through a material with a volume of 1 cm^3 , while the mass resistivity, ρ_m , is the resistance when the length of a material is 1 cm and the mass of the material is 1 g . The relationship between volume resistivity and mass resistivity is shown below:

$$\rho_m = d\rho_v \quad (2.13)$$

The unit of mass resistivity is $\Omega\cdot\text{g}/\text{cm}^2$, and its value is calculated as follows:

$$\rho_m = R \frac{m}{L^2} \quad (2.14)$$

The electrical resistivity of the fibers can also be obtained directly by measuring the resistance of the monofilament that is fixed on the paper frame and is calculated according to Eq. 2.10.

2.8.2.3 Coefficients of Thermal Conductivity and Thermal Expansion

Heat conduction is based on the thermal property of the materials coefficient of thermal conductivity. Heat conduction along an infinite flat material with a thickness of x can be described using the Fourier equation as shown below in a one-dimensional manner:

$$Q = -\lambda \cdot \Delta T / \Delta x \quad (2.15)$$

Q represents the unit area heat flow caused by the temperature gradient ΔT over the thickness Δx . Two factors are related to the coefficient of thermal conductivity, λ . Under stable temperature gradient and material geometry conditions, λ expresses the amount of heat required to maintain the temperature gradient.

Many methods and instruments exist to measure the coefficient of thermal conductivity. The Fourier equation is used to describe steady-state conditions, and instruments using this equation are only suitable for testing low thermal conductivity at middle-range temperatures. Equipment that use dynamic (transient) methods such as the hotline or laser light scattering method can be used to measure high thermal conductivity at high temperatures.

A fiber's coefficient of thermal expansion is of great significance in the selection of fibers for matching with ceramic matrixes. For example, reinforcements should have at least the same high-temperature performance as the matrix, and the fiber coefficient of thermal expansion should be slightly higher than that of the matrix. Some thermal expansion testing instruments such as the DIL 402C produced by NETZSCH (temperature range -180 to 2000 °C) can provide a special monofilament support, which is convenient when determining the fiber's coefficient of thermal expansion.

2.9 Whiskers

Whiskers are single-crystal short fibers grown under controlled conditions. They are usually defect-free with diameters ranging from $0.1 \mu\text{m}$ to several microns, and their lengths range from dozens to thousands of microns [52].

Each whisker has a characteristic shape and structure relevant to its intrinsic material property. Good whiskers have perfect crystal structures, highly ordered atomic structures, and contain the least internal defects, e.g., dislocations and impurities. Therefore, they are high-purity short fibers with strengths close to the atomic bonding strength. They are regarded as a pillar reinforcement family for advanced composite materials.

Whisker-reinforced composites have enhanced microstructures, leading to excellent resistance to sliding and wearing. Some whiskers also have special physical properties such as electrical insulation or a negative coefficient of thermal conductivity. Whisker-reinforced high-performance composites have become an important integration composite in structural and functional materials [53].

Recent applications of whisker-reinforced composites have spread greatly, which in turn has promoted research and development into a variety of whiskers, particularly in the manufacturing of cost-effective whiskers.

More than 100 species of various whiskers have been developed to date, and these include organic whiskers, metal whiskers and ceramic whiskers. These are the

Table 2.58 Physical properties of general whiskers

Whisker	Melting point/ $^{\circ}\text{C}$	Density/ (g/cm^3)	Tensile strength/GPa	Young's modulus/GPa
BeO	2570	2.85	13	350
B ₄ C	2450	2.52	14	490
α -SiC	2316	3.15	–	480
β -SiC	1600	3.19	3–14	400–700
Si ₃ N ₄	1690 (sublimation)	3.18	13.7	380
C(graphite)	3650	1.66	19.6	710
TiN	–	5.20	7	200–300
AlN	2199	3.30	6.9	340
MgO	2799	3.60	–	340
K ₂ O[TiO ₂] _n	760–1370	3.29	5.7–7.0	280
Cr	1890	7.20	9	240
Cu	1080	8.91	3	120
Fe	1540	7.83	13	200
Ni	1450	8.97	4	210
9Al ₂ O ₃ ·B ₂ O ₃	1420–1480	2.93	7.8	392
ZnO	1720 (sublimation)	5.78	>10	354
Polyoxymethylene	184	1.42	–	>100

three major categories, among which ceramic whiskers are superior to the other two in terms of strength, modulus, heat resistance and wear resistance. Therefore, ceramic whiskers have more industrial use and have become the focus of research and development. The physical properties of general whiskers are listed in Table 2.58.

2.9.1 Ceramic Whiskers

As a kind of special fibrous single-crystal material, the growth mechanisms of whiskers are also unique as they are completely different to the formation of continuous fibers. The vapor–solid (VS) mechanism and the vapor–liquid–solid (VLS) mechanism are the two most common types. However, whisker growth mechanisms and their preparation methods are closely linked. For example, in the VS mechanism, in addition to the chemical reaction conditions and the choice of raw materials, oversaturation in the vapor reactant also plays an important role. The growth mechanisms of selected whiskers and their preparation methods are listed in Table 2.59.

In the VLS mechanism, catalysts are necessary for the fast growth of whiskers. A good catalyst should be able to form a low-melting eutectic liquid, which can

Table 2.59 Growth mechanisms of selected whiskers and their preparation methods

VS mechanism		VLS mechanism		
Whisker	Preparation method	Whisker	Preparation method	Catalyst
Al ₂ O ₃	AlF ₃ hydrolysis	Si ₃ N ₄	CVD	Fe
β-SiC	Carbon thermal reduction	β-Si ₃ N ₄	CVD	Cr
Mullite	Vapor	α-Al ₂ O ₃	CVD	Mo, Fe
Mullite	Sol-gel	β-Sialon	Carbon thermal reduction	Fe

significantly reduce the growth energy. This is why the VLS growth rate is faster than the VS growth rate, because no catalyst takes part in the VS mechanism. By properly controlling the droplet location, type and chemical composition of the low eutectic liquid, a variety of whiskers with different shapes, types and properties can be obtained. Therefore, the VLS growth mechanism is currently the most important and mostly used approach to a number of commercialized whiskers. Typical ceramic whiskers and their performance are listed in Table 2.60.

In addition to basic whisker properties such as high tensile strength, high Young's modulus and high heat resistance, the typical ceramic whiskers listed in Table 2.60 also have unique characteristics such as high hardness (SiC) or a low coefficient of thermal expansion (Si₃N₄) [53]. It is very important to select appropriate whiskers to meet the specific requirements of different composites.

2.9.1.1 SiC Whiskers

There are two kinds of crystal isomers in SiC whiskers, hexagonal α-SiC and cubic β-SiC [54]. Compared with α-SiC whiskers, β-SiC whiskers maintain whisker length better because of the lower likelihood of fracture upon loading; therefore, they are preferred in most industrial fields. In addition to their high strength, high modulus, high hardness and good chemical stability, SiC whiskers also have good wear resistance, corrosion resistance and high-temperature anti-oxidation properties. For these reasons, they are known as “king of the whiskers.”

SiC whiskers are at the practical application stage, and many satisfactory results have been obtained. For example, SiC whiskers can greatly improve the Young's modulus and wear resistance in aluminum matrixes. Additionally, it improves their low-temperature and high-temperature strength and their fatigue strength. These composites are now widely used in the automotive, aerospace and military industries as structural parts and wear-resistant parts such as engine pistons, connecting rods, bearings, bulletproof plates and shielding materials.

Research into SiC whiskers started in the 1960s, and in the 1980s SiC whiskers were extensively applied as polymer, metal and ceramic matrix reinforcements. Many production reports have been published, and most come from the USA and Japan. In addition to their successful application as cutting tools (SiCw/Al₂O₃), piston engines (SiCw/Al), aircraft landing gear parts and sporting equipment such as golf clubs (SiCw/polymer), SiC whisker composites have begun to be used as

Table 2.60 Some typical ceramic whiskers and their performance

Whisker	Density/ (g/cm ³)	Diameter/ μ m	Length/ μ m	Tensile strength/GPa	Young's modulus/GPa	Mo's hardness	Coefficient of thermal expansion/ (10 ⁻⁶ /K)	Melting point/ $^{\circ}$ C	Thermal stability/ $^{\circ}$ C
SiC	3.18	0.05-7	5-200	21	490	9	4.0	2690	1600
K ₆ Ti ₁₃ O ₆	3.30	0.1-1.5	10-100	7	280	4	6.8	1370	1200
Al ₁₈ B ₄ O ₃₃	2.93	0.5-1	10-20	8	400	7	4.2	1950	1200
ZnO	5.78	5	2-300	10	350	4	4.0	1720	-
Si ₃ N ₄	3.20	0.1-0.6	5-200	1.4	350	-	3.0	1900	1700
MgO	3.60	3.0-10	200-300	1-8	-	-	13.5	2850	2800

Table 2.61 Manufacturers and brand names of SiC whiskers in the USA and Japan

Manufacturer	Brand name
Advanced Composite Materials Co. (ACMC)	AC ₁ , AC ₂
American Mterix Co.	AM ₁ , AM ₂ , AM ₃ , AM ₄ , AM ₅ , AM ₆ , AM ₇ , AM ₈
Advanced Ceramic Technologies	AI ₁
Alcan Co.	CN ₁
Huber Co.	Hu ₁ , Hu ₂ , Hu ₃
Clermont Co.	KE ₁
Kobe Steel Co.	KS ₁ , KS ₂ , KS ₃ , KS ₄
Tateho Chemical Industries Co.	TA ₁ , TA ₂ , TA ₃
Tokai Carbon Co.	TK ₁ , TK ₂ , TK ₃ , TK ₄ C, TK ₅ , TK ₆ , TK ₇
Los-Alamos Co.	ARCo

Table 2.62 Typical properties of SiC whiskers

Property	ARCo	Tateho	ToKai	BP, China
Tensile strength/GPa	8.4	–	3–14	4–13
Young's modulus/GPa	580	–	400–700	–
Diameter/ μm	0.6	0.05–0.20	0.2–1.0	0.1–1.0
Length/ μm	10–80	10–40	30–200	10–200
Crystal type	α	$\alpha + \beta$	β	β

filter materials in the chemical industry recently. However, since they are carcinogenic, it is necessary to take protective measures during production and application.

Research into these materials started in China in the early 1970s, and a number of SiC whisker products have been produced. The carbon thermal reduction method has also been used to prepare SiC whiskers, and a pilot plant was commissioned and delivered a product quality close to that of other countries. In addition, using carbon black and rice husk as a carbon source for the growth of SiC whiskers has also been reported.

Manufacturers, brand names and typical properties of SiC whiskers in the USA, Japan and China are listed in Tables 2.61 and 2.62. Morphological characteristics of typical SiC whiskers are listed in Table 2.63. All the products have similar mechanical properties but with some obvious differences in morphology.

2.9.1.2 Si₃N₄ Whiskers

Morphologies of Si₃N₄ whiskers vary according to preparation methods. In general, there are three types of preparation methods:

Table 2.63 Morphology characteristics of typical SiC whiskers

Characteristic	US AM ₁	USAC ₁	China BP	Japan TK ₁	Japan TA ₁
Extremely straight crystal/%	97	99	97	54.5	98
Straight crystal/%	3	1	3	35.5	2
Bent crystal/%	–	–	–	8.5	–
Extremely bent crystal/%	–	–	–	1.5	–
Extremely smooth whisker/%	10.5	89.5	16.5	47.5	5.0
Smooth whisker/%	20.5	5.0	19.5	6.5	45.0
Coarse whisker/%	48.5	5.0	54.5	44.5	19.0
Extremely coarse whisker/%	20.5	0.5	9.5	1.5	31.0
Particle content/%	4	1.0	4.0	1.0	4.0

- ① In the vapor-phase method, a mixed gas of SiCl₄, H₂ and N₂ is used, and Si₃N₄ whiskers are grown on an Fe-coated graphite base heated to 1250 °C. These whiskers are amorphous with regular spiral bodies and spherical ends and are thus the smallest coil springs;
- ② In the liquid-phase method, silicon is heated to 1550–1600 °C to a liquid state and reacts with the nitrogen atmosphere to give Si₃N₄ whiskers;
- ③ In the solid-phase method, a mixture of solid SiO₂ and C is heated in nitrogen or a mixture of solid SiO₂ and Si is heated in a N₂ and H₂ atmosphere affording the target Si₃N₄ whiskers.

Another method exists for the preparation of defect-free Si₃N₄ whiskers; that is, Si₃N₄ and high-pressure NH₃ are mixed at room temperature and then heated to remove the ammonium nitrogen, and this is further heated gradually to decompose the amide affording Si₃N₄ ultra-fine powders with high activity and high purity. If they are further heated to 1400–1450 °C, straight and smooth Si₃N₄ whiskers are obtained. Their oxygen content is less than 1%, and their aspect ratio depends on the heating temperature. For example, at a heating temperature of 1400 °C, the diameter and length are 0.02–0.08 and 50–100 μm, respectively, whereas at 1450 °C these parameters are 0.1–0.3 and 10–30 μm, respectively. In addition, their typical tensile strength, Young's modulus and coefficient of thermal expansion are 13.8, 390 GPa, and $2.75 \times 10^{-6} \text{ K}^{-1}$, respectively.

Si₃N₄ whiskers can be used to reinforce aluminum matrix composites and also to reinforce a large number of various ceramics such as glass, aluminum, silicon nitride and silicon carbide. These ceramic matrix composites have good high-temperature performance and excellent toughness; for example, Si₃N₄ whisker-reinforced SiC ceramic has a maximum working temperature up to 1400 °C. In addition, the toughness of 20%(wt) Si₃N₄ whisker-reinforced Al₂O₃ is 1.5 times that of its matrix.

2.9.1.3 Potassium Titanate Whiskers

Even though their tensile strength and Young's modulus are relatively low, potassium titanate whiskers are a kind of low-cost material with good integrated performance. Their aluminum composites are easily cut-processed, which is attractive. They are mainly used in the manufacture of polymer matrix composites because they improve the friction and insulation properties of the polymers.

Potassium titanate whisker reinforcement composites meet the requirements of automobile, chemical and military applications such as high strength, low attrition rate, good high-temperature and low-temperature stability, and good resistance to strong acids and strong bases.

Additionally, potassium titanate whiskers have high infrared reflectivity and very low thermal conductivity and are thus widely used in the automobile, electrical, electronic and instrumentation industries as corrosion resistance paints, lubricants, insulation materials and anti-corrosion materials.

As a kind of general reinforcement, there is a demand for a further reduction in the production cost. According to expert analysis, only when the price reaches 11,100 US dollars/ton, large-scale use will be possible in the automobile industry. A conductive potassium titanate whisker recently produced in Japan can apparently be used in the manufacture of static electricity prevention or electromagnetic shielding electronic components.

Since potassium titanate whiskers have been adopted as reinforcements in resins such as POM, PBT, Nylon 66, Nylon 6, specialty Nylon, PPS, ABS, PVC and PP, there are many applications for these plastic composites: ① reinforced POM as watch gears, camera gears, micromotor gears and tape recorders; ② reinforced PBT as telegraph key switches, posts, motor parts, relays, cams and plugs; ③ reinforced Nylon 66 as bearings, cams, gears, winding pipes, wheels and bearing retainers; ④ reinforced Nylon 6 as bearings, gears, industrial posts, automatic closing door devices, winding pipes and buttons; ⑤ reinforced specialty Nylon as sliding parts, silence gears, thin-walled parts, and sporting goods; ⑥ reinforced PPS as copier parts, sliding parts and auto parts; ⑦ reinforced ABS as copier parts, electroplating products, watches and clock parts and sporting goods; ⑧ reinforced PVC as pearls, decorative bands and coating pipes; ⑨ reinforced PP, as audio components, vacuum-forming parts and auto parts.

The general formula of potassium titanate whiskers is $K_2O(TiO_2)_n$ in which $n = 1, 2, 4, 6$ and 8 . Best stability is usually obtained when $n = 6$. Typical characteristics of one type of stable potassium titanate whiskers are listed in Table 2.64.

The biggest drawback of these whiskers is that they readily react with metal melts at the interface, and furthermore, these whiskers are not stable at higher temperatures because of decomposition. Further in-depth studies are needed to extend their application in reinforcing metals.

Table 2.64 Typical characteristics of potassium titanate and aluminum borate whiskers

Property	$K_2O \cdot 6TiO_2$	$9Al_2O_3 \cdot 2B_2O_3$
Appearance	White, needle-like	White, needle-like
Density/(g/cm^3)	3.3–3.4	2.93
Melting point/ $^{\circ}C$	1370	1440
Young's modulus/GPa	280	400
Tensile strength/GPa	7	8
Mo's hardness	4	7
Linear expansion coefficient/($\times 10^{-6}/K$)	–	4.2
Axial direction	–	2.6
Cross-sectional direction	–	5–6
Coefficient of thermal conductivity/[$W/(cm \cdot K)$]	–	0.04–0.05
Thermal diffusion coefficient/(cm^2/s)	–	0.01
Dielectric constant	3.5–3.7	5.6

2.9.1.4 Aluminum Borate Whiskers

Aluminum borate whiskers have two kinds of structures, namely $9Al_2O_3 \cdot 2B_2O_3$ and $2Al_2O_3 \cdot B_2O_3$. They are new emerging high-tech whiskers with high performance and low price. For example, their production cost is only 1/10th to 1/30th that of SiC whiskers.

Aluminum borate whiskers are widely used as new inorganic fillers in light-metal alloys, functional plastic composites, ceramic fibers and coatings. Because of resource conditions in China, the state attaches great importance to the further research and development of these whiskers.

Typical physical properties of $9Al_2O_3 \cdot 2B_2O_3$ whiskers are listed in Table 2.64. These whiskers have good tensile strength, Young's modulus, heat resistance, chemical resistance, neutron absorption and electrical insulation properties. They are not only used for insulation and heat-resistant materials but also used as reinforcements in thermoplastic resin, thermosetting resins, cements, ceramics and metals.

After treatment with coupling agents such as silane, aluminum borate whiskers can significantly improve the mechanical properties of a variety of engineering plastics such as Nylon 6 and polycarbonate. Aluminum borate whiskers improve the tensile strength, wear resistance and heat resistance and also result in isotropic products with smooth surfaces. Satisfactory results have also been obtained in a number of small precise parts with complicated shapes such as the components of clocks, watches and cameras.

Aluminum borate whiskers can be used as reinforcements in metals and alloys, especially aluminum alloys, which have good abrasion resistance and a low thermal expansion rate. These have found application in cycling operation components in vehicles and compressors.

Aluminum borate whisker-reinforced aluminum composites have competitive strength, modulus and thermal expansion properties compared with SiC and Si₃N₄ whisker-reinforced aluminum and even have better wear resistance. For example, whisker-reinforced aluminum composites can be used to manufacture automobile engine pistons that substantially increase engine power, save fuel and reduce noise and exhaust emissions.

These high-performance, low-cost whiskers are important composite reinforcements, especially in the automotive industry [53]. However, measures must be taken to control the interface between the whiskers and alloys. They also can be used in ceramic matrix composites as they improve their mechanical properties and high-temperature stabilities. In addition, they are also applied to flame-retardant or fire-resistant coatings, electronic materials and electromagnetic shielding materials.

2.9.1.5 ZnO Whiskers

As a kind of *n*-type semiconductor, ZnO whiskers are mainly divided into two categories, mono-needle-like and multi-needle-like. Mono-needle-like ZnO whiskers have similar properties and applications to those of SiC whiskers or potassium titanate whiskers. Tetra-needle-like ZnO whiskers, which are typical multi-needle-like ZnO whiskers, have more interesting properties and applications [55].

They have a central body and four protruding needle-like crystals with a general length of 3–300 μm, a root diameter of 0.1–14 μm and an angle between protruding crystals of about 109°. Their crystal structure is a hexagonal Wurtzite structure, and the protruding needles grow along the *c* axis of hexagonal crystal. Their typical physical properties are listed in Table 2.65. Their average volume resistance is 10⁴–10⁸ Ω·cm indicating a semiconductive property.

ZnO whiskers have many functional properties such as electrical conductivity, thermal conductivity, piezoelectric activity, pressure sensitivity, microwave absorption, sound absorption, vibration attenuation and anti-bacterial and catalytic properties. They are widely used as reinforcements in metals, ceramics and polymers, with the ability to improve their tensile strength, bending strength, shear

Table 2.65 Typical physical properties of tetra-needle-like ZnO whiskers

Property	Value
Formula	ZnO
Shape	Tetra-needle-like
Intrinsic density/(g/cm ³)	5.78
Apparent density/(g/cm ³)	0.05–0.50
Boiling point/°C	1720
Length of protruding needle/μm	3–300
Root diameter of protruding needle/μm	0.1–14
Volume resistance/Ω·cm	7.14
Coefficient of thermal expansion/ (×10 ⁻⁶ /K)	4.0

strength, abrasion resistance and high-temperature chemical stability, as well as many other functional properties [56].

For example, because of their conductive and piezoelectric properties, ZnO whiskers are widely used as conductive fillers, conductive layers, anti-electrostatic materials, radio wave-absorbing materials and piezoelectric materials [56]. Also, because of their good isotropic structures and isotropic physical properties, tetra-needle-like ZnO whisker-reinforced composites have good isotropic mechanical properties, electrical properties and optical properties, which are unmatched by other whiskers, particularly in the field of functional materials. Furthermore, the whiskers are also widely used as noise shielding, sound absorption and damping materials in the automotive, construction, industrial equipment, office equipment and household appliance fields.

In addition, ZnO whiskers are also sensitive to combustible gases, especially when doped with Li^+ , which can significantly increase their sensitivity. The apparent density of ZnO whiskers is very low, and they are thus attractive fillers for insulation materials as well as unique vibration attenuation fillers in music instruments.

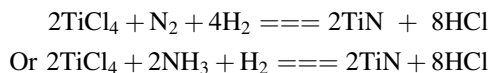
ZnO whisker research began in the mid-1980s, and Matsushita Electric Industrial is one of the most successful companies in the preparation of ZnO whiskers, devices and their applications.

Research started in China in the early 1990s, and the tetra-needle-like ZnO whiskers obtained have an average protruding needle length of 51 μm , a root diameter of 15 μm , a specific heat of 5.52 J/g·K, heat resistance of 1720 $^{\circ}\text{C}$, an apparent density of 0.01–0.50 g/cm³, electrical resistivity below 50 $\Omega\cdot\text{cm}$, bending strength of 12 GPa and a Young's modulus of 350 GPa.

2.9.1.6 TiN Whiskers

TiN whiskers are cubic crystals, and their density is 5.21 g/cm³ at 25 $^{\circ}\text{C}$, their specific conductivity is 8.7 $\mu\Omega^{-1}\cdot\text{m}^{-1}$ at 20 $^{\circ}\text{C}$, their microhardness is 2000–2400 kg/mm², and they have melting points up to 2950 $^{\circ}\text{C}$. They have low-temperature superconductivity and excellent thermal conductivity, and their linear expansion coefficient is as high as $9.4 \times 10^{-6}/\text{K}$.

TiN whiskers are prepared by chemical vapor deposition (CVD) at 1000–1450 $^{\circ}\text{C}$ using a mixed vapor system of $\text{TiCl}_4\text{--H}_2\text{--N}_2$ or $\text{TiCl}_4\text{--H}_2\text{--NH}_3$ [57] as follows:



The TiN whiskers thus prepared are cubic crystals with high purity and good chemical stability. The macroscopic shape of the whiskers is four-prism or eight-prism. In the 1980s, much research was carried out in the USA, Japan, Poland, the former Soviet Union and China. The TiN whiskers produced in China

have a tensile strength distribution of 1.5–10 GPa and a Young's modulus distribution of 30–200 GPa. Their Young's modulus is a magnitude of order higher than that of the bulk crystal and is 10 GPa.

TiN whiskers have good compatibility with alumina, boron nitride, tungsten carbide and stainless steel, as well as a number of metal alloys. In particular, they are ideal reinforcements in zirconia ceramic matrix composites because their coefficients of thermal expansion are very close; for example, the coefficient of thermal expansion of zirconia is $9.5 \times 10^{-6}/\text{K}$. The whiskers can greatly improve the high-temperature toughness of zirconia.

In addition, TiN whiskers have high hardness and good abrasion resistance and can thus be used to improve the hardness of super-tough ceramics. For example, TiN whisker-reinforced WC cutting tools have a higher bending strength of 750–1050 MPa compared with 650 MPa without reinforcement and also show a reduced wearing rate of the cutting edge.

2.9.2 Carbon Whiskers

Carbon (graphite) whiskers are prepared from low boiling point hydrocarbon compounds, which act as carbon resources. Oxygen or an inert gas is used as the carrier gas, and transition metals such as Fe, Co or Ni are used as the catalyst in the form of ultra-fine powder. The whiskers are grown at 500–1100 °C in the form of monocystals [58, 59].

Carbon nanotubes are seamless hollow tubes formed by rolling graphite sheets. They are classified as single-walled nanotubes or multi-walled nanotubes. They are a new kind of carbon material with chirality. They can be considered to be special hollow carbon whiskers because of their diameter, length, as well as their single-crystal form.

2.9.2.1 Carbon (Graphite) Whiskers

Carbon (graphite) whiskers are also referred to as carbon (graphite) nanofibers because their diameters are about 50–200 nm, and they have a relatively longer length than general whiskers [58]. For example, their length varies from 50 μm to several millimeters.

The growth of carbon whiskers from hydrocarbon gases was observed more than 100 years ago, and in the mid-1950s they began to receive much more attention. Over the last two decades, a considerable amount of research has been carried out mainly in Japan, the USA and France.

The vapor growth of carbon whiskers has been mostly studied in Japan and the USA. Currently, the production and sales of carbon (graphite) whiskers are dominated mainly by Showa Denko, Hyperion Catalysis International and Applied Sciences Inc. No extensive research has been carried out or reported in China.

Because vapor growth carbon whiskers are obtained at high temperature from hydrocarbon compounds, their structures are denser than general carbon fibers. They have a much smaller surface and less internal defects as well.

Additionally, carbon whiskers have a high aspect ratio and a large surface area and are easily graphitized. This makes them superior to other carbon fibers in mechanical properties, electrical conductivity, thermal conductivity and chemical and thermal stabilities. Table 2.66 lists some typical characteristics of carbon whiskers (preheat treatment) and graphite whiskers (post-heat treatment).

Additionally, carbon (graphite) whiskers are excellent heat insulation materials, brake sealing abrasion materials, corrosion-resistant chemical filtration materials and electromagnetic shielding materials [58]. Carbon (graphite) whiskers are mainly used as additives to increase conductivity, as reinforcements to improve mechanical properties and additives to control the coefficient of thermal expansion. Their specific applications are listed in Table 2.67.

Carbon (graphite) whiskers are thus a new kind of sub-micron additive material. In the current market, they are mainly used as electromagnetic shielding materials for automotive fuel tanks, semiconductor and electronic products. There is also a large market in lithium batteries, large-capacity capacitors and fuel cells. They are not generally used as reinforcements in structural components yet but are used as additives to improve mechanical properties, electrical and thermal conductivities, interlaminar shear strength (ILSS) and the coefficient of thermal expansion. Over the next 10 years with large-scale production and lower prices, carbon (graphite) whiskers are expected to become major reinforcements of composite structures.

2.9.2.2 Carbon Nanotubes

It was generally believed that there are three kinds of carbon allotropes existed, namely diamond, graphite and amorphous carbon. Kroto, a professor in Britain, and Curl and Smalley, two professors in the USA, discovered C_{60} in 1985 [60] and received the Nobel Prize for Chemistry in 1996. Professor Iijima from Japan discovered carbon nanotubes (CNTs) in 1991 using a high-resolution transmission electron microscope [59]. These two new allotropes were thus included in the carbon family as fullerenes and carbon nanotubes. Recently, a two-dimensional graphene was also added [61].

Since the discovery of CNTs, widespread interest has been expressed because of their excellent performance and their potential applications, which then makes them a very hot topic around the world. In the USA, large investments have resulted and much research has been carried out in fields from medical to electronics and composite materials. The response has been similar in Japan and China, with a focus on electronics.

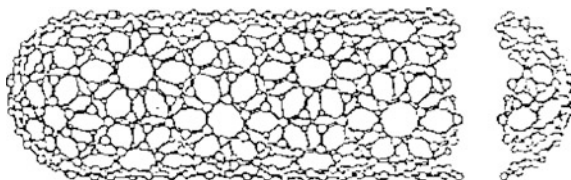
Significant progress has been made in preparation methods and in the study of CNT characteristics. Mass production has begun, and studies continue into the application of CNTs.

Table 2.66 Typical characteristics of carbon whiskers and graphite whiskers

State	Tensile strength/GPa	Young's modulus/GPa	Tensile strain/%	Density/(g/cm ³)	Electrical resistivity/ $\mu\Omega\cdot\text{cm}$	Thermal conductivity/W/(m·K)
Carbon whiskers	2.7	400	1.5	1.8	1000	20
Graphite whiskers	7.0	600	0.5	2.1	55	1950

Table 2.67 Specific applications of carbon (graphite) whiskers

Role	Area	Specific applications
To increase electrical conductivity	Static electricity dissipation	Oil pipelines, automotive systems, electronic assembly, weapons and electrostatic control of satellites
	Electrostatic painting	Aircraft, vehicle body components, vessels and other vehicles
	Anti-EMI	High-speed computers, communication systems, aerospace control systems and electronic systems
	Anti-lightning	Aircraft, ground structures, ships, radomes and weapon warehouses
	Soft contact	Scanning electron microscopes and fuel cells
To improve mechanical properties	Synthetic rubber	Tires, vessels, ship structures and sporting goods
	Thermoplastic components	Aircraft, vehicles, satellites, ships and sporting goods
	Thermosetting components	Aircraft, vehicles, satellites, ships and sporting goods
	Carbon/epoxy components	Aircraft bodies, automobiles, aerospace components and sporting goods
To control the coefficient of thermal expansion	Optical	Injection molding low-cost optical components and laser components
	Frames	Frames of aircraft, vehicles, satellites and ships
	Electrical	Electronic equipment, instrument panels, computers and controlling equipment

Fig. 3.21 Synthesis of PT resins

Carbon nanotubes are seamless nanotubes spirally coiled from single- or multilayered graphite sheets at a certain angle along the central axis [62, 63]. As shown in Fig. 2.12, each layer of the nanotube is a cylinder surface composed of many hexagonal planes, which are formed from carbon atoms by SP^2 hybrid bonding. The border length of the planular hexagonal cell is 0.246 nm, and the shortened C–C bond is 0.142 nm, which is close to the atomic stacking distance of 0.139 nm. Both ends of the cylinder are closed with pentagon or heptagon atomic cycles. During graphite sheet rolling, suspended bonds on the border combine randomly, which leads to randomness in the tube axis. As a result, the carbon atoms are arranged spirally in the hexagonal lattice in the general structure of carbon nanotubes, and there is thus a certain degree of spirality in the CNTs.

Based on the number of layers, CNTs can be divided into two categories: single-walled carbon nanotubes (SWCNTs) and multi-walled carbon nanotubes (MWCNTs). MWCNTs are composed of a number of coaxial cylindrical structures with inter-layer stacking like ABAB, and its layer distance of 0.34 nm approximates that of graphite.

Studies on the electrical properties of SWCNTs have shown that their performance is strongly dependent on their geometric structure, that is, their diameter or chirality (i.e., m , n). When the difference between m and n is an exact integer dividable by 3, the SWCNTs act as metals or semimetals. For example, (n, n) “chair” structural SWCNTs are metallic. In other cases, SWCNTs are semiconductors and the band gap is proportional to the inverse of the diameter. Among all CNTs, about one-third are metallic and two-thirds are nonmetallic.

For practical applications, their preparation should meet the following requirements: continuous mass production, low cost and environmental friendliness. Additionally, the products obtained should be of high purity and have uniform structures with good control. Currently, three main methods are used: arc discharging, catalytic pyrolysis and laser evaporation.

The arc discharging system mainly consists of a power supply, a graphite electrode, a vacuum system and a cooling system. Catalysts are usually introduced to the cathode to increase production efficiency, and sometimes laser evaporation is also applied. For arc discharging, the temperature inside the reaction vessel can be as high as 2700–3700 °C, and the CNTs generated have a high degree of graphitization close to the expected theoretical state. However, the CNTs prepared this way have uncertain growth directions as well as a high impurity content, and they are easily sintered. Research shows that discharge stability is the key to high yields and high-quality CNTs. The adoption of a uniformly rotating progressing anode or cathode can improve the discharge conditions, which promotes the mass production of CNTs.

Catalytic pyrolysis is a widely applied method for the preparation of CNTs. The necessary equipment and processes are relatively simple, while the key is the preparation and dispersion of the catalysts, which are mainly transition metal catalysts. It is suitable for the large-scale preparation of CNTs with the advantage of a high content of CNTs in the final products. However, many defects exist in these CNTs.

Current research into catalytic pyrolysis is mainly focused on two areas: the large-scale preparation of disordered, randomly directed CNTs and the preparation of discretely distributed, order directed arrays of CNTs. The former process gives SWCNTs or MWCNTs in large quantities at 530–1130 °C when using Fe, Co, Ni or their alloys as catalysts and using clay, silica, diatomite, alumina or magnesium oxide as carriers as well as acetylene, propylene or methane as carbon sources, and hydrogen, nitrogen, helium, argon or ammonia as dilution gases. Free carbon ions form nanotubes under the effect of catalysts.

Research into arrays of CNTs is also currently a hot topic, and the important step is the preparation and dispersion of catalyst nanoparticles. Currently, catalysts and catalyst supports with a high density of active sites, a high surface area and a high

pore volume are mainly used. For example, Pan successfully prepared a very long array of CNTs of more than 2 mm using catalyst nanoparticle-incorporated porous silica gel, which was prepared by the hydrolysis of a TEOS solution mixed with a transition metal salt [64]. There is no doubt that this is an important step toward the application of CNTs.

Laser evaporation is an effective method for the preparation of SWCNTs, and a high-energy CO₂ laser or a Nd/YAG laser is used to evaporate the carbon target that has been mixed with Fe, Co, Ni or their alloys resulting in SWCNTs and their bundles. The diameter of the SWCNTs can be controlled by laser pulses. However, the shortcomings of laser evaporation (ablation) are the low content of SWCNTs in the products as well as excessive tangling of the SWCNTs. Solar energy has also been reportedly used for preparation of SWCNTs.

Since the emergence of CNTs much interest has been shown in their special morphologies and structures. The nature of the various forms has been of interest to ultimately realize their applications. Based on theoretical calculations and experimental studies, CNTs have been found to have important physical properties and attractive applications in the following areas:

(1) Electrical Properties and Their Applications

The electrical properties of CNTs are very strange. Their axial resistance is very small, and they can be transformed into superconductors at low temperatures and can thus be observed as one-dimensional quantum wires. In 1992, researchers discovered semiconducting or conducting properties that vary according to the different rolling structures. Deforer and coworkers have successfully prepared horizontal carbon nanotube transistors that work at room temperature. The volume of the carbon nanotube transistor is only one-tenth that of the semiconductor transistor. This is bound to lead to a new computer revolution if computer chips are replaced with carbon-based molecular electronic devices. CNTs can also be used as nanowires, as coherent electronic sources in electron microscopy, as efficient electronic sources in field emission and as super-capacitors.

(2) Mechanical Properties and Their Applications

Experimental and theoretical calculations show that carbon nanotubes have high strength and great toughness. The Young's modulus of SWCNTs is estimated to be as high as 5 TPa, and the experimentally measured average Young's modulus and bending strength of MWCNTs are 1.8 TPa and 14.2 GPa, respectively. Although their density is only one-seventh that of steel, their tensile strength is 100 times that of steel.

As one-dimensional materials and compared with carbon fibers, CNTs have less defects, higher purity, higher strength and a higher modulus. Their aspect ratio is as high as 100–1000. They have self-resilience after bending, and scientists use them as CNT tips in scanning tunneling microscopes as well as in nanometer balances that can weigh a single virus of 2×10^{-16} g in weight, making use of the excellent rigidity and flexibility of CNTs.

Because of their excellent mechanical properties, CNT-reinforced composites are expected to have excellent strength, flexibility, anti-fatigue and isotropic properties. For example, carbon fiber sports equipment can easily fracture under low amounts of stress with a tensile strain of only 1%. For MWCNTs, the tensile strain before fracture can be as high as 15%.

(3) Siphon Phenomenon and Its Applications

CNTs with open ends possess a siphon phenomenon, which can be used as a particle absorbent. If highly active particles are adsorbed, CNTs become molecular-scale catalysts, which are in high demand and are widely applied in the oil industry.

CNTs also have excellent hydrogen storage properties, and a hydrogen storage capacity up to 4.2%(wt) was reported based on a large amount of SWCNTs with a diameter of 1.85 nm. These could release 80% of the absorbed hydrogen at ambient pressure [65].

(4) Other Properties and Their Application

CNTs are resistant to acid and alkali, with good high-temperature stabilities. In addition, they can be modified to become soluble, and so can be used in the preparation of composite materials, chemical sensors and artificial muscles. If added to light-emitting polymers, they can improve light-emitting performance.

CNTs are also a good thermal conductive material. However, heat does not transfer from one tube to another even when a bundle of nanotubes are bound together, which means that CNTs can only transfer heat in one dimension.

CNTs can also be used in stealth materials and batteries. For example, helical CNTs absorb light with a higher absorbing capacity than general materials. Therefore, they can be used in stealth weapons. CNTs with a layered structure can also be used as cathodes in lithium batteries.

References

1. Zou ZW (ed) (1999) Composite structures and properties. China Science Press, Beijing (in Chinese)
2. Chou TW (ed) (2000) Comprehensive composite materials, Volume 1: Fiber reinforcements and general theory of composites. Kelly A, Zweben C, Editors-in-Chief. Pergamon Press, Elsevier Science Ltd., Oxford
3. Hearle JWS (ed) (2001) High performance fibers. CRC Press, Woodhead Publishing Ltd., Cambridge
4. Zhang BD, Wu ZM (eds) (1998) Continuous glass fiber processing basics. China Architecture and Building Press, Beijing (in Chinese)

5. Editorial B (1993) Introduction to high technology materials. China Science Press, Beijing (in Chinese)
6. Morgan P (ed) (2005) Carbon fibers and their composites. CRC Press, Taylor & Francis Group, New York
7. Wu RJ (ed) (2000) Composites. Tianjin University Press, Tianjin (in Chinese)
8. Zhao JX (2001) A brief introduction to Nippon graphite fiber corporation, Japan. *Jpn Hi-tech Fiber & Appl* 26(4):28 (in Chinese)
9. Wo XY (2000) Comparison and elemental analysis of the performance of domestic and abroad carbon fiber. *Hi-tech Fiber & Appl* 25(2):30 (in Chinese)
10. Peebles LH, Yanovsky YG, Sirota AG, Bogdanov VV, Levit PM (1998) Mechanical properties of carbon fibers. In: Donnet JB, Wang TK, Peng JCM and Rebouillat S (eds) *Carbon Fibers*, 3rd edn. Marcel Dekker, New York
11. Luo YF (2000) New developments in hi-tech synthetic fibers. *Hi-tech Fiber & Appl* 25(4):1 (in Chinese)
12. Zhang WX (2001) New development of polyacrylonitrile-based carbon fibers. *Hi-tech Fiber & Appl* 26(5):13 (in Chinese)
13. He F, Zhang JG (2000) The rapid development of carbon fiber industry. *Hi-tech Fiber & Appl* 25(4):11 (in Chinese)
14. Zhang HB, Liu HB, Xu ZY (2001) High temperature heat treatment technology prepared PAN-based high modulus carbon fibers. *Hi-tech Fiber & Appl* 26(3):6 (in Chinese)
15. Li SH (1992) Preparation of high strength and high modulus polyacrylonitrile-based carbon fibers. *Carbon Tech* 5:39 (in Chinese)
16. Li RY (1982) Preparation of HS-I type polyacrylonitrile-based carbon fibers. *China Synth Fiber Ind* 2:15 (in Chinese)
17. Beijing University of Chemical Technology (2001) Newsletter: Preparation of polyacrylonitrile fibers via DMSO. *Hi-tech Fiber & Appl* 26(2):48 (in Chinese)
18. Chang WP (1996) Newsletter: Preparation of high modulus of carbon fibers. *New Carbon Mater* 11(11):19 (in Chinese)
19. Yu SF (1992) Composition and structure characterization of raw materials for high-performance pitch-based carbon fibers. *New Carbon Mater* 7(4):25 (in Chinese)
20. Shi Y, Cha QF, Liu L (1995) Melt spinning of Y-shaped pitch-based carbon fiber. *New Carbon Mater* 10(3):33 (in Chinese)
21. Gu W, Pan D (1996) Rayon-based carbon fiber. *New Carbon Mater* 11(3):10 (in Chinese)
22. Li XD, Peng P (1999) Preparation of rayon-based carbon fiber infiltrated with SiC coating. *New Carbon Mater* 14(3):41 (in Chinese)
23. Feng CX, Fan XL, Song YC (1999) Prospect and challenge of high performance fibers in the 21 century. Part I, silicon-based ceramic fibers. *Hi-tech Fiber & Appl* 24(3):8 (in Chinese)
24. Feng CX, Fan XL, Cao F (1999) Prospect and challenge of high performance fibers in the 21 century. Part II, aluminum-based oxide fibers. *Hi-tech Fiber & Appl* 24(6):8 (in Chinese)
25. Song YC, Feng CX, Xue JG (2002) The progress of research on silicon nitride fiber. *Hi-tech Fiber & Appl* 27(2):6 (in Chinese)
26. Bunsell AR, Piant A (2006) A review of the development of three generations of small diameter silicon carbide fibers. *J Mater Sci* 41:823
27. Chu ZY, Feng CX, Song YC, Xiao JY, Li XD, Wang YD (2002) Advances in polymer-derived SiC fibers. *J Inorg Mater* 17(2):193 (in Chinese)
28. Gareis PJ, Mohr PH (1961) Process for depositing beta SiC. US Patent 3011912
29. Shi NL (2000) Preparation of high performance CVD SiC filaments. *Mater Rev* 14(7):53 (in Chinese)
30. Ichikawa H (2006) Development of high performance SiC fibers derived from polycarbosilane using electron beam irradiation curing, a review. *J Ceram Soc Jpn* 114(6):455
31. Chu ZY, Wang L, Song YC, Xu YS, Fu YB (2001) Synthesis and irradiation crosslinking reaction of polysilazane fibers. *Polym Mater Sci & Eng* 17(4):37 (in Chinese)
32. Hasegawa Y, Feng CX, Song YC, Tan ZL (1991) Ceramic fibers from polymer precursor containing Si-O-Ti bonds. *J Mater Sci* 26(13):3657

33. Wang YF, Feng CX, Song YC (1999) Study of the preparation and electric properties of Si-Ti-C-O fibers. *Chin High Technol Lett* 9(5):45 (in Chinese)
34. Yu YX, Tai JH, Tang XY, Guo YD, Tang M, Li XD (2008) Continuous Si-C-O-Al fiber derived from aluminum-containing polycarbosilane precursor. *Compos A* 39:1101
35. Tang Y, Wang J, Li XD, Li WH, Wang H, Xie ZF (2008) Synthesis and characterization of polyborosilazane as novel precursor to SiBNC ceramic. *Acta Chim Sin* 66(11):371 (in Chinese)
36. Tang Y, Wang J, Li XD, Xie ZF, Wang H, Li WH, Wang XZ (2010) Polymer-derived SiBN fiber for high-temperature structural/functional applications. *Chem A Eur J* 22(16):6458
37. Yamamura T, Ishikawa T, Shibuya M (1990) Electromagnetic wave absorbing material. US Patent 5094907
38. Wang YD, Feng CX, Wang J, Song YC, Wang J, Yao M, He YC, Xue JG, Long JF (2001) Preparation of trilobal SiC fibers with radar-absorbing properties. *Acta Mater Compos Sinica* 18(1):42 (in Chinese)
39. Feng CX, Liu J, Song YC (2001) Preparation of SiC fibers with low electrical resistance by simple mixing. *J Funct Mater* 32(4):269 (in Chinese)
40. Wang J, Song YC, Feng CX (1997) Preparation of a mixed SiC fiber for microwave absorbent. *Aerosp Mater & Technol* 27(4):61 (in Chinese)
41. Wang J, Feng CX, Song YC (1996) Preparation of SiC Ceramic fiber mixed with nano Ni particle. *Chin High Technol Lett* 6(11):33 (in Chinese)
42. Ouyang GE, Liu XW (1994) Preparation of SiC-C fibers. *J Funct Mater* 25(4):300 (in Chinese)
43. Re W, Zhang QW (1991) Approaches to improve mechanical properties of BN fibers. *Chin High Technol Lett* 1(10):3 (in Chinese)
44. Cornu D, Bernard S, Duperrier S, Toury B, Miele P (2005) Alkylaminoborazine-based precursors for the preparation of BN fibers by the polymer-derived ceramics (PDCs) route. *J Eur Ceram Soc* 25(2-3):111
45. Kotek R (2008) Recent advances in polymer fibers. *Polym Rev* 48(2):221
46. Wo DZ (ed) (2000) *Comprehensive Composites*. China Science Press, Beijing (in Chinese)
47. Huang XC, Zhang JC (2000) The present and the development trend of the high-strength & high-modulus aramid fibers of Russia. *Hi-tech Fiber & Appl* 25(1):14 (in Chinese)
48. Luo YF (2002) Look around the recent R&D in world's high-tech fibers. *Hi-tech Fiber & Appl* 27(3):7 (in Chinese)
49. Afshari M, Sikkema DJ, Lee K, Bogle M (2008) High performance fibers based on rigid and flexible polymers. *Polym Rev* 48(2):230
50. Wang DR (2001) Application and synthesize technics of transform PBO. *Hi-tech Fiber & Appl* 26(6):27 (in Chinese)
51. Li ZJ (2000) The high-powered UHMWPE fiber and its applications foreground in ground radome. *Hi-tech Fiber & Appl* 25(4):24 (in Chinese)
52. Zhou ZW, Hu SC (2002) Characteristics and industrialization prospects of whiskers. *Adv Mater Ind* 6:71 (in Chinese)
53. Bi G, Wang HW, Wu RJ (1999) Ceramic whiskers and their applications in composites. *Mater Rev* 5:56 (in Chinese)
54. Xu H, Guo MX (1994) The property of SiC whisker. *Acta Mater Compos Sinica* 1:15 (in Chinese)
55. Xu CX, Sun XW, Dong ZL, Zhu GP, Cui YP (2006) ZnO hexagram whiskers. *Appl Phys Lett* 88(9):093101
56. Zhang ZC, Zhou ZW (2001) Application of ZnO whiskers in functional rubbers. *J Funct Mater* 32(4):1263 (in Chinese)
57. Huang JT, Zhang BZ, Zhu JG, Yang B, Xu SJ (1988) Vapor growth TiN whiskers. *Chin J Mater Res* 2(1):39 (in Chinese)
58. Zhao JX (2003) Carbon nanofiber and its applications. *Hi-tech Fiber & Appl* 28(2):7 (in Chinese)
59. Iijima S (1991) Helical microtubules of graphitic carbon. *Nature* 354:56

60. Kroto HW, Heath JR, O'Brien SC, Curl RF, Smalley RE (1985) C₆₀: buckminsterfullerene. *Nature* 318:162
61. Novoselov KS, Geim AK, Morozov SV, Jiang D, Zhang Y, Dubonos SV, Grigorieva IV, Firsov AA (2004) Electric field effect in atomically thin carbon films. *Science* 306:666
62. Meyyappan M (ed) (2004) Carbon nanotubes: science and applications. CRC Press, Boca Raton, FL
63. Cui C, Li HY (2002) Research actualities of preparing carbon nanotubes. *Chem Ind Eng* 19 (1):59 (in Chinese)
64. Pan ZW, Xie SS, Chang BH, Wang CY, Lu L, Liu W, Zhou WY, Li WZ, Qian LX (1998) Very long carbon nanotubes. *Nature* 394:631
65. Liu C, Fan YY, Liu M, Cong HT, Cheng HM, Dresselhaus MS (1999) Hydrogen storage in single-walled carbon nanotubes at room temperature. *Science* 286:1127

Chapter 3

Polymer Matrix Materials

Xiangbao Chen, Jianwen Bao, Chao Shen, Baoyan Zhang, Yahong Xu
and Zhen Shen

Advanced resin matrix composites are referred as a class of composites constructed by matrix resins and continuous fiber reinforcements. Advanced resin matrix composites can provide a series of extraordinary advantages including high specific strength and stiffness, designable properties, fatigue and corrosion resistance as well as special electric–magnetic performance. Compared with traditional steel and aluminum alloys, the density of composites is only about 1/5 that of steels and 1/2 that of aluminum. Therefore, the specific strength and modulus of these composites are obviously higher than those of steel and aluminum alloys. Using composites to replace aluminum and other metal materials can significantly decrease structure weights [1].

In addition to superior performance in processing technologies, advanced resin matrix composites can provide integrated one-step processing even for complex structural shapes and for large size parts. They offer many benefits in terms of significantly reducing the number of components in structural parts, eliminating too many joints, greatly decreasing stress concentrations, saving processing steps and machining work, thus reducing raw material quantities and costs. Because of their unique advantages, advanced resin matrix composites are applied in the aerospace, sporting goods and other industries. They have become a class of important composite materials with fast-growing and widespread applications [2].

The mechanical and physical properties of advanced resin matrix composites depend on the types and content of fibers, fiber orientations, laminating sequences and numbers and are also closely related to the resin matrixes used. The maximum service temperature, environmental effect resistance, mechanical and electric performance will largely depend on the resin matrix used.

X. Chen (✉) · J. Bao · C. Shen · B. Zhang · Y. Xu
Beijing Institute of Aeronautical Materials, Beijing 100095, China
e-mail: Xiangbao.chen@biam.ac.cn

Z. Shen
China Institute of Aircraft Strength, Xi'an, Shaanxi 710065, China

In this chapter, we introduce the types and features as well as the suitable ranges and applicable technologies of the resin matrix materials selected for advanced resin matrix composites. Some achievements from high-performance resin matrix studies and applications in China will also be discussed.

3.1 The Performance of Composite Resin Matrixes

When used for composite matrixes, high-performance resin systems must satisfy the requirements of practical engineering applications including processing ability, thermal, physical and mechanical properties. The processing performance of resin matrixes will include their dissolution in solvents, melting viscosity (flow ability) and change in viscosity behavior (processing windows). The thermal resistance includes the glass transition temperature (T_g), thermal-oxidant stability, thermal decomposition temperature, flame-retardant performance and thermal deformation temperature, which can dominate the composite service temperature ranges. The discussion about the mechanical properties of resin matrixes will cover their property specifications under service conditions such as tensile strength, compression, bending properties, impact resistance and fracture toughness. Resin matrixes should have very good electric properties and chemical resistance including solvent resistance, self-lubrication and anti-corrosion properties. For resins to be used in optical fields, their refractive index, transparency, color, weather and optical-chemical stabilities should be taken into account [3, 4].

3.1.1 Thermal Resistances

(1) Glass transition temperature

The glass transition is a secondary transition in which polymers will transit from a glass state into an elastic state. At temperatures lower than the glass transition temperature, polymers will be subject to a series of changes including sudden changes in specific heat and capacity, movement of molecular chain segments and the fast growth of linear expansion coefficients. In polymer chains, the existence of strong polar groups will increase the interaction forces between molecules, which further increases chain densities, and as a result, polar polymers will possess a higher T_g . In polymer main chains and side groups, huge rigid groups can inhibit chain segment free rotation, which is useful for an increase in T_g , while flexible side groups can increase the distance between chains and allow them to move more easily, resulting in a decrease in T_g . Therefore, to increase the T_g and the thermal resistance the resin matrixes of advanced composites will normally be designed to contain a large quantity of chains with huge rigid groups.

(2) Thermal–oxidant stability

To meet the requirements of aerospace applications, high-temperature-resistant resin matrixes that can tolerate long-term temperature exposure, even as high as 300 °C, have been developed. Dynamic thermal gravimetric analysis (TGA) can be used to determine the short-term thermal resistance and the thermal–oxidant stability. The long-term thermal–oxidant stability of resin matrixes should be determined by a high-temperature long-term aging test. Thermal–oxidant stability depends on the bond energy between the atoms that constitute the molecular chains. Aromatic and heterocyclic structures like phenyl and nitrogen hetero-naphthalenes have a high bond energy and can provide high thermal–oxidant stability.

The most stable polymers are ladder polymers composed of heterocyclic and aromatic conjugate structures. The most stable flexible chain groups are aliphatic compounds in which all the hydrogens are substituted by fluorine and phenyl. –O–, –S–, –CONH– and –CO– can also give good thermal–oxidant stability; –SO₂–, –NH–, hydroxyl and chloride groups impart lower thermal–oxidant stability. The thermal–oxidant stability of xylene-containing polymers increases as follows: $p > m > o$. Generally, cross-linking can improve polymer thermal–oxidant stability.

3.1.2 Coefficient of Thermal Expansion (CTE)

The combination of two materials with different CTE will cause interface stress when the temperature changes. If this difference in CTE is large, the interfacial bond can be damaged. Composites are composed of resins and reinforcing fibers. Stress can be generated at the resin and fiber interface as the temperature changes, possibly resulting in delamination by severe stresses. Adhered structures are also easily damaged at the adhering interface. Therefore, for high-performance resin matrixes, CTE matching of reinforcing materials should be seriously taken into account.

CTE can be determined by thermal mechanical analysis (TMA). In Table 3.1, some commonly used composite resin matrixes and reinforcing materials are given with their CTE. In general, inorganic materials have a lower CTE than polymeric materials. To decrease the CTE of polymers, the following methods can be adopted:

- (1) Introduce ordered structures such as crystals into the polymers.
- (2) Use huge rigid structures like aromatic heterocyclic structures to reduce polymer molecular segment movement.
- (3) Increase cross-linking density.

Table 3.1 CTE of selected resins and reinforcing materials

Materials	CTE/ $\times 10^{-6} \text{ K}^{-1}$	Materials	CTE/ $\times 10^{-6} \text{ K}^{-1}$
Polyester	70–101	Phenolic	16–25
Polysulfone	59–86	Carbon fiber	3.2–12.1
Epoxy	59	Glass fiber	8.46
Polyimide	45–50	Quartz fiber	0.31

3.1.3 Mechanical Properties

The mechanical properties of high-performance resin matrixes are mainly characterized by tensile strength and modulus, fracture elongation, bending strength and modulus, impact strength and surface hardness. These properties will change as the temperature, processing and cure conditions change. Compared with other structural materials, an important property of a high-performance resin matrix is its viscoelasticity, that is, its behavior is dependent on applied temperature and time. Because of the existence of viscoelasticity, polymeric materials, especially thermoplastic resin matrixes, will be subject to creep and stress relaxation during working processes.

High-performance resin matrixes with a rigid backbone will have a macromolecular main chain that contains a large amount of aromatic heterocyclic structures, and some conjugated double bonds will be arranged in an ordered ladder structure, and the molecules will have good regularity or a high cross-linking density. Therefore, high-performance resin matrixes generally have a high modulus, but their fracture elongation and toughness are relatively lower. Table 3.2 lists some high-performance resin matrixes and their mechanical properties.

Table 3.2 Selected high-performance resins and their mechanical properties

Resin matrix	Tensile strength/MPa	Bending strength/MPa	Bending modulus/GPa
Polyetheretherketone (PEEK)	99	145	3.8
Polyetherimide (PEI)	107	148	3.37
Thermoplastic polyimide (PI(TP))	87	134	3.16
Bismaleimide (BMI)	84	45	3.3
Thermosetting polyimide (PI(TS))	75	40	3.5
Epoxy	85	50	3.3

Improving the toughness of high-performance resin matrixes can be carried out by two ways:

- (1) Introduction of a flexible chain segment into main chain structures or reducing the cross-linking density, but this may result in a decrease in resin thermal resistance.
- (2) Introduction of a secondary phase into the resin matrix.

3.1.4 Electric Properties

High-performance resins are increasingly used in the electronics industry as insulating materials and wave transparent materials. Therefore, understanding the electric properties of high-performance resins is of great significance.

For engineering materials, the electric properties of interest are the dielectric properties and the electric breakdown intensity. The dielectric constant of materials is the storage of energy in a unit material volume under a unit of electric field intensity. The magnitude of the dielectric constant is related to the extent of dielectric polarization (electronic polarization, atom polarization and orientation polarization).

For polymeric materials used in insulating applications, their insulating performance should be considered in addition to their satisfied thermal resistance and mechanical properties. For example, when the heat generated by dielectric loss under a certain electric field exceeds the material's dispersed heat, local overheating will be induced and subsequently cause a breakdown in materials. The deformation of polymers under stress can also affect the breakdown behavior causing a decrease in the breakdown intensity. This kind of breakdown behavior, under these circumstances, is referred to as electric–mechanical breakdown. Table 3.3 lists some polymers and their electric properties [5].

Apart from the physical, mechanical and electrical properties in high-performance resin development, other important issues should be taken into account such as the feasibility of processing technologies, stable bulk production and costs.

Table 3.3 Selected polymers and their electric properties

Resin matrix	Electric breakdown intensity/V·mil ⁻¹	Dielectric constant (60 Hz)	Dielectric loss tangent (60 Hz)
Epoxy	400	4.02–4.79	0.005–0.038
Nylon 6	385	4.0–5.3	0.014–0.06
Polyester	300–400	2.8–4.4	0.003–0.04
Cyanate acid ester	390	2.7–3.2	0.001–0.005
BMI	400	4.0–4.8	0.004–0.035
Polyethylene	480	2.3	<0.0005

Note 1 mil = 25.3 μm

3.2 Characterization of Composite Resin Matrixes

3.2.1 *Characterization of Curing Behavior in Composite Resin Matrixes*

The curing behavior of composite resin matrixes is the basis for establishing composite curing processing techniques. These curing behaviors involve the cure reaction temperature parameters, reaction enthalpy, gel time and viscosity–temperature curves.

Differential scanning calorimetry (DSC) and differential thermal analysis (DTA) are most commonly used to characterize the curing behavior of resin matrixes. They can measure and monitor the reaction heat and temperature in the curing reactions of the composite resin matrixes and can also characterize resin decomposition and oxidant degradation. For composite resin matrixes, DSC and DTA primarily determine reaction parameters such as curing reaction onset and peak temperatures, reaction enthalpy and peak shape. Both DSC and DTA can be used for isothermal and dynamic (constant heating) operation models.

For the heating and curing processes, composite resin matrixes will undergo state changes from solid to flow states because of the application of heat. A change back to the solid state will result from resin curing, and this will cause significant changes to the resin's dielectric properties. Dynamic dielectric thermal analysis (DETA) can be used to characterize the curing behavior by allowing the determination of cure temperatures.

For reactions with mass changes, TGA can be used to study the curing processes. For example, the phenolic resin curing reaction depends upon the imidization of polyimide resins.

Gel time is an important parameter for the determination of the pressure application point in composite curing processes. The commonly used method is referred to as “knife” testing, that is, heating a gel plate to a predetermined temperature, adding some resin and recording time while stirring the resins with a probe tool. Initially, for a small molecular mass resin the probe does not detect the filament resin; however, when the resin reacts and the molecular mass becomes large enough, the probe can detect the filament resin. The operation continues until no filament resin is detected, and at this point, the resin has been transformed from a linear molecular structure to a 3D network structure and the resin has thus reached the gel point.

The curing degree is referred to as the cure reaction extent in resin matrixes. It is the percentage of functional groups that took part in the curing reaction versus the total number of functional groups that should have taken part in the curing reaction. Theoretically, all methods that can characterize group concentration can be used to determine the resin curing degree. The most commonly used methods are the chemical analysis method, Fourier transform infrared spectrometry and thermal analysis.

In the chemical analysis method, the functional group concentration in the resins is determined before and after resin curing and the curing degree can thus be determined. Chemical analysis is limited to those resin systems that can be dissolved in a solvent during the early curing stage or after full curing.

In the FTIR method, the resin curing degree is determined by the relative intensity changes in the characteristic peaks of the reacting groups in the resin system before and after curing. For this method, two basic requirements have to be met: One is that the characteristic peaks of the reacting groups should not be influenced by other group characteristic peaks and the other is that there should be a proper and stable reference standard peak on the resin's infrared spectrum. The standard peak should be independent of other group characteristic peaks. For example, in epoxy resin curing the epoxy group's characteristic peak is at 915 cm^{-1} and the benzene ring peak is at 1500 cm^{-1} ; this peak can be used as the reference standard peak. These two peaks can be represented by S_{915} and S_{1500} , and S_{915}/S_{1500} is thus the relative intensity of the epoxy group's peak. Before and after curing, the epoxy group will give the relative intensities of $(S_{915}/S_{1500})_0$ and $(S_{915}/S_{1500})_t$, and the resin curing degree α will be:

$$\alpha = 1 - (S_{915}/S_{1500})_t / (S_{915}/S_{1500})_0$$

Since reaction heat will be released during the resin curing process and the curing reaction heat is proportional to the resin curing degree, the curing degree can be determined by thermal analysis to also give the residual heat of the cured resin:

$$\alpha = \Delta H_t / \Delta H_0$$

where ΔH_0 is the total released reaction heat and ΔH_t is the reaction heat over a certain curing time.

3.2.2 *Characterization of Physical Properties in Composite Resin Matrixes*

The physical properties of resin matrixes will dramatically influence the final performance of the composites. The physical properties of resin matrixes mainly include the resin melting point, softening point, rheological behavior, CTE, water absorption and volatile content.

For crystallized resin monomers such as crystal BMI monomers and cyanate acid ester resin, the melting point can be determined by standard determination methods for organic polymers such as the capillary method and the microscopy melting point method (heat stage microscopy).

The basic principle of the capillary method is that a little resin is added to a 40–50-cm-long capillary with one end closed. After sealing and placing into a transparent heating medium (petroleum ether or paraffin wax), heat is applied at 2 °C/min and the temperature is observed and recorded where the sample begins to become to transparent liquid. The temperature at which a fully transparent liquid is realized is referred to as the resin melting point.

The microscope melting method is similar to the capillary method, but the resin sample is placed on a microscope thermal stage to observe and record the resin melting history. This method is suitable for organic small molecules and also for polymer melting point determinations. Detailed test procedures can be found in ASTM D2117 “the standard testing method for half-crystallized polymer melting point determination by thermal stage microscopy.”

Resin matrixes and thermoplastic (crystallized or half-crystallized) polymers need to absorb ambient heat upon melting. Therefore, thermal analysis (DSC and DTA) can be used to determine the melting points of resin monomers and thermoplastic resins. In these analyses, resin melting points and melting heat can be determined. The related standard method is ASTM E794.

Softening points are also an important physical parameter of resins with non-crystallized solids or half-solid states. These types of resins include solid epoxy resins and phenolic resins. National standard GB/T 12007.6-1989 specifies the “ring-and-ball” method to determine resin soft points (especially for epoxy resins) as follows: evaluate the resins in a horizontal copper ring under the action of a steel ball in a water bath or in a glycol alcohol bath heated at a specified rate and determine the temperature where the steel ball fell by 25 mm.

Composite processing performance basically depends on the rheological behavior of resin matrixes. In fact, resin rheological behavior will include solid and fluid rheological behavior, but only fluid rheological behavior can directly influence the composite processing techniques. The parameters characterizing resin rheological behavior include shear viscosity, tensile viscosity and melting index. For composite resin matrixes, the rheological behavior is essentially characterized by resin shear viscosity. Shear viscosity is determined by capillary, co-axis cylinder, cone plate and fall ball viscometers.

Dynamic analysis test methods (DMTA, TBA) can be also used to characterize resin rheological behavior, resin test frequency, temperature and curing conditions. Data are collected from their corresponding dynamic spectra. Based on the dynamic spectra parameters such as the storage modulus, loss modulus, dielectric loss angle and complex viscosity can be directly determined, and these data can be used for resin morphological change analysis during the curing processes.

In composite resin matrix curing processes, electric performance parameters such as dielectric constants and loss angles will change as the resin viscosity and morphology change. Therefore, DETA can also be used to characterize resin viscosity and physical state changes by characterizing dielectric performance changes with different test frequencies, temperatures and times.

The volatile component of composite resin matrixes can influence the void content in composite structures. The volatile component can be determined by

thermal gravity analysis (TGA) or by referring to the ASTM standard test methods. In ASTM D4526 “The testing method to determine the volatile content in polymers by gas chromatography analysis,” standard methods to qualitatively and quantitatively determine the volatile in thermoplastic polymers are given. ASTM D3530 “The determination of volatile content in carbon fiber prepregs” can be used to determine the volatile component in most thermosetting resin matrixes.

The water absorption rate in composite resin matrixes will dominate the water absorption rate in composites and directly influence the hot/wet resistance, insulating performance, dielectric loss and dimension stability. Water absorption in resin matrixes depends on the resins and on the specimen shape, specific surface area and machining procedures. The specimen for the water absorption experiment can be prepared by molding or machining. The specimen surface should be flattened, made smooth and cleaned to remove defects, and for molding or machining preparation, at least three specimens should be prepared for each test. Before water absorption testing, the specimen should be subjected to equal-weighting treatment to guarantee test reliability.

The water absorption test conditions for different materials can be determined based on the required service, for example, for high-temperature curing and high-performance resin matrixes, general hot/wet test conditions will be boiling water ($97\text{ }^{\circ}\text{C} \pm 2\text{ }^{\circ}\text{C}$) for 48 h. For medium-temperature curing systems, the general test conditions will be water immersion or R.H. environmental exposure. Detailed test methods and conditions can be found in the standard GB/T 1034-1998.

The resin matrix coefficient of thermal expansion (CTE) can be determined by measuring specimen length changes under a specific temperature difference and calculating the changes in length before and after. Detailed testing, calculation methods and equipment principles can be found in GB/T 1036-1989.

3.2.3 Characterization of Resin Thermal Resistance and Stabilities

(1) Characterization of resin thermal resistance

The thermal resistance of composite resin matrixes is usually characterized by the glass transition temperature (T_g) and the thermal deformation temperature. Theoretically, all the obvious changes or the sudden physical property changes taking place during the glass transition processes can be used to measure the glass transition temperature of polymer materials. Currently, the instruments or devices used for polymer glass transition temperature measurement rely on physical property changes in polymers including volume changes, thermal-dynamic property changes, mechanical changes and electric-magnetic property changes.

A typical test method to measure the polymer glass transition temperature on the basis of volume changes is the dilatometer method (including the volume and linear dilatometer), which is a classic test method for the glass transition temperature. Other parameters related to volume changes such as density, refractory index, diffusion coefficient and thermal conductivity can also be used to measure the glass transition temperature.

In glass transition processes, because of changes in molecular movement, resin matrixes are subjected to exothermal or endothermal phenomena. DSC and DTA are used for T_g measurements by quantifying the thermal–dynamic performance of polymers. In these methods, the test procedure is simple and samples are easily prepared. However, since glass transition is a secondary transition in polymers, the enthalpy change during the transition is not very clear, and the glass transition enthalpy is easily shielded by other physical or chemical reaction enthalpies. Additionally, the curve baseline is not flat and no plateau is observed resulting in a difficult glass transition temperature determination. Thermal analysis will encounter more difficulties in thermosetting resin glass transition temperature measurements. The heating rates will largely influence the test results.

For mechanical performance, especially thermal–dynamic performance, changing the temperature is one of the principal methods to measure the polymer glass transition temperature. Dynamic thermal mechanical analysis (DTMA) and thermal braiding analysis (TBA) are currently the most used thermodynamic test methods. In DTMA, the generated thermodynamic temperature spectra will contain three curves (Fig. 3.1): the storage modulus (E'), loss modulus (E'') and loss tangent ($\tan \delta$). Based on polymer glass transition theory, both E'' and $\tan \delta$ can have maximum values and the maximum value will be related to T_g . In general, the temperature of E'' will lower than that of $\tan \delta$. The initial lower temperature of the storage modulus (E') has been used to evaluate the thermal resistance of polymers in previous studies, and it is believed that using this temperature to evaluate the thermal resistance is a more

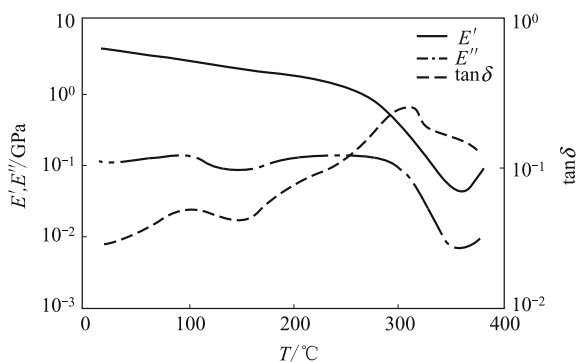


Fig. 3.1 Thermodynamic/temperature curves of polymers

reasonable approach to determining whether polymer materials can be used as structural materials. The initial decrease results in a temperature of the storage modulus (E') that is lower than the temperature at which the maximum value of E'' was found. The heating rate, test frequencies and stress level will directly affect the DTMA test results. Additionally, the specimen sizes and the thermal conductivities of the test materials will also influence the DTMA test results. Because polymer molecular movement shows multiple behaviors, a study into the α transition (T_g) in DTMA can also be extended to characterize the β , γ and δ transitions. DTMA can also be used to study the damping performance of materials (including polymers, ceramics and metals) for the development of various damping materials.

The static mechanical performance of resin matrixes will also show obvious changes in the glass transition zones. Using TMA to measure resin matrix deformation or relative deformation as a function of temperature is another important method for T_g characterization. The factors that can affect TMA test results include the heating rate and specimen sizes. The test instrument is simple and can be self-made. The test procedures are simple; however, for highly cross-linked or highly rigid thermosetting resins, the deformation is not very clear in the glass transition zones. Therefore, their T_g is often not accurate and the generated test results may possibly give the thermal deformation temperature.

Resin matrixes will apparently undergo changes in electric conductivity and dielectric performance in the glass transition zones, which can be used to measure the glass transition temperature. DETA is a test method that exploits the correlation between dielectric constant, changes in dielectric loss and temperature to give a resin's T_g . Nuclear magnet resonance (NMR) will obviously change the spectral line width in polymer glass transition zones, which is used to measure the resin matrix T_g value.

Several thermal resistance test methods are used in industry such as Martin's thermal resistance temperature, the thermal deformation temperature and the Vicat thermal resistance temperature. These are unified standard test methods for the measurement and evaluation of the maximum service temperature of resin matrixes, which do not provide definite physical significance such as T_g does.

(2) Thermal stability

TGA is the main technique used to evaluate resin matrix thermal stability. TGA is normally used to characterize the relationship between resin matrix weight change and temperature, to monitor resin matrix thermal decomposition processes, to study the resin matrix thermal decomposition mechanism and to evaluate resin matrix ultimate service temperature and life.

TGA provides the resin's initial decomposition temperature and the weight loss temperature. Other parameters include the resin thermal decomposition rate, the extrapolated initial weight loss temperature (cross between the maximum slope point tangent line and the baseline), the terminated weight loss temperature or

the extrapolated terminated weight loss temperature, the turning point temperature or the maximum weight loss rate temperature and preset weight loss percentage temperatures (usually preset to 3, 5, 10, 20 and 50%). The heating rate and the atmosphere in the oven will be the main factors that can affect TGA test results.

3.2.4 Characterization of Composite Resin Matrix Electric Performance

Polymer electric performance is usually characterized by its dielectric constant, dielectric loss angle tangent, specific volume resistance, specific surface resistance, breakdown voltage and breakdown intensity. For composite resin matrixes, the important electric performance parameters include the dielectric constant, dielectric loss angle tangent and breakdown intensity.

The dielectric constant and the dielectric loss angle tangent are significant in wave penetrating composites. The related measurements can be taken as stipulated in the national standard GB/T 1409-1988. The dielectric constant and dielectric loss angle tangent test results can be influenced by test frequencies, temperature, wetness and electric field intensity.

The electric breakdown intensity will become an important standard for the use of composite resin matrixes in insulation applications. This characterization can be carried out according to the national standard GB/T 1408.1-1999. The measurement of polymer electric resistance parameters can be taken according to the national standard GB/T 1410-1989.

3.2.5 Characterization of Composite Resin Matrix Mechanical Performance

(1) Preparation of a resin matrix specimen for mechanical testing

- (1) Direct casting: direct casting of the resin prepared according to the resin formulation and processing specifications into specimen molds, and curing by following the standard curing procedure.
- (2) Plate casting and machining: direct casting of the resin prepared according to the resin formulation and processing specifications into plate molds with a specific thickness, and curing by following the standard curing procedure. The cast plates are cut and machined into a specimen according to the test method requirements.
- (3) Specimen requirement: Smooth surface, no defects like air bubbles, flaws or impurities.

(2) **Resin matrix tensile testing**

- (1) Large specimen test methods: A cast resin tensile test specimen is shown in Fig. 3.2.

In the test operation, the test load application rate is 10 ± 0.5 mm/min for tensile strength determinations and 2 mm/min or handle operation for tensile modulus determinations.

Standard GB/T 2568-1995 is a test method to determine resin casting tensile properties.

- (2) Small specimen test methods: To simplify specimen preparation and to save raw materials, small specimens can be used to determine the tensile properties of resin matrixes.

Specimen requirement: Since all composite resin matrixes are hard thermoplastic or thermosetting plastics, small specimens for their tensile property determinations are selected as the model I specimen, as specified in GB/T 16421-1996; typical specimen dimensions are shown in Fig. 3.3 and Table 3.4.

(3) **Resin matrix compression test**

The typical shape and dimensions of the resin matrix compression test specimen are shown in Fig. 3.4.

The compression strength testing requires a specimen of height $H = (25 \pm 0.5)$ mm, and the compression modulus testing requires a specimen of height $H = 40-60$ mm. The specimen is a square section either of column type or of

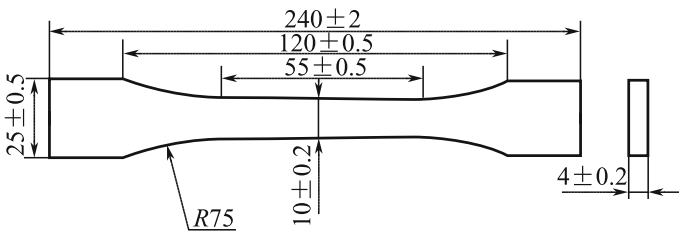


Fig. 3.2 Cast resin tensile test specimen

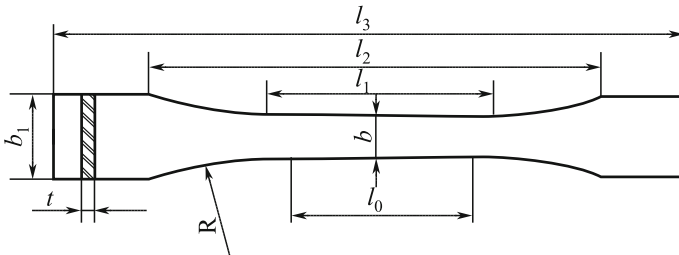


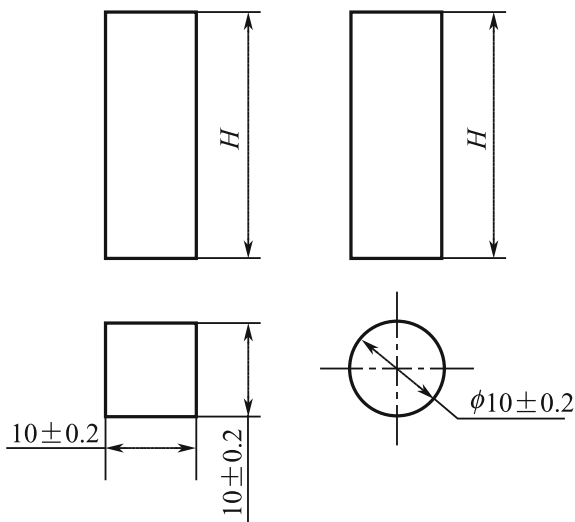
Fig. 3.3 Small specimens for the cast resin tensile test

Table 3.4 Small specimen requirements for the cast resin tensile test/mm

Symbol	Dimensions	Specimen	
		I 1	I 2
l_3	Minimum total length	75	30
b_1	End width	10 ± 0.5	4 ± 0.2
l_1	Narrow parallel section length	30 ± 0.5	12 ± 0.5
b	Narrow parallel section width	5 ± 0.5	2 ± 0.2
R	Minimum radius	30	12
l_0	Distance between metric lines	25 ± 0.5	10 ± 0.2
l_2	Distance between clamps	58 ± 2	23 ± 2
t	Minimum thickness	2	2

Standard: GB/T 16421-1996 Small specimen test method for plastic tensile properties

Fig. 3.4 Shape and dimensions of the resin matrix compression testing specimen



cylinder type. The top and bottom end surfaces need to be parallel and vertical to the axes, and the non-parallel dimension of the end surface should be less than 0.04 mm. Standard: GB/T 2569-1995 Compression testing method for cast resins.

(4) **Resin matrix shear test (open-hole method)**

Principle: Use a cylinder hole puncher and apply a compression-type shear load onto the specimen to cause shear deformation or failure. This way the shear strength of the thermoplastic or the thermosetting plastics can be determined. Requirements for the resin matrix shear testing specimen are given as follows:

- (1) Uniform thickness, smooth and clean surface, no machining damage or impurities.

- (2) Specimen is either a square plate with a side length of 50 mm or a circular plate with a diameter of 50 mm. The thickness is 1.0–1.25 mm and the central hole diameter is 11 mm. The standard specimen will be 3–4 mm thick, as shown in Fig. 3.5.
- (3) Specimen preparation.

Injection molding, press molding, extrusion or machining can be used to prepare the specimen, but the test results obtained using different methods cannot be compared with each other.

Standard: GB/T 15598-1995 The shear test method for plastics.

(5) **Resin matrix bending test**

The specimen for the resin matrix bending test is a rectangular column with the dimensions shown in Fig. 3.6.

Test method: Three-point bending with a span of 100 mm, the loading head radius of 5 ± 0.1 mm and the specimen support top half-sphere radius of 5 ± 0.2 mm.

Standard: GB/T 2570-1995 The bending test method for casting resins.

(6) **Resin matrix impact testing**

Principle: Use a simple support beam pendulum impact tester to measure the resin matrix impact strength and to evaluate the resin matrix toughness.

Specimen requirement: The specimen should include a notched and an un-notched impact specimen. For thermoplastic or tougher thermosetting resins, the notched specimen will be used while the un-notched specimen should be used for lower toughness thermosetting resins. The specimen dimension requirements are shown in Fig. 3.7.

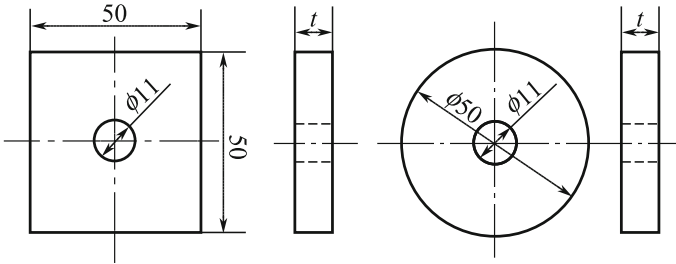


Fig. 3.5 Shear test specimen

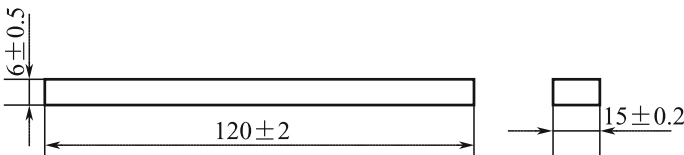


Fig. 3.6 The bending test specimen

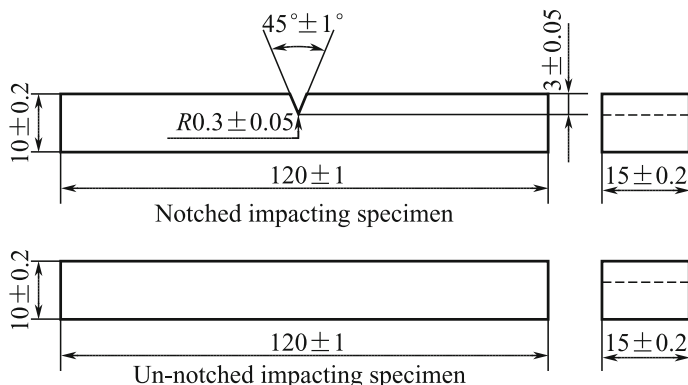


Fig. 3.7 The casting resin impact test specimen

The simple support beam span is 70 mm when the pendulum impacts the center of the specimen and the impact speed should be 2.9 m/s. For notched impacting testing, when failure occurs in non-notched area, the test results are not valid, and a compensation test is necessary. For an un-notched specimen, when fracture occurs beyond 1/3 of the span from the central line, the testing results are not acceptable, and a compensation test is needed. Standard: GB/T 2571-1995 The impact test method for casting resins.

3.3 High-Performance Phenolic Resin Matrixes

Phenolic resins are prepared by condensing phenyl and aldehyde compounds. Among them, the most important phenolic resins are condensed phenols and methyl aldehyde. Among the condensed plastics, phenolic base plastics are the most widely applied and produced in the highest volume.

Phenolic resins are the earliest synthesized polymers [6]. In 1872, A. Bayer first discovered that phenol and aldehyde can interact and generate a resin-like product under acid catalysis. In 1910, Bachland submitted a patent on phenolic curing by “applied heat and pressure,” successfully establishing prepolymer curing technology. This is condensation under “applied heat and pressure.” He further pointed out that the thermoplastic characteristics of phenolic resins will depend on the ratio of phenyl to aldehyde, as well as the catalyst. He also indicated that wood powder and other fillers can improve resin brittleness and thus industrial production and other applications were realized. In 1911, Aylesworth discovered that phenolic resins could be cured by adding hex-functional tetramine. In 1913, a German chemist K. Albert discovered a manufacturing method for oil-soluble phenolic resins, which advanced synthetic resin coating industrial applications.

It has been more than 80 years since the initial use of phenolic resins and their plastics as raw materials. They are abundant, are of low cost and have good performance that meets the requirements of hi-tech fields such as the aerospace, electronics and automobile industries. Much innovative work has been carried out by researchers and engineers to exploit the potential and increase the performance of phenolic resins. Many new materials have been developed. In this chapter, modern achievements in phenolic resins will be discussed.

3.3.1 The Synthesis of Phenolic Resins

3.3.1.1 Linear Phenolic Resins

The synthesis of phenolic resins should be carried out at pH values less than 3.0. Phenolic resins are prepared by the condensation of methyl aldehyde and trifunctional (phenol, resorcin) or difunctional (orthocresol, paracresol, 2,3-dimethyl phenol, etc.) phenols. For trifunctional phenols, the quantity of phenol must be in excess (mol ratio of phenol to aldehyde of 6:5 or 7:6) as less phenol could result in thermosetting resins. An increase in phenol could decrease the relative molecular weight of resins, as shown in Fig. 3.8. The linear phenolic resins prepared by acid catalysis generally have a number average molecular weight of 500 with five phenol rings in the molecules. This is a mixture containing variable and dispersed compositions, as given in Table 3.5.

Fig. 3.8 Correlation of relative molar mass to raw materials in linear phenolic resins

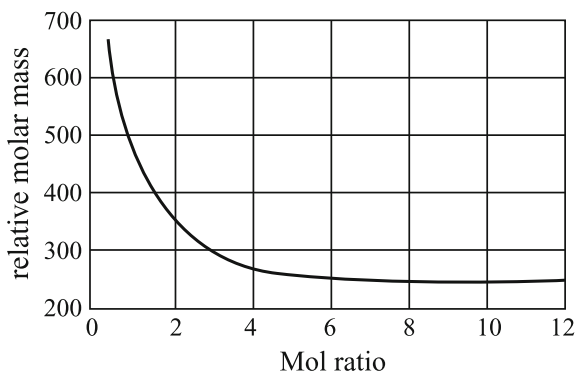


Table 3.5 Resin performance with different relative molar mass

Compositions	1	2	3	4	5
Mass/g	10.7	37.5	16.4	19.5	116.0
Molar weight	210	414	648	870	1270
Melting point/ $^{\circ}$ C	50–70	71–125	96–125	110–140	119–150
Solubility (30% alcohol)/%		3.27	6.12	7.83	9.8

Because unreacted species are present in the phenol core, thermosetting resins could result upon methyl aldehyde or hexamethylenetetramine reactions and can further condense into infusible and insoluble bulk products.

3.3.1.2 Thermosetting Resins

Thermosetting phenolic resins are produced by the condensation of phenol and methyl aldehyde (overloaded) under alkali or acid media, and they are referred to as fusible thermosetting resins [7]. For condensations in alkali medium, the mol ratio of phenol to aldehyde is usually 6:7 (pH = 8–11). If the amount of methyl aldehyde is increased, hydroxymethyls will be present in the resin systems. Therefore, thermosetting phenolic resins can self-heat to form infusible and insoluble cured products.

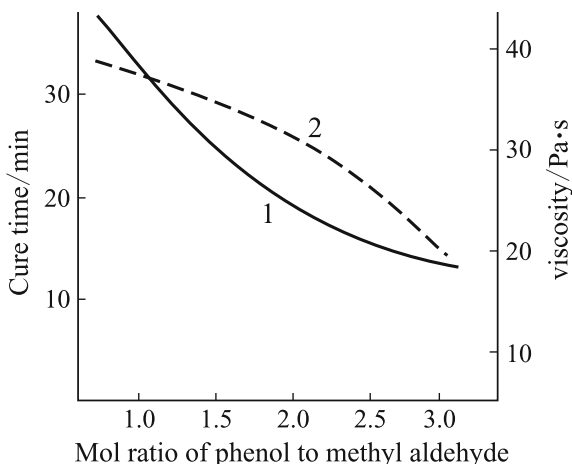
In addition, the hydroxyphenol produced by the additive reaction between phenol and aldehyde in stable alkali medium has been found to be stable. Therefore, 2-hydroxy methyl phenol or 3-hydroxy methyl phenol can be obtained using any mol ratio, as given in Table 3.6. By increasing the reaction temperature or extending the reaction time, they can be further condensed into solid resins; even with insufficient aldehyde, they can produce thermosetting resins.

At this point, a part of the phenol will be dissolved in the resin and exist in “free phenol” states. Under alkali catalysis, it will only be possible to form thermosetting resins, which is independent of the phenol to methyl aldehyde mol ratio. However, the mol ratio will affect the cure rate of the phenolic thermosetting resins, as shown in Fig. 3.9. With an increase in methyl aldehyde, the resin viscosity will decrease and the cure time will decrease.

Table 3.6 Correlation between mol ratio of phenol to methyl aldehyde and 3-hydroxy methyl phenol content

Mol ratio of phenol to methyl aldehyde	1:0.5	1:1	1:1.5	1:2	1:2.5
3-hydroxy methyl phenol content/%	3.38	9.24	22.16	31.00	40.70

Fig. 3.9 The mol ratio of phenol to methyl aldehyde versus the resin viscosity and cure time (viscosity measured at 25 °C). 1—Cure time; 2—Viscosity



3.3.1.3 Innovation in Phenolic Resin Synthesis

Although there have been no major advances in phenolic resin synthesis recently, much work has been done on the current processing techniques and raw materials. Some innovative progress and breakthroughs have been reported [8, 9]. For example, the new suspension process changes in reaction media, increases the molecular mass in phenolic resins and changes in the reactants of the prepolymers of phenolic resins.

(1) New synthetic processes

Currently, the features of phenolic resin synthesis are a large-scale reaction pot, computerized process control, continuity in product output and cooling and the suspension method for the synthesis of granular phenolic resins [10, 11]. For the suspension method, the synthetic procedures include: suspension polymerization \rightarrow solid and liquid separation \rightarrow drying \rightarrow products. In comparison with traditional processes, the suspension method consumes less energy and has processing continuity, grain uniformity, low free phenol content in the end products and superior quality. In China, research into the suspension method has been carried out recently [12], and suspension processing techniques to produce fusible phenolic resins have been successfully developed [13]. The products conform to the technical standards of phenol-amine-modified phenolic resins.

(2) Linear phenolic resins with high relative molar mass

Phenolic resins were generally prepared by phenol and aldehyde reactions in water containing an alkali (NaOH, KOH or ammonia water) or acid (oxalic acid, hydrochloric acid) as catalysts. The relative molar mass was lower because of product branching and heterogeneity. To increase the molecular weight of phenolic resins, many studies have been carried out and linear phenolic resins with high molar weight were obtained when using a strong acid in highly polar solutions. *o*-Cresol or *p*-cresol was reacted with methyl aldehyde, and the basic properties of the resins are given in Table 3.7 [14]. Table 3.8 lists data characterizing the performance of the cured products obtained by the reaction of these linear phenolic resins and diglycidyl ethers of bisphenol A in equivalent mixtures. Phenol and methyl aldehyde were used as reactants (mol ratio 1:1), acetic as the reaction medium and hydrochloric acid as

Table 3.7 Performance of high molar mass phenolic resins

Properties	Value
Hydroxyl content/ $\text{g}\cdot\text{mol}^{-1}$	120
M_n	2000–3000
Soft point	150–180
Water content/%	<1.0
M_w	5000–10,000
Free phenol content/%	<0.2

Table 3.8 Performance of cured products

Properties	Value
Density/g·cm ⁻³	1.2
Tensile strength/MPa	43
Bending strength/MPa	106
Modulus/MPa	2700
Compression strength/MPa	200
Impact toughness/kJ·m ⁻²	2.0
Thermal deformation temp./°C	190–210
Volume electric resistance/Ω·cm	
Normal state	8×10^{15}
Boiling water, 2 h	3×10^{15}
Dielectric loss tangent	0.03

the catalyst. Phenolic resins with a very high relative molar mass can be prepared with (M_n) values up to 63,600 and a M_w/M_n of 6.21. Another method is to use a metal or P, S nonmetal catalysis to replace the traditional alkali or acid catalysis to generate phenolic resins [15].

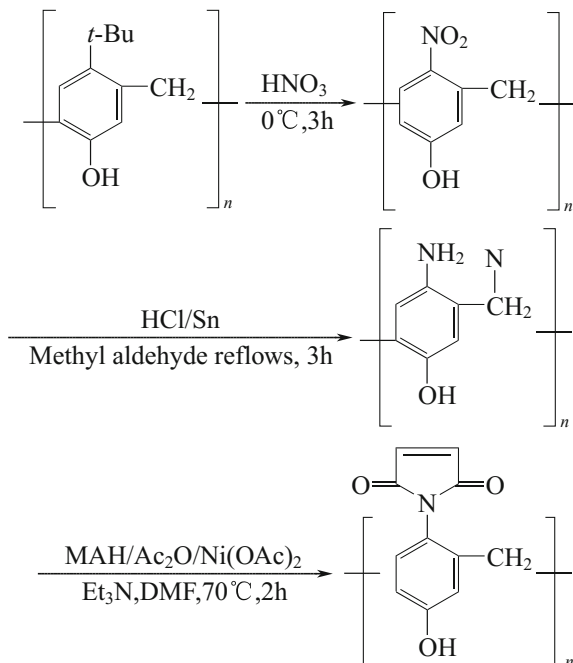
Results indicate that when Mg, Ca, Cu and Zn were used as catalysts, the reaction time was shortened and activation increased, while P, Fe, Al, and Ni as catalysts will result in longer reaction times and lower activation. However, both can generate high molecular mass phenolic resins. If oxalic acid is used together with Al, the system does not gel, even if too much methyl aldehyde is added. Using these catalysts to catalyze naphthol, phenol and methyl aldehyde co-condensed systems can produce phenolic resins with a high molar mass and naphthol content. This type of resin has very good thermal resistance.

Recently in Japan, a new phenolic resin with high molar weight has been developed. This resin can generate grains in water and can be used for injection molding without hexamethylenetetramine as a curing agent. Its starting weight loss temperature is 338 °C, its bending strength is 31.9 MPa, its impact strength is 11.0 kJ·m⁻², and its water absorption rate is 0.05%.

(3) Prepolymers in phenolic resin synthesis

During the curing of phenolic resins, low molecular weight volatiles can escape and affect the processing performance. Therefore, it is of great significance to prepare phenolic resins that will retain low molecular weight volatiles during the curing process [16–18]. In the early 1950s in the USA, GE used allyl chloride to prepare oxide-allyls and carbon-allyls on aromatic rings and in phenolic resins. Curing at high temperature and upon catalysis by an inorganic acid [19] is another way to use an unsaturated carboxylic halide ester liner phenolic resin low molecular weight polymer together with dilution and initiating agents to enable cross-linking and curing. Recently in Japan, phenolic resin low molecular weight polymers containing maleimide (synthesis in Fig. 3.10) were developed. The results have indicated good processing abilities,

Fig. 3.10 Synthesis of phenolic resins containing maleimide



heat resistance and mechanical properties, which bodes well for this application's future [19].

(4) **Benzoxazine compounds**

Benzoxazine compounds are new ring-opening polymerized phenolic resins that have been receiving plenty of attention. They have the advantages of ring-opening polymerization including: retaining low molecular weight volatiles during curing, low viscosity of the uncured small monomers and lower curing stresses. They will become a new phenolic resin product with wide applications in future. Details about their synthesis and performance will be discussed in Sect. 3.2.

3.3.2 Phenolic Resin Curing

Curing is a chemical process in which linear molecular structures are transformed into bulk structures. These chemical reactions are usually complete by the part forming process. Therefore, the curing of phenolic resins will greatly affect part processing and performance.

3.3.2.1 The Curing of Thermosetting Phenolic Resins

Thermosetting phenolic resins are prepared by the reaction of excess methyl aldehyde and phenols under alkali catalysis. The reaction mixture contains a large amount of reactable hydroxyl methyls. Curing can be conducted at high temperature and also low temperature when using an acid.

Curing reactions under applied heat in thermosetting phenolic resins are very complex because of the temperatures applied and also the raw material chemical compositions and catalysts. Research has shown that hydroxymethyl condensation will mainly generate methine bonds and ether bonds. Low molecular weight water is released at temperatures lower than 170 °C [13]. When the temperature is increased from 170 to 200 °C or higher, a more complex second-phase reaction will occur in the resins. This is basically the decomposition of dibenzyl ether and the escape of a small quantity of methyl aldehyde. Almost no water is generated. Pressure is needed for the curing of thermosetting phenolic resins (laminating 10–12 MPa, molding 30–50 MPa). The purpose is to avoid the escape of low molecular weight volatiles (solutions, water and activated methyl aldehyde generated during thermal curing) as this will cause voids and increase flowability.

Thermal setting phenolic resins can be also cured by adding appropriate inorganic or organic acids such as hydrochloric, phosphoric, sulfuric, dichloride p-toluene sulfonic acid and mahogany acid. The basic reaction during curing will be the formation of methine ether bonds. Other features include a strong reaction and a large amount of heat release. Acid-cured thermosetting phenolic resins are used as castings or adhesives and also in flame-retardant composite applications. Details are given in Sect. 3.2.

3.3.2.2 Linear Phenolic Resin Curing and Curing Agents

Linear phenolic resins are stable and require curing agents for curing into bulk structures. Commonly hexamethylenetetramine and paraformaldehyde are used as curing agents, and the curing agents in industry include trimethylol, polymethylol melamine resins, polymethylol bimeric cyanamide and epoxy resins. Hexamethylenetetramine curing agents have many advantages: fast curing speed, short press molding time, good stiffness of cured parts at high temperature and minimum buckling after release from molds. Different curing agents can be used for other applications.

To produce high-performance phenolic resin materials, new curing agents have been developed and applied. Oxazoline compounds are used to cure phenolic resins and give cured parts with increased toughness without a loss in flame retardant, low smoke and high thermal resistance. In Japan, research in this field is actively carried out and some reports on the oxazoline curing of polyamide have been published. Culbertson et al. have used phenylene bioxazoline (PBOX) as curing agents and have developed a series of phenolic resins using 1,3-PBOX as a curing agent. They

Fig. 3.11 Molecular structure of 1,3-PBOX

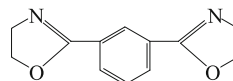


Fig. 3.12 Effect of linear phenolic resin and benzoxazine content on gel time

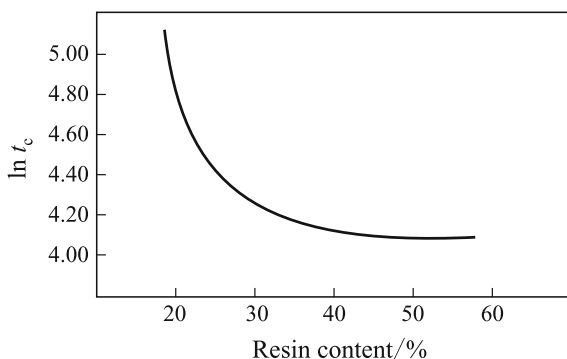
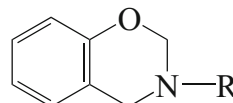


Fig. 3.13 Typical molar structure of benzoxazine compounds



prepared linear phenolic resins with a low free phenol content using dilution methods for processing to prepare high-performance composites (Fig. 3.11).

Apart from PBOX, benzoxazine and bismaleimide (BMI) are special cross-linking agents. In Fig. 3.12, the effects of linear phenolic resin and benzoxazine content on gel time were evaluated by the plate knife method at 180 °C. When the phenolic resins were cured using benzoxazine, no low molar weight volatiles escape and the end parts have a light color. Figure 3.13 shows typical molar structures of benzoxazine compounds.

Since the hydroxyl and the activated hydrogen on the phenol core (p or o-hydroxyls) can give additive reactions with the bi-bonds in BMI, the BMI can also be used as a cross-linking agent for phenolic resins. No volatiles are released during curing, and the cross-linking reaction proceeds very quickly at higher than 150 °C. Reports indicate that the starting weight loss temperature of the cured parts of linear phenolic resins and BMI is higher than 400 °C, and the bending strength at 220 °C can be 75%. The low molecular weight polymers have very good shelf stability.

3.3.3 Modification of Phenolic Resins

Phenolic resins have a good adhering ability, and the cured parts have high thermal resistance and good dielectric properties. Phenolic composites have excellent

mechanical properties, and glass and phenolic composites have bending strengths up to 110–150 MPa. Conversely, phenolic resins have structural drawbacks that should be improved. The main drawbacks of phenolic resins are that the hydroxyl and phenol groups in the molecular structures are very easily oxidized and this will affect the thermal and oxidation resistance; the cured resins will be brittle because methylene linkages are only found between the phenol cores. Therefore, it is necessary to enhance their toughness. Hydroxyl and phenol groups absorb moisture easily, which will affect the electric and mechanical performance and alkali resistance of cured parts. The medium or high pressures used for processing will also limit the application as resin matrixes are required in high-performance composites. Therefore, phenolic resins need to be improved in terms of thermal resistance, toughness and processing performance.

3.3.3.1 Toughening of the Phenolic Resins

Increasing the toughness of phenolic resins can be done in three ways: ① adding tough materials such as natural rubbers, nitrile-butadiene rubber (NBR) or styrene-butadiene rubber (SBR); ② adding an internal tough substance like a modified phenolic resin; ③ using reinforcements like wood powder, glass fiber or fabrics, plasma or cotton to improve brittleness.

(1) External toughening of phenolic resins

Research on the rubber toughening of phenolic resins has been reported since early times. Rubbers are a kind of elastomer that can improve the brittleness and adhering ability of phenolic resins; however, to achieve optimum improvement, the chemical reaction between the rubber and the resin must form primary bonds. However, this will result in a loss of other properties of the phenolic resins. In the rubber toughening of phenolic resins, a certain quantity of elastic latex is added at any stage to phenol to give a distribution of grain size in 0.01–0.1 μm . In two-phase structures, the phenolic resins prepared this way have higher toughness without any apparent decrease in thermal resistance, bending strength, fracture elongation rate or hardness. Another toughening method is to add a conjugated diene glue solution containing positive-ion activation agents during dehydration in fusible phenolic resins, and to disperse the phenolic resins to give grain sizes less than 10 μm , two-phase structures are formed. Using thermoplastic resin mixtures with solvent parameters of 7–15 and with good compatibility is another toughening method. Some parameters are given in Table 3.9. In Table 3.10, the mechanical properties of mixtures blended with polybutylene terephthalate (PBT), polyamide, polyphenyl ether, etc. and melted phenolic resins are given.

(2) Internal toughening of phenolic resins

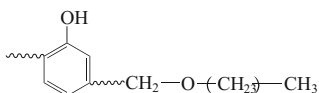
Polyvinyl acetaldehyde improved phenolic resin is a modified phenolic resin applied in industry since early times, as shown in Fig. 3.14. Polyvinyl acetaldehyde can improve the brittleness of phenolic resins, increase their

To reduce the thermal resistance loss, a higher thermal resistance polyvinyl acetaldehyde is often used with a certain ratio of organic silicon monomer. A typical formulation is given as follows:

Methyl-order phenolic resin	135 (mass ratio)
Polyvinyl acetaldehyde	100 (mass ratio)
Orthosilicon ethyl	30 (mass ratio)

Upon blending with fusible linear phenolic resins, NBR containing carboxyls is added because the methylol in the fusible linear phenolic resins can react with divinyl butadiene bonds or with the carboxyls in NBR giving strong bonds between the phenolic resins and NBR. Therefore, the bending and tensile strengths are increased, as are the impact strength and the fracture elongation. Table 3.11 lists some properties of the cured parts of the phenolic resins toughened by NBR or carboxyl NBR.

The use of ethylene glycol to dissolve phenolic resins and blended polyurethane oligopolymers has been reported. Linear phenolic resins were blended and cured with liquid butadiene containing an epoxy group, hexamethylenetetramine and free groups, which gave high impact strength phenolic resins. Another common toughening method is the use of ether alcohol phenol and the hydroxyl in aldehyde prepolymers, for example:



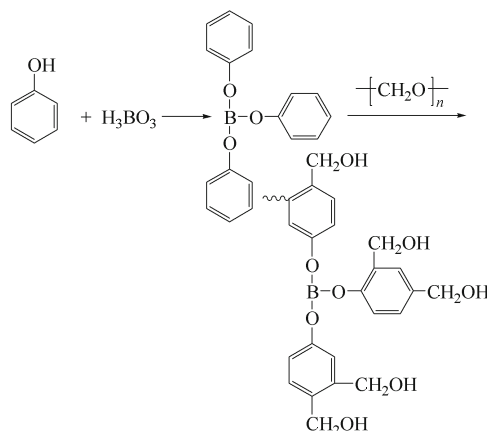
This is because they can form hydroxyl benzyl positive ions. A high hydroxyl phenol content and excess alcohol can avoid self-condensation.

The above reactions are commonly carried out at pH 5–7 at 100–120 °C using methyl alcohol, butyl and isobutyl alcohol. Butyl alcohol is most commonly used. The generated water is separated upon co-boiling with excess butyl alcohol. The etherized methyl-order phenolic resins can be far more soluble in aromatic solvents.

Table 3.11 Properties of phenolic resins toughened by NBR or carboxyl NBR (CTNN)

Performances	CTNN	NBR
Pendulum impact strength/ $\text{kJ}\cdot\text{m}^{-2}$	11.5	4.0
Bending strength/MPa	240	160
Tensile strength/MPa	110	70
Thermal deforming temp./°C	285	235

3.3.3.2 The Structural Modification of Phenolic Resins and New Products



Boron phenolic resins have much better thermal resistance, an instant anti-high-temperature ability and better mechanical properties than phenolic resins [5].

Prepolymers can be transformed into molding compounds by hexamethylenetetramine and some filler, and cured at high temperature (200 °C) to obtain the required high thermal resistance. If hexamethylenetetramine is replaced by epoxy compounds, the curing reaction can take place at lower temperature (100–120 °C). Since the hydrogen in the hydroxyl phenol is substituted by boron, its waterproof properties are improved. The more flexible –B–O– bond is incorporated into the molecules resulting in an increase in brittleness and strength because of the 3D cross-linking structure of the cured products. Their anti-ablating and quantum resistance are higher than those of common phenolic resins.

Boron-modified paraaminebenzylic aldehyde resins are kind of very high anti-ablating material. They are prepared by adding 3 mol of paraaminephenyl and 1 mol of boron acid into boiling dimethylphenyl. Water can be evaporated as a co-boiled compound. Triparaamine–boron compounds can be dissolved in water and are blue. Furthermore, a trialdehyde (or aldehyde water solution) upon reaction for 3 h at 70 °C under acid catalysis conditions yields a red solid resin that can be cured by hexamethylenetetramine. This resin shows a small weight loss under very high temperatures or stresses and can yield a nitrogen compound similar to boron at temperatures higher than 2500 °C.

Typical bisphenol A boron phenolic resins are not affected by the drawbacks of a decrease in dielectric property under wet conditions, which would happen because of the phenol in aldehyde boron phenolic resins. It can thus be widely used in rockets, missiles and space vehicles as a superior ablating material [20]. Its synthesis comprises two steps: First NaOH is catalyzed to generate the additive and a condensation reaction between bisphenol A and an aldehyde with proper dehydrate and then boronic acid or boron sand is added for further reaction and dewatering

Table 3.12 Properties of glass fiber and boron phenolic resin composites

Performance	Laminates of phenol aldehyde B-phenolic resins	High Si-O G-fiber/bisphenol A boron phenolic resin molding
Density/g·cm ⁻³	1.8	0.25–0.26
Poisson's ratio	0.192–0.196	0.38–0.39
Water absorption/%	0.089	159–191
Bending strength/MPa	502	68–97
Tensile strength/MPa	367–426	226–248
Compression strength/MPa	417–579	
Surface resistance/ Ω	Normal	9.15×10^{14}
	In water	3.26×10^9
Volume resistance/ $\Omega \cdot \text{cm}^3$	Normal	7.1×10^{15}
	In water	3.05×10^9
Dielectric loss tangent	0.007	0.010–0.022

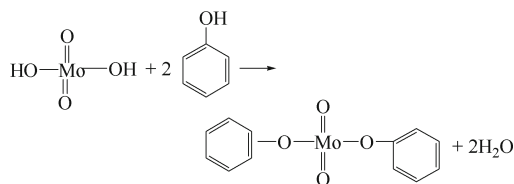
occurs under vacuum to give thermosetting phenolic resins. In Table 3.12, the properties of glass and boron phenolic resin laminates and fiber composites are given.

(1) **Mo acid-modified phenolic resins** [21, 22]

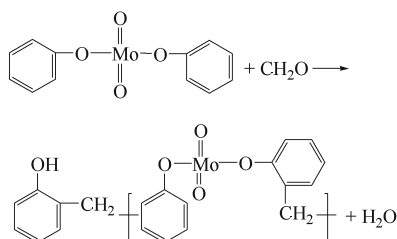
The Mo acid-modified phenolic resin is a new resin with ablating features and can be used in ablating, thermal isolation, smoke removal and flame arresting, for example, its high silicon-oxygen glass cloth (fiber) composites can be used to make jet pipes in missile engines, fire guide tubes and their isolating liner materials.

The synthesis of Mo-phenolic resins comprises a chemical reaction wherein the intermediate molybdenum is chemically incorporated into the backbone of the phenolic resin. Using Mo oxidations, chloride and its acids can be used to react a phenol and an aldehyde to yield phenolic resins containing Mo. In general, Mo-phenolic resins require a two-step reaction:

- ① Under catalysis, Mo acid and phenol will react to form an atomic linkage between Mo atoms and the oxygen atoms in phenol.



- ② Further additive and condensation reactions will take place between the Mo acid phenol ester and an aldehyde to yield Mo-phenolic resins.



(2) Phosphorous-modified phenolic resins

Phosphorous-modified phenolic resins can be prepared by phosphoric acid esterification or by a phosphorous oxychloride reaction. A bifunctional phosphorous oxychloride reaction is shown in Fig. 3.15 and will take place at 20–60 °C for the bioxazole alkyl group. Phosphorous-modified phenolic resins show superior thermal resistance and are flame proof under oxidation conditions, but they are not readily available presently.

(3) Heavy metal-modified phenolic resins

Phenolic resins can react with metal halides (Mo trichloride, Ti tetrachloride, W hexachloride) and metal alcoholates (acetylaceton compounds) to obtain thermal resistance and flame arresting resins. The phenolic resins containing metals can have a far slower decomposition speed at high temperature. In general, the metal can yield metal carbon compounds with carbon atoms in the resins. These resins are colored and possibly contain 20% ion-bonded metals. Under acid catalysis, a reaction will take place to give ether aromatic-hydride aldehyde resins similar to linear phenolic resins. The addition of powder or fiber fillers together with a curing agent such as hexamethylenetetramine, a promoter such as MnO_2 or CaO_2 as well as pigment and release agents into the resins and then mixing, rolling and grinding into molding compounds gives

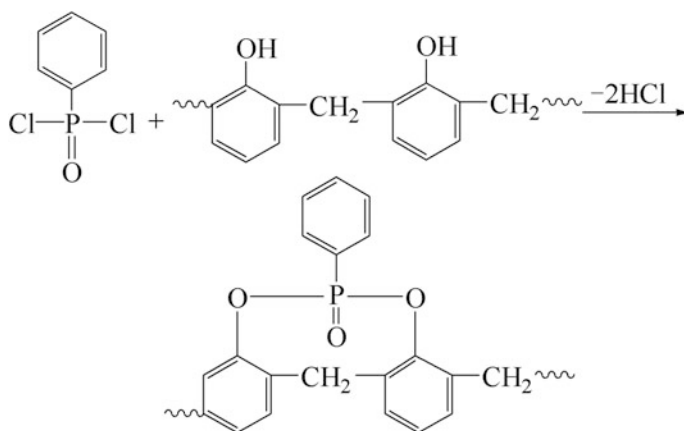


Fig. 3.15 Synthesis of phosphorous-modified phenolic resins

resins suitable for press molding, transfer molding and injection or casting processes.

These molding compounds have high mechanical strength, low water absorption, high electric resistance and dielectric strength as well as stability toward acid and alkali. They can be used over long periods at 200–220 °C in the military, transportation and electricity industries.

Under alkali catalysis, ether aromatic hydrides will react with aldehydes to generate thermosetting resins, which can be used to impregnate glass fibers or fabrics. Usually, these resins are supplied as commercial methylethyl ketone solutions with a solids content of 50–60%.

Aromatic-hydride aldehyde resins need 150–180 °C and 8–28 MPa for curing and are post-cured at 170 °C for 4–6 h to further increase performance. Post-curing at 170–250 °C for 12 h will be necessary. The glass composites made from these types of resins have a higher retention rate and bending strength after aging at 250 °C for 1000 h. The bending strength is still more than 80% after exposure to 275 °C for 750–1000 h, and at 300 °C for 300 h the bending strength is more than 50%. Therefore, aromatic-hydride aldehyde resins are good high-temperature-resistant materials and are used in rocket shells and in engine main body materials.

(4) **Organic silicon-modified phenolic resins** [23]

Organic silicon-modified phenolic resins have been used for decades because of their superior thermal and moisture resistances, but they have a low mechanical strength. Modification will mainly increase the heat resistance and waterproof characteristics. Organic silicon-modified phenolic resins undergo the typical reaction shown in Fig. 3.16.

To simplify modification processes in industry, impregnation, drying and thermal compression are commonly used. If ethyl silicate is used to modify glass or phenolic resin composites, 100 units of amine-catalyzed phenolic resin,

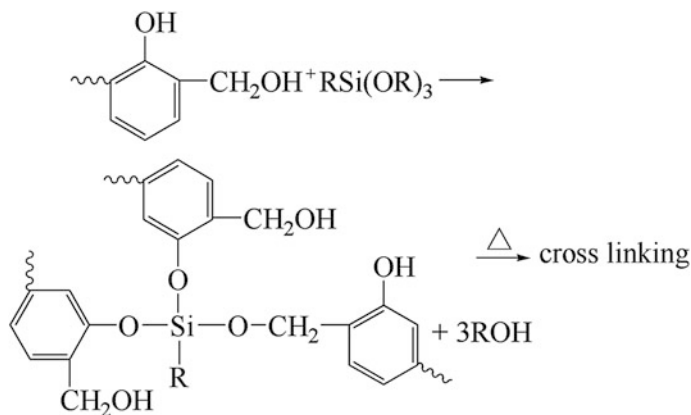


Fig. 3.16 Typical reaction of organic silicon-modified phenolic resins

32 units of ethyl silicate and water diluted into a glue solution with a 55–60% solids content are used and impregnation occurs on vertical machine at 90–95 °C. After drying, press molding into high-temperature glass cloth, lamination is carried out for aero applications. It is a very good ablating material and has a long service life at 200–300 °C. It has largely been used in rockets, missiles and spacecraft. Phenolic resins can also be modified by phenol silicon monomers or aromatic silicon hydrides, which can be used to impregnate glass fibers or cloths, in addition to plasma or carbon fiber fabrics to make structural materials or heat-proof, electric isolation and ablating materials.

In organic silicon-modified phenolic resins, the phenolic resins are generally subjected to allylation and then an additive reaction with organic polymers, as shown in Fig. 3.17.

(5) Ether aromatic-hydride-modified phenolic resins

For the synthesis of phenolic resins, phenyl hydroxide will not normally take part in the reaction. Therefore, the resistance toward alkali, solution and thermal oxidation is affected. To overcome these drawbacks in the phenolic resin structure, aromatics or aromatic hydrides can be incorporated to protect the phenyl hydroxide and can then be reacted with an aldehyde to yield phenolic resins. This kind of resin has good alkali resistance, low moisture absorption and high mechanical strength in addition to superior thermal and oxidation resistance. They can be used over long periods at 180–200 °C.

Ether aromatic-hydride aldehyde resins are prepared by the dichloride-methylation of aromatic hydrides and then methanol-etherized in an ether exchange reaction with phenol under Fourier catalysis to form aramid ether compounds containing two phenol rings. The reaction with an aldehyde to generate the ether aromatic-hydride aldehyde resin is shown in Fig. 3.18.

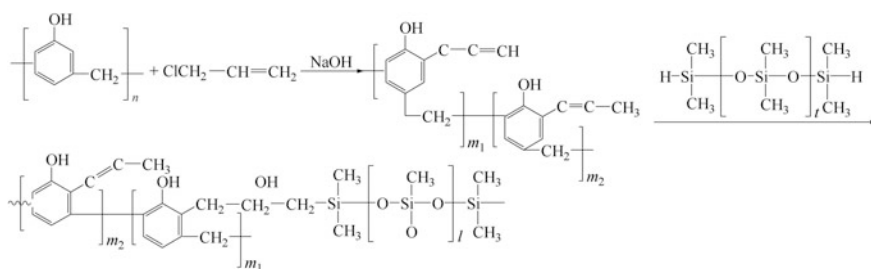


Fig. 3.17 Organic silicon-modified phenolic resins

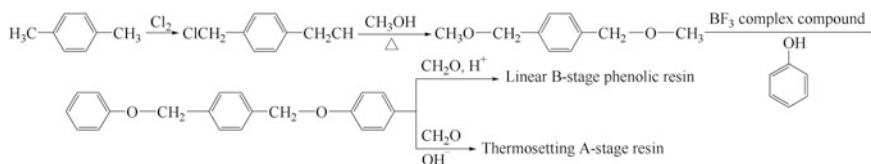


Fig. 3.18 The synthesis of ether aromatic-hydride aldehyde resins

Table 3.13 Properties of Mo-phenolic resins

Performance	CTNN
Appetency	Dark green
Solid content/%	98–99
Melting point/°C	–100
Polymerization speed/s	50–60
Water content	Mini

Table 3.14 Thermal properties of Mo-phenolic resins with varied Mo content

Mo content/%	Cure temp./°C	Discomposed temp./°C	Thermal loss at 700 °C
6.0	145	460	46.2
8.0	150	475	41.1
10.0	150	560	41.9

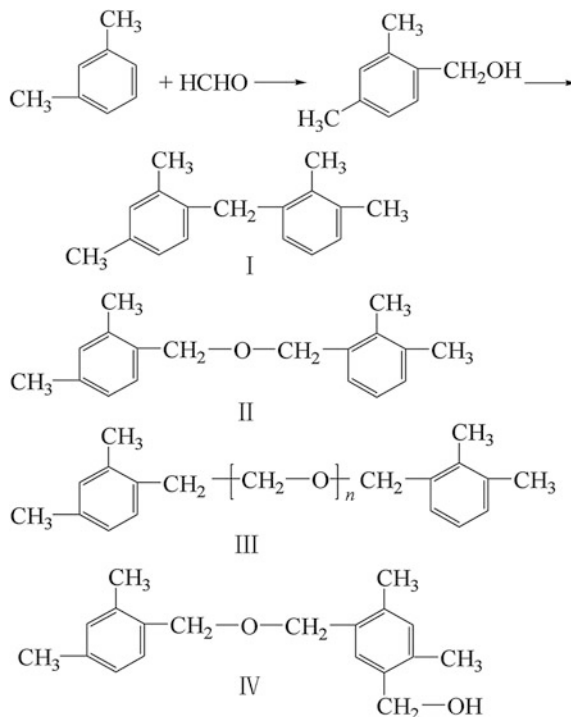
Phenol and Mo acid are added into the reaction vessel and stirred upon heating at 60 °C. Stirring is maintained for 30 min, and a 37% aldehyde water solution is added upon proper catalysis. Stirring is continued upon heating. The isothermal reaction continues for 2 h, and then the water is removed from the resin under vacuum to yield a dark green Mo-phenolic resin. After cooling, a green solid is obtained. This Mo-phenolic resin can be dissolved in alcohol and acetone, showing bright purple without any suspensions. The resin can be cured by hexamethylenetetramine, which is commonly used in linear phenolic resin curing.

Mo-phenolic resins are new ablating resins (see Table 3.13 for properties). As the Mo content in the resins is increased, the decomposition temperature increases (Table 3.14). Mo-phenolic resins are cured at 150–160 °C and decompose at 460–560 °C. A thermal weight loss of 40% occurs at 700 °C, while B-phenolic resins have a weight loss of more than 50% at 700 °C. As the Mo content in the phenolic resins is increased, the thermal resistance will increase. Glass fiber composites made from this resin have the ability to resist ablating and erosion, and they also possess high mechanical strength and good processing performance. They can be used to make ablating and thermal materials for rockets and missiles.

(6) **Dimethylbenzene-modified phenolic resins**

Since phenolic resins have hydrophilic phenol groups that easily absorb moisture and have no resistance to oxidation, they possess poor electric properties and thermal resistance. Dimethylbenzene-modified phenolic resins (also referred to as phenol-modified dimethylbenzene aldehyde resins) have been developed. Its synthesis includes the use of dimethylbenzene and an aldehyde to synthesize dimethylbenzene aldehyde resins under acid catalysis. A further reaction is carried out between a phenol and an aldehyde.

Fig. 3.19 Reaction between dimethylbenzenes and aldehydes



- (1) Synthesis of dimethylbenzene aldehyde resins: Sulfuric acid, phosphoric acid, hydrofluoric acid and aluminum trichlorides are used as industrial catalysts. The reaction between m-xylene and an aldehyde will take place as shown in Fig. 3.19.

Industrial dimethylbenzenes have a relative molar mass of 250–700, and compounds I–IV containing 3–6 dimethylbenzene rings are shown in Fig. 3.19.

With excess dimethylbenzene and a high concentration of sulfuric acid (catalyst), the reaction will mainly give compound I. When the aldehyde is in excess, and the catalyst has a low concentration, compound III will be dominant.

- (2) Phenol-modified dimethylbenzene aldehyde resins: Modified dimethylbenzene aldehyde resins are formally similar to thermoplastic phenolic resins but cannot be cured with hexamethylenetetramine, and only their relative molar mass is increased. If they further react with a phenol and an aldehyde, thermosetting phenolic resins are generated as shown by the reactions in Fig. 3.20.

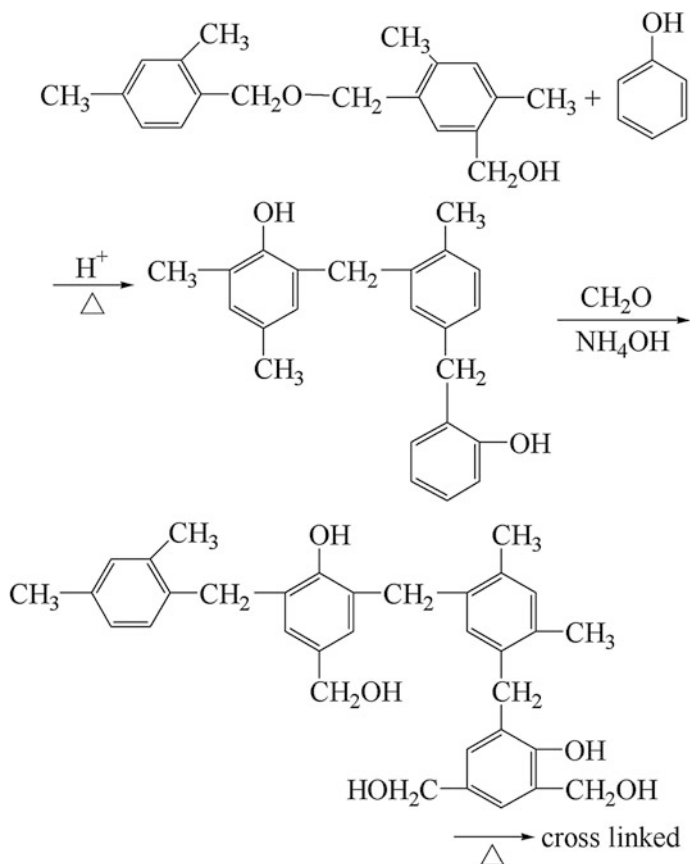


Fig. 3.20 Synthesis of dimethylbenzene-modified aldehyde resins

Industrialized phenol-modified dimethylbenzene aldehyde resins have superior performance and have been used in glass laminates, glass laminated pipes and glass fiber composites.

In Table 3.15, the properties of glass cloth laminates made using phenol-modified dimethylbenzene aldehyde resins are listed. These laminates were tested at 200 °C for 400 h or 250 °C for 24 h, as well as being subjected to X-ray radiation of 10^3 – 10^9 R, and no changes in their bending property were found. Additionally, they are resistant to acid, alkali and organic solutions.

Dimethylbenzene aldehyde resins are of industrial interest for press molding. Their preparation is similar to that of linear phenolic resins: Phenol and dimethylbenzene are blended in an appropriate ratio and then reacted with aldehyde under acid catalysis, which yields a fusible and soluble A-stage solid resin. The product is obtained after grinding, mixing

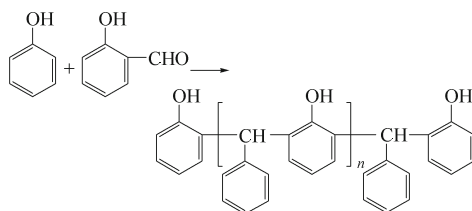
Table 3.15 Properties of glass cloth laminates made using phenol-modified dimethylbenzene aldehyde resins

Performance		Test results
Bending strength/MPa		400–500
Tensile strength/MPa		300–350
Martin's thermal temp./°C		>250
Tearing strength/MPa		300–450
Surface resistance/ Ω	Dry	5.9×10^{14}
	Wet	5.7×10^{12}
Dielectric strength/kV·mm ⁻¹	Dry	20.0
	Wet	17.3
Dielectric loss tangent		0.005–0.009
Dielectric constant		4.2–4.6
Volume resistance/ $\Omega\cdot\text{cm}^3$	Dry	6.9×10^{14}
	Wet	4.2×10^{13}

with hexamethylenetetramine and adding fillers, pigments and release agents. The plastic parts produced by the plastic machine-milled press molding powder have high thermal resistance, good surface finishing and good dielectric properties after wetting and can be used for injection and casting. The main disadvantage is a slow cure speed and the need for further improvements.

(7) Phenol salicylaldehyde phenolic resins

Phenol salicylaldehyde phenolic resins are prepared by the reaction between phenol and salicylaldehyde as follows:



The preparation of phenol salicylaldehyde phenolic resins is done using excess phenol in the reaction with salicylaldehyde under acid catalysis conditions and dehydration at 160–180 °C. Because of the many phenol rings in their molecular structure, these resins have high thermal resistance and good storage stability.

In Table 3.16, the properties of the cured products of mixtures of phenol salicylaldehyde phenolic resins, diaminodiphenylmethane and bismaleimide (BMI) are compared with BMI cured by diaminodiphenylmethane, and their thermal resistance, mechanical performance and storage stabilities are very good.

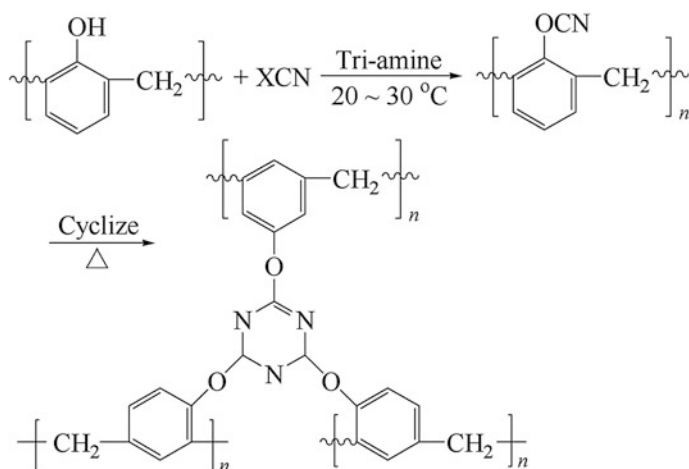
(8) Phenol-triazine (PT) resins [24]

Phenol-triazine (PT) resins are a kind of modified phenolic resin with good thermal resistance. They have good processing performance similar to those in epoxy resins, and a high-temperature resistance ability similar to bismaleimide

Table 3.16 Properties of phenol salicylal phenolic resin-cured bismaleimide resins

Performance	BMI/phenol salicylal resins	BMI/diaminodiphenylmethane
Thermal deforming temp./°C	300	262
Bending Strength/MPa	R.T.	85
	250 °C	71
Weight loss (300 °C, 2 h)/%	12.3	15.3
Viscosity (30 °C, 30 d)/Pa·s	0.05	Gel

Note Cure condition: 180 °C/3 h, 250 °C/5 h; NMP solvent

**Fig. 3.21** Synthesis of PT resins

(BMI) as well as excellent flame-retardant properties similar to that of phenolic resins. A typical synthesis is shown in Fig. 3.21.

PT resins are a new matrix system that can be used in high-performance composites. It is a self-curing system with advantages like a low shrinkage rate, retention of volatiles, a glass transition temperature higher than 300 °C and an elongation limit of up to 3.5%. Their main drawback is that the raw materials used for resin synthesis are toxic and require by-product recycling, which is environmentally unfriendly. Therefore, industrial-scale production still requires further research. In Tables 3.17 and 3.18, some PT resin composite performance data are presented.

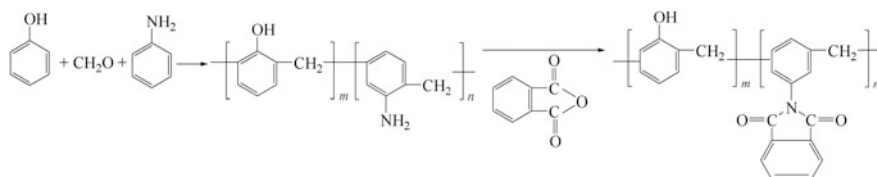
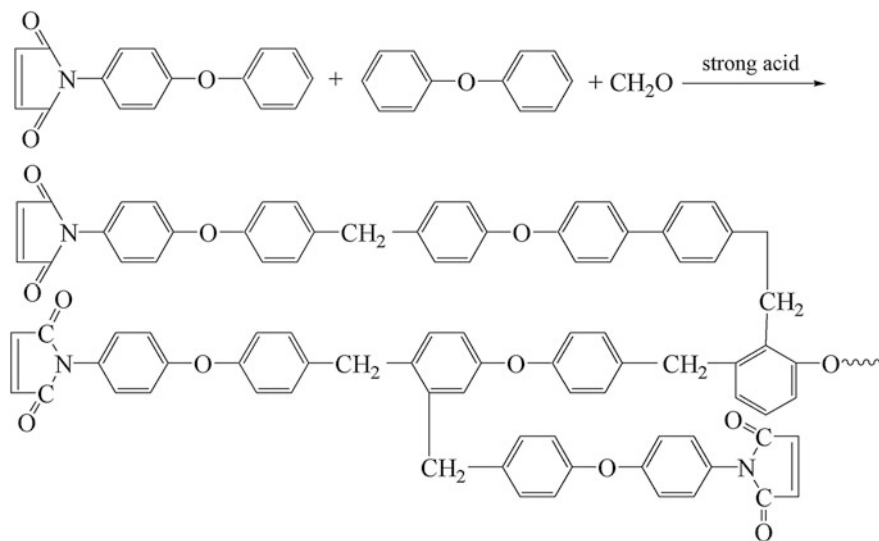
The phenolic resins synthesized by the condensation of phenols, aromatic amines and aldehydes can react with aromatic hydroxyl-anhydrides to give modified phenolic resins containing imide groups. It is a new phenolic resin with superior performance in terms of thermal resistance, curing behavior and storage stability. Typical reactions are shown in Fig. 3.22.

Table 3.17 Bending test results of unaged unidirectional CF/PT laminates

Carbon fibers	Room temp.			216 °C			316 °C		
	Bending strength/MPa	Bending modulus/GPa	Bending strength/MPa	Bending strength/MPa	Bending modulus/GPa	Bending strength/MPa	Bending strength/MPa	Bending modulus/GPa	
T-400-UC309	1786	174				591		158	
T650/42UC322	1919	152				559		152	
T650/42UC323	1444	175	686		163	559		155	
T650/42-AS1	1371	175	988		170	824		166	
T650/42-AS2	1417	179	896		166	788		156	
T650/42-AS3	1483	171	922		167	884		160	

Table 3.18 Bending test results of unidirectional CF/PT laminates aged at 260 °C for 600 h

Carbon fibers	Room temp.		260 °C	
	Bending strength/MPa	Bending modulus/GPa	Bending strength/MPa	Bending modulus/GPa
T650/42-UC322	1840	187	1264	161
T650/42-UC323	1398	185	871	171
T650/42-AS1	1603	190	1085	186
T650/42-AS2	1655	184	1052	179
T650/42-AS3	1649	173	1022	170

**Fig. 3.22** Synthesis of imide-containing phenolic resins**Fig. 3.23** Synthesis of BMI-modified ether-diphenyl-type phenol resins(9) imide-containing phenolic resins

The hydroxyls and phenols in p-hydroxyl BMI are oxidized to form 4-phenoxy maleimide, which are then further reacted with ether-diphenyl or polyaldehyde to generate BMI-modified ether-diphenyl-type phenol resins with excellent thermal resistance, impact toughness and hydrophobic properties (see Fig. 3.23 for synthesis) [25].

(9) **Benzoxazine compounds [5]**

Benzoxazine compounds are a new kind of ring-opening polymerization phenol resin monomer. They can be used to produce polymers that are similar to phenolic resin structures upon ring-opening polymerization. Low molecular weight volatiles are retained during curing, and the products have a low void content and shrinkage rate. This can reduce internal stresses and microcracks. They exist as ring monomers with a low molar mass and viscosity, and they form composites easily. Since some phenols and hydroxyls are present in these resins, they have an improved thermal resistance. At high reaction temperatures, the phenols and hydroxyls convert into molar ether bonds, which increases their toughness. Therefore, they can be widely used in many areas as new types of phenolic resins.

- (1) Benzoxazine compounds are commonly referred as 2H-dihydro-1,3-benzoxazine and are synthesized as shown in Fig. 3.24.

In 1973, Schreiber introduced benzoxazine compounds to polymer science for use in ring-opening polymerization. Much development has taken place in terms of the synthesis and applications of benzoxazine compounds. From the synthesis by Holly and Cope, by changing the reaction media and improving the synthesis processes, intermediate compounds were developed as shown in Fig. 3.24.

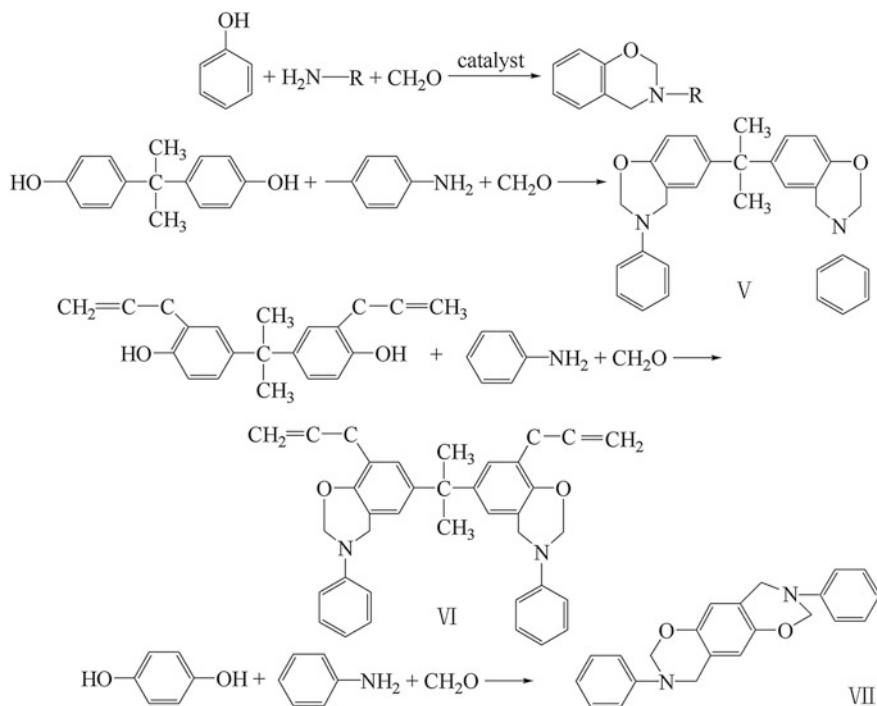
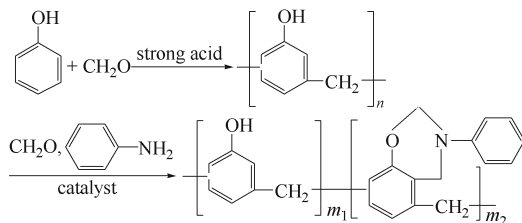
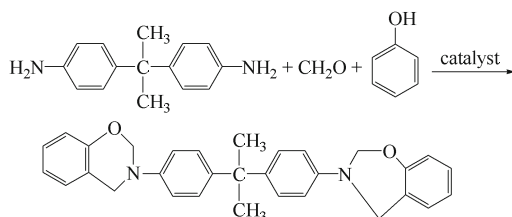


Fig. 3.24 Synthesis of dibenzoxazine intermediate compounds

The following synthesis uses polyhydric phenol, phenol amine and an aldehyde as reactants to prepare intermediate products for polybenzoxazine:



Using diamine and phenol amine as reactants to prepare intermediate products for polybenzoxazine is done as follows:



Because the reactants can differ, and organic media or water can be used as reaction media for the preparation of suspensions, the obtained intermediate compounds will have different physical states. Therefore, wet or dry processing methods can be used to produce superior performance benzoxazine rings.

- (2) Structural characteristics of benzoxazine intermediate compounds Quantum chemistry calculations have indicated that benzoxazine intermediate compounds have odd-shaped chair structures (oxazine rings) and also that their electronic charges are non-uniformly distributed. The methylenes in the oxazine rings have positive charges, while the hetero atoms (N,O) have negative charges. Analyses have been carried out on the model benzoxazine compounds (3-phenol-6,8-dimethyl-3,4-2H-1,3-benzoxazine compounds, 3-phenol-6,8-2Cl-3,4-2H-1,3 benzoxazine compounds, 3-phenol-6-methyl-3,4-2H-1,3 benzoxazine compounds) and have indicated that the oxazine rings show an infrared characteristic absorption peak near 945 cm^{-1} , while in H-NMR analysis, peaks are present near 4.7×10^{-6} and 5.3×10^{-6} . These analyses are consistent with classic calculations.
- (3) The solubility of benzoxazine intermediate compounds As matrix resins, benzoxazine intermediate compounds require good solubility, apart from dry processing applications, as given in Table 3.19. Test results of intermediate solubility in different solvents are listed, indicating that a small difference exists between the intermediates and common phenolic resins. Oxazine rings are only slightly soluble in water-free alcohol.

Table 3.19 Solubility of intermediates

Solvent	Solubility
<i>N,N</i> -di-methyl-methane Amide	Yes
Acetone	Yes
THF (tetrahydrofuran)	Yes
Dimethyl phenol	Partly
Butanone	Yes
<i>N</i> -methyl-2-ketoyrrolidine	Yes
Dehydrated alcohol	Little
Methyl phenol	Yes
Trichloromethane	Yes
Carbon tetrachloride	Little

Thermal ring polymerization under activated hydrogen: Intermediates contain imperfect points in closed rings within phenol-hydroxyl (activated H). The phenol cores contain activated H and ring-opening polymerization can take place. In Table 3.20, the curing temperature of the above-mentioned intermediates is listed (DTA analysis).

The cured products have superior thermal resistance and the indexes range from 230 to 270 °C (in nitrogen). The residual carbon rate is 60–70% (in nitrogen), and the mechanical properties and T_g of their castings are given in Table 3.21.

Apart from the thermal ring opening caused by the activation of H, intermediates be polymerized under ionic catalysis conditions when using intermediate compounds as matrix resins. Aluminum trichloride can be used as a catalyst for the production of automobile brake materials with good processing performance, stable high-temperature braking coefficients and high toughness. In Table 3.22, several properties of glass cloth

Table 3.20 Curing temperature of intermediates

Intermediate	DTA data/°C		
	Onset temp.	Peak temp.	Terminal temp.
a	190	220	265
b	233	273	303
c	205	233	252
d	129	219	265
e	167	230	265

Table 3.21 Properties of cured intermediates

Intermediate	Bending strength/MPa	Fracture elongation/%	Impact toughness/kJ·m ⁻²	T_g /°C
a	33.4	2.0	1.87	190
b	44.7	1.5		229

Table 3.22 Performance of glass/intermediate laminates

Performance		Resin matrix	
		Intermediates/epoxy resins (ETA)	Polyamine/BMI
Density/g·cm ⁻³		1.78	≥ 1.70
Water absorption (24 h)/%		0.057	
Bending strength/MPa	Normal	517	≥ 343.1
	180 °C	267	≥ 176.5
Interlaminar shear strength/MPa		67.4	≥ 49
Surface electric resistance/Ω	Normal	6.5 × 10 ¹²	≥ 1.0 × 10 ¹²
	180 °C		≥ 1.0 × 10 ¹⁰
Volume electric resistance/Ω·cm	Normal	7.3 × 10 ¹¹	≥ 1.0 × 10 ¹¹
	180 °C	1.4 × 10 ¹⁰	≥ 1.0 × 10 ⁹
Dielectric loss tangent	Normal	0.00124	≤ 0.5
	180 °C	0.435	

laminates fabricated using benzoxazine intermediates with epoxy resins under tri-amine catalysis conditions are given and compared with glass/polyamine-bismaleimide (BMI) laminate standards (thermal resistance: H grade, compliance with HB/Z308-1997). Glass/benzoxazine intermediate laminates have outstanding high-temperature mechanical properties. The bending strength at 180 °C is 267 MPa, and the residual strength can be 50% or higher. The thermal resistance index is higher than 200 °C, and therefore, benzoxazine intermediates are suitable as 180 °C long-term exposure structural materials.

3.3.4 Progress in Phenolic Resin Composites and Processing Techniques

In the 1980s with the urgent demand for fire-retardant materials, a new generation of phenolic resin composite system was developed at large chemical companies including the US's West Chemical Co., Dow Chemical Ltd., OCF Company, INDSPEC Co. and the UK's Imperia Chemical Co. Compared with traditional phenolic resin composites, the new generation of phenolic resin composites has fire-retardant properties, a low amount of smoke release, low toxicity and outstanding mechanical properties. Their most favorable feature is their suitability for current composite processing techniques including SMC, BMC, XMC, DMC, HMC, RTM, SRTM, SRIM [26], filament winding (FW), pultrusion, spraying and handy laying.

3.3.4.1 Resin Processing Requirements

To suit the many composite processing techniques, a variety of new phenolic resins have been developed for use in different production processes. For traditional phenolic resins, the redesign of constituent materials in phenolic resins has been investigated to achieve good processing and mechanical performance. Table 3.23 shows a performance comparison between new and traditional phenolic resins.

The principles for the synthesis of new phenolic resins are: Resins should have a high molar mass to reduce the amount of condensed water during curing; redesigned molecules, the addition of unsaturated bonds or other functional groups to increase the reaction speed; the use of activated solutions to reduce volatiles; the use of composed catalysis to increase catalyst selection.

- (1) Acid curing systems: Acid curing systems are widely used in FRP processing techniques. The resins are synthesized under alkali catalysis conditions, and curing by aromatic carboxylic acid can be accelerated. These resins have good processing performance and electronic properties. The processing times can be reduced to those of thermoplastics. The manufactured parts have high thermal stiffness and a small buckling deformation. In the UK, acid curing phenolic resins with different viscosities are commercially available and a variety of curing agents can thus be selected. Thixotropy phenolic resins can especially be used for central vertical part surfaces using convenient processes. This is similar to polyester gel coating and can improve part surface quality by avoiding pinholes on the part surface. The only drawback is the limited selection of product colors.
- (2) Thermosetting phenolic resins have great potential. To increase reactivity, a highly ortho-synthesis should be adopted to obtain a 2–4 mol ratio O/P methylene in the phenol-hydroxyl. If necessary, polyaldehyde/resorcinol catalysis can be used to process FRP at lower reaction temperatures. In the USA, a general A-stage phenolic resin is used and blended with a modified phenolic, and then cured into dark brown products (different from the acid cured yellow/brown).

Table 3.23 Performance comparison between new and traditional phenolic resins [5]

Performance	Domestic thermosetting resins	US SMC	US pultrusion	Handy laying-up
Appearance	Brawn thick liquid	Light yellow liquid		
Viscosity/Pa·s	1–1.5	0.135	3	0.75–2
Free phenol content/%	≤ 6	1.4	2.2	
Solid content/%	57–62	69	88–99	90
Gel time/s	90–120 (160 °C)	33 (165 °C)		

- (3) To improve the brittleness of phenolic resins, epoxy and isocyanic resins are most commonly blended with phenolic or thermosetting phenolic resins and then blended with thermoplastics for copolymerization.

3.3.4.2 Composite Processing Performance

Research and development into new phenolic resins have greatly advanced the processing technologies of phenolic resin matrix composites (FRP). Traditional filament winding, laminating and press molding processing were further improved. Convenient operation, spraying, pultrusion and SMC/BMC processes can also be used for phenolic composites. Therefore, the FRP products of the phenolic resins have been extensively developed.

In Table 3.24, a processing performance comparison between traditional and new phenolic resin FRP is given indicating the superior processing performance of the new phenolic resins.

3.3.4.3 Phenolic Resin Composite Applications [27]

Phenolic resins have been used with a variety of reinforcements to develop many innovative materials. Because of their low cost and acceptance as thermosetting engineering plastics or thermal resistance engineering plastics, phenolic resin matrix composites are widely applied in different fields.

Electric industries: isolating structural component touch switches and high pressure parts.

Transportation industries: automobile and train braking materials, wind tunnels for trains and subway trains, internal decorating panels, worktable top surfaces, front nose-shaped parts and integrated drive chambers. Internal decoration panels in ships and boats will be another large market.

Aerospace: Modified phenolic resin-impregnated paper, fabrics and Nomex honeycombs have been largely used in internal cabin fire-retardant and decorate composites, rocket nose cones and bottles, and engine jet pipes are also made of phenolic resin composites.

In general, phenolic matrix composites have great potential in civil and military applications.

Table 3.24 Processing comparison between traditional and new phenolic resin FRP

Processing parameters	Traditional FRP	New handy process	Pultrusion	SMC/BMC	RTM
Processing pressure/MPa	5.5–280	Contact	13–27	3.5–10	9.8–11.7
Processing temp./°C	160–180	60	130–205	135–180	150–180
Processing time/min	1440	60	0.3–1.0	4–10	1–4

3.4 High-Performance Epoxy Resin Matrixes

Epoxy resins are a kind of polymer containing two or more epoxy functional groups. Since the 1940s, they have been developed into a wide variety of thermosetting resins including glycidol amines, glycidol esters and aliphatic-ester epoxy resins. Because of their superior processing performance, mechanical and physical properties and low cost, epoxy resins have been extensively applied in the mechanical, electronic, aerospace, chemical, transportation and infrastructure industries as coating materials, adhesives and composite matrixes.

General purpose epoxy resins such as bisphenyl-A resins and their modified resins are cured by common curing agents but have some disadvantages like high moisture absorption, poor dimensional stability and poor dielectric properties as well as brittleness. These resins do not meet the much higher demands of epoxy resins in terms of performance such as thermal resistance, water absorption, dielectric property, impact toughness and curing behavior. Therefore, epoxy resin modification and the development of new types of resin are growing fast. The use of new curing agents for epoxy resins has been used to produce high-performance epoxy resins. In this chapter, highlights of the development of high-performance epoxy resins that are used as composite matrixes will be discussed.

3.4.1 *Synthesis of Epoxy Resins*

High-performance epoxy resins are prepared by the condensation of multiple activated H-containing compounds such as polyamines, polyalcohols or epoxy chloropropane under strong alkali (KOH, NaOH) conditions. In the synthesis of epoxy resins, the reaction between the epoxy groups and activated H will take place resulting in molar chain elongation. By controlling the mol ratio of epoxy chloropropane and the activated H compounds, and using the proper reaction conditions, resins with different molar masses can be synthesized. In the synthesis of low molar mass resins, excess epoxy chloropropane can be added and the epoxy equivalent can be determined by chemical titration, relative absorbing quantitative infrared spectroscopy and NMR. In the synthesis of epoxy resins, some side reactions will occur such as the hydrolysis or branching of end groups in epoxy chloropropane or the resins will affect the epoxy qualities and the performance of the cured products. Control standards for epoxy resins include epoxy values, inorganic chloride content, total chloride content, volatiles content, molar mass, the viscosity of the liquid resins and the softening temperature of the solid resins.

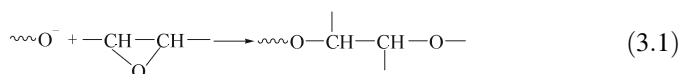
3.4.2 Curing of Epoxy Resins and Curing Agents

3.4.2.1 Curing Reaction

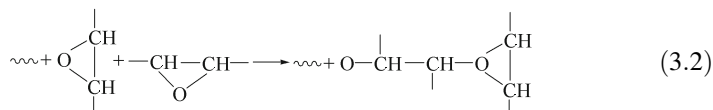
Epoxy resins contain extendable tri-rings, which easily undergo cross-linking reactions with various cross-linking agents. Curing properties depend on the epoxy resin structure and also the type and proportions of the curing agents used. The curing speed of epoxy systems is controlled by the type of curing agent and the quantity as well as the curing processing parameters. Epoxy values can also affect the curing speed. The positions of the epoxy groups will be the principal factor that affects the epoxy resin reaction activity.

Epoxy groups can be homopolymerized into polyether chains through the following three mechanisms: negative ion (Lewis alkali catalysis), positive ion (Lewis acid) and coordination polymerization [28]:

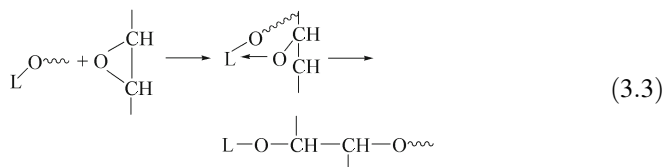
Negative ion:



Positive ion:



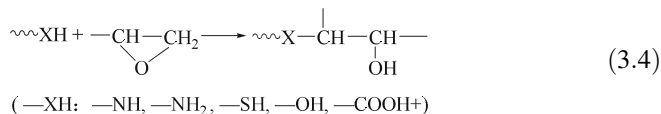
Coordination:



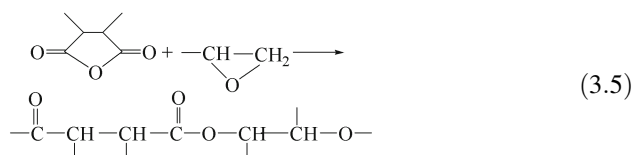
Organic alkali like tri-amine is typical Lewis alkali epoxy resin curing agents. The simplest Lewis acid positive-ion curing agents are BF_3 complex compounds. Metal alkyl-oxidations can follow the coordination polymerization mechanism to cure epoxy resins. This research is actively being pursued and will hopefully result in practical applications.

The gradually additive reaction in epoxy resins is very critical in practical applications, and the reactions include [29]:

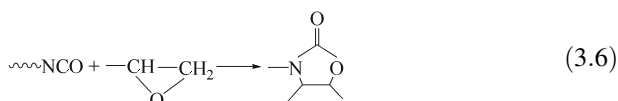
Activated H:



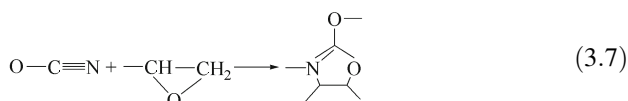
Acid anhydride



Isocyanate ester



Cyanate ester



Curing agent types include polyamines, polyalcohols, anhydrides and polyphenols. All these agents can be catalyzed by acid or alkali catalytic agents. The ratio of curing agents to epoxy resins determined the properties of the cured materials.

3.4.2.2 New Curing Agents

For high epoxy resin matrixes, diaminodiphenylsulfone (DDS) is the most commonly used curing agent. Epoxy/DDS systems have high thermal resistance (T_g) but allow a high amount of absorption and give poor hot/wet performance. In addition, these systems are brittle because of their high cross-linking density. To improve their hot/wet performance and toughness, the following polyetherdiamine cure agents have been developed: bietherdisphenylaminesulfone (BDAS), bietherdiphenylamine oxide (BDAO), bietherdisphenylaminebisphenyl-A (BDAP) and bietherdisphenylamine-6F-bisphenyl-A (BDAF). Their structures are shown in Fig. 3.25 [30].

Cured 4-functional epoxy resins (TGDDM) upon curing by these agents have performances as listed in Table 3.25.

Since polyetherdiamine contains longer molecular chains and more flexible ether bonds than DDS, the resins cured by polyetherdiamine will possess increased toughness but their dry thermal resistance will be slightly lower. Furthermore, because of their lower moisture absorption, the effect of absorbed water will be mitigated. Therefore, the cured resins will have a higher thermal resistance than those cured by DDS.

The Shell Co. in the USA developed the ether-bond-free curing agents Epon HPT 1061 and 1062 with structures as follows. Because of the large quantity of carbon-hydrogen bonds, their water absorption rates are much smaller than that of DDS [31, 32].

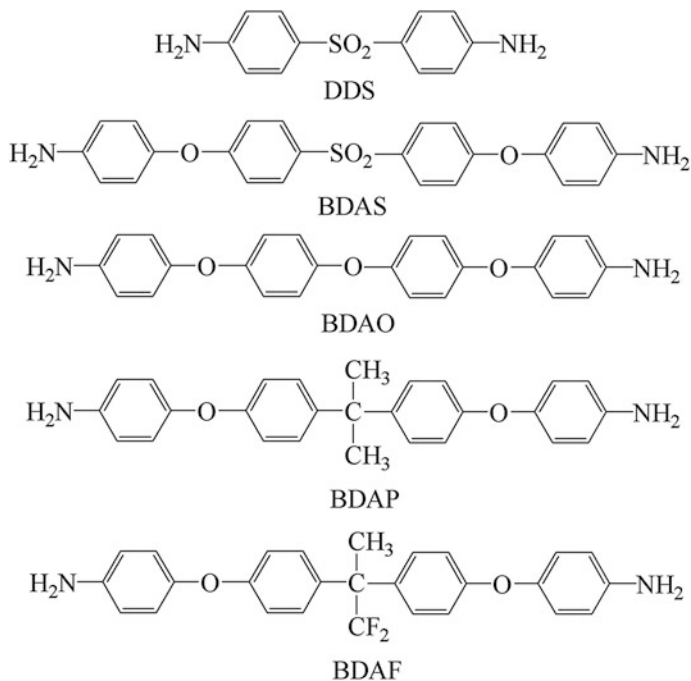
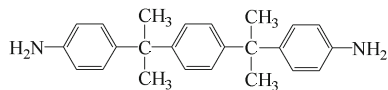


Fig. 3.25 Chemical structures of DDS and polyetherdiamine curing agents

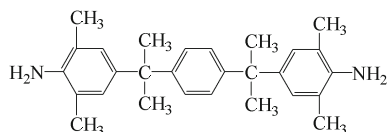
Table 3.25 Performance of TGDDM upon curing by polyetherdiamine

Cure agents	Water absorption/%	Dried $T_g/^\circ\text{C}$	Wetted $T_g/^\circ\text{C}$	$\Delta T_g/^\circ\text{C}$
DDM	3.3	220	151	69
BDAS	2.3	211	158	53
BDAO	1.7	202	163	39
BDAP	1.5	204	164	40
BDAF	1.3	200	170	30

Epon HPT 1061

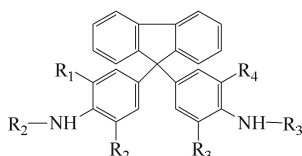


Epon HPT 1062



Epon HPT 1071 and 1072 resins are produced with the 1061 and 1062 curing agents. Their dry thermal resistance (T_g) is about 10 °C lower than that of DDS and is in the range of 241–250 °C, while their water absorption rates are only 1.4–1.6%.

3M has developed a variety of biamine compounds with a fluorine-containing backbone, and they are used in epoxy curing as thermal and moisture-resistant curing agents. These agents give superior high-temperature performance and have very small water absorption rates. Fluorine–amines have the following chemical structure [30]:



In Fig. 3.26, the performance of bisphenol A epoxy (DGEBA) and fluorine epoxy (DGEBF) upon curing by blended I and II amines is shown [33]. Curing agent I contains two secondary amines for chain extension. II is an epoxy resin curing agent, and as the cure agent II content is increased, T_g also increases because the cross-linking density increases. When the cross-linking densities are equivalent, the cured DGEBF has a much higher T_g than DGEBA (210 °C) because of the stiff fluorine structures. Despite the existence of a stiff suspended fluorine group, the cured DGEBF shows a slightly higher toughness than DGEBA. As the cross-linking density is decreased, both DGEBA and DGEBF showed higher toughness while T_g did not significantly decrease.

The DGEBF cured by curing agents I or II or a mixture of these agents has a water absorption of only 2.2% at 100% relative humidity and at 95 °C, and this shows that the fluorine group is strongly hydrophobic. As the content of curing

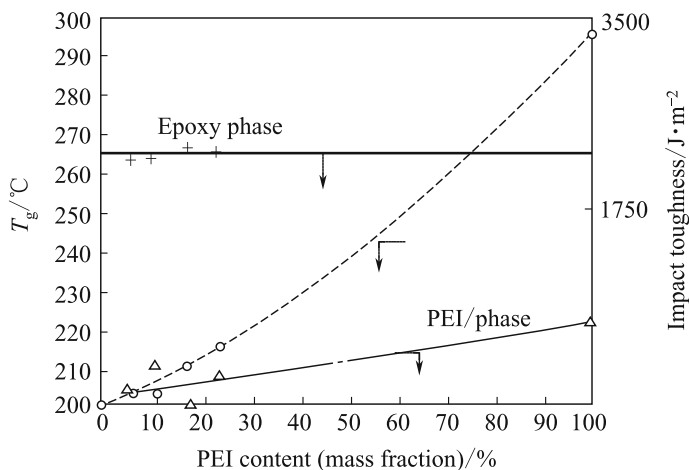
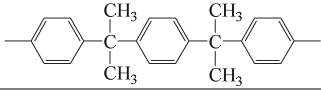
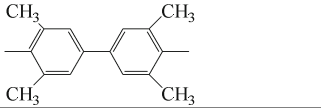
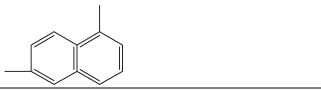
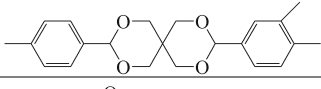
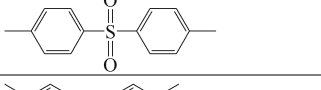
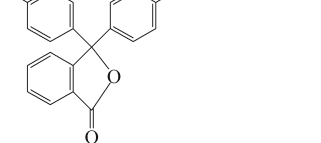
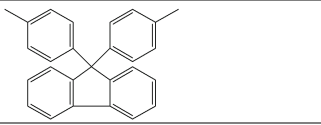
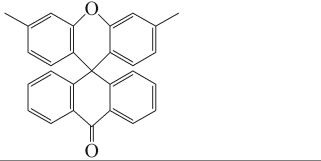
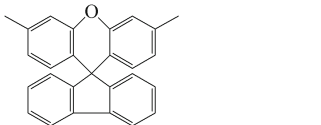
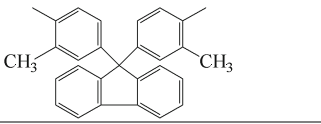


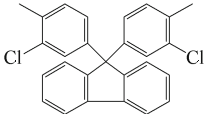
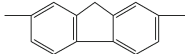
Fig. 3.26 Performance of the fluorine–amine-cured resins

Table 3.26 Basic properties of diglycidyl ether resins

General structural formula: $\text{CH}_2-\text{CH}-\text{CH}_2-\text{Ar}-(\text{O}-\text{CH}_2-\text{CH}-\text{CH}_2-\text{Ar})_n-\text{O}-\text{CH}_2-\text{CH}-\text{CH}_2$					
Resin	-Ar-	n	Epoxy equivalent/g·mol ⁻¹	Resin T _g /°C	Melting point/°C
DGEIB			240–250	1.195 Pa·s (30 °C)	
YX-400			185		105
EXA4032			147		1.160 Pa·s (25 °C)
YX-7			292		80
DGEBS			305		75
DGEPP		0.24	260	30	
DGEBF		0.36	305	50	132
DGEA		0.45	343	48	163
DGEFX		0.87	416	58	
DGEBF-DiMe		0.06	257		85–95

(continued)

Table 3.26 (continued)

General structural formula: $\text{CH}_2-\text{CH}-\text{CH}_2-\text{Ar}-(\text{O}-\text{CH}_2-\text{CH}-\text{CH}_2-\text{Ar})_n-\text{O}-\text{CH}_2-\text{CH}-\text{CH}_2$					
$\begin{array}{c} \text{O} \qquad \qquad \qquad \text{OH} \qquad \qquad \qquad \text{O} \\ \diagdown \quad \diagup \quad \quad \quad \diagdown \quad \diagup \quad \quad \quad \diagdown \quad \diagup \end{array}$					
Resin	-Ar-	n	Epoxy equivalent/g·mol ⁻¹	Resin T _g /°C	Melting point/°C
DGEBF-DiCl		0.02	270		198
DGEBD			202	125	135–145

Shell's YX-7-cured resins have spiral ring structures, and a mechanical relaxation zone exists between 50 and 100 °C as determined by the dynamic viscosity–elastic method. This is a low-temperature relaxation (β relax) that is not found in bisphenyl-A epoxy resins, and this comes from the aromatic rings connected to the P/O spiral rings. Because of this relaxation, its tensile strength and fracture elongation are double that of the corresponding epoxy resins.

Bisphenyl-S diglycidyl ether (DGEBS) is an epoxy resin containing a bisphenyl-S backbone with a low linear expansion coefficient. The reason for this is that the sulfuryls within the additives interact and hydrogen bonds form between the sulfuryl and hydroxyl group. This confines any sliding motion between the molecules. The commercial available resins of this type are the EXA 4023 resins supplied in Japan by the Printing Ink Chemical Industry Ltd.

Lo was the first to prepare phenolphthalein epoxy resins (DGEPP) [36], and they predicted that four possible structures exist for these synthesized resins, based on a balanced reaction between phenolphthalein and NaOH. Because of their yellow color and an IR absorption shift of phthalidyl (1725–1780 cm⁻¹), the quinone structures were initially thought to be the main component in these resins, but Lin and Pearce discovered that only a basic structure, orthophthalate, was present in the DGEOO resin based on HPLC, IR, UV and NMR results. Pure phenolphthalein diglycidyl ether extracted by HPLC is a white thick resin with a soft point at 15 °C. Because of the long molecular chains and the increase in relative molar mass, the yellow color comes from the interaction between the secondary hydroxyl and the phthalate and this is initiated through H bonds.

Korshak was the first to prepare 9,9-bi(4-hydroxyl-benzol)-p-fluorine-diglycidyl ether (DGEBF) and discovered that this resin can be transformed into a very stable thermal–oxidation material after curing by benzene-hex-carboxylic-tri-anhydride. Lin and Pearce created a processing technique to produce crystalline DGEBA with a melting point of 132 °C [37]. The monomers can be melted after quick cooling, and they have a softening temperature of 38 °C on a DSC curve. The softening and melting temperatures of DGEBF depend on resin crystallization and molar mass. Since the introduced fluorine structures give increased stiffness, this epoxy resin will have a higher thermal resistance than traditional DGEBA epoxy resins.

Table 3.27 Performance of cured fluorine epoxy resins

Resin/epoxy equivalent/g.mol ⁻¹	Formula 1	Formula 2	Formula 3	Formula 4	Formula 5
DGEBA/175	50	50	50	50	50
DGEBF/245					50
DGEBF-DiMe/257		50			
DGEBF-DiCl/270				50	
DGEBF-Mix/269	50				
DGEBF-Mix/268			50		
DDS	43.9	44.6	43.9	43.8	45.8
Modulus (25 °C)/ GPa	3.0	3.1	3.2	3.3	2.9
$T_g/^\circ\text{C}$	223	205	215	187	205

Note In DGEBF-Mix/269: 25% in 9,9-bi-(4-hydroxyl-benzol)-fluorine, 25% in 9,9-bi(3,5-dimethyl-4-hydroxyl-benzol)-fluorine, and 50% in 9-(4-hydroxyl-benzol)-9-(3,5-dimethyl-4-hydroxyl-benzol) fluorine-diglycidyl ether

In DGEBF-Mix/268: 25% in 9,9-bi-(3-methyl-4-hydroxyl-benzol)-fluorine, 25% in 9,9-bi-(3,5-dimethyl-4-hydroxyl-benzol)-fluorine, and 50% in 9-(4-hydroxyl-benzol)-9-(3,5-dimethyl-4-hydroxyl-benzol) fluorine-diglycidyl ether

Table 3.27 shows the properties of these fluorine-containing epoxy resins cured at 175 °C for 4 h and post-cured for 2 h at 225 °C. If cured by DDS, these resins will have a higher T_g (>187 °C) and stiffness (modulus > 2.9 MPa). Bi (o-replaced 4-hydroxyl-benzol)-fluorine-diglycidyl ether (DGEBF-DiMe and DiCl) has a higher T_g and modulus than DGEBF [38].

Fluorine epoxy resins can be used in coatings and composite matrixes because of decreased water absorption. However, their high prices are the main obstacle for application.

3.4.3.2 Poly-Glycidyl Ether Resins

The purpose of polyfunctional group epoxy resin development is to increase heat resistance. In Table 3.28, some polyfunctional group glycidyl epoxy resins are listed [31, 32].

Compared with traditional epoxy resins, bisphenol A phenolic-type epoxy resins give higher thermal resistance cured products, and the T_g can reach 224 °C when cured by DDS. They also have a good balance of properties. The available resins are supplied by Shell Epoxy Co. and Japan Printing Ink Chemical Ltd. The epoxy equivalent is 201 g/mol, and the melting point is 65 °C.

The naphthol-ring backbone-containing epoxy resins have good thermal resistance because of the hydrophobic naphthol-ring backbone, and they also have low

Table 3.28 The basic properties of diglycidyl ether resins

Resins	General structural formulate: $\begin{array}{c} \text{CH}_2-\text{CH}-\text{Ar}-\text{CH}-\text{CH}_2 \\ \diagup \quad \diagdown \quad \diagup \quad \diagdown \\ \text{O} \quad \quad \quad \text{O} \end{array}$ -Ar-	Epoxy equivalent/(g·mol) ⁻¹	Resin T _g /°C	Melting point /°C
BisphenoI A phenolic		201	65	
Naphthol-ring phenolic		240-275		110-150
Bi-cyclopenta-diene phenolic		310		65
DGE-GF				56-58
TGEPM		162-220	55-85	

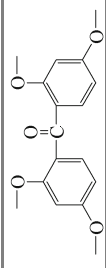
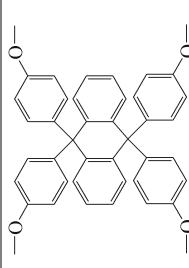
(continued)

Table 3.28 (continued)

Resins	General structural formulate: $\begin{array}{c} \text{CH}_2-\text{CH}-\text{Ar}-\text{CH}-\text{CH}_2 \\ \quad \quad \\ \text{O} \quad \quad \text{O} \end{array}$ -Ar-	Epoxy equivalent/g·mol ⁻¹	Resin T _g /°C	Melting point /°C
PCTGE		135		
VG3101		219		61
TGIC		103		100-104
E-1031s		196		92

(continued)

Table 3.28 (continued)

Resins	General structural formulate: $\begin{array}{c} \text{CH}_2-\text{CH}-\text{Ar}-\text{CH}-\text{CH}_2 \\ \diagup \quad \diagdown \quad \diagup \quad \diagdown \\ \text{O} \quad \quad \quad \text{O} \end{array}$	Epoxy equivalent/(g·mol) ⁻¹	Resin T _g /°C	Melting point /°C
BPTGE	---Ar--- 	143		
TGETA		204	143	

melting viscosity, low water absorption and an excellent adhering ability. Curing by DDS gives resins with a T_g as high as 300 °C.

Bi-cyclopentadiene epoxy resins, because of introduced cyclopentadiene in the backbone, are multifunctional epoxy resins with well-known toughness.

Tri-glycidyl ether epoxy resins, compared with phenolic-epoxy, have the advantages of narrow molar mass distribution and low melting viscosity.

1,3,5-Tri-(hexfluorine-bihydroxyl-2-propyl) benzol tri-glycidyl ether epoxy resins have superior hydrolysis stability and curing performance. To further increase their performance and reduce costs, tri-(4-hydroxyl-benzol) methane tri-glycidyl ether has undergone further development.

PGTGE epoxy resins have three epoxy groups connected to the aromatic rings and have a high T_g and elastic modulus, and good water resistance.

VG3101 was developed by Japan Mitsui Petrochem Co. and is a tri-glycidyl ether epoxy resin with an epoxy equivalent of 219 g/mol and a melting point of 61 °C. These resins use methyl-tetrahydrophthalic anhydride as a curing agent and 2-vinyl-4 methylimidazole as a promoter. After curing at 100 °C for 3 h and 230 °C for 2 h, the cured resins have a T_g of 250 °C and a thermal deformation temperature (HDT) of 235 °C.

In caustic dispersed inert media, isocyanic acid can react with excess epoxy-chloropropane to yield isocyanic acid tri-glycidyl ether (TGIL) crystal products [39]. 1 mol isocyanic acid requires at least 9 mol epoxy-chloropropane. Non-crystalline products can be purified according to the standards and extracted as two racemized products. Using methanol as a solution to extract and recrystallize poly-soluble products and low solubility isomers can generate poly-soluble isomers with a melting point of 103–104.5 °C and low-soluble isomers with a melting point of 156–157.5 °C. Commercially available products of this resin are Araldite PT-810 as supplied by Ciba-Geigy, and they are white crystal products with a melting range of 85–110 °C and an epoxy equivalent of 101–111 g/mol.

TGIC has excellent weather resistance, adhering ability, chemical stability, high thermal degradation temperature and good thermal aging performance. It can be used in powder coatings, castings, molding, structural laminates and adhesives [40]. TGIC can be cured by acid, anhydride, aromatic amines and isocyanic acid. TGIC blended with selected curing agents can be used in casting, for example, a casting material consisting of 41.7% TGIC and 58.3% hexhydrobenzol dianhydride can provide intermediate thermal resistance ($T_g = 160$ – 180 °C), good bending strength (59–117 MPa) and good impact properties.

To further increase the cross-linking density, many tetra-glycidyl ether resins have been developed and commercialized. Since no hydrophilic N atoms are contained within the molecules, these resins have low water absorption and good hot/wet performance.

Commercial products containing tetra-styrene tetra-glycidyl ether resins are E-1031s as supplied by Shell with an epoxy equivalent of 196 g/mol, a melting point of 92 °C and a T_g of 235 °C after curing with DDS. The tetra-styrene tetra-glycidyl ether prepared by the condensation of terephthalic aldehyde and benzene has a high cross-linking density and low water absorption.

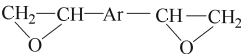
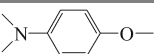
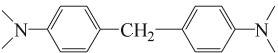
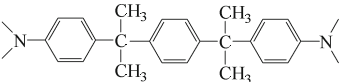
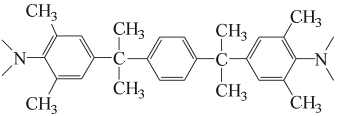
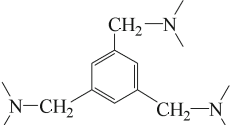
BPTGE is a kind of tetra-styrene tetra-glycidyl ether resin with good thermal resistance and toughness after curing by DDS. Its T_g can reach 260 °C. 9,9',10,10'-(4-hydroxyl-benzol)-anthrene (TGETA) is a white solid with a softening point of 143 °C.

3.4.3.3 Glycidyl Amine Resins

Glycidyl amine resins are still a commonly used resin in advanced composites. They have good thermal resistance but high water absorption because of the presence of N atoms. In Table 3.29, some modified glycidyl amine resins are given [41–47].

Tri-glycidyl p-aminophenol amines (TGAP) such as Araldite MY 0500 and 0510 from Ciba are low-viscosity liquids and have a very fast cure speed. The cured resins have superior thermal and chemical stabilities [42, 43]. This kind of resin is mainly used in adhesives, laminates and high-performance coatings. They are also used as viscosity modifiers or copolymerizing agents to increase the curing speed in low activity resins. However, because of the very fast curing speed, attention should be given to the selection of curing agents and curing conditions. Even a medium quantity of aliphatic amine curing can release a great amount of heat resulting in carbonization and smoke release. Problems can also arise when aromatic amines are gelled at high temperatures or with catalysis agents such as BF_3 ethylamine.

Table 3.29 Glycidyl ether resins

General structural formula: $\text{CH}_2\text{---CH---Ar---CH---CH}_2$ 				
Resin	–Ar–	Epoxy equivalent /g.mol ⁻¹	Viscosity/Pa.s	Melting point/°C
TGAP		110 95–107	3 (25 °C) 0.55–0.85 (25 °C)	
TGDDM		117–134	8–18 (50 °C) 3–6 (50 °C)	
TGBAP		150–170		50
TGMBAP		185–205		656
Hex-functional		96	9.2 (25 °C)	

DSC analysis shows that the reaction between TGAP and an aromatic biamine depends on the selected curing agent and the curing speed. The onset curing temperature can be decreased to 70 °C. The curing behavior is given in Table 3.30 [48], and the onset and peak temperatures are elevated as the DSC heating rate increased. If the correct ratio of curing agents selected, aromatic biamines will have the following order in terms of curing speed: *m*-benzene biamine > diaminodiphenylmethane > bietherdiphenylamine > disphenylaminesulfone. The curing reaction activation energy of this resin and the aromatic amine will be 40–70 kJ/mol.

Using aromatic anhydride as a TGAP curing agent is another developing trend in high-performance resin systems. Some bisphenol anhydrides such as benaophenonel-tetra-dianhydride (BPTA) and its derivatives can dissolve and cure TGAP at room temperature. The cured resins have better physical properties. TGAP and bisphenol-dianhydride systems can be used as structural adhesives [49].

4,4-Tetra-glycidyl-amine-diaminodiphenylmethane (TGDDM), because of its high performance/price ratio, may be the most practical high-performance epoxy resin and includes products like Araldite My 720 and 721 as supplied by Shell. These resins have good rheological behavior and a high degree of functional groups. They are suitable as resin matrixes in high-performance composites. They have very good thermal resistance, long-term high-temperature performance and mechanical property retention, low curing shrinkage, good chemical and radiation resistance and can be used as structural adhesives and laminates, and high-energy-resistant materials [50].

The TGDDM and DDS system, because of its high strength/density ratio, is commonly used in aerospace composites. TGDDM and DDS show an initial reaction at 80 °C, as shown by an exothermic peak on a DSC curve. Since the

Table 3.30 Curing behavior of TGAP and the aromatic biamine

Biamine	Heating up rate/°C·min ⁻¹	Reaction peak temperature/°C			Exothermic /J·g ⁻¹
		On-set	Peak	Terminal	
<i>m</i> -benzene biamine	5	70	110	160	465.6
	10	80	130	175	447.1
	20	98	149	197	422.6
4,4-diaminodiphenylmethane	5	85	138	168	443.2
	10	95	156	190	428.5
	20	102	168	205	399.2
4,4-bietherdiphenylamine	5	100	149	180	382.7
	10	112	169	205	335.2
	20	128	184	235	318.6
4,4-disphenylaminesulfone	5	110	186	235	325.8
	10	115	201	245	302.3
	20	130	220	268	285.9

blending temperature is high, the reaction onset temperature will be also high. The peak temperature of the resin system is about 275 °C. BF₃-ethylamine can accelerate the curing reaction yielding a high T_g of 240 °C. In FTIR, at a temperature of 177 °C, three principal reactions occur in the TGDDM/DDS system. Initially an amine-epoxy and then epoxy-hydroxyl reactions occur and basically form ethers in the last reaction stages [51].

The performance of the TGDDM resin upon curing by an equivalent of DDS is given in Table 3.31 [43–45]. The cured resins have high-performance retention at 150 °C.

Curing parameters are as follows: for A and B, 80 °C/2 h, 100 °C/1 h, 150 °C/4 h, 200 °C/7 h and for C, 180 °C/2 h, 210 °C/2 h.

α,α' -Bi-(4-hydroxyl-benzol)-p-diisopropyl benzene- N,N, N',N' -tetra-glycidyl ether (TGBAP) and α,α' -bi-(3,5-dimethyl-4-amine-1-benzol)-p-diisopropyl benzene- N,N, N',N' -tetra-glycidyl ether (TGMBAP) are two other commercialized high-performance four-functional epoxy resins and include Epon HPT 1071 and 1072 [46, 47]. They are low melting point dark brown resins with a T_g of 23 °C and 41 °C, respectively. Because of the molar chain extension, the hydrophilic N atom content in the resins decreases and the sensitivity of resin flow to temperature also

Table 3.31 Performance of the cured TGDDM/DDS system

Resin ratio and property	A	B	C
My720	100		
My721		100	
XU My 722			100
DDS	44	49	50
Tensile strength/MPa			
25 °C	59	48	58
150 °C	45	52	
Tensile modulus/GPa			
25 °C	3.7	3.9	4.2
150 °C	2.6	2.6	
Fracture elongation/%			
25 °C	1.8	1.3	1.6
150 °C	1.9	2.3	
Bending strength/MPa	90	127	125
Bending modulus/GPa	3.5	3.7	4.0
Compression strength			
Limit strength/MPa	230		
Yielding strength/MPa	130		
Compression modulus/GPa	1.9		
Thermal deforming temp/°C	238		
T_g /°C	177	265	240
Water absorption/%			3.7

Table 3.32 Performance comparison between cured TGBAP and TGMBAP

Resin ratio and property	A	B	C	D
Epon HPT 1071	100			
Epon HPT 1072		100		
Epon 825			100	
Epon HPT 1061				100
Epon HPT 1062				100
DDS	41.5	53.8	53.2	110
$T_g/^\circ\text{C}$	429	241	239	232
Water absorption/% ^①	3.6	2.1	1.4	1.2
Bending strength/MPa ^②				
Room temperature				
93 °C	140	140	130	124
Bending modulus/GPa ^②	90	97	90	90
Room temperature				
93 °C				
Bending strength retention/%	3.9	3.4	3.4	3.0
Bending modulus retention/%	3.0	2.9	3.2	2.7
	6.5	70	68	72
	7.0	86	96	89

① In boiling water for 48 h. ② In water for 2 weeks at 93 °C

decreases. The viscosity at 100 °C is within 0.02–0.03 Pa·s. Compared with TGBAP, TGMBAP has been further improved in terms of hot/wet performance and thermal resistance. In Table 3.32, the performance of these two resins cured by high-performance aromatic amines is included. Since large amounts of methyl aromatic amine curing agents were used and water absorption was further decreased, the hot/wet performance retention rate increased significantly.

Because these two resins exist in the solid state at room temperature, the application of heat or a diluting agent is needed to improve processing performance (e.g., DGEBA). Basically, resins or blended resins are heated to 150–170 °C, and aromatic curing agents added to give uniform blended resins.

An alternative approach to increasing thermal resistance and to decreasing moisture absorption is to introduce halogen groups into the epoxy molecular backbone [52].

3.4.4 Epoxy Resin Toughening

The most serious drawback of epoxy resins is their poor toughness. Cured epoxy resins are brittle and crack easily because of their low impact resistance. For high-performance composite applications, epoxy resins need to be improved. At present, the toughening of epoxy resins includes the following approaches [53]:

- (1) Use of a secondary phase such as elastomers, thermoplastics or stiffening particles for toughening.
- (2) Use of thermoplastic resins to continuously penetrate the thermosetting resins to form interlaced networks.
- (3) Changing the chemical structures in the cross-linking networks (adding “flexible segments” into the cross-linking network) to increase cross-like molecular activity.
- (4) Controlling the heterogeneity of molar cross-linking to form inhomogeneous structures that are helpful for plastic deformation.

3.4.4.1 Rubber Elastomer Toughening

Elastomer molecules with activated end groups can react with epoxy groups and can block into epoxy crossed networks. They will have much better toughening efficiency than common rubbers. Commonly used toughening elastomers include liquid carboxylic-terminal butadiene-nitrile (CTBN), liquid irregular carboxylic butadiene-nitrile rubbers, carboxylic-terminal polybutadienes, liquid carboxylic-terminal silicon rubbers, liquid-phase polysulfide rubbers and polyether-terminal elastomers. To achieve toughening, the elastomers should be compatible with the uncured resins, but they also need to form elastomer dominated particular dispersion phases in the cured resins. Rubber elastomer toughening efficiency on epoxy resins will depend on the dispersion phase (matrix) structures as well as interfacial bonding [54].

Among the various toughening agents, carboxylic-terminal butadiene-nitrile rubbers (CTBN) were developed first. In high cross-link density and network chain rigid epoxy resins, the consumed energy upon rubber tensile peering can be substantial. In lower cross-link systems, the particle-induced matrix energy consumption will characterize the critical fracture process. Fracture mechanics studies have indicated that the plasticized expansions caused by the holes formed after CTBN particle debonding or fracturing, as well as the shear yield deformations induced by particles or holes will be a critical toughening mechanism. The principal factors that can affect CTBN toughening efficiency include the acrylic nitrile content in CTBN, the CTBN ratio, curing agents, curing temperature, average net chain length and the number of functional groups [55].

CTBN-toughened epoxy resins will provide a notable improvement in mechanical properties (see Table 3.33 [56]). However, only a small amount of

Table 3.33 Mechanical performance of CTBN (15)-modified epoxy resins

Property	Unmodified	Modified
Tensile strength/MPa	73.1	95.8
Fracture elongation/%	4.8	9.0
Elastic modulus/GPa	2.8	2.7
Fracture toughness/kJ·m ⁻²	0.18	5.3–5.8

modifying rubbers can be dissolved in these resins, and this may result in a decrease in the modulus and T_g of the resin system. This effect can be eliminated by using core-shell rubber toughening agents. For example, if 7.5% core-shell rubbers are added to a blended epoxy system composed by 50% DGEBA and 50% DGEBF, the toughness will be significantly increased because of the added toughening agents, while T_g will not be decrease.

3.4.4.2 Thermoplastic Resin Toughening

To increase epoxy resin toughness and guarantee the modulus, thermoplastic resins with a relatively high molar mass or containing low molar functional copolymers can be used to toughen and improve epoxy resins. Bridging-crack anchoring models are suitable to demonstrate qualitatively or quantitatively the toughening behavior of strong and tough thermoplastic particles [54].

(1) Bridging confinement

Most thermoplastic resins have a similar elastic modulus and much larger fracture elongation compared with epoxy resins, which will cause the extendable thermoplastic particles that are bridged on the brittle cracked epoxy surface to become confined resulting in close crack growth.

(2) Crack anchoring

Bridging particles can confine or stop the crack frontiers from extending forward, and the bridging forces can anchor the cracks positioned on the bridging points, and this causes the crack leading frontier to stretch out in bow-wave patterns.

Polyethersulfone (PES)-modified amine can be used to cure epoxy resins, and the typical formula and curing procedures are: to 100 units of tetra-functional epoxy resin blended with 15 units of PES are added 80 units of aromatic amine curing agent. Upon dissolution in methylene dichloride and adding 1 unit of 2-vinyl-1,4-biether methyl, the mixture is heated for 8 h at 50 °C under vacuum and then heated for 2 h at 150 °C. A final cure is carried out for 2 h at 180 °C. In the cured resin, a double-phase microstructure distribution is observed. These dispersed phases can suppress crack generation and growth by increasing the fracture energy so that the toughness and adhering strength of the cured resins are improved [57].

Using high thermal resistance thermoplastic polyetherimide (PEI) to modify epoxy resins can also increase toughness. PEI is predried for 2 h at 120 °C under vacuum, then dissolved in methylene dichloride and blended with TGDDM at room temperature, and the mixture is heated to 100 °C in an oil bath to remove methylene dichloride. When the mixture enters a glassy state from the uniform and clean glue liquid, it is heated to 150 °C and DDS is added slowly while stirring. In Fig. 3.27, the effect of PEI content on fracture energy and glass transition temperature T_g is shown [58].

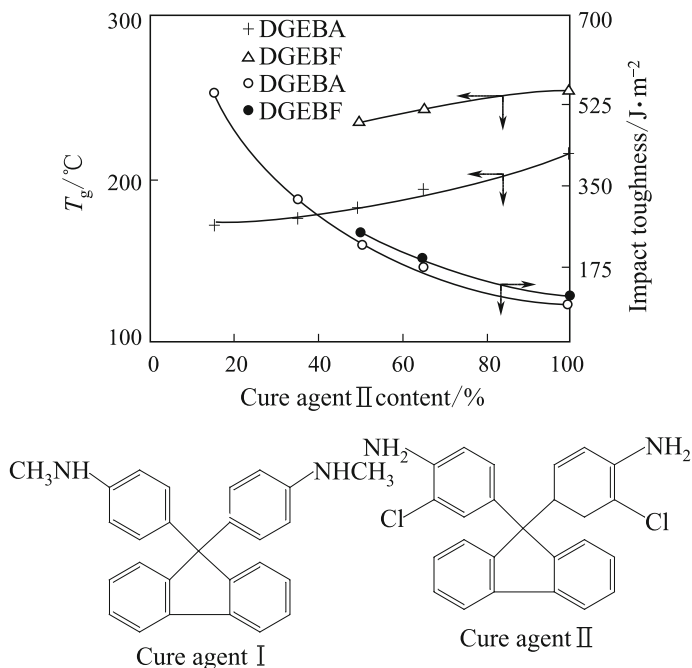


Fig. 3.27 Impact toughness and T_g of PEI-modified epoxy resins

In general, the toughening efficiency of thermoplastic resins will be lower than rubber toughening, but the selection of a proper thermoplastic resin can improve toughness and maintain the modulus and T_g of the epoxy resin system. Amine-terminated aryletherketones have very good toughening effects. They are condensed using 4,4'-bifluorine-diphenyl ketone and bisphenol A and then copolymerized using 4-aminephenyl end closing. The copolymer molar mass is controlled by the ratio of 4,4'-bifluorine-diphenyl ketone and bisphenol A. Figure 3.28 shows the copolymer molecular structures [59].

The amine-terminated copolymer of hydroquinone and methyl hydroquinone is a half-crystallized polymer, and the amine-terminated copolymer of butyl hydroquinone and bisphenol A is non-crystalline. Non-crystalline polymers can be blended with epoxy resins at 120–150 °C, and half-crystalline hydroquinone copolymers do not dissolve in any commercial epoxy resins. Methyl hydroquinone can only be blended with Epon 828 at higher than its melting point of 230 °C.

The curing agents DDS and DDM should be added based on the epoxy equivalent. The thermal, mechanical and structural performance of epoxy resins toughened by different amine-terminated aryletherketone copolymers is given in Table 3.34. As the copolymer ratio is increased, the fracture energy increases and T_g decreases. The phase separation during cross-linking and curing is the origin of the process. These resin structures depend on the quantity of toughening agent used.

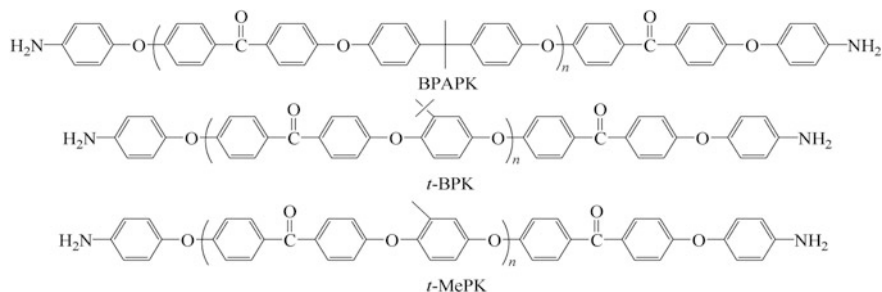


Fig. 3.28 Chemical structures of amine-terminated aryetherketones

Table 3.34 Performance of amine-terminated aryetherketone-modified Epon 828 resins

Blended system	Ratio/%	$T_g/^\circ\text{C}$	Modulus/GPa	Fracture toughness/ $\text{J}\cdot\text{m}^{-2}$	Phase separation
700-Mn BPAPK/Epon 828-DDS	0	213	2.5	315	–
	20	145	2.5	903	A
	30	145	2.5	1386	B
	40	145	2.5	2338	B
21000-Mn BPAPK/Epon 828-DDM	0	185	2.3	280	–
	10	175	2.4	516	A
	20	160	2.4	891	–
	25	160	2.4	1348	B
3200-Mnt-BPK/Epon 828-DDS	0	213	2.5	315	–
	30	180	2.7	905	B
	40	160	2.7	875	B
4600-Mnt-BPK/Epon 828-DDS	30	165	2.6	880	A/B
	40	165	2.7	1274	B
5000-Mnt-MePK/Epon 828-DDS	0	213	2.5	315	–
	10	195	2.6	318	–
	20	195	3.0	359	–

Note A—matrixes in continuous phase; B—toughening agents in continuous phase

3.4.4.3 Thermal Liquid Crystal Toughening

Thermal liquid crystal polymer (TLCP) toughening can both increase epoxy toughness and guarantee other mechanical properties and thermal resistance. They have been commonly used since the 1990s [60]. For example, adding 2% TLCP to toughen epoxy resins can result in a 20% increment in fracture toughness. As the TLCP content increases, the material toughness will be significantly enhanced

while the bending modulus will remain unchanged, and T_g will increase slightly. The cured system is a double-phase structure, and the TLCP in the fibril pattern remains in continuous epoxy resin phases while the TLCP morphology depends on the blending process. Small amounts of TLCP fibrils can inhibit cracking and increase the toughness of brittle matrixes, but this does not decrease the material thermal resistance or stiffness. Compared with thermoplastic resins, similar toughening effects can be achieved when the ratio of TLCP is 25–30% of the thermoplastic resin.

3.4.5 High-Performance Epoxy Composites

3.4.5.1 High-Performance Epoxy Composite Properties

The improvement in epoxy resins basically focuses on two aspects: One is to improve hot/wet performance to increase the service temperature, which could be realized by the synthesis of new structural epoxy resins and curing agents and the other is to enhance the toughness to increase the composite's damage tolerance. This could be realized using new curing agents or toughening agents. Many high-performance epoxy resin matrixes have been successfully developed, for example, the Hercules 8552 resin, R6376 from Ciba-Geigy, 977-3 from ICI, 3234, 5228 5288 and LT-01 from the Beijing Institute of Aeronautical Material (BIAM). Apart from the higher thermal stability and hot/wet performance, a critical feature of these resins is the significant increase in toughness.

In Tables 3.35, 3.36, 3.37, 3.38, 3.39, 3.40, 3.41, 3.42, 3.43, 3.44, 3.45, 3.46, 3.47 and 3.48, the maximum service temperature, typical mechanical properties and hot/wet performance of some high-performance epoxy resins are listed [61–66].

Table 3.35 Maximum service temperature of high-performance epoxy resins

Resin designation	Service temp./°C	Manufacturers
977-1	82	ICI
977-2	93	ICI
977-3	132	ICI
8552	121	Hercules
R6376	130	Ciba-Geigr
3234	80	BAIM
5228	130	BIAM
5288	130	BIAM
LT-01 ^①	80–130	BIAM

① LT-01 is a low-temperature curable (70–80 °C) high-performance epoxy composite matrix

Table 3.36 G803/3234 C fabric-reinforced epoxy composite mechanical performance

Performances	Testing temp./°C			Testing method
	Room temp.	80 °C	-55 °C	
Longitudinal tensile strength/MPa	756	748	733	Q/6S 1138-1994
Longitudinal tensile modulus/GPa	69	65	64	
Poisson's ratio/%	0.064	0.063	0.061	
Longitudinal compression strength/MPa	557	437	538	Q/6S 1143-1994
Longitudinal compression modulus/GPa	64	60	61	
L/T shear strength/MPa	118	99	120	GB/T 3355-1982
L/T shear modulus/GPa	4.2	4.0	4.7	
Interlaminar shear strength/MPa	68	56		Q/6S 1142-1994
Longitudinal bending strength/MPa	924	772		Q/6S 1141-1994 Z9-1279-1992
Longitudinal bending modulus/GPa	59	62		

Table 3.37 G803/3234 C fabric-reinforced epoxy composite hot/wet performance

Performances		Testing temp./°C		Testing method
		Room temp.	80 °C	
Longitudinal tensile strength/MPa	Typical value ^C	421	343	Q/6S 1143-1994
	Typical value ^D	328	340	
Longitudinal tensile modulus/GPa	Typical value ^C		51	
	Typical value ^D		52	
Longitudinal bending strength/MPa	Typical value ^A	696		Q/6S 1141-1994
	Typical value ^B	890		
	Typical value ^C	712		
	Typical value ^D	600		
	Typical value ^A	58		
	Typical value ^B	60		
	Typical value ^C	61		
	Typical value ^D	57		

(continued)

Table 3.37 (continued)

Performances		Testing temp./°C		Testing method
		Room temp.	80 °C	
Interlaminar shear strength/MPa	Typical value ^A	52		Q/6S 1142-1994
	Typical value ^B	62		
	Typical value ^C	45		
	Typical value ^D	47		
L/T shear strength/MPa	Typical value ^C	97	68	GB/T 3355-1982
	Typical value ^D	96	60	
L/T shear modulus/GPa	Typical value ^C	4.0	3.5	
	Typical value ^D	4.0	4.7	

Note A—Specimen put in distilled water container and heated for 48 h in a 100–105 °C chamber
 B—Specimen after A treated and immediately dried for 24 h at 100–105 °C
 C—Specimen treated for 750 h at 70 °C and R.H. > 95%
 D—Specimen treated for 1000 h at 70 °C and R.H. > 95%

Table 3.38 T300/5228 epoxy composite mechanical performance

Performances	Testing temp.			Testing method
	Room temp.		130 °C	
	Min. value	Typical value	Typical value	
Longitudinal tensile strength/MPa	1650	1744		GB/T 3354-1994
Longitudinal tensile modulus/GPa	110	137		
Transverse tensile strength/MPa	60	81		
Transverse tensile modulus/GPa	7.0	8.8		
Longitudinal compression strength/MPa	1000	1230		GB/T 3856-1983
Longitudinal compression modulus/GPa	100	110		
Transverse compression strength/MPa		212		
Transverse compression modulus/GPa	7.0	9.3		
L/T shear strength/MPa		124		GB/T 3355-1982
L/T shear modulus/GPa		4.4		
Interlaminar shear strength/MPa		106	63	JC/T 7733-1982 (1996)
Longitudinal bending strength/MPa	1500	1780	1250	GB/T 3356-1999
Longitudinal bending modulus/GPa	110	130	137	

Table 3.39 T300/5228 epoxy composite toughness performance

Performances		Testing temp.		Testing method
		Room temp.		
Transverse tensile strength/MPa	Typical value	81		GB/T 3354-1999
Transverse tensile modulus/GPa	Typical value	8.8		
Transverse tensile fracture strain/%	Typical value	0.96		
Open-hole tensile strength/MPa	Typical value	333		HB 6740-1993
Open-hole compression strength/MPa	Typical value	341		HB 6741-1993
Edgy delamination/ $J \cdot m^{-2}$	Typical value	348		HB 7071-1994
Model I fracture toughness, $G_{IC}/J \cdot m^{-2}$	Typical value	227		HB 7402-1996
Model II fracture toughness, $G_{IIc}/J \cdot m^{-2}$	Typical value	1105		HB 7403-1996
Compression strength after impact (6.67 J/mm^2)/MPa	Typical value	190		NASA-RP-1142

Table 3.40 T800/5288 epoxy composite mechanical performance

Performances		Testing temp.		Testing method
		Room temp.	130 °C	
Longitudinal tensile strength/MPa	Typical value	2630		GB/T 3354-1999
Longitudinal tensile modulus/GPa	Typical value	172		
Longitudinal tensile Poission's ratio	Typical value	0.35		
Transverse tensile strength/MPa	Typical value	62		
Transverse tensile modulus/GPa	Typical value	7.0		
Longitudinal compression strength/MPa	Typical value	1480		GB/T 3856-1983
Longitudinal compression modulus/GPa	Typical value	169		
Transverse compression strength/MPa	Typical value	213		
Transverse compression modulus/GPa	Typical value	8.1		
L/T shear strength/MPa	Typical value	109		GB/T 3355-1982
L/T shear modulus/GPa	Typical value	3.9		
Interlaminar shear strength/MPa	Typical value	107	58	JC/T 773-1982 (1996)
Longitudinal bending strength/MPa	Typical value	1830	1780	GB/T 3356-1999
Longitudinal bending modulus/GPa	Typical value	151	134	

Table 3.41 T800/5288 epoxy composite toughness performance

Performances		Testing temp.	Testing method
		Room temp.	
Open-hole tensile strength/MPa	Typical value	464	HB 6740-1993
Open-hole compression strength/MPa	Typical value	274	HB 6741-1993
Edgy delamination/ $J \cdot m^{-2}$	Typical value	371	HB 7071-1994
Model I fracture toughness, $G_{IC}/J \cdot m^{-2}$	Typical value	470	HB 7402-1996
Model II fracture toughness, $G_{IIC}/J \cdot m^{-2}$	Typical value	765	HB 7403-1996
Compression strength after impact (6.67 J/mm^2)/MPa	Typical value	272	BSS-7260

Table 3.42 T300/LT-01 low-temperature curing epoxy composite mechanical performance

Performances		Testing temp.		Testing method
		Room temp.	130 °C	
Longitudinal tensile strength/MPa	Typical value	1560	1550	GB/T 3354-1999
Longitudinal tensile modulus/GPa	Typical value	136	130	
Longitudinal tensile Poisson's ratio	Typical value	0.31	–	
Longitudinal compression strength/MPa	Typical value	1380	1224	GB/T 3856-1983
Longitudinal compression modulus/GPa	Typical value	136	130	
In-plane shear strength/MPa	Typical value	83.7	67.9	GB/T 3355-1982
In-plane shear modulus/GPa	Typical value	4.90	4.11	
Short beam shear strength/MPa	Typical value	94.6	65.5	JC/T 773-1982 (1996)
Longitudinal bending strength/MPa	Typical value	1627	1321	GB/T 3356-1999
Longitudinal bending modulus/GPa	Typical value	135	133	
Transverse compression strength/MPa	Typical value	215	–	GB/T 3856-1983
Transverse compression modulus/GPa	Typical value	8.1	–	
Transverse tensile strength/MPa	Typical value	43.7	–	GB/T 3354-1999
Transverse tensile modulus/GPa	Typical value	8.1	–	

Table 3.43 T300/LT-01 low-temperature cure epoxy composite hot/wet performance

Performances		Testing temp.		Testing method
		130 °C		
Longitudinal compression strength/MPa	Typical value	964		GB/T 3856-1983
Open-hole compression strength/MPa	Typical value	272		HB 6740-1993
Short beam shear strength/MPa	Typical value	43.6		JC/T 773-1982 (1996)
Bending strength/MPa	Typical value	1045		GB/T 3356-1999
Bending modulus/GPa	Typical value	121		

Note Wet specimen boiled in water for 48 h at 95–100 °C

Table 3.44 T700/LT-03 low-temperature curing epoxy composite mechanical performance

Performances		Testing temp.		Testing method
		Room temp.	80 °C	
Longitudinal tensile strength/MPa	Typical value	2377	2310	GB/T 3354-1999
Longitudinal tensile modulus/GPa	Typical value	120	120	
Longitudinal tensile Poisson's ratio	Typical value	0.316	–	
Longitudinal compression strength/MPa	Typical value	1074	926	GB/T 3856-1983
Longitudinal compression modulus/GPa	Typical value	128	7.2	
In-plane shear strength/MPa	Typical value	104	83.8	GB/T 3356-1982
In-plane shear modulus/GPa	Typical value	4.7	4.1	
Short beam shear strength/MPa	Typical value	75	62	JC/T 773-1982 (1996)
Longitudinal bending strength/MPa	Typical value	1497	1198	GB/T 3356-1999
Longitudinal bending modulus/GPa	Typical value	120	113	
Transverse compression strength/MPa	Typical value	128	96	GB/T 3856-1983
Transverse compression modulus/GPa	Typical value	7.2	6.8	
Transverse tensile strength/MPa	Typical value	42.8	34.6	GB/T 3354-1999
Transverse tensile modulus/GPa	Typical value	7.3	6.78	

Table 3.45 T700/LT-03 low-temperature curing epoxy composite toughness performance

Performances		Testing temp.	Testing method
		Room temp.	
Model I fracture toughness, $G_{IC}/J \cdot m^{-2}$	Typical value	309	HB 7402-1996
Model II fracture toughness, $G_{IIC}/J \cdot m^{-2}$	Typical value	761	HB 7403-1996
Edgy delamination/ $J \cdot m^{-2}$	Typical value	241	HB 7071-1994
Open-hole tensile strength/MPa	Typical value	482	HB 6740-1993
Open-hole compression strength/MPa	Typical value	277	HB 6741-1993
Compression strength after impact (6.67 J/mm ²)/MPa	Typical value	195	BSS 7260

Table 3.46 IM-7/977-3 epoxy composite mechanical performance

Performances		Testing temp./°C	
		Room temp.	-60 °C
Longitudinal tensile modulus/GPa	Average value	2510	2430
Longitudinal tensile strength/MPa	Average value	162	158
Transverse tensile strength/MPa	Average value	64.1	
Transverse tensile modulus/GPa	Average value	8.34	
Longitudinal compression strength/MPa	Average value	1680	
Longitudinal compression modulus/GPa	Average value	154	
L/T shear modulus/GPa	Average value	4.96	
Interlaminar shear strength/MPa	Average value	127	
Longitudinal bending strength/MPa	Average value	1765	
Longitudinal bending modulus/GPa	Average value	150	

Table 3.47 IM-7/8552 epoxy composite mechanical performance

Performances		Testing temp.			
		-55 °C	25 °C	91 °C	93 °C
Longitudinal tensile strength/MPa	Typical value	2570	2721	2535	
Longitudinal tensile modulus/GPa	Typical value	163	164	163	
Transverse tensile strength/MPa	Typical value	174	111		92
Transverse tensile modulus/GPa	Typical value	19	11.7		10.3
Longitudinal compression strength/MPa	Typical value		1688	1481	
Longitudinal compression modulus/GPa	Typical value		149	162	
Transverse compression strength/MPa	Typical value		304	226	
Transverse compression modulus/GPa	Typical value		12.9	10.8	
L/T shear strength/MPa	Typical value		120		106
Interlaminar shear strength/MPa	Typical value		137	93.7	
Longitudinal bending strength/MPa	Typical value		1860		
Longitudinal bending modulus/GPa	Typical value		151		
Compression after impact/MPa	Typical value		213		

Table 3.48 T800H/R6376 epoxy composite mechanical performance

Performances		Testing temp.		
		-55 °C	Room. temp.	82 °C
Longitudinal tensile strength/MPa	Average value	2480	2480	2480
Longitudinal tensile modulus/GPa	Average value	156	147	
Longitudinal tensile strain/%	Average value	1.44	1.50	1.41
Poisson's ratio	Average value	0.31	0.31	0.32
Transverse tensile strength/MPa	Average value	64	78	63
Transverse tensile modulus/GPa	Average value	10.7	8.7	8.4
Transverse tensile strain/%	Average value	0.62	0.93	0.80
Longitudinal compression strength/MPa	Average value		1791	1584
Longitudinal compression modulus/GPa	Average value		147	157
L/T shear strength/MPa	Average value		200	200
L/T shear modulus/GPa	Average value		16.7	15.6
L/T tensile strain/%	Typical value		5.94	7.17
Interlaminar shear strength/MPa	Typical value		125	82
Longitudinal fracture strength/GPa	Typical value		2.5	

3.4.5.2 High-Performance Composite Applications

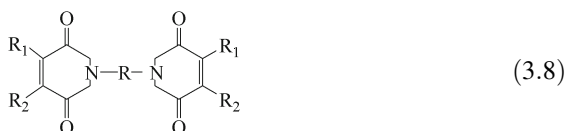
Composite applications in the aero industries can be split into three stages: Initially, using an equivalent design to select airplane non-load-bearing or secondary structures made using low toughness composites to make items like movable hatch caps, wall panels and cabin doors. The next stage is using an optimized design to select composites with the required toughness for load-bearing vertical tails, rudders and horizontal tails. In the late 1980s to early 1990s, high-performance composite applications were extended to primary structures such as wings and fuselages. Advanced fighter jets including the Rafale, EFA, JAS39, Lavi, F22 and F35 mainly contain composites in their primary structures. Their content ranges from 25 to 30% of the total structure mass. High-performance epoxy composites used in aircraft applications are given in Table 3.49.

Table 3.49 High-performance epoxy composites in aircraft applications

Composites	Manufacturer	Aircraft type	Applications
IM7/977-2	ICI	Jet fighters	Wing, skin
IM7/8552	Hercules	Helicopters	Primary structures
T300/R6376	Ciba	Large commercial planes	Central wing boss
G803/3234	BAIM	Helicopters	Load-bearing structures
T300/5228	BAIM	Jet fighters	Secondary structures
T300/LT-01	BAIM	Large commercial planes	Fin and other load-bearing structures
T300/LT-03	BAIM	Unmanned planes	Wing and fuselage

3.5 Bismaleimide (BMI) Resin Matrixes

Bismaleimide (BMI) is a double-functional containing active maleimide terminal groups with a general formula as follows:



In late 1960s, the Rhone-Poulenc Company in France developed the M-33BMI resin and its composites. Since then, BMI resins prepared from BMI monomers have received an increasing amount of attention. BMI resins have similar flow and processing abilities to typical thermosetting resins, and furthermore, BMI resins have the advantages of high-temperature resistance, radiation resistance, hot/wet resistance, low water absorption and small thermal linear expansion coefficients (TEC). Overcoming the drawbacks of the low hot/wet resistance in epoxy resins and the high temperatures and pressures required for polyamide resin processing has resulted in BMI resins recently undergoing fast development and wide application [5, 67]. In Sect. 3.4 of this chapter, the main commercial BMI resin products available for high-tech applications are discussed.

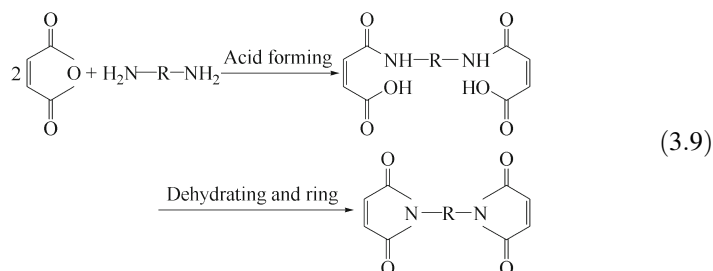
In China, preliminary research into BMI resins started in the 1970s for use in electric isolation materials, sand wheel adhesives, rubber cross-linking agents and plastic additives. In the 1980s, the development of BMI for advanced composite matrixes was initiated and some progress has been made. The commercial BMI resins available in China include QY8911, QY9511, 5405, 5428, 5429 and 4501 [68, 69].

3.5.1 BMI Physical Properties

3.5.1.1 BMI Monomers

(1) Synthesis of BMI monomers

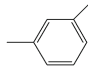
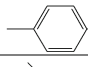
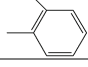
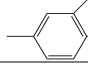
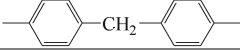
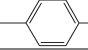
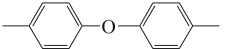
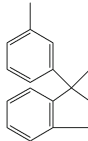
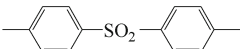
In 1948, US scientist Searle acquired the patent for BMI synthesis. Improved Searle methods were used to prepare various BMI resins with different structures and performances. BMI monomers can be synthesized by the pathway shown in Scheme 3.2: Typically, 2 mol maleic anhydride and 1 mol biamine are used to prepare bismaleimide acids, and then ring reactions take place between the bismaleimide acids to produce BMI monomers. By selecting different structural biamines and maleic anhydrides, using proper reaction conditions, material formulae, purification and separation processes, BMI monomers with different structures and properties can be prepared.



(2) Physical properties

BMI monomers are mostly crystalline solids, and aliphatic BMI generally have lower melting points, while aromatic BMI have relatively higher melting points. Asymmetric factors like introduced substituent groups will cause defects in BMI crystals and subsequently affect the melting point. In general, to improve BMI resin processing performance, they require lower melting points to guarantee BMI curing performance. In Table 3.50, some common diphenylmethane BMI monomers are listed together with their melting points. Commonly used BMI monomers are generally not soluble in common organic solvents like acetone and alcohol, and only dissolve in strong polar solvents such as dimethyl polyamide (DMP) or N-methyl ketopyrrolidine (NMP).

Table 3.50 Common diphenylmethane BMI monomer melting points

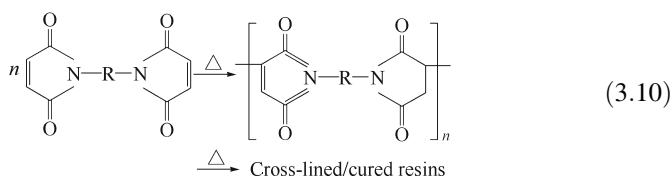
R	Melting point/°C	R	Melting point/°C
CH ₂	156–158	(CH ₂) ₈	113–118
(CH ₂) ₂	190–192	(CH ₂) ₁₀	111–113
(CH ₂) ₄	171		198–201
(CH ₂) ₁₂	110–112		>340
–CH ₂ –C(CH ₃)–CH ₂ –			307–309
–C(CH ₃)–(CH ₂) ₂ –	70–130		172–174
	154–156		307–309
	180–181		>300
	251–153		
(CH ₂) ₆	137–138		

(3) Chemical properties

Because of the electronic attraction between the two O-hydroxyls in the BMI monomer, its double bonds are electron poor. Therefore, through their double bonds, BMI monomers can undergo additive reactions with active H-containing polymers such as diamines, hydrazides, amides, sulfhydryls, cyanuric acids and hydroxyls. They can also copolymerize with epoxy resins, unsaturated bond contained polymers and other BMI monomers. Self-polymerization in BMI monomers can also take place under catalysis or applied heat. Their curing behavior and post-curing conditions are closely related to their chemical structures.

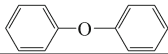
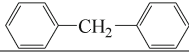
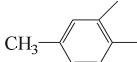
3.5.1.2 BMI Curing

BMI monomers can self-polymerize and cross-link under proper conditions as shown by the basic reactions given as follows:



Because of their constituent imides and high cross-linking density, cured BMI have superior thermal resistance and their service temperature can reach 177–230 °C

Table 3.51 Thermal resistance of some cured BMI

R	$T_d/^\circ\text{C}$	Weight loss rate/%	Polymerization condition/h·K ⁻¹
(CH ₂) ₂	435	—	1/195 + 3/240
(CH ₂) ₆	420	3.20	1/170 + 3/240
(CH ₂) ₈	408	3.30	1/170 + 3/240
(CH ₂) ₁₀	400	3.10	1/170 + 3/240
(CH ₂) ₁₂	380	3.20	1/170 + 3/240
	438	1.10	1/170 + 3/240
	452	1.40	1/185 + 3/(240–260)
	462	0.10	1/(175–181) + 3/240

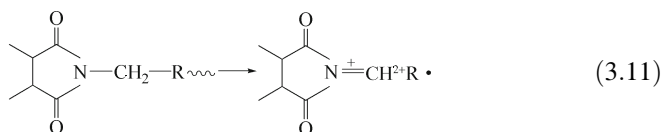
with a T_g generally higher than 250 °C. Table 3.51 lists some cure BMI resins with their thermal properties. In terms of aliphatic cured BMI, as the number of methyls increases, the initial thermal degradation temperature (T_d) of the cured BMI will decrease.

Aromatic BMI have a higher T_d than aliphatic BMI, and their T_d is closely related to the cross-linking density. Within a certain range, the T_d will increase as the cross-linking density increases.

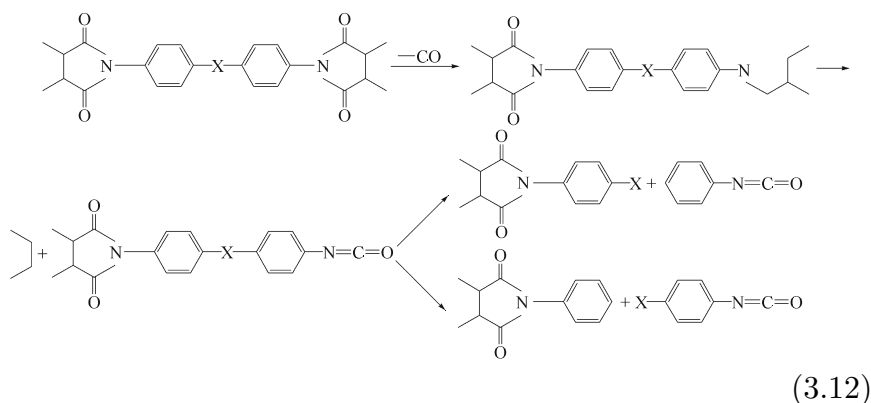
Cured BMI have dense structures and less defects, in addition to much higher strength and modulus. However, their higher cross-linking density results in an increase in molar chain rigidity giving higher brittleness. Therefore, cured BMI have poor impact resistance, lower fracture elongation and toughness.

Cured BMI show complex thermal degradation behavior, and different structures will give different thermal degradation behavior, and this can be summarized as follows:

- (1) In cured aliphatic BMI, thermal degradations generally occur at the C–C bonds between the R-chains in the imide rings, but mostly at the C–C bonds closest to the imide rings. The reaction is shown in Scheme 3.11.



- (2) For cured aromatic BMI, the thermal degradation has a different mechanism compared with that of aliphatic BMI. The degradation will initially produce maleimide rings as shown in Scheme 3.12



Many factors will affect the cured BMI thermal degradation. To increase the thermal degradation temperature, the monomer quality, cross-linking extent and molecular structures should be taken into account.

3.5.2 BMI Resin Modification

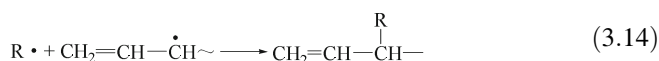
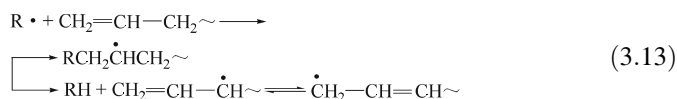
Although BMI has good mechanical properties and thermal resistance, unmodified BMI resins have some drawbacks such as high melting points, dissolution difficulties, high processing temperatures and brittleness of cured resins; among these, poor toughness is the main obstacle to BMI resin application and development. With BMI modification, much attention has been given to the following issues: ① increasing toughness. As a result of continuous development in advanced science and aerospace technologies, stricter demands have been placed on material performance; for example, tougher composites are required in aeronautics, to increase the composite weight-saving efficiency; ② improving processing performance. Although the processing temperatures of BMI resins are far lower than those required for polyimide (PI) resins, they are much higher than those required for epoxy resins. BMI prepregs have poorer viscosity than epoxy prepregs, and this will result in difficulties during composite preparations. Innovative processing techniques such as resin transfer molding (RTM) and resin film infusion (RFI) also require BMI resins to have improved processing performance. Therefore, improving processing performance is an important aspect in BMI modification [5, 70]; ③ decreasing costs. Price is a common concern for all products. Apart from increasing the production volume to reduce raw material prices, high-efficiency and low-cost processing technologies are also becoming more interesting [68].

A number of modifications are available for BMI resins, and the most interesting is to improve resin toughness. Toughening modification for BMI resins includes the following approaches [5, 68]: ① copolymerization with allyl compounds; ② aromatic biamine chain extension; ③ epoxy modification; ④ thermoplastic resin toughening; ⑤ aromatic cyanic ester modification; and ⑥ new monomer synthesis. In addition, studies on BMI processing improvements have been carried out, and in the following sections, some main modifications of BMI resins will be briefly presented.

3.5.2.1 Copolymerization with Alkenyl Compounds

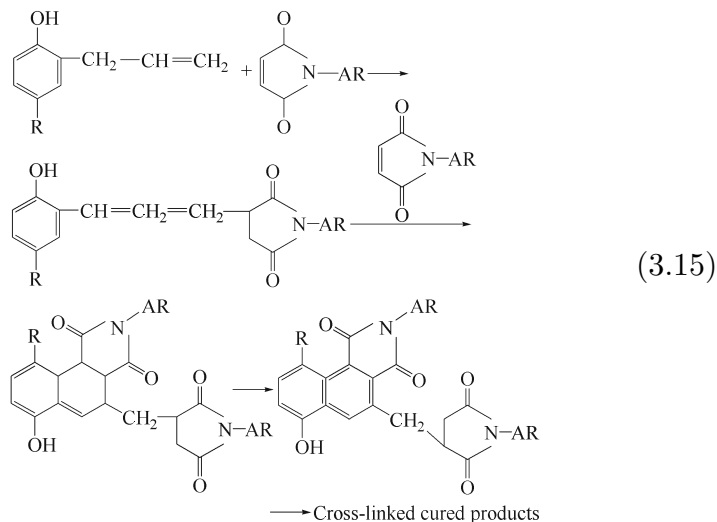
Several types of alkenyl compounds are available for BMI resin modification; the most commonly used compounds in BMI resin toughening and modification are allyl compounds. The prepolymers obtained by the copolymerization of BMI monomers and allyl compounds are stable, dissolve easily, adhere well, are hard and tough cured products, are resistant to wet/hot conditions as well as have superior electric properties, and they are suitable for coatings, molding compounds, adhesives and matrixes of advanced composites.

Allyl compounds are generally very stable at room temperature, and they self-polymerize with difficulty, even at high temperatures or upon the addition of initiators. This is because the free radicals and allyl monomers give additive and transfer reactions, as shown in Schemes 3.13 and 3.14.



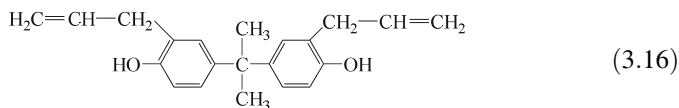
In the additive reactions, the generated free radicals are more active and can further react with allyl monomers resulting in the above-mentioned reactions. In transfer reactions, the free radicals are very stable because of conjugation, and no additive or transfer reactions will occur. Most often these reactions are terminated by initial free radicals or self-double radicals, resulting in retarded or inhibited reactions.

The curing reaction mechanism of BMI monomers and allyl compounds is generally more complicated. The double bonds (C=C) in the maleimide rings initially undergo additive reactions with the allyl compounds to form intermediate phases at a ratio of 1:1. At higher temperatures, the double bonds in the maleimide rings and the intermediate phases will undergo Diels-Alder reactions and negative ion imide oligo-polymerization to generate highly cross-linked toughened resins as shown in Scheme 3.15.



(1) Allyl-bisphenol A-modified BMI

Many types of allyl compounds exist. The most commonly used allyl compounds for BMI modifications are *O,O'*-diallyl-bisphenol A (DABPA) (see 3.16). Diallyl-bisphenol S (DABPS) allyl-aralkyl phenol resins, allyl-ester-ketone resins and allyl epoxy resins are made using *N*-allyl aryl-amine and other allyl compounds [67].



DABPA is an amber liquid at ambient temperature with a viscosity of 12–20 Pa·s. The most typical DABPA-modified BMI resin is the XU292 system. The XU292 system was developed by the Ciba-Geigy Company in 1982, and it mainly consists of biphenyl methyl bismaleimide (MBMI) and the DABPA oligopolymer. With a proper ratio during preparation the prepolymers can dissolve in acetone and can be maintained for more than one week at ambient temperature without demixing. These prepolymers have a low softening point within 20–30 °C, and the prepared prepregs have a good adhering ability. Tables 3.52, 3.53, 3.54 and 3.55 list the XU292 system viscosity, basic properties of the cured resins, the hot/wet resistance and the XU292/graphite composite performance. For the MBMI/DABPA system, the gel-cure curve (Fig. 3.29) shows two reaction transition peaks and they indicate an additive reaction (low-temperature peak) and a ring-forming reaction (high-temperature peak).

System I, system II and system III represent mol ratios of 1:1, 1:0.87 and 1:1.12, respectively.

Table 3.52 The viscosity of the XU292 system

Prepolymerization time at 100 °C/h	System I	System II	System III
Initial	0.75	0.85	0.64
2	0.89	0.99	0.71
4	0.95	1.01	0.78
6	1.04	1.13	0.87
8	1.10	1.24	0.98
16	2.00	–	–

Table 3.53 Properties of the cured XU292 system

Properties	System I	System II	System III
Tensile strength/MPa			
25 °C	81.6	93.3	76.8
149 °C	50.7	69.3	–
204 °C	39.8	71.3	–
Tensile modulus/GPa			
25 °C	4.3	3.9	4.1
149 °C	2.4	2.8	–
204 °C	2	2.7	–
Fracture elongation/%			
25 °C	2.3	3.0	2.3
149 °C	2.6	3.05	–
204 °C			
Bending strength/MPa	2.3	4.6	–
Bending modulus/GPa	166	184	154
Compression strength/MPa	4.0	3.98	3.95
Compression modulus/GPa	205	209	–
Compression yield rate/%	2.38	2.47	–
HDT/°C	16.8	13.6	–
T_g (TMA)/°C	273	285	295
T_g (DMA)/°C	273	282	287
Dried	295	310	–
Wetted	305	297	–

Note Wetted is 2 weeks at 30 °C/100% R.H. Cure cycle: 180 °C/2 h + 250 °C/6 h

Table 3.54 Wet/hot properties of the XU292 system

Properties	System I	System II
Tensile strength/MPa		
25 °C	66	88.2
149 °C	29.6	47.5
Tensile modulus/GPa		
25 °C	3.77	3.78
149 °C	1.86	2.15
Fracture elongation/%		
25 °C	2.1	3.4
149 °C	1.95	3.2
Water absorption/%		
	1.4	1.47

Note 2 weeks at 30 °C/100% R.H.

Table 3.55 XU292/graphite composite performance

Properties	System I	System II
Interlaminar shear strength/MPa		
25 °C	113	123
177 °C	75.8	82
232 °C	59	78
177 °C (wet) ^①	52	53
25 °C (aged) ^②	–	105
177 °C (aged) ^②	–	56
Bending strength/MPa		
25 °C	–	1860
177 °C	–	1509
177 °C (wet) ^①	–	1120
Bending modulus/GPa		
25 °C	–	144
177 °C	–	144
177 °C (wet) ^①	–	142

① 2 weeks at 71 °C/95% R.H.

② Aged for 1000 h at 232 °C

Note Fiber AS-4-12K; cure cycle: 177 °C/1 h + 200 °C/2 h + 250 °C/6 h

The MBMI/DABPA system prepared using domestic raw materials (mol ratio = 1:0.87) gives the properties given in Table 3.56. This system has good mechanical properties and thermal resistance, but its overall performance is slightly worse than the XU292 system because of poorer raw material quality. Recently, the Ciba-Geigy Company developed another type of BMI monomer referred to as RD85 (see Scheme 3.17). After copolymerizing with DABPA,

Fig. 3.29 MBMI/DABPA resin gel-cure curve

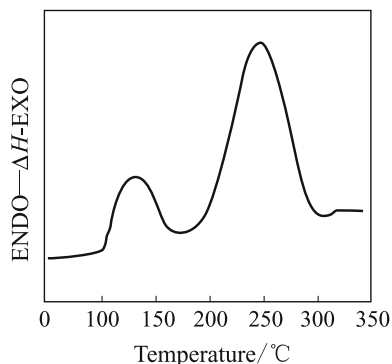
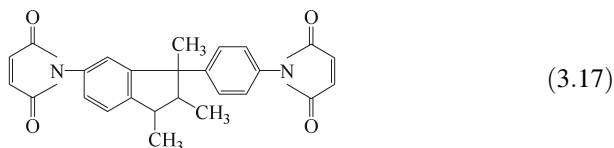


Table 3.56 Properties of the MBMI/DABPA-copolymerized resin system

Properties	Testing results
Tensile strength/MPa	69
Tensile modulus/GPa	4
Fracture elongation/%	1.73
Bending strength/MPa	170
Bending modulus/GPa	3.9
Simply-support-beam	
Impact strength/MPa	8.4
$T_g/^\circ\text{C}$	310
Thermal deflect temp./ $^\circ\text{C}$	280
$T_d/^\circ\text{C}$	370
Water absorption/%	3.5
CAI of T300/BMI composites/MPa	156

Note Resin cure cycle: 150 $^\circ\text{C}$ /1 h + 180 $^\circ\text{C}$ /3 h + 250 $^\circ\text{C}$ /4 h

the generated prepolymers have low viscosity and are suitable for prepreg production. Apart from their superior mechanical properties and thermal resistance, this resin system also shows good processing performance.

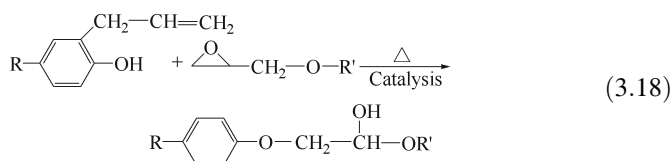


Although DABPA modification can significantly increase the BMI resin toughness, these resins can still not be considered to have high toughness levels. For example, their CAI values evaluated using T300/MBMI-DABPA composites are only in the range of 140–170 MPa, and this resin needs a much higher post-treatment temperature. Despite these shortcomings, further studies

have indicated that the MBMI/DABPA system can still become a fundamental resin system for further toughening modification.

(2) **Allyl phenol-oxidant resin (AE)-modified BMI [68]**

To improve the BMI resin impregnation property and its adhering ability to fibers, allyl phenol-oxidant resin (AE) with a higher number of $-OH$ groups can be used for BMI modification. AE can be synthesized by the following approach:



Using different epoxy and allyl compounds with different chemical structures, allyl phenol-oxidant resins with different structures and properties can be generated. The author has himself used allyl-bisphenol A, bisphenol A and epoxy E51 to synthesize AE BMI resins under catalysis conditions and further modified BMI/PEK-C (thermoplastic-modified polyetherketone-PEK) resins. Tables 3.57 and 3.58 list the main properties of this resin system and its composites.

For the BMI/PEK-C resins, before and after AE modification, the T_g are 245 and 246 °C, respectively, and the initial thermal degradation temperatures T_d are 376 and 374 °C, respectively, indicating that AE modification has little effect on the thermal resistance of the BMI/PEK-C resin.

Table 3.57 Properties of the BMI/PEK-C resin modified by AE

System	Impact strength/ $\text{kJ}\cdot\text{m}^{-2}$	$T_g/^\circ\text{C}$	$T_d/^\circ\text{C}$
Without AE	17.0	245	376
With AE	19.0	246	374

Note Resin cure cycle: 150 °C/2 h + 180 °C/2 h + 230 °C/4 h

Table 3.58 Properties of the AE-modified BMI/PEK-C/T300 composite

Performance	PEK-C-modified BMI/T300	AE+PEK-C-modified BMI/T300
CAI/MPa	185	202
Damage delaminated area/ mm^2	700	550
Short beam shear (SBS)/MPa	93	116
Bending strength at room temp./MPa	1720	1750
Bending modulus at room temp./GPa	114	112
Bending strength at 150 °C/MPa	1100	1050
Bending modulus at 150 °C/GPa	112	110
$T_g/^\circ\text{C}$	280	273
Water absorption/%	0.6–0.8	0.6–0.8

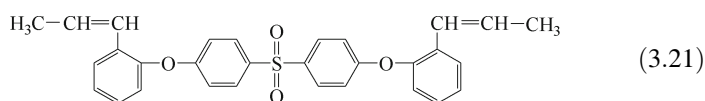
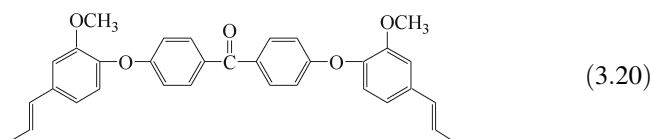
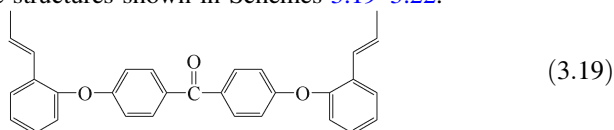
Note Fiber volume fraction 60–63%

Cure cycle: 150 °C/2 h + 180 °C/3 h + 250 °C/4–6 h

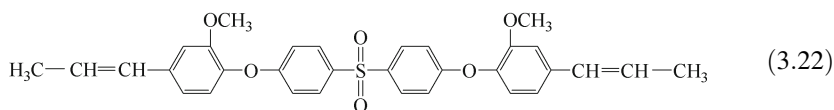
Table 3.58 shows that pure PEK-C-modified T300/BMI composites have a SBS strength of 93 MPa, while the damaged delaminated areas before and after AE modified are 700 and 550 mm², respectively. The above results indicate that the added AE can apparently improve the interface bonding between BMI resin matrix and fibers and increase the impact-resistant ability of composites. Therefore, composite CAI values have been significantly increased (from 185 MPa increased to 202 MPa).

(3) Toughening by propenyl ether (PPE) copolymerization with BMI

The reaction between BMI and PPC is different to the reaction between BMI and DABPA. For BMI and PPC, Diels–Alder reactions will take place and then an “alkene” additive reaction will occur to form high density cross-linked “ladder like” copolymers. A typical BMI/PPC system is the Compimide 796/TM-123 resin system. TM-123 is 4,4'-bi (O-propenyl phenyl group) diphenyl ketene, and it is an amorphous solid at room temperature with a low viscosity at 80 °C. It mixes easily and can be prepolymerized with Compimide 796. In the Compimide 796/TM-123 system, the toughness and thermal resistance depend on the ratio of TM-123. At a mass ratio of Compimide 796/TM-123 of 60/40, its toughness will reach a maximum value ($G_{IC} = 439 \text{ J/m}^2$), and its T_g is 249 °C with higher thermal resistance. The main PPC compounds used for BMI modification have the structures shown in Schemes 3.19–3.22.



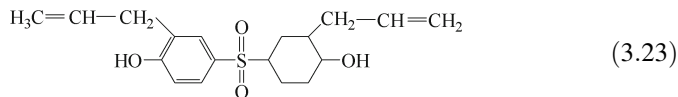
As for the BMI/DABPA system, BMI/PPC can also become a fundamental resin system for further toughening.



(4) Allyl-bisphenol S-modified BMI

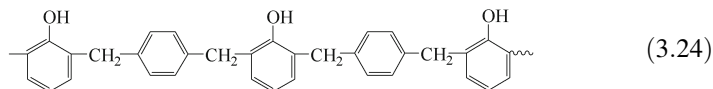
For different applications, different allyl compounds with different structures can be used for BMI modification; for example, to increase and improve the BMI thermal stability, allyl-bisphenol S (Scheme 3.23) can be used to copolymerize with diphenyl methane BMI. The prepared resin system has a softening point at 60 °C and a viscosity of 1.2 Pa·s at 110 °C. This resin system

has good storage stability. The reaction activity of allyl-bisphenol S and BMI is similar to that of the BMI/DABPA system.



(5) Allyl-aralkyl phenol-modified BMI

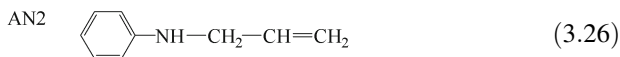
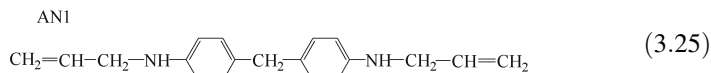
If allyl groups are introduced into aralkyl resins, allyl-aralkyl phenol can be generated as shown in Scheme 3.17. The allyl-aralkyl phenol resin is a brown solid at room temperature with a softening point within 30–40 °C. It dissolves in organic solvents like alcohol, acetone and methylbenzene. After copolymerization with BMI, the obtained prepolymers have a lower softening point (60 °C) and they can then dissolve in acetone. The cured product of allyl-aralkyl phenol and BMI has superior mechanical performance and thermal resistance. Its HDT is 309 °C, T_g 325 °C and T_d 490 °C. It has good hot/wet resistance, and after 100 h in boiling water, its HDT and water absorption are 282 °C and 2.3%, respectively. The glass fiber molding compounds prepared by allyl-aralkyl phenol-modified BMI have superior dielectric properties and hot/wet mechanical performance.



(6) Other alkenyl-modified BMI compounds

Apart from the above-mentioned allyl compounds, many other types of allyl compounds can be used for BMI modification, for example, *N*-allyl aromatic amine. Therefore, it is possible to select specific allyl compounds to modify BMI for different purposes.

Two *N*-allyl aromatic amines are commonly used as shown in Schemes 3.25 and 3.26.



3.5.2.2 Binary Amine-Modified BMI

Binary amine modification was an earlier approach to improving BMI brittleness. Generally binary amines can copolymerize with BMI as shown in Scheme 3.27.

BMI and binary amines will initially undergo Michael linear additive block copolymerization; the double bonds in the maleimide rings will then open resulting in a free-radical-type curing reaction. Cross-linked networks will form and the second amine generated in the linear polymers after the Michael additive reaction

can also undergo a further additive reaction with other double bonds in the molecular chain-extended polymers.

Kerimide 601 resin was developed by the Rhone-Poulenc Company and is prepared using MBMI and 4,4'-diaminodiphenyl methane at a mol ratio of 2:1. Its melting point ranges from 40 to 110 °C and its curing temperature is 150–250 °C with good processing performance. The prepregs prepared with the Kerimide 601 resin can be stored for 3 months at 25 °C and for 6 months at 0 °C. The performance of the Kerimide 601 resin composites is given in Tables 3.59, 3.60 and 3.61.

Table 3.59 Properties of Kerimide 601/glass cloth 181E composites

Properties	Data
Short beam shear strength/MPa	
25 °C	59.6
200 °C	51
250 °C	44.8
Bending strength/MPa	
25 °C	482
200 °C	413
250 °C	345
Bending modulus/GPa	
25 °C	27.6
200 °C	22.7
250 °C	20.7
Tensile strength/MPa	
344	
Compression strength/MPa	
344	
Delaminated strength/MPa	
14.8	
Impact strength/kJ·m ⁻²	
With notch	
232	
Without notch	
267	

Table 3.60 Electric properties of Kerimide 601 resin and its composites

Properties	Cured resin	K601/GF-181E	K601/GF-112E
Dielectric strength/kV·mm ⁻¹			
Normal state		25	
In water 24 h		20	
180 °C aged 1000 h		>16.5	
200 °C aged 1000 h		>16.5	
220 °C aged 1000 h		12	
Volume resistance rate/Ω·cm			
Normal state	1.6×10^{16}	6×10^{14}	4×10^{14}
In water 24 h	1.6×10^{13}	1.5×10^{13}	5×10^{13}
250 °C aged 2000 h		2.2×10^{15}	
Dielectric constant (1 kHz)			

(continued)

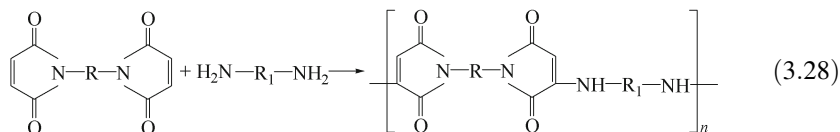
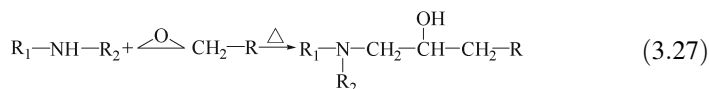
Table 3.60 (continued)

Properties	Cured resin	K601/GF-181E	K601/GF-112E
Normal state	3.5	4.5	
In water 24 h		5.4	
180 °C aged 1000 h		5.5	
200 °C aged 1000 h		5.5	
220 °C aged 1000 h		4.7	
Dielectric loss factor (1 kHz)			
Normal state	2×10^{-2}	1.2×10^{-2}	0.6×10^{-2}
In water 24 h	1×10^{-2}	1.6×10^{-2}	7.2×10^{-2}

Table 3.61 The hot/wet properties of Kerimide 601/glass cloth composites

Properties	Time in filtered steam vapor/h			
	0	170	340	500
Bending strength/MPa				
25 °C	496	475	482	503
250 °C	392	268	255	227
Bending modulus/GPa				
25 °C	34.9	24.7	24.7	24.5
250 °C	22.3	18.4	18.4	17.4
Water absorption/%	0	0.8	0.8	0.9

Kerimide 601 resins have good thermal resistance, mechanical and electric properties, however, their prepreps have almost no tack, and the toughness of composites is low. In addition, the second amine group ($-\text{NH}-$) generated after the chain extension reaction between the binary amine and BMI can often cause a decrease in the thermal-oxidant stability. Therefore, on the basis of binary amine chain extension modification, an epoxy resin can be added to improve the viscosity of the BMI system. Since epoxy groups can react with $-\text{NH}-$ bonds (see Scheme 3.27) to form cross-linked cured networks, the thermal-oxidant stability of the system can be simultaneously improved.



Although the processing performance can be significantly improved by introducing an epoxy resin into the BMI system, epoxy resins can often decrease the thermal resistance of BMI resins. Therefore, the operating temperature of BMI

resins modified by an epoxy resin cannot exceed 150 °C. Not much improvement in toughness can be expected either.

3.5.2.3 Thermoplastic Resin-Modified BMI

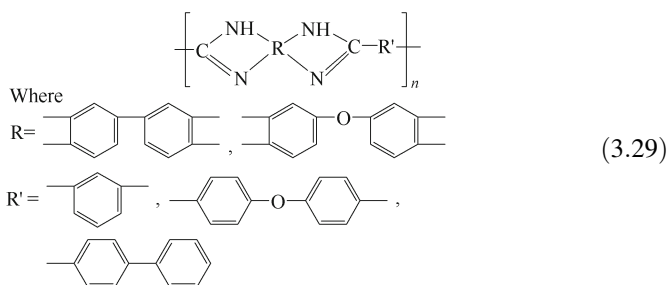
It is possible to improve resin toughness without losing thermal resistance and mechanical properties using higher thermal resistance thermoplastics (TP) to modify the BMI resin system. The currently used TP resins include polybenzimidazole (PBI), polyethersulfone (PES), polyetherimide (PEI), polyhydantoin (PH), modified polyetherketone (PEK-C) and modified polyethersulfone (PES-C) [68, 69].

Factors that can affect toughening efficiency include primary molecular chain structures, relative molar mass, resin grain size, terminal group structure and content, as well as solvent types and processing techniques. Recent research indicates that the TP toughening of BMI resin has achieved great success and is the principal approach to BMI resin toughening and modification.

In the next section, the main TP used for toughening and modifying BMI resins will be briefly introduced.

(1) Polybenzimidazole (PBI)

The PBI chemical structure is shown in Scheme 3.29.



PBI is an industrial and commercial thermoplastic aromatic heterocyclic material with superior low-temperature resistance and thermal resistance. Its T_g is 480 °C and it starts to degrade at 550 °C in air. PBI easily dissolves into strong polar solvents such as concentrated sulfate acid, dimethylformamide, dimethyl sulfoxide, *N*-methyl pyrrolidone and 6-methylphosphonic amide. The properties of PBI-toughened BMI resin and its composites are given in Tables 3.62 and 3.63.

The data in Table 3.62 indicate that adding 10% of three different PBI grain sizes has no effect on the T_g and modulus but that G_{IC} increases significantly.

(2) PES, PEI and PH

Other typical TP for toughening BMI resin include PES (Udel P1700), PEI (Ultem) and HP (PH10), which is used for Compimide 796/TM-123 system toughening. The structure and properties of these three TP are given in Table 3.64.

Table 3.62 Formula and properties of PBI-modified BMI resins

Materials and properties		CM-1	CM-2	CM-3	CM-4
Formula	Matrimide 5292B/%	33.35	30	30	30
	Compimide 795/%	60.65	60	60	60
	PBI < 10 ^① /μm	–	10	–	–
	PBI 15-44 ^① /μm	–	–	10	–
	PBI 32-63 ^① /μm	–	–	–	10
Properties	T_g /°C (DMTA, dried)	251	250	250	252
	Modulus at room temp./GPa	4.53	3.97	3.85	3.87
	Temp. at which modulus lost 50%/°C	211	211	213	211
	T_g /°C (DMTA, wetted ^②)	182	175	181	178
	Modulus at room temp./GPa	3.86	3.6	4.27	3.5
	Temp. at which modulus lost 50%/°C	151	150	152	151
	Shear modulus at room temp./GPa	1.97	1.98	1.98	1.92
	G_{IC} /J·m ⁻²	128	272	247	242
	Water absorption/%	3.24	3.93	4.03	3.98

① Grain unit μm

② 14 days at 71 °C and 100% R.H.

Table 3.63 Mechanical properties of apollo43-600/PBI-modified BMI composites

Properties	Resins	25 °C dried	25 °C wetted	177 °C dried	177 °C wetted	204 °C wetted	219 °C wetted	232 °C dried
Interlaminar shear strength/MPa	CM-1	99.3	88.2	53.4	39.4	29.9	26.2	37.2
	CM-2	115	103	58.3	39.3	26.8	24.8	37.2
0° bending strength/MPa	CM-1	1372	1294	997	529	369	359	655
	CM-2	1386	1290	980	427	336	341	341
0° bending modulus/GPa	CM-1	140	150	136	105	81.8	88.7	118
	CM-2	142	150	139	87.5	76.3	77.9	95.9
0° compression strength/MPa	CM-1	1462	1485	1186	650	450	426	398
	CM-2	1407	1358	1193	571	410	253	391
0° tensile strength/MPa	CM-1	2676	–	–	–	–	–	–
	CM-2	2538						
0° tensile modulus/GPa	CM-1	188	–	–	–	–	–	–
	CM-2	177						
edge peel strength/MPa	CM-1	142	–	–	–	–	–	–
	CM-2	165						
G_{IC} /J·m ⁻²	CM-1	182	–	–	–	–	–	–
	CM-2	212						

Note Fiber volume fraction 57 ± 1%; cure cycle: 177 °C/4 h + 218 °C/8 h

The properties of the BMI resin and its composites modified by the above-mentioned TP resins are listed in Tables 3.65, 3.66, 3.67. The results in these tables show that the lower T_g of TP resins is not good enough for high-performance modified BMI resins. The toughness improves as the TP

Table 3.64 Structure and properties of some TP resins

Resin properties	Structural formula	Specific viscosity/MPa	$T_g/^\circ\text{C}$
UdelPES1700 Ployethersulfone		0.38	190
Ultem 100 Polyetherimide		0.50	220
PH10 Polyhydantoin (PH)		0.76	>250

Table 3.65 Properties of the Compimide 796/Tm-123/Tp system

Properties	Temp./ $^\circ\text{C}$	TP/%						
		0 ^①	0 ^②	13.04U	25.9U	20PH	33PH	20PS
0° bending strength/MPa	23	132	115	117	139	115	126	95
	177	103	84	97	64	95	110	37
	250	74	77	45	22	91	83	–
0° bending modulus/GPa	23	3.92	3.86	3.72	3.77	3.65	3.40	3.49
	177	2.90	3.27	3.02	3.08	2.88	2.81	1.97
	250	2.42	2.39	1.71	0.41	2.77	2.40	–
Bending strain/%	23	3.75	3.04	3.35	3.96	3.09	3.92	2.67
	177	3.72	2.73	3.38	2.12	3.44	4.20	–
	250	4.69	4.77	2.99	4.07	4.52	5.20	–
$G_{IC}/\text{J}\cdot\text{m}^{-2}$		182	225	462	841	454	1091	440

① Cure cycle: 190 $^\circ\text{C}/2\text{ h} + 230\text{ }^\circ\text{C}/10\text{ h}$ ② Cure cycle: 170 $^\circ\text{C}/2\text{ h} + 190\text{ }^\circ\text{C}/2\text{ h} + 230\text{ }^\circ\text{C}/10\text{ h}$ **Table 3.66** Properties of CF(T800)/Ultem-modified BMI

Properties	Temp./ $^\circ\text{C}$	Ultem/%				
		0 ^①	0 ^②	4.76	9.0	13.04
0° bending strength/MPa	23	1474	1833	1630	1670	1682
	250	1268	1243	1317	1177	780
0° bending modulus/GPa	23	155	153	144	156	162
	250	182	146	163	158	128
90° bending strength/MPa	23	99	92	84	95	95
	250	55	69	55	42	29
90° bending modulus/GPa	23	8.7	8.6	8.5	9.8	9.7
	250	7.3	9.2	7.9	7.0	4.9
0° SBS strength/MPa	23	103	103	97	84	93
	120	78	81	84	78	79
	175	68	70	76	70	63
	200	65	60	75	63	50
	250	48	51	56	43	22
0 ± 45° SBS strength/MPa	23	81	62	62	76	72
	250	43	51	44	30	14
$G_{IC}/\text{J}\cdot\text{m}^{-2}$	23	319	319	369	352	585

① Cure cycle: 190 $^\circ\text{C}/2\text{ h} + 230\text{ }^\circ\text{C}/10\text{ h}$ ② Cure cycle: 170 $^\circ\text{C}/2\text{ h} + 190\text{ }^\circ\text{C}/2\text{ h} + 210\text{ }^\circ\text{C}/3\text{ h} + 230\text{ }^\circ\text{C}/10\text{ h}$; resin system: Compimide 796/TM-123 = 65/35; fiber volume fraction = 60%

Table 3.67 Properties of CF(T800)/polyhydantoin (PH)-modified BMI

Properties	Temp./°C	PH/%				
		0 ^①	0 ^②	13.04	20	30
Bending strength/MPa	23	1747	1747	1661	1571	1590
	250	1268	1268	1401	1258	–
Bending modulus/GPa	23	155	155	155	156	147
	250	182	182	208	165	–
90° bending strength/MPa	23	99	99	91	97	91
	250	75	75	52	57	–
90° bending modulus/GPa	23	8.7	8.7	9.3	9.3	7.5
	250	7.3	7.3	7.2	6.3	–
SBS strength/MPa	23	103	103	101	96	93
	120	78	78	75	77	–
	175	68	68	69	70	–
	200	65	60	66	62	–
	250	48	51	59	45	40
L/T SBS strength/MPa	23	81	62	66	57	79
	250	43	51	39	44	39
$G_{IC}/J\cdot m^{-2}$	23	319	319	335	640	1011

① Cure cycle: 190 °C/2 h + 230 °C/10 h

② Cure cycle: 170 °C/2 h + 190 °C/2 h + 210 °C/3 h + 230 °C/10 h; resin system: Compimide 796/TM-123 = 65/35

content increases, but the modulus decreases as the TP content increases, or as the T_g decreases. Because the T_g of PES is only 190 °C, Ultem and PH TP resins were the first to be selected for BMI modification. These two TP have T_g values of 220 °C and higher than 250 °C, respectively. For example, the lower Ultem content resin system of Compimide 796/TM-123/Ultem (ratio = 65/35/13.04) has very high toughness ($G_{IC} = 1281 J/m^2$), strength and modulus. The unidirectional composite made using this resin system and T-800 carbon fiber has very good thermal resistance (the retention rate of interlaminar shear strength is greater than 50%) and toughness ($G_{IC} = 585 J/m^2$). On the other hand, TP modification and toughening will cause a decrease in prepreg tack. Some prepreps will have no tack at all, and this will significantly affect the resin's processing abilities.

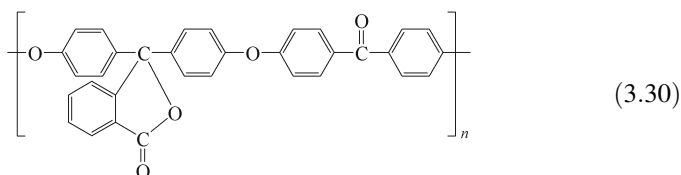
(3) Modified polyetherketone (PEK-C)

The structural formula of PEK-C is shown in (3.30). PEK-C has been used to modify the typical two-phase BMI/DABPA system, and the properties of a pure BMI resin are listed in Table 3.68.

Table 3.68 Properties of PEK-C-modified BMI resin

System	I	II	III	IV	V	VI
PEK-C/%	0	5	1.0	20	30	40
Impact strength/ $J \cdot m^{-2}$	7.1	8.2	8.9	18.9	13.0	13.0
$T_g/^\circ C$	310	231	238	225	225	228
Initial thermal degradation temp./ $^\circ C$	375	–	374	–	–	378

Cure cycle: 150 $^\circ C/2$ h + 230 $^\circ C/4$ h

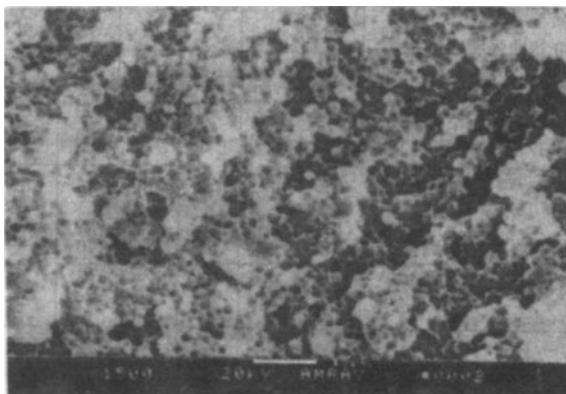


Based on research results, added PEK-C can obviously increase the impact strength of resins. As the PEK-C content is increased, the impact strength of resin casts will initially show an increase and then reach a peak value, after which it decreases. At a PEK-C content of 20%, the impact strength of the resins will have a maximum value of 18.9 kJ/m^2 , which is a 2.5 times increase compared with the 7.1 kJ/m^2 of unmodified BMI without PEK-C. As the PEK-C content is increased, the TP grains in the system will increase and the distance between the grains will become shorter. The distance between the grains and cracks will also become shorter, and the cracks will have more of a chance to encounter TP grains. Therefore, the cracks will terminate more easily. This enhanced ability to terminate cracks is useful in increasing resin toughness. Therefore, as the PEK-C content increases, the toughening will become more significant, and the impact strength will be also increased. The PEK-C that contains hydroxyl groups is more efficient at toughening than end-terminated PEK-C. This may be because the end hydroxyl groups can react with BMI and the two phases of interfacial strength may thus increase.

As shown in Fig. 3.30, a single system phase can be observed by scanning electronic microscopy (SEM). This was obtained from the impact fracture surface of the BMI resin without PEK-C modification. Many clear stripe patterns are present on the surface indicating brittle fracture behavior. Upon the addition of PEK-C, especially a larger amount of PEK-C, the stripe patterns disappeared, which means that tough fracture behavior can be expected. Since the PEK-C grains were dispersed in the BMI matrix, the system displayed two-phase characteristics.

When the PEK-C content reached a certain ratio, a further increase in the amount of PEK-C will result in non-uniform distribution and large dumped grains will be formed. This will result in stress concentration. On the other hand, a too high TP content will result in too many grains, and a too-dense

Fig. 3.30 SEM image of the impact fracture surface of a BMI resin modified by PEK-C



similar grain distribution resulting in fracture cracking exceeding a threshold value. The resin toughness will decrease as the TP content increases.

The T_g of the BMI resins modified by PEK-C is listed in Table 3.68, which shows that the T_g values decreased 70–80 °C after modification. The reason may be the lower T_g of PEK-C (about 230 °C). TGA was used to study the thermal degradation behavior of a modified BMI system, and they found that the degradation initial temperature, termination temperature and maximum degradation rate temperature are 371, 500 and 415 °C, respectively (see Fig. 3.31).

However, PEK-C increased the viscosity of the system resulting in a difficult resin mixing process. Therefore, to obtain a BMI resin system with good mixing, toughness and thermal resistance, an appropriate selection of PEK-C content is very critical. For example, when the ratio of BMI/DABPA/PEK-C is 100/75/15, the resin system can give $G_{IC} = 403.8 \text{ J/m}^2$ and HDT = 271 °C, while its composites made using CF T300 have $G_{IC} = 512 \text{ J/m}^2$, which is much higher than that of the T300/XU292 system ($G_{IC} = 210 \text{ J/m}^2$).

Fig. 3.31 TG analysis of BMI resins modified by PEK-C

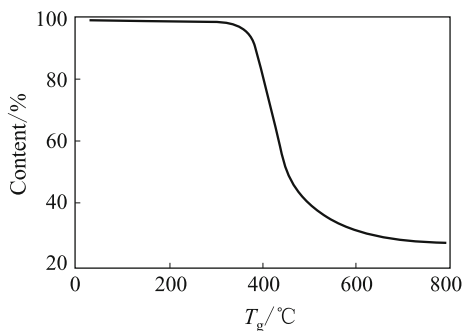


Table 3.69 Properties of the T300/BMI composite modified by PS

Properties	PS modified	Unmodified
Bending strength/MPa		
23 °C	1935	–
250 °C	1250	–
Bending modulus/GPa		
23 °C	150	–
250 °C	151	–
Interlaminar shear strength/MPa		
23 °C	112	103
250 °C	52	69
Impact strength/MPa	159	85

Note Cure cycle: 180 °C/2 h; post-treatment: 200 °C/6 h + 250 °C/4.5 h

(4) Polysulfone (PS)-modified BMI

The properties of the T300/BMI composites modified by polysulfone are listed in Table 3.69.

3.5.2.4 Epoxy Resin-Modified BMI

Epoxy modification is an earlier and more matured approach, and it can improve BMI resin system processing performance and increase the interfacial adhering strength between reinforcements. It can also improve BMI resin system toughness. Epoxy resin reacts with BMI monomers with difficulty, and approaches to modifying BMI system toughness will mainly be the following:

- (1) On the basis of binary amine modification, epoxy resins can be added. In this system, the copolymerization between BMI and an epoxy resin can be carried out using a binary amine additive reaction. A cross-linked network will be generated, and chain propagation will take place in BMI and, therefore, the toughness of BMI can be improved. A BMI resin modified by an epoxy/binary amine has good processing ability, for example, prepolymers can dissolve in acetone and prepregs have good adhering and drape abilities.
- (2) Use of an epoxy group-containing BMI resin: BMI containing epoxy groups are prepared by the prepolymerization of excess epoxy resins and binary amines. Epoxy groups function as terminal groups, and this BMI can give much improved performance if cured by amine curing agents. For example, 3 mol of BDM, 1 mol of DDM and 7.5 mol phenolic-type epoxy resin (BEN 438) are mixed together in 2-methyl alcohol and left to react for 90 min at 95 °C. After cooling to room temperature, 1 mol of 2,4-biamine-6-phenol-1,3,5 triazine (BG) is added and stirred thoroughly, and then the solution is dried for 24 h under vacuum. BMI prepolymers containing epoxy groups are thus produced.

As for other common BMI resins, this kind of BMI gives good thermal resistance after curing under proper conditions. However, the curing temperature required by this BMI is usually lower.

- (3) Synthetic modifiers: One such modifier is allyl phenol-oxidant resin which is prepared by epoxy reaction with allyl compounds. It is useful to improve the interface performance between a resin matrix and carbon fiber reinforcements such as the previously mentioned allyl phenol-oxidant resin AE, and this can provide effective modification.

However, the added epoxy resin can often cause a decrease in thermal resistance in the BMI system, and the important point in this modification is the optimization of the constituent ratios and the polymerization procedures to deliver a balance of toughness, thermal resistance and processing ability.

In the 1980s, a very good epoxy-modified BMI system was successfully developed and was designated 5245C resin. To decrease water absorption and increase toughness, bicyanate ester was added to the system. The outstanding feature of this resin system is its superior processing performance, which is similar to epoxy resins, and its good thermal resistance retention rate between 93 and 132 °C with $G_{IC} = 158 \text{ J/m}^2$.

3.5.2.5 Cyanate Ester (CE)-Modified BMI

Generally, the binary amine can be used for chain propagation modification or the allyl compound can be used for modification. Increase in the toughness by decreasing the resin cross-linking density will often compensate for the loss in material stiffness and thermal resistance. Using epoxy to improve the BMI will result in some thermal resistance loss. For the TP toughening of BMI, although the toughness of the resin system can be significantly increased, the viscosity of the modified resin system can also increase significantly. This will cause the adhering ability of the carbon fiber prepregs to decrease, which means a poorer processing ability for the resin systems. However, the above-mentioned drawbacks can be eliminated by cyanate ester (CE) modification of BMI resin systems.

In the mid-1980s, much attention was given to cyanate ester resins because of their superior combined performance. Cyanate ester resins have an overall performance between that of epoxy and BMI. They can provide the superior processing performance of epoxy resins and the thermal resistance of BMI resins. Their flame-retardant and dielectric properties are also very good, and water absorption is very low. Using CE to modify BMI maintains good thermal resistance and increases toughness in addition to improving the dielectric properties and decreasing the water absorption rate. Generally, two mechanisms can explain the behavior of CE-modified BMI: One is copolymerization between BMI and CE and the other is the formation of an interpenetrated network between BMI and CE resulting in effective toughness. For example, the BT resin from Mitsubishi is regarded to be an interpenetrated system.

CE-modified BMI resin systems have higher toughness, thermal resistance, dielectric properties, wet resistance, anti-abrading, good dimension stability and combined mechanical performances. However, excess halogen cyan is required for the synthesis of cyanate esters. The produced toxic waste liquids are difficult to handle, and this is a main obstacle that limits the wide application of CE-modified BMI systems.

3.5.2.6 New BMI Monomer Synthesis

In previous sections, a number of BMI monomers have been mentioned, but the most commonly used monomer is MBMI, and the second is RD85-101 from Ciby-Geigy. Other types of BMI monomers are not widely used. No specific definition exists with regard to new BMI monomers, but in general the main types will include chain extension, substitution, condensed ring and thiophene BMI monomers. Multi-maleimide BMI monomers such as linear phenolic multi-maleimide monomers also exist.

(1) Chain-extended BMI

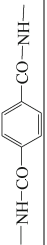
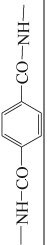
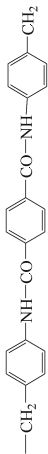
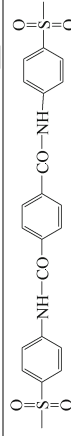
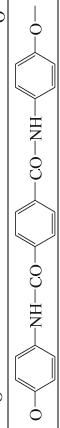
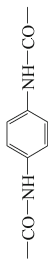

In chain extension modification, based on molecular design, by extending the R chain length the chain flexibility and self-spiraling can be increased. Additionally, the cross-linking density of cured resins can be decreased and resin toughness can be improved. Based on the different functional groups and chemical elements contained in the extended chains, chain-extended BMI can be further divided into different types including amide, allanturic, epoxy backbone, ether linkage, sulfate ether bond, imide, and aromatic ester bond BMI as well as silicon contained BMI. In the following sections, the synthesis and performance of some BMI will be discussed.

- (1) Amide BMI: A number of methods are available for amide BMI synthesis, but only three are commonly used and these are given below (see Scheme 3.31).

Type I and II can react with maleic dianhydride, dehydrate and cyclize to generate amide linkage BMI.

In amide BMI, the curing temperature will usually increase as the distance between the chains increases, and the initial thermal degradation temperature will decrease. This type of BMI has a series of advantages including flame retardation, thermal resistance, excellent mechanical properties, anti-abrading and electric isolation (see Table 3.70).

Table 3.70 Structure and properties of BMI resins containing amide linkages

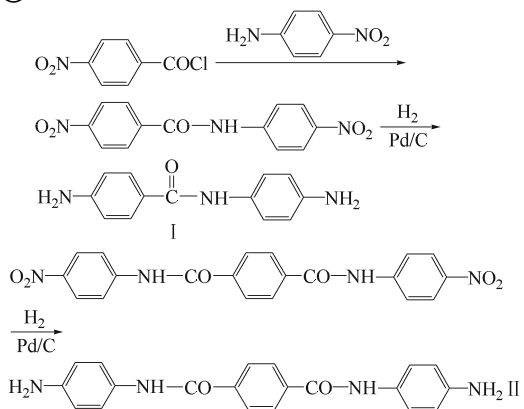
No.	Structural formula (R)	T_1 /°C	T_2 /°C	T_3 /°C	T_{di} /°C	T_{dp} /°C	Y_c /°C	Melting point/°C
1		197	225	249	363	487	56	–
2		215	236	261	344	462	56	–
3		224	286	308	337	480	67	–
4		235	303	331	334	465	50	–
5		221	290	324	345	465	57	–
6		289	–	315	380	–	56	260
7		–	320	–	–487	553	–	312

Note 1. Y_c in 1–5 is the residual carbon rate under nitrogen at 800 °C. Cure cycle: 160 °C/0.5 h + 220 °C/0.5 h + 260 °C/0.5 h

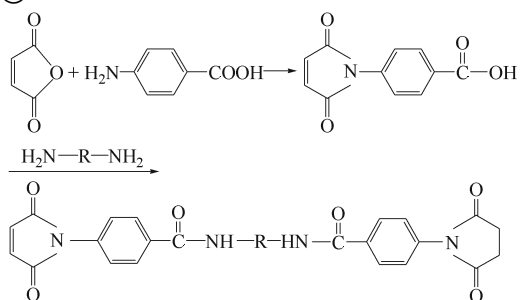
2. Y_c in 6–7 is the residual carbon rate under nitrogen at 700 °C. Cure cycle: 220 °C/1 h + 250 °C/10 h

3. T_1 , T_2 , T_3 are the onset, peak and termination temperatures on the DSC cure curve; T_{di} is the initial degradation temperature, T_{dp} is the maximum degradation temperature

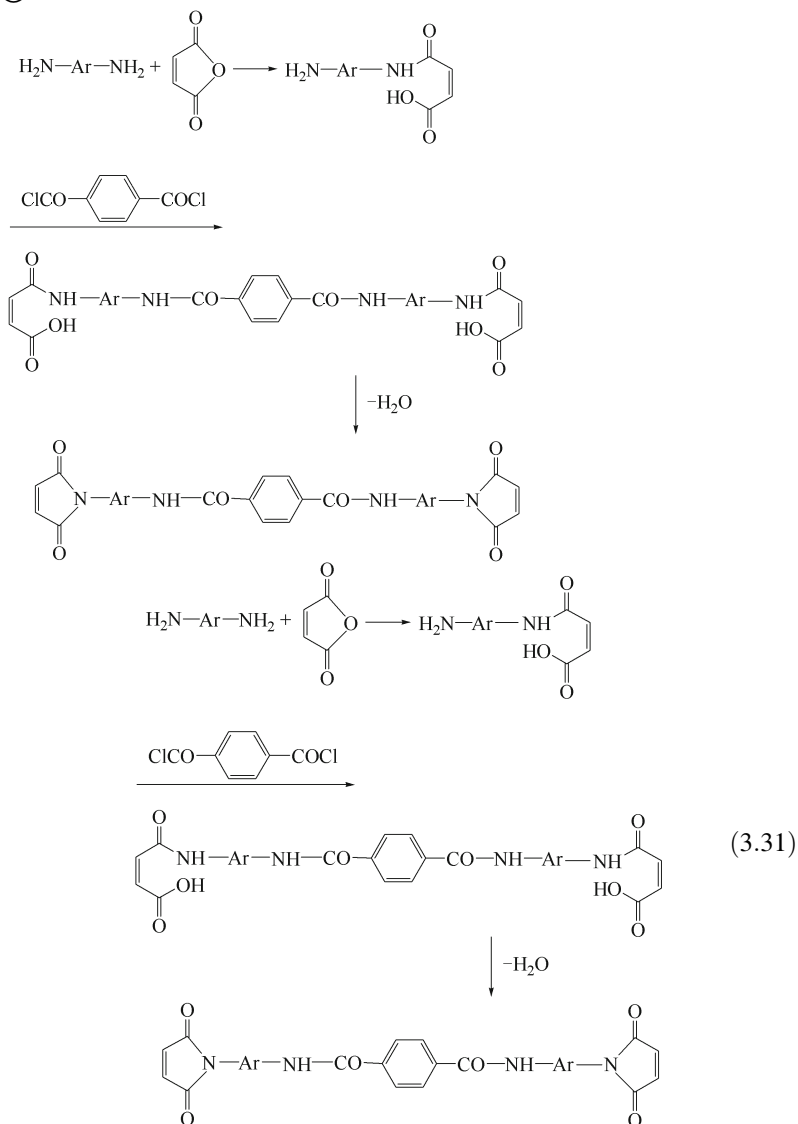
①



②

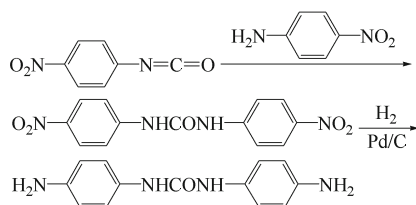


③

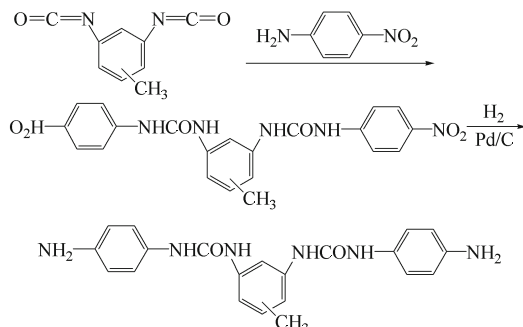


(2) Allanturic BMI: BMI containing allanturic linkages can be synthesized by the following reactions:

①

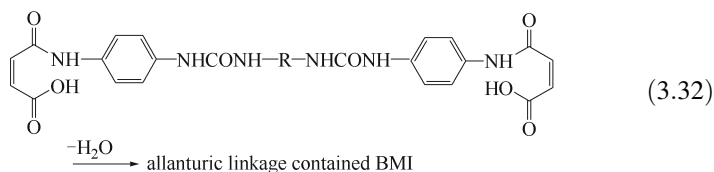


②



In ① and ②, amine and maleic anhydride react, dehydrate and cyclize to form allanturic linkage containing BMI.

③



Allanturic BMI requires a higher curing temperature, generally in the range of 203–297 °C, and its initial degradation temperature is equivalent to that of amide BMI. Its maximum degradation temperature and residual carbon rate at 800 °C are lower than those of amide BMI, but its thermal stability is the same as that of common aromatic BMI resins (see Table 3.71).

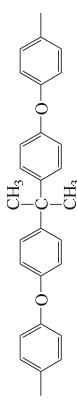

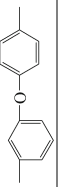


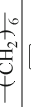

- (3) Ether linkage BMI: The introduction of ether linkages can increase chain flexibility resulting in an increase in the mechanical properties and flexibility of the BMI resin as well as a decrease in its melting point. Additionally, the reaction activity will decrease, the gel time will be extended and the curing temperature will increase. The introduced ether bonds decrease the T_g of the resin system. Table 3.72 shows the structures and performance of some ether linkage BMI.
- (4) Imide BMI: Flexible chain segments introduced into BMI are useful to increase its toughness, but they also cause a decrease in the thermal resistance and stability of the resin system. Using imide linkages can eliminate this problem as the BMI toughness can be increased and the thermal resistance can be maintained without any loss after the introduction of imide bonds. Imide BMI can be produced by the following synthetic reactions:

Table 3.71 Structure and properties of BMI resins containing allanturic bonds

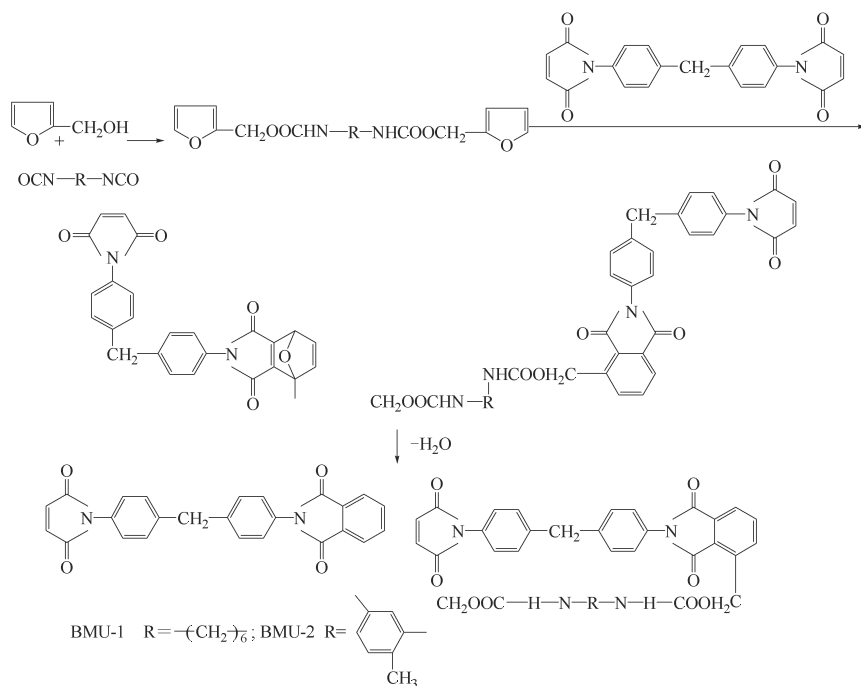
No.	Structural formula (R)	T ₁ /°C	T ₂ /°C	T ₃ /°C	T _{di} /°C	T _{dp} /°C	Y _e /°C
1		228	255	181	332	426	49
2		242	270	294	334	401	41
3		244	276	297	331	402	54
4		249	272	288	324	416	52
5		229	266	289	334	432	61
6		203	223	256	331	431	49

Note Y_e is the residual carbon rate under nitrogen at 800 °C. Cure cycle: 160 °C/30 min + 230 °C/120 min + 250 °C/40 min

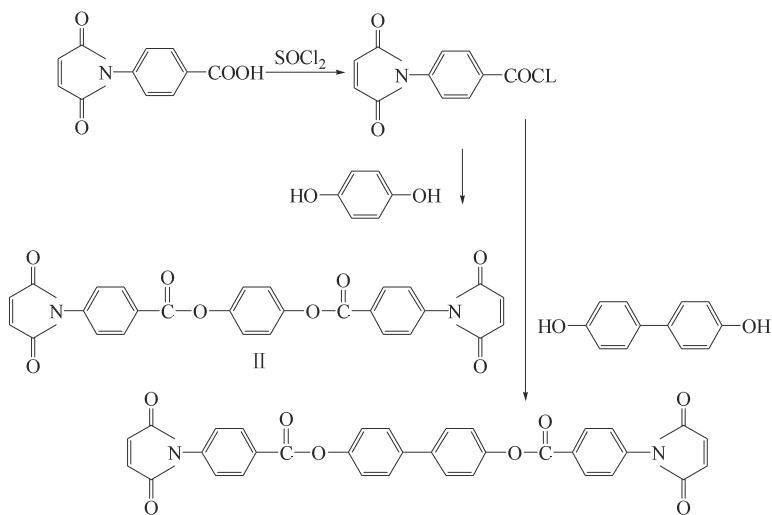
Table 3.72 Structure and properties of BMI resins containing ether linkages

No.	Structural formula (R)	$T_m/^\circ\text{C}$	$T_1/^\circ\text{C}$	$T_2/^\circ\text{C}$	$T_3/^\circ\text{C}$	GT/min	$T_{d11}/^\circ\text{C}$	$T_{d12}/^\circ\text{C}$	$T_g/^\circ\text{C}$
1		121	203	302	344	8.5	412	464	312
2		104	198	272	330	17.6	414	436	288
3		212	217	318	365	–	431	483	313
4		230	240	245	280	–	385	436	317
5		176	236	274	334	28.5	334	394	285
6		143	177	234	322	0.33	392	468	–
7		158	174	233	316	2.17	416	500	342

Note GT is the gel time at 200 °C. T_{d11} and T_{d12} are the initial degradation temperature in air or nitrogen, respectively; cure cycle: 280 °C/10 h



(3.34)



(3.35)

The introduced urethane bonds will increase BMI reaction activity resulting in a lower curing temperature in the range of 187–248 °C. The cured resins have better toughness, but their thermal resistance is lower than that of commonly modified BMI, and its initial degradation temperature is relatively lower.

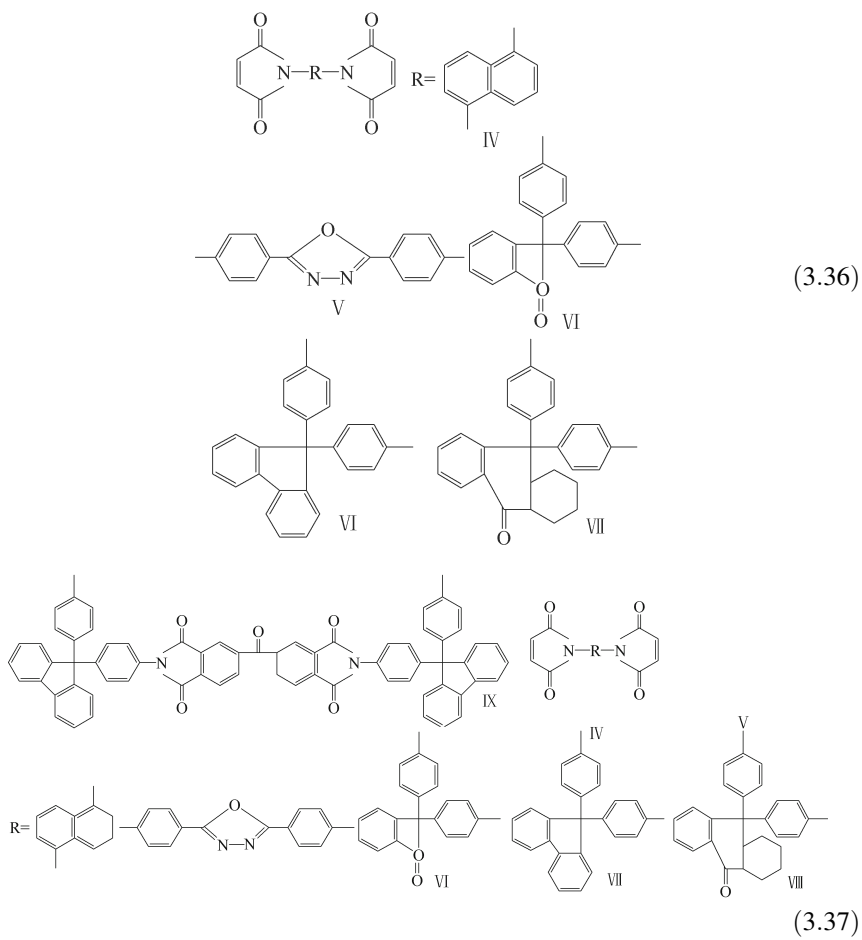
- (6) **Aromatic ester BMI:** The BMI containing stiffened rod-pattern aromatic ester groups can be used as thermosetting thermotropic liquid crystal (TLC) polymers and can be prepared by the following synthetic reactions: Cured BMI containing aromatic ester bonds have superior thermal stability and an initial degradation temperature higher than 500 °C, but they dissolve with difficulty in organic solvents. Their melting points are high, and the range between the melting degradation and the melting temperature is small.
- (7) **Silicon-containing BMI:** In the BMI backbone chain, the introduction of organic silicon structural units can generate cured polymeric products with good processing performance, high flexibility and thermal stability. This is because of the higher Si–O linkage energy and the larger bond spiral degree of freedom. Silicon-containing BMI are usually produced by the condensed polymerization of silicon-containing bisfuran monomers and BMI monomers.

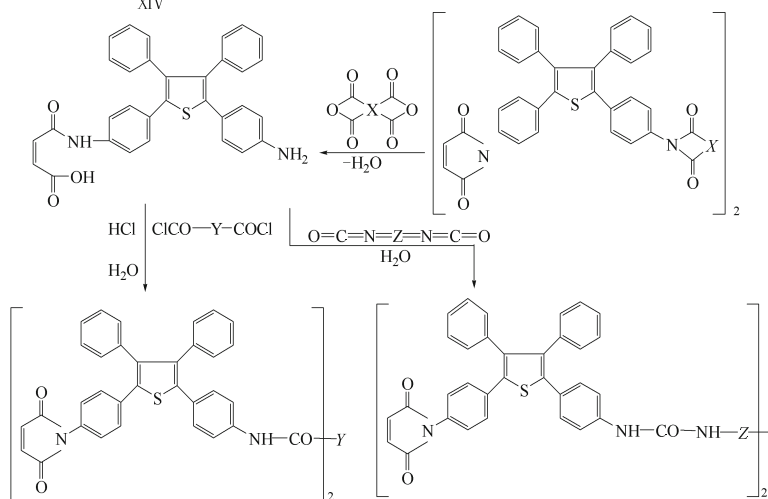
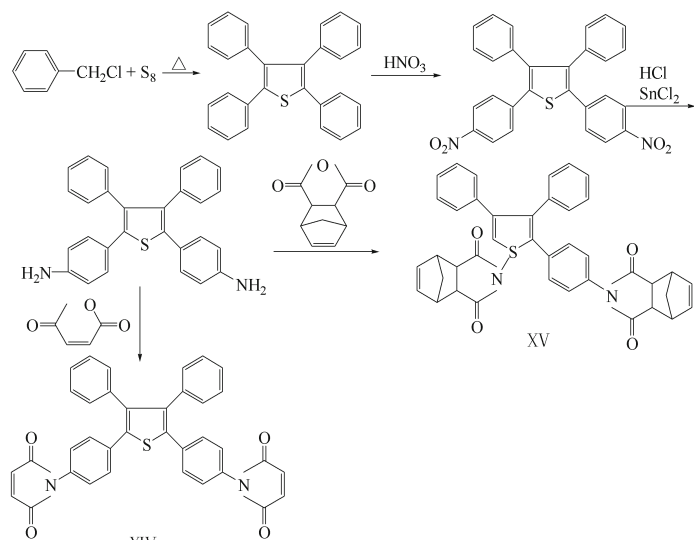
(2) **Substituted BMI**

In this type of BMI, the hydrogen atoms in the bismaleimide group groups are substituted by other groups to form BMI monomers. For their synthesis, the related diacid will be synthesized first and then further reacted with binary amine to obtain the BMI. Aliphatic and aromatic group substitution will consist of two basic reactions. The structures and properties of the substituting groups significantly affect BMI reaction activity, thermal resistance and dissolution behavior. Some functional groups, after introduction, can impart special functions onto BMI, for example, bromium-substituted BMI will have a very good flame-retardant ability.

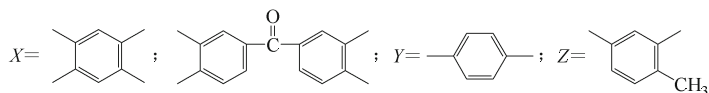
(3) **Condensed ring BMI**

To obtain superior thermal resistance BMI, a condensed ring binary amine and maleic dianhydride can be used to synthesize condensed ring BMI by traditional processing methods. Their structural formulae are given as follows:





where



Condensed ring BMI have superior thermal stability, and their maximum degradation temperature ranges from 450 to 520 °C with a higher residual carbon rate at 800 °C. Its glass cloth-reinforced composites have excellent mechanical performance and flame-retardant properties.

(4) Thiophene BMI

Thiophene BMI has high thermal–oxidation stability and thermal stability. Its synthetic reaction formula is given below: Thiophene BMI usually requires high temperature for curing, and oxygen has little effect on its thermal degradation temperature. Its residual carbon rate at 800 °C is 64–66%.

(5) Special element containing BMI

For special applications of BMI, hydroxyl amine and elemental organic compounds (such as boronic acid, silicon acid ester and titanate acid butyl) are reacted to form special element containing BMI such as those containing boron, silicon, molybdenum and titanium (BBMI, SiBMI, MBMI and TiBMI).

3.5.2.7 Processing Modification**(1) Decreasing the curing and post-treatment temperature**

Many modified BMI resin systems are currently available with high-temperature resistance, high strength and toughness. They have good dissolution and viscosity properties. However, these resin systems usually need high-temperature treatment (220–250 °C). High-temperature post-treatment requires processing equipment and molds with higher thermal resistance resulting in an increase in production cost and a decrease in production efficiency. In addition, high-temperature curing may cause an increase in product internal stresses or cracking. The combined curing performance will significantly decrease. To decrease the curing and post-treatment temperature, the following methods can be considered:

- (1) Increasing BMI monomer reaction activity: Principally, select and use nucleophilic monomers with higher activity to copolymerize with BMI monomers. Since the double bond on the imide rings in the BMI molecules is affected by adjacent carbonyl groups and becomes electrophilic, the nucleophilic monomers selected to copolymerize with them will result in a larger copolymerization rate. Therefore, the required curing temperature can be decreased. At the North West University in China, Professor Lan Liwen, etc. used styrene and divinyl benzene, with high activity constituents, to copolymerize with the BMI system, and the generated resins have good reactivity between 80 and 120 °C. The gel time is only 9 min at 120 °C, but the shelf life is short at ambient temperature, being only 48 h at 30 °C. Post-treatment at 220 °C is required to obtain products with high performance and cross-linking densities. This means that high activity constituents can reduce the BMI resin gel time at medium or low temperatures, but they cannot absolutely decrease its post-treatment temperature. This problem can often occur when studying increasing reactivity or decreasing post-treatment temperatures and attention should be paid to:

(2) Adding a catalyst or promoter: Adding a catalyst or promoter is another approach to decreasing the processing temperature. For different modified BMI resin systems, suitable catalysts or promoters are different. In Japan, researchers used 2-vinyl-4-methyl imidazole (2E4MZ), triethylamine, triphenylphosphonate and peroxidate diisopropylphenol (DCP) to study the catalysis mechanism of *N*-maleimide phenol/allyl phenol ether, indicating that the former three catalysts are suitable for this resin system. DCP is an effective catalyst. Prof. Lan Liwen et al. studied an imidazole catalyzed MBMI/DABPA systemic reaction and found that imidazole can dramatically accelerate the system gel reaction, but the cured resins have very low thermal resistance after post-treatment for 10 h at 200 °C. The thermal deflection temperature was only 156 °C. A further tracing study found that imidazole can only catalyze BMI self-polymerization and does not catalyze BMI/DABPA system copolymerization, resulting in an unmatched BMI/DABPA ratio. Therefore, DABPA was used in excess. Since DABPA self-polymerizes with difficulty, excess DABPA will result in free states and this causes a dramatic decrease in the thermal resistance and mechanical properties of the resin system. Therefore, proper catalysts or promoters should be able to catalyze or promote the copolymerization of a whole modified system rather than individual constituents in the system.

(2) **Special BMI for resin transfer molding (RTM)**

RTM is a liquid composite molding (LCM) technique and a low-cost processing technique for high-performance composites [70]. RTM requires resin systems to have low viscosity, long-term suitability and short curing cycles. Currently, the BMI resins used in RTM are prepared by adding allyl or vinyl groups to the system, and then prepolymerization may or may not be used to obtain the required viscosity suitable for RTM. The main commercially available resins include: Compimide 65 FWR from the Shell Co., RTM-BMI used for wheel bosses from the BP Co. The DESBIMID resin is used for cabin cover back beams in FORKKR50 airplane engines and supplied by the DSM Co. In this resin, BMI is dissolved in methacrylate and styrene and injected with a promoter at room temperature. Post-treatment is at 60, 130, 200 and 260 °C for high performance. The typical properties of these resins are given in Table 3.73.

Table 3.73 Properties of some BMI resins

Properties	BP RTM-BMI	DESBIMID	COMPIMIDE
Bending strength at R.T./MPa	118	100	102
Bending modulus at R.T./GPa	3.6	3.4	4.5
Fracture strain at R.T./%	–	3.0	–
Bending strength at 200 °C/MPa	63	–	–
Bending modulus at 200 °C/GPa	2.0	–	–
$G_{IC}/J \cdot m^{-2}$	–	500	–
$T_g/°C$	–	250	260

3.5.3 BMI Application

3.5.3.1 Main Commercial BMI Resins

Some commercial BMI resins with their designation and compositions are given in Table 3.74.

Table 3.74 BMI resins with their designations and compositions

Resin designation	Manufacturer	Basic composition	Features
Kerimide 601	Rhone-Poulenc (France)	Diphenyl methane BMI/methane diphenyl biamine	$T_m = 40\text{--}110\text{ }^\circ\text{C}$, good processing ability
Kerimide 353	Rhone-Poulenc (France)	The low co-melted resin of diphenyl methane BMI, phenyl methane BMI and 3-ethyl 6-methylene BMI	$T_m = 70\text{--}125\text{ }^\circ\text{C}$, melted viscosity is 0.15 MPa·s at 120 °C, suitable for melting impregnating fibers and the thermal winding, thermal stability of cured resin is lower
FE7003 and FE7006 (modified Kerimide)	Rhone-Poulenc (France)	Diphenyl silicone glycol-modified BMI	Amine-solvent-free system, thermally resistant to 250 °C, good hot/wet resistance and superior electric properties
Compimide-183,353, 795, 796, 800, 65FWR	Boots Technochemic (Germany)	Low co-melted BMI or added aminophenol formohydrazide and modifiers	Solvent-free and low co-melted resin, cured resins have high strength at 250 °C, good thermal resistance and dimensional stability, small linear expansion
Compimide-453 Boots Tech-	Boots Technochemic (Germany)	Compimide 453 with CTBN added	Solvent-free and thermal melting resins
F-178	Hexcel (US)	The copolymers of BMI, DDM and a little 3-allyl cyanuric ester	$T_m = 24\text{ }^\circ\text{C}$, can impregnate fiber melted or in butanone, cured at 130 °C, curing resin $T_g = 260\text{--}275\text{ }^\circ\text{C}$, water absorption = 3.7%, brittle

(continued)

Table 3.74 (continued)

Resin designation	Manufacturer	Basic composition	Features
V-378	Polymeric (US)	Bivinylic compound BMI resin	Processing similar to epoxy, cured resins have 3 classes at 230 °C, 315 °C and 371 °C, its composites have high hot/wet strength
V-391	Polymeric (US)	Modified BMI	Good toughness, thermal resistance and mechanical performance
R6451	Ciba-Geigy (US)	Modified BMI	Superior tacky and drape, hot/wet resistance in its prepregs, suitable for automatic winding large and complex structures, the retention rate of tensile strength is 35% at 300 °C
XU292	Ciba-Geigy (US)	Copolymer of diphenyl methane BMI and biallylic bisphenol A	Prepolymer has low viscosity and is stable at 100 °C, $T_g = 273-287$ °C after curing at 180–250 °C, the max. service temp. is 256 °C, superior hot/wet performance
RD85-101	Ciba-Geigy (US)	The copolymer of new BMI synthesized with biamine phenol indan/maleic anhydride and allyl benzene	Low viscosity at 90–100 °C, soluble in acetone, good processing ability, superior hot/wet performance
RX130-9	Ciba-Geigy (US)	Innovative BMI	Superior impact toughness
X5245C	Narmco (US)	Bicyanate ester and epoxy-modified BMI	Easy processing, curing temperature is 180 °C, good toughness of cured resins, $T_g = 228$ °C, suitable for high strain carbon fiber (1.8%) composites applied as airplane primary structures

(continued)

Table 3.74 (continued)

Resin designation	Manufacturer	Basic composition	Features
X5250	Narmco (US)	X5345C modified	Long shelf life, good compatibility with different fibers, hot/wet resistant, superior impact resistance and high-temperature mechanical performance, can be used for thermal resistance structures at 205 °C
QY8911	Beijing aeronautical processing institute of AVIC I (CN)	Modified BMI	Suitable for wet prepreg preparation, superior thermal resistance, toughness and oxidant resistance of cured resins, its composite can be used at 150–230 °C
QY9511	Beijing aeronautical processing institute of AVIC I (CN)	Modified BMI	Suitable for wet prepreg preparation, high toughness and superior thermal resistance and oxidant resistance of cured resins, its composite can be used at 170 °C
5405	North west Polytech university/Beijing Inst. of aero materials (CN)	Modified BMI	Good processing ability, composite can be used under long-term hot/wet conditions and at 130–150 °C
5428	Beijing Inst. of aero materials of AVIC I (CN)	High-toughness BMI	Suitable for thermal melting, preparing prepreps, high toughness of cured resins, good processing ability, composite can be used under long-term hot/wet conditions and at 170 °C

(continued)

Table 3.74 (continued)

Resin designation	Manufacturer	Basic composition	Features
5429	Beijing Inst. of aero materials of AVIC I (CN)	High-toughness BMI	Suitable for thermal melting, preparing prepregs, good processing ability, high toughness of composite, and can be used under long-term hot/wet conditions and at 150 °C
4501A	North west polytech university (CN)	Modified BMI	Low resin softening point, soluble in acetone, superior dielectric properties of cured resins, suitable for artificial medium materials and high-performance composite matrixes
4501B	North west polytech university (CN)	Modified BMI	Good tacky and drape ability of prepregs, superior dielectric properties of composites, possible low-temperature processing, used for the radome in advanced jet fighters

3.5.3.2 BMI Composites and Their Performance

In Tables 3.75, 3.76, 3.77, 3.78, 3.79, 3.80 and 3.81, some high-performance BMI resin composites with their mechanical properties and toughness are presented.

3.5.3.3 BMI Resins and Their Composite Application

BMI resins are widely applied in the following high technology fields:

(1) Isolation materials

They are mainly used as high-temperature impregnation paints, laminates, copper cladding plates and press molding plastics. For example, BMI can be blended with an epoxy resin and active diluting agents to produce H-grade solvent-free impregnated paintings with superior aging, thermal, adhering and chemical corrosion resistance.

Table 3.75 Mechanical properties of the T300/5405 BMI composites

Properties		Testing temperature			Standard
		R.T.	130 °C	150 °C	
Longitudinal tensile strength/MPa	Classical value	1841			GB/T 3354-1999
Longitudinal tensile modulus/GPa	Classical value	157			
Poisson's ratio	Classical value	0.36			
Transverse tensile strength/MPa	Classical value	88.6			GB/T 3354-1999
Transversal tensile modulus/GPa	Classical value	9.19			
Longitudinal compression strength/MPa	Classical value	1102			GB/T 3856-1983
Longitudinal compression modulus/GPa	Classical value	144			
Transverse compression strength/MPa	Classical value	186			
Transverse compression modulus/GPa	Classical value	10.3			
L/T shear strength/MPa	Classical value	126			
L/T shear modulus/GPa	Classical value	4.59			GB/T 3355-1982
Interlaminar shear strength/MPa	Classical value	101	70.6	64.4	JC/T 773-1982 (1996)
Bending strength/MPa	Classical value	1810	1440	1340	GB/T 3856-1983
Bending modulus/GPa	Classical value	122	125	126	

Table 3.76 The toughness of T300/5405 BMI composites

Properties		Testing temperature		Standard
		R.T.		
Open-hole tensile strength/MPa	Classical value	286		NASA PR 1142
Open-hole compression strength/MPa	Classical value	293		
Interlaminar fracture toughness (G_{IC})/J·m ⁻²	Classical value	236		
Fracture strength/MPa	Classical value	315		
Interlaminar fracture toughness (G_{IC})/J·m ⁻²	Classical value	172		
Fracture strength/MPa	Classical value	557		

(continued)

Table 3.76 (continued)

Properties			Testing temperature		Standard
			R.T.		
Compression after impact (CAI)	Compression strength/MPa	Classical value	170		NASA PR 1142 (impact energy 27.10 J)
	Acuminated delaminated area/mm ²	Classical value	1400		
	Fracture strain/ $\mu\epsilon$	Classical value	3498		
Compression strength after impact (solution method)/MPa		Classical value	191		BSS 7260
Compression strength after impact (thermal melting method)/MPa		Classical value	207		BSS 7260

Table 3.77 Mechanical properties of the T700/5428 BMI composites

Properties		Testing temperature		Standard
		R.T.	170 °C	
Longitudinal tensile strength/MPa	Classical value	2150		GB/T 3354-1999
Longitudinal tensile modulus/GPa	Classical value	125		
Poisson's ratio	Classical value	0.32		
Transverse tensile strength/MPa	Classical value	65		
Transversal tensile modulus/GPa	Classical value	7.8		
Transversal tensile strain/%	Classical value	0.85		
Longitudinal compression strength/MPa	Classical value	1210		GB/T 3856-1983
Longitudinal compression modulus/GPa	Classical value	107		
Transverse compression strength/MPa	Classical value	220		
Transverse compression modulus/GPa	Classical value	10		
L/T shear strength/MPa	Classical value	111		GB/T 3355-1982
L/T shear modulus/GPa	Classical value	5.6		
Interlaminar shear strength/MPa	Classical value	97	64	JC/T 773-1982 (1996)
Longitudinal bending strength/MPa	Classical value	1640	1240	GB/T 3356-1999
Longitudinal bending modulus/GPa	Classical value	120	120	

Table 3.78 Toughness of the T700/5428 BMI composites

Properties		Testing temperature		Standard
		R.T.		
Transverse tensile strength/MPa	Classical value	65		GB/T 3354-1999
Transversal tensile modulus/GPa	Classical value	7.8		
Transversal tensile strain/%	Classical value	0.85		
Open-hole tensile strength/MPa	Classical value	454		NASA PR 1142
Open-hole compression strength/MPa	Classical value	280		
Edgy delamination/J·m ⁻²	Classical value	301		
Model I strain energy release rate (G _{IC})/J·m ⁻²	Classical value	780		
Compression strength after impact (CAI)/MPa	Classical value	260		BSS 7260

Table 3.79 Mechanical properties of the T700/5429 BMI composites

Properties		Testing temperature		Standard
		R.T.	150 °C	
Longitudinal tensile strength/MPa	Classical value	2010		GB/T 3354-1999
Longitudinal tensile modulus/GPa	Classical value	129		
Poisson's ratio	Classical value	0.31		
Longitudinal compression strength/MPa	Classical value	1430		GB/T 3856-1999
Longitudinal compression modulus/GPa	Classical value	116		
Interlaminar shear strength/MPa	Classical value	103	55	JC/T 773-1982 (1996)
Longitudinal bending strength/MPa	Classical value	1530	1130	GB/T 3356-1999
Longitudinal bending modulus/GPa	Classical value	100	105	

(2) Aerospace structural materials

BMI is mainly combined with carbon fibers to make continuous fiber-reinforced composites, which are mainly used for load-bearing structures in military or commercial airplanes and space vehicles, such as wing skins, tails, vertical tails, fuselages and frames.

(3) Anti-abrading materials

They are used for diamond sand wheels, heavy duty sand wheels, brake pads and high-temperature-bearing adhesives.

Table 3.80 Toughness of the T700/5429 BMI composites

Properties		Testing temperature		Standard
		R.T.		
Open-hole tensile strength/MPa	Classical value	587		NASA PR 1142
Open-hole compression strength/MPa	Classical value	291		
Edgy delamination/J·m ⁻²	Classical value	281		
Model I strain energy release rate (G _{IC})/J·m ⁻²	Classical value	764		
Compression strength after impact (CAI)/MPa	Classical value	296		BSS 7260

Table 3.81 Mechanical properties of the T300/QY9511 BMI composites

Properties		Testing temperature		Standard
		R.T.	150 °C	
Transverse tensile strength/MPa	Classical value	75		GB/T 3354-1999
Transverse tensile modulus/GPa	Classical value	10		
Longitudinal compression strength/MPa	Classical value	1530		GB/T 3856-1999
Interlaminar shear strength/MPa	Classical value	121		JC/T 773-1982 (1996)
Longitudinal bending strength/MPa	Classical value	1868	1685	GB/T 3356-1999
Longitudinal bending modulus/GPa	Classical value	128	119	
Transverse bending strength/MPa	Classical value	106	71	
Transverse bending modulus/GPa	Classical value	10	8.9	

(4) Functional composites

BMI has a far higher thermal resistance than epoxy resins, and its processing ability is similar. Their hot/wet resistance is excellent, and BMI resin matrix composites are widely used in the aerospace field, for example, the wings, fuselages, tails, various ribs, beams and horizontal stabilizers in F-22 fighter jets are made from high-toughness BMI composites. Table 3.82 lists some high-performance BMI resin composites that are used in airplane applications.

Table 3.82 BMI resins in airplane applications

CF/resin	Application
IM7/5250-2	Mid fuselage, frame and operation surface in F-22
T700/5248	Horizontal tail, mid fuselage
T700/5249	Wings
IM7/5250-4	Wing skin, stabilizer surface in F-22
T300/QY8911-1	Wing, front fuselage, tail
T300/QY8911-2	Space structures
T300/540	Wing, tail skin

3.6 Cyanate Ester Resin Matrixes

In the second half of the nineteenth century, the production of cyanate ester (CE) was attempted using hypochlorite ester with cyanides or phenate compounds with cyanogen halides, but these attempts were not successful [71]. The obtained products were only the isocyanate ester or other compounds. In the late 1950s and early 1960s, R. Stroh and H. Gerber reported the first successful synthesis of a real cyanate ester. In 1963, a Germany chemist E. Grigat developed a simple method in which phenol compounds and cyanogen halides were used to synthesize cyanate esters. Since then, E. Grigat and his company have carried much research into this subject. However, since the cyanate ester synthesis as well as the polymerization mechanism was not fully understood in the early stages, the processing and operating capabilities of cyanate ester resins were influenced, and the promotion and application of cyanate ester resins was severely limited. In 1976, the Miles Co. introduced a resin to the market that could be applied in the electronics industry. This was a butanone solution containing 70% cyanate ester. However, this resin was inconsistent during vapor welding immersion testing, and it was withdrawn from the market by Miles in 1978. Research continued and with the advancement of science and technology in the 1980s products with future applications were successfully developed.

Cyanate ester resin is usually defined as a phenol derivative containing two or more cyanate ester functional groups. They can undergo tri-ring reactions under applied heat and catalysis and form highly cross-linked networks and structural macromolecules containing triazine rings. Cured cyanate ester resins can provide low dielectric constants (2.8–3.2) and a very small dielectric loss tangent (0.002–0.008), a high glass transition temperature ($T_g = 240\text{--}290\text{ }^\circ\text{C}$), low shrinkage and water absorption (<1.5%), good mechanical performance and adhering ability. Cyanate ester resins have a similar processing ability to epoxy resins, and no small molecular volatiles are released during the curing processes. Cyanate ester resins are mainly used in the following industries: as printed circuit boards in high speed and frequency digital applications, high-performance wave penetration materials and aerospace high-performance structural composite matrices.

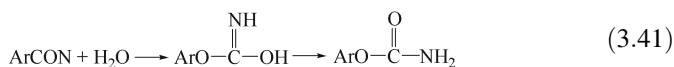
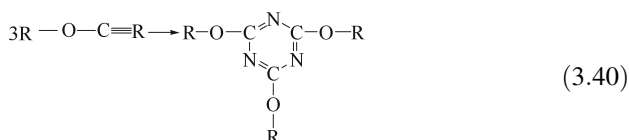
3.6.1 Synthesis of Cyanate Ester Resin Monomers

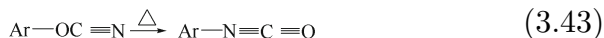
Extensive research has been reported regarding cyanate ester resin synthesis, and many approaches are currently available. Only one method has been commercialized [72–74] for the preparation of high-temperature-resistant cyanate ester resin. This method consists of alkali catalysis using cyanogen halides and phenol compounds to prepare cyanate ester monomers:



In Eq. 3.39, Hal can be Cl, Br and I but bromine cyanide is most popular because it is a stable solid at ambient temperature. Its reaction activity is adequate and it has low toxicity. ArOH can be a single phenol, a multi-phenol or aliphatic hydroxyl compounds. The alkali in the reaction medium is usually an organic alkali like triethylamine that can accept protonic acid. This type of reaction is usually carried out in organic solution at -30 to 20 °C. The reaction temperature may differ slightly depending on the phenol used, for example, the reaction temperature required for the reaction between bisphenol A and bromine cyanide is usually controlled at approximately -30 °C [75]. The initial products generated in the reaction will be subject to vacuum distillation or recrystallization to yield purified products. The 4,4'-dicyanate ester-diphenyl methane is a low-viscosity liquid, and all the other commercialized cyanate ester monomers are crystallized solids. For the synthesis of cyanate ester monomers, two main side reactions take place: One is the tri-polymerization of some of the cyanate ester monomers under alkali catalysis to form cyanate ester monomer oligopolymers in non-crystallized half-solid states [Eq. (3.40)], which occurs because the synthesis is carried out under alkali ambient conditions. Under alkali conditions, the small amount of water in the system or in the phenol may continuously react with the generated cyanate ester to form amine formic ether or an imino-carbonic ester [Eqs. (3.41) and (3.42)]. The small amount of impurities will affect the storage stability of the synthesized products and the service performance of the end products (such as their thermal resistance and hydrolysis resistance) [76].

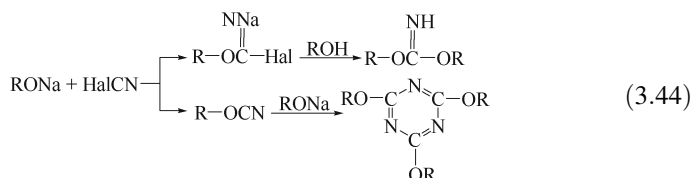
It is necessary to point out that aliphatic cyanate esters can easily undergo isomeric reactions to form isocyanate esters:





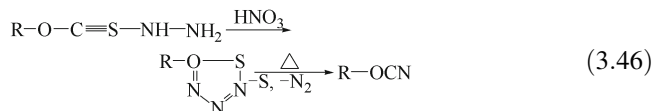
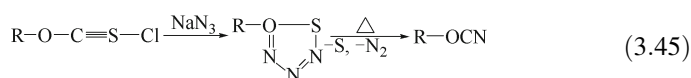
This synthesis method for cyanate esters is highly suitable for industrial production with its simple production procedures, high output rate and product purity. Additionally, the cyanate ester produced can provide very good stability, and their end products can give superior service performance.

The second synthesis method for cyanate esters is also the earliest method used for cyanate ester synthesis. It comprises the reaction between alkaline phenate (phenol sodium) compounds and cyanogen halides. In these syntheses, the generated cyanate ester can undergo tri-polymerization easily, or react with phenol to form imino-carbonic esters under strong alkali catalysis [77]:



When these syntheses were developed, the production rate was very low, and the purity of the products was not high either. Therefore, the scaling of this synthetic method to commercial production was not feasible. However, according to some literature reports, high-purity aromatic cyanate esters can be prepared by this method if proper processing conditions are selected. For example, amine catalysis at low temperature using polyalkylphenol amine salt to react with the abundant cyanogen halides in organic solution can also give high-purity cyanate esters.

A year after the preparation of the cyanate ester shown in Eq. 3.39 by E. Grigat, D. Martin and Berlin also developed a new method for cyanate ester preparation. They used the thermal decomposition of phenoxy 1,2,3,4-thiaziazole and oxethyl 1,2,3,4-thiaziazole to prepare cyanate esters [78]:



In Eqs. 3.45 and 3.46, the R group can be aromatic groups or aliphatic groups, and thus aromatic cyanate esters as well as aliphatic cyanate esters can be produced at a high production rate and product purity. However, cyanate ester production using this method is often lower than that given in Eq. 3.39. The cyanate ester yielded by the method given in Eq. 3.45 is only 60%, while that from Eq. 3.46 is 70–80%. Additionally, the synthetic process for this type of synthesis is very complex.

Cyanate ester synthesis can also be conducted by adding bromine to potassium cyanide or sodium cyanide aqueous solutions. In the presence of tert-amine, the solution is dispersed in a phenol carbon tetrachloride solution and the reaction will occur as follows (3.47) [72]:



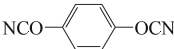
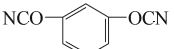
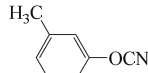
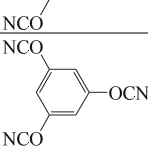
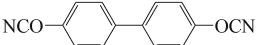
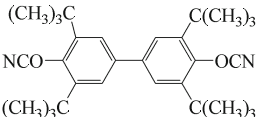
The advantages of this method are the elimination of the very toxic cyanogen halides, which vaporize easily or undergo sublimation during preparation. This process is a one-step simple reaction, but the purification of the final cyanate ester products is difficult.

Jesen and Holm tried to use thiocarbamic acid ester with heavy metal oxidants to eliminate sulfide hydrogen for the preparation of cyanate ester, but the yield is only 40%, and it is not a successful synthetic approach [72].



In Table 3.83, some applicable cyanate ester resins are given with their structures and thermal performance. Bisphenol F cyanate ester is a low-viscosity liquid, and the other monomers are crystallized solids. These crystals have lower melting points than those of the phenol compounds used for these preparations, and thus, the cyanate ester has a good processing ability.

Table 3.83 Some resins and reinforcing materials with their CTE

Cyanate ester structures	Melting point/ $^{\circ}\text{C}$	$T_{\text{od}}/^{\circ}\text{C}$	$T_{\text{wt}}/^{\circ}\text{C}$
	78–79.5	360	390
	115	395	390
	72–74	–	–
	102	–	–
	133	380	390
	263	–	–

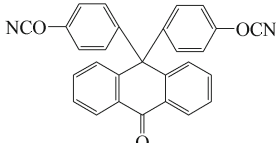
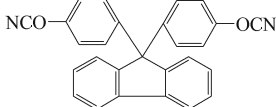
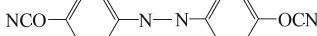
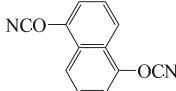
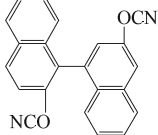
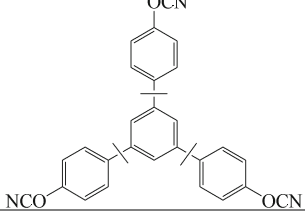
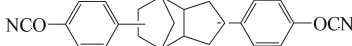
(continued)

Table 3.83 (continued)

Cyanate ester structures	Melting point/°C	$T_{od}/^{\circ}\text{C}$	$T_{wt}/^{\circ}\text{C}$
	108	370	400
	89	400	380
	94	—	400
	106	—	403
	206	—	—
	182	360	360
	79	385	411
	77–78	280	280
	Low-viscosity liquid, 0.1 MPa·s (R.T.)	—	408
	Light yellow liquid (possible crystallization during storage, T_m is 68 °C)	$(T_g = 192^{\circ}\text{C})$	—
	Half-solid and non-crystallized	$(270^{\circ}\text{C} < T_g < 350^{\circ}\text{C})$	—
	88	360	431
	73	410	410
	88	370	395
	191	360	400
	135	385	405

(continued)

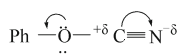
Table 3.83 (continued)

Cyanate ester structures	Melting point/°C	$T_{od}/^{\circ}\text{C}$	$T_{wt}/^{\circ}\text{C}$
	170	395	400
	163	375	400
	163	–	–
	Not melted	–	–
	149	–	–
	Crystals	–	–
	Half-solid, 0.7 Pa·s (85 °C)	–	405

3.6.2 Curing Reaction of Cyanate Ester Resins

3.6.2.1 Curing Reaction Mechanism

Research has shown that highly purified aromatic cyanate esters cannot polymerize even under applied heat conditions. However, for functional groups containing partial negative charges like oxygen and nitrogen, the adjacent carbon atoms show strongly electrophilic behavior.



Therefore, with a nucleophilic reactant the reactions of cyanate ester functional groups can be catalyzed either by acid or by alkali.

Model cyanate ester compounds with a single functional degree react in aqueous solutions containing active hydrogens (or acids) with difficulty. It has been reported that at 100 °C for 5 h in butanone and acetone solutions and without any catalysis, a reaction mixture containing the model compounds and tert-butyl phenyl cyanate ester (PTBPCN) was evaporated to remove the solvent followed by N-NMR analysis. The results showed that no reactions took place. The same system showed apparent tri-polymerization after the addition of 200×10^{-6} zinc octoate catalyst and heating for 1 h. Additionally, a hydration reaction gave a small amount of cyanate ester (Eq. 3.41), as shown in Fig. 3.32 [79].

- (1) **No catalysis (100 °C × 5 h); (2) 200×10^{-6} zinc octoate catalysis (100 °C × 1 h)**

Some of the cyanate esters prepared by different synthetic methods will not contain residual phenols, while others will contain a little. The curing reaction is very slow, even for the residual phenol-containing cyanate esters. To polymerize high-purity cyanate ester monomers, two kinds of catalysts should be added to the system: One is an active hydrogen-containing compound such as a single phenol in water (2–6%) and the second is a metal catalyst such as a Lewis acid or organic metal salts. Since cyanate ester functional groups contain lone-pair electrons and they donate electron π bonds, they easily form complexes with metal compounds. Therefore, metal compounds like metal carboxyl

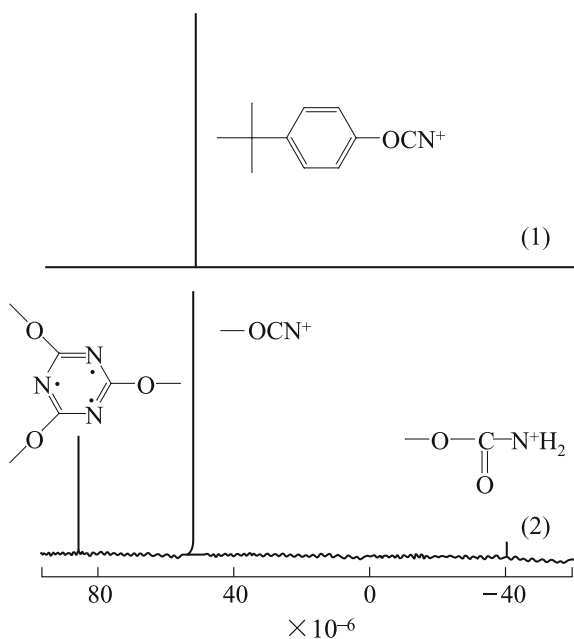


Fig. 3.32 N-NMR spectrum of the nitrogen-rich PTBPCN reaction

acid salts, $ZnCl_2$ and $AlCl_3$ can be used as catalysts to catalyze cyanate ester functional group tri-polymerization. However, these metal salts have very poor solubility in cyanate ester resins resulting in very low catalysis efficiency. To increase the catalysis efficiency, organic metal compounds that can dissolve in cyanate ester resins should be used. In Fig. 3.33, the polymerization mechanisms of cyanate ester reactions under metal salt or phenol catalysis are given [80–82]. In these reaction processes when using cyanate esters with good flow ability, the metal ions will first concentrate the cyanate ester molecules and surround the ester upon which the phenol hydroxyl will undergo a nucleophilic addition reaction with the cyanate ester in the surrounding metal ions to form an imide carbonized ester, and undergo a continuous addition reaction with the two cyanate esters.

Finally, the ring will close and remove the molecular phenol to form a triazine ring. In this reaction process, the metal salt is the principal catalyzing agent, and phenol is the coordinating catalyzing agent, which promotes the ring-closing reaction by proton migration.

3.6.2.2 Curing Reaction Kinetics of the Cyanate Ester

In the tri-ring reaction, the polymerization consists of four fundamental reactions related to the cyanate ester monomers, metal catalyzing agents and the cyanate ester/catalyzing agents. The cyanate ester functional groups will react first with the metal catalyzing agent ions to form a complex. A chain expansion by the complex

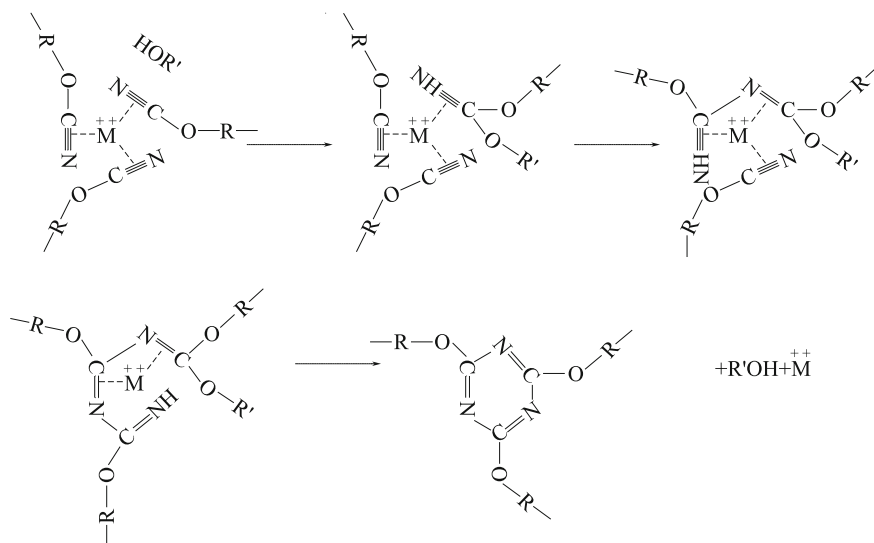
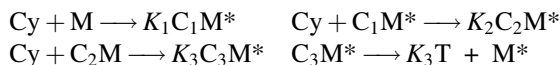
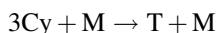


Fig. 3.33 The reaction mechanism of cyanate ester polymerization under catalysis

will take place and promote a ring-closing reaction by proton migration because of the active hydrogen-containing compounds. The four basic reactions are as follows:



where Cy is the unreacted unit; T is the triazine ring; M is the metal ions; C_1M^* , C_2M^* and C_3M^* are the metal ion/cyanate ester complexes with ratios of 1:1, 1:2 and 1:3, respectively; K_1 is the reaction speed constant of the basic reaction. The general reaction can be expressed as:



In the reaction process, assuming that the complexes have the same concentrations at all reaction stages, that is, $[\text{C}_1\text{M}^*] = [\text{C}_2\text{M}^*] = [\text{C}_3\text{M}^*]$, and considering the above-mentioned reaction equations, it can be concluded that $K_2 = K_3 \geq K_1$ ($[\text{M}] \geq [\text{CM}]$). The consumption rate of the cyanate ester functional groups is thus:

$$\frac{d[\text{Cy}]}{dt} = \frac{2K_2K_1}{K_4} [\text{M}][\text{Cy}]^2 \quad (3.49)$$

Additionally, assuming that the metal ion concentration is nearly equal to the initial concentration of the metal catalyst, which is $[\text{M}] = [\text{M}_0]$, Eq. (3.49) can be expressed as:

$$\frac{d[\text{Cy}]}{dt} = \frac{2K_2K_1}{K_4} [\text{M}_0][\text{Cy}]^2 = -[\text{Cy}]^2 \quad (3.50)$$

From Eq. (3.50), the reaction kinetics of the cyanate ester tri-polymerization obeys a secondary reaction kinetic model. From the deduction of the kinetic equation, the reaction speed constant of the tri-polymerization will be proportional to the ion concentration of the metal catalysts. Based on the Arrhenius equation and the different reaction speeds of the different catalysts at different temperatures, the reaction activation energies of the polymerization with different metal catalysts can be calculated. In Table 3.84, the reaction speed constants, activation energies and frequency factors of several BPACy formulae are given. In terms of the reaction speed constants, the catalysis abilities of the metal catalyzing agents will be

Table 3.84 Some BPACy formulae with their kinetic parameters

Resin formulae	$E_a / \text{kJ}\cdot\text{mol}^{-1}$	LnA/s^{-1}	Reaction speed constant $k/10^{-3}$			
			130 °C	150 °C	157 °C	200 °C
BPACy/ $100 \times 10^{-6}\text{Zn}/4 \text{ OH}$	80.2	16.5	0.60	2.1	8.97	19.1
BPACy/ $100 \times 10^{-6}\text{Mn}/4 \text{ OH}$	76.2	15.2	0.47	1.52	6.48	12.3
BPACy/ $100 \times 10^{-6}\text{Co}/4 \text{ OH}$	103.4	22.3	0.13	0.62	5.47	10.95

Zn > Mn > Co, and the reactivity of the metal catalysis is related to the coordination number of the metal ions. The Zn salts have the lowest coordination number, and their complexes will give a higher diffusing ability in the cyanate ester ring-forming processes. Therefore, its catalyzed BPACy resins will have higher reactivity. Based on these experimental results, the resins prepared using various catalysts have reactive activation energies of 75–104 kJ/mol. It is necessary to point out that the kinetic equation given in Eq. 3.50 is only applicable to the sections controlled by reaction kinetics while the kinetics controlled sections are found where the curing temperature is about 30 °C higher than the glass transition temperature.

For cyanate ester curing, IR spectra can be used to monitor the reaction and the band at 2270 cm^{-1} disappears while new absorption bands appear at 1565 and 1370 cm^{-1} . The band at 2270 cm^{-1} is a $\text{C}\equiv\text{N}$ tension vibration, while those at 1565 and 1370 cm^{-1} are vibration absorptions of the triazine rings from the cyanate ester tri-ring reactions. Figure 3.34 shows that under catalysis by a $100 \times 10^{-6}\text{ mol/L}$ Zn salt and a 4% single phenol solution, concentration fraction changes in the cyanate ester functional degree in the BPACy resins at different temperatures are obtained. This shows the cyanate ester reaction extent, as monitored by IR. From Fig. 3.35, when the transformation of the cyanate ester function is higher, that is, when the resin is gelled, the flow ability of the reaction system decreases and the reaction does not fit the kinetics model any more. The reaction will thus be controlled by mass transfer. After the reaction system becomes gelled, the active hydrogen-containing compounds, especially nonyl phenol, will be more efficient at catalyzing the cyanate ester functional group transformation compared with metal ions, and this may be because the nonyl phenols undergo mass transfer better in this system.

3.6.2.3 Effect of Catalyst on the Curing Reaction

In cyanate ester curing processes, the type of metal ion and the concentration of catalysts can have a significant effect on the curing reactions. Additionally, the organic ions of the catalysts and the concentrations and types of activated hydrogen compounds in the coordinated catalysts will greatly affect the curing reactions.

Fig. 3.34 Correlation between speed constant and metal catalyst concentration. ●, ■ are the Co and Mn catalysts (containing 4% phenol hydroxyl)

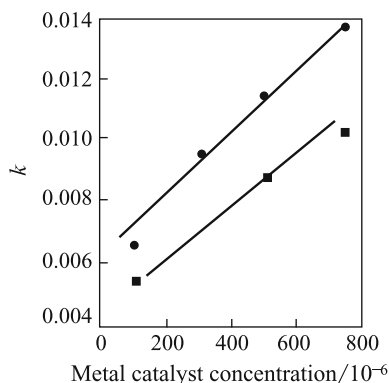


Fig. 3.35 Comparison between model and experimental results—model of calculated results. ●, ■, □, ▲ are the experimental results obtained at 130, 150, 175 and 200 °C, respectively

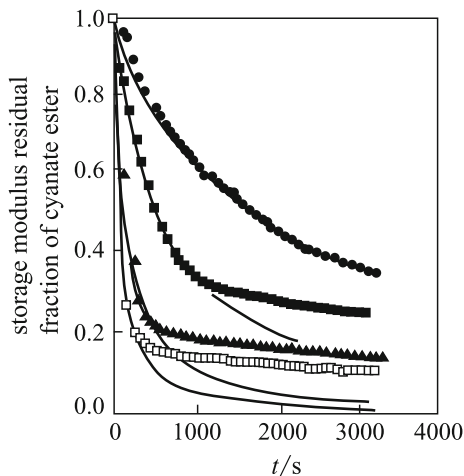
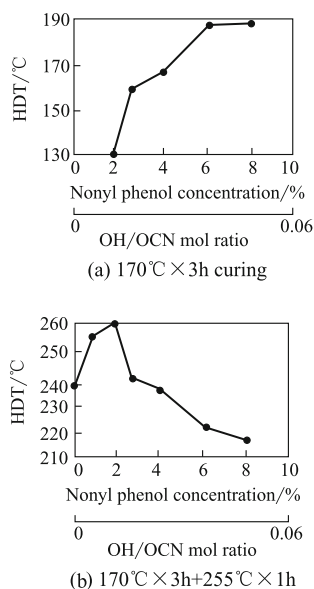


Figure 3.36 shows the effect of nonyl phenol concentration on the thermal deformation temperature of the BPACy cast resins cured under copper naphthenate catalysis [81]. At a nonyl phenyl concentration less than 2% (0.013 OH/OCN mol ratio), the system is not fully cured at 170 °C for 3 h as determined by FTIR and DSC analysis. The curing degree is only in 70–75%. At a phenol concentration of 6%, the curing degree is 91%, and the HDT is 186 °C. This is because the reaction speed is controlled by nonyl mass transfer after the resin has gelled. Therefore, a higher concentration of nonyl phenol will be more effective during the curing reaction of the gelled cyanate ester. Curing at 250 °C for 1 h gives a cyanate ester cast resin containing 2% nonyl phenol that gives a HDT of up to 260 °C (transfer rate = 97%).

Fig. 3.36 Effect of nonyl phenol concentration on the heat deformation temperature (HDT) of the BPACy cast resins cured under copper naphthenate catalysis



For the 6% nonyl phenol cast resin, the HDT was only 220 °C (transfer rate > 98%). The reason is that a proper amount of nonyl phenol can cause –OCN to be sufficiently tricyclized into triazine rings, and this will prevent phenol reacting with –OCN to form an imide carbonized ester (cause resin cross-linking density to decrease), resulting in very high HDT. A high concentration of phenol (6%) can cause –OCN to be fully transferred, but the phenol can react with –OCN and cause a decrease in the resin's cross-linking density, resulting in a lower HDT. In Fig. 3.37 [83], the BPACy resins cured under various post-curing conditions and their T_g changes with different nonyl phenol concentrations are shown. These results indicate that the 250 °C post-cured samples will show a decrease in T_g as the nonyl phenol concentration increases. If the post-curing temperature is increased to 285 °C, the resin T_g (2% nonyl phenol) does not increase by comparison with 250 °C post-curing. However, for resins without nonyl phenol, their T_g increases from 270 to 295 °C. Therefore, at a nonyl phenol content less than 2%, high-temperature post-treatment is necessary for a high transfer rate. The nonyl phenol concentration will also significantly influence the cured resin's mechanical, thermal resistance and chemical resistance performance. Table 3.85 lists some BPACy resins and their mechanical and thermal resistance performance [81].

The active hydrogen compounds can also dramatically affect the curing reaction as well as the cured resin's performance. Table 3.86 lists the effects of several different phenols on the cyanate ester cure reaction and the cured resin's performance. The type of phenol can influence both the reaction speed and the mechanical properties. The formula containing o-phenyl bisphenol gave higher thermal resistance, but its mechanical properties are far poorer than those of the other formulae, and its toughness is also lower [84].

Figure 3.38 shows gel time curves for the BPACy reaction catalyzed by different acetylacetone cobalt concentrations [85]. From this figure, cobalt salts of the same concentration and with different negative ions gave different corresponding gel times. Carboxylic salts provide a far better catalyzing efficiency than acetylpropyl salts. In fact, acetylpropyl salts can be considered to be a potential catalyst because the catalyzed and cured resins will have a higher hydrolyzing resistance than that

Fig. 3.37 Correlation between BPACy resin T_g and nonyl phenol concentration. Maximum curing temperature: □ –175 °C; ▲ –285 °C; ● –300 °C

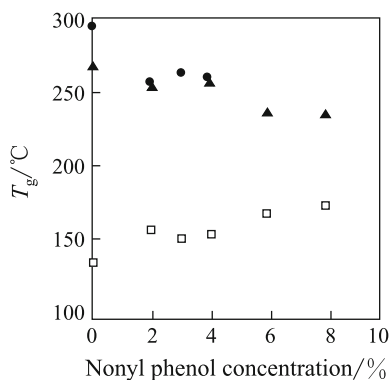


Table 3.85 Some polymers and their electrical properties

Nonyl phenol concentration/%	1.7		6.0	
Curing temp./°C	177	250	177	150
CE functional group transfer rate/%	72	97	91	>98
HDT (dried)/°C	108	206	186	222
HDT ^① (wet)/°C	(Failure)	172	161	174
Water absorption ^① /%	(Failure)	1.9	1.1	1.4
Tensile strength/MPa	(Brittle)	82.7	70.3	78.5
Tensile modulus/GPa	(Brittle)	3.24	3.24	2.96
Tensile strain/%	(Brittle)	3.6	2.5	2.8
MeCl ₂ water absorption ^② /%	(Failure)	5.8	15.5	7.6

① Wet conditions: 92 °C, 95% R.H. for 64 h; ② R.T., 3 h

Table 3.86 Effects of different phenols on cured cyanate esters

Curing processing	Performance	Nonyl phenol	o-cresol	o-phenyl bisphenol
170 °C × 3 h	Gel time (104.4 °C)/min	40	35	40
	HDT (dried)/°C	162	169	188
	HDT ^① (wet)/°C	133	134	156
	Water absorption/%	1.5	1.6	1.7
	Tensile strength/MPa	83.4	79.9	57.9
	Tensile fracture elongation/%	2.6	2.4	1.7
170 °C × 3 h + 232 °C × 1 h	HDT (dried)/°C	209	205	211
	HDT ^① (wet)/°C	156	151	168
	Water absorption/%	1.5	1.7	1.6
	Bending strength/MPa	135.7	131.6	94.4
	Bending fracture elongation/%	4.5	4.0	3.0

Note All resins used copper naphthenate as catalyst, mol fraction of active hydrogen was 3.2% (related to cyanate ester functional groups)

Fig. 3.38 Correlation between gel time and cobalt salt types and concentrations. 1—Acetylacetonate cobalt; 2—naphthenate cobalt; 3—octoate cobalt

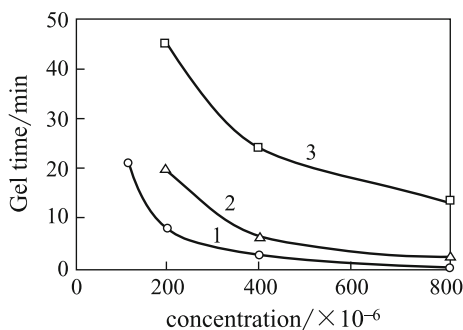


Table 3.87 Effects of different copper ion complexes on BPACy reactivity

Catalyst	CuCl ₂	Cu(Sal) ₂	Cu(AcAc) ₂	Cu(Bac) ₂	Cu(F ₆ Ac) ₂
Gel time/min	116	31	34	100	54

produced using other types of catalysts. Table 3.87 shows the effects of several copper ion complexes on the curing reactions. In Table 3.87, the time needed for resin gel hardening with less than 2% mol/CON catalyst and at 25 °C is listed. These results also show the effect of negative ion types on resin reactivity [86].

The effect of different metal ions on the cyanate ester curing reaction is important [80, 84]. In Table 3.88, the effects of acetylacetonate metal ions on the cyanate ester cure reaction are listed. At 104 °C, the gel time upon catalysis by Mn²⁺, Mn³⁺ and Zn²⁺ was only 20 min, while Co³⁺ required 240 min. The mechanical performance of the cured resins catalyzed by these metal salts showed large differences as their bending strengths varied from 178 to 119 MPa. Their bending strains varied from 4.8 to 7.7%. Among these catalysts, Zn²⁺, Cu²⁺, Mg²⁺, Co²⁺ and Co³⁺ were found to be good catalysts although Fe³⁺, Ti³⁺, Mg²⁺, Pb²⁺ and Sn²⁺ also gave high catalysis efficiencies, and their catalysis upon cross cyanate ester hydration should also be considered.

The effects of different metal ion types and concentrations on the thermal stability of cyanate ester cross-linked networks will be also different [83]. Under catalysis by 4% nonyl phenol and metal catalysts at 170 °C for 1 h or 255 °C for 1 h as curing conditions, the glass transition temperature T_g was found to be related to the catalyst type and concentration (shown in Fig. 3.39). At a metal catalyst concentration of 100×10^{-6} mol/L, the maximum glass transition temperature reached 250–260 °C. However, using Zn salts as catalysts for these resins resulted in a decrease in the T_g as the catalyst concentration increased. At a Zn catalyst concentration of 750×10^{-6} mol/L, the resin's T_g decreased to 190 °C, while using Mn and Co salts as catalysts did not give a change in T_g with different catalyst concentrations. Figure 3.40 shows TGA results [87, 88] for BPACy resins after curing with 4% nonyl phenol and catalysis by 100×10^{-6} mol/L Zn, 750×10^{-6} mol/L Zn and 750×10^{-6} mol/L Mn. The sample obtained using 750×10^{-6} mol/L Mn gave 450 °C or higher in terms of initial thermal decomposition temperature, while for 750×10^{-6} M Zn the initial thermal decomposition temperature was 250–300 °C. Even for the 100×10^{-6} mol/L Zn sample, the initial thermal decomposition temperature only reached about 400 °C. In addition, the samples catalyzed using 100×10^{-6} mol/L Zn and 750×10^{-6} mol/L Mn showed a second weight loss stage at 600 °C, while the 750×10^{-6} mol/L Zn-catalyzed samples had second and third stages at 500 and 600 °C. Based on GPC catalysis studies, single functional group model compounds may generate a certain amount of cyanate ester dimers, and the generation of dimers may be a reason for the lower glass transition temperature and the thermal decomposition temperature of the Zn salt catalyzed and cured resins.

Table 3.88 Effects of acetylacetone salts on BPACy reactivity

Catalyst concentration/ 10^{-6}	Metals										
	Cu (II)	Co (II)	Co (III)	Al (III)	Fe (III)	Mn (II)	Mn (III)	Ni (II)	Zn (II)		Zn (II)
104 °C Gel time/min	60	190	240	210	34	20	20	80	20		20
177 °C Gel time/min	2.0	4.0	4.0	4.0	1.5	0.83		3.5			0.83
Cure degree/%	96.6	95.7	95.8	96.8	96.5	93.8		96.0			95.8
HDT (dried)/°C	244	243	248	238	239	242		241			243
Bending strength/MPa	173.63	178.45	126.78	124.71	142.62	156.40		119.2			119.2
Bending modulus/GPa	2.96	3.1	3.1	2.9	2.96	2.96		3.1			3.03
Bending strain/%	7.7	6.7	5.5	4.6	5.3	6.0		4.8			6.0

Fig. 3.39 T_g changes with different catalyst types and concentrations. ■, ○, ▲, □, ● are zinc acid salt, naphthenate zinc, zinc acid manganese, naphthenate manganese and acetylacetone cobalt

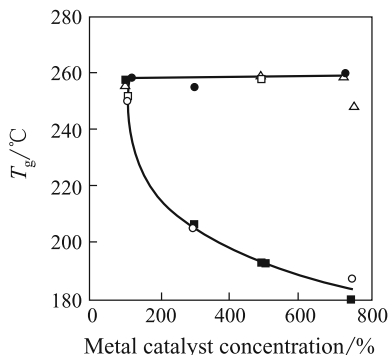
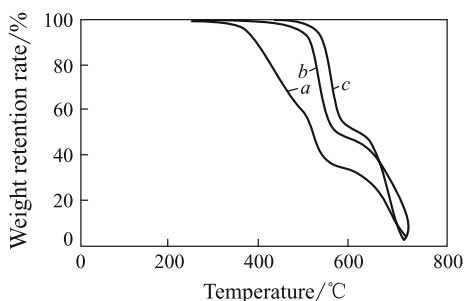


Fig. 3.40 TGA analysis of the BPACy resins catalyzed by 4% nonyl phenol and Zn^{2+} or Mn^{2+} . *a*— $750 \times 10^{-6} Zn^{2+}$; *b*— $100 \times 10^{-6} Zn^{2+}$; *c*— $750 \times 10^{-6} Mn^{2+}$



3.6.3 Cyanate Ester-Modified Epoxy and BMI Resins

As discussed in section one, cyanate ester resins can provide superior service performance and processing abilities compared with other resins. Therefore, using cyanate esters to modify epoxy, BMI and other thermosetting resins can improve the service performance of these resins (hot/wet resistance and impact resistance) and also their processing abilities.

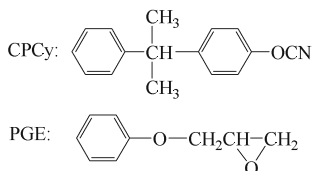
3.6.3.1 Cyanate Ester-Modified Epoxy Resins

Epoxy resins are a class of thermosetting resins with good combined performances and have gained wide application. However, common epoxy resin matrixes contain a large amount of polar groups like hydroxyls that are generated during the curing reactions resulting in higher water absorption for the resin matrixes. This may cause a significant decrease in the mechanical properties of the composites under hot/wet environments. Using cyanate ester resins to modify (cure) epoxy resins eliminates the possibility of hydroxyl and amine polar groups in the cured resins. Therefore, water absorption is lower, and the resins will have good hot/wet resistance. The cured resins contain five oxazoline heterocyclic and six triazine structures and thus

have good thermal resistance. The large amount of $-C-O-$ ether bonds contained in the cured resins can provide good toughness. In general, adding 30% cyanate ester can cure bisphenol A epoxy resin at less than $180\text{ }^{\circ}\text{C}$, and the composites will have good processing performance.

(1) **The curing reaction in cyanate ester-modified epoxy resins**

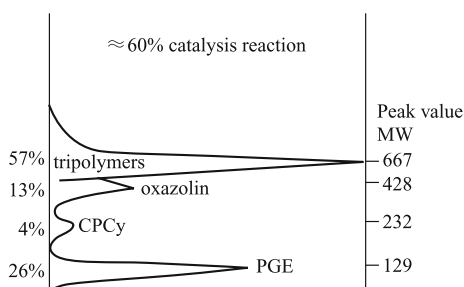
To study the copolymerization mechanism of cyanate ester/epoxy mixtures, a single functional degree cyanate ester model compound, CPCy and epoxy PGE were used to carry out a copolymerization mechanism study.



Under catalysis by titanate acid ester, equal molar quantities of CPCy and PGE were reacted at $177\text{ }^{\circ}\text{C}$, and it was found that 60% of the cyanate ester functional groups were transformed into tri-polymers. GPC analysis showed that the reacted products of equal molar quantities of CPCy and PGE consist of 57% cyanate ester tri-polymers, 13% oxazoline, 4% cyanate ester compounds and 26% PGE. Figure 3.41 shows the instant composition distribution of the CPCy and PGE reaction [80, 89, 90]. When HPLC was used to monitor the residual compound distribution of the CPCy/PGE system as well as the distribution of newly generated compounds under different reaction times (Fig. 3.42) [91], it was found that PGE was consumed at a lower rate than CPCy. Additionally, as the reaction proceeded, the tri-polymer content will reach a maximum value over a short reaction time and will then gradually decrease. It will finally reach a lower equilibrium value at the end of the reaction (this equilibrium value is related to the CPCy to PGE ratio). When the tri-polymer content began to decrease, oxazoline was generated.

FTIR is an important method for the study of reactions in the cyanate ester/epoxy resin system. The following table lists the infrared absorbing characteristic frequencies that correspond to the chemical functional groups in cyanate ester/epoxy co-curing:

Fig. 3.41 GPC peak distribution of equal molar quantities of blended CPCy and PGE reactants



The FTIR spectra of the CPCy/PGE blended system indicate that unreacted CPCy, PGE and generated CPCy tri-polymers, oxazoline and polyether structures are present in the blended reaction compounds.

From FTIR analyses (Fig. 3.43), the consumption rate of cyanate esters is much faster than that of epoxy. During the early reaction stage, tri-polymerized cyanate ester structures are apparent in the FTIR. As the curing reaction proceeded, the characteristic peaks of the tri-polymerized cyanate ester (1565 and 1372 cm^{-1}) were dramatically reduced, and even disappeared, while the characteristic peak intensities of the oxazoline structures (1760 and 1690 cm^{-1}) increased gradually. Therefore, when the ratio of BPACy/bisphenol A is less than 1, oxazoline and polyether will be the main structures present in the cured resins while low amounts of the triazine structures survived.

In summary, it has been found that the copolymerization of cyanate ester and epoxy resin will basically follow the mechanism as given as follows:

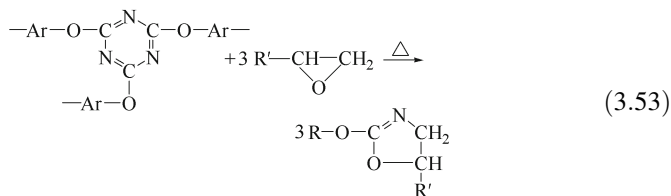
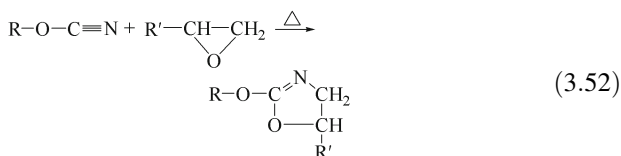
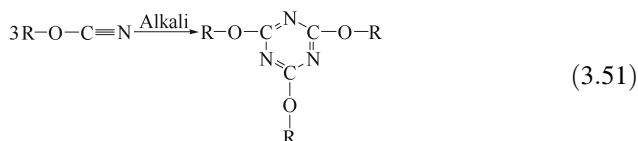


Fig. 3.42 The compound content distribution in the CPCy and PGE system. +—CPCy; ☒—PGE; ■—tri-polymers; ○—oxazoline

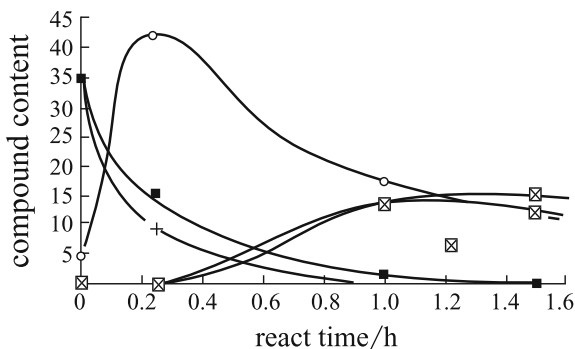
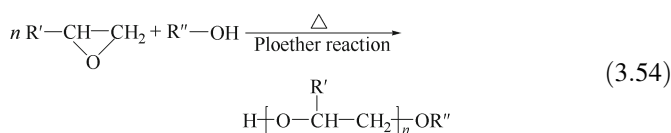
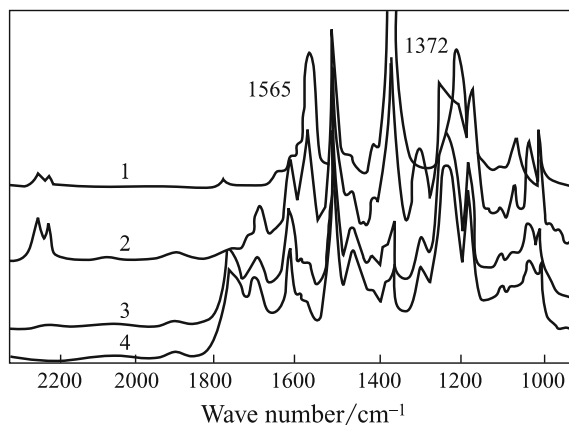
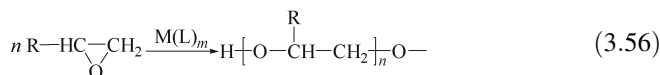
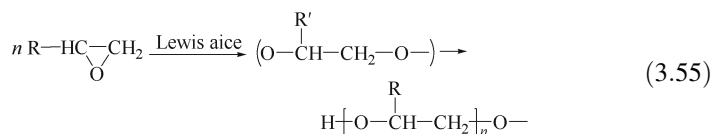


Fig. 3.43 FTIR spectra of cyanate ester/epoxy copolymerization. 1—Cured cyanate ester; 2—epoxy/cyanate ester 180 °C for 15 min; 3—epoxy/cyanate ester 180 °C for 1 h; 4—epoxy/cyanate ester 180 °C for 1 h and 200 °C for 2.5 h



From the FTIR analyses, a ring-opening reaction to form polyether will essentially occur during the later reaction stages in the epoxy functional groups. When organic metal catalysts were used, the epoxy compound PGE can undergo either positive-ion polymerization or coordination polymerization to form polyether structures:



It is well known that cyanate esters and epoxy resins do not undergo curing reactions independently without catalysts and curing agents. However, when blended compounds of cyanate ester and epoxy resin undergo curing reactions, only a small quantity of cyanate ester is required to promote epoxy resin curing. Additionally, a small quantity of epoxy resin can also promote the curing of cyanate ester; in other words, cyanate esters and epoxy resins can intercatalyze each other (Fig. 3.44) [92].

Using cyanate ester to cure epoxy resin can give fully cured resins without catalysts, but catalysts can also be used for curing reactions. When catalysts are added, the resin will have a different curing mechanism and molecular structure. Table 3.89 shows the effect of various catalyst concentrations on the

Fig. 3.44 Cyanate ester/epoxy mixed compounds with various ratios and their viscosities

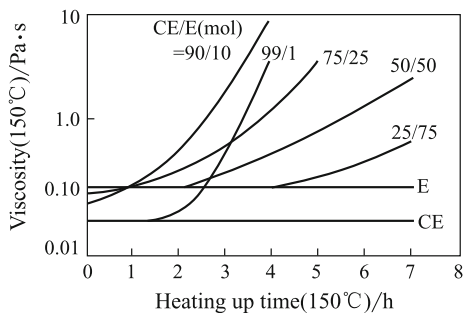


Table 3.89 Activities of the cyanate ester/epoxy with different catalyst contents

Formula	Gel time (177 °C)/min	Metal catalysts	Catalyst concentration/ $\times 10^{-6}$ M
A	24.2	CuAc Ac	37
B	10.0	CuAc Ac	152
C	5.7	CuAc Ac	267
D	1.2	CuNaPh	500
E	92	No	—

reaction activity of this resin system. In Table 3.89, formula D gives a very short gel and cure time (1.2 min) and very large reaction activity. This formula almost meets the RTM processing requirement for resins. Figure 3.45 shows curves showing the curing degree changes with curing time (FTIR was used to determine the epoxy curing degree). The resins are both catalyst-free and contain 500×10^{-6} M acetylacetone catalyst, and were cured at 180 °C. For the catalyst-free resin, after 30 min of curing the curing degree of the epoxy functional groups only reached 72% while 97.5% was obtained for the resin containing 500×10^{-6} M acetylacetone as a catalyst. However, the resin containing the catalyst was subject to a 3.5 h reaction to reach a certain curing degree (97%). The different catalysts will cause the cured resins to have a slight difference in structure. Table 3.90 shows FTIR peaks at 1695 and 1760 cm^{-1} with intensity changes. The resins used in this analysis were catalyzed by

Fig. 3.45 Effect of catalysts on epoxy functional group curing degree

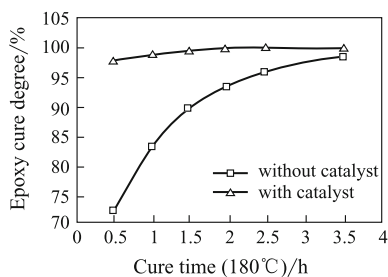


Table 3.90 Structure change in cured resins catalyzed by various catalysts

Catalyst	Mass fraction/%	Oxazone ratio/%		Reaction transformation rate/%	
		1695 cm^{-1}	1760 cm^{-1}	CE	Epoxy
No	—	0.71	0.49	>99	>95
Titanic ester	0.5	0.85	0.54	>99	>95
Acetylacetone copper	0.05	0.75	0.18	>99	>95
Oxidant methyl pyridine	1.0	0.55	0.53	>99	>95
Octoate Cr	1.0	0.44	0.75	>99	>95
Naphthenate V	1.0	0.34	0.52	98	>95
Neodecanoate i	1.0	0.29	0.39	97	>95
Naphthenate Pb	0.25	0.24	0.68	94	93

Note In Tables 3.89 and 3.90, BADCy/DGEBA is an equal mol ratio

different catalysts. These differences in structure will influence the physical and mechanical properties as well as the thermal stabilities of the cured resins.

(2) The physical and mechanical performance of cyanate ester-modified epoxy resins

As discussed before, epoxy resins after modification by cyanate esters can offer good hot/wet resistance and impact resistance, and this will depend on the molecular structures of the cured resins. Cyanate ester-modified epoxy cured resins will give a much lower water absorption rate than aromatic amine-cured epoxy resins and can reach an equilibrium state in a short time. Therefore, the decrease in HDT will also be smaller than for other resins. Figure 3.46 shows a comparison between several resins in terms of their water absorbing abilities. Cyanate ester-modified epoxy resins have a much lower water absorption rate than the AG-80/DDS resin system, the hot/wet resistant epoxy 5228 system and the BMI-MDA system. This is because of the high amount of generated hydrophilic hydroxyl groups from the curing processes of the epoxy resins (such as AG-80/DDS, 5228). Additionally, there will be some trialkylamine as well as incompletely reacted polar groups such as primary amine and secondary amine trialkylamine contained in the cross-linked network structures. In the cyanate ester-cured epoxy resin systems, no hydroxyls will be generated during

Fig. 3.46 Comparison between resins with their water absorption. 1—Cyanate ester/epoxy; 2—5228 epoxy; 3—BMI-MDA; 4—AG-80/DDS

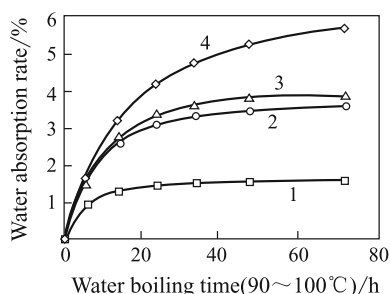
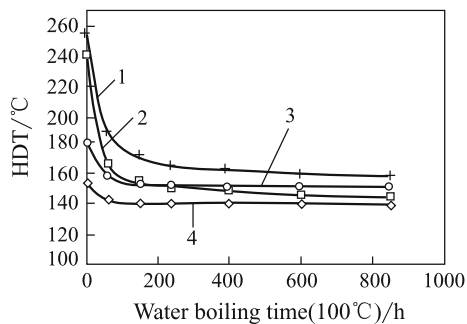


Fig. 3.47 HDT changes for several resins with different boiling water times. 1—BADCy homopolymer; 2—My720/DDS epoxy; 3—BADCy/DGEBA 43%/57%; 4—BADCy/DGEBA 35%/65%



the resin curing processes, and not many polar groups will be present either. The resin castings will thus have a lower water absorption rate, and the main water absorption model is water dissolved in the resin matrixes.

Figure 3.47 shows the effect of water boiling time on resin HDT. For cyanate ester homopolymers and the MY720/DDS resin system, HDT is still slightly lower after 500 h in boiling water, while the HDT of the cyanate ester-modified epoxy resin reaches equilibrium after 60 h in boiling water. The HDT difference between dry and wet conditions ranges from 10 to 20 °C.

Table 3.91 shows the cyanate ester epoxy resin's physical and mechanical properties [90]. Different structures will give different epoxy resin mechanical properties. The cyanate ester-cured DGEBA gives higher bending strength and fracture elongation.

The cyanate ester improves the epoxy resin's mechanical properties and also its electrical performance. Its electrical performance is superior to that of amine-cured epoxy resins and BMI-MDA resins as given in Table 3.92.

Table 3.91 Effect of epoxy resin structure on the performance of CE-modified epoxy cured resins

Epoxy type	Epoxy ratio/% (mass ratio)	Cure temp./°C	HDT/°C		Bending properties		
			Dried	Wet	Strength/MPa	Modulus/GPa	Elongation/%
DGEBA	56.8	200	196	167	147.6	3.45	6.2
DGETBBA	71.6	200	192	172	124.9	3.59	3.6
MY720	47.4	235	237	188	73.1	3.04	2.1

Table 3.92 Dielectric performance of CE-modified epoxy and other resins

Performance	DGEBA/BADCy	My720/BADCy	BADCy homopolymers	BMI-MDA	TGMDA/DDS
D_k (1 MHz)	3.1	3.3	2.9	3.5	4.1
D_f (1 MHz)	0.013	0.017	0.005	0.015	0.033

Note D_k —Dielectric constant; D_f —dielectric loss factor

Using the cyanate ester functional group to react with electron-deficient unsaturated olefinic compounds is an important cyanate ester modification approach [80]. In Japan, Mitsubishi's commercialized BT resin series is a major class of reactant for cyanate ester and BMI resins. In BT resins, the main constituents are the bisphenol A dicyanate ester and diphenyl methane bismaleimide. Figure 3.48 shows the major reaction equation of cyanate ester and BMI. For cyanate ester-modified BMI, the addition of epoxy, unsaturated polyester, acrylate and thermosetting fire-retardant agents can give various materials that meet different special application needs. BT-cured resins can increase the impact, electric and processing performance of BMI resins, or improve the hydration resistance of cyanate ester resins. In terms of thermal resistance, the cured BT resin series will range between the BMI and cyanate ester resins. Figure 3.49 shows the glass transition temperature of the BMI/CE resins with different ratios. Using a blended compound of CE, BMI and epoxy to carry out co-curing, the generated resins offer much better processing ability and toughness while the service temperature can be further decreased. Figure 3.50 shows the correlation between glass transition temperature and different constituents in a co-cured BMI/CE/epoxy resin system.

Group	CH ₂	-C≡N	-C-O-	C=N	Oxazoline ring	Triazine ring	Triazine ring ≡C-O-	Aromatic ether	Epoxy
Wave number/cm ⁻¹	2875	2230	1760	1695	1608	1565	1365	1245	915

3.6.3.2 Cyanate Ester-Modified Bismaleimide Resin (BMI)

The Chemical Department of Surrey University in the UK reported the copolymerization of allyl cyanate ester and bismaleimide as a systematic study [92–94].

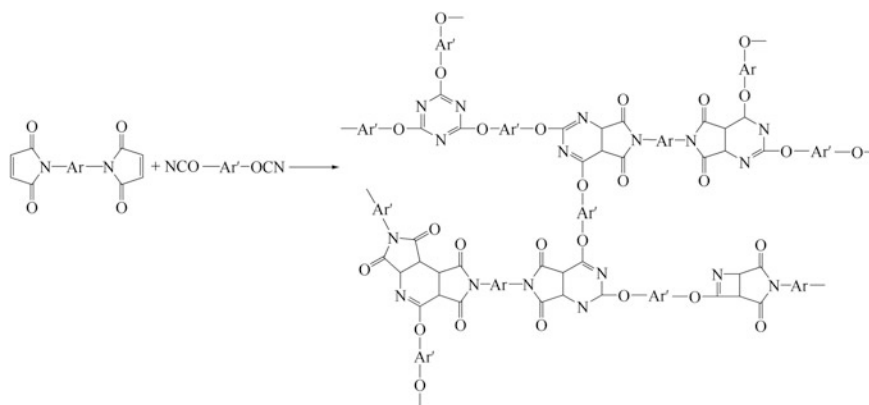


Fig. 3.48 BMI/CE copolymerization mechanism

Fig. 3.49 BMI/CE resins with various BMI mol ratios and their T_g

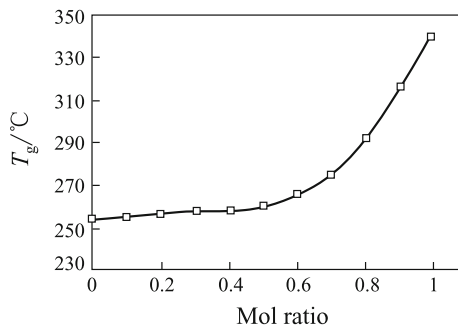
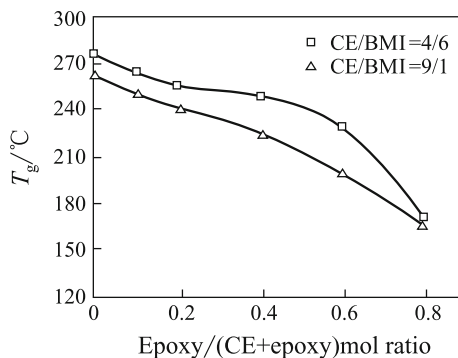


Fig. 3.50 Various BMI/CE resins with their T_g



A 1-cyano-2-allyl phenyl and *N*-phenyl maleimide (*N*-PNMI) model mixture was subjected to 140 °C for 4 h and 150 °C for 5 h. A C-NMR analysis showed a very strong absorbing carbon atom shift with 174.51×10^{-6} M triazine, as well as two different carbon atom shifts with 178.85×10^{-6} M and 175.75×10^{-6} M for the weaker asymmetric hydroxyls (for the allyl phenyl and *N*-phenyl maleimide reactants, the same two chemical shifts are shown in the C-NMR spectrum). In this set of C-NMR spectra, very strong carbon atom chemical shifts from unreacted carboxyl groups (Fig. 3.51) were also present. This indicated that the major reaction in this process is a tricyclization reaction of the cyanate ester functional groups. The allyl then further reacted with maleimide, and the reaction mechanism is shown in Fig. 3.52. In dynamic mechanical thermal analysis (DMTA), allyl cyanate ester and BMI blends gave a T_g of 350 °C after curing, while diphenyl methane BMI only gave a T_g of 210 °C after curing by the same curing process. This shows that this BMI is not completely cured using this process as shown in Fig. 3.53.

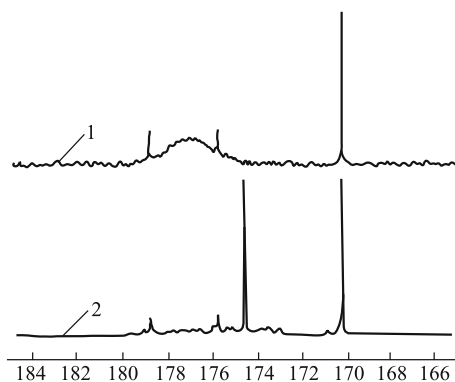


Fig. 3.51 C-NMR of the allyl cyanate ester and *N*-PNMI cured resins. 1—Allyl phenyl and *N*-PNMI reaction; 2—allyl CE and *N*-PNMI reaction

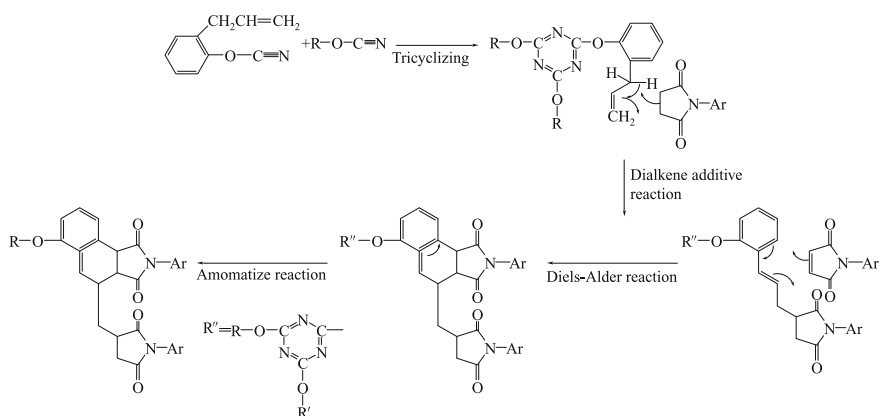
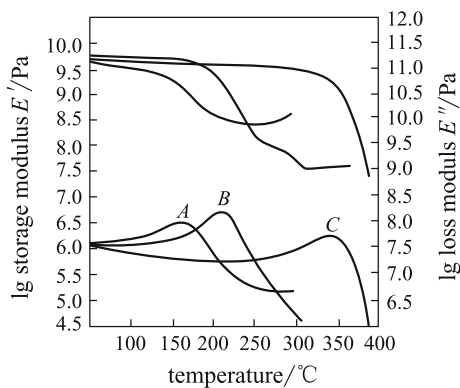


Fig. 3.52 Allyl cyanate esters and BMI copolymerization mechanism

Fig. 3.53 DMTA curves for allyl CE/BMI. BMI and CE resins. *C*—Allyl CE/BMI copolymer; E' —storage modulus; E'' —loss modulus; the top 3 are storage modulus curves; the bottom 3 are loss modulus curves



3.6.4 Cyanate Ester Resin and Its Composite Performances and Applications

3.6.4.1 Cyanate Ester Resin Structure and Performance

Extensive triazine and aromatic rings or rigid ester rings (such as in the Xu-71787 resin system) are contained in cured cyanate ester resin molecular networks, and the triazines as well as the aromatic rings are joined by ether linkages, and cured cyanate ester resins can thus give good thermal and chemical resistance and good impact resistance as well as dielectric properties.

Since different cyanate ester monomer structures exist, the physical states and processing behavior of these monomers will be very different. Table 3.93 lists some commercialized cyanate ester monomers and their physical properties [80]. Some of these monomers are crystalline and have different melting points as there are slight variations between the different structures in CE crystals. ArocyL-10 and RTX-366 are supplied as liquids, and ArocyL-10 can be used as a RTM resin. RTX-366 is crystalline with a melting point of 68 °C. It crystallizes from a light yellow liquid during storage. Xu-71787 is a half-solid material containing some oligopolymers. To improve the crystallized cyanate ester monomer's processing ability, the cyanate ester monomer should be partly homopolymerized into amorphous prepolymers with physical states ranging from tacky half-solids to brittle solids. Table 3.94 lists some cyanate ester resins supplied with prepolymers [80, 95, 96].

Table 3.93 Commercial CE monomers and their physical properties

X=	C(CH ₃) ₂	CH ₂	S	C(CF ₃) ₂	CH(CH ₃)	a	b
R=	H	CH ₂	H	H	H	H	H
Supplier	Rhône-Poulenc Arocy					Dow	
Resin products	B-10	M-10	T-10	F-10	U-10	RTX-366	Xu-71787
State	crystal	crystal	crystal	crystal	liquid	yellow liquid	non-crystal
Melting point/°C	79	106	94	87	low-viscosity liquid	68 ^①	half-solid
Viscosity/Pa·s	0.015 (90 °C)	0.02 (110 °C)	–	0.02(90 °C)	0.14(25 °C)	8(25 °C)	0.7 (25 °C)
CE equivalent (EW) ^②	139	153	134	193	132	198	–
Enthalpy/J·g ⁻¹	732	594	–	418	761	508	–

① RTX-366 can crystallize during storage

② Refer to the resin weight containing 1 mol of CE functional groups

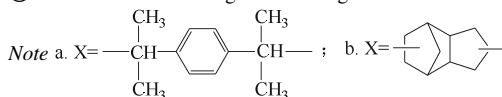


Table 3.94 Commercial CE prepolymers and their physical properties

X=	C(CH ₃) ₂		CH ₂		S		C(CF ₃) ₂	
R=	H		CH ₃		H		H	
Supplier	Rhone-Poulenc Arocy							
Resin products	B-30	B-40 s	B-50	M-30	M-40 s	M-50	T-30	F-40
Viscosity/Pa-s	0.45 (82 °C)	0.19 (25 °C)	3.6 (149 °C)	3.1 (82 °C)	0.09 (25 °C)	0.6 (149 °C)	16.7 (82 °C)	0.21 (25 °C)
Tri-polymer percentage/%	30	40	50	30	39	42	44	32
Physical state	Half-solid	Butanone solution	Solid	Half-solid	Butanone solution	Solid	Half-solid	Butanone solution
CE equivalent (EW)	200	232	278	218	243	262	240	284

Table 3.95 CE resins with their T_g and HDT [97–99]

Performance	Arocy					RTX-366	Xu-71787	REX-371 ^①	AG80/DDA
	B	M	T	F	L				
T_g (DMTA)/°C	289	252	273	270	258	192	244	270–400	246
HDT/°C dried	254	242	243	238	249				232
Wet ^②	197	234	195	160	183				167

① Rex-371 is a phenolic cyanate ester

② At 95 °C and >95% R.H. for 64 h

(1) Cyanate ester environmental resistance

The environmental resistance of cured cyanate ester resins will depend on the chemical structures of the CE monomer backbones, the catalysts used and the curing conditions. In this section, the effect of chemical structures on thermal resistance will be discussed. Table 3.95 lists cyanate esters with different chemical structures and their glass transition temperature T_g (DMA analysis) as well as their dry and wet HDT. In terms of T_g , the Arocy series cyanate esters range from 250 to 290 °C. Arocy M with four side methyl groups is the lowest, and asymmetric structure Arocy L is also low. However, the HDT difference in the Arocy series cyanate esters will not be as large as T_g . Arocy M has the highest wet HDT, and the difference between its dry and wet HDT is only 8 °C, which indicates that Arocy M will have the best hot/wet resistance, while Arocy F, which contains fluorine, will only give a wet HDT of 160 °C. The difference between the dry and wet HDT is 78 °C and, therefore, Arocy F is the lowest in the series in terms of hot/wet resistance.

For all the listed cyanate esters, RTX-366 has the lowest thermal resistance because the distance between the cross-linkages in its molecular structure is the longest. Xu-71787 also has a long distance between molecular cross-linkages, but it contains a very strong ester ring in between and, therefore, it gives a similar thermal resistance as the Arocy series. The T_g of the phenolic cyanate ester REX-371 ranges from 270 to 400 °C, and its thermal resistance can be adjusted by controlling the degree of esterification of the phenolic resins or the relative molecular masses of the half-cured resins. The different cured cyanate ester resins with different structures will give different thermal stabilities. Table 3.96 lists several cyanate esters with their initial decomposing temperatures measured by TGA. Apart from Arocy F at 431 °C the other esters range from 400 to 410 °C. They provide a much higher thermal decomposition temperature compared with epoxy resins, and these are also significantly higher than those of BMI resins.

Table 3.96 CE resins and their TGA initial decomposition temperatures

Arocy					Xu-71787	AG-80/DDS	BMI-MDA
B	M	T	F	L			
411	403	400	431	408	405	306	369

Fig. 3.54 Several commercial cyanate ester resins and their water absorption curves

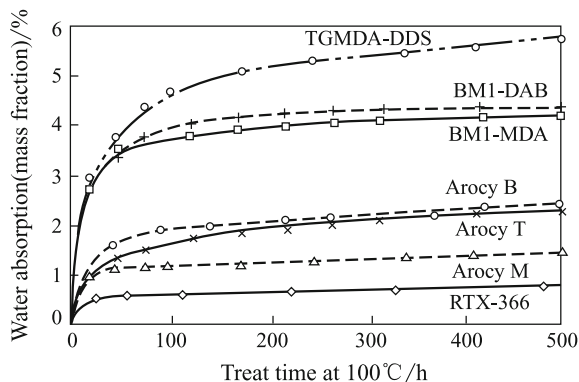


Figure 3.54 lists several commercial cyanate ester resins and their water absorption curves [97]. In the Arocy series, because of *o*-methylation, Arocy M can provide far better thermal resistance and hydrolysis resistance than Arocy B and Arocy T. Its water absorption curves are similar to those of Xu-71787, and its equilibrium water absorption is lower than that of Arocy B and T. Arocy M shows no hydrolysis upon treatment at 150 °C in steam for 100 h, while Arocy B undergoes hydrolysis very quickly at 150 °C by steam, as shown in Fig. 3.55 [81].

Table 3.97 lists various cyanate esters and their flame performance as well as chemical resistance [97, 100]. Arocy T-containing ether-linked phenyl rings and Arocy F-containing fluorine atoms offer very good fire-retardant performance. Arocy is basically non-burning, and REX-371 can give a high limit oxygen index (LOI) of up to 45%, indicating that it is also a non-burning resin. Other cyanate esters offer different burning performance, and Xu-71787 has very poor fire-retardant performance.

Arocy T's chemical resistance is obviously superior to that of other cyanate ester resins. REX-371 maintains the excellent ablating resistance of phenolic resins, and its residual carbon rate is high at 58% at less than 800 °C under oxygen conditions.

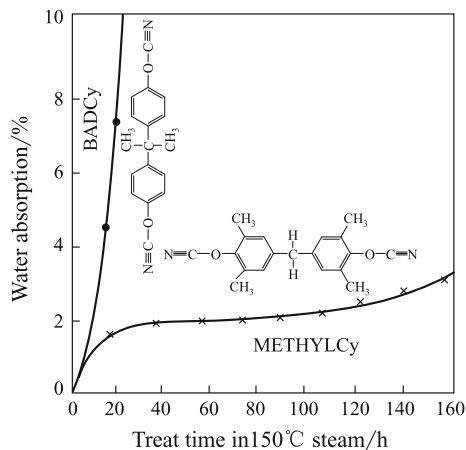
Table 3.97 Several CE homopolymers and their fire-retardant property and chemical resistance

Performance	Arocy					Xu-71787	REX-371
	B	M	T	F	L		
Burning behavior ^①							
First spot burning	33	20	1	0	1	>50	LOI:
Second spot burning	23	14	3	0	>50	–	45%
Residual carbon rate/%	41	48	46	52	43	32	58 ^②
Chemical resistance (MeCl ₂ , 3 h, R.T.)	5.8	4.9	0.8	–	–	–	–

① UI-94 standard

② 800 °C with oxygen

Fig. 3.55 The effect of O-methylizing on steam resistance



(2) Cyanate ester electrical performance

In curing processes, cyanate ester resins will undergo cyclization reactions and generate triazine ring network structures, which can cause the entire molecule to form an integrated system. This kind of structure can make cyanate esters susceptible to electric-magnetic fields, and they thus have a very low D_f and a very stable dielectric constant. Upon a change in frequency, this molecular structure will not be sensitive to polar relaxation. Therefore, cyanate esters offer a wide band (8–100 GHz) service. Figure 3.56 shows the correlation between thermosetting resin dielectric constants and testing frequencies [98]. Additionally, cyanate esters show very small dielectric performance changes over a very wide temperature range [–160 °C to its ($T_g - 50$ °C)], for example, Arocy B resin castings can give $D_f = 0.005$ and dielectric constant $D_k = 2.74$ at ambient temperature. At 232 °C, the dielectric constant is unchanged and D_f is only 0.009. Because of their different structures, cyanate ester-cured resins will give very different dielectric performance. RTX-366 and Arocy F have the lowest dielectric constants, while Arocy M and Xu-71787 have the smallest D_f as

Fig. 3.56 Correlation between resin matrix dielectric constants and testing frequencies

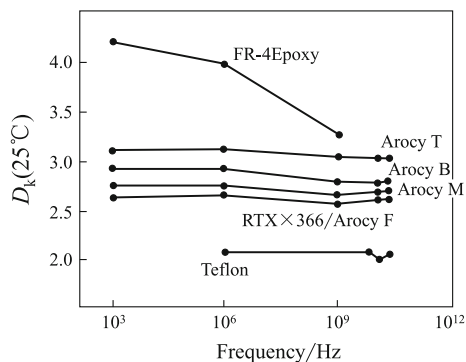


Table 3.98 Dielectric performance of various resins

Dielectric performance	Arocy					Xu-71787	RTX-366	Ag80/DDS	BMI-MDA
	B	M	T	F	L				
D_k	2.9	2.75	3.11	2.66	2.98	2.8	2.64	4.1	3.5
$D_f/10^{-3}$	5	2	3	3	—	2	—	—	—

Note D_k —Dielectric constant; D_f —dielectric loss factor

indicated in Table 3.98. Water absorption can also influence the resin castings dielectric performance [97].

(3) Cyanate ester mechanical performance

Cyanate ester resins also offer good mechanical performance because the large amount of ether linkages between the phenyl rings and the triazine rings can result in cyanate ester resins having very good impact resistance. Theoretically, this is because the C–O–C ether bond is a freely rotating α bond with a long bond length. This allows C–O–C to rotate more easily. Table 3.99 lists some thermosetting resins and their mechanical properties. From the data in Table 3.99, cyanate esters show very good toughness, as indicated by their bending strains, impact strength and tensile strains, or by G_{IC} . The Arocy series of cyanate ester resins can provide 2–3 times the bending strain and impact strength G_{IC} compared with AG80/DDS and BMI-MDA. Xu-71787 has a far lower impact resistance ability than the Arocy series, and this may be because of the half-ladder rigid ester ring in Xu-71787. Because of the difference in structure, the Arocy series will have different mechanical performance, especially Arocy L because its bending strain, tensile fracture elongation, impact strength and G_{IC} are much higher than those of the other Arocy resins.

(4) Modified cyanate ester performances

Although cyanate ester resins can provide good impact resistance, their toughness does not satisfy the requirements of aerospace high-performance structural materials. The main methods that can be used for cyanate ester toughening and improvement include:

- ① Copolymerize with single functional degree cyanate esters to reduce the cross-linking density of the networks.
- ② Blend with rubber elastomers.
- ③ Blend with thermoplastic resins to form half-interpenetrating networks (HIPN).

The common toughening methods are similar to those used for the rubber toughening of other thermosetting resins, which will be not discussed in this section. One type of new rubber-toughened cyanate ester resin system is Xu-71787.02L, which is toughened by core-shell rubber grains. Core-shell toughening will not affect the thermal resistance of cyanate ester resins, and it only has a small influence on rheological properties. A small amount of core-shell rubber can give significant toughening efficiency. Table 3.100 lists Xu-71787.02L resin performance after toughening by core-shell rubbers.

Table 3.99 Mechanical performance of various resins [97, 98]

Performance	Arocy						Xu-71787	RTX-366	AG80/DDS	BMI-MDA
	B	M	T	F	L					
Bending strength/MPa	173.6	160.5	133.7	122.6	161.9		121	95.6	75.1	
Bending modulus/GPa	3.1	2.89	2.96	3.31	2.89		2.82	3.79	3.45	
Bending strain/%	7.7	6.6	5.4	4.6	8		5.1	2.5	2.2	
Izod impact strength/J·m ⁻¹	37.3	43.7	43.7	37.3	48		—	21.3	16	
G_{IC} /J·m ⁻²	138.9	173.6	156.3	38.91	191		60.8	69.4	69.4	
Tensile strength/MPa	88.2	73	78.5	74.4	86.8		—	—	—	
Tensile modulus/GPa	3.17	2.96	2.76	3.1	2.89		—	—	—	
Fracture elongation/%	3.2	2.5	3.6	2.8	3.8		—	—	—	

Table 3.100 Core-shell rubber/Xu-71787 blended system and its performance

Standard	Performance			
Rubber content/%	0	2.5	5.0	10.0
Glass transition temp./°C	250	253	254	254
Water absorption/%	0.7	0.76	0.95	0.93
Bending strength/MPa	121	117	112	101
Bending modulus/GPa	3.3	3.1	2.7	2.4
Bending strain/%	4.0	5.0	6.2	7.5
$k_{IC}/\text{MPa}\cdot\text{m}^{1/2}$	0.522	0.837	1.107	1.118
$G_{IC}/\text{J}\cdot\text{m}^{-2}$	0.07	0.20	0.32	0.63

Note 1. Cure cycle: 175 °C × 1 h + 225 °C × 2 h + 250 °C × 1 h

2. Wet condition: in boiling water for 48 h

Similar to the modification of other thermosetting resins to improve their impact resistance, some amorphous or half-crystallized thermoplastic resins with glass transition temperatures (T_g) from 170 to 300 °C can be used to modify cyanate ester resins [97, 101]. These include PEI, PS, PES, PEK-C and PI. These thermoplastic resins can dissolve in cyanate ester monomers but can undergo phase separation during the curing processes. Research has indicated that at a content of more than 15%, the phase-separated thermoplastic resins will be in continuous phases, which allows the cured resins to form half-interpenetrated network structures. Figure 3.57 shows G_{IC} curves obtained by testing the cyanate ester resins modified by thermoplastic resins of different content. Table 3.101 lists the performance of Arocy B/thermoplastic resins (1:1). From the figure and table, it is obvious that thermoplastic resins with a high T_g can greatly increase the cyanate ester resin's toughness. If thermoplastic resins terminated with activation end groups (hydroxyl and amine) were used to modify these cyanate esters, the interface between the thermoplastic resin and the cyanate ester can be further improved. Additionally, solvent resistance can also be increased; for example, PES with activated end hydroxyls used to

Fig. 3.57 Effect of TP content on Arocy B cast resin toughness

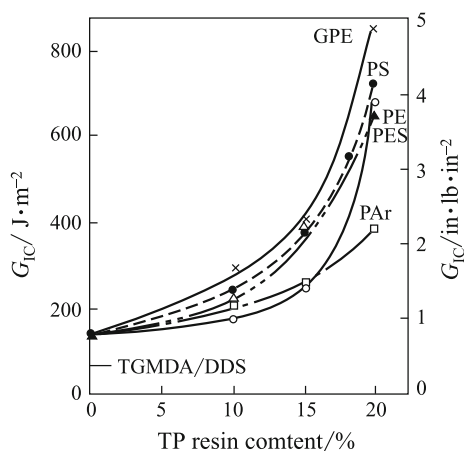


Table 3.101 Arocy B/thermoplastic resin (1:1) and its performance

Material	Strain/%	Tensile strength/MPa	Tensile modulus/GPa	$T_g/^\circ\text{C}$
Arocy B/PC	17.3	84.8	2.06	195
Arocy B/PSF	12.7	72.4	2.05	185
Arocy B/PES	9.6	71.7	2.34	–

modify the Arocy L-10 resin can increase its dichloride methane resistance and this is far superior to the PES with cyanotic end groups. Its bending strain can also be increased from 69 to 10.1%.

(5) Cured cyanate ester resin thermal stability

Although cured cyanate esters offer extraordinary physical and thermal resistance, each kind of material will have a limited service life under a specific service environment. Materials are usually exposed to air, water, heat and other chemical environments. Therefore, to increase their performances and extend their service ability it is very important to understand the material's behavior under varied environments. In general, cured cyanate ester resins have initial thermal decomposition temperatures above 400 °C, and glass transition temperatures above 250 °C, but they will slowly undergo hydrolytic reactions under hot/wet conditions and catalysis [81].

Using gas chromatography (GC) and mass spectroscopy (MS), the thermal decomposition of the cyanate ester model triphenoxyazine compound was carried out and it was found that the main decomposition materials were CO₂ and phenols. However, at temperatures higher than 400 °C some phenyl, cyanuric acids, phenyl cyanate, water, hydrogen and a small quantity of phenyl amine and HCN were obtained. At high-temperature and under hot/wet conditions, the CO₂ and phenols formation rate increases quickly. During degradation, the cured cyanate ester will be subjected to water and the ether linkages will hydrolyze to generate phenyl. The phenyl can undergo further hot/wet decomposition to give CO₂ and amines. Based on the decomposed products, two degradation models, homolytic and heterolytic decomposition, were proposed [80].

If a certain phenol is added to the model cyanate ester compounds, the CO₂ generation rate can increase at either 400 °C or under hot/wet conditions. This shows that the phenol generated during hydrolysis will take part in the cyanate ester decomposition reaction. In hot/wet decomposition studies, the phenol generation rate increased as the temperature increased, but this decomposition rate reached a maximum value at 450 °C. This also further indicated that phenol plays an important role in cyanate ester thermal degradation. As discussed before, when cured at a high temperature (250 °C), the HDT of cured resins will reach a maximum value as the phenol content in the catalyst is increased to 2%. The HDT decreases as the phenol content increases, and this may be because the phenol participates in cyanate ester degradation during the early stages. In cyanate ester hot/wet degradation, the uncured –OCN functional groups will possibly be the reason for cyanate ester degradation during the early stages. In summary, the thermal decomposition mechanism of the cyanate ester is as follows [80, 102, 103]:

Fig. 3.58 Dielectric constant changes of quartz fiber/CE composites with various frequencies. 1—Epoxy resin; 2—BMI resin; 3—CE resin

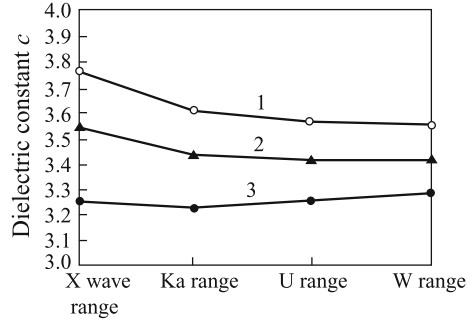


Fig. 3.59 Dielectric loss tangent changes of quartz fiber/CE composites with various frequencies. 1—Epoxy resin; 2—BMI resin; 3—CE resin

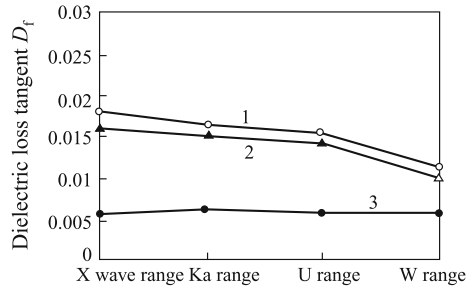
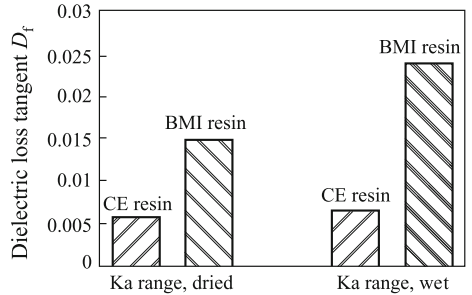


Fig. 3.60 Effect of water absorption on the CE and BMI CE composite dielectric loss tangents



content in cyanate esters, BMI-MDA and FR4 epoxy composites reinforced by E-glass fibers. All the composites have lower D_k values, which decrease in a linear manner as resin content increases. Table 3.102 lists several composites with their electrical performance, and this shows that the dielectric loss tangents are independent of resin content [97].

Cyanate ester resin composites can possess remarkable impact damage resistance and hot/wet resistance. Table 3.103 shows a comparison between BMI, cyanate ester and epoxy resin matrix composite performances. From this table, the CAI value of the cyanate ester resin matrix composite can reach 236–276 MPa. Cyanate ester resin composites have a hot/wet resistance that is superior to epoxy and BMI.

Fig. 3.61 Correlation between dielectric constants and resin content in CE/E glass fiber composites

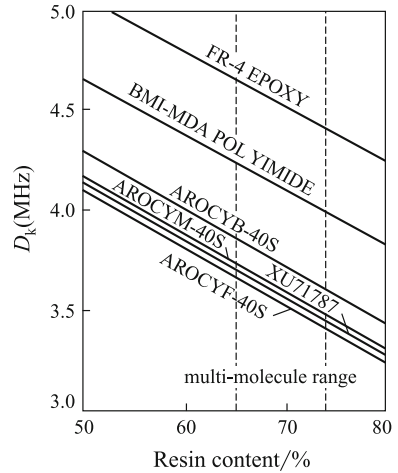


Table 3.102 CE/E glass fiber composites and their dielectric performance

Resins		ArocyF-40s	ArocyM-40s	ArocyB-40s	Xu-71787	BMI-MDA	FR-4
D_k (1 MHz)	70% ^①	3.5	3.6	3.7	3.6	4.1	4.9
	50%	3.9	4.0	4.1	4.0	4.5	4.9
$D_k/\times 10^{-3}$		2	2	3	3	9	20

① Resin volume content

Table 3.103 Comparison between CE and epoxy resin composite performance

Properties	BMI	CE	Epoxy
Cure temperature/°C	180–200	177	177
Post-treating Temperature/°C	240	204	–
Cure time/h	16–24	3–4	3–4
T_g (dried)/°C	2.93	1.56	4.13
T_g (wet)/°C	300	250–290	≤ 250
Reduction rate/%	200	214	–
Shear strength difference between dried/wet	33	9	–
20 °C	Water absorbed < 0.6%	Water absorbed < 0.6%	No effect
100 °C	Much decreased	Some changed	Linear decreased
CAI/MPa	214 ^①	236–276	–
Service temperature/°C	<250	<177	<177

① BMI composite impact strength 4.45 kJ/m. CE composite 6.67 kJ/m. Figure 3.62 shows the core-shell rubber-toughened Xu-71787/AS4 composite’s toughness. The core-shell rubber grain can significantly increase the composite’s toughness without decreasing its thermal resistance, and the rubber grain content was optimized to 5% [105]. Figure 3.63 shows several cyanate ester resin matrix composites and their short beam shear strength (SBSS) changes with temperature [97]

Fig. 3.62 Xu71787/AS4 composite toughness

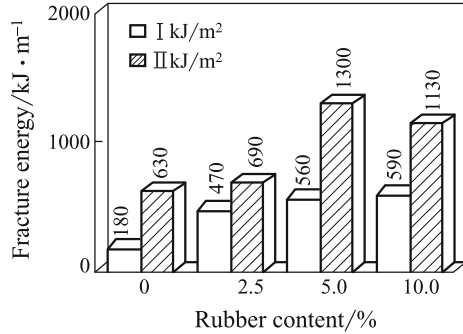


Fig. 3.63 CE composite short beam shear strength (SBSS) changes with temperature

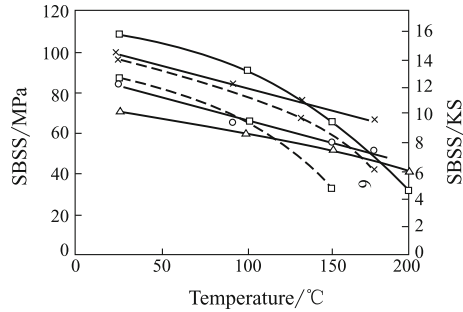


Table 3.104 lists several cyanate ester resin matrix composites with their performance, as developed by Hexcel. Tables 3.105 and 3.106, respectively, show the X54-2/IM7 composite’s basic mechanical properties and hot/wet properties [106]. Table 3.107 shows the Arocy B/quartz composite mechanical performance. Cyanate ester resin matrixes have good hot/wet resistance and fracture toughness, and therefore, their composites also have good mechanical performance. Table 3.108 shows the hot/wet mechanical properties of the 5228/T300 composite. The data indicate that the 5228/T300 composite has good hot/wet resistance and that the long-term service temperature under hot/wet conditions could be 150 °C [107].

(2) **Cyanate ester resin matrix composite applications**

Cyanate ester resin matrix composites have remarkable performance and wide applications in high-speed and high-frequency printing digital circuits, high-performance wave transparent materials and aerospace structural materials. Cyanate ester resin matrix composites can offer good electrical and mechanical performance and can be used in high-performance radar antenna domes and in smart structure skins. Because of their wide band features and low and stable dielectric constant and loss tangent, they are used in stealth vehicles. Cyanate ester resins are also widely applied in modern electronic communications. Table 3.109 lists some commercial cyanate ester resins with their basic performances and applications.

Table 3.104 CE composite performance of Hexcel resins

Properties		Composites		
		561-66/IM7	HX1553/IM7	HX1562/IM7
Tensile strength/MPa		2618	2753	2606
Bending strength/MPa	R.T.	1529	1662	1571
	135 °C	–	1076	1035
	149 °C	1118	866	923
	204 °C	961	–	–
	R.T. (wet) ^①	1369 ^①	1544	1521
	135 °C (wet)	–	631	779
	177 °C (wet)	847 ^②	–	–
Shear strength/MPa	R.T.	98.7	106.4	106.4
	135 °C	–	63.4	66.8
	149 °C	72.8	61.4	67.9
	204 °C	55	–	–
	R.T. (wet) ^①	88.9 ^②	99.5	94.3
	135 °C (wet)	–	54.6	54.9
	177 °C (wet)	45.6 ^②	–	–
Compression strength/MPa	R.T.	1806	1660	1800
	135 °C	–	1268	1241
	147 °C	–	1021	1003
	R.T. (wet) ^①	–	1674	1638
	135 °C (wet)	–	935	866

① Wet condition: 71 °C, 95% R.H. for 14d; ② wet condition: in boiling water for 96 h
Note Composite fiber volume content: 60%

3.7 Thermosetting Polyimide Resin Matrixes

The thermally stable resin matrix composites made using thermosetting polyimide resins as matrixes can be used as load-bearing structural components under high-temperature conditions to satisfy the requirements of aerospace and electronic industrial applications. Over the last 30 years, this kind of high-temperature resin matrix composite has undergone rapid development. Their thermal–oxidation stability, processing techniques and combined mechanical properties have advanced significantly.

Based on their activated terminal radical groups, thermosetting polyimides can be divided into three main types: PMR polyimide (mainly Nadic anhydride-terminated polyimide), acetylene-terminated polyimide and bismaleimide (BMI). Since BMI will be discussed in a separate chapter, PMR and acetylene-terminated polyimide will be introduced in this chapter.

Table 3.105 X54-2/IM7 composite's mechanical performance

Properties	Temperature/°C			
	R.T.	121	149	177
Longitudinal tensile strength/MPa	2811			
Longitudinal tensile modulus/GPa	161			
Longitudinal compression strength/MPa	1571	1288	1337	
SBSS/MPa	98.5	73	66	49.6
Interlaminar shear strength/MPa	116.4			
Interlaminar shear modulus/GPa	4.68			
L/T bending strength/MPa	1694	1282	1123	1061
L/T bending modulus/GPa	140	137	124	128
Open-hole tensile strength ^① /MPa	428			
Open-hole compression strength ^② /MPa	291			
Open-hole compression strength ^③ /MPa	397			
CAI/MPa	258.5			

① Laminating code: [+45/0/-45/90]s

② Laminating code: [+45/0/-45/90]2s

③ Laminating code: [$\pm 45/0/0/90/0/0 \pm 45$]s

Table 3.106 X54-2/IM7 composite hot/wet performance

Properties	Temperature/°C			
	121	149	163	177
L compression strength ^① /MPa	1330	1288		
SBSS/MPa ^①	60.6	51		42
Interlaminar shear strength ^② /MPa	77	66	55.8	
Interlaminar shear modulus/GPa	3.51	2.55	2.41	
L bending strength ^① /MPa	1116	930		686
L bending modulus ^① /GPa	128.8	126		122.6
Open-hole compression strength ^③ /MPa	241.8	230		
Open-hole compression strength ^④ /MPa	323.8	321		

① 71 °C immersed for 3d

② Equilibrated under 65.5 °C and 85% R.H.

③ 71 °C immersion for 14d

④ The laminating code is the same as in ② and ③ in Table 3.105

Table 3.107 Arcoy B/quartz fiber composite mechanical performance

Tensile S/MPa	Tensile M/GPa	Compression S/MPa	Compression M/GPa	Bending S/MPa	Bending M/GPa	Shear S/MPa
696	26.2	524	23.4	793	26.9	81

Table 3.108 5228/T300 composite hot/wet performance

Testing condition ^②		R.T. (Dried)	130 °C (Dried)	130 °C (Wet)	150 °C (Dried)	150 °C (Wet)
Bending	Strength/MPa	1680	1390	1200	1310	1082
	Retention rate/%	100	82.74	71.4	77.8	64.4
Interlaminar shear	Strength/MPa	104	69.6	61.4	61.4	51.5
	Retention rate/%	100	66.92	59.04	59.04	49.5
Compression ^①	Strength/MPa	659.5	556.4	497.6	–	–
	Retention rate/%	100	84.4	75.4	–	–

① Lamination code: [+45/0/–45/90]4s

② Hot/wet condition: in boiling water for 48 h

3.7.1 PMR Polyimide

In 1972, PMR technology (in situ polymerization of monomeric reactants) was developed at the Lewis center, NASA in the USA and used to manufacture high-temperature polyimide composites [108].

The features of the PMR technique include:

- (1) Using low relative molar mass and low-viscosity monomers;
- (2) Using low boiling point solvents;
- (3) Since imidization is complete before curing cross-linking, no or little volatile substances are released in the end cure stages [109].

In the PMR techniques, the composite preparation procedures usually include the following steps: first, the dissolution of the terminating radicals/aromatic biamine/aromatic dianhydride derivatives in low boiling point solvents at a specific ratio to obtain a PMR polyimide solution and then preparation of prepregs using a wet process. Heat is applied to advance the imide reaction and to give PMR polyimide prepolymers. Finally, heat is applied for cross-linking and curing to obtain the composites (Fig. 3.64). Carbon fiber-reinforced PMR polyimide composites have been widely used in aerospace applications.

The commonly used monomers in the synthesis of PMR polyimide are aromatic biamines, aromatic dianhydrides and Nadic anhydride. In Fig. 3.65, the synthesis of PMR polyimide prepolymers is given. Different mol ratios of the three monomers will affect the relative molecular masses of the intermediate amide acid and polyimide prepolymers. Since the imidization temperature in Nadic anhydride-terminated amide acid is much lower than its cross-linking and curing temperature, the imidization can be fully completed before curing and, therefore, no

Table 3.109 Commercial cyanate ester resins with their performances and applications

Supplier/resin system	Untoughened Toughening agent	Cure temp./service temp/°C	$T_g/^\circ\text{C}$	Water absorption/%	D_f	Dielectric constant	Application
Rhone-Poulenc (resin)							
B-10	U	177/177	290	2.5	0.003	2.9	High-speed electric circuits, airplane structures, radar domes and antennae
M-10	(TP or epoxy resin)	177/177	270	1.3	0.003	2.75	
F-10		177/177	290	1.3	0.003	2.66	
L-10 (liquid)		177/177	260	2.4		2.98	
RTX-366 (liquid)		121/121	192	0.6		2.6–2.8	
Dow-Plastics (resin)							
Xu71787.02	U	177/177	252	1.2	0.002	2.8	Radar domes and antennae, space structures
Xu71787.07	Rubber	177/177	265	1.2	0.002	2.9	
Xu71787.09L	TP	177/177	220–250	0.6	0.002	3.1	
ICI Fiberite (pregreg)							
954-1	TP	177/177	266	0.4			Radar domes and antennae, aerospace structures
954-2	TP	177/177	240	0.5			
954-3	TP	177/177	258	0.4			
BASF (pregreg)							
5445C		177/177	216				Load-bearing structures, radar antennae
5575-2	TP	177/177	232	1.0	0.005	3.25	

(continued)

Table 3.109 (continued)

Supplier/resin system	Untoughened Toughening agent	Cure temp./service temp/°C	T_g^p °C	Water absorption/%	D_f	Dielectric constant	Application
X6555 Syntactic core		177/177	250		0.005	1.8	Radar domes and antennae, space structures
X6555-1 Syntactic core		177/177	250		0.005	1.6	
Amico (prepreg)							
ERL-1939-3	TP	177/177	240	1.6	0.004	3.04	
ERL-1999	U	177/177	201	0.99			
Hexcel (prepreg)							
HX1566	U	177/177	240	0.5	0.005	2.74	Military jets, antennae and space structures, low-temperature service
HX1553	TP	177/177	180	0.8			
HX-1584-3	U	177/177	210	0.3	0.004	2.74	
YLA Lnc. (prepreg)							
RS-3							Satellite structures, radar domes
RS-12 (120 °C curing)	U	177/177	254	1.45	0.005	2.6	
Bryte Techn. (prepreg)							
BTCY-1	U	177/177	270	1.0	0.003	2.7-2.8	High-temperature Radar domes/antennae, Super low loss radar domes, space applications
BTCY-2	U	177/177	190	0.6	0.004	2.6	
BTCY-3	U	121/163	166	0.6	0.004	2.7	
EX1515 (toughened)		121/135					
EX1505	U	177/260	330		0.007	2.8	

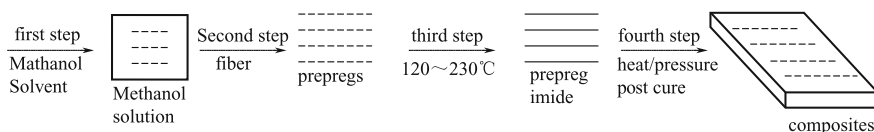


Fig. 3.64 Schematic showing PMR polyimide composite preparation processes

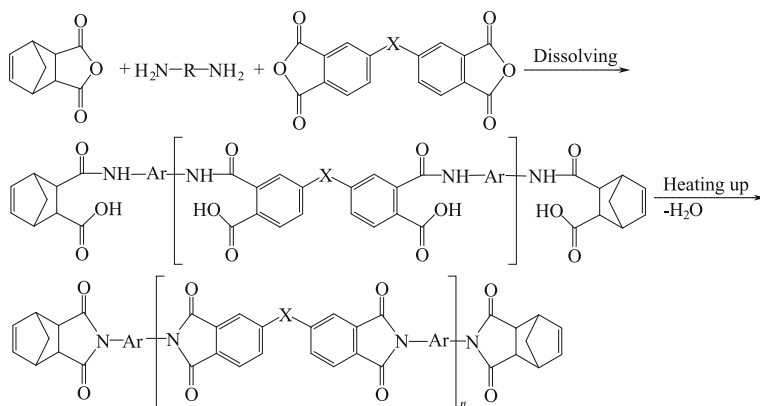


Fig. 3.65 Synthesis of PMR polyimide prepolymers

volatiles are produced in the end curing stages. Low-void-containing composites are thus prepared.

(1) Synthesis of the PMR-15 polyimide

PMR-15 is the most commonly used polyimide, and it is prepared using Nadic acid methyl ester (NE), 4,4'-bimethyl diphenyl amine (MDA) and 3,3',4,4'-bisphenyl ketone tetraanhydride dimethyl ester (BTDE) as monomers. When the mol ratio of the reaction monomers is NE:MDA:BTDE = 2.000: 3.078:2.087, the relative molar mass of the generated prepolymers will be 1500. Changing the monomer mol ratio can give different PMR polyimide pre-0072 polymers with different relative molar masses, as shown in Fig. 3.66[110].

3.7.1.1 Synthesis of PMR Polyimide

In common applications, BTDE solutions can be prepared by dissolving BTDE in methanol and then heating and circulating for several hours. Other monomers are then added to the prepared BTDE solution to obtain the PMR polyimide resin solution. If the BTDE/methanol solution is heated and circulated for an excessive amount of time or the BTDE solution is stored for too long, it is possible that tri-methanol or

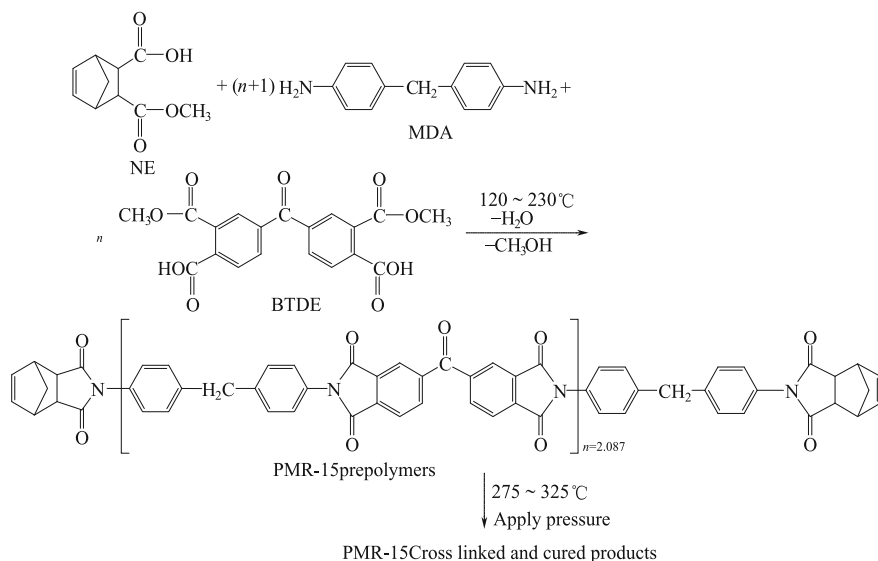


Fig. 3.66 Synthesis of the PMR-15 cured polyimide resin

tetra-methanol will be formed resulting in chain propagation. This will restrict the curing process, and the relative molar mass of the prepolymers will decrease.

It was believed that the reaction between diamine and aromatic biester-biacid was a directly substitution of the ester for the amine to form an imide acid and finally imide linkages (Fig. 3.67) [111]. High ester (tri-ester, tetra-ester) inhibition on imidization will apparently result in a change in reaction mechanism, as shown in Fig. 3.68. In a simulated reaction between phthalic acid methyl ester and phenol amine at 80 °C, methanol will be released very quickly, indicating that a direct fast substitution reaction between them occurred. However, no methanol will be released during the interaction between isophthalic acid methyl ester and phenol amine under the same reaction conditions. Therefore, the direct substitution reaction mechanism will not be applicable to the fast reaction between BTDE and MDA. Upon heating BTDE, any existing anhydride can be observed. At lower

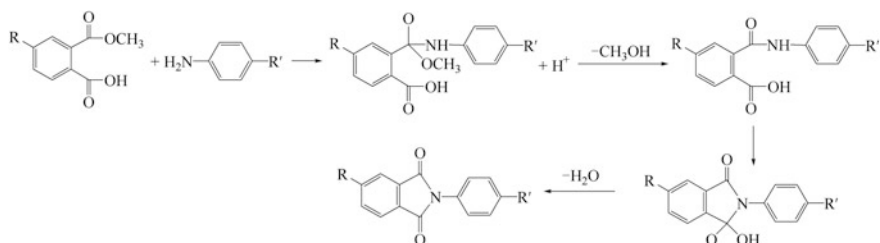


Fig. 3.67 The reaction mechanism of the biester-diacid formation of polyimide (1)

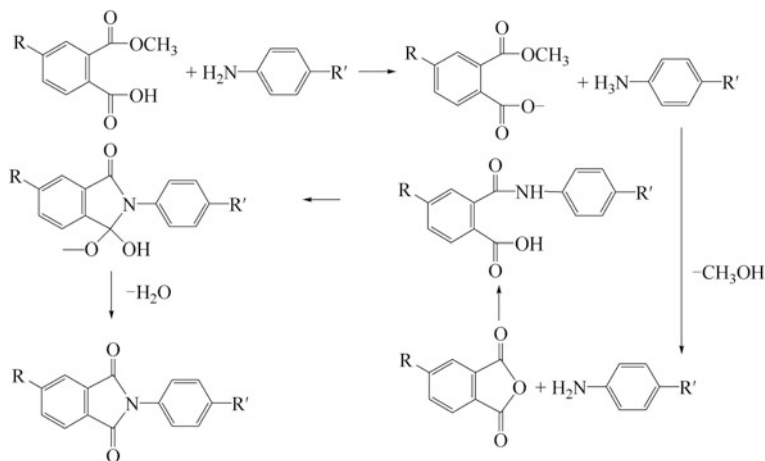


Fig. 3.68 The reaction mechanism of the biester-diacid formation of polyimide (2)

temperatures, the reversible ester acid to anhydride reaction will result in a corresponding quick amide acid formation, and then the corresponding imide prepolymers will be produced upon further imidization [112].

A study into the curing reaction of the PMR-15 polyimide at different temperatures indicated that imidization may take place in two steps. In the first step, the reaction will occur very quickly, while the slower second step reaction is a first-order reaction with an activation energy of 100 kJ/mol.

The imidization rate can be expressed as follows:

$$k = 1.4 \times 10^7 \exp[(-100\text{kJ/mol})/RT] \text{s}^{-1}$$

The reaction mechanism for the PMR-15 polyimide is very complicated and consists of several possible curing reaction processes. When the temperature is higher than 175 °C, imine formation is dominant, while at lower temperatures equal amounts of imide and imine are formed. At 175–275 °C, anhydride is obviously formed. Isothermal kinetic studies carried out by DSC at higher than 275 °C have shown that the PMR-15 polyimide curing reaction can be expressed as a first-order reaction:

$$k = 4.24 \times 10^3 \exp[(-84\text{kJ/mol})/RT] \text{s}^{-1}$$

This indicates that the control processes in the PMR-15 polyimide curing reaction are a reversible first-order reaction of norbornylene end groups. Since changes will take place in the constituents at different temperatures, the performance of PMR-15 polyimide will also change under different curing conditions. Therefore, to achieve superior performance, the curing processing parameters need to be carefully controlled.

(2) Synthesis of high-temperature (370 °C) PMR polyimide

PMR-15 polyimide has a good processing ability and combined mechanical performance. It has been widely applied as a composite matrix. Its main drawback is its high curing cross-linking temperature and its long-term service temperature is lower than 316 °C, which does not meet long-term service requirements at higher temperature. To further increase the thermal-oxidation stability of PMR polyimide use can be made of 4,4'-hexafluoro-trimethylene di-*o*-phenyl dimethyl ester (6FDE) as a high thermal resistance monomer to replace BTDE in PMR-15 polyimide, or *p*-phenyl diamine (*p*-PDA) and 3,4'-diamine phenylate (3,4'-ODA) can be used to replace MDA. The use of *p*-amine phenyl to replace NE gives a second-generation PMR polyimide resin with much higher thermal resistance, and these resins been developed and commercialized [113]. Second-generation PMR polyimide resins mainly include PMR-II [114], V-CAP [115], AFR-700 [116] and LaRC-RP-46 [117] [114–117]. In Figs. 3.69, 3.70, 3.71 and 3.72, the reaction principles used for these resins are illustrated [118, 119]:

Another problem in the synthesis of PMR-15 polyimide is the use of carcinogenic MDA, which is a hazard to operation safety and human health. For the

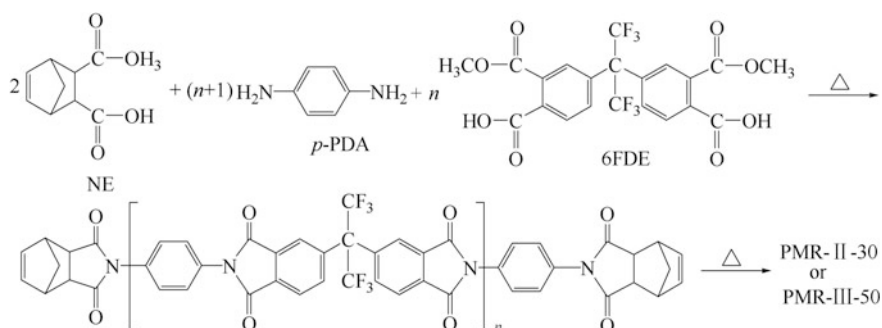


Fig. 3.69 Synthesis of PMR-II polyimide $n = 5$ resulting in PMR-II-30; $n = 8.9$ resulting in PMR-II-50

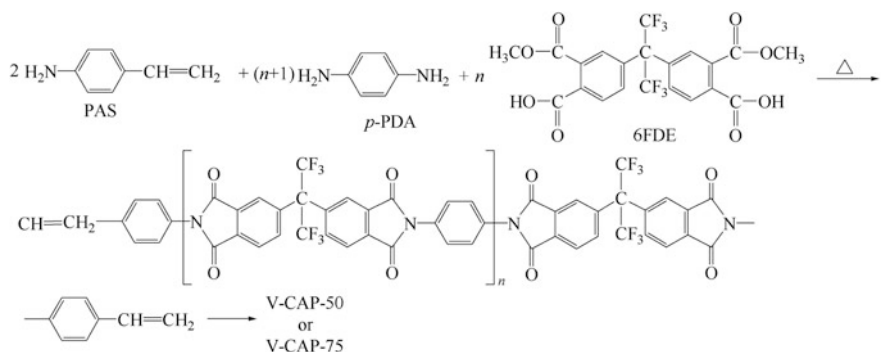


Fig. 3.70 Synthesis of V-CAP polyimide $n = 9$ resulting in V-CAP-50; $n = 14$ resulting in V-CAP-75

polyimides retain their superior processing ability and combined mechanical performance while their thermal-oxidation stability is equal to or slightly worse than that of PMR-15. In Figs. 3.73 and 3.74, the synthetic reaction principles of the LaRC-160 and LP-15 polyimide resins are shown [120].

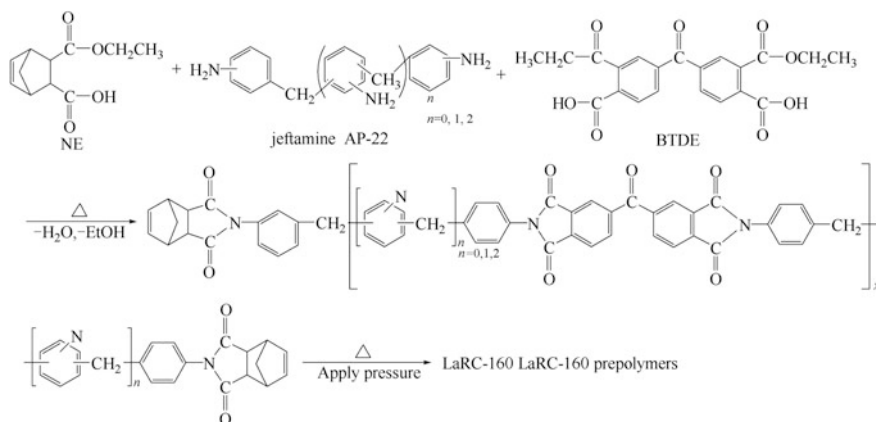


Fig. 3.73 Synthesis of the LaRC-160 polyimide

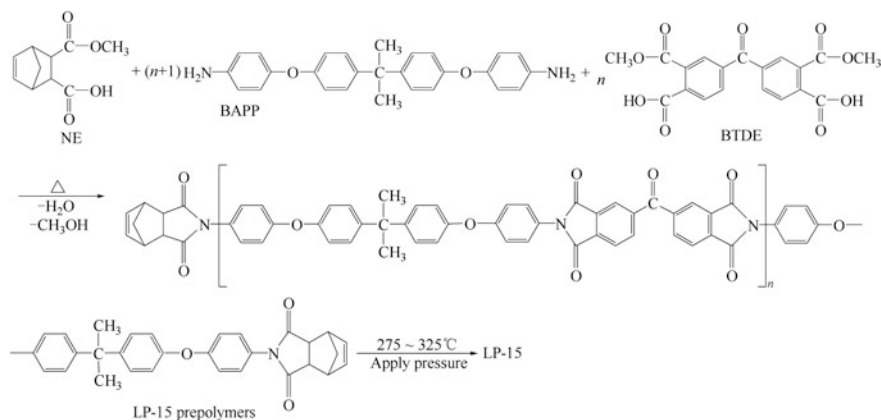


Fig. 3.74 Synthesis of the LP-15 polyimide

3.7.1.2 Performance of PMR Polyimide

(1) Thermal–oxidation stability of PMR polyimide

One of the principal applications of PMR polyimide is to manufacture high-temperature-resistant structural composites such as the cool end components in advanced aeronautical engines. Therefore, the thermal–oxidation stability is a very critical factor that will directly determine the operation temperature and time as well as application ranges.

Thermal aging in PMR polyimides includes physical aging and chemical aging. Physical aging will result in a change in the physical states of polymers such as an increase in density, a decrease in creep compliance and an increase in brittleness. In general, physical aging only has a little effect on polymer performance. In thermal aging, chemical aging that consists of cross-linkage and oxidation degradation will occur under high aging temperatures and this will significantly affect the polymer's physical properties. In Fig. 3.75, the T_g changes in the PMR-15/G30-500 composites caused by thermal aging under 316 and 343 °C are shown. In the early aging stages, the T_g of the composites increases quickly as the aging proceeds. This is because further cross-linking takes place in the polyimide matrix at temperature during the early aging stages. The cross-linking density in the resin matrix will subsequently increase resulting in an increase in the T_g of the composites. As aging continues, this cross-linking will gradually terminate and the T_g of the composites will become consistent [121].

The weight loss rates for the PMR-15 polyimides under different thermal aging temperatures are shown in Fig. 3.76. The weight loss rates for the PMR-15 polyimides are very low below 288 °C but increase at 343 °C. As aging continues, the weight loss rate decreases slightly and then remains unchanged. In Figs. 3.77 and 3.78, weight changes in the PMR-15 polyimide composites after different thermal aging times are shown. After aging for 1000 h at 316 °C, the weight loss for the PMR-15 polyimide composites is still less than 10%, but when aging for 200 h at 317 °C a weight loss of up to 20% was found. Therefore, the long-term service temperature of the PMR-15 polyimide composites is less than 316 °C [122].

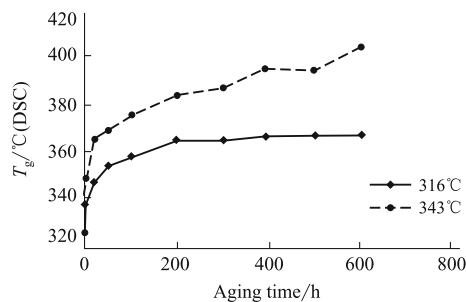


Fig. 3.75 Aging effect on the T_g of the PMR-15 composites

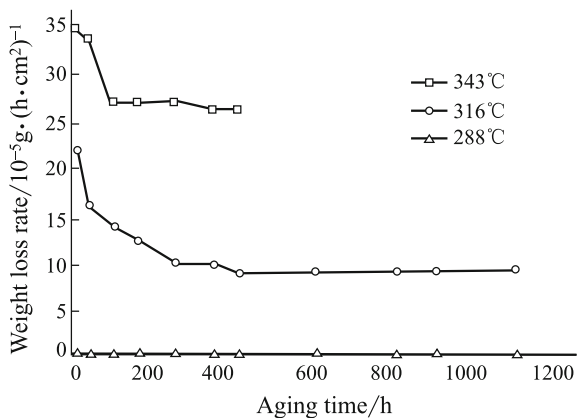


Fig. 3.76 Weight loss rates of PMR-15 resins at various temperatures

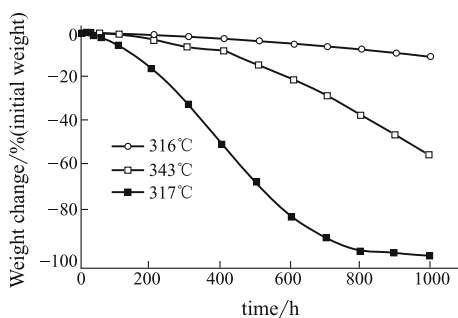


Fig. 3.77 Weight change for PMR-15/G30-500 composites at various temperatures

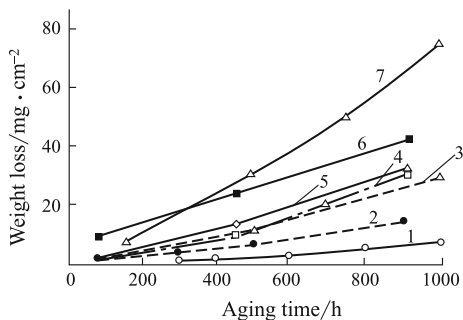


Fig. 3.78 Weight change for different PMR-15 composites at 316 °C aging. 1—Unsized Celion 6K fiber; 2—unsized T-40R fiber; 3—unsized (T-40R/Celion 6K) blend fiber; 4—sized Nextel 312 fiber; 5—unsized Nicalon fiber; 6—sized Nicalon fiber; 7—PMR-15 resin

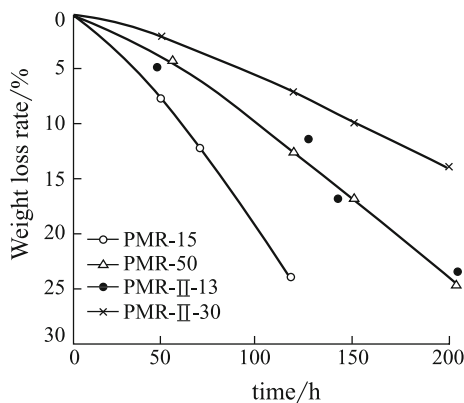


Fig. 3.79 Weight loss for different PMR resin/Celion 6K composites

The PMR-15 polyimide composites made using different reinforcing fibers will have different weight loss rates during the aging processes (Fig. 3.79). For Celion-6, PVA, T-40R, Nextel 312 and Nicalon, the composites reinforced by T-40R fibers will have minimum weight loss. There will not be a corresponding relationship in the thermal-oxidation stability of composites and reinforcing fibers. In fact, for PMR polyimide composites a resin matrix cladding on the fiber surface can be a protective layer and different interface structures will exist between the different fibers and the resin matrixes. Because of these different interface structures, composites with different thermal-oxidation stabilities will be produced.

Different PMR polyimide resins will have different thermal-oxidation stabilities. Second-generation high-temperature PMR resins such as PMR-II have thermal-oxidation stabilities that are superior to the PMR-15 polyimides.

For the same molecular structure PMR polyimides, the thermal weight rates will decrease as the molar mass of the prepolymers increases (Table 3.110).

This is because thermal degradation in the polyimides terminated by Nadic

Table 3.110 Effect of different prepolymer molecules on the thermal weight loss in polyimide resins

Resins	Weight loss rate after aging/%	
	371 °C, 300 h/0.1 MPa in air	371 °C, 75 h/0.4 MPa in air
PMR-15	18.0	18.2
PMR-30	12.0	14.0
	371 °C, 300 h/0.1 MPa in air	
	371 °C, 75 h/0.4 MPa in air	
PMR-II-13	13.0	12.3
PMR-II-50	5.5	5.0
	280 °C, 500 h/0.1 MPa in air	
	280 °C, 1000 h/0.4 MPa in air	
LP-15	11.0	22.0
LLP-30	9.0	16.0

anhydride will mainly occur at the terminating groups on the chain ends. Large prepolymer molecular mass polyimides will have a lower content of terminating groups, which are not easily exposed, and this will result in smaller thermal weight losses under the same aging conditions.

(2) Mechanical performance of PMR polyimides

Apart from their excellent thermal–oxidation stability, PMR polyimide composites also have good combined mechanical performances. Table 3.111 shows a comparison of the mechanical properties at room temperature between LP15, KH304 polyimide composites and high-performance epoxy composites. From this table, the room-temperature tensile and bending properties of the PMR composites are equivalent to that of epoxy composites, while the interlaminar shear strength of LP-15/AS₄ is slightly lower. This may be because the reinforcing fiber LP-15/AS₄ used in these composites had not undergone sizing treatment. The interface bonding between the fiber and the matrix is lower than that in the T300/epoxy composites resulting in lower interlaminar shear strength in the LP-15/AS₄ composites [120].

After curing, the PMR polyimides can form highly cross-linked thermosetting polymers with much better high-temperature mechanical performance than that of BMI and epoxy, as given in Table 3.112.

In this table, X5250-4 and DK-bis-BCB are a high-temperature BMI and polyphenol cyclobutylene resin system. At room temperature, the bending properties of the PMR-15 composites are similar to those of the BMI composites. However, the bending strength retention rate in the BMI composites is less than 50% at lower than 191 °C, while the bending strength retention rate for the PMR-15 composites is still higher than 50% at lower than 316 °C.

For the PMR composites, the different structures will give different mechanical performance retention rates. In Table 3.113, the bending properties and the interlaminar shear strength of the LP-15 and PMR-15 composites at different

Table 3.111 Mechanical properties of different composites at room temperature

Properties	LP-15/AS ₄	KH304/T300 ^①	5228/T300 ^②
0° bending strength/MPa	1950	1589	1780
0° bending modulus/GPa	134	116	130
0° tensile strength/MPa	1850	1605	1740
0° tensile modulus/GPa	140	137	135
90° tensile strength/MPa	45	41	40
90° tensile modulus/GPa	9.8	8.8	10.3
0° compression strength/MPa	980	1035	1230
0° compression modulus/GPa	138	112	110
ILIS/MPa	87	103	105
Poisson's ratio	0.32	0.294	0.28

① KH304—PMR-15 modeled by the Chemical Research Institute of China Academic

② 5228—high toughness and hot/wet resistance epoxy resin matrix developed at the Beijing Institute of Aero Materials

Table 3.112 Bending property comparison between the different composites

Properties		Composites		
		AS ₄₈ HS/DK-bis-BCB	IM7 5HS/X5250-4	Celion22 48HS/PMR-15
25 °C	Bending strength/MPa	1180	828	1076
	Bending modulus/GPa	58.5	67.6	57.2
191 ° C (wet)	Bending strength/MPa	814	393	–
	Bending modulus/GPa	54.5	41.7	–
316 °C	Bending strength/MPa	420	–	600
	Bending modulus/GPa	46.3	–	48.3

Table 3.113 Properties of the LP-15/AS₄ and PMR-15/AS₄ composites

Properties	Materials	Testing temp.			
		R.T.	260 °C	280 °C	300 °C
Bending strength/MPa	PMR-15/AS ₄	1850	1690	1200	930
	LP-15/AS ₄	1960	1670	1080	510
Bending modulus/GPa	PMR-15/AS ₄	118	119	115	104
	LP-15/AS ₄	136	132	117	82
Interlaminar shear strength/MPa	PMR-15/AS ₄	98	92	69	65
	LP-15/AS ₄	87	85	58	46

temperatures are listed. At lower than 260 °C or 280 °C, the bending properties and interlaminar shear strength of the LP-15 composites are similar to those of the PMR-15 composites, but at lower than 300 °C the bending properties and interlaminar shear strength of the LP-15 composites are lower than those of the PMR-15 composites. The difference between LP-15 and PMR-15 comes from the use of BAPP in LP-15 instead of MDA. The use of BAPP in the LP-15 polyimide can result in a large quantity of flexible ether bonds being attached to the resin main chain structures, and therefore, LP-15 polyimide has a lower T_g [123].

For the second-generation PMR polyimides with a much higher temperature resistance such as the V-CAP-75 and AFR-700B polyimide composites, the rigidity of the molecular structure is better since fluorine-containing monomers were used, and the T_g of these composites will also be higher. The property retention rate is high, even at temperatures up to 371 °C (Table 3.114).

Different prepolymer relative molecular masses can affect PMR polyimide cross-linking densities. A larger prepolymer relative molecular mass results in a lower cross-linking density. As the polyimide prepolymer relative molecular mass is increased, the T_g of the polyimide composites will decrease and their high-temperature mechanical performance will also decrease. In Table 3.115, the bending properties and shear strength of the LP series of PMR composites with different prepolymer relative molecular masses under different temperatures are compared. In this table, the prepolymer relative molecular masses of LP-15, LP-21 and LP-30 of 1500, 2100 and 3000, respectively, are given.

Table 3.114 Mechanical properties of the different PMR polyimide composites

Composites	Bending strength/MPa		Interlaminar shear strength/MPa			
	R.T.	361 °C	361 °C	R.T.	316 °C	371 °C
Celion 6K/PMR-15	1750	710	317	120	45	21.4
HT-SLaRC™-160 (3)	2130			96	–	–
T40-R/PMR-11-50 (11)	–		320	–	–	20
T40-R/V-CAP-50 (11)	–		190	–	–	20
QuaHZ-AFR-700B (12)	848		420	59	–	51.7
Celion 6K/LaRC™-RP46 (13)	1724	917	793	131	51	32.4

Thermal aging can have a significant effect on the performance of the PMR composites. In general, during the early aging stages the mechanical properties of the PMR polyimide composites will increase slightly as aging progresses. The mechanical properties will begin to decrease upon further progress (Figs. 3.80 and 3.81). The effect of the thermal aging process on composite mechanical properties will mainly be further cross-linking and thermal-oxidation degradation. Further cross-linking and curing will perfect the cross-linking network and increase the T_g of the composites, and this may lead to an increase in the composite's mechanical properties. Thermal-oxidation degradation can cause the composite matrix to decompose because of oxidation, weight loss, and damage to the resin/fiber interface structures, which results in a decrease in the composite's mechanical properties. The combined effects of further cross-linking together with thermal-oxidation degradation will cause PMR polyimide composite mechanical performance changes that would be slightly enhanced at first and then subsequently decrease.

Table 3.115 Effects of prepolymer relative molecular masses on composite mechanical properties

Properties	Materials	Testing temp.		
		R.T.	260 °C	280 °C
Bending strength/MPa	LP-15/AS ₄	1960	1670	1090
	LP-21/AS ₄	1900	1600	900
	LP-30/AS ₄	1890	1400	810
Bending modulus/GPa	LP-15/AS ₄	136	132	117
	LP-21/AS ₄	125	120	106
	LP-30/AS ₄	115	122	106
Interlaminar shear strength/MPa	LP-15/AS ₄	87	85	58
	LP-21/AS ₄	91	83	45
	LP-30/AS ₄	85	81	40

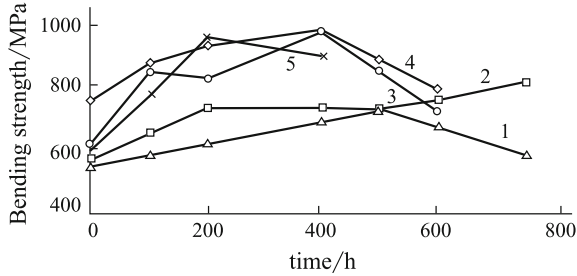


Fig. 3.80 Bending strength of the PMR composites after aging at 343 °C. 1—PMR-II-50/T-40R; 2—PMR-II-30/T-40R; 3—PMR-II-50/C-6; 4—PMR-II-30/C-6; 5—PMR-15/C-6

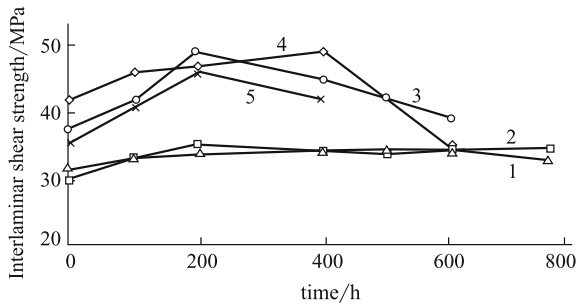


Fig. 3.81 Interlaminar shear strength of the PMR composites after aging at 343 °C. 1—PMR-II-50/T-40R; 2—PMR-II-30/T-40R; 3—PMR-II-50/C-6; 4—PMR-II-30/C-6; 5—PMR-15/C-6

3.7.1.3 Modification of PMR Polyimide

(1) Toughening of PMR polyimide

Despite their superior thermal-oxidation stability, good processing performance and combined mechanical properties, in general, PMR polyimides are brittle resins. For example, the G_{IC} of the PMR-15 composites is only 87 J/m^2 . Because of their low toughness, microcracks are easily produced in PMR-15 composites under thermal fatigue processes.

PMR polyimide can be toughened by a number of approaches. The most commonly used toughening methods include: thermoplastic polyimide blending toughening and the introduction of flexible chain segments to increase toughness. In thermosetting resin systems toughened by thermoplastic resins, an inhomogeneous phase system is usually generated. Fine thermoplastic grains can disperse into the thermosetting resin matrixes, and when cracks grow, the thermoplastic grains can produce “anchorage” to inhibit crack propagation and to increase the fracture toughness of the resin matrix. At NASA’s Langley Center, the thermoplastic polyimide powder Matrimid 5218 was used to toughen PMR-15 and LaRC-RP-46. The homogeneous and interpenetrating

network structural PMR-15/5218 and LaRC-RP-46/5218 resin systems were thus developed.

To prepare PMR-15 (LaRC-RP-46)/5218 polyimide prepregs, NASA Langley Center developed a wet powder coating prepreg preparation technique. Initially, the solution method was used to prepare PMR-15 (LaRC-RP-46)/IM7 [124] unidirectional prepreg tapes, and then, these tapes were guided to pass through a funnel in which the thermoplastic polyimide powder Matrimid 5218 was loaded. The 5218 powder was uniformly spread over the prepreg tapes. The thermoplastic resin content (mass fraction) was controlled to within 12% by adjusting the 5218 powder falling velocity. After most of solvents were evaporated, the prepregs were cut and laminated and then placed in an oven to carry out imidization treatment for 1 h at 200 °C. They were finally press molded and cured according to the PMR-15/5218 and LaRC-RP-46/5218 curing specifications, and PMR-15/5218 and LaRC-RP-46/5218 composites were produced.

No two-phase structures were found on the toughened composite fracture surface by scanning electronic microscopy (SEM), but some trenches, voids and crushed matrixes were present in the crack growing zones on the fracture surface. Even under high-power SEM observations, no phase separation between the thermosetting and thermoplastic polyimides was found. In a TMA, only a single transition peak was found for the PMR-15 (LaRC-RP-46)/5218 polyimide system. The specimen was placed in a solvent to dissolve Matrimid 5218 by extraction treatment for 48 h. No significant weight loss was found for either specimen. The above analysis infers that only a single-phase half-interpenetrated network structure exists in the PMR-15 (LaRC-RP-46)/5218-toughened polyimide resins.

In the PMR-15 (LaRC-RP-46) curing process, the resin matrix will subject to a series of reactions including amidation, imidization, cross-linking and curing. The resin viscosity will be at its lowest when the temperature is initially increased and it will increase as the resin's relative molecular mass increases upon reaction progression. Matrimid 5218 is a polymerized thermoplastic resin with a huge relative molar mass. Its melting viscosity is also much higher than that of PMR-15 and LaRC-RP-46. During processing, the low-viscosity PMR-15 and LaRC-RP-46 can disperse and penetrate the high-viscosity Matrimid 5218 thermoplastic resin zones. Since these two constituents show good compatibility, no phase separation will occur until cross-linking and curing are complete. A single-phase half-interpenetrated network structure geometry is thus formed.

The bending strength and modulus, and shear strength of the toughened PMR-15 (LaRC-RP-46)/5218 polyimide composites are lower than those of the untoughened composites, but its nut toughness is significantly higher, as given in Table 3.116.

To evaluate composite toughness, the compressing strength after impact (CAI) is commonly used. The specimen was initially subjected to impact at an

Table 3.116 Mechanical properties of toughened and untoughened polyimide composites

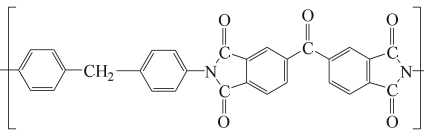
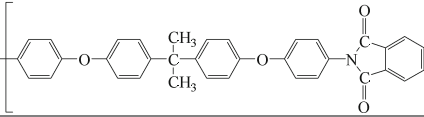
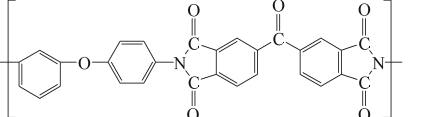
Properties	Composites			
	PMR-15/IM7	PMR-15 + 5218/IM7	LaRC-RP-46/IM7	LaRC-RP-46 + 5218/IM7
0° bending strength/MPa	1508	1185	1659	1443
0° bending modulus/GPa	120.6	111.6	137.1	119.6
0° short beam shear strength/MPa	104	91	135	85
0° tensile strength/MPa	2458	1960	2623	2766
0° tensile modulus/GPa	144	145.4	155.8	155.0
0° compression strength/MPa	1384	1254	1491	1446
0° compression modulus/GPa	142.6	147.5	168.8	173
90° tensile strength/MPa	29	31	28	26
90° tensile modulus/GPa	8.6	8.7	8.8	9.0
In-plane shear Strength/MPa	85	7.5	76	64
In-plane shear Modulus/GPa	5.5	4.9	5.1	4.5
CAI/MPa	150	161	185	208

energy of 6.8 kJ/m, and large damage delamination was found on the untoughened polyimide composites and this was reduced in the toughened polyimide composites. In PMR-15 polyimide composites, the CAI value increased by 8% after toughening while it increased by 12% for the toughened LaRC-RP-46 polyimide composites to give a value of 208 MPa, as given in Table 3.116 [125].

Also, the toughness was improved by modifying the backbone chain in the PMR polyimide. By introducing flexible chains into the PMR polyimide backbone chains to reduce rigidity, the toughness can be effectively improved. In the LaRC-RP-46 and LP-15 polyimide resins, 3,4'-ODA and BAPP were used to replace MDA because flexible ether bonds exist in 3,4'-ODA and BAPP. Compared with PMR-15, the main chain flexibility in LaRC-RP-46 and LP-15 had improved resulting in an improvement in toughness (Table 3.117) [126].

One of the major applications of polyimide is their use as PMR composite matrixes. To meet the composite processing requirements, PMR polyimide requires a low processing temperature, low resin viscosity, good flow ability and proper tack and drape in prepregs.

Table 3.117 Effect of main chain structure on polyimide composite toughness

Resin system	Composites	$G_{IC}/J\cdot m^{-2}$
PMR-15		87
LP-15		187
LaRC-RP-46		177

The temperature for PMR polyimide curing and cross-linking can reach 300 °C and, therefore, the current BMI and epoxy composites processing techniques are not satisfactory for PMR polyimide composite processing. If the curing temperature can be effectively decreased, PMR polyimides will find wider application.

Earlier studies have indicated that *m*-amine phenol can be used as a terminating radical group and can reduce the curing temperature from 316 °C to 260 °C. However, *m*-amino benzene-terminated polyimide can only be used below 260 °C because its T_g ranges from 270 to 280 °C. When blends of *p*-amino benzene and NE, in an equal mol ratio, are used as terminating groups, the generated PMR-NV polyimide can be also cured and cross-linked at 260 °C. However, the T_g of the cured PMR-NV polyimide will exceed 325 °C. Carbon fiber-reinforced PMR-NV polyimide composites are equivalent to PMR-15 composites in terms of short-term mechanical properties at 318 °C. The drawback of PMR-NV polyimide is its poor resin flow ability. To obtain high-quality and void-free composites, the processing pressure required should be double that of the PMR-15 composites. Based on some reports, PN can be used to modify PMR-NV polyimide according to the synthesis shown in Fig. 3.82 [127].

A further study has indicated that if *N*-benzene-5-dinorbormene-2,3-dicarboxylic imino (PN) is blended with PMR-NV polyimide (Fig. 3.83), the flow ability of the PMR-NV polyimide is effectively improved at a PN content (mol fraction) of 5–10% (Fig. 3.83). In Table 3.118, compositions of PMR-NV polyimide modified with different PN contents are listed. From Fig. 3.83, when the PN content (mol fraction) is 5%, the PMR-NV polyimide resin will have a flow ability of more than 2% and when the PN content (mol fraction) is 10%, PMR-NV will have the same flow ability as PMR-15.

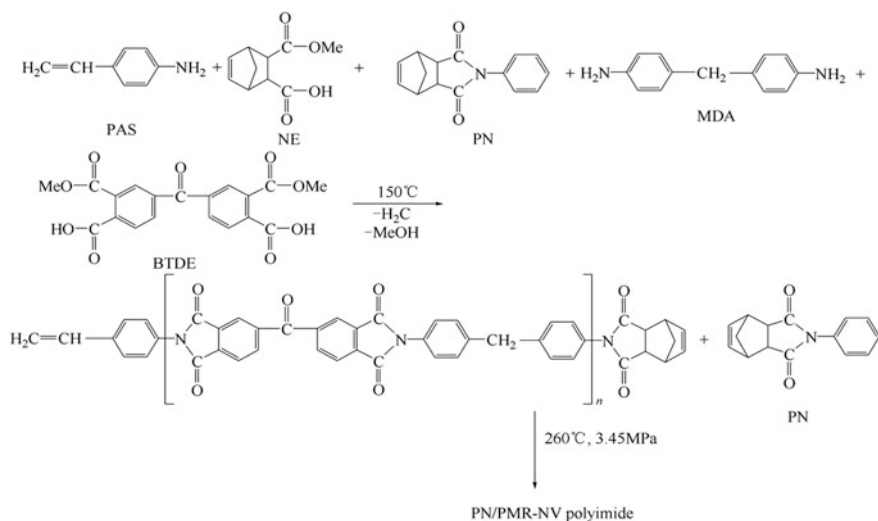


Fig. 3.82 Synthesis of PN-modified PMR-NV polyimide (2) processing modification of PMR polyimide

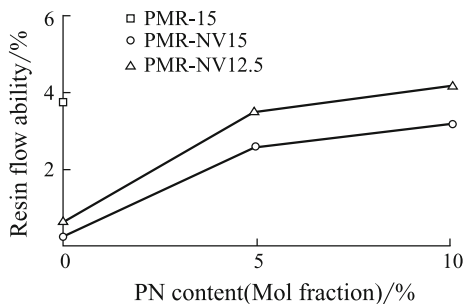


Fig. 3.83 The flow ability of PN-modified PMR-NV polyimide

PN-modified PMR-NV polyimide composites can be cured at lower than 3.45 MPa and 260 °C. No voids are present in composite laminates as determined by supersonic C-scan inspection. After post-treatment for 24 h at 316 °C, the T_g of the PN-modified PMR-NV polyimide composites can reach 300 °C or higher, which is slightly lower than that of unmodified PMR-NV polyimide composites. If post-treatment is continued for 16 h at 343 °C, the T_g of the modified PMR-NV polyimide composites can reach 340 °C or higher, which

Table 3.118 Different compositions of PMR-NV polyimide

Resins	PN content (mol fraction)/%	Reactant monomer ratio/mol				
		PAS	NE	MDA	BTDE	PN
PMR-NV15	0	1	1	2.5	2.5	0
PMR-NV15-PN5	5	1	1	2.5	2.5	0.368
PMR-NV15-PN10	10	1	1	2.5	2.5	0.778
PMR-NV12.5-PN5	5	1	1	2	2	0.316
PMR-NV12.5-PN10	10	1	1	2	2	0.667

fully meets long-term service requirements at 316 °C. Tables 3.119 and 3.120 list the different PMR-NV polyimide composites with their T_g and mechanical properties [128].

Low boiling point solvents can be easily removed during PMR polyimide processing and, therefore, high-quality and void-free composites can be produced. However, the ease of evaporation of low boiling point solvents can make it difficult for polyimide preregs to maintain their required tack and drape abilities. The tack and drape abilities are very important for large and complex composite parts.

Using reactive diluting agents or high boiling point solvents can improve prepreg tack and drape abilities. However, reactive diluting agents cannot significantly improve the prepreg's tack, while high boiling point solvents are not easily removed during processing resulting in many problems. Recent research has indicated that the use of blended low boiling point solvents or alkyl ester monomers instead of methyl ester monomers can provide a significant improvement to PMR polyimide prepreg track and drape abilities.

In Table 3.121, the effects of various alkyl esters and mixed solvents on PMR-15 polyimide prepreg tack and drape abilities are given. The tack retention period for PMR-15 polyimide preregs is only 2–3 days, and 2 days for drape ability. When propyl ester and propyl alcohol/methane alcohol were blended as solvents, the retention period for the tack and drape abilities of prepreg fabrics and tapes exceeded 12 days.

Since low boiling point solvent mixtures are easily removed during processing the alkyl ester-modified reactive monomer does not affect the curing reaction

Table 3.119 Different Celion 6K/PMR-NV polyimide composites with their T_g values

Resin	T_g after different post-treatment/°C		
	24 h/316 °C	48 h/316 °C	24 h/316 °C + 16 h/343 °C
PMR-NV15	328	332	358
PMR-NV15-PN5	314	320	353
PMR-NV15-PN10	303	308	324
PMR-NV12.5	330	335	358
PMR-NV12.5-PN5	316	321	344
PMR-NV12.5-PN10	304	310	341

Table 3.120 Mechanical properties of different Celion 6K/PMR-NV polyimide composites

Resins	Interlaminar shear strength/MPa		Bending strength/MPa		Bending modulus/GPa	
	25 °C	316 °C	25 °C	316 °C	25 °C	316 °C
PMR-NV15	113	50.3	1740	960	127	116
PMR-NV15-PN5	109	49.6	1750	950	121	112
PMR-NV15-PN10	112	49.6	1710	910	120	112
PMR-NV12.5-PN5	112	49.6	1850	940	123	115
PMR-NV12.5-PN10	110	48.9	1860	900	125	113

Note Post-treatment: 316 °C/24 h + 343 °C/16 h. A thermal aging study indicated that PN-modified PMR-NV polyimide composites will have slightly higher weight loss at 316°C by comparison with unmodified PMR-NV polyimide composites. Their interlaminar shear strength, bending strength and modulus retention rates were a little lower (Figs. 3.84, 3.85, 3.86 and 3.87). However, this difference is not apparent and, therefore, a small quantity of added PN does not significantly affect the PMR-NV polyimide in terms of thermal-oxidation stability and mechanical properties. This can extensively improve resin flow ability, which makes it possible to process composites under lower pressure

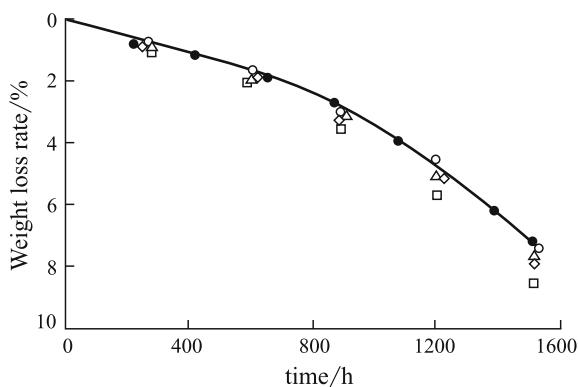


Fig. 3.84 Weight loss rates of various PMR-NV/Celion composites upon 316 °C aging. ●—PMR-NV 15; ○—PMR-NV 15-PN 5; △—PMR-NV 15-PN 10; ◇—PMR-NV 12.5-PN 5; □—PMR-NV 12.5-PN 10

history. Therefore, using this process to improve prepreg tack and drape ability will not affect the composite's performance. Table 3.122 and Figs. 3.88 and 3.89 show the mechanical properties of various PMR-NV/Celion 6K composites modified by different alkyl esters and blended solvents [128].

The use of different alkyl esters and blended solvents will affect PMR polyimide resin flow ability during the curing reaction. For example, when propyl ester and ethanol/propanol mixed solvents were used, propanol was generated as a by-product during imidization. This propanol by-product and the original propanol in the solvents caused a significant decrease in viscosity during the early stage of resin imidization. This resulted in the resin flow ability

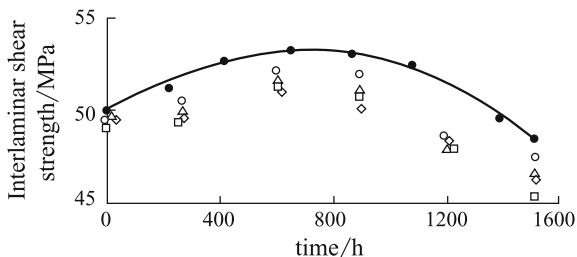


Fig. 3.85 Effect of 316 °C aging on the interlaminar shear strength of various PMR-NV/Celion composites. ●—PMR-NV 15; ○—PMR-NV 15-PN 5; △—PMR-NV 15-PN 10; ◇—PMR-NV 12.5-PN 5; □—PMR-NV 12.5-PN 10

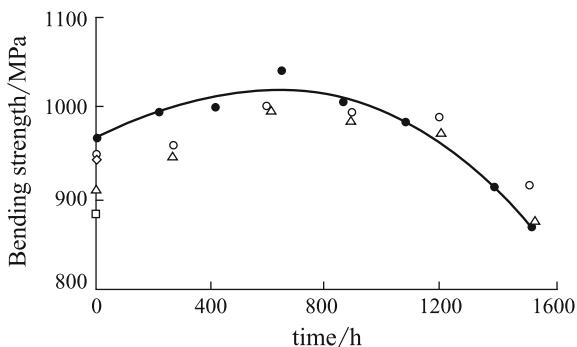


Fig. 3.86 Effect of 316 °C aging on the bending strength of various PMR-NV/Celion composites. ●—PMR-NV 15; ○—PMR-NV 15-PN 5; △—PMR-NV 15-PN 10; ◇—PMR-NV 12.5-PN 5; □—PMR-NV 12.5-PN 10

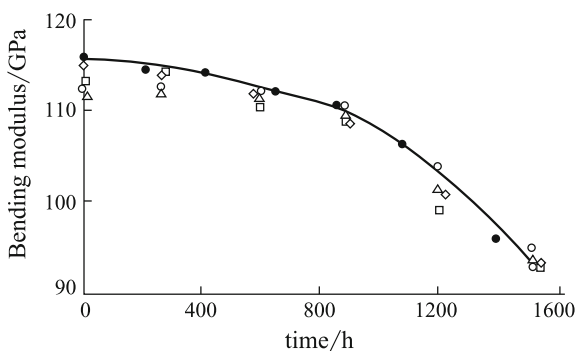


Fig. 3.87 Effect of 316 °C aging on the bending modulus of various PMR-NV/Celion composites. ●—PMR-NV 15; ○—PMR-NV 15-PN 5; △—PMR-NV 15-PN 10; ◇—PMR-NV 12.5-PN 5; □—PMR-NV 12.5-PN 10

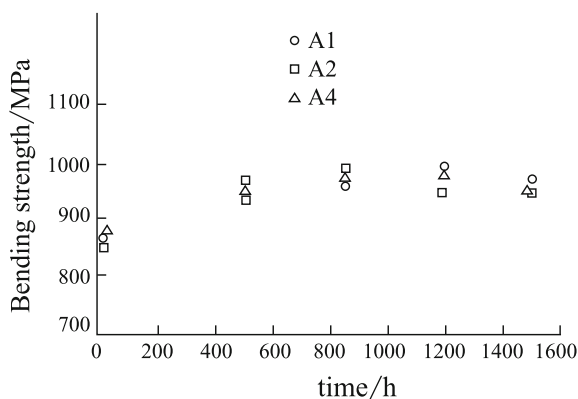
Table 3.121 Tack and drape of PMR-15 prepreg using various alkyl ester and blended solvents

Prepreg code	Ester type	Solvent	Tack/d		Drape/d	
			Fabric	Tape	Fabric	Tape
A1			2–3	2–3	2	2
A2			6–7	7–8	5	6
A3	Methane ester		3–4	–	2	–
A4	Methane ester		12	15	7	8
A5			12	15	12	15
A6			12	21	12	21

Note Prepreg fabric: PMR-15/T300 fabric; prepreg tape: PMR-NV/Celion 6K; Testing at R.T.

Table 3.122 Mechanical properties of the PMR-15/Celion 6k composites

Prepreg code	Store time at R. T./d	Fiber volume (content)/%	Interlaminar shear strength/MPa		Bending strength/MPa	
			R. T.	316 ° C	R.T.	316 ° C
A1	1	62.7	103	44.8	1532	834
A2	1	65	90	42.7	1632	861
A3	1	63	100	46.2	1639	841
A4	1	66	96	46.1	1612	875

**Fig. 3.88** Bending strength change at 316 °C of PMR-15/Celion 6K composites upon 316 °C aging

increasing. Therefore, if modified PMR-15 prepreps are to be used, proper adjustments during curing processing will be required and the heating rates should be reduced during the early imidization stage to prevent the resin from flowing too much.

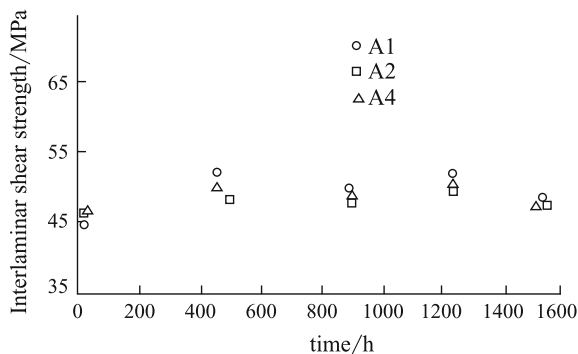


Fig. 3.89 Interlaminar shear strength change at 316 °C for PMR-15/Celion 6K composites upon 316 °C aging

(3) Safety in PMR polyimide applications

In the most commonly used PMR-15 polyimide, the reactive monomer ratio used is 2NE/3MDA/3BTDE, which implies a MDA content in the resin solid of about 34%. During resin synthesis, prepreg preparation, storage and shipping, some chemical reactions will take place. These are mainly NE monomers reacting with MDA to form NI-MDA. BTDE has a very low reaction activity and has little chance of reacting with MDA. Therefore, before PMR-15 polyimide prepreg cutting and lamination about 25% MDA will still be present. Based on toxic experiments, long periods of contact with MDA will damage the lungs, stomach, blood and spleen. Animal experiments indicate that MDA is potentially carcinogenic. Therefore, strict regulations about MDA operational safety have been established by the Health and Safety Organization in the USA.

- (1) In workplaces, the MDA content in air should be lower than $10 \times 10^{-7}\%$.
- (2) Personnel should be trained in operational safety.
- (3) Health should be inspected regularly.
- (4) Written emergency procedures should be established.
- (5) Good ventilation required at work sites.
- (6) Protective clothing and masks should be worn during working hours.
- (7) Washing and cleaning facilities should be provided in case of exceedances.

To reduce PMR-15 toxicity and lower its cost, non-toxic or low toxicity aromatic diamines have been used to replace MDA. Many non-MDA PMR polyimides have been developed. These low-cost non-MDA PMR polyimides are equivalent to PMR-15 in terms of processing performance and room-temperature mechanical properties. However, their thermal-oxidation stability and high-temperature mechanical properties are worse than that of PMR-15 [129].

The Rohr Company developed a MDA-free PMR polyimide, PMR-15 MDAF. This resin is produced using MDA, NE and BTDE as reactive monomers. The use of a step reaction causes MDA to fully react with NE (or BTDE) to form NI-MDA (or BTDI-MDA) compounds. Finally, these two compounds are dissolved in organic solvents and it is then possible to use standard PMR processing techniques to prepare prepregs and composites. Rohr's monomer prepreg tapes produced by PMR-15MDAF/Celion G30–500 are commercially sold as Cycom X 3009 [130].

Compared with PMR-15, PMR-15MDAF provides equivalent composite mechanical properties and thermal–oxidation stability (Table 3.123). From animal consumption toxicity experiments, skin irritation and salmonella/fine particle induction experiments, no toxic effects have been found for PMR-15MDAF. No free MDA was found in the PMR-15MDAF system. Animal consumption testing indicated that the safe consumption limit of PMR-15MDAF is more than 5 g/kg. This means that the safe consumption limit is more than 300 g for a 60 kg person, confirming that PMR-15MDAF is very safe during operation.

3.7.2 Acetylene-Terminated Polyimide

Acetylene-terminated polyimides are high-performance thermosetting resins developed simultaneously with PMR-15. They can be used as molding compounds or composite matrixes with superior thermal–oxidation stability and dielectric properties. Their glass or carbon fiber-reinforced composites, chopped carbon fiber-reinforced molding compounds, self-lubrication composites and abrading resistant materials are widely applied. Acetylene-terminated polyimides mainly consist of the Thermid series of polyimides and the Thermcon series of polyimides.

Table 3.123 Composites performance of Celion G30-500/PMR-15 and PMR-15MDAF

Properties	Composites	
	Celion G30-500/PMR-15	Celion G30-500/PMR-15 and PMR-15MDAF
	342	340
$T_g/^\circ\text{C}$	1655	1650
0° bending strength/MPa	118	114
Short beam shear strength/MPa	1586 (R.T.)	1590 (R.T.)
0° compression strength/MPa	896 (260 °C)	895 (260 °C)
	848 (316 °C)	745 (316 °C)

The former can be prepared by the reaction between aromatic diamines, 3-acetylene phenol amine and 1,3-di-(3-amine phenoxy) phenyl. The latter can be obtained by simply treating amine aromatic acetylenes and acetylene aromatic acetylenes.

3.7.2.1 Synthesis of Acetylene-Terminated Polyimide

(1) Synthesis of Thermid polyimides

The earliest Thermid polyimide was developed in the USA by the Hughes Aircraft Company. This technology was transferred to Gulf and commercialized in the USA by the State Starch and Chemicals Co. Ltd. In the Thermid series of polyimides, aromatic dianhydride, 3-acetylene phenol amine (APB) and 1,3-di-(3-amine phenoxy) phenyl (APA) are used as reactive monomers and reacted to obtain the corresponding acetylene-terminated polyimide. It is then heated and imidized in cresol to yield acetylene-terminated polyimide prepolymer resins. Figure 3.90 shows the synthesis of the Thermid series of polyimides [131].

3-Acetylene phenyl is a major raw material in the synthesis of Thermid polyimides and can be prepared by different synthetic approaches. The most commonly used method is to react 3-bromo nitrophenol and methylbutynol under catalysis of $(\text{Ph}_3\text{P})_2\text{PdCl}_3$ to generate 2-methyl-4-nitrophenol-3-butanol-2-alcohol. Under Al_2O_3 catalysis, the above-mentioned compounds are subjected to dehydrogenation and dehydration to yield 3-acetylene phenyl amine. The total yield of reaction products is about 85% (Fig. 3.91) [132].

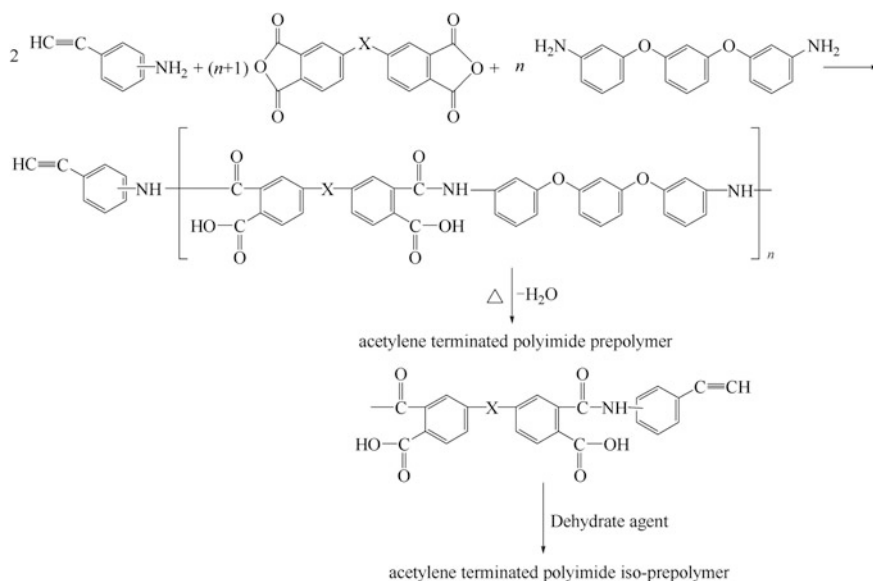


Fig. 3.90 Synthesis of Thermid polyimides

Another major monomer in Thermid polyimide synthesis is 1,3-di-(3-amine phenoxy) phenyl. *m*-Phenol bisphenyl and sodium carbonate react to form *m*-phenol bisphenyl sodium, and using cupric chloride as a catalyst, *m*-phenol bisphenyl sodium will react with 3-bromo nitrophenol in pyrrole solution to form 1,3-di-(3-nitryl phenoxy) phenyl. Finally, under platinum oxide catalysis, 1,3-di-(3-nitryl phenoxy) phenyl is dehydrogenated under reduced pressure to yield 1,3-di-(3-amine phenoxy) phenyl (Fig. 3.92).

The Thermid series of polyimides mainly includes Thermid MC-600, Thermid LR-600, Thermid AL-600, Thermid IP-600 and Thermid FA-600 (Fig. 3.93). Thermid MC-600 is the earliest commercialized polyimide resin. It is synthesized by reacting 3,3',4,4'-diphenyl ketone tetraacid dianhydride, 3-acetylene phenyl amine and 1,3-di-(3-amine phenoxy) phenyl to obtain the corresponding acetylene-terminated amide acid. Heating the blended solution of amide acid and cresol results in imidization and condensed water is continuously removed so that the acetylene-terminated polyimide prepolymers are obtained. Thermid MC-600 is a brown solid with a softening temperature between 157 and 210 °C. It can be cured above its softening temperature without catalysis and can be dissolved in polar solvents such as *N*-methyl pyrrolidone, *N,N'*-bimethyl amide and Me₂SO₃ [133].

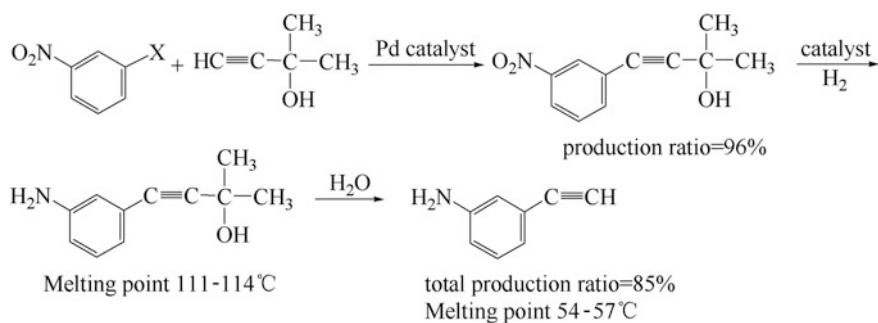


Fig. 3.91 Synthesis of acetylene phenyl amine

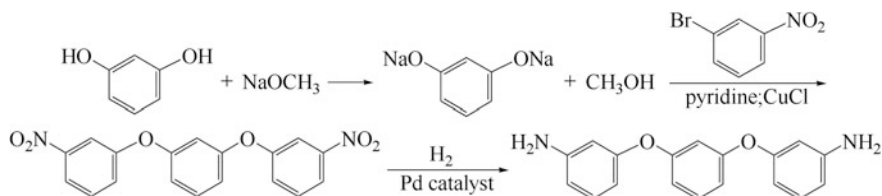


Fig. 3.92 Synthesis of 1,3-di-(3-amine phenoxy) phenyl

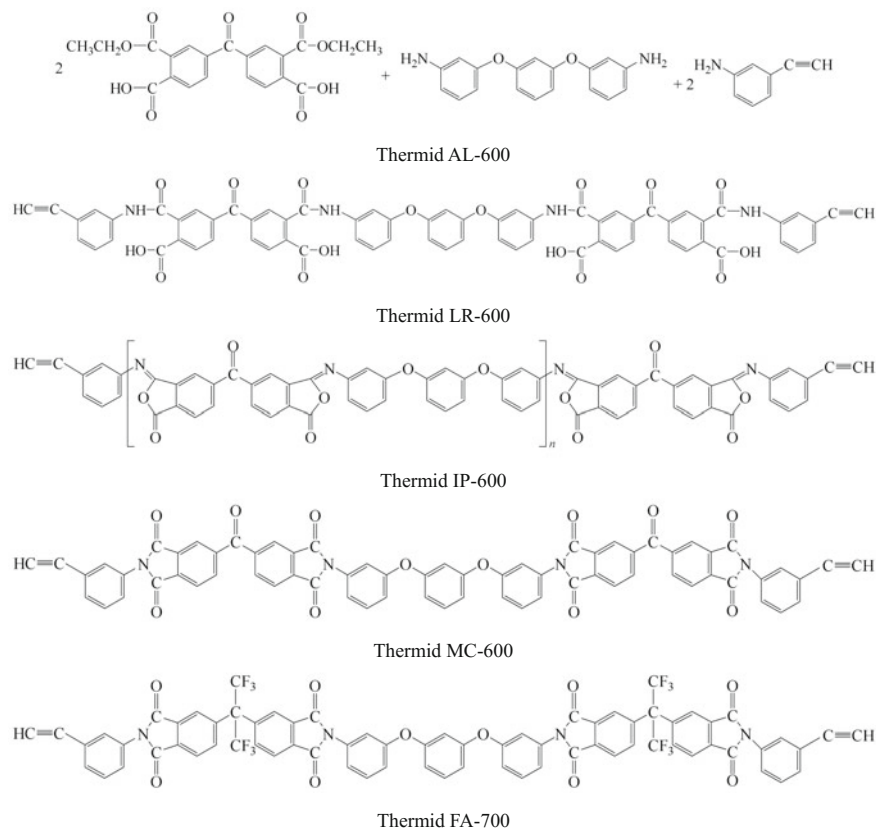


Fig. 3.93 Thermid series polyimide structures

Thermid Al-600 and Thermid LR-600 are acetylene-terminated amide acids produced by the reaction of a mixed solution of three reactive monomers such as 3,3',4,4'-diphenyl ketone tetraacid dianhydride, 3-acetylene phenyl amine and 1,3-di-(3-amine phenoxy) phenyl. Thermid AL-600 and Thermid LR-600 have improved solubility and processing ability, but during the curing process, the condensation and imidization of amines and esters in Thermid AL-600, and the imidization in Thermid LR-600 will generate some condensed water and alcohol or condensed water volatiles, which can result in voids forming in the cured resins. The difference between Thermid IP-600 and Thermid MC-600 is that the iso-imide chain is used to replace the imide chain in prepolymers. Therefore, the melting point of Thermid IP-600 is lower and it has a longer gel time while its processing window is longer. The ring iso-imide structure is formed by a cyclization of the corresponding amide acid and dehydration with appropriate chemical reagents (Fig. 3.92). In general, the imide and iso-imide generated by N-substituted amide acid chemical dehydration will depend on the reactant

ratios, the reaction conditions, amide acid behavior and the chemical dehydrating agents used. Trifluoroacetic anhydride (TFAA) and *N,N'*-dicyclohexylcarbodiimide (DCC) can effectively dehydrate amide acids and transform them into their corresponding iso-imides. Compared with TFAA, DCC will generate fewer by-products and is more widely used. After heating at 230 °C for 2.5 min, the Thermid IP-600 resin infrared spectrum shows a decreasing absorption peak at 940 cm^{-1} and this corresponds to an iso-imide chain. Another absorption peak at 1375 cm^{-1} corresponding to an imide chain increases. This indicates that iso-imide quickly transforms into imide under proper curing conditions. At 371 °C, Thermid IP-600 and Thermid MC-600 give the same infrared spectrum after curing for 2 h in air.

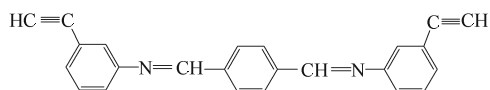
For Thermid FA-700, 4,4'-(hexafluoroisopropylidene)-di-*o*-phenyl dicarboxylic dianhydride replaced 3,3',4,4'-diphenyl ketone tetraacidic dianhydride, but the other structures are same as those in Thermid MC-600. This change in structure greatly improves prepolymer solubility in solvents like methylene dichloride, acetone, tetrahydrofuran, cyclic hexether, *N,N'*-dimethyl methane amide, *N,N'*-dimethyl acetylamine and *N*-methyl pyrrolidone. With a high solid content, these resin solutions still have very low viscosity, for example, at 22 °C, the viscosity of the Thermid FA-700/cyclic hexether resin solution with a 50% solids content is 0.21 Pa·s. In addition, these high solid content resin solutions are very stable at room temperature.

(2) Synthesis of Thermcon polyimide

The Thermcon resin was developed by Bilow and Walton with features like superior dielectric performance in cured resins, and these can be used as insulating materials. After proper treatment, Thermcon resins will become conductive plastics with stable performance in ambient conditions.

The Thermcon resin can be synthesized by various methods, for example, by the condensation of aromatic diacetylenes and aromatic biamines, and termination by amine acetylene or acetylene aromatic acetylenes.

Thermcon 1000



In its infrared spectrum, Thermcon 1000 shows a strong absorption peak of acetylene hydrogen at 3278 cm^{-1} and weak absorption peaks for $\text{C}\equiv\text{C}$ and amine at 2110 and 1622 cm^{-1} , respectively. Upon recrystallization in alcohol, Thermcon 1000 will melt at 138.5–139.5 °C. Upon methyl benzene recrystallization, its melting point is 149–150 °C. The curing onset temperature of the Thermcon 1000 resin is about 190 °C, and its peak temperature is 209 °C with a high reaction heat of 761 J/g. If the polymerization rate is too high, the resins strongly decompose during the curing process because of their very high reaction heat. To control the reaction rate, a multiple-step curing process should be

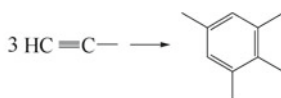
adopted, for example, first cured for 2 h at 155 °C and then for 94 h at 200 °C, which can yield strong and brittle materials with good dielectric performances.

3.7.2.2 Curing of Acetylene-Terminated Polyimide

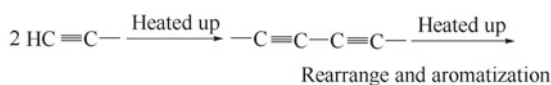
The curing reactions that can possibly occur in acetylene-terminated polyimide are listed in Fig. 3.94. The acetylene end groups in acetylene-terminated polyimide can possibly undergo a simple tri-polymerization reaction to form aromatic cross-linked structures. Other reaction paths also lead to tri-polymerized cross-linked structures. The Glaser reaction between two acetylene end groups gives diacetylene chain segments, and the Strauss reaction between two acetylene end groups gives acetylene-ethylene structures. In the Diels–Alder reaction, this kind of conjugate structural chain segment can react with acetylene end groups or the main chain of aromatic polymers. Acetylene end groups can also take part in free-radical-induced polymerization.

No tri-polymerized products are formed when using acetylene-terminated analog compounds after heating at 275 °C in nitrogen. Apart from the main products (90%), some complex products containing terphenyl and phenyl groups are formed. The reaction enthalpy and infrared spectrum analysis indicate that acetylene end

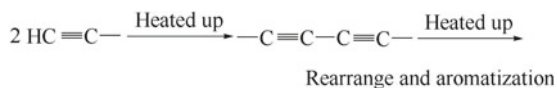
1) Acetylene group tri-polymerization



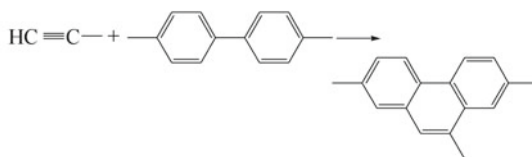
2) Glaser reaction



3) Strauss reaction



4) Diels-Alder reaction



5) Free radical induced polymerization

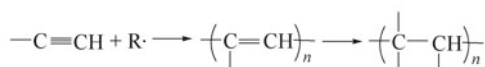
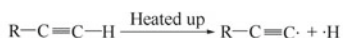


Fig. 3.94 Possible cure reactions in acetylene-terminated polyimides

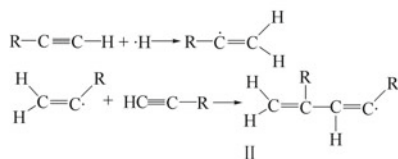
group tri-polymerization is not the main cross-linking path. NMR analysis showed that no aromatic Diels-Alder reactions took place. For acetylene-terminated analog compound curing, the C–H absorption peak (3300 cm^{-1}) and $\text{C}\equiv\text{C}$ absorption peak ($2100\text{--}2109\text{ cm}^{-1}$) disappeared and the conjugated $\text{C}=\text{C}$ peak increased. Therefore, the main curing reaction in acetylene-terminated resins at high temperature will result in reverse-conjugated polyenes. However, from infrared, NMR and kinetic analyses upon low-temperature curing or upon a low polymerization degree, 4,4'-diacetylene phenyl methane can form ring tri-polymers by a fast zero-order reaction. At a higher reaction extent, the degree of cross-linking increased and a slow almost linear polymerization reaction took place to form polyene structures.

Based on the above discussion, the curing reaction mechanism is illustrated in Fig. 3.95. This explains the formation of the polyene structures upon the thermal polymerization of acetylene-terminated resins. Further studies into the thermal polymerization of phenyl acetylenes indicated that a bi-polymerization between two phenyl acetylene molecules occurs to form a head-end-end-head 1,4'-diphenyl butadienyl free radical, and then chain growth and extension occurs as shown in Eq. 3.57. The double free radical formation mechanism has been found in a study on 3-phenoxy ethylene thermal polymerization. In compounds that are generated by thermal polymerization at $127\text{--}327\text{ }^\circ\text{C}$, their relative molecular mass will not change with different polymerization temperatures. The reaction kinetics and molecular chain lengths will be controlled by a first-order termination reaction upon polymeric chain cyclization [134].

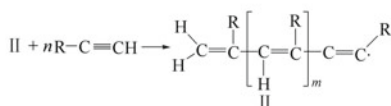
1) Free radical induction



2) Chain growth



3) Chain extension



4) Chain termination

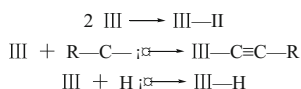
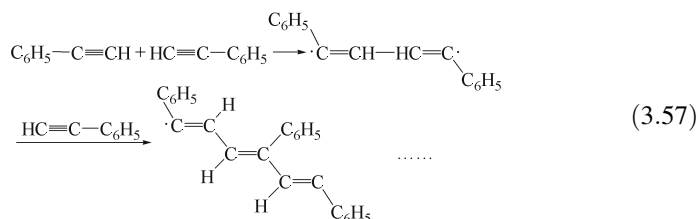
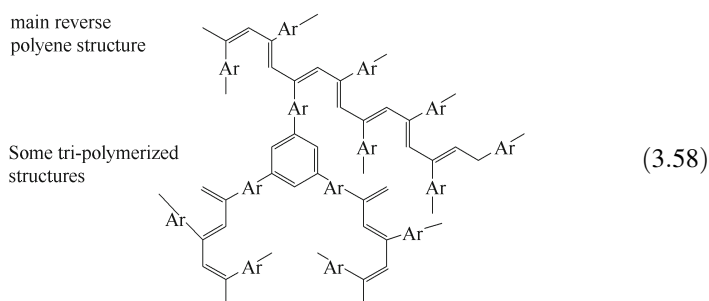


Fig. 3.95 Thermal polymerization of acetylene-terminated resins



In summary, the curing reaction mechanism of acetylene-terminated polyimides will be:

The main curing reaction at high temperature is the linear polymerization of acetylene end groups, and this gives reverse-polyene structures in cross-linked materials (Eq. 3.58).



- (3) In the early stage, the curing reaction is dominated by acetylene end group tri-polymerization.
- (4) Two acetylene end groups will form double free radicals and induce resin thermal polymerization.
- (5) The termination of polymerization is controlled by cyclization.

3.7.2.3 Performance of Acetylene-Terminated Polyimides

(1) Thermid polyimide performance

Thermid polyimides have excellent thermal-oxidation stability and dielectric properties, good hot/wet resistance and little performance change over long-term service at 188 °C. Table 3.124 lists the performance of Thermid 600 polyimide. Thermid MC-600 has a melting temperature from 195 to 205 °C, curing onset and peak temperatures of 221 and 251°C, respectively. A molded specimen made at 246 °C and 15 MPa gives a T_g of 255 °C, and after 371 °C

Table 3.124 Thermid 600 polyimide performance

Properties	Tested values
Mechanical and physical properties	
Bending strength/MPa	
Bending modulus/GPa	131
Tensile strength/MPa	4.49
Tensile modulus/GPa	82.8
Fracture elongation/%	3.66
Compression strength/MPa	2
Water absorption (mass fraction) %	17.3
50 °C, R.H. 95%,1000 h	2.1
Electric properties	
Dielectric constant	
Dielectric loss tangent	3.88 (10 MHz), 3.13 (9 GHz), 3.12 (12 GHz)
Thermal resistance	0.0006 (10 MHz), 0.0068 (9 GHz), 0.0048 (12 GHz)
316 °C aging weight loss/%	
500 h	
1000 h	2.89
316 °C aging strength retention rate/%	4.4
1000 h	72 (R.T.), 62 (316 °C)

post-treatment, its T_g increases to 349 °C. The thermal decomposition temperature of Thermid MC-600 is higher than 500 °C.

The drawbacks of Thermid MC-600 include very high melting temperatures, short gel times (gel time at 190 °C is about 3 min), insolubility in low boiling solvents, which results in poor impregnation and processing abilities.

Thermid IP-600 is produced using iso-imide to replace the imide chain in Thermid MC-600 and, therefore, the melting temperature decreases from 200 to 160 °C, and its solubility increases and it can dissolve in many solvents such as tetrahydrofuran, glycol dimethyl ether, a mixed solvent of ethyl methyl ketone and methylbenzene (4:1), *N*-methyl pyrrolidone and *N,N'* dimethyl methyl amide. Its gel time increases from 3 min to more than 15 min, and its reaction heat release peak is wider (190–320 °C). This means that Thermid IP-600 will have a more constant reaction and a wider processing window. The above-mentioned processing improvement allows the use of conventional impregnation and autoclave processing methods for Thermid IP-600 for the fabrication of large structural composites. Figures 3.96 and 3.97 show a comparison of the gel time and DSC results for Thermid IP-600 and Thermid MC-600.

When used as composite matrix, Thermid IP-600 can be processed at lower temperature and can then be post-treated under normal conditions. After 370 °C

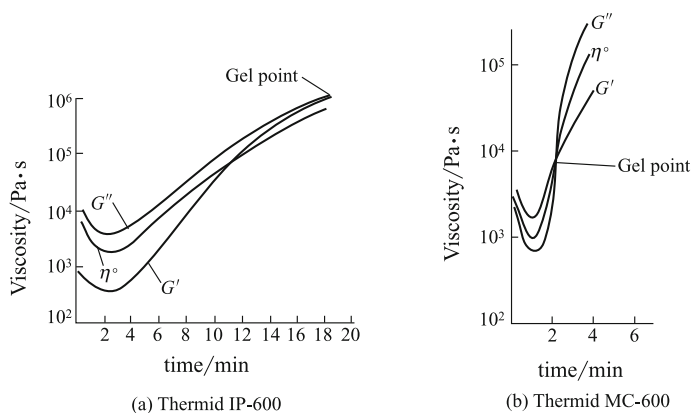


Fig. 3.96 Thermid IP-600 and Thermid MC-600 gel times

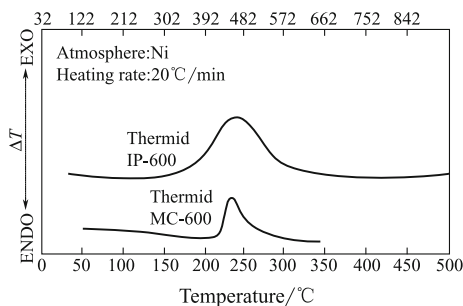


Fig. 3.97 Thermid IP-600 and Thermid MC-600 thermal analysis curves

Table 3.125 Thermid IP-600 polyimide performance

Properties	Tested values
Tensile strength/MPa	58.6 (R.T.)
	29.3 (316 °C)
Tensile modulus/GPa	5.03 (R.T.)
	1.24 (316 °C)
Fracture elongation/%	1.2 (R.T.)
	4.2 (316 °C)
T_g (MDA)	300 °C (370 °C, 6 h post-treated)
	350 °C (370 °C, 15 h post-treated)
	330 °C (400 °C, 4 h post-treated)
	354 °C (400 °C, 8 h post-treated)
Density/g·cm ⁻³	1.34

post-treatment for 8 h, Thermid IP-600 has a T_g up to 350 °C, which is similar to that of Thermid MC-600 (Table 3.125).

Figures 3.98 and 3.99 show the effect of thermal aging on the performance of the CF/Thermid IP-600 composites. After aging more than 700 h at 288 °C, the room-temperature bending and shear strength retention rates are greater than 60%, while the bending and shear strength at 288 °C do not change. The above-mentioned aged composites have not undergone processing optimization, and their void content is high at 5–7% [135].

Using 6FDA to replace BTDA, the generated Thermid AF-700 gives a T_g of 95 °C and its cure onset and peak temperatures are 228 and 244 °C, respectively. The cure reaction heat is equivalent to that of Thermid MC-600, but its peak temperature range is wider. This means that the curing reaction of Thermid AF-700 is more consistent and its curing window is wider. The cured Thermid AF-700 resins have a T_g of 350 °C and a thermal decomposition temperature of 500 °C.

Thermid AF-700 has very good dielectric performance. Figure 3.100 shows the dielectric performance of Thermid MC-600 and Thermid AF-700 at different frequencies. For Thermid AF-700, the dielectric constant and the loss factor increase as the curing time increases. The dielectric performance can be different at different frequencies. Compared with Thermid MC-600, the performance of Thermid AF-700 is better before and after curing [134].

(2) Thermcon resin performances

Table 3.126 lists the physical properties of the Thermcon-1000 resins and includes the high reaction heat of Thermcon-1000. To avoid the thermal decomposition that may be induced during resin curing, a step curing procedure is required. A typical curing process will be 155 °C curing for 2 h and then at 200 °C for 94 h. In this way, insulating materials with very stable dielectric

Fig. 3.98 Effect of thermal aging on the bending strength of the CF/Thermid IP-600 composites. —Tested in air ambient; ●—●—● tested at 288 °C

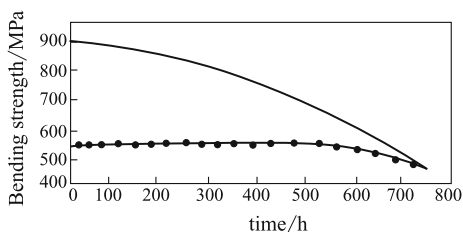


Fig. 3.99 Effect of thermal aging on the interlaminar shear strength of the CF/Thermid IP-600 composites. —Tested in air ambient; ●—●—● tested at 288 °C

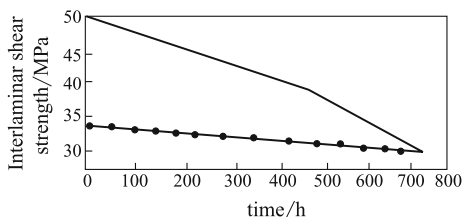
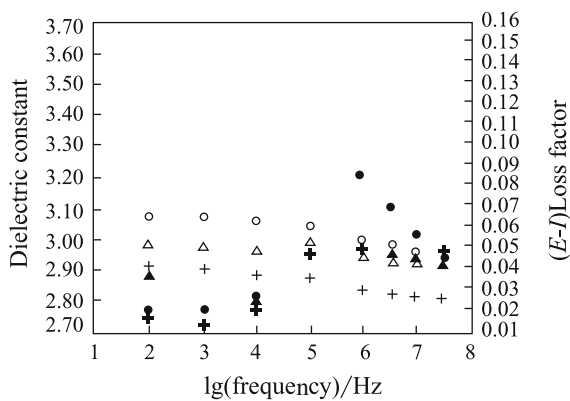
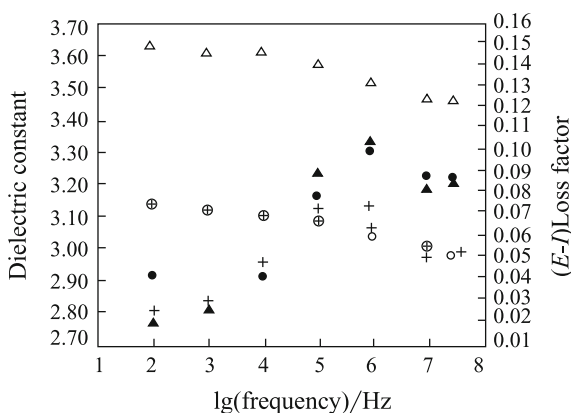


Fig. 3.100 Dielectric performance of acetylene-terminated polyimides. \oplus —Cold pressed, dielectric constant K ; +—cold pressed, loss factor; \triangle —cured, dielectric constant K ; \blacktriangle —cured, loss factor; \circ —post-cured, dielectric constant K ; \bullet —post-cured, loss factor



(a) Thermid Af-700

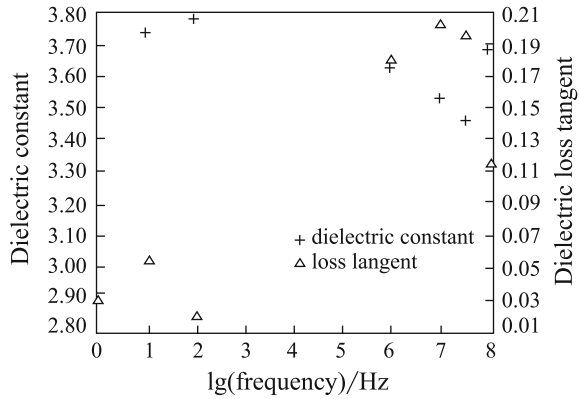


(b) Thermid MC-600

Table 3.126 Thermcon 1000 physical performance

Properties	Tested values
Appearance	Yellow solid
Density/g·cm ⁻³	0.75
Melting point (DSC)/°C	139.1
Crystal temperature (DSC)/°C	140
Reaction peak temp. (DSC, 10 °C/min)/°C	761
Curing heat/J·g ⁻¹	Diethylene dimethylether
Solubility	<i>N</i> -methyl pyrrolidone
	Tetrahydrofuran
	Methyl benzene
Cured resin thermal decomposed temp./°C	450 (onset), 590 (turn point)

Fig. 3.101 Dielectric performance of Thermcon 1000



constants and loss factors as well as very good dielectric properties over a wide frequency range are obtained (Fig. 3.101).

Cured Thermcon resins can undergo further high-temperature post-treatment and can be fabricated into conductive plastics with very stable performance under ambient conditions. After curing at 150 °C/2 h + 200 °C/1 h + 250 °C/1 h + 300 °C/50 h, its conductivity will depend on the post-treatment temperature and time, for example, after 600 °C post-treatment for 100 h, the conductivity of Thermcon 1000 can reach 5 S/cm.

3.7.3 Polyimide Composite Application

Polyimide composites have high specific strength and modulus as well as superior thermal–oxidation stability, which allow them to be used as replacements for metals

Table 3.127 Different resin composites with their service temperature ranges

Service temperature	<130 °C	130–230 °C	>230 °C
Composite types	Epoxy composites (1) 3501 (2) 8552 (3) 977 (4) PR500	BMI composites (1) V378A (2) 5245 (3) 5250 (4) 5260	Polyimide composites (1) PMR-15 (2) LaRC-RP-46 (3) LP-15 (4) V-CAP-75
Features	(1) Rich design data (2) Wide application in aerospace industry (3) Good processing ability (4) Long-term service at 130 °C	(1) Rich design data (2) Less experience than epoxy composites (3) Similar to epoxy composites (4) Lack of hot/wet data	(1) Need high-temp. molding (2) Superior thermal–oxidation stability (3) Lack of design and use experience (4) High resin cost

at higher than 230 °C. Table 3.127 lists different resin composites with their service temperature ranges.

Polyimide composites in aircraft engine applications can significantly reduce the engine weight and increase the thrust–weight ratio. For example, polyimide composites are used extensively in aeronautical turbine engines. Engine parts made of polyimide composites include F404 by-pass air duct, CF6 core cap, F100 flap, YE-120 static blade, PLT-210 condenser case and the F110AFT fairing. The polyimide resin matrixes in these composite engine parts are PMR-15 and V-CAP-75. Some of them have been certified by airworthiness testing and are in service.

The F404 by-pass air duct was the first composite engine part made of T300 fabric/PMR-15. It is a coning cylinder with a diameter and length of 76 and 102 cm, respectively. The composite part weighs about 13 kg.

The processing molds for the F404 by-pass air duct are made of molding steel (Fig. 3.102). The mold is made during frame construction and installed on a support stand. The mold can be rotated on an axis shaft for easy lamination. The F404 by-pass air duct is manufactured by autoclave curing processing with curing parameters as follows:

- (1) Apply vacuum at 13 kPa.
- (2) Heat to 204 °C at a rate of 23.5 °C/min
- (3) Hold for 12 min at 204 °C and then apply full vacuum.
- (4) Heat to 238 °C at a rate of 2–3 °C/min and apply pressure at 1.277 MPa.
- (5) Heat to 252 °C within 30 min, pressure at 1.277 MPa and then vacuum.
- (6) Hold for 30 min at 252 °C, pressure at 1.277 MPa and vacuum.
- (7) Heat to 307 °C at a rate of 1 °C/min, pressure at 1.277 MPa and vacuum.

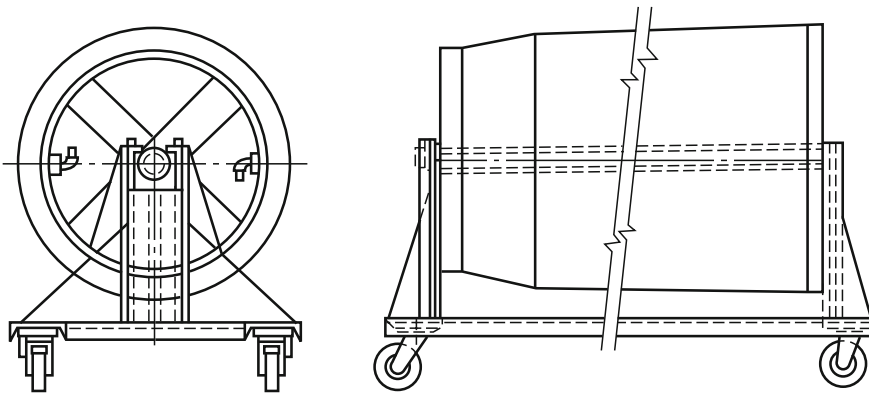


Fig. 3.102 Processing molds for F404 composite by-pass air duct

- (8) Hold for 180 min at 307 °C, pressure at 1.277 MPa and vacuum.
- (9) Slowly cool to below 80 °C, remove pressure and vacuum.

After being released from the mold, the part is inspected by C-scan. Both the delamination and void content are lower than 3%. After static and operational testing, the part can be put into service. Compared with the Ti alloy by-pass air duct, the F404 composite part weighs 15–20% less and its cost is 30–50% lower [136, 137].

Although polyimide composites have obvious weight-saving advantages for airplane engines and enhance engine performance, for several reasons polyimide composites are still in small scale trials before use in airplane engines. Airplane engines are flight power devices and very high reliability requires very mature materials. As new materials, especially high-temperature-resistant polyimide composites, both experience and accumulated data are still insufficient. For small and complex composite engine parts, there are currently no reliable nondestructive inspection methods available. Additionally, engine parts require a higher service temperature than other airplane parts, and for high-temperature-resistant polyimide composites, the application ranges are limited to the cool ends of engines and to external parts. Finally, the market requirements for airplane engines are limited, and engine parts are produced in small volumes and have complex shapes and structures resulting in high production costs for engine composite parts.

Apart from their application in airplane engines, polyimide composites have been also applied in other airplane parts, for example, the ice-proof air pressure pipe system in the B747, the flap in the F-15 jet, etc.

In the B747, Ti alloy pipes were previously used and were 200 kg in total weight. These pipes have varied diameters and were required to meet the following conditions:

- (1) Pressure resistance: 0.5 MPa.
- (2) Max. service temperature: 232 °C.
- (3) Max. air flow: 12.4 m³/s.
- (4) Service term: 50,000 h.

For the service temperature and term, common composites do not meet these requirements and carbon-reinforced PMR-15 polyimide composites were selected. After replacing the Ti alloy pipes with the composites, the ice-proof air pressure pipe system in an airplane weigh 125 kg less, and the weight reduction is thus 35% or more [138].

(Translated by Jianmao Tang)

References

1. Chen XB (2000) Development of advanced polymer composites. *J Aeronaut Mater* 20 (1):46–54 (in Chinese)
2. Chen XB (2003) Development and applications of advanced polymer matrix composites. *J Aeronaut Mater* 23(suppl):198–204 (in Chinese)
3. Chen XB, Zhang BY (2009) Application and development of advanced polymer matrix composites. *Mater China* 28(6):2–12 (in Chinese)
4. Du SY (2007) Advanced composite materials and aerospace engineering. *Acta Mater Compos Sinica* 24(1):1–2 (in Chinese)
5. Chen XB et al (1999) High performance phenolic resin. Chemical Industry Press, Beijing (in Chinese)
6. Yin RZ (1990) Phenolic resin and its application. Chemical Industry Press, Beijing (in Chinese)
7. Shananz ZM (1994) Thermosett Resin 15(3):27 (in Chinese)
8. Ren GG (1993) A new generation of phenolic resin and its composites. China FRP Industry Association, Beijing (in Chinese)
9. Jiang LX et al (1990) Heat resistant polymer. Press of University of Electronic Science and Technology of Chengdu, Chengdu (in Chinese)
10. Regina-Mazzuca Alba M, Fong Ark W, Jones Thomas R (1982) Novel process for the production of particulate phenolic resins. *Ind Eng Chem Prod Res Dev* 21:139
11. Brode GL, Kopf PW, Chow SW (1982) Phenolic thermospheres. Chemical design and principles. *Ind Eng Chem Prod Res Dev* 21:142
12. Yang YG et al (1988) Study on reaction kinetics of suspension polymerization of phenolic resin. *J Beijing Univ Chem Technol* 3:33 (in Chinese)
13. Wang LC et al (1993) Resorcin modified phenolic resin to reduce its flame, smoke and toxicity. *Polym Mater* (2):49 (in Chinese)
14. Bian JX (1991) Development of molding technology of phenolic resin. *New Chem Mater* 3:21 (in Chinese)
15. Phenolic Resin. Insulating Material and Technology Committee (1993) (in Chinese)
16. Pei DF (1996) Research on synthesis and ring-opening polymerization of benzoxazine-precursor of a new phenolic resin. Dissertation for Doctor's Degree of Sichuan University (in Chinese)
17. Lu ZJ (1995) Dissertation for Master's Degree of Sichuan University (in Chinese)
18. Kang YJ et al (1996) New type phenolic resin and its process development. *GRP/Compos Mater* 2:43 (in Chinese)
19. Pei DF et al (1994) Synthesis and modification of high performance phenolic resin. *New Chem Mater* 10:12 (in Chinese)
20. Xiao CR et al (1997) Study on performance of composite material based on FB resin (in Chinese)
21. Liu XH et al (1997) Study on friction materials based on heat resistant phenolic resin containing molybdenum. *Eng Plast Appl* 3:30 (in Chinese)
22. Lu ZJ et al (1995) Study on ring opening polymerization of composites materials based on phenolic resin—preparation of laminate of MDAPF1-EGF Glass Cloth. *Eng Plast Appl* 2:1 (in Chinese)
23. Lu FC (1993) Adhesive with high heat resistance. Science Press, Beijing (in Chinese)
24. Jiao YS (1994) Phenolic triazine resin, *Fiber Reinf Plast/Compos* (1):10 (in Chinese)
25. Liang GZ et al (1996) The BMI modifier—ally compounds. *New Chem Mater* 3:27 (in Chinese)
26. Canfield A, Clinton RG (1992) Improved ablative materials for the ASRM Nozzle. In: AIAA/SAE/ASEE 28th joint propulsion conf and exhibit, Nashville, 3057
27. Chen MY (1990) Application status and prospect of advanced materials used in solid rocket motor of strategic missile. *Aerosp Mater & Technol* 4:1 (in Chinese)

28. ShangHai Chemistry College Lab (1979) Synth Resin, 208 (in Chinese)
29. Liu TD, Wang XC, Xu XP (1989) Thermosett Resin (2):38 (in Chinese)
30. Zou SO (1996) New Chem Mater (3):26 (in Chinese)
31. Shell Chemical Co (1988) Epon HPT Curing agent 1061-M, product data
32. Shell Chemical Co (1988) Epon HPT Curing agent 1062-M, product data
33. Schultz WJ et al (1988) Polym Prepr Am Chem Soc (1):136
34. Yao KD, Liu G (1992) Thermosetti Resin (3):52 (in Chinese)
35. Sun QL (1990) Thermosett Resin (4):48 (in Chinese)
36. US Patent 3015648
37. US Patent 4707534
38. Lin SC, Pearce EM (1979) J Polym Sci 17:3095
39. US Patent 3910908
40. Ciba-Geigy (1984) Araldite PT810, product data
41. Ciba-Geigy (1987) Araldite MY 0510, product data
42. Ciba-Geigy (1983) Araldite MY 0510, product data
43. Ciba-Geigy (1987) Araldite MY 720, product data
44. Ciba-Geigy (1987) Araldite MY 721, product data
45. Ciba-Geigy (1990) Araldite MY 722, product data
46. Shell Chemical Co (1988) Techn Bull SC:875–888. Epon HPT Resin 1071
47. Shell Chemical Co (1988) Tech Bull SC:876–888. Epon HPT Resin 1072
48. Patel RD et al (1988) J Therm Anal 34:1283
49. US Patent 4002599
50. Fornes RE et al (1991) Polym. Prepr (2):40
51. Pyun E (1991) Sung CSP. Macromolecules 24:855
52. Eur. Patent 76584
53. Cheng P, Hang LJ (1996) Thermosett Resin (2):42 (in Chinese)
54. Sun YS, Yang W (1990) Thermosett Resin (3): 1 (in Chinese)
55. Lu HB, Fu ZL (1990) J Tsinghua Univ (5): 22 (in Chinese)
56. Zhong XJ (1992) Adhesives (5):11 (in Chinese)
57. Bucknall CB, Partridge IK (1986) Polym Eng Sci (26):54
58. Gilert AH, Bucknall CB (1991) Makrojol Symp 45:289
59. Bennett GS et al (1991) Polymer 9:1633
60. Wang HM, Yi XS (1992) Thermosett Resin (4):35 (in Chinese)
61. ICI Fiberite (1991) 977-2 Epoxy Resin
62. Ciba-Geigy Composite Materials. R6376, product data
63. Hercules. 8552 Epoxy Resin, product data
64. Li B, Tang BM (1996) 5228 research report (in Chinese)
65. Cheng QB (2003) J Aeron Mater (S1): (in Chinese)
66. Zhang FF (1995) J Mater Eng (5):3 (in Chinese)
67. Liang GZ, Gu YJ (1997) Bismaleimide Resin. Chemical Industry Press, Beijing (in Chinese)
68. Zhang BY, Li P, Chen XB (1998) Studies of modified BMI resin (I) the Influence of resin composition on the thermal and mechanical properties. J Mater Sci 33:5683–5687
69. Zhang BY, Chen XB, Li M et al (2002) Discussion on the compression strength after impact of carbon fiber reinforced BMI resin matrix composite. J Aeronaut Mater 22(1):36–40 (in Chinese)
70. Yi XS (2006) Progress of advanced composite. National Defense Industry Press, Beijing (in Chinese)
71. Houben-weyl (1952) Methoden der Organischen Chemie, Vol 8/3, Thieme, Stuttgart: 89 and 125
72. Grigat E, Putter R (1967) Chem A. (International edition) 6(2):206
73. Grigat E, Putter R (1963) (Farbenfabriken Bayer AG). German patent 1195764
74. Grigat E, Putter R (1963) (Farbenfabriken Bayer AG). German patent 1201839
75. Zhou ZHM (University of Leeds) (1993). WO 95/07309
76. Grigat E, Chem A (1972) Chem A (International edition) 11(11):949

77. Stroh R et al (1960) *Angew Chem* 72:1000
78. Martin D et al (1964) *Angew Chem* 76:303
79. Fyfe CA et al (1992) *Macromolecules* 25:6289
80. Lin SC, Elim P (1994) High performance thermosets, Hanser publisher, New York, p 68
81. Shimp DA (1986) *Polym Mater Sci Eng* 58:107
82. Barton JM et al (1991) *Polym Bull* 25:475
83. Osei-Owusu A et al (1991) *Polym Eng Sci* 31(22):1604
84. Shimp DA (Celanese Corporation) (1986) U.S.P. 4, 604, 453; U.S.P. 4, 608, 434
85. Woo EP et al (The Dow Chemical Company) (1985) U.S.P. 4, 528, 366
86. Oehmke RW et al (Minnesota Mining and Manufacturing Company) (1972) U.S.P. 3, 694, 410
87. Osei-Owusu A et al (1992) *Polym Eng Sci* 32(8):535
88. Osei-Owusu A et al (1991) *Polym Mater Sci Eng* 65:304
89. Shimp DA et al (1988) In: 33th International SAMPE symposium, March 7–10, 754
90. Shimp DA et al (1992) In: 33th International SAMPE symposium, March 9–12
91. Marie F, Grenier L et al (1995) *Eur Polym J* 31(11):1139
92. Morio G (1994) *Plym Mater Sci Eng* 71:621
93. Ian H et al (1994) *Polym Mater Sci Eng* 71:807
94. Fyfe CA et al (1995) *J Polym Sci A: Polym Chem* 33:1991
95. Carig, WM Jr (INTEREZ, Inc.) (1987) E.P.O, 269,412
96. Bogan WW et al (1988) *SAMPE J* 24(6):19
97. Shimp DA et al (1989) In: 34th international SAMPE symposium, May 8–11, 222
98. Shimp DA et al (1990) In: 35th international SAMPE symposium, April 2–5, 1045
99. Tanigaichi M et al (1977) U.S.P. 4, 022, 755
100. Delano CB et al (1979) NASA-CR-159724
101. Sung et al (1997) 6th SPSJ Internat Polym Conf 46 (preprints)
102. Korshak VV et al (1980) *Vysokomol Soedin Ser A* 22(8):1714
103. Bauer M et al (1987) *Acta Polymerica* 38(12):658
104. Monnerat GA et al (1989) International SAMPE Electron Conf Sec (4):132
105. Yang PC et al (1990) 35th International SAMPE Symposium, April 2–5, 1131
106. Almen G, et al (1990) 35th International SAMPE Symposium, April 2–5, 408
107. Bao JW et al (1998) First Asian-Australasian conference on composite materials, Oct 7–9
108. Yang HX, Liu JG, Chen JS et al (2006) Synthesis and properties of RMR-type polyimide composites with improved flexibility. *J Aeronaut Mater* 26(3):173–176
109. Zhao WD, Wang L, Dong B et al (2009) PMR-type polyimide matrix composites and their applications. *Aerosp Mater & Technol* 4:1–5
110. Mohamed O, Abdalla Derrick Deana et al (2002) Viscoelastic and mechanical properties of thermoset PMR-type polyimide-clay nanocomposites. *Polymer* 43:5887–5893
111. Conreur C, Francillette J, Laupretre F et al (1997) Synthesis and processing of model compound of PMR-15 resin. *J Polym Sci A: Polym Chem* 35(1):123–136
112. Ding YH (2011) Polymerization approach for polyimide preparation. *Chem Intermed* 5:36–43
113. Allred RE, Wesson SP, Shin EE (2003) The influence of sizings on the durability of high-temperature polymer composites. *High Perform Polym* 15(4):395–419
114. Bowman CL, Sauer JK, Thesken JC (2001) Characterization of graphite fiber/polyimide composites for m applications. *Int SAMPE Symp Exhib (Proceedings)*, 46(2):1515–1529
115. Ahn MK, Stringfellow TC, Bowles KJ (1993) Investigation of stable free radicals in polyimides using EPR spectroscopy. *Mater Res Soc Symp Proc* 305:217–227
116. Morgan RJ, Shin EE, Lincoln J (2001) Overview of polymer matrix composites performance and materials development for aerospace applications. *SAMPE J* 37(2):102–107
117. Pater Ruth H, Curto Paul A (2007) Advanced materials for space applications. *Acta Astronaut* 61(11–12):1121–1129
118. Chen JS, Zuo HJ, Fan L et al (2006) Development of high temperature polyimide. *Aerosp Mater & Technol* 2:7–12
119. Yang SY, Gao SQ, Hu AJ et al (2000) Progress in high temperature polyimide matrix resins and carbon fiber reinforced composites. *Aerosp Mater & Technol* 1:1–6

120. Chen XB, Fu Y, Shen C et al (1998) Study on LP-15 non-MDA polyimide composite. *Acta Mater Compos Sinica* 15(1):7–13
121. Tandon GP, Pochiraju KV, Schoeppner GA (2006) Modeling of oxidative development in PMR-15 resin. *Polym Degrad Stab* 91(8):1861–1869
122. Tandon GP, Pochiraju KV, Schoeppner GA (2008) Thermo-oxidative behavior of high-temperature PMR-15 resin and composites. *Mater Sci Eng, A* 498:150–161
123. Tan B, Xiaosu YI (2001) High-temperature polyimide composites and its application in aeronautical engine. *J Aeronaut Mater* 12(1):55–62
124. Hou H, Wilkinson SP, Johnston NJ et al (1996) Processing and properties of IM7/LARCTM-RP46 polyimide composites. *High Perform Polym*, December, 89(4):491–505
125. Tiwari SN, Srinivasan K (1991) Toughening of PMR composites by semi-interpenetrating networks. NASA Report, NASA-CR-189468
126. Johnston NJ, Srinivasan K, Pater RH (1992) Toughening of PMR composites by gradient semi-interpenetrating networks. 37th Int SAMPE Symp Exhib, 37:690–704
127. Delvigs P (1985) PMR polyimides from solutions containing mixed endcaps. NASA Conference Publication, 23–24
128. Hurwitz FI, Daniel Whittenberger J (1984) Effect of a coating on the thermo-oxidative stability of Celion 6000 Graphite Fiber/PMR-15 polyimide composite. *Compos Technol Rev* 5(4):109–114
129. Mitrovic Milan, Carman Greg P (1996) Effect of fatigue damage in woven composites on thermo-mechanical properties and residual compressive strength. *J Compos Mater* 30 (2):164–188
130. Delaney E, Riel F, Vuong T et al (1992) Preliminary physical, mechanical and toxicological properties of a benign version of the PMR-15 polyimide resin system. *SAMPE J* 28(1):31–35
131. Koenig JL, Shields CM (1985) Spectroscopic characterization of acetylene-terminated sulfone resin. *Polym Sci: Polym Phys Ed* 23(5):845–859
132. Landis AL, Naselow AB (1985) Improved processible acetylene-terminated polyimide for composites. NASA Conference Publication
133. Huang WX, Wunder SL (1994) FTIR investigation of cross-linking and isomerization reactions of acetylene-terminated polyimide and polyisoimide oligomers. *J Polym Sci, B: Polym Phys* 32(12):2005–2017
134. Wu LY (2005) The high performance/high temperature polymer an overview (V) polyimides oligomer terminated with reactive groups and its curing process. *Thermosett Resin* 20(5):41–47
135. Bott RH, Taylor LT, Ward TC (1986) Cure chemistry of acetylene-terminated polyimides. *Am Chem Soc (Polymer Preprints, Division of Polymer Chemistry)* 27(2):72–73
136. Mcdanels DL, Serafini TT, Dicarolo JA (1985) Polymer, metal, and ceramic matrix composites for advanced aircraft engine applications, N86-13407
137. Pratt RD, Wilson AJ (1985) Fabrication process of a high temperature polymer matrix engine duct, N86-11620, 401–407
138. Tan B, YI XS (2001) High-temperature polyimide composites and its application in aeronautical engine. *J Aeronaut Mater* 12(1):57–62

Chapter 4

Composite Structure Design and Analysis

Zhen Shen, Xianxin Tong, Naibin Yang, Mingjiu Xie,
Ye Li and Puhui Chen

4.1 General

4.1.1 Overview

The term advanced composite materials is given to an innovative range of materials that were developed toward the end of the 1960s. These material systems have since found a wide range of applications and continue to be widely developed. Currently, advanced composites, in particular, polymer matrix composites, are widely used in aerospace structures. Such composites are considered one of the four aerospace structural materials together with Al, Ti, and steel alloys.

Reducing structural weight is particularly important for modern aerospace vehicles. Advanced composite materials offer many advantages, such as high specific strength and specific modulus, tailorable performance, good resistance to fatigue and corrosion, and the potential for integrated processing. These factors may permit weight reductions of up to 25–30%, if composites are used to replace conventional metal structures in aerospace applications. Furthermore, air-elastic properties can be considerably improved, which is difficult or impossible to achieve with the use of other materials. Some advanced composites may facilitate stealth and intelligent flight structures in aerospace applications. Owing to their superior performance, advanced composite materials are also widely applied in infrastructures such as bridges and pipelines, and other vehicles including automobiles and

Z. Shen (✉) · X. Tong · M. Xie · Y. Li
Aircraft Strength Research Institute of China, Xi'an, Shaanxi 710065, China
e-mail: Shenzhen623@yahoo.com.cn

N. Yang
Beihang University, Beijing 100191, China

P. Chen
Nanjing University of Aeronautics and Astronautics, Nanjing, Jiangsu 210016, China

ships. Applications of composite began in aerospace structures. Hence, resources for design and analysis of advanced composite materials have been adopted from aerospace experiences to benefit other transportation industries in both military and commercial sectors.

4.1.2 Applications of Advanced Composite Materials in Aircraft Structures

In the USA and Europe, development of advanced composite materials began in the 1960s and was first applied in the early 1970s. Fighter jets in service in the 1980s used advanced composite materials in their wing and tail structures, comprising 20–30% of the total aircraft weight. The wing structures of the stealth B-2 developed in the 1980s was made up of ~60% composite materials.

Applications of advanced composite materials in civil aircraft proceeded more cautiously because of safety and cost considerations. To promote confidence in composite technologies for civil aerospace applications, many programs were implemented in the USA in the 1970s. These include the Aircraft Energy Efficiency (ACEE) and Advanced Composite Technology (ACT) programs, and the Composite Affordability Initiative (CAI). In Europe, the Technology Application to the Near-Term Business Goals and Objectives (TANGO) project was initiated with the aim of producing composite wing and fuselage components at a competitive cost. In the recently launched A380, A350, and Boeing 787, contributions of advanced composite materials to the structural weight were 22, 52, and 50%, respectively.

In helicopters, the use of composites has reached 50–60% of the total structure weight in military helicopters. Advanced composite materials make up 41% of the structural weight of the US RAH-66. The vertical landing and tilt rotor V22 Osprey contains up to 51% composite materials by weight and is considered to be a full-composite vehicle. To date, many small full-composite airplanes have been launched. Among these, the well-known passenger-goods dual-purpose “ship star” has passed the airworthiness certification. The world-famous “voyager” has set the world record for a continuous flight around the world without refueling or landing. These successes are an excellent showcase for the effectiveness of advanced composite materials.

In China, research and development of advanced composite materials and their applications in aircraft structures were initiated in the late 1960s. In the mid-1970s, the first composite structural components were successfully used in the air duct wall of aircraft fighter. In 1985, a jet fighter with a composite vertical tail made its first flight. In 1995, a composite wing with an integrated fuel tank was successfully developed. This advance marked a new milestone in composite material applications in aircraft structures in China. Almost all aircraft currently in service now use composite parts to some extent. In 2000, the commercial airplane-Y7, with a

composite vertical tail, passed the airworthiness certification ushering in a new era of composite material applications in civil aircraft. Many large-scale commercial aircrafts currently being planned will feature large proportions of advanced composite materials. Applications of composite materials in helicopters have also considerably advanced. Imported manufacturing technologies have been replaced by native design approaches to next generation helicopters in China.

4.1.3 Properties of Advanced Composite Materials

4.1.3.1 Structural Performance

(1) Specific strength and specific modulus

Carbon fiber/epoxy resin composites are most often used in aircraft structures. The use of these materials can greatly reduce the structural weight because of their high specific strength (σ_b/ρ) and specific modulus (E/ρ). In Table 4.1, the performance of unidirectional composites and conventional metals is compared. The advanced T800/modified epoxy resin can, respectively, provide specific strength and specific modulus 10 and 4 times as high as that of aluminum alloys [1, 2].

(2) Anisotropy and tailorable performance

Currently, laminated structures, prepared by unidirectional prepreg laying-up and curing, are the main materials used in aircraft structures. Unidirectional prepreg tapes are strongly orthotropic, i.e., performance in the fiber direction is different to that vertical to fibers. To satisfy the performances requirements in specific directions in a structural plane, it is necessary to place unidirectional tape in different directions at certain ratios. The designed laminates may be either isotropic or anisotropic and may be either symmetrically balanced or asymmetrically balanced. This unique feature offers considerable flexibility to designers. The use of low-density advanced composite materials requires new structural design methods to be applied at an early stage to fully take advantage of the properties of composite materials. Composite forward-swept aircraft wing and the zero thermal expansion coefficient structures are typical applications of laminating anisotropy, which offers tailorable performance. However, anisotropy also presents some challenges for structural design, analysis, and manufacture of composite structures.

Another characteristic of composite laminate anisotropy is that interlaminar performance is typically much lower than that in-plane. There are also large differences in the performance of different constituents, i.e., the mechanical properties of the fiber and matrix. These factors typically contribute to failure mechanisms of laminated composite structures, which are to very different from those of metal structures. Impact damage and delamination are key design considerations.

Table 4.1 Comparison between composite and metal materials

Materials	T. strength/MPa	T. modulus/GPa	Specific strength/MPa·g ⁻¹ ·cm ³	Specific modulus/GPa·g ⁻¹ ·cm ³	Density/g·cm ⁻³
Al alloy	420	72.0	151.1	25.9	2.78
Steel (structure)	1200	206.0	152.9	26.3	7.85
Ti alloy	1000	116.7	221.2	25.8	4.52
H.S/C/epoxy	1471	137.3	1014	94.7	1.45
H.M/C/epoxy	1049	235.0	656.0	146.9	1.60
Kevlar/epoxy	1373	78.4	981.0	56.0	1.40

(3) Damage, fracture, and fatigue behavior

Features of advanced composite materials often include anisotropy, brittleness, and inhomogeneity. These features, and the inferior interlaminar properties compared with those in-plane, cause the failure mechanisms of laminate composites are very different from those of metals. Their damage, fracture, and fatigue performances are also very different. Although the laying-up and autoclave processing used for composite components is simple, impacts by foreign objects during machining and delivery are more likely to damage or induce defects in composite parts than equivalent metal parts. Table 4.2 summarizes the fatigue and damage tolerance of metal and composite structures.

- ① Main defect/damage types: Cracks are the main damage mode of metal structures. For composite structures, the critical defect/damage modes include interlaminar debonding, delamination, and low-energy (low-speed) impact damage. Impact damage can cause critical damage to composites by significantly decreasing their actual compression load-bearing ability. While no visible damage may be apparent from inspection of the outer surface, impacts may induce cracking of the internal matrix or delamination. Visible checks are only reliable once the compression strength has decreased to 40% of its original value after an impact. Delamination is a unique damage mode of laminated composites. Impacts from tools, and foreign bodies such as runway chippings, hail stones, and birds, together with the local interlaminar stress concentration and over-loading, may all contribute to internal delamination. The occurrence and growth of this type of damage greatly reduce the strength and stiffness of laminate components.

Table 4.2 Comparison of factors affecting fatigue and damage tolerance

Content		Metal	Composites
Main damage cause		Fatigue, corrosion and stress corrosion	Foreign impact, processing defects
Critical damage		Crack	Impact damage/delamination
Danger loads		Tensile	Compression
Stress-strain behavior		Show yielding	Linear until final failure
Notch sensitivity	Static strength	Insensitive	Very sensitive
	Fatigue	Very sensitive	Insensitive
Damage check before failure		Possible for visible check	Impossible for visible check
Damage growth		Along main crack with regularity	Multi-damage propagation without regularity
Dispersion for static and fatigue strength		Small	Large

- ② Notch sensitivity: Generally, metals possess a yielding stage; however, composites typically show a linear stress–strain curve up until final failure occurs. Hence, composites have much higher static strength notch sensitivity than metals. Conversely, composites show much lower fatigue notch sensitivity than that of metals. The fatigue notch coefficient (i.e., the ratio of the fatigue strength between a non-notched and notched specimen under a certain number of fatigue cycles) is much smaller than the static stress coefficient and close to 1 over the long term.
- ③ Fatigue performance: Metals are often sensitive to fatigue. For notched structures, in particular, the fatigue strength will quickly decrease under a tensile–tensile fatigue load; composites can offer much better fatigue resistance. Fiber-dominated multi-direction laminates can pass 10^6 cycles in a tensile–tensile fatigue test under a maximum stress equal to 80% of the ultimate tensile load. Under tensile–compression, or compression–compression fatigue, the fatigue strength decreases slightly; however, after 10^6 cycles the fatigue strength remains at approximately 50% of the static strength value. For notched specimens subjected to compression–compression fatigue tests, the fatigue strength corresponding to 10^6 cycles will be greater than 60% of the static strength. Although impact damage and delaminated composites do not usually show crack growth under high fatigue loads, such damage may occur at later stages of the component life. It remains challenging to determine the probability of crack propagation in composite materials.
- ④ Stiffness reduction: For metal structures, the stiffness changes caused by fatigue load are usually not accounted for; however, this factor must be considered for composite structures bearing high-cycled fatigue, in particular, helicopter components such as rotor blades.
- ⑤ Dispersion: The dispersions in static strength and fatigue strength for composite materials are more than for metals. So, not only the life dispersion coefficient, but also the load enlarging coefficient should be considered in composite structure fatigue certification.

(4) Environmental effects

Besides extreme high temperatures, the effects of hot/wet environments on metals are generally not considered. For composites, the combination of environmental effects must be carefully considered. Composite matrices are made of polymer materials, which can be affected by heat and moisture. The glass transition temperature (T_g) of a composite may be decreased on environmental exposure resulting in a considerable decrease in matrix-dominated mechanical properties, such as compression and shear. Although corrosion is a serious problem for metals, composites typically show good corrosion resistance.

(5) **Electrical Conductivity**

Compared with metals, composites have very low electrical conductivity. Special lightning-proof measures must be considered in composite component design and special attention should be given to the oil tank design and to avoid static electrical shocks to compartments containing electrical instruments and devices.

4.1.3.2 Structure Design and Processing

Metal airplane structures usually consist of parts such as the skin, beams, stringers, rib, and frame. These parts are mechanically assembled with a large quantity of fastening components. Metal parts can be processed by machining, rolling, forging, casting, and welding.

For composites, the material and structure can be manufactured simultaneously. Structural elements can be connected simultaneously with material processing through co-curing, knitting, braiding, and Z-pin technologies. Thus a large and integrated structure can be designed and manufactured in one time. The number of elements and fastening parts as well as the machining and assembling work can be greatly reduced. Hence, the structure weight and production costs can be considerably reduced. Owing to the above features, integration of design and processing is a serious concern for composite structures.

4.1.4 Overview of Composite Structure Design and Certification

4.1.4.1 Design Essentials

According to specifications for composites in military or civil airplanes applications, the design and certification of composite aircraft structures involve the following working phases: structural materials selection, determination of design allowables, structural type selection, quality assurance, and building block approach (BBA) certification. The composite structure design workflow includes the following steps [1, 2].

(1) Material selection

In addition to a material's fundamental properties, processing ability, and cost, for composite part design, the toughness, i.e., compression strength after impact (CAI), and the maximum service temperature and environmental effects should also be considered.

(2) **Determination of design allowables**

A typical laminating code and skin thickness are used for testing and determination of the design allowables. Critical issues include the structural properties of laminate specimens with typical stacking, such as compression failure strain, open hole tensile/compression, filled hole compression failure strain, and assembly allowables. Furthermore, the effects of heat and moisture should be included, as well as fatigue properties. Defects are unavoidable in composites, and initial defects (in particular impact damage) can greatly affect the strength of the component. Thus, the effect of initial defects should be considered even if the design allowables only consider the static strength certification.

(3) **Structure type selection**

On the basis of the structure design requirements and an outline of the external load conditions, proper structure types are selected. If necessary, selection tests should be performed to determine the optimized structure type. For the critical damage tolerance locations, the structures should be designed with the ability to resist impact damage. In the detailed design, special attention should be paid to out-of-plane loads that could be applied to the structures. Care should also be taken for open hole strengthening design. Honeycomb structures and thin skin structures, are susceptible to impact damage and should receive special attention.

(4) **Certification of typical structures and assemblies with key structural features**

BBA certification tests, from simple to complex in different phases, can verify that a selected structure type can meet the design requirements in key areas. The durability/damage tolerance of the composite components should be verified in this phase particularly for blended metal/composite structures.

(5) **Full-size part certification**

To verify that a part meets its structural integrity requirements, full-size part static strength verification is typically performed. The durability and damage tolerance of metal structures in blended metal/composite structures are assessed.

4.1.4.2 Affordability of Composite Structures in Low-Cost Design and Manufacture

Although composites can satisfy the high-performance requirements of aircraft structures and effectively reduce the structural weight, processing of this material is expensive. In large-scale aerospace applications, lowering the cost of design and manufacture are key goals of composite research. Currently, areas for cost-saving in composite technologies include lowering the cost of materials and molding. Automatic fiber placement technologies have also been developed, including automated tape-lying (ATL), automated tow placement (ATP), and liquid

composite molding (LCM), such as resin transfer molding (RTM), resin film infusion (RFI), and vacuum assisted RTM (VARTM). More affordable ACM structures have received considerable attention for integrated structure design and manufacture.

4.2 Requirements of Structure Design

4.2.1 General Requirements of Structure Design

The following requirements should be satisfied in composite structure design, in addition to the general requirements for metal structure design.

- ① Co-curing, knitting, or adhering should be used as much as possible to reduce the number of components and eliminate stress concentration sources. Structure integration should be considered as much as possible to take full advantage of composites. For large parts, it is also necessary to consider delivery and repair.
- ② Out-of-plane loading should be avoided as much as possible in composite structures. Special attention should be paid to the out-of-plane load caused by off-axis or structural deformation.
- ③ It is necessary to consider the detectability of damage in manufacture and service. If reliable inspection methods are not available, the potential for large defects or damage should be considered in the design.
- ④ Environmental effects on materials should be considered, including heat, moisture, and the largest potential impact damage that may be encountered in service.
- ⑤ If all the possible failure modes have been considered, buckling or twisting may be allowed in thin laminated composites; however, buckling in thick laminates should be avoided.
- ⑥ Owing to the lower conductivity of composites than that of metals anti-static electrical, lightning proofing, and electromagnetic compatibility design and certification should be performed for certain parts of the airplane to satisfy the safety requirements.
- ⑦ The cost of the design should be considered at all phases of the structure design.

4.2.2 Requirements of Military Aircraft Structure Design

4.2.2.1 Static Strength

The static strength design requirements of metal structures can also be applied to composite structures. Additional special requirements for composite structures include: the combined effects of operation temperature and moisture absorption to

determine the allowables for the composite structures. The uncertainty coefficient used in this case (the original safety coefficient) will remain as 15. The strength of composite structures is related to the laminating code, geometrical shape, and applied load. Hence, these factors should be also considered in the determination of B-allowables. Large numbers of complex structural tests are used to determine which of the B-allowables of composite structures are not applicable. It is acceptable to use a specimen that can replicate the structure laminating code, geometrical shape, and load to determine the B-allowables.

4.2.2.2 Durability

(1) General requirements

The durability design requirements of metal structures can be generally be applied for composite structures. The key consideration for composite durability design is to control the matrix strain level. Unlike metal structures, the fatigue life and corrosion are not major factors to consider in the design of composite structure durability; however, for the impact damage resistance, the following requirements should be satisfied:

- ① The design should allow for checking and repair of damage caused by low-energy impacts such as tool dropping.
- ② Special attention should be paid to the organic polymer matrix composites, taking into account damage induced during services such as low-energy impacts, and the potential for damage during production, delivery, and maintenance. The repair of damage, maintenance, and function of the component should be carefully investigated.
- ③ It should be confirmed that no invisible surface defects exist, which may contribute to performance degradation of a part, requiring repair.
- ④ It should be confirmed that any impact will not result in damage to structures that may become critical over two designed life cycles under typical environmental conditions.

(2) Requirements for impact damage resistance

- ① Tool impact: On the basis of the probability of tool impact occurring, composite structures can be divided into two categories. The different structural requirements in durability design of these two structural zones are listed in Table 4.3.
- ② Hail stones and runway chippings: There are two possible impact sources that could bring about serious effects to structures; hail stone impacts during parking time, and stone impacts during aircraft movement on a runway. The selection of hail sizes will depend on the aircraft capacity and should cover a range greater than 90% of possible hail

Table 4.3 Low-energy impact damage and durability testing requirements (tool impact)

Zone	Damage source	Damage level	Requirement
Zone 1 Easily impacted	Impactor diameter, in 12.7 mm low speed	Impact energy less than 8.1 J, or visible damage (energy not below 5.5 J)	No functional problems, no need for structure repair, and no water leakage over two designed life cycles
	Vertical to surface		No visible damage caused by a single impact of 5.5 J
Zone 2 Not easily impacted	Same as zone 1	Impact energy less than 8.1 J, or visible damage	No functional problem over two designed life cycles, no visible damage, no water leakage after site repair

Table 4.4 Low-energy impact damage and its durability testing requirement (hail stones and runway chippings)

Zone	Damage source	Damage level	Requirement
All vertical surfaces and upward horizontal surfaces	Hail: Diameter: 20.3 mm Specific weight = 0.9 27.4 m/s Vertical to horizontal surface 45° angle with vertical surface	Uniformly distributed Central distance between impact points 20 mm	No functional problem over two designed life cycles, no need for structure repair No visible damage
Possibly impacted structures	Runway: Diameter: 12.7 mm Specific weight = 3 Equivalent to aircraft speed	None	No functional problem over two designed life cycles, no visible damage, no water leakage after site repair

stone sizes. The majority of stones that will likely be encountered by aircraft moving on a runway will be small and the speed of their impact will depend on the aircraft performance. In Table 4.4 the requirements of durability design for these two impact sources are given.

- ③ Load from operation and stampede: Apart from the impact load, it is necessary to consider the resistance on the operation and pedal loads encountered in manufacturing processes or in a service environment. The requirement on loads should be considered as follows:
 - a. Operation load:
 - Very difficult to reach, i.e., finger touching.
 - Easy to reach from top, i.e., one-hand catching and hanging.
 - b. Pedal load:
 - Very difficult to reach, i.e., difficult to stand on structure with one foot.

Easy to reach from top, i.e., two feet can be placed on the structure.
Note: It is necessary to define the contact zone, position, and weight related to each of the conditions above.

(3) Honeycomb sandwich structure control

This type of structure should be used in design elements requiring very light weight, and in parts that can be easily replaced or be accessible for repair. These structures are not permitted for use in environments exposed to water or for parts that require immediate replacement. The impact energy level acceptable for this kind of structure could be appropriately decreased, for example, to the level where no visible damage 2.5 mm in depth or penetration could be produced by an impact of 0.5–0.7 J.

(4) Damage sensitive zone and details

Special care should be paid to some damage sensitive zones of the airplane, including the lower fuselage and the radome, inside the flap lower surface, and cabin doors. These zones need to be strengthened with thicker structures, possibly using glass-fiber to replace carbon fiber. Furthermore, the potential for a tire burst necessitates special attention to be paid to the damage sensitivity of the tire zone. Similar structures include components near the jet thrust reverser, which are sensitive to damage from ice and debris on the runway.

- ① Minimum-weight structure: Components such as the radome structure may not operate if the weight is designed to be too small. Another example is sandwich structures with low core density. The surface plates should have the minimum required thickness built into the design to prevent water invading the core. Surface coatings should not be considered as the only water resistance measure. Coatings may become corroded or abraded exposing the component to water.
- ② Joints of thin skin honeycomb sandwich structures are easily damaged during assembly and disassembly. Thus, it is necessary to use solid laminated structures in appropriate joining areas.
- ③ The rear edge of control surfaces is very sensitive to damage, the area located 102 mm from the back may be easily damaged by ground impact, loading and unloading impact, or by lightning strikes. These components are difficult to repair because of the need to strengthen the skin and the rear edge. It is acceptable in the design to add a load-bearing element to resist the load ahead of the rear edge. The rear edge itself or its surface should be reinforced with a material that is easily repaired, which will not endanger the functional parts when damaged. Considering the possibility of cracking leading to sealing problems, sealing agents should not be used at the ends of components.
- ④ The edge of laminates should not be directly exposed to an air stream to avoid delamination.

Possible measures include:

- (a) Use of corrosion-resistant edge protection, such as co-cured metal edge element.
- (b) Use of an easily replaced sacrificial material to wrap the edge.
- (c) The pre-cruise edge of wall plates should be placed in a lower position than the after-air edge of adjacent preceding wall plates.

4.2.2.3 Damage Tolerance

Damage tolerance design principals of metal structures can generally be adopted for composite aircraft structures. The major source of damage to composite structures is impact damage. The feature of impact damage is that damage may not be visible on the component's surface, but underlying delamination can considerably decrease the compression strength of the component. Composite structures are defined as undetectable structures in design. In this section, some particular requirements of composite structures are outlined [1–3].

(1) Assumption of defect dimensions

The damage tolerance of a component containing a defect should be sufficient that the component has enough residual strength over the specified operation period. Here defect refers to both initial and service defects. Defects caused by foreign low-speed impacts can occur at any time during service, including directly after being put into service. It is very difficult to detect such defects visibly over the service time, and thus, this type of defects is defined as an initial defect for the purposes of damage tolerance analysis and certification.

- ① Initial defect size assumption: Initial defects may be divided into three types: impact damage, delamination, and scratches.
 - a. Impact damage: Considering the features of composite impact damage, composite structures are defined as undetectable structures to ensure structure safety. The initial defect size can be determined by the basic concept defined as barely visible identification (BVID). The following standards can be used in general cases:
 - (a) The BVID dent caused by a half-sphere impactor with 25.4-mm diameter (depth less than 2.5 mm).
 - (b) The damage caused by a half-sphere impactor, with 25.4 mm diameter, at the maximum energy possibly encountered in service (typically less than 136 J).

The required energy for a BVID dent is related to the structure thickness. The former of the conditions mentioned above is used for medium thickness structures (less than 6 mm), while the latter is used for thicker structures (greater than 6 mm). For general cases, the smaller value is selected from the above two conditions.

When structures are not exposed to external impact or under threat of damage or the parts can be checked carefully before the structure is closed a lower impact damage requirement can be adopted. To pass certification under such decreased impact energy criterion, the proposed impact energy should be approved by the users; the impact damage, including damage which expanded to critical dimensions over a two-life-cycle spectrum load, can be detected by NDI techniques that have been verified for manufacture acceptance.

b. Delamination and scratches: The initial defect/damage size assumptions can be selected from Table 4.5.

- ② Service damage size assumption: Service damage refers to visibly detectable damage caused by high-energy impacts with foreign objects such as bird impacts or lighting strikes. The size assumption for this kind of damage should be determined and analyzed supported by testing.

(2) Residual strength requirements

The structural residual strength should meet the following requirements:

- ① Initial defect-contained structures: The requirement for residual strength of composite structures containing initial defects is specified in the section above and is the same as those for metal structures, i.e., the ability to stand a maximum load occurring over 20 life cycles. If the load is smaller than the limit load, the residual strength should meet the requirements of the retaining load. If this load is larger than the limit load, it will not be restricted by 1.2 times the maximum load occurring over the structure life. This requirement is different from that of metal structures.
- ② Service defect-contained structures: The requirements are the same as those of metal structures.

(3) Damage propagation requirements

Usually, composite structures are considered as slow-growing “crack” structures. No damage propagation models are currently used. In general, the absence of damage propagation should be verified by analysis supported by testing. Fatigue tests of small parts, elements, or substructural components may be used. Cycle numbers of zero damage propagation should consider the dispersion of the composite fatigue data and environmental effects. If structures designed with no consideration of damage propagation show obvious defects or damage at inspection intervals, the component should be re-designed.

Table 4.5 Initial defect assumption

Defect/damage	Defect/damage dimensions
Scratch	Surface scratch of 100 mm in length, 0.50 mm in depth
Delamination	Delaminated area equal to a circle 50 mm in diameter

4.2.3 Requirements for Civil Aircraft Structure Design

The requirements for military aircraft structure design are generally suitable for civil aircraft with the following differences.

4.2.3.1 Advisory Circular AC 20-107A “Composite Structure”

Some items involved in AC 20-107A “Composite Structure” are given below. (The following has been simplified, the reader can refer to the original.)

5.d Impact damage is generally accommodated by limiting the design strain level.

6.g It should be shown that impact damage that can be realistically expected from manufacturing and service (but not more than the established threshold of detectability) for the selected inspection procedure will not reduce the structural strength below ultimate load capability.

7. Verification of structure fatigue/damage tolerance: The evaluation of composite structure should be based on the applicable requirements of FAR 23.571, 23.572, 25.571, 27.571, and 29.571. The following considerations are unique to the use of composite material systems and should be observed for the method of substantiation selected by the applicant. When selecting the damage tolerance or safe life approach, attention should be given to geometry, inspectability, good design practice, and the type of damage/degradation of the structure under consideration.

(1) Damage tolerance (fail-safe) evaluation.

- ① Structural details, elements, and subcomponents of critical structural areas should be tested under repeated loads to define the sensitivity of the structure to damage growth.
- ② The extent of initially detectable damage should be established and be consistent with the inspection techniques employed during manufacture and in service. Flaw/damage growth data should be obtained by repeated load cycling of intrinsic flaws or mechanically introduced damage.
- ③ The extent of damage for residual strength assessments should be established. Residual strength evaluation by component or sub-component testing or by analysis supported by test evidence should be performed considering that damage.
- ④ An inspection program should be developed consisting of frequency, extent, and methods of inspection for inclusion in the maintenance plan.
- ⑤ The structure should be able to withstand static loads (considered as ultimate loads) which are reasonably expected during a completion of the flight on which damage resulting from obvious discrete sources occurs (i.e., uncontained engine failures).

- ⑥ The effects of temperature, humidity, and other environmental factors which may result in material property degradation should be addressed in the damage tolerance evaluation.
- (2) Fatigue (safe-life) evaluation fatigue substantiation should be accomplished by component fatigue tests or by analysis supported by test evidence, accounting for the effects of the appropriate environment. The test articles should be fabricated and assembled in accordance with production specifications and processes so that the test articles are representative of production structure. Sufficient component, subcomponent, element, or coupon tests should be performed to establish the fatigue scatter and the environmental effects.

4.2.3.2 Differences from Military Aircraft Requirement

(1) Residual strength level

For civil aircraft structures with defects and damage that have not been detected during manufacture and in service, the structure should be able to withstand the ultimate load in its expected life, without any effects on its operation function. For military aircraft structures, the requirement is lower; the load to be withstood will be the maximum internal element load occurring once in 20 life cycles of undetectable structures [1–5].

(2) Initial defect dimension assumptions

For military aircraft, the impact damage dimension is clearly specified, either as the maximum impact energy (136 J for thicker panels), or by the defined dent depth detectability (deep dent in 1.5 mm for thin panels). For civil aircraft, there is no such specification, and it is defined only by the impact damage that can be realistically expected from manufacturing and service (but not more than the established threshold of detectability). Although a visual check is not specified for inspection, it is commonly used, and lighting should be considered. Some civil aircraft composite structures (such as the horizontal stabilizer box in the Boeing 7J7) have used the military aircraft initial defect dimension assumption. This is currently based on a statistical analysis, and a smaller initial defect size assumption has been adopted, i.e., 0.3–0.5 mm. A smaller impact energy cutoff value (36 J) has also been certified by the FAA.

(3) Particular conditions for adhesive joint damage tolerance (with reference to military aircraft)

If currently available manufacture technologies cannot ensure each adhesive joint can meet its designed strength, and NDI cannot detect debonding and weak adhering defects, one or two of the methods described below should be used to

verify the adherence of any joint regarded as a key safety flight element and any joints that have a load-bearing ability not lower than their design limit load:

- ① Use analysis, testing or both to determine the maximum acceptable debonding area of each joint under the load in the most serious case. The detailed design should avoid the possibility of debonding over a greater area.
- ② Proof testing should be performed for each end product, i.e., the largest potential load should be applied to each key adhered joint.

4.2.3.3 AC20-107A Conformity Requirements

(1) Static strength [1–6]

- ① The impact damage possibly occurring during manufacture and in service should be considered as inherent damage of the structure to be assessed. It is necessary to consider locations where a tool box or repair tool may drop and impact.
- ② Evaluation of the static strength should include the expected critical failure areas, the corresponding failure mode, and the strain level. If the failure modes under the expected different environmental conditions (such as R.M. Dried and hot/wet) have the same probability of occurring, these two ambient conditions are both needed for verification, or one case should be eliminated from the design, without implementing verification.
- ③ Special attention should be paid to out-of-plane loads caused by design elements such as local thickening, which could induce early damage.

Figure 4.1 shows a flowchart of composite structure static strength verification, in which the items in brackets are cited from AC 29-107A.

(2) Damage tolerance

In establishing structure verification plans, the damage tolerance requirements of FAR AC25.471 and Item 7(a) in AC20-107A should be considered. Figure 4.2 is a flowchart for composite aircraft structure damage tolerance evaluation, in which the items in brackets are cited from AC 29-107A.

For example, the following aspects should be verified:

- ① Accidental damage (Failure-Safety) evaluation: Serious accidental damage (Failure-Safety) evaluation should be performed. The primary structural components or part of primary structure components should be cut off to verify that the other structures can withstand design load limits.
- ② Check intervals: By following the intervals defined by 7.a(4) in AC20-107A, the possibility of a missed inspection should be considered in the regular damage inspection.

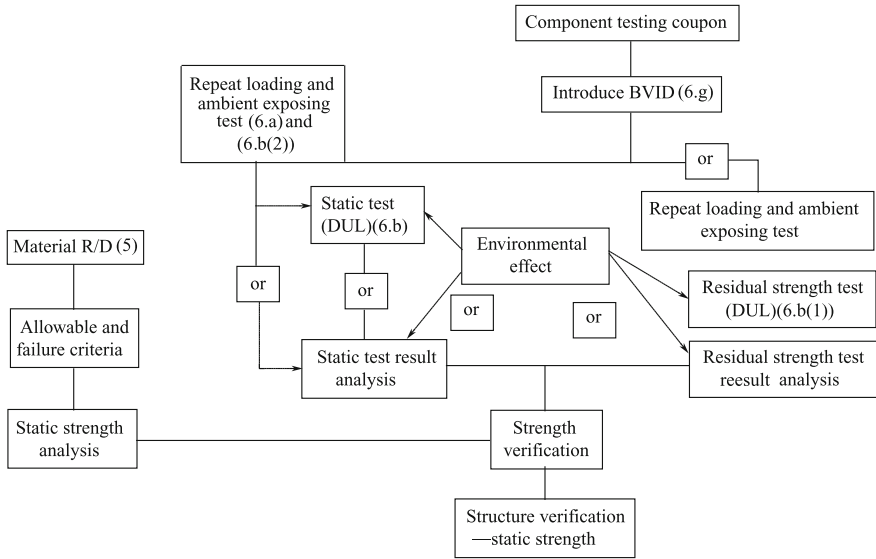


Fig. 4.1 Flowchart of composite structure static strength verification

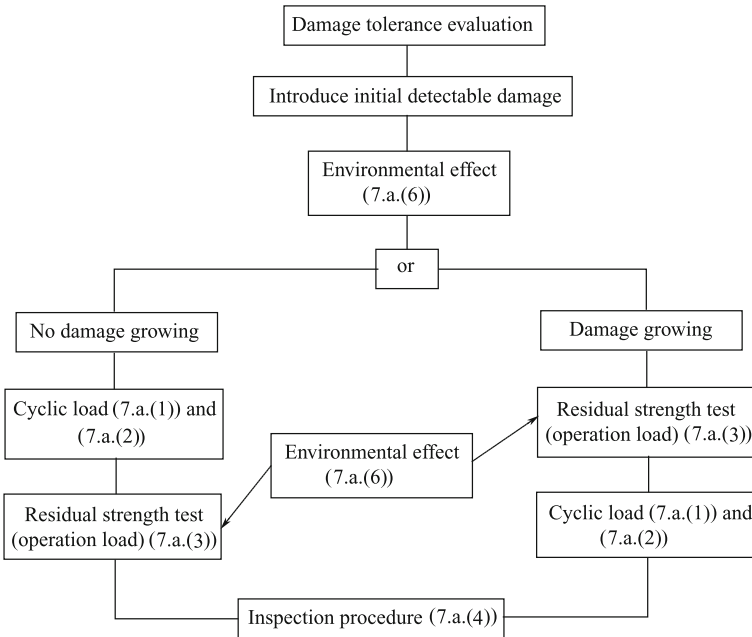


Fig. 4.2 Flowchart of composite structure damage tolerance verification

- ③ The load spectrum and load removal method as well as all other aspects related to damage tolerance evaluation should be written into testing programs, and submitted for FAA certification.
- ④ The B-allowable repeated load verification on flight safety redundant structures as well as the single-load transferring route structures should have Failure-Safety capacity. Here, the Failure-Safety capacity refers to the capacity to withstanding the designed limit load after a major part of a single-load transferring route structure is damaged.
- ⑤ Ice hail impact should be included in damage analysis items.

4.3 Material Selection in Structure Design and Structural Processing

4.3.1 Principles of Structural Material Selection

4.3.1.1 General Principles

- ① We should prefer materials with adequately characterized performance, service experience, and reliable supply sources as much as possible. If a new material that has been used in structures, is selected, it should pass “building block approach” verification including element, typical component, and structural assemble tests, according to the structure production [2].
- ② Similar to metal materials, we should select cheap materials when possible if structural integrity can be satisfied. The cost assessment should cover the following aspects: material cost, processing cost (consider processing feasibility, processing temperature and pressure, as well as the requirement for auxiliary materials) and maintenance costs.
- ③ Materials should have good processing ability. Consider processes such as curing, machining, and repair. Processing and curing performances include: resin viscosity, tack and drape, curing method, temperature and pressure, pressure applying window, shelf life, and flow ability.
- ④ Materials should meet the requirements of the service environment and mechanical properties of structures, including:
 - (a) The service temperature should be higher than the maximum operation temperature of the structure. Under most ambient operation environments (hot/wet), the mechanical performance cannot obviously decrease, and should remain stable in long-term service.
 - (b) Can resist impacts, including impact damage resistance, as well as the residual strength after defect/damage.

- (c) Open-hole tensile and compression strength, and joining bearing strength.
 - (d) Fuel resistance, anti-medium, aging resistance, sand abrasion, and rain corrosion proof.
- ⑤ Materials should meet some special requirement in certain structures.
- (a) Requirements for electromagnetic performances such as electromagnetic shielding, overlap resistance.
 - (b) Requirements as fire retardants, smoke and toxic release behaviors.
 - (c) Good compatibility with related materials.
 - (d) Low input to ensure environment protection.

In general, it is necessary to select resins and fibers of different types and grades to meet the requirements of different applications and structures, even at different locations within the same structure. This allows materials to be utilized to their full potential to reduce costs. Avoid over estimation of the temperature and toughness, which may increase the material and production costs.

4.3.1.2 Property Data Sources

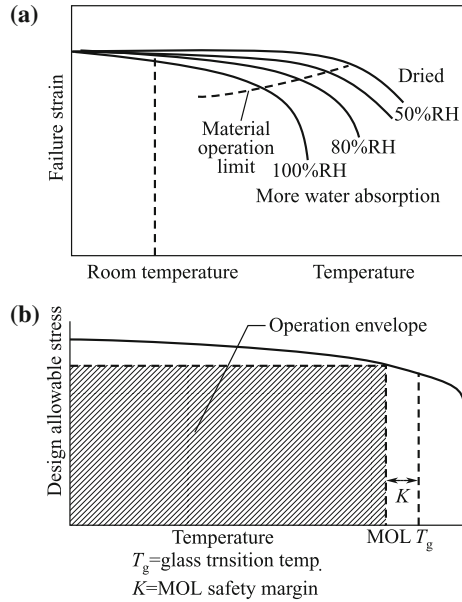
Data sources for mechanical properties of composite materials system and sandwich composite should be authorized and approved for design purposes. The adopted data should meet the following requirements:

- ① Performance characterization based on statistics should be used to establish design data.
- ② All factors affecting the required strength, stiffness, and reliability should be adequately considered in performance characterization, especially the combined action of moisture and high temperature, as well as the effect of defects/damage possibly occurring during manufacture or in service (mainly open hole and low-speed impact).

4.3.1.3 Evaluation of Replacement Materials

- ① Before using replacement materials in production, an evaluation of the equivalence of the replacement and original materials should be performed in accordance with related standards, to ensure no harmful effects on structural performance.
- ② Changes in the original material constituents, material formula, elimination of a processing step, use of alternate processing equipment, or other procedure change should be considered as a major modification, and properties of the new material should be re-evaluated. The necessary evaluation of the effects of changes should be performed in accordance with related standards, to ensure no harmful effects on the structural performance.

Fig. 4.3 Material selection criterion after considering the effect of hot/wet ambient conditions. **a** Temperature/wetness effect on the matrix-dominated failure; **b** Material selection criterion



4.3.2 Environmental Effects of Material Performances

The properties of composite materials are resin matrix-dominated and sensitive to ambient conditions. To reduce environmental problems in a verification program as much as possible, it is necessary to consider environmental effects in the material selection phase of structure design. The materials selection should be performed based on the relationship between the aircraft hot/wet envelope and the material’s maximum operation temperature or material operation limit (MOL). The material’s maximum operation temperature can be defined as shown in Fig. 4.3. The gray area indicates the material operation envelope, in which the aircraft operates.

The envelope helps guide the selection of materials that can be used under typical normal conditions, and environment issues in the verification program to be reduced. The difference K between the glass transition temperature T_g under the maximum moisture absorption conditions and MOL is defined as the basis for the determination of the maximum operation temperature. The determination of a K is related to design considerations. For an epoxy resin matrix, the K value will be no less than 30 °C.

4.3.3 Selection and Use of Matrices and Fibers

Resin matrices have an important influence on mechanical properties of composites. The transverse performance, compression, and shear properties are all resin

Table 4.6 Comparison of commonly used resin matrices and their performance

Performance	Resin				
	Epoxy	Phenolic	BMI	Polyimide	High performance thermoplastics
Processing ability	Excellent	Good	Good	Bad	Good
Mechanical property	Excellent	Medium	Excellent	Good	Excellent
Heat resistance (°C)	Below 130	Below 177	Below 230	Above 288	Above 120
Toughness	Good	Bad	Good	Bad	Excellent
Dimension stability	Excellent	Excellent	Excellent	Excellent	Excellent
Cost	Low	Low	Medium	High	High

dependent. Toughened resin can improve the damage resistance of a composite, and absorb energy simultaneously.

Composite performances such as heat resistance, aging resistance, fire retardant, hot/wet behavior, anti-corrosion, and electromagnet performance are mainly determined by the resin matrix.

Composite processing abilities such as rheological properties, tack and drape, gel time, prepreg shelf stability, processing temperature, pressure, and time are also directly dominated by the resin matrix. Common requirements of advanced composite resin matrices are: high strength, good toughness, medium-proofing, low processing temperature and pressure, long prepreg shelf life, a wide applied pressure window, low cured shrinkage, low toxicity, and suitability for prepreg solution or melting preparations. The performances of commonly available resin matrices are given in Table 4.6.

Reinforcing fibers offer composites with high strength and moduli and can also greatly increase damage resistance. Fiber selection should be optimized through a combined evaluation of performance and cost. Table 4.7 lists some aspects to consider for fiber selection. Table 4.8 includes data on environmental effects on the materials.

4.3.4 Structural Processing Ability

Structural processing ability includes the ability to use cure processing and assembling processing methods. Different processing methods have different requirements and different structural processing capabilities. Critical issues in considering structural processing capability will vary depending on the structure, so it is important to select a proper curing processing method during design. The curing process of a composite structure can be simultaneously completed with the

Table 4.7 Evaluation of different fibers

Criterion	Powering factor 1–3	Nominated value for different fiber powering		
		Carbon fiber	Kevlar	E-glass-fiber
Tensile strength	3	9	9	9
Compression strength	2	6	0	4
Modulus	3	9	6	3
Long-term performance	3	9	6	3
Fatigue properties	2	6	4	2
Density	2	4	6	2
Alkali proof	2	6	4	0
Price	3	6	6	9
Total		55	41	32

Table 4.8 Ambient powering factor of materials

Performance	Materials			
	Steel	Kevlar fiber composite	Carbon fiber composite	Glass-fiber composite
Relaxation and creep	3	1	3	2
Wet resistance	2	2	3	1
Alkali proof	3	2	3	1
Thermal stability	2	2	3	1
Salt water resistance	1	2	3	2
Fatigue behavior	1	3	3	2
Total	13	12	18	8

Note power factor (3, very good; 2, good; 1, meets requirements; 0, cannot meet requirements)

material processing. Hence, the design of the structure and its processing are linked. Structure design should consider the feasibility of processing methods, particularly for integrated part processing.

4.3.4.1 Principles of Processing Method Selection

The feasibility of processing methods should be considered in the structure design phase, to determine the structure processing capability. Principles for processing method selection include the following:

- ① The selected processing method should be able to ensure the structure performance can satisfy design standards and that the fitting accuracy meets the assembly requirements.
- ② Equipment requirements should be satisfied, including currently used and new added equipment. Autoclave size, in particular, should be considered.

- ③ The cost over the lifetime of the component should be considered, including the production continuity, end product rate, and maintenance.
- ④ Processing methods with the greatest level of operation experience should be prioritized.

4.3.4.2 Typical Structure Processing Methods

- ① Autoclave processing is mainly selected for panel structures but liquid resin molding (LCM) processes, such as RTM and RFI, are also widely applied.
- ② Sandwich structures mainly use vacuum bag and pressure bag methods.
- ③ Cylinder structures use filament winding (FW).
- ④ Co-curing, secondary curing or secondary adhering is suitable for integrated part manufacturing.

4.4 Structure Design—Determination of Design Allowables

4.4.1 Allowables and Design Allowables

Allowables are mainly used to characterize material performance and are defined as characteristic values of material performance, with a certain confidence and reliability, determined by statistical analysis of coupon testing data under certain loads and environmental conditions. Design allowables are mainly used in structural design. These are defined as the design limits determined on the basis of material allowables and the testing results of typical coupons, elements, and structures. These allowable may be determined for project requirements and structure integrity, and also based on previous design and operation experiences. Designers should follow requirements for structural integrity, such as static strength, stiffness, durability, and damage tolerance to specify design allowables. The design allowables of a composite system are commonly expressed as strain values. The components are subject to the testing verification performed on subcomponents and full-size scale parts, to guarantee that structures designed by following the design allowables can meet these requirements [1, 2].

Material allowables are characteristic mechanical properties of material systems, and mainly used for material selection, acceptance, and equivalence evaluation. These values are usually not directly used in design except for the modulus, which needs detailed analysis of open hole, delamination, and impact damage in analytical models. When performing structural strength verification, design allowables should be used rather than material allowables.

4.4.2 General Principles for Design Allowables Determination

To determine design allowables, the following principles should be followed:

- ① The tensile design allowables of skin structures should mainly derive from test results on hole-contained specimens with typical structural laminating code. The compression design allowables of skin structures should mainly derive from the testing results of impact damage containing and filled hole-containing specimens with typical structural laminating code.
- ② For thin skin or surface honeycomb sandwich structures, the determination of design allowables should account for buckling effects. If the design allowables mainly depend on buckling effects, the additional coefficient (less than 1) of impact damage effect should be taken into account.
- ③ The mechanical fastener bearing design allowables should derive from the bearing strength allowables of single pin specimens and should consider the effects of the degree of importance, structural features, load type, durability, and operation environment.
- ④ The design allowables of important joints, and details should derive from test results of corresponding typical structures, or from practically verified past experiences.
- ⑤ Combinations of extreme environmental conditions should be considered for design allowables of composite structures.

4.4.3 Current Status

On the basis of documents available from aircraft companies, for current carbon fiber resin matrix composites, the allowable strain values under the designed ultimate loads are as follows:

Compression $[\varepsilon_c] = 4000 \mu\varepsilon$; tensile $[\varepsilon_t] = 5500 \mu\varepsilon$; Shear $[\gamma] = 7600 \mu\varepsilon$.

Table 4.9 indicates some design allowables of current aircraft structures for reference.

4.4.4 Approach to Increasing Design Allowables

Currently used design allowables have been lowered, to further reduce weight and fully utilize the high specific strength and specific stiffness of composite materials [7].

In aircraft primary structures, it is necessary to increase the structural design allowables, especially the compression design allowables. This approach can be summarized as:

Table 4.9 Part of design allowables of current aircraft structures

Co.	Structure component	Material	T. design		C. design	
			Uni.	Fabric	Uni.	Fabric
Lockheed	L-1011 vertical stabilizer	T300/5208	4500	3900	4000	4000
Boeing	B727 horizontal stabilizer	T300/5208			4000	
Boeing	B1 horizontal stabilizer	AS/3501			3600	
M.D.	F18A/B wing	AS4/3501-6	4000		4000	
M.D.	AV-8B wing	AS4/3501-6	4000		4000	
BAe	Stabilizer	XAS/914C	4500	3530	3900	2830
MBB	A310 vertical stabilizer	T300/913C	2800		2800	
MBB	A320 vertical stabilizer	T300/913C	3200		3200	
DA	TORNADO main cabin door	T800/5245	5500		4200	

(1) Increase the damage tolerance of the composite system

The design allowables of composite structures mainly depend on the properties of the composite that can meet requirements for structural damage tolerance. Attention should be paid to the ability of composites to resist impact damage (damage resistance), which is different to the physical damage tolerance of composites. Damage resistance refers to the ability of a component to resist an impact event, while damage tolerance refers to the effect of a certain damage state on the performance of the structure. In the past, the compression strength of standard specimen impacted by 6.7 J/mm (denoted as CAI) was used to evaluate composite damage tolerance. Some studies have shown that this method can give conflicting results. Hence, in recent years, the compression strength after impact by several energy levels is evaluated. Alternatively the compression strength of a standard specimen can be evaluated after impact and induction of a 1-mm dent. The relevant evaluation methods for composite impact resistance can be seen in Sect. 4.9 of this chapter.

(2) Increase the damage tolerance of the structure through design

This approach includes the application of soften and harden bands, soft skin and stiffened plates with mechanical fasteners.

(3) Modify the damage tolerance requirements

Currently used damage tolerance requirements have strict specifications for initial defect dimensions, especially for military aircraft structures. If these specifications can be guaranteed, i.e., supported by extensive studies on manufacture and operation in an ambient environment, or by taking effective measures, the specifications can be decreased, and the design allowables can be increased. For civil aircraft, the

design allowables could be increased based on statistical data of processing composite structures and the use of a lower impact energy threshold, such as 35 J.

4.5 Building Block Approach for Composite Structure Design Verification

4.5.1 Introduction and Philosophy

Owing to the lack of effective analysis and extensive design and use the experience of composite structures the structural integrity needs to be ensured in some way [1–3]. The BBA consists of multiple level testing and certification, at the level of coupons, structural elements, subcomponents, components, and finally a complete full-scale product. This approach is used to solve (and certify) challenging issues such as environmental effects and damage. This approach can also reduce the complexity of full-size tests, qualify the safety of cost reduction measures, and ensure a pass on full-size verification.

For widely used composite/metal structures, the BBA verification approach can also be applied for testing below the substructure component level, and used to complement verification of composite durability and damage tolerance.

For the static strength verification tests of full-size parts, it is difficult to simulate a full range of combined ambient effects, thus the verification may not be fully comprehensive. However, the overall integration can be guaranteed for composite structure static verification, if a BBA verification test program is properly organized.

On the basis of the maturity of materials and design, and the accumulation of experience, the testing content and coupon numbers may be reduced to decrease development costs.

The application of the BBA has not yet been standardized. Relationships between numbers of specimens and material bases values are well defined for specimen tests at the lowest level (see part 15), the numbers of specimens required at higher levels of complexity are somewhat arbitrary and largely based on historical experience, structural criticality, engineering judgment, and economic considerations. Thus, there is currently no standardized methodology for statistically validating each level of the process, although some attempts have been made to develop models that relate specimen quantities to overall reliability.

The sensitivity to out-of-plane loads, failure mode multiplicity, sensitivity to ambient operation conditions, and the absence of mature and reliable analysis for comparing composite and metal structures, motivate the use BBA for structural certification of composite structures [1–3].

The multiplicity of potential failure modes is perhaps the main reason that the BBA is essential for the development of composite structural substantiation. The

many failure modes in composite structures are mainly caused by defects, environmental effects, and out-of-plane sensitivities of the materials.

4.5.2 General Procedures for BBA Implementation

Figure 4.4 shows the building block integration. BBA analysis/testing verification is generally divided into five steps described as follows [3]:

- ① Coupon: Small dimension test specimens used for the evaluation of laminar and laminate performances, as well as general structural characteristics. Test specimens including commonly used laminate strips, and adhered or mechanically joined strip joints, may be used to gain material allowables. This approach is also used for evaluation of material notch sensitivity, ambient effects, and specimen failure modes. At this level, the number of specimens is usually large, sometimes on the order of thousands.
- ② Element: Includes elements and typical structures, i.e., typical load-bearing units in complex configuration structures, such as skin,

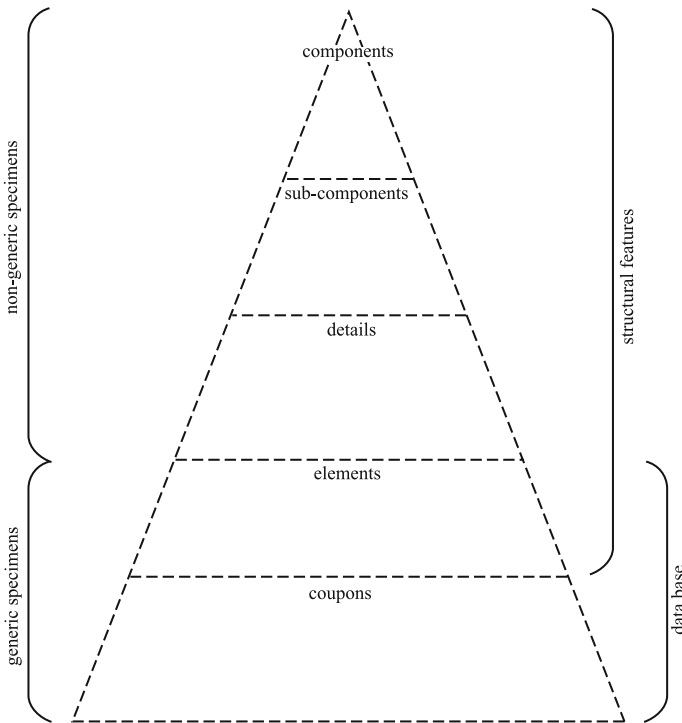


Fig. 4.4 Pyramid of tests

spars, shear panels, laminate and varied joints. Elements also include weaker components in complex configuration structures such as specially designed complex configuration joints, mechanical fasteners, stranger ends, and large inspection ports. The purpose is to verify the load-bearing ability, failure modes, environmental effects, and analysis methods for a variety of elements. Design allowables will be generated at this testing level on the basis of the material allowables, with a large number of specimens on the order of hundreds.

- ③ Subcomponent: Large 3-dimensional structures that feature all the properties of an integral structure section, such as a box segment, frame segment, wing panel, fuselage panel, wing rib, cabin sector, or frame. These features all represent a typical section of an integral structure and their load-bearing ability, environmental effects, damage tolerance, durability, and analytical methods can be verified. The determination of design allowables is also generated at this testing level. Fewer specimens are used at this level, usually of the order of tens, but occasional hundreds.
- ④ Component: Refers to the main structural section of a wing, fuselage, vertical tail, and horizontal stabilizer, which can be used as an integral aircraft body structure in verification tests. A small number of specimens will be used at this level, usually one or more. Considering current application status, verification of structural integrity can be performed at this level.
- ⑤ Full-size scale: At this level, full-size scale aircraft structures are used for analysis and verification and full-size scale static and fatigue tests should be performed to verify structural integrity and the internal load distribution, deflection, and entire structure failure modes predicted by finite element analysis (FEA). The requirements for full-size tests should be proposed by the customer, verification agency, or by the airworthiness certification body, based on safety and durability requirements. The numbers of specimens at this level is usually one or two. For metal/composite combined structures, the main purpose of verification at this level is to verify the metal structure. Full-size tests can also include testing content at the component level, which may overlap with lower levels.

The BBA has been accepted by all composite designers and manufacturers globally; however, different individuals may use different procedures. On the basis of the different tasks, verification levels, and test items, the numbers of specimens may change. Furthermore, the testing sequence may change or overlap. For example, testing and analysis at the element or subcomponent levels should be performed in advance, to gain knowledge of potential risks as soon as possible. In this sense, the current BBA/verification approaches are not yet fully standardized or documented and certain flexibility is allowed in practical use.

4.5.3 Boeing 777 Aircraft Composite Primary Structure Building Block Approach

In Boeing 777, 9.9 t composites have been used to make up 11% of the total structural weight [3]. The horizontal and vertical stabilizers of Boeing 777 are all made of carbon fiber-reinforced composites. The horizontal tail is a main torque box main torque box structure consisting of two spar and multi-rib construction. The BBA for Boeing airplane primary structures (Fig. 4.5) include the following tests.

- (1) Specimens and elements;
- (2) Subcomponents (Table 4.10);
- (3) Components;
- (4) 777 Pre-production horizontal stabilizer test (Table 4.11);
- (5) Stabilizer root attachment test;
- (6) 777 Horizontal stabilizer tests;
- (7) 777 Vertical stabilizer test.

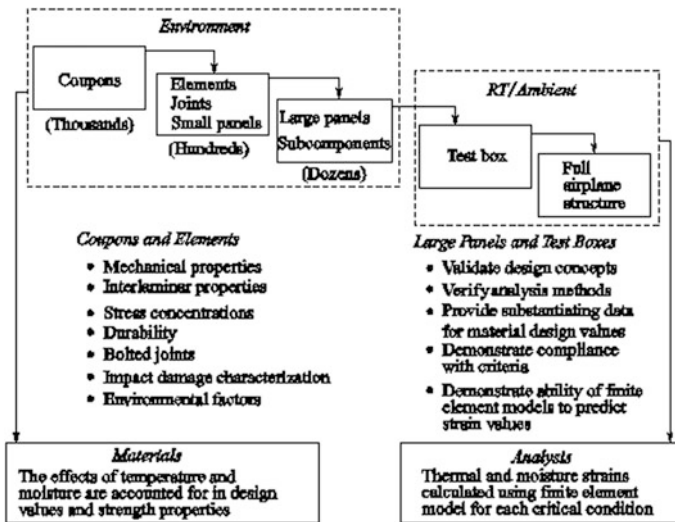


Fig. 4.5 Building block approach for commercial aircraft primary structure

Table 4.10 Summary of subcomponent tests for 777 empennage

Test type	Number of tests
Bolted joints (major splices)	110
Rib details	90
Spar chord crippling	50
Skin/stringer compression panels	26
Skin/stringer tension panels	4
Skin/stringer shear/compression	6
Skin/stringer repair panels	6
Skin splice panels	2
Stringer runouts	4
Spar shear beams	6
Total	305

Table 4.11 Pre-production test box load and damage sequence

Test sequence	Damage types and test loadings
1	Perform all small (BVID) damages
2	Design limit load static strain survey
3	One lifetime fatigue spectrum, 50,000 flights, including 1.15 LEF (Load Enhancement Factor)
4	Design limit load static strain survey
5	One lifetime fatigue spectrum, 50,000 flights, including 1.15 LEF
6	Design limit load static strain survey
7	Design ultimate (select cases) load static strain survey
8	Two (C) check fatigue spectrum (8000 flights) with small and visible damages, including 1.15 LEF
9	“Fail-safe” test; 100% design limit load static strain survey with small and visible damage
10	“Continued safe flight \pm loads test”: 70% design limit load static strain survey with small, visible, and element damages
11	Visible and element damages repaired. Design ultimate load static strain survey
12	Destruction test. Strain survey up to destruction

4.6 Structural Design and Strength and Stiffness Analysis

4.6.1 Composite Structure Design Concepts

To reduce structural weight and to meet load-bearing requirements, most aircraft bodies are designed as a thin-wall construction consisting of several curved planar thin-wall structures. Traditional metal aircraft frames have a thin-wall construction

consisting of a large number of thin-wall components such as skin, beam, stringer, and rib (frame) joined by a large number of mechanical fasteners.

Fiber composites are a kind of artificial structural material. The main advantage of this material is its very high specific strength and stiffness along the fiber direction, which offers great potential for structural weight reduction. Composites also have very different processing techniques from metal materials. Most thin plane structures must withstand in-plane loads, and composites are typically used as laminates or laminated structures in aircraft structures. Laminated composites can offer advantages such as high specific strength and specific stiffness, tailorable properties, and easy processing. On the other hand, composites also have some drawbacks such as low interlaminar strength, stress concentration at open holes, and the occurrence of electrochemical corrosion at composite/aluminum joints. The design concepts used for composite structures are different from those of traditional metal structures. Composite materials are better suited to innovative design concepts.

4.6.2 *Laminate Design and Analysis*

4.6.2.1 **Ply Design Guidelines**

After the determination of laminate total thickness and its local variation based on the application requirements, ply laminate design should be performed [2, 3, 11, 13]. This step will mainly involve:

- ① Selection of proper ply angles;
- ② Determination of the ply ratio at different angles;
- ③ Provision of proper laminating stacking sequence (LSS).

In addition, ply design also includes local ply alternation, such as the ply design in connecting zones and at the edges of open hole, as well as the ply transitions for sudden changes in the thickness of the structure. It may be said that ply design is one of main factors influencing the characteristics of composite materials. Rational design will directly affect the composite structural strength, stiffness, stability, and other important properties such as delamination, damage, failure, and dimensional stability, as well as processing performance. These factors have direct implications for load-carrying capacity and operation functions. The critical issues of laminate ply design are as follows:

- (1) A LSS is said to be homogeneous if the ply angles are evenly distributed throughout the laminate thickness. Homogeneous LSS is recommended for strength controlled designs.
- (2) A laminate is considered to be symmetric if the plies and property parameters are symmetrical to the mid-plane. A balanced laminate is defined as having equal numbers of $+\theta$ and $-\theta$ plies, where θ is measured from the primary

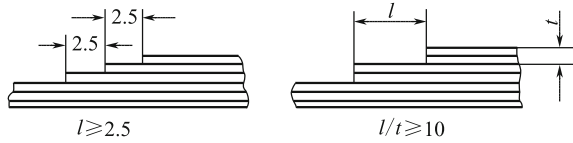
load direction. A laminate having both balanced and symmetrical plies is referred to as balanced and symmetric. If possible, laminates should be balanced and symmetric about the mid-plane to avoid warpage caused by couplings. If this is not possible due to other requirements, locate the asymmetry or imbalance as near to the laminate mid-plane as possible.

- (3) A LSS should have at least four distinct ply angles (e.g., 0° , 90° , $\pm 45^\circ$) with a minimum of 10% of the plies oriented at each angle.
- (4) Minimize groupings of plies with the same orientation. For tape plies, stack no more than four plies of the same orientation together (i.e., limit stacked ply group thicknesses 0.03 in. (0.8 mm). In addition, stacked ply group thicknesses with orientations perpendicular to a free edge should be limited to 0.015 in. (0.38 mm) to avoid delamination, matrix cracking, and shear-out failure in bolted joints.
- (5) The ply orientation should be consistent with the primary load direction. That is, 0° ply should be preferentially used for laminates that are primarily subjected to tensile or compressive loads. For the laminates primarily under shear load, ply with $\pm 45^\circ$ is preferred. In addition, the plies for primary load transmission should not be placed on outer surfaces.
- (6) For ply design in joint zones, the ratio of the ply in $\pm 45^\circ$ against the pin load direction should not be less than 40%. The ply ratio in the direction consistent with the pin load should be greater than 25%, to ensure enough shear strength and bearing strength in the joint zone, and reduce stress concentration.
- (7) For the laminates subject to buckling as a critical condition, the outer surface should be a feature $\pm 45^\circ$ plies. To enhance impact resistance, hybrid composite layers should be used such as aromatic or glass-fiber plies.
- (8) The $\pm\theta$ plies should be placed as close to each other as possible to reduce bending/twisting coupling and avoid the negative effects on the effective stiffness and stability. However, separation of $\pm\theta$ plies can offer the benefits in terms of reducing interlaminar stress.
- (9) Attention should be paid to avoid the high interlaminar stress (σ_z) that may occur at the free edges of laminates. The stacking sequence should be properly selected to reduce the delaminating stress and strain levels at free edges.
- (10) Mismatch of the Poisson's ratio between two laminates co-cured or adhered together should be reduced as much as possible. Otherwise, delamination and/or debonding can easily take place. The following equation is recommended for assessing this risk:

$$|v_{xy}(\text{laminat e 1}) - v_{xy}(\text{laminat e 2})| < 0.1$$

- (11) Usually, ply decreasing is used to realize laminate thickness alternation. The step length of each ply transition zone should not be less than 2.5 mm, or be followed by $l/t > 10$ to realize a ply decrease, as illustrated in Fig. 4.6. In general, there should be no more than two ply numbers simultaneously decreasing and no ply decreasing is allowed on the width direction of a raised

Fig. 4.6 Requirements for ply decreases



flange of a beam, frame, or rib of skin. It is specified that certain continuous plies should be used on laminate surfaces to avoid ply tear-off.

Ply splicing is allowed in the direction parallel to the applied load but not permitted in the load vertical direction. The splicing gap should be less than 2 mm, with no overlap. The spliced plies should be separated by four other layers, if less than four layers are applied the intersplicing width should be at least 15 mm, to reduce weak laminating.

The above-mentioned guidelines for ply design cannot always be completely achieved and are sometimes even conflict with the principal needs of satisfying the primary load-bearing and operation functions requirements.

4.6.2.2 Laminate Stiffness Analysis

Laminate stiffness is not only dependent on its thickness, but also related to its constituent lamina and their stacking sequence. The stiffness of laminate can be calculated by classical laminate theory [8–10, 12].

(1) Lamina on-axis and off-axis stiffness

Lamina on-axis stiffness (also known as on-axis modulus) refers to the lamina stiffness along the fiber direction (1). The matrix for laminar on-axis stress–strain is given as:

$$\begin{Bmatrix} \varepsilon_1 \\ \varepsilon_2 \\ \gamma_{12} \end{Bmatrix} = \begin{bmatrix} \frac{1}{E_1} & -\frac{\nu_2}{E_2} & 0 \\ -\frac{\nu_1}{E_1} & \frac{1}{E_2} & 0 \\ 0 & 0 & \frac{1}{G_{12}} \end{bmatrix} \begin{Bmatrix} \sigma_1 \\ \sigma_2 \\ \tau_{12} \end{Bmatrix} \tag{4.1}$$

where $\varepsilon_1, \varepsilon_2, \gamma_{12}$ are on-axis strains; $\sigma_1, \sigma_2, \tau_{12}$ are on-axis stresses; E_1, E_2, ν_1, G_{12} are the four independent stiffness coefficients;

$$\frac{\nu_1}{E_1} = \frac{\nu_2}{E_2}$$

From the lamina on-axis stiffness matrix expression, then:

$$\begin{Bmatrix} \sigma_1 \\ \sigma_2 \\ \tau_{12} \end{Bmatrix} = \begin{bmatrix} Q_{11} & Q_{12} & 0 \\ Q_{21} & Q_{22} & 0 \\ 0 & 0 & Q_{66} \end{bmatrix} \begin{Bmatrix} \varepsilon_1 \\ \varepsilon_2 \\ \gamma_{12} \end{Bmatrix} \tag{4.2}$$

where Q_{11} , Q_{22} , Q_{12} , Q_{21} , and Q_{66} are the lamina on-axis stiffness coefficients:

$$Q_{11} = mE_1$$

$$Q_{22} = mE_2$$

$$Q_{12} = Q_{21} = mvE_1 = mv_1E_2, v_1/v_2 = E_1/E_2$$

$$M = 1/(1 - v_1v_2)$$

$$Q_{66} = G_{12}$$

$$Q_{16} = Q_{26} = Q_{61} = Q_{62} = 0$$

Lamina off-axis stiffness (also known as the off-axis modulus) refers to the lamina stiffness along the direction forming an angle θ with the fiber direction. The off-axis stiffness of a lamina at angle θ can be expressed by the matrix:

$$[\bar{Q}] = \begin{bmatrix} \bar{Q}_{11} & \bar{Q}_{12} & \bar{Q}_{16} \\ \bar{Q}_{21} & \bar{Q}_{22} & \bar{Q}_{26} \\ \bar{Q}_{61} & \bar{Q}_{62} & \bar{Q}_{66} \end{bmatrix} \tag{4.3}$$

where \bar{Q}_{11} , \bar{Q}_{12} , \bar{Q}_{22} , \bar{Q}_{16} , \bar{Q}_{26} and \bar{Q}_{66} are lamina off-axis stiffness coefficients.

$[\bar{Q}]$ is a symmetrical matrix, so that the off-axis stiffness coefficient $\bar{Q}_{12} = \bar{Q}_{21}$; $\bar{Q}_{16} = \bar{Q}_{61}$; $\bar{Q}_{26} = \bar{Q}_{62}$.

The conversion between the off-axis stiffness coefficient and the on-axis stiffness coefficient can be expressed by trigonometric functions of the off-axis angle as given in the table:

	Q_{11}	Q_{22}	Q_{12}	Q_{66}
\bar{Q}_{11}	m^4	n^4	$2m^2n^2$	$4m^2n^2$
\bar{Q}_{22}	n^4	m^4	$2m^2n^2$	$4m^2n^2$
\bar{Q}_{12}	m^2n^2	m^2n^2	$m^4 + n^4$	$-4m^2n^2$
\bar{Q}_{66}	m^2n^2	m^2n^2	$-2m^2n^2$	$(m^2 - n^2)^2$
\bar{Q}_{16}	m^3n	$-mn^3$	$mn^3 - m^3n$	$2(mn^3 - m^3n)$
\bar{Q}_{26}	mn^3	$-m^3n$	$m^3n - mn^3$	$2(m^3n - mn^3)$

where $m = \cos\theta$, $n = \sin\theta$.

Note:

- ① \bar{Q}_{11} and \bar{Q}_{22} have an intermirror relationship, i.e., $\bar{Q}_{11}(\theta + 90^\circ) = \bar{Q}_{22}(\theta)$.
- \bar{Q}_{16} and \bar{Q}_{26} have an intermirror relationship, i.e., $\bar{Q}_{16}(\theta + 90^\circ) = -\bar{Q}_{26}(\theta)$.

- ② $\bar{Q}_{11}, \bar{Q}_{22}, \bar{Q}_{12},$ and \bar{Q}_{66} are even functions and thus independent of the polarity of the angle θ , \bar{Q}_{16} and \bar{Q}_{26} are odd functions, and thus dependent on the polarity of the angle θ .
- ③ $\frac{\partial \bar{Q}_{11}}{\partial \theta} = 4\bar{Q}_{16}, \frac{\partial \bar{Q}_{22}}{\partial \theta} = 4\bar{Q}_{26}.$

Hence, only four of the six off-axis stiffness coefficients are independent.

Off-axis stiffness coefficients can also be expressed as a combination of the on-axis stiffness coefficients as listed in the table:

	1	U_2	U_3
\bar{Q}_{11}	U_1	$\cos 2\theta$	$\cos 4\theta$
\bar{Q}_{22}	U_1	$-\cos 2\theta$	$\cos 4\theta$
\bar{Q}_{12}	U_4		$-\cos 4\theta$
\bar{Q}_{66}	U_5		$-\cos 4\theta$
\bar{Q}_{16}		$\frac{1}{2} \sin 2\theta$	$\sin 4\theta$
\bar{Q}_{26}		$\frac{1}{2} \sin 2\theta$	$-\sin 4\theta$

The combination of on-axis stiffness coefficients in the table:

$$U_1 = \frac{1}{8}(3Q_{11} + 3Q_{22} + 2Q_{12} + 4Q_{66})$$

$$U_2 = \frac{1}{2}(Q_{11} - Q_{22})$$

$$U_3 = \frac{1}{8}(Q_{11} + Q_{22} - 2Q_{12} - 4Q_{66})$$

$$U_4 = \frac{1}{8}(Q_{11} + Q_{22} + 6Q_{12} - 4Q_{66})$$

$$U_5 = \frac{1}{8}(Q_{11} + Q_{22} - 2Q_{12} + 4Q_{66}) = \frac{1}{2}(U_1 - U_4)$$

From the lamina stiffness expression, it can be seen that the off-axis stiffness coefficient \bar{Q}_{ij} is a function of the off-axis angle θ . Thus, the off-axis angle θ can determine the lamina off-axis stiffness. In general, i.e., when $\theta \neq 0^\circ$ or 90° , the lamina off-axis coupling stiffness coefficients \bar{Q}_{16} and \bar{Q}_{26} will not be zero. This means that tensile–shear coupling or compression–shear coupling will exist, as shown in Fig. 4.7.

The off-axis angle also refers to the ply laminating angle. The design the lamina off-axis stiffness based on the laminating angle is the main approach to tailoring laminate properties.

Fig. 4.7 Schematic of unidirectional laminate off-axis tensile deformation ($\bar{Q}_{16} \neq 0$)

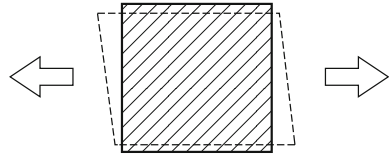


Fig. 4.8 Laminate stiffness analysis model

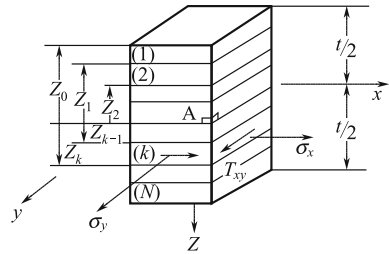


Fig. 4.9 Resultant force on laminate

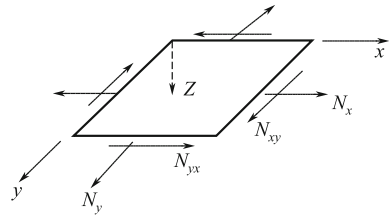
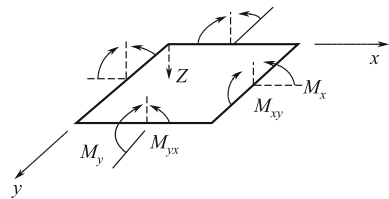


Fig. 4.10 Resultant moment on laminate



(2) Laminate stiffness analysis

In the laminate stiffness analysis model, the mid-plane resultant force $\{N\}$, and mid-plane resultant moment $\{M\}$ scheme are given in Figs. 4.8, 4.9 and 4.10.

In the analysis, the lamina is assumed to be a homogeneous material, and their properties can be determined from unidirectional composite testing.

On the basis of classical laminate theory, the physical equation of laminate can be expressed as:

$$\begin{Bmatrix} N \\ M \end{Bmatrix} = \begin{bmatrix} A & B \\ B & D \end{bmatrix} \begin{Bmatrix} \varepsilon^0 \\ k \end{Bmatrix} \tag{4.4}$$

where

- $\{N\}$ laminate mid-plane resultant force array;
- $\{M\}$ laminate mid-plane resultant moment array;
- $\{\varepsilon^0\}$ laminate mid-plane strain array;
- $\{k\}$ laminate mid-plane curvature array;
- $[A]$ laminate tensile stiffness matrix (3×3 matrix), where each tensile stiffness coefficient can be calculated from the equation:

$$A_{ij} = \sum_1^N (\bar{Q}_{ij})_k (Z_k - Z_{k-1}) = \sum_1^N (\bar{Q}_{ij})_k h_k l \quad (4.5)$$

where $(\bar{Q}_{ij})_k$ is the off-axis stiffness coefficient of layer k and $h_k l$ is the area of layer k .

$[B]$ —laminated coupling stiffness matrix (3×3 matrix), wherein each coupling stiffness coefficient can be calculated by the equation:

$$B_{ij} = \frac{1}{2} \sum_1^N (\bar{Q}_{ij})_k (Z_k^2 - Z_{k-1}^2) = \sum_1^N (\bar{Q}_{ij})_k \bar{Z}_k h_k l \quad (4.6)$$

where $\bar{Z}_k h_k l$ is the static moment from layer k to the mid-plane.

$[D]$ —laminated bending stiffness matrix (3×3 matrix), wherein each bending stiffness coefficient can be calculated by the equation:

$$D_{ij} = \frac{1}{2} \sum_1^N (\bar{Q}_{ij})_k (Z_k^3 - Z_{k-1}^3) = \sum_1^N (\bar{Q}_{ij})_k \left(\frac{h_k^3}{12} + \bar{Z}_k h_k l \right) \quad (4.7)$$

where $\left(\frac{h_k^3}{12} + \bar{Z}_k h_k l \right)$ is the inertia moment from the layer k to mid-plane.

The strain on laminate cross section $\{\varepsilon\}_Z$ is expressed as:

$$\{\varepsilon\}_Z = \{\varepsilon^0\} + Z\{k\} \quad \left(-\frac{t}{2} \leq Z \leq \frac{t}{2} \right) \quad (4.8)$$

Clearly, the strain on cross section changes continuously and linearly.

The strain on layer k is:

$$\{\varepsilon\}_k = \{\varepsilon^0\} + Z\{k\} \quad (Z_{k-1} \leq Z \leq Z_k) \quad (4.9)$$

The stress of each lamina depends on the lamina strain and stiffness. The stress in layer k $\{\sigma\}_k$ can be expressed as:

$$\{\sigma\}_k = [\bar{Q}]_k \{\varepsilon\}_k = [\bar{Q}]_k \{\varepsilon^0\} + [\bar{Q}]_k Z \{k\} \quad (Z_{k-1} \leq Z \leq Z_k) \quad (4.10)$$

It can be seen that the stress in cross section is not constant and may be summarized based on the analysis of stiffness matrices $[A]$, $[B]$, and $[D]$:

- ① The expected laminate stiffness and strength can be derived from the proper selection of each lamina laying-up angles, ply percentages and stacking sequences, similar to cloth tailoring, and so-called tailoring design.
- ② Coupling is a unique feature possessed by laminates, and it is the basis of aeroelastic tailoring design of aircraft wing surfaces.

Laminate stiffness design analysis generally begins from the matrix $[A]$ and goes through parameter adjustment (ply sequence, laying-up angle and axis moving) to generate matrices $[D]$ and $[B]$.

With the use of symmetrical laminating sequences, where each lamina is of the same material and has the same thickness, then $[B] = 0$; however, in-plane tensile–shear coupling ($A_{16} \neq 0$, $A_{26} \neq 0$) and bending–twisting coupling ($D_{16} \neq 0$, $D_{26} \neq 0$) will exist.

If an asymmetrical laminating sequence is used, when each lamina has the same material and thickness, then $[B] \neq 0$. Thus, in-plane tensile–shear and out-of-plane bending–twisting coupling will take place in the laminates.

If a symmetrical and balanced stacking sequence is used, such as $[\pm\alpha/-\alpha]$, or $[\pm\alpha]_{ns}$, $[0/90/\pm\alpha]_s$, where each lamina is composed of the same material and has the same thickness, symmetrical laminating will make $[B] = 0$. Simultaneously, balanced laminating will make $A_{16} = A_{26} = 0$. The values of D_{16} and D_{26} will depend on the number of plies (i.e., the more the plies, the smaller the coupling effect). When the ply number is equal to or greater than 12, D_{16} and $D_{26} \approx 0$. In this type of laminate, there will be no in-plane tensile–shear coupling, and no out-of-plane bending–twisting coupling. It is also possible to obtain larger in-plane shear stiffness and out-of-plane twisting stiffness. Hence in structural design, symmetrical and balanced laminating is usually preferred.

Symmetrical laminating or symmetrical unbalanced laminating may be used to give unique composite coupling deformation features, and gives great freedom to composite structural designs, for example, to meet the aerodynamic tailoring requirements.

(3) Typical laminate stiffness

Typical laminate stiffness is an example of how to describe the designed ability of laminate stiffness. Common laminates are listed below to illustrate the concept of laminate stiffness.

- ① Stiffness of quasi-isotropic laminates: For example, laminates with a ply sequence of $[0/\pm 45/90]$, $[0/\pm 60]$ are quasi-isotropic laminates. The stiffness coefficients A_{11} , A_{22} , A_{12} , and A_{66} in the in-plane stiffness matrix will correlate as:

$$A_{11} = A_{22} = U_1t; A_{12} = U_4t$$

$$A_{66} = U_5t = \frac{1}{2}(U_1 - U_2)t = \frac{1}{2}(A_{11} - A_{12})$$

where, $U_1, U_2, U_4,$ and U_5 —material on-axis stiffness coefficient combination,

t —laminate thickness.

This equation indicates that only two of the four stiffness coefficients $A_{11}, A_{22}, A_{12}, A_{66}$ are independent. This is similar to the case of isotropic materials, where only two of four properties $E, G, \nu,$ and $G = \frac{E}{2(1+\nu)}$ are independent. Thus laminates $[0/\pm 45/90], [0/\pm 60]$ are referred to as quasi-isotropic laminates.

The stiffness coefficients in the matrix $[A]$ are independent of the laminating sequence when it is symmetric and balanced; however, in matrix $[B]$ and $[D]$, the stiffness coefficients are dependent on the laminating sequences. Quasi-isotropic laminating has the stiffness matrix:

$$\begin{bmatrix} A_{11} & A_{12} & 0 & & & \\ A_{12} & A_{11} & 0 & & & [B] \\ 0 & 0 & \frac{1}{2}(A_{11} - A_{12}) & & & \\ & [B] & & & & [D] \end{bmatrix}$$

- ② Stiffness of symmetrical orthotropic laminates: Symmetrical laminates consisting of 0° and 90° plies are referred to as symmetrical orthotropic laminates, for example $[0/90]_s, [0_2/90]_s$.

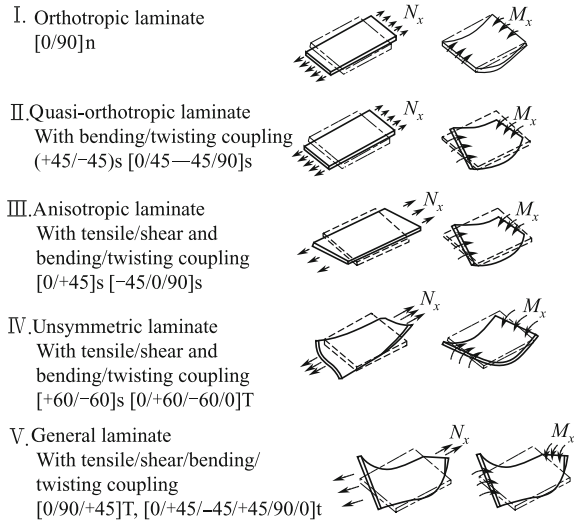
In this type of laminates, each lamina (in 0° or 90°) will not have tensile–shear coupling in their off-axis stiffness, namely $(\bar{Q}_{16})_k = (\bar{Q}_{26})_k = 0$. Accordingly, the in-plane stiffness cross term $A_{16} = A_{26} = 0$ and bending–twisting stiffness cross term $D_{16} = D_{26} = 0$ can be derived. Again, for symmetrical laminated plies, $[B] = 0$.

The deformation of symmetrical orthotropic laminates is shown as in Fig. 4.11(I). Because of the absence of cross-ply, symmetrical orthotropic laminates have very small in-plane shear stiffness and out-of-plane twisting stiffness. These systems are only suitable for withstanding in-plane biaxial loads.

The stiffness matrix of symmetrical orthotropic laminates is given as:

$$\begin{bmatrix} A_{11} & A_{12} & 0 & & & \\ A_{12} & A_{22} & 0 & & & 0 \\ 0 & 0 & A_{66} & & & \\ & & & D_{11} & D_{12} & 0 \\ & 0 & & D_{12} & D_{22} & 0 \\ & & & 0 & 0 & D_{66} \end{bmatrix}$$

Fig. 4.11 Schematic illustration of typical laminate deformations



③ Stiffness of symmetrical and balance laminates: Laminates consisting of $[\pm\alpha]_s$ ply combinations are referred to as symmetrical and balanced laminates.

For lamina with $+\alpha$ and lamina with $-\alpha$, $\bar{Q}_{16}(\alpha) = -\bar{Q}_{16}(-\alpha)$, $\bar{Q}_{26}(\alpha) = -\bar{Q}_{26}(-\alpha)$. If the number of lamina with $+\alpha$ is equal to that with $-\alpha$, then $A_{16} = A_{26} = 0$, laminates will show in-plane orthotropic behaviors.

For symmetrical laminating, then $[B] = 0$ and each stiffness coefficient D_{ij} is independent of the stacking sequence. Generally, $D_{16} \neq 0$, $D_{26} \neq 0$. Only in laminates with a sufficient number of plies (12 or more plies), can D_{16} and D_{26} be reduced and ignored.

The deformation of symmetrical and balanced laminates is shown as in Fig. 4.11(II). Balanced laminates with $[\pm\alpha]_s$ are referred to as cross-ply laminates, with large in-plane shear stiffness and out-of-plane twisting stiffness. If 0° and 90° plies are arranged, laminates will be enhanced with improved positive stress bearing ability. This arrangement can be used to meet the design requirements of complex load-bearing conditions. The difference between symmetrical and balanced laminates and quasi-isotropic laminates is that the former is not limited by $A_{11} = A_{12}$ and $A_{66} = (A_{11} - A_{12})/2$, which allows greater design freedom. However, owing to their low degree of processing deformation and the ease of quality control, symmetrical and balance laminates are most commonly used in composite structures.

$$\begin{bmatrix} A_{11} & A_{12} & 0 & 0 & 0 & B_{16} \\ A_{12} & A_{22} & 0 & 0 & 0 & B_{26} \\ 0 & 0 & A_{66} & B_{16} & B_{26} & 0 \\ 0 & 0 & B_{16} & D_{11} & D_{12} & 0 \\ 0 & 0 & B_{26} & D_{12} & D_{22} & 0 \\ B_{16} & B_{26} & 0 & 0 & 0 & D_{66} \end{bmatrix}$$

- ⑥ Stiffness of unsymmetrical orthotropic laminates: Laminates containing alternative arrangement of 0° and 90° plies, and with an even total ply number, such as $[0/90/0/90]$, are referred to as unsymmetrical orthotropic laminates.

The analysis of matrix $[A]$ and $[D]$ is the same as that used for symmetrical orthotropic laminates. It can be proven that $B_{11} = -B_{22}$, $B_{12} = B_{66} = B_{16} = B_{26} = 0$ in matrix $[B]$. As ply number increases, the coupling stiffness coefficient $B_{11} = -B_{22}$ tends to zero when the ply number is less than eight such that $B_{11} = -B_{22} = 0$. Unsymmetrical orthotropic laminates have a stiffness matrix given by:

$$\begin{bmatrix} A_{11} & A_{12} & 0 & B_{11} & 0 & 0 \\ A_{12} & A_{22} & 0 & 0 & -B_{11} & 0 \\ 0 & 0 & A_{66} & 0 & 0 & 0 \\ B_{11} & 0 & 0 & D_{11} & D_{12} & 0 \\ 0 & -B_{11} & 0 & D_{12} & D_{22} & 0 \\ 0 & 0 & 0 & 0 & 0 & D_{66} \end{bmatrix}$$

- ⑦ Stiffness of general laminates: General laminates, referred to as asymmetrical and unbalance laminates, feature a stiffness matrix containing all the coupling terms. The deformation of these laminates is illustrated in Fig. 4.11(V), and the stiffness matrix is given by:

$$\begin{bmatrix} A_{11} & A_{12} & A_{16} & B_{11} & B_{12} & B_{16} \\ A_{12} & A_{22} & A_{26} & B_{12} & B_{22} & B_{26} \\ A_{16} & A_{26} & A_{66} & B_{16} & B_{26} & B_{66} \\ B_{11} & B_{12} & B_{16} & D_{11} & D_{12} & D_{16} \\ B_{12} & B_{22} & B_{26} & D_{12} & D_{22} & D_{26} \\ B_{16} & B_{26} & B_{66} & D_{16} & D_{26} & D_{66} \end{bmatrix}$$

4.6.2.3 Laminate Strength and Failure Analysis

(1) Ply strength criterion

The strength criterion provides an analytical relationship (mathematical model) of the strength under a combination of stresses. The aim of establishing strength criterion (failure criterion) is to create a material failure envelope under combined stresses based on a simple load-bearing strength index [8–10, 12, 13].

(1) Maximum (on-axis) stress criterion and maximum (on-axis) strain criterion

- ① Maximum (on-axis) stress criterion: All on-axis stresses in a ply should be low, or equal to zero. The corresponding material strength and failure are determined by the ply. Expressions of maximum stress criterion are given by:

$$\begin{aligned} \sigma_1 &\leq X_t & |\sigma_1| &\leq X_c \\ \sigma_2 &\leq Y_t & |\sigma_2| &\leq Y_c \\ & & |\tau_{12}| &\leq S \end{aligned} \quad (4.11)$$

If one of these inequalities cannot be satisfied, a corresponding failure will occur in the ply.

- ② Maximum (on-axis) strain criterion: All the on-axis strain in a ply should be less than the correspond material ultimate strain, otherwise failure will take place in the ply. The expression for maximum strain criterion is given by:

$$\begin{aligned} \varepsilon_1 &\leq X_{te} = X_t/E_1 & |\varepsilon_1| &\leq X_{ce} = X_c/E_1 \\ \varepsilon_2 &\leq Y_{te} = Y_t/E_2 & |\varepsilon_2| &\leq Y_{ce} = Y_c/E_2 \\ & & |\gamma_{12}| &\leq S_e = S/G \end{aligned} \quad (4.12)$$

If one of the inequalities cannot be satisfied, then corresponding failure will occur in the ply.

- ③ Discussion: Each component with maximum (on-axis) stress criterion and maximum (on-axis) strain criterion should have independent criterion. Each criterion has five subcriteria, such that the failure envelope described by the criterion shows a tipping point. The difference between these criteria is that Poisson's effect is involved in the strain criterion.

(2) Tsai–Hill criterion: The Tsai–Hill criterion follows the expression:

$$\left(\frac{\sigma_1}{X}\right)^2 + \left(\frac{\sigma_2}{Y}\right)^2 - \frac{\sigma_1\sigma_2}{X^2} + \left(\frac{\tau_{12}}{S}\right)^2 = 1 \quad (4.13)$$

The Tsai–Hill criterion can give a smooth and continuous failure envelope, with small differences between the theoretical values and testing results. The main problem is that the interaction terms σ_1 and σ_2 are only related to

X and have no first power terms (without considering $X \neq X'$, $Y \neq Y'$). Under the reduced conditions, $Y = Z$ and $S_{12} = S_{13} = S$ are used in derivation, such that this expression cannot be used for biaxial woven reinforcement. More details are given in Tsai's published work.

- (3) Tsai–Wu criterion: In stress space, unidirectional composite failure can be expressed by the quadratic tensor of the failure envelope:

$$F_{ij}\sigma_i\sigma_j + F_i\sigma_i = 1, \quad (4.14)$$

referred to as the quadratic interaction criterion.

For plane stress conditions, the expression can be simplified as:

$$F_{11}\sigma_1^2 + 2F_{12}\sigma_1\sigma_2 + F_{22}\sigma_2^2 + F_{66}\sigma_6^2 + F_1\sigma_1 + F_2\sigma_2 = 1 \quad (4.15)$$

In the equation, there are four quadratic strength parameters and two linear strength parameters. Of these six material strength parameters, five can be determined by simple tensile, compression, and shear tests.

$$F_{11} = \frac{1}{XX'} \quad F_1 = \frac{1}{X} - \frac{1}{X'}$$

$$F_{22} = \frac{1}{YY'} \quad F_2 = \frac{1}{Y} - \frac{1}{Y'}$$

$$F_{66} = \frac{1}{S^2}$$

It is more complex to determine F_{12} , because of the interaction of σ_1 and σ_2 is involved. Tsai recommended the use of:

$$F_{12} = -\frac{\sqrt{F_{11}F_{22}}}{2}$$

Compared with the Tsai–Hill criterion, the Tsai–Wu criterion can give more information about strength standards, such as the inequality between tensile and compression strength and how the interaction terms σ_1 and σ_2 depend on X , X' , Y , and Y' values.

Tsai–Wu criterion can also be expressed in terms of strain parameters (refer to Tsai's publication for details).

- (4) Strength ratio: Strength criterion gives the material failure criterion under operation stress. To describe the safety margin of materials under proportional loading conditions, the concept of the strength ratio is introduced. The strength ratio is defined as the ratio between allowable and operation stress:

$$R = \frac{\sigma_i(\alpha)}{\sigma_i}$$

When the strength ratio is used to describe the safety margin under proportional loads, it is assumed that the deformation of a composite is linear until its final failure.

If $R = 1$, $\sigma_i = \sigma_i(\alpha)$, failure occurs.

When $R > 1$, $\sigma_i < \sigma_i(\alpha)$, R denotes an operation stress σ_i smaller than the allowable stress $\sigma_i(\alpha)$. Hence the factor of proportional load increases, within the safety margin. When $R = 2$, the operation stress doubles and failure occurs. Hence, if a load is proportionally applied and doubled material failure will occur.

When $R < 1$, $\sigma_i > \sigma_i(\alpha)$ material failure occurs, or the situation is not physically possible.

The strength ratio can be also used in strain space. The Tsai–Wu criterion in strain space can be expressed as:

$$G_{11}\varepsilon_1^2 + 2G_{12}\varepsilon_1\varepsilon_2 + G_{22}\varepsilon_2^2 + G_{66}\varepsilon_6^2 + G_1\varepsilon_1 + G_2\varepsilon_2 = 1 \quad (4.16)$$

where

$$\begin{aligned} G_{11} &= F_{11}Q_{11}^2 + 2F_{12}Q_{11}Q_{12} + F_{22}Q_{12}^2G_{22} \\ &= F_{11}Q_{11}^2 + 2F_{12}Q_{12}Q_{22} + F_{22}Q_{12}^2 \end{aligned}$$

$$G_{12} = F_{11}Q_{11}Q_{12} + F_{12}(Q_{11}Q_{12} + Q_{12}^2) + F_{22}Q_{12}G_{22}$$

$$G_{66} = F_{66}Q_{66}^2$$

$$G_1 = F_1Q_{11} + F_2Q_{12}$$

$$G_2 = F_1Q_{12} + F_2Q_{22}$$

When using the strength ratio, then

$$\begin{aligned} (G_{11}\varepsilon_1^2 + 2G_{12}\varepsilon_1\varepsilon_2 + G_{22}\varepsilon_2^2 + G_{66}\varepsilon_6^2)R^2 \\ + (G_1\varepsilon_1 + G_2\varepsilon_2)R = 1 \end{aligned} \quad (4.17)$$

This expression can also be used to obtain R , to determine if failure occurs in a ply.

(2) Strength estimation of laminates

- (1) Strength failure features of laminates: Laminate strength is based on that of individual ply. Under loading, laminate failure will begin first at a single ply, and will then take place at other ply successively, until total failure occurs, as shown in Fig. 4.12. The failure process proceeds from single ply

failure to total failure. In estimating the laminate strength, it is necessary to determine the first ply failure (FPF) load and the final failure ultimate load. The estimation of laminate strength involves the following aspects:

- ① Select the ply failure criterion,
 - ② Determine the FPF load,
 - ③ Laminate stiffness modification,
 - ④ Calculate ultimate load.
- (2) Determination of FPF load: When a laminate is under loading (including additional temperature loading), the load causing a FPF ($R = 1$) is defined as the FPF load.
- (3) Modification of laminate stiffness: After FPF, the following models can be used for laminate stiffness modification:
- ① Ply-deeply model: Set the stiffness of failure ply ($R = 1$) in the laminate to zero, i.e., $[\bar{Q}]_{k(R=1)} = 0$.
 - ② Fiber successive load-bearing model: Longitudinal cracks usually occur during failure ply ($R = 1$). The ply will separate into fiber bundles, which can only withstand loads in the fiber axial direction, as shown in Fig. 4.13. Hence the stiffness matrix becomes $\bar{Q}_{11} \neq 0$ and all other terms zero:

$$[\bar{Q}]_{k(R=1)} = \begin{bmatrix} \bar{Q}_{11} & 0 & 0 \\ 0 & 0 & 0 \\ 0 & 0 & 0 \end{bmatrix}$$

- ③ Shear failure model: When shear failure occurs in a ply of laminate ($R = 1$), let the shear stiffness Q_{66} and the tensile–shear coupling stiffness Q_{16} and Q_{26} be zero, such that:

$$[\bar{Q}]_{k(R=1)} = \begin{bmatrix} \bar{Q}_{11} & \bar{Q}_{12} & 0 \\ \bar{Q}_{12} & \bar{Q}_{22} & 0 \\ 0 & 0 & 0 \end{bmatrix}$$

Fig. 4.12 Load versus displacement curve of laminate

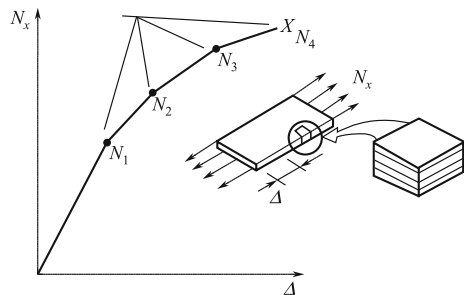
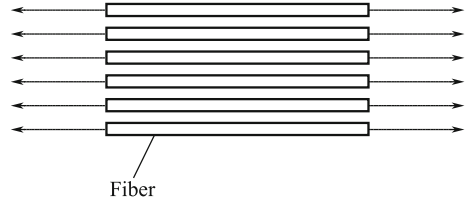


Fig. 4.13 Fiber successive load-bearing model

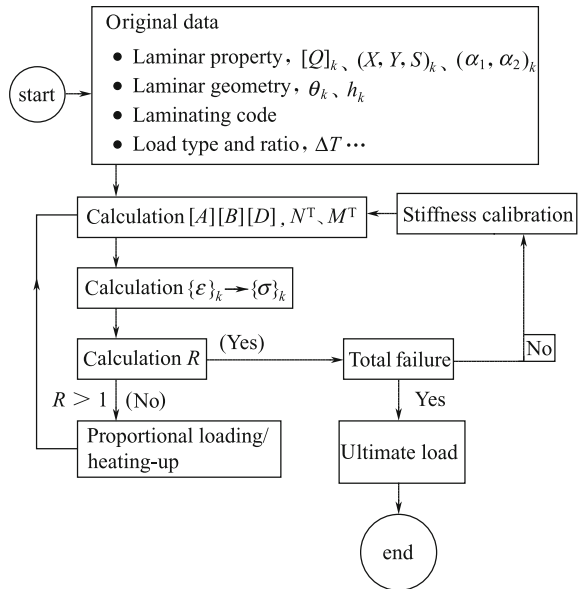


(4) Determination of laminate ultimate load: Fig. 4.14 shows a frame chart of the process from ply successive failure to total damage. This is an iterative calculation process.

Note:

- ① Ply failure criterion is considered suitable for other laminate plies.
- ② Assume that Kirchhoff hypothesis can be always applicable in laminate successive ply failure.
- ③ Decide and select stiffness modification models based on the ply failure modes.

Fig. 4.14 Analytical chart of laminate ultimate load



4.6.2.4 Examples of Laminate Structure Design

(1) Symmetrical and unbalance composite skin design

Figure 4.15 shows the canard wing of a jet plane. Symmetrical and unbalanced skin is used in the composite to achieve bending–twisting effects, which allow the canard wing to meet many requirements in terms of strength, stiffness, aerodynamics, and weight reduction [2].

The design steps of symmetrical and unbalanced skin are as follows:

- ① On the basis of static strength requirements, determine the coordinate system (in the 0° ply direction) and perform preliminary ply design. The 0° ply direction in a symmetric and balanced skin is usually consistent with the structural primary load direction, as shown if Fig. 4.16a.

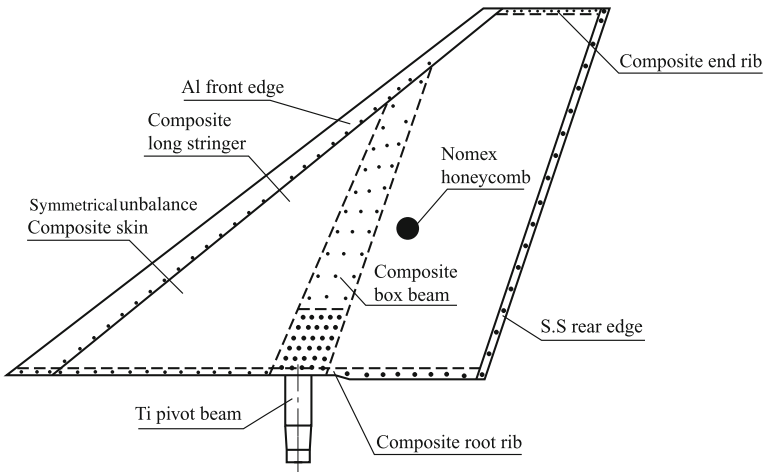


Fig. 4.15 Schematic of rudder canard wing with symmetrical and unbalanced full-height honeycomb

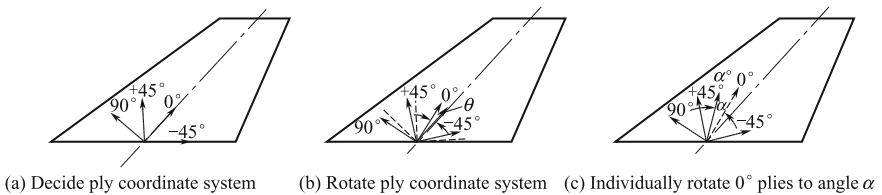


Fig. 4.16 Conversion of coordinate system during symmetrical and balance skin design

- ② Rotate the symmetrical and balance coordinate system to an angle θ , as shown in Fig. 4.16b, and adjust the ply numbers to fully meet the requirements of strength, stiffness, and aerodynamics. The obtained skin laminating is still symmetric and balanced.
- ③ Individually rotate 0° plies to angle α , as shown in Fig. 4.16c (or $\pm 45^\circ$ plies), and optimized the design to minimize the weight. The obtained skin laminating will be symmetrical and balanced.

(2) Aeroelastic tailoring design of a composite forward-swept wing [13]

Because isotropic metal materials encounter insurmountable forces in forward-swept wing designs caused by twisting divergence, great attention should be given to aluminum forward-swept wings in terms of structural weight (Fig. 4.17).

Controlling forward-swept wing wash-in, and changing it into wash-out is the fundamental approach to increasing divergence speed. Wing surface cross-coupling stiffness and the coupling stiffness between bending curvature and twisting curvature play a key role in the control of wing wash-in and wash-out.

When the bending–twisting coupling stiffness coefficients D_{16} and D_{26} in the composite laminated wing skin bending–twisting stiffness matrix have different values, different bending–twisting coupling deformations will take place. These effects can produce wash-in or wash-out effects, as shown in Fig. 4.18.

When $D_{16} = D_{26} = 0$, there will be no bending–twisting coupling in wing skin laminates (Fig. 4.18a).

When D_{16} and D_{26} take negative values, and up-forward bending occurs in the wing skin, twisting will cause the front edge to deform down and forward such that a wash-out effect will take place (Fig. 4.18b).

When D_{16} and D_{26} take positive values, and up and forward bending occurs in the wing skin. Twisting will cause the front edge to deform in this manner giving rise to wash-in effects (Fig. 4.18c).

The basis of forward-swept wing aerodynamic tailoring design is to engineer bending–twisting coupling stiffness coefficients D_{16} and D_{26} with negative values.

Symmetrical and unbalanced ply design can be used to make D_{16} and D_{26} with a negative value. This is the main approach in composite forward-swept wing aerodynamic design. Symmetrical plies can make $[B] = 0$, in which no deformation exists coupling between the in-plane and out-of-plane loads. This is useful for cure

Fig. 4.17 Correlation between wing weight and sweep angle

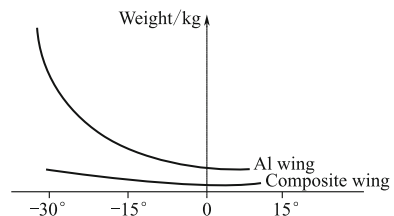
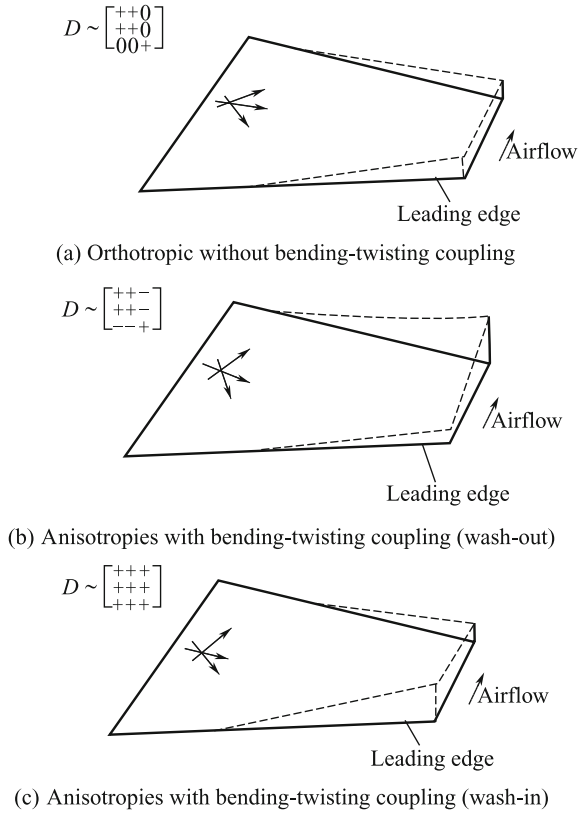


Fig. 4.18 Correlation between positive/negative values of bending–twisting coupling stiffness and wing skin wash-in/wash-out



deformation control. Unbalanced ply design can be realized with unequal numbers of plies with ply angles $+\theta$ and $-\theta$, or by changing the ply angle in balanced laminates. These choices will depend on the requirements of the design program.

In the above discussion on forward-swept wing design, the focus is on a technical approach to increase the divergence speed. In fact, aeroelastic tailoring is the height of a combined design approach, giving many benefits in aeroelastic performances, besides increasing divergence speed. For forward-swept wings, this approach can also increase buffet speed, improve operational safety, reduce motor load, and improve the lift-to-drag ratio in aerodynamic quality curves. These performances are closely related to aeroelastic deformation control, reflecting wash-in, washout, and chord wise deflection, simultaneously. There is often conflict between these technical approaches, for example, the contradiction between divergence and buffet speed. In general, wing washout is useful for divergence prevention, while wash-in is useful to increase buffet speed. Hence aero elastic tailoring should try to reach a combined optimized design.

(3) Hollow step grid structure [15]

This design includes skin and hollow step grids. Grids are mounted on a skin as shown in Fig. 4.19. The grid width and thickness can be changed based on the application requirements. It can be manufactured as an integrated component without additional fasteners, and weight reduction can be realized, with guaranteed strength and stiffness. In Fig. 4.20, the design concept of a cabin door design is shown.

4.6.3 Sandwich Structure Design and Analysis

4.6.3.1 Basic Design Concept of Sandwich Structure

(1) Load-bearing and failure modes of sandwich structures

Owing to their light weight and high bending stiffness, sandwich structures are widely used in aircraft structures, as shown in Fig. 4.21. Sandwich structures consist of a pair of thin surface panels and a honeycomb core. Core materials

Fig. 4.19 Step grid design concept

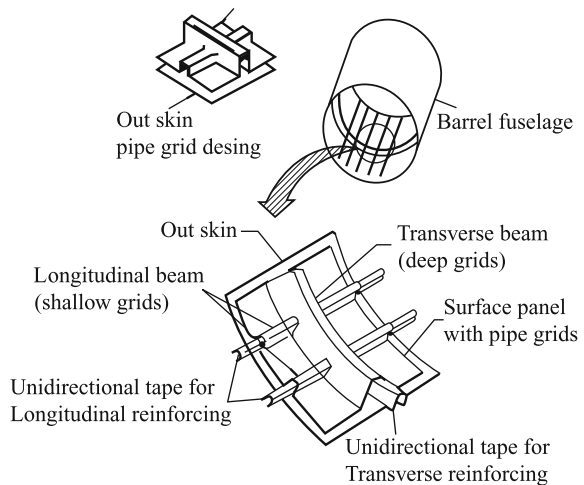


Fig. 4.20 Hollow step grid cabin door design

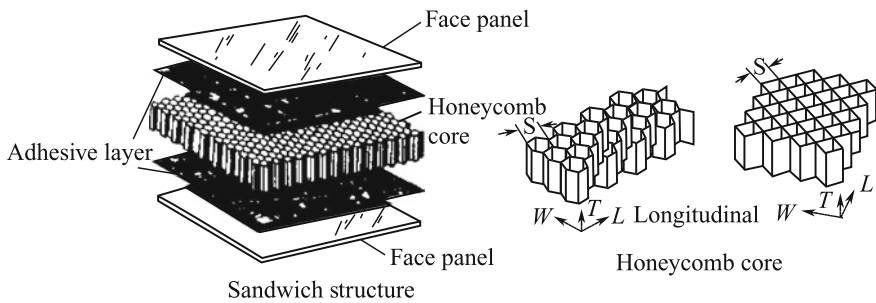
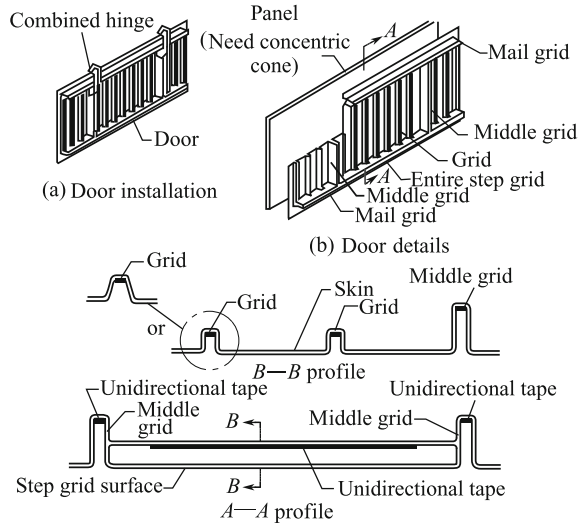
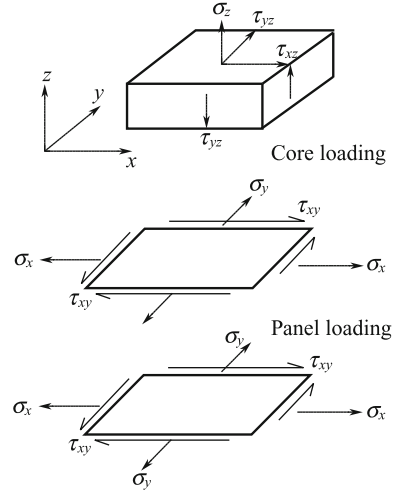


Fig. 4.21 Honeycomb sandwich construction

may be classed as longitudinal (L) and transverse (W), and have very low stiffness in the LW plane, i.e., $G_{LW}, E_L, E_W = 0$, and give a definite value to E_T and G_{LT} and G_{WT} . The load-bearing conditions are shown in Fig. 4.22, surface panels will withstand tensile, compression, and shear loads in the xy plane, where the xy axes are in the same plane as LW. Core materials provide support to the surface panels and can only withstand transverse shear load and loads vertical to the xy plane [2].

The failure modes of sandwich structures include: total buckling, surface panel wrinkling and buckling, surface bending failure, transverse shear failure, local crash, and impact damage failure. Several failures can occur at the same time during practical applications, and hence strength corrections should be performed for several failure modes.

Fig. 4.22 Load-bearing of sandwich structure component



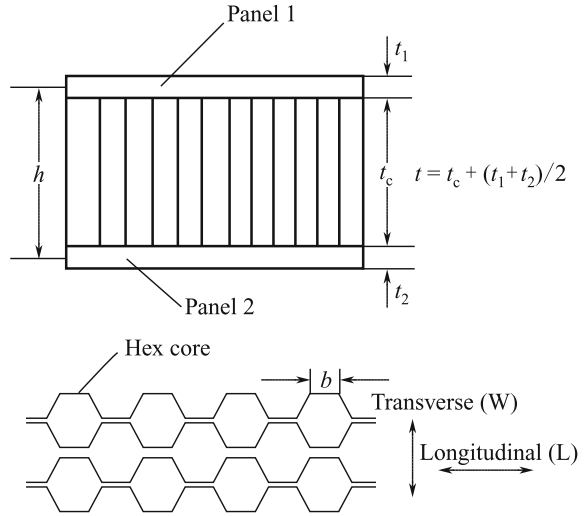
(2) Sandwich structure preliminary design—engineering beam approach

Sandwich structures have similar load-bearing features to I-cross-section beams. Thus, in preliminary design, the simple engineering beam approach can be used to determine the preliminary dimensions of sandwich structures. The dimensional definition of sandwich structures is shown as in Fig. 4.23.

- ① Mechanical properties of sandwich panels: First use laminate theory to determine the mechanical properties of the surface panels: E_x , E_y and ν_{xy} , ν_{yx} . The mechanical properties of the core materials include: longitudinal shear modulus G_{TL} , transverse shear modulus G_{TW} , longitudinal shear strength $[\tau_{TL}]$, transverse shear strength $[\tau_{TW}]$, compression modulus E_c , tensile modulus E_T (usually replaced by E_c), compression strength $[\sigma_c]$, tensile strength $[\sigma_c^t]$ (usually replaced by $[\sigma_c]$), and normal tensile modulus. Subscripts L, W, and T represent the longitudinal, transverse, and normal directions, as shown in Fig. 4.23.

In some references, several equations are provided for the calculating the mechanical properties of sandwich structures, but in engineering, test results should be used in the structure design.

Fig. 4.23 Dimensional definition of sandwich structures



The followings should be taken into account in the application of the above properties:

- (a) $[\tau_{TL}]$ and $[\tau_{TW}]$ are related to core thickness and highly reliable test results should be used, or, thickness modification should be engineered in. A value of 0.7 is recommended as a conservative correction factor.
- (b) The normal tensile modulus is usually replaced by the compression modulus.
- (c) The property data of core materials should be based on material specifications.

② Sandwich panel stiffness

- (a) The bending stiffness of sandwich panels: The bending stiffness per unit width of a panel in the i direction ($i = x, y$) (units N-mm) can be calculated by:

$$D_i = \frac{E_{i1}t_1E_{i2}t_2h^2}{(E_{i1}t_1 + E_{i2}t_2)\lambda} + \frac{1}{12\lambda}(E_{i1}t_1^3 + E_{i2}t_2^3) \quad (4.18)$$

where $\lambda = (1 - \nu_{xy}\nu_{yx})$,

ν_{xy}, ν_{yx} are the panel Poisson's ratio, and subscripts 1 and 2 denote the top and bottom surface panels. When the panel is very thin, the second term in the equation can be ignored.

- (b) The shear stiffness of sandwich panels: The transverse shear stiffness of a unit width of panel (N/mm) can be calculated by the following equation:

$$U = h^2 G_c / t_c \quad (4.19)$$

where G_c is the core shear modulus. In some special cases ($G_c = G_{TL}$ or G_{TW})

$$U = h^2 G_{TL} / t_c \quad (4.20)$$

$$U = h^2 G_{TW} / t_c$$

- ③ Core material density: Core density is an important index reflecting the core mechanical properties and weight. Core density is the same concept as volumetric weight, a dimensional unit. A regular hexagon honeycomb cell has a core density (kg/m^3) given by:

$$\rho = \frac{8}{3\sqrt{3}} \rho_m (t_m / b) \quad (4.21a)$$

A square honeycomb cell has a core density given by:

$$\rho_c = \frac{2t_m}{b} \rho_m \quad (4.21b)$$

where

- ρ_m —core cell wall material density, kg/m^3 ;
 t_m —core cell wall material thickness, mm;
 b —cell side length, mm.

In general, the above equations underestimate the actual core density.

- ④ Sandwich beam design and analysis: When sandwich panels have an aspect ratio (length versus width) greater than or equal to 3:1, the system can be simplified as a sandwich beam for design purposes. The shorter side can be considered to be the beam width. Following the external load, material selection and preliminary design can be performed to determine the sandwich beam dimensions. Following the local pressure (or absorbing force), core density can be determined from the following equation:

$$[\sigma_c] / \sigma_c = 3$$

Preliminary design of sandwich beams can be performed by following the engineering beam equations:

(a) Bending stress on a surface panel given by:

$$\sigma_{\bar{n}} = M / (t_{\bar{n}}hb) \quad (4.22)$$

(b) Shear stress on core cell is given by:

$$\tau_c = V / (hb) \quad (4.23)$$

(c) Deflection is given by:

$$\Delta = \frac{2k_b PL^3 \lambda}{E_f t_f h^2 b} + \frac{k_b PL}{h G_c b} \quad (4.24a)$$

or

$$\Delta = \frac{k_b PL^3}{D} + \frac{k_b PL}{h G_c b} \quad (4.24b)$$

(d) The wrinkle stress on a surface panel is given by:

$$\sigma_{cr} = \frac{2E_f}{S} \left(\frac{t_f}{S} \right)^2 \quad (4.25)$$

(e) The buckling stress on a surface panel is given by:

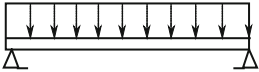
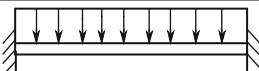
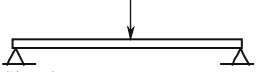
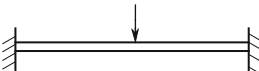
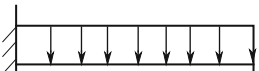
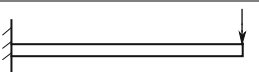
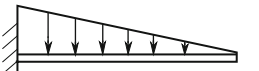
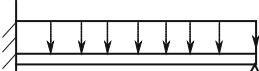
$$\sigma_{cr} = 0.82E_f \left(\frac{E_c \cdot t_f}{E_f \cdot t_c} \right)^{\frac{1}{2}} \quad (4.26)$$

where M , V , K_b , and K_s are given in Table 4.12.

- M maximum bending moment;
- V maximum shear force;
- k_b bending deflection constant;
- D bending stiffness;
- P total load;
- $\sigma_{\bar{n}}$ surface panel stress;
- t_f surface panel thickness;
- τ_c core shear stress;
- Δ deflection;
- E_f surface panel modulus, taking the values in beam axial direction;
- σ_{cr} surface critical stress;
- λ $1 - \nu_{xy}\nu_{yx}$;
- S core cell dimensions (core cell inscribed circle diameter);
- E_c core compression modulus;
- t_c core thickness.

Others variables are shown in Fig. 4.23.

Table 4.12 Calculation of V , M , K_b , and K_s of beams

Beam type	Max. shear force V	Max. bending moment M	Bending deflection constant K_b	Shear deflection constant K_s
 Simple support Uniform force	$0.5P$ ($P = qL$)	$0.125PL$	0.01302	0.125
 Two-point Fixed-support Uniform force	$5P$ ($P = qL$)	$0.08333PL$	0.002604	0.125
 Simple support Concentrated force	$0.5P$	$0.25PL$	0.02083	0.25
 Two-point Fixed-support Concentrated force	$0.5P$	$0.125PL$	0.00521	0.25
 Suspend beam Uniform force	P ($P = qL$)	$0.5PL$	0.125	0.5
 Suspend beam Concentrated force	P	PL	0.3333	1
 Suspend beam Triangle distribution	P ($P = 0.5qL$)	$0.3333PL$	0.06666	0.3333
 One end fixed, one end uniform force	$0.625P$ ($P = qL$)	$0.125PL$	0.005403	0.07042

shear modulus in two directions, and G_{ij} is zero. To avoid value overflow in the calculation, G_{11} , G_{22} , G_{44} use 1% of the minimum values of G_{33} , G_{55} , and G_{66} .

$$G_{11} = G_{22} = G_{44} = \min(G_{33}, G_{55}, G_{66}) \times 0.001$$

For the coordinate system in arbitrary X , Y , Z axes the stiffness coefficients in the stress–strain relationship should be calculated by tensor algorithms, which are automatically processed by FEM programs.

② Use of MSC/NASTRAN program

- (a) Separation between a panel and core. The panel uses plate elements; the core uses a special body unit.
- (b) The core special body unit can be divided into hexahedron (CHEXH), pentahedral (CPENTA) or tetrahedron (CTETRA) units. For a sandwich panel with a rectangular projection, either QUAD4 or HEXA units can be used, based on the sandwich structure construction.
- (c) Use the MAT9 card to denote the core modulus G_i in the coordinate system L , W , T_j .
- (d) Define the material coordinate system.

When the volume unit orientation is in an arbitrary coordinate system, the correlation between MAT9 and the arbitrary orientation should be established through a CORDM domain in the PSOLID card. In such a case, the output special body unit stress components will be the components in the defined coordinate axes in CORDM domain.

③ Finite element mesh partition concept

- (a) For full-height sandwich structures, external loads will be mainly distributed asymmetrically. If the core material strength is critical, the core special body unit should be analyzed as a multiple-layer partition from top to bottom. If the core material strength is not critical, a single-layer partition can be used.
- (b) For in-plane load sandwich structures, the core can be analyzed as a single-layer partition for total buckling analysis.
- (c) In buckling analysis, the mesh partition should be of an appropriate size to properly reflect the buckling behavior. Attention should be paid to the rational modeling of boundary conditions.

(2) **Sandwich strength corrections**

A design load is used for stress analysis, and the results can be used for strength correction and structural design modifications.

① In-plane strength correction

- (a) Operation strain \leq allowable strain.
 - (b) Modification of operation stress under design load should be performed with the modifying factor is f_m .
Operation stress $\times f_m \leq$ panel allowable strength.
For composite panels, $f_m = 1.06\text{--}1.15$.
- ② Core material strength correction: The FEM results σ_z (stress at cell center) should be modified by the factor f_c .

$$\sigma_z \times f_c \leq [\sigma_c]$$

where

$[\sigma_c]$ —core material allowable compression strength,
 f_c —modification factor, depending on the core partition layer number as well as loading conditions usually $f_c = 1.0\text{--}2.0$,

In the case of a core “single-layer” partition and a normally distributed load applied to a sandwich panel, then $f_c \approx 2.0$.

Core shear strength can be corrected by the following equation:

$$\begin{aligned}\tau_{LT} &\leq [\tau_{LT}] \times 0.7 \\ \tau_{WT} &\leq [\tau_{WT}] \times 0.7\end{aligned}$$

where $[\tau_{LT}]$ $[\tau_{WT}]$ —core allowable shear strength.

4.6.4 Composite Structure Anti-crash and Energy Absorption Design

4.6.4.1 Aircraft Body Structure Crash Resistant Design Features

When an aircraft crashes, the body structure is subjected to a large instantaneous deformation to absorb the impact energy. Theoretical analysis of large structural impact deformation involves multiple complex fields of study, such as collision mechanics and material high strain rate and impact damage mechanics. Hence, body structure anti-crash and energy absorbing design should be performed by combining digital stimulation analysis and testing verification. Testing plays a particularly important role. The design should be started from the crash/absorption of structural components [3].

The measures taken for structural crash absorption will increase structural weight. This increase is considered to be a fixed additional weight, so low mass composites with high energy absorption are important for structural crash/absorption design. Many studies have indicated that energy absorption components, such as agamid/epoxy composite sine-wave beams, offer better energy

absorption capacities than that of aluminum alloy components. Use of composite components may also reduce the weight requirements of crash absorption designs.

4.6.4.2 Composite Crash Absorption Component Design

Composite body structures should be able to provide at least the same level of crash safety as metal structures. The design of energy absorption components provides a basis for materials selection and selection of configuration parameters in crash absorption structure designs. Thus, composite crash/absorption component design is an important part of the design process. Anti-crash and energy absorption components can be classified as follows:

(1) Metal crash absorption components

Structural metal materials such as Al alloy are the tough materials, which can produce large deformations to absorb crash impact energies. The toughness of metals can be used to design crash/absorption body structures.

(2) Composite crash/absorption components

Fiber-reinforced composites show linear elastic behaviors at 0° tensile and compression loads with a small failure strain. However, nonlinear $\pm 45^\circ$ off-axis tensile and compression loads have a large failure strain and show tough material behavior. Thus, in composite crash/absorption component design, a design scheme with tube and wave beams with $\pm 45^\circ$ plies as the base, and 0° plies as supplements are preferred, as shown in Fig. 4.24. Tube components may be easily manufactured at low cost, and the test result analysis is straightforward.

Composite sine-wave web beams are a high stiffness and stability structural component with both load-bearing and energy absorption abilities. The shapes of sine waves and ply stacking can be designed to give good processing ability. An energy absorption component made of a sandwiched web beam with a ladder core is shown in Fig. 4.25. This structure is used in the helicopter NH90. Its absorbing ability is equivalent to that of a sine-wave web beam, but it can be processed more easily.

Fig. 4.24 Composite crash/absorption components

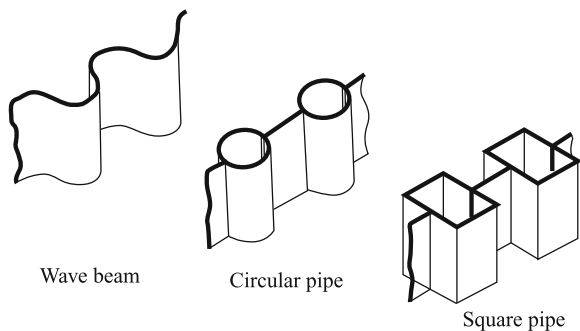
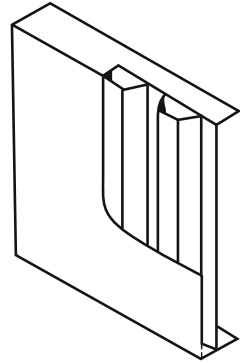


Fig. 4.25 Energy absorption component made of sandwich web beam with ladder cores



Material selection for crash absorption components and common structural components requires materials with high toughness and energy absorption capacity, which also have good mechanical properties and processing ability. Currently, Kevlar/carbon hybrids or woven Kevlar are selected as reinforcing materials and an epoxy or thermoplastic (such as PEEK) resin matrix is selected with high toughness. For RTM processing, a special resin matrix is required. Test-based verification is needed for all selected composite systems.

4.6.4.3 Structural Design of Composite Crash/Absorption Floor

Crash/absorption floor structures are an important part of aircraft crash resistance design. In designing these structures, the first consideration is energy absorption and the second is their load-bearing ability. With a selection of a proper structural configuration, parameters, and materials a balance between the load-bearing and crash absorption requirements can be realized.

(1) Structural design principle of crash/absorption composite floor

Crash/absorption composite floor structures consist of a fuselage structural floor and energy absorbing structure as shown in Fig. 4.26. In an airplane crash, the impact energy to the aircraft body will be mainly absorbed by an energy absorption structure. The floor deformation will absorb part of the residual energy. The energy absorption ability of the energy absorption structure is controlled through its structural design.

(2) Structural design of sine-wave beam crash/absorption floor

As an energy absorbing component, sine-wave beams are commonly used in crash/absorption floor design. The sine-wave beam crash/absorption floor construction used in the front body of a “Tiger” helicopter is shown in Fig. 4.27. Crash

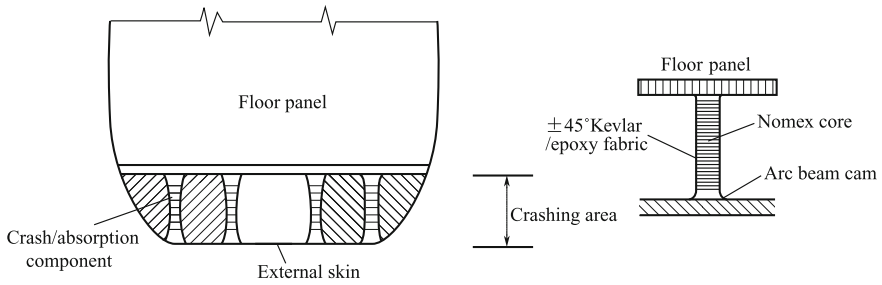


Fig. 4.26 Structural design principle of crash/absorption floor

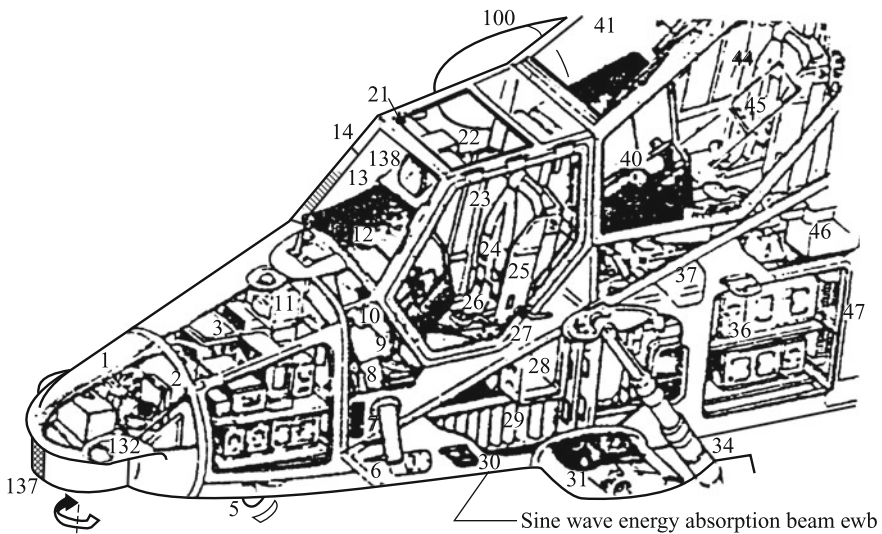


Fig. 4.27 Crash/absorption floor in "Tiger" front helicopter body

absorption structures feature a longitudinal/transverse cross-beam construction, which can be a single component in a single cross, double cross, or well-shape configuration, as shown in Fig. 4.28. A recommended configuration is shown in Fig. 4.29.

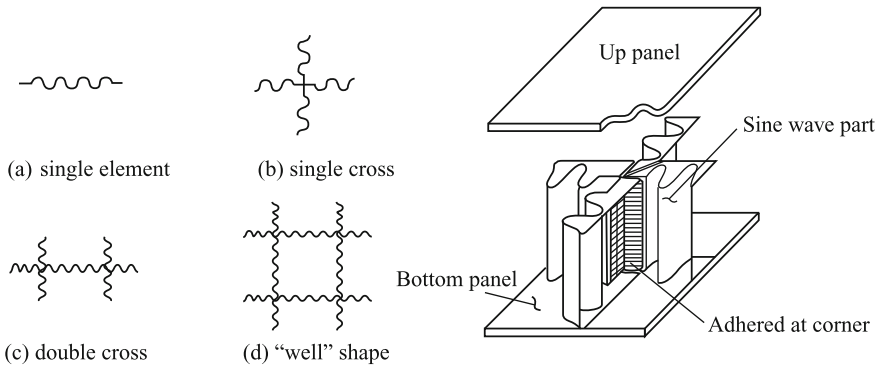
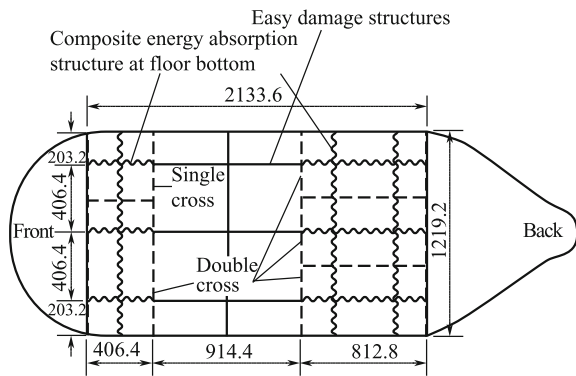


Fig. 4.28 Basic pattern of a sine-wave web assembly

Fig. 4.29 Recommended optimized energy absorption construction configuration



4.6.5 Analysis of Thick Cross-sectional Composite (Thick Laminate)

Thick cross-section composites refer to thick laminates containing a large number of plies.

Currently, thin composite laminates are most often used in aerospace engineering. However, thick composite laminates are becoming more common. For example, the panel thickness in the wing root of a large commercial airplane is 30–45 mm.

In an A380, some panels of the central wing critical joints have thicknesses up to 160 mm and the number of plies is of the order of hundreds or thousands.

Compared with thin laminates, thick laminates can offer higher impact and damage resistances. Their damage tolerance is a less serious concern and thick laminates can also provide improved thermal resistance and hot/wet properties, and

operation performances. However, in terms of processing and property testing, the analysis and design of thick laminates require special care to be taken.

4.6.5.1 Features of Thick Cross-section Composites

Owing to the dimensional increase in the thickness direction, the stress component in this direction cannot be ignored. Hence, 3D stress analysis should be performed on thick laminates. Even under a single in-plane load, thick laminates will also show a 3D stress distribution. Any stress components reaching a critical state can result in thick laminate failure. Therefore, the above-mentioned thin laminate 2D stress analysis and the corresponding failure criteria are not appropriate for thick laminates.

In addition, the 3D effects in thick laminate composite are more significant than those in uniform isotropic materials. The strength along the thickness direction is very low, and has a high sensitivity to matrix cracking and delamination. Thus, it is necessary to perform 3D stress analysis to establish the failure criterion for thick laminates. The failure modes governed by the fiber, matrix, and interface should all be considered.

Many new problems will be encountered in thick composite processing, such as decreasing residual stress, reducing void content, and ensuring full curing. To minimize these effects, it is necessary to use special resin matrices, processing techniques, modes, and curing conditions. Special attention should be given to two main issues in thick composite processing: A low-level residual stress should be achieved; the production efficiency should be high, i.e., the time required for full curing should be as short as possible. Rapid heating and cooling can reduce the curing time, but can also induce higher residual stress. Slow curing cycles will result in a low production rate and high cost; however, a fully cured part can be expected. Cure modeling is very important for thick composite manufacture and can provide a good understanding of the cure kinetics and instant cure degree in the cure cycle. This knowledge is useful for predicting the processing stress and is an important approach to guaranteeing processing quality.

In thick composite laminate analysis and design, it is necessary to understand the multi-axial strength and stiffness to fully take advantage of thick composites. Currently, there is a lack of studies on thick composite design, analysis, and materials testing.

In Fig. 4.30, a flowchart of thick composite analysis is given.

4.6.5.2 3D Stress Analysis of Thick Composites

As mentioned above, 3D stress analysis should be performed for thick composites. The effects of interlaminar tensile stress and shear stress should be considered when thick laminate is under out-plane loading conditions. Furthermore, 3D stress

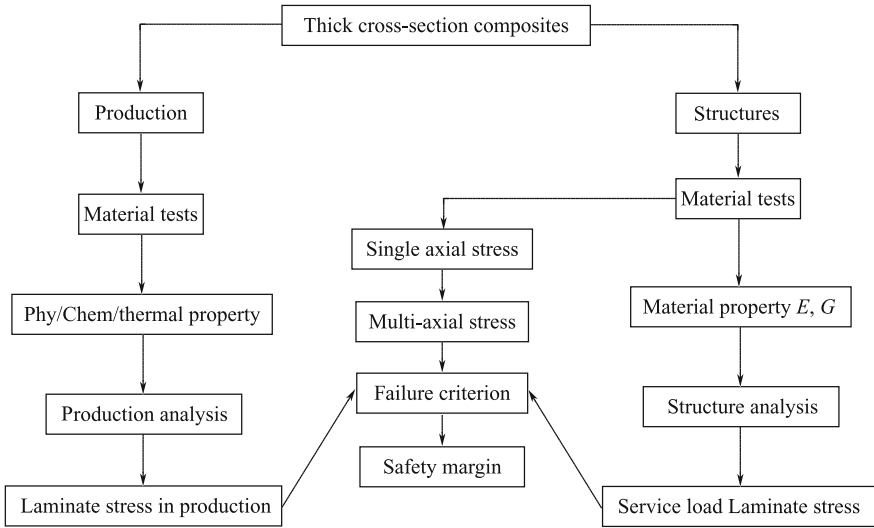


Fig. 4.30 Flow chart of thick composite analysis

analysis is needed in unidirectional isotropic laminates. The stress–strain expression is given as:

$$\begin{Bmatrix} \varepsilon_1 \\ \varepsilon_2 \\ \varepsilon_3 \\ \gamma_{23} \\ \gamma_{31} \\ \gamma_{12} \end{Bmatrix} = \begin{bmatrix} S_{11} & S_{12} & S_{13} & 0 & 0 & 0 \\ S_{12} & S_{22} & S_{23} & 0 & 0 & 0 \\ S_{13} & S_{23} & S_{33} & 0 & 0 & 0 \\ 0 & 0 & 0 & S_{44} & 0 & 0 \\ 0 & 0 & 0 & 0 & S_{55} & 0 \\ 0 & 0 & 0 & 0 & 0 & S_{66} \end{bmatrix} \begin{Bmatrix} \sigma_1 \\ \sigma_2 \\ \sigma_3 \\ \tau_{23} \\ \tau_{31} \\ \tau_{12} \end{Bmatrix} \quad (4.28)$$

If engineering constants are used, then:

$$\begin{Bmatrix} \varepsilon_1 \\ \varepsilon_2 \\ \varepsilon_3 \\ \gamma_{23} \\ \gamma_{31} \\ \gamma_{12} \end{Bmatrix} = \begin{bmatrix} \frac{1}{E_1} & -\frac{\nu_{21}}{E_2} & -\frac{\nu_{31}}{E_3} & 0 & 0 & 0 \\ -\frac{\nu_{12}}{E_1} & \frac{1}{E_2} & -\frac{\nu_{32}}{E_3} & 0 & 0 & 0 \\ -\frac{\nu_{13}}{E_1} & -\frac{\nu_{23}}{E_2} & \frac{1}{E_3} & 0 & 0 & 0 \\ 0 & 0 & 0 & \frac{1}{G_{23}} & 0 & 0 \\ 0 & 0 & 0 & 0 & \frac{1}{G_{13}} & 0 \\ 0 & 0 & 0 & 0 & 0 & \frac{1}{G_{12}} \end{bmatrix} \begin{Bmatrix} \sigma_1 \\ \sigma_2 \\ \sigma_3 \\ \tau_{23} \\ \tau_{31} \\ \tau_{12} \end{Bmatrix} \quad (4.29)$$

where

$$\frac{\nu_{12}}{E_1} = \frac{\nu_{21}}{E_2}, \frac{\nu_{13}}{E_1} = \frac{\nu_{31}}{E_3}, \frac{\nu_{23}}{E_2} = \frac{\nu_{32}}{E_3} \quad (4.30)$$

Nine independent elastic parameters are involved: $E_1, E_2, E_3, G_{12}, G_{13}, G_{23}, \nu_{12}, \nu_{13},$ and ν_{23} .

If a difference exists between the tensile modulus and compression modulus, the mean value of the two should be used for small differences; for large differences, the applied external load should be used for the tensile and compression moduli.

Symmetrical and balanced laminates can be treated as orthotropic laminates, by changing the subscripts 1, 2, 3 in the above equation to x, y, z coordinate axes to derive the laminate stress–strain relationship. Hence, the laminate takes the nine independent elastic parameters: $E_x, E_y, E_z, G_{xy}, G_{xz}, G_{yz}, \nu_{xy}, \nu_{xz}, \nu_{yz}$.

4.6.5.3 Determination of the Properties of Thick Composites

For design and establishing failure criterion of thick composites, it is necessary to determine their properties and behavior. Determination of the 3D properties of thick composites is more complex than that of thin 2D laminates. The use of testing supported by theoretical calculations is the main approach to analyzing these structures:

(1) Testing Methods

Problems may arise with the testing methods, specimens, equipment, and fixtures used for thick composite testing. In general, the following aspects should be considered:

- Fixtures and clamping
- Specimen design and optimization
- Computer control interface
- Proper control of displacement in the central zone of the specimen
- The internal stress state of thick composites
- Multi-axial extensometers and other measuring devices
- Environmental considerations
- Data collection and processing
- Multi-axial yielding and failure criterion
- Dimensional effects and magnifications
- Static and dynamic testing, including fatigue and impact
- Sensitivity of stress concentration
- NDT evaluation

- ① Single-axis testing: Conventional 2D single-axis testing of unidirectional laminates includes measurements of in-plane tensile moduli (E_{1t}, E_{2t}), compression moduli (E_{1c}, E_{2c}), shear modulus (G_{12}), and tensile–compression strengths ($T_X, X_{-C}, \bar{Y}_t, \bar{Y}_c$) and tensile–compression failure strains ($\varepsilon_{1t}, \varepsilon_{1c}, \varepsilon_{2t}, \varepsilon_{2c}$). In 3D single-axis testing, new characteristics for testing, include: the tensile modulus in the thickness direction (E_{3t}); compression modulus (E_{3c}) and shear

moduli (G_{13}, G_{23}) related to thickness; and the tensile–compression strengths (T_{zu}, Z_c) and tensile–compression failure strain ($\epsilon_{3t}, \epsilon_{3c}$).

In compression testing of thick composites, special attention should be paid to the design and bonding of the specimen end tabs as well as the end supports. Any impact, end cracking or improper fixturing, may negatively affect the material’s properties and give inconclusive data. Tables 4.13 and 4.14 present typical room-temperature testing data from medium modulus C-fiber/epoxy unidirectional laminates and multi-directional laminates.

- ② Multi-axis testing: Multi-axis testing is needed to evaluate the behavior of thick laminates under 3D loading conditions. Two- or three-axis testing machines are needed. The load can be applied along two intervertical or three intervertical axes. Figures 4.31 and 4.32 show two-axis and three-axis tensile–compression testing systems, respectively.

Specimens for multi-axis testing should be specially designed, having a 3D construction, as shown in Fig. 4.33.

(2) **Calculation Methods**

When theoretical methods are used to calculate composite mechanical properties, the constituent mechanical properties and micromechanics should be considered.

Table 4.13 Typical 3D test data of medium modulus C-fiber/epoxy unidirectional laminates

Item	x_t	E_{1t}	ϵ_{1t}	x_c	E_{1c}	ϵ_{1c}	\bar{Y}_t	E_{2t}	ϵ_{2t}
Property	1720	114	15,200	1170	114	10,300	55.2	9.65	5700
Item	\bar{Y}_c	E_{2c}	ϵ_{2c}	S	G_{12}	r_{12}	Z_t	E_{3t}	ϵ_{3t}
Property	207	9.65	21,500	103	6.0	17,000	55.2	9.65	5700
Item	z_c	E_{3c}	ϵ_{3c}	S_{13}	G_{13}	r_{13}	S_{23}	G_{23}	γ_{23}
Property	207	9.65	21,500	82.7	6.0	4000	82.7	3.8	22,000

Note 1. Units: Strength in MPa, modulus in GPa, strain in $\mu\epsilon$; 2. Laminate thickness: >6.35 mm; 3. Assume transverse isotropy in 2–3 plane

Table 4.14 Typical 3D test data of medium modulus C-fiber/epoxy cross-ply laminates $[0_3/90]_n$

Item	σ_{xt}	E_{xt}	ϵ_{xt}	σ_{xc}	E_{xc}	ϵ_{xc}	σ_{yt}	E_{yt}	ϵ_{yt}
Property	965	103	9330	765	88.9	8600	241	39.0	12,900
Item	σ_{yc}	E_{yc}	ϵ_{yc}	S_{xy}	G_{xy}	γ_{xy}	σ_{zt}	E_{zt}	ϵ_{zx}
Property	503	39.0	12,900	105	4.8	22,000	23.4	7.72	3040
Item	σ_{zc}	E_{zc}	ϵ_{zc}	S_{xz}	G_{xz}	γ_{xz}	S_{yz}	G_{yz}	γ_{yz}
Property	414	11.3	3600	28.0	3.7	7700	42.4	4.6	9300

Note 1. Units: same as above; 2. Laminate thickness: 15 mm; 3. $V_f = 61.4\%$, void content 0.04%

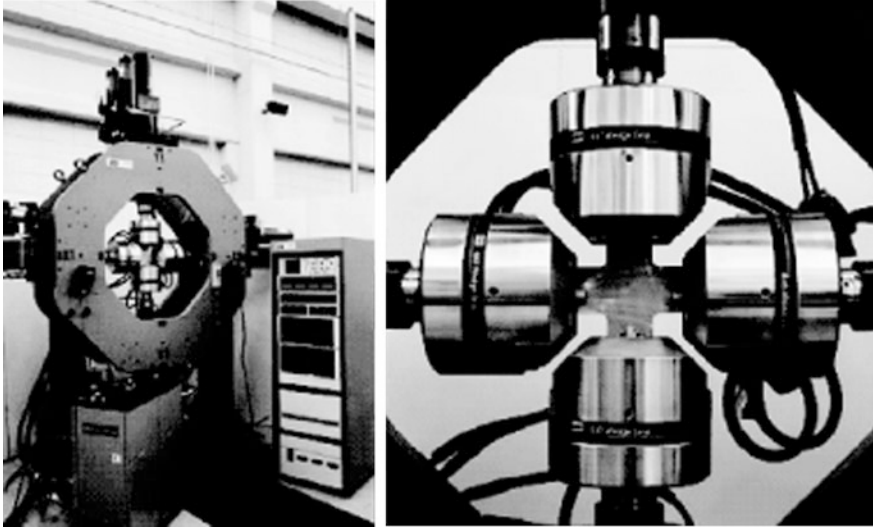


Fig. 4.31 Two-axis tensile-compression testing (I)



Fig. 4.32 Three-axis tensile-compression testing (II)

A data processing method is introduced below.

- ① 3D properties of unidirectional laminates: As mentioned above, unidirectional laminates have nine material properties, i.e., E_1 , E_2 , E_3 , G_{12} , G_{13} , G_{23} , ν_{12} , ν_{13} , ν_{23} . The values of E_1 , E_2 , G_{12} and ν_{12} are

Fig. 4.33 Two-axis testing specimen

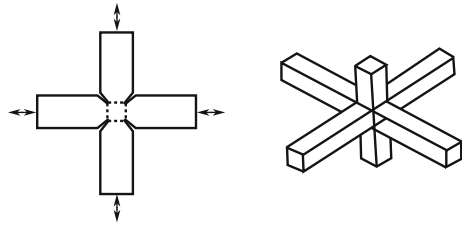


Table 4.15 3D elastic constants of composite materials

Material	Performance								
	$E_1/$ GPa	$E_2/$ GPa	$E_3/$ GPa	$G_{12}/$ GPa	$G_{13}/$ GPa	$G_{23}/$ GPa	ν_{12}	ν_{13}	ν_{23}
AS4/3501-6	113.6	9.65	9.65	6.0	6.0	3.1	0.334	0.328	0.540
S2/3501-6	49.3	4.7	4.7	6.8	6.8	4.9	0.296	0.306	0.499

easily derived from conventional testing. For a calculation, assuming that the 2–3 plane is transverse isotropic, then:

$$E_3 = E_2, G_{13} = G_{12}, \nu_{13} = \nu_{12}, G_{23} = \frac{E_2}{2(1 + \nu_{23})}.$$

In this way, only the term ν_{23} needs to be experimentally determined. The test values of ν_{23} can be found in some sources. Table 4.15 presents the 3D elastic constants of CF and GF S2 reinforced epoxy composites. The values of $E_1, E_2, \nu_{12}, \nu_{13},$ and ν_{23} are derived from thick composite compression testing.

② 3D properties of multi-directional laminates (thick laminates):

As mentioned above, multi-directional laminates have nine material properties. The values of $E_x, E_y, G_{xy}, \nu_{xy}$ can be easily derived from conventional testing or calculated by classical laminate theory; however, determining the out-of-plane properties is complex by both testing and theoretical approaches. Hence, there are fewer test data available for multi-directional laminates. Several theoretical methods are available; however, these approaches are based on unidirectional in-plane properties. Owing to the lack of available 3D testing data, it is difficult to verify theoretical calculations.

4.7 Analysis of Structural Stability

4.7.1 Stability Analysis of Laminates

The failure mode of thin panel structures of composite materials under compressive or shear loads is an instability known as buckling. Therefore, stability analysis is required to design these structures [2, 14].

For analysis the structure may be simplified as three components: ① rectangle laminates; ② stiffened stringers; ③ stiffened laminates.

Rectangular flat plates are widely used in numerous aerospace structures in the form of unstiffened panels and panels between the stiffened stringer of a stiffened panel, elements of a stiffened stringer and the skin of the air foil. The bending of the air foil skin is usually ignored in the analysis. The results of simulations with this assumption are relatively safe, but not conservative. The bending of fuselage skin cannot be ignored; however, in this section, only the air foil structure is discussed.

The stiffened stringer is an important component for enforcing the stability of the air foil skin. Commonly used section configurations include angle-, T-, Z-, I-, channel-, and hat-shaped stiffened stringers. It can be assumed that there is no shear load on the stiffened stringer; hence, only the compressive stability needs to be considered.

The skins of airfoils and the empennage are usually made of stiffened laminates. Hence these are the most widely studied components in stability analysis. Although global analysis is highly complex, programs based on the FEM are frequently used for calculations performed by computer. The performance of a preliminary design can be estimated by considering the rectangular plate and stiffened stringer separately.

Next, the stability analysis of three typical components/elements will be introduced.

4.7.1.1 Buckling Analysis of Rectangular Flat Plates

Stability analysis of rectangle plates, also known as buckling analysis, is mainly concerned with the initial buckling load (or simply the buckling load).

Buckling load is related to the stiffness of the laminate, its dimensions (i.e., thickness, length, and width), and peripheral supporting conditions. Compared with isotropic metal plates, the stiffness of anisotropic laminates made from composite materials is complex. Stiffness not only depends on the thickness of laminates but also on the stacking sequence. In the case of symmetrical and balanced laminated plates, if $\pm\theta$ cross-layers are stacked adjacently there are many layers with rigidity coefficients $B_{ij} = 0$, $D_{16} \approx 0$, and $D_{26} \approx 0$. Commonly used laminated plates are orthotropic and can be simply considered under ideal boundary conditions (i.e., simply supported, fixed, and free) and under an evenly distributed load for axial pressure, and shear and transverse compression. With these assumptions, the

buckling load has a closed analytical solution. Therefore, the four edges of orthotropic laminated plate in supported conditions can be properly simplified: The ideal conditions are simply supported, fixed supported, and free boundary conditions. Engineers can apply existing closed formulae to calculate the buckling loads.

The calculation of buckling load in unbalanced and asymmetrical laminates is difficult. Calculations based on numerical methods are commonly used.

The next eight sections introduce calculations used to determine the buckling load of orthogonal anisotropic laminates under different loads and boundary conditions.

(1) Uniaxial load, rectangular flat plate with all sides simply supported

In the case of a rectangular flat plate with all sides simply supported and a compressive pressure applied equally to the two edges of a rectangular flat plate (Fig. 4.34), the formula of the buckling load is:

$$N_{xcr} = \frac{\pi^2}{b^2} \left[D_{11} \left(\frac{b}{a} \right)^2 m^2 + 2(D_{12} + 2D_{66}) + \left(\frac{a}{b} \right)^2 \frac{D_{22}}{m^2} \right] \quad (4.31)$$

In this formula:

- N_{xcr} —axial compressive buckling load per unit length;
- m —buckling half-wave number along the x -axis of plate;
- a, b —length and width of the plate;
- D_{ij} ($i, j = 1, 2, 6$) —bending stiffness factor of plate.

The parameter m can take the values 1, 2, 3, ... in the calculation, to determine a corresponding set. The minimum value of the set is the buckling load of the laminate, N_{xcr} .

(2) Uniaxial load, laminates with loaded edges simply supported and unloaded edges fixed

The case of a uniaxially loaded plate with the loaded sides simply supported and unloaded sides fixed is considered in Fig. 4.35. In this case, the calculation formula of the buckling load is:

Fig. 4.34 Uniaxial load, rectangular flat plate with all sides simply supported

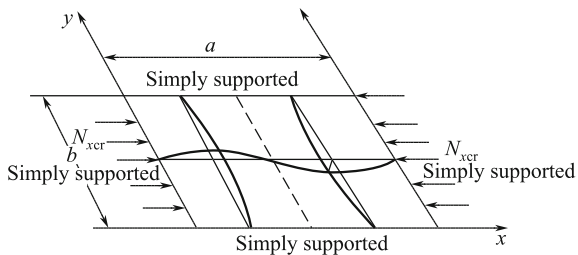


Fig. 4.35 Uniaxial load, rectangular flat plate with loaded edges simply supported and unloaded edges fixed

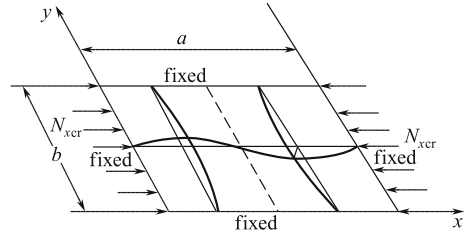
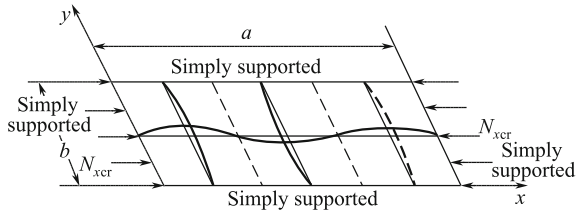


Fig. 4.36 Uniaxial load, long plate with all sides simply supported



$$N_{xcr} = \frac{\pi^2}{b^2} \left\{ \begin{array}{l} D_{11} \left(\frac{b}{a}\right)^2 m^2 + 2.67D_{12} + \\ 5.33 \left[D_{22} \left(\frac{a}{b}\right)^2 + D_{66} \frac{1}{m^2} \right] \end{array} \right\} \quad (4.32)$$

The parameter m can be 1, 2, 3, ... in the calculation to determine a corresponding set. The minimum value of the set is the buckling load of the laminate, N_{xcr} .

(3) Uniaxial load of a long plate with all sides simply supported

To calculate the buckling load of a long plate with a length-to-width ratio of $a/b > 4$ and all sides simply supported under a compressive pressure applied equally to two edges (Fig. 4.36), the following formula is used:

$$N_{xcr} = \frac{2\pi^2}{b^2} \left[\sqrt{D_{11}D_{22}} + D_{12} + 2D_{66} \right] \quad (4.33)$$

This formula can also be applied under the conditions when the two compressed edges are fixed.

Supporting experiments have demonstrated that the error of this calculation is within 10% for a long plate with a width-to-thickness ratio of $b/t > 35$; however, in the case of a narrow plate with $b/t < 35$, the transverse shear effect must be considered and the calculation results should be revised.

(4) Uniaxial load, long plate with all sides fixed

In the case of a long plate with a length-to-width ratio $a/b > 4$ and all edges fixed, when an even compressive pressure is applied to two edges (Fig. 4.37), the buckling load can be calculated from the formula:

Fig. 4.37 Uniaxial load, long plate with all sides fixed

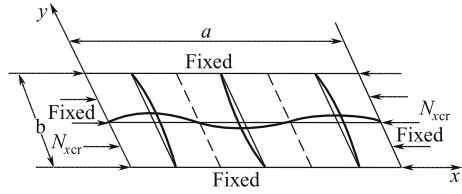
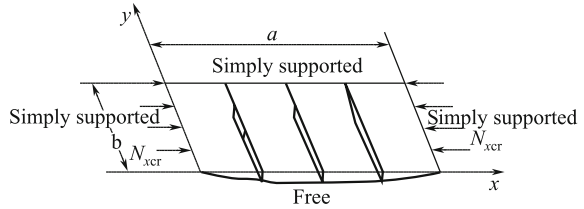


Fig. 4.38 Uniaxial load, rectangular plate with three edges simply supported and one unloaded edge free



$$N_{xcr} = \frac{\pi^2}{b^2} (4.6\sqrt{D_{11}D_{22}} + 2.67D_{12} + 5.33D_{66}) \quad (4.34)$$

This formula can also be applied in the situation of two simply supported loading edges.

In the case of a narrow flat plate with a width-to-thickness ratio of $b/t < 35$, it is also necessary to consider the transverse shear effect and correct the calculation result.

(5) Uniaxial load, long plate with three edges simply supported and one unloaded edge free

When an equal compressive pressure is applied to two edges of a long plate with a length-to-width ratio of $a/b > 4$ having three edges simply supported and one free unloaded edge (Fig. 4.38), the calculation to determine the buckling load is:

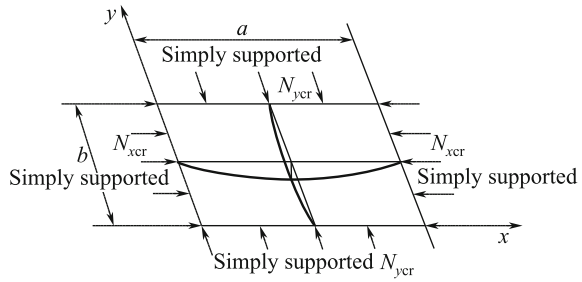
$$N_{xcr} = \frac{12D_{66}}{b^2} + \frac{\pi^2D_{11}}{a^2} \quad (4.35)$$

For a narrow flat plate, with a width-to-thickness ratio $b/t < 20$, it is also necessary to correct the calculation for the transverse shear effect.

(6) Biaxial load, rectangular flat plate with all edges simply supported

In the case of a rectangular flat plate with all edges simply supported and the short edges under an equal longitudinal compressive pressure N_x and the long edges under an equal transverse compressive pressure N_y (Fig. 4.39), the buckling load can be calculated from the formula:

Fig. 4.39 Biaxial load, rectangular flat plate with all edges simply supported



$$N_{xcr} = \frac{\pi^2}{b^2} \left[\frac{D_{11} \left(\frac{b}{a}\right)^4 m^4 + 2(D_{12} + 2D_{66}) \left(\frac{b}{a}\right)^4 m^2 n^2 + D_{22} n^4}{\left(\frac{b}{a}\right)^2 m^2 + \phi n^2} \right] \tag{4.36}$$

$$N_{ycr} = \phi N_{xcr}$$

In this formula: ϕ —ratio of loading, i.e., the ratio of applied transverse to longitudinal loading;

$$\phi = N_y/N_x$$

m —longitudinal buckling half-wave number;
 n —transverse buckling half-wave number.

For calculations, with $m = 1, 2, 3, \dots$ and $n = 1, 2, 3, \dots$, then a corresponding set of N_x can be determined and the minimum value of N_x is N_{xcr} . The calculation gives good results with the use of $n = 1$ and $m = 1$.

(7) Shear load, flat laminate with all edges simply supported or fixed

In the case of all four edges of rectangular flat laminate under an equal shear pressure (Fig. 4.40), the buckling load values of the four edges, in simply supported or fixed cases, can be calculated from the following formula:

$$N_{xycr} = K_s \frac{\pi^2 \sqrt{4D_{11}D_{22}^3}}{b^2} \tag{4.37}$$

where K_s —shear buckling load factor.

The K_s values of the four edges simply supported or fixed are different, and can be determined from the nine variables as the dimensionless parameters α and β as illustrated in Figs. 4.41 and 4.42.

Fig. 4.40 Shear load, rectangular flat plate with all edges simply supported or fixed

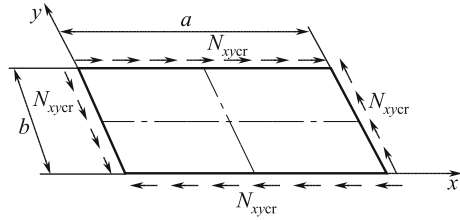


Fig. 4.41 Shear buckling coefficient of rectangular flat plate with all edges simply supported

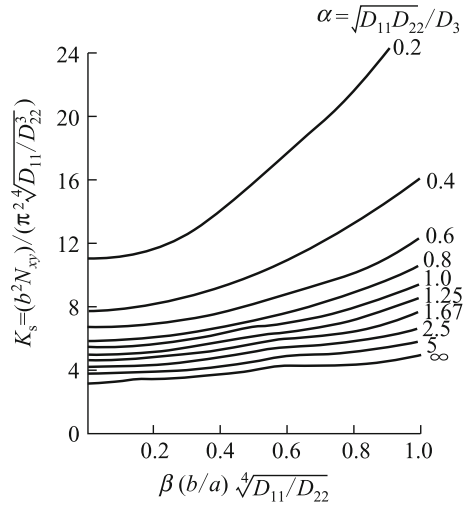


Fig. 4.42 Shear buckling coefficient of rectangular flat plate with all edges fixed

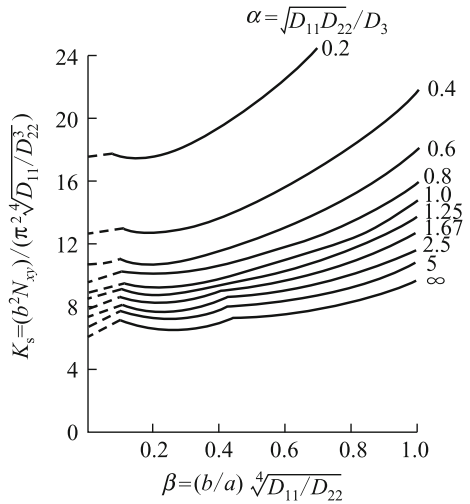
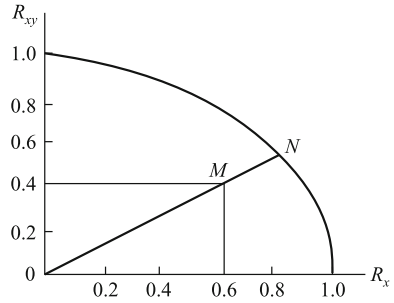


Fig. 4.44 Diagram used to identify buckling safety margin of a rectangular flat plate with shear and compressive complex load



component, stiffened stringers can be decomposed or simplified into two kinds of laths: first, one long lath with one edge free, i.e., one unloaded edge simply supported, while another unloaded edge (or flange) is free; second, a long lath with no free edges, i.e., a web plate with two unloaded edges simply supported, as shown in Fig. 4.45. Analysis of stiffened stringer buckling and crippling should integrate estimated characteristics for all the constituent laths.

(1) Buckling analysis of stiffened stringer components

The buckling load values of two laths can be calculated with the formula presented in Sect. 4.1.1 of this chapter.

The buckling load of a web plate of a long lath with no free edge is given by:

$$N_{xcr} = \frac{2\pi^2}{b^2} [\sqrt{D_{11}D_{12}} + D_{12} + 2D_{66}] \tag{4.39}$$

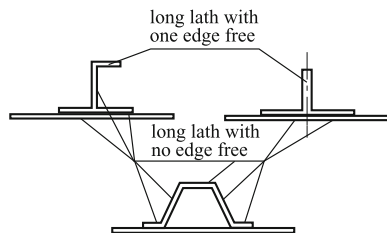
The buckling load of the flange of long lath with one free edge is given by:

$$N_{xcr} = \frac{12D_{66}}{b^2} + \frac{\pi^2 D_{11}}{L^2} \tag{4.40}$$

In these formula, the length of the stiffened stringer L is used instead of the length of the lath a, which appeared in the initial formula.

Equations (4.39) and (4.40) are only suitably for use with orthogonal anisotropic laminates and do not consider the effects of bending and torsion rigidity of laminates, i.e., D_{16} and D_{26} . However, these two formulae are correct for most

Fig. 4.45 Separation of stiffened stringer into long lath with one free edge and long lath with no free edges



symmetrical and balanced laminated plates. If the layering of laminates is slightly asymmetrical, the following equation can be applied for asymmetrical laminates to give results equivalent to those for orthogonal anisotropic laminates. Use the equivalent bending rigidity \bar{D}_{ij} in place of D_{ij} in previous formula, calculated as:

$$[\bar{D}] = [D] - [B][A]^{-1}[B] \tag{4.41}$$

In this formula: $[A]$, $[B]$, $[D]$ —(tension) stiffness matrix, coupling stiffness matrix, bending stiffness matrix of in-plane laminate, respectively;

$[\bar{D}]$ —equivalent bending stiffness matrix of an equivalent orthotropic plate.

The partial buckling load of a stiffened stringer corresponds to the minimum buckling value of the constitute laths and can be determined by the following method:

It is assumed that the initial buckling stress σ_{cri} of the n th component of a stiffened stringer, where k -plate buckling stress σ_{crk} is minimum, is given by $\sigma_{cri} = N_{xcri}/t_i$, $\sigma_{crk} = N_{xcrk}/t_k$.

The partial buckling stress of a stiffened stringer σ_{cr}^{st} is:

$$\sigma_{cr}^{st} = E_{xc}^{st} \left(\frac{N_{xcrk}}{t_k E_{xc}k} \right) \tag{4.42}$$

where:

- N_{xcri} buckling load of i th plate element;
- N_{xcrk} buckling load of k th plate element;
- σ_{cri} buckling stress of i th plate element;
- σ_{crk} buckling stress of k th plate element;
- $E_{xc}k$ equivalent compressive modulus along x -axial of k th plate element.

$$E_{xc}k = \frac{1}{t_k} \left(A_{11k} - \frac{A_{12k}^2}{A_{22k}} \right)$$

E_{xc}^{st} —equivalent compressive modulus along x -axial of stiffened stringer;

$$E_{xc}^{st} = \frac{\sum_{i=1}^n \left(A_{11i} - \frac{A_{12i}^2}{A_{22i}} \right) b_i}{\sum_{i=1}^n b_i t_i}$$

- t_k thickness of k th plate element;
- t_i thickness of i th plate element;
- b_i width of i th plate element;
- $A_{11k}, A_{12k}, A_{22k}$ in-plane stiffness coefficient of k th plate element;
- $A_{11i}, A_{12i}, A_{22i}$ in-plane stiffness coefficient of i th plate element.

(2) Crippling of stiffened stringer

After one layer of a stiffened stringer undergoes initial buckling, i.e., an externally applied load reaches the partial buckling load, the stiffened stringer may continue to bear some load. For a stiffened stringer in this post-buckling phase, further increases in the externally applied load, i.e., the axial compressive load, may induce two modes of deterioration. One mode is an overall buckling instability for long stiffened stringers; another is deterioration through partial crippling for a short stiffened stringer, also known as crippling.

Post-buckling analyses of the two kinds of laminated plates that are used in stiffened stringers involve geometric nonlinearities. Furthermore, the stress–strain curve of a laminate with a higher percentage of $\pm 45^\circ$ layers shows considerable nonlinear behavior before initial buckling. Thus, specific programs based on nonlinear buckling theory are required to analyze the intensity of crippling.

At the beginning of the design, designers are reluctant to or unwilling to analyze the complicated nonlinear characteristics of a large number of preselected laminates, including the layering characteristics and width-to-thickness ratio of b/t . Thus, to estimate the intensity of crippling, a better solution is to apply the results of experiments and semiempirical relationships.

Here we introduce experiments used to determine the crippling intensity of a stiffened stringer, and calculation methods used to estimate the crippling intensity of a long stiffened stringer.

- (1) Crippling intensity experiments of a stiffened stringer: Fig. 4.46 shows the shape deformation of angle- and channel-shaped stiffened stringers undergoing crippling. The in-plane cross section of a stiffened stringer becomes distorted because part of the plate elements is buckled. However, the whole stiffened stringer is not deflected and cross lines (i.e., crest lines) of all the plate elements remain straight.

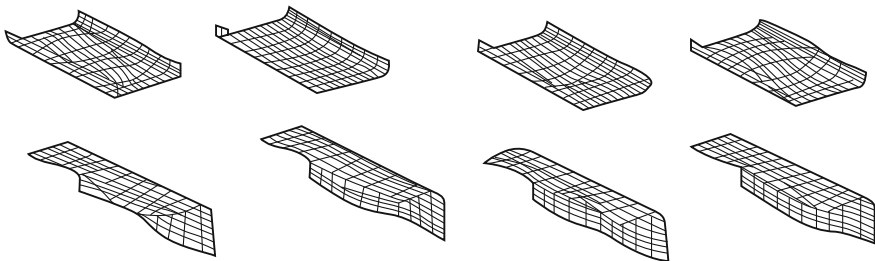


Fig. 4.46 Crippling deformation of angle- and channel-shaped stiffened stringers

Fig. 4.47 Loading–displacement diagram of a plate element with no free edge

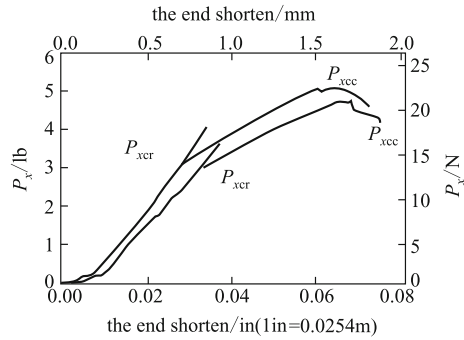
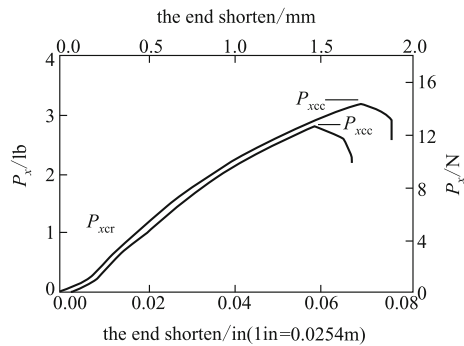


Fig. 4.48 Loading–displacement diagram of a plate element with one free edge



An experiment, which is specific to two typical plate elements of the stiffened stringers, may be performed. Figures 4.47 and 4.48 show loading displacement diagrams for no free edge and one free edge test specimens, respectively, under axial compression. After the phase of initial buckling (P_{xcr}), the rigidity of the plate considerably decreased in the post-buckling phase. When the pressure reached P_{xcc} , the test specimens were destroyed.

Figures 4.49 and 4.50 show experimental dimensionless crippling curves, $\sigma_{cc}/\sigma_{cu} \sim b/t$, of laminates with no free edge and one free edge, respectively. In these dimensionless curves the y-coordinate is the ratio of the crippling stress to the compressive strength limit of the materials comprising the laminate. The x-coordinate is the width-to-thickness ratio b/t of the laminate. However, in these crippling curves, the compressive ability of the laminate is dimensionless and the effects of bending rigidity of the laminates are not considered. Although the compressive ability of materials may be similar, the buckling and crippling may be different owing to different layering order, which gives different bending rigidity.

For this reason, the curves in Figs. 4.49 and 4.50 have little practical value, and further work is necessary to determine the effect of the layering order of laminates on bending rigidity.

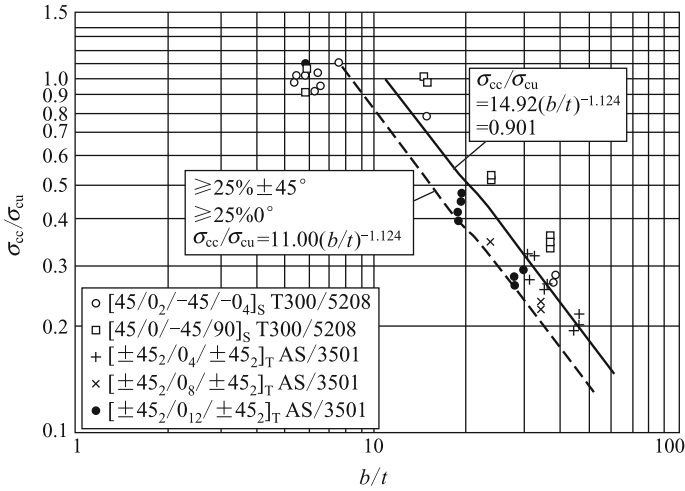


Fig. 4.49 Crippling curve of plate element with no free edge

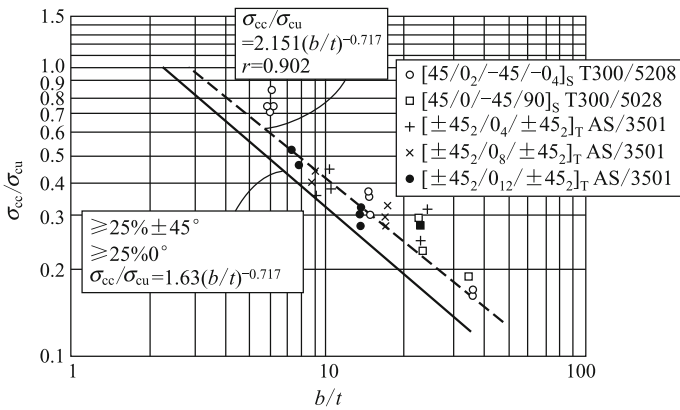


Fig. 4.50 Crippling curve of plate element with one free edge

The crippling curves in Figs. 4.51 and 4.52 are corrected crippling curves of two kinds of laminates with one free edge and no free edge, respectively.

The y-coordinate is the dimensionless crippling stress $\frac{\sigma_{cc}}{\sigma_{cu}} \left(\frac{E_{yc}}{E} \right)$; the x-coordinate is the dimensionless ratio of width to thickness $\frac{b}{t} \left(\frac{\bar{E}}{E_{xc}} \sqrt{\frac{\sigma_{cu}}{E_{xc} E_{yc}}} \right)$, and

$$\bar{E} = \frac{12D_{11}}{t^3} (1 - \nu_{xy}\nu_{yx}) \tag{4.43}$$

Fig. 4.51 Corrected crippling curve of laminated plate element with one free edge

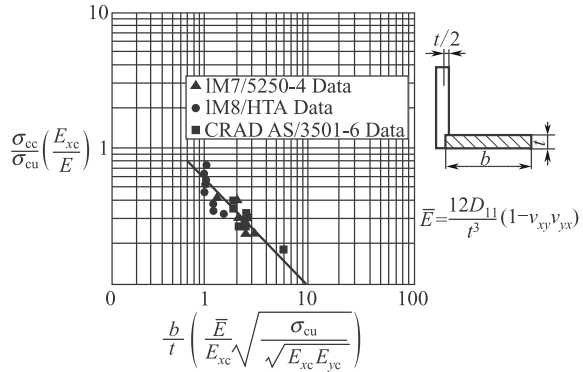
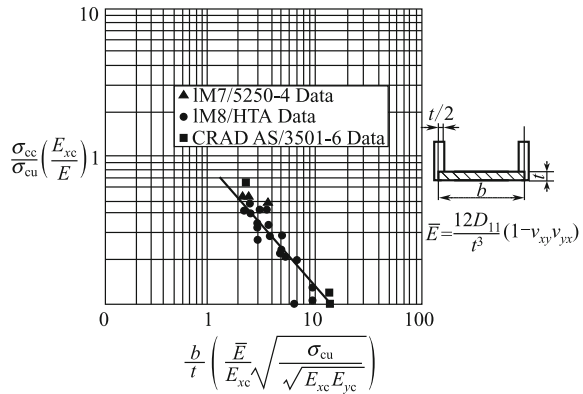


Fig. 4.52 Corrected crippling curve of laminated plate element with no free edge



where

- D_{11} —bending stiffness coefficient of laminate;
- ν_{xy}, ν_{yx} —Poisson’s ratio of the laminate;
- E_{xc}, E_{yc} —equivalent longitudinal and transverse compressive moduli of laminate;
- b —laminated width;
- t —laminated thickness;
- σ_{cu} —compressive strength (ultimate);
- σ_{cc} —crippling strength (stress).

The values of E_x (E_{xc}), E_y (E_{yc}), ν_{xy} and ν_{yx} of a symmetric laminated plate can be calculated from the following formulae.

$$E_x = \frac{1}{t} \left(A_{11} - \frac{A_{12}^2}{A_{22}} \right)$$

$$E_y = \frac{1}{t} \left(A_{22} - \frac{A_{12}^2}{A_{11}} \right) \quad (4.44)$$

$$\nu_{xy} = \frac{A_{12}}{A_{22}}$$

$$\nu_{yx} = \frac{A_{12}}{A_{11}}$$

(2) Identification of crippling rigidity of a stiffened stringer: According to curves from previous experiments, the crippling rigidity of a stiffened stringer can be identified by the following procedures:

- ① Break down the stiffened stringers into two plate element groups, i.e., one-free-edge and no-free-edge groups.
- ② Certify the crippling stress of every plate element according to Figs. 4.51 and 4.52; when applying the width-to-thickness ratio determine σ_{cc} for every plate element, the values of E_x , E_y , ν_{xy} , ν_{yx} , and \bar{E} should be calculated from Eqs. 4.44 and 4.45 to determine the value of σ_{cu} .
- ③ The limiting value of the crippling stress of a laminated plate σ_{cu} can be determined experimentally or estimated from the following formula:

$$\sigma_{cu} = E_{xc} \varepsilon_c$$

where

E_{xc} —equivalent longitudinal modulus of elasticity of laminate;

ε_c —compressive strain design allowable value of composite laminate.

- ④ Apply the following formula to determine the weighted contribution of crippling stress of each plate element of the composite laminated plate. The crippling stress of a stiffened stringer can be determined from:

$$\sigma_{cc}^{st} = \frac{\sum_{i=1}^N \sigma_{cci} b_i t_i}{\sum_{i=1}^N b_i t_i} \quad (4.45)$$

where

σ_{cci} —crippling stress of i th stringer;

b_i —width of i th stringer;

t_i —thickness of i th stringer;

N —number of stringer.

Note: if the value σ_{cc} of one plate element is higher than its σ_{cu} , the whole calculation should use σ_{cu} instead.

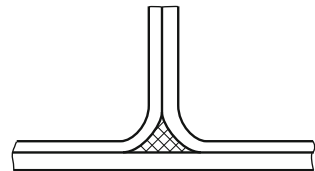
- (3) Some issues should be considered when calculating the crippling stress of a stiffened stringer.
- ① The data in Figs. 4.51 and 4.52 are taken from experiments based on a stiffened stringer with uniform thickness. If the thickness of a single plate element in the stiffened stringer differs greatly, the thicker plate elements will give greater resistance than the thinner plate elements and enhance the buckling and crippling stress of the thinner plate elements. However, the buckling and crippling stress of the thicker plate elements will also be reduced. Therefore, the crippling stress of the affected plate element should be modified. The crippling stress of a stiffened stringer depends on the plate elements that will undergo buckling or crippling first.
 - ② Consideration of fillets: As shown in Fig. 4.53, a 0°-material is used to fill the corners of stiffened stringers, and these materials can boost the crippling rigidity of the stiffened stringer. The area of the fillets under pressure is directly proportional to the square of the corner radius. Thus, the larger the corner radius, the greater the enhancement on the crippling rigidity. The following formula can be used to estimate the enhanced crippling stress:

$$\bar{\sigma}_{cc}^{st} = \left(\frac{1 + \frac{E_f A_f}{\sum E_i b_i t_i}}{1 + \frac{A_f}{\sum b_i t_i}} \right) \sigma_{cc}^{st} \quad (4.46)$$

where

- σ_{cc}^{st} crippling stress of stiffeners (without fillets);
- $\bar{\sigma}_{cc}^{st}$ crippling stress of stiffeners (with fillets);
- A_f cross-sectional area of fillets;
- E_f equivalent longitudinal modulus of elasticity of fillets.

Fig. 4.53 Sketch of corner stuffing in a stiffened stringer



- ③ Modification of the slenderness ratio: A stiffened stringer may become unstable as its length is increased, but it will not undergo partial crippling. A modification engineering method is introduced to adjust the crippling stress by considering the slenderness ratio. The slenderness ratio L'/ρ of a stiffened stringer can be considered as a pressured column, where $L' = L/\sqrt{C}$ is a valid length of a stiffened stringer, and C is the supporting coefficient of the end of the stiffened stringer. The value of C can be in the range 1–4, but it is generally assumed that C is 2.0. ρ is the gyration radius of the cross section of the stiffened stringer. With the use of the formula:

$$\rho = \sqrt{\frac{(EI)_{st}}{(EA)_{st}}} \tag{4.47}$$

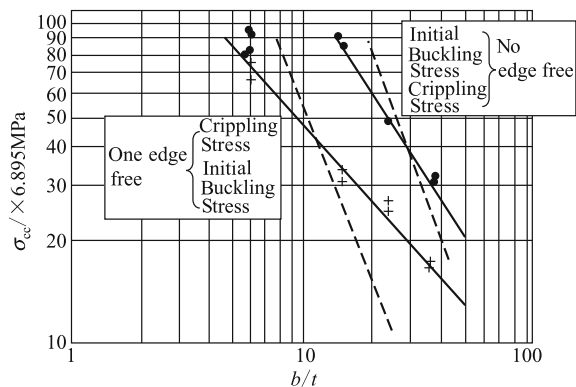
where $(EA)_{st}$ and $(EI)_{st}$ are the tensile or compression rigidity and the bending rigidity, respectively. These two values may be calculated from Eqs. (4.53) and (4.54), given in Sect. 4.7.2.3 of this chapter. The critical stress of a stiffened stringer is:

$$\sigma_{cr} = \sigma_{cc} \left[1 - \frac{\sigma_{cc}}{4\pi^2 E_{xc}} \left(\frac{L'}{\rho} \right)^2 \right] \tag{4.48}$$

If the value of L'/ρ is greater than 12, this formula may require some modifications.

- ④ In Fig. 4.54, the broken line represents the calculated initial buckling stress compared with experimental results from plate elements with one free edge and with no free edges. The solid lines show crippling stress data from corresponding experiments. The calculated initial buckling stress is smaller than the experimental values when b/t is great, i.e., in the case of a thin plate. The value of the calculated initial buckling stress is larger than the experimental value when b/t

Fig. 4.54 Comparison of calculated initial buckling and crippling stresses with experiment results for plate elements with one free edge and no free edge



t is small, i.e., in the case of a thick plate. Thin plates undergo buckling at a lower stress; however, thin plates can undergo greater loading in the post-buckling phase. Therefore, the estimate of the loading of a thin plate from its initial buckling stress is conservative. For the thick plate, the loading will recede because of the crosswise shear effect and these calculations do not give reliable results.

In summary, it is necessary to consider partial buckling and crippling intensity together when analyzing the stability of a stiffened stringer. If the laminated plate elements are thin, the lower initial partial buckling stress is a conservative estimate of the loading of a plate element. If the laminated plate elements are thick, applying the initial partial buckling stress without consideration of the crosswise shear effect will overestimate the loading of the stiffened stringer.

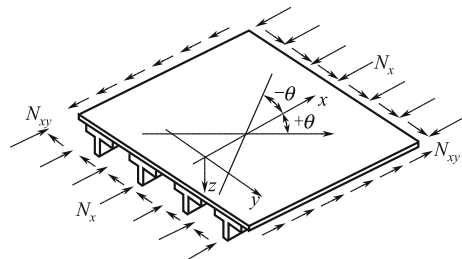
4.7.1.3 Stability Analysis of Stiffened Stringer

Stiffened stringers are a typical component used in airfoil structures. The stability of a stringer is enhanced when it is reinforced with a cover. Part of the stiffened stringer between two wing ribs and two wing spars should be analyzed to consider the stability of the whole design. For convenience, the structure can be simplified as a set of parallel stringers and the dimensions and materials (i.e., layering) of a section plane of the stringers are same, with equal spacing. The slight lateral curvature of a stiffened stringer may be ignored, as shown in Fig. 4.55. This approach is widely accepted by engineers.

The loading situations of stiffened stringers can be divided into three categories: axial compression loading (along the length direction of the stiffened stringer), shear loading, and combinations of shear and compression loadings.

Failure modes of instability can be divided into four categories: ① covers between stringers or parts of the stringers buckling; ② general instabilities of the stiffened stringer. A long stiffened stringer can be considered as a wide column with the use of Euler instability under axial compression; ③ crippling damage that may occur in a short stiffened stringer under axial pressure; ④ a combination of the previously mentioned Modes ① and ②.

Fig. 4.55 Diagram of laminated reinforced stringer



Medium long stiffened stringers, widely used in airfoils, typically undergo failure through Mode ④. The covers between stringers become partially buckled and enter into the post-buckling phase. Under greater loading, the partial flexural wave of the cover gradually expands and passes through the stiffened stringers. These stringers are subjected to strong bending and torsion, leading to instability. Sometimes, the load on damaged stiffened stringers may be reduced by damage to the cover or stringer before general instability occurs.

The stability analysis of stiffened stringers is complex and requires special programs based on FEMs, including: MSC/NASTRAN, BAFLCP, CPANDA, and COMPOSS. These programs have different merits and scopes of application. Most of these programs are based on linear buckling theory and thus can only be applied to calculate the partial buckling load of covers or stringers and the general buckling load of a stiffened stringer. Only the COMPOSS program can be used to analyze the loading of a stiffened stringer in the post-buckling phase and give the limiting loading of a reinforced stringer.

In the initial design phase, the following simplified methods are used to estimate the stability of a stiffened stringer:

- (1) A dense stiffened stringer, which has a compact arrangement of stringers, can be considered to be a smooth plate for estimates of its general buckling load. The method for calculating the equivalent rigidity of a stiffened stringer is given in Appendix A: Directory of structural stability analysis of composited materials.
- (2) In the case of widely spaced stiffened stringers, the partial initial buckling load and crippling intensity of the covers between the stringers and that of the reinforcing stringer can be estimated separately.
The partial initial buckling load of covers between stringers can be calculated from the formula given in Sect. 4.7.1.1 of this chapter. Initially, the supporting conditions of all sides of the covers should be regarded as ideal boundary (supporting) conditions. The ideal boundary of a reinforced stringer or wing rib is the supported boundary condition. The reinforced stringer or wing rib can be regarded as a fixed supported boundary condition.
The subjacent end of a reinforced stringer connected with the cover can be regarded as a no free edge plate element, with two edges simply supported, when calculating the initial buckling load and crippling intensity of a stiffened stringer.
- (3) Some specific programs can be applied to the simplify the methods for estimating the general stability of a whole stiffened stringer.
- (4) Continuous loading analysis of covers or parts of reinforced stringers in the post-buckling phase can only be estimated for the limiting loading of a reinforced stringer at a certain axial pressures. This topic will be introduced in Sect. 4.7.2.3.

4.7.1.4 Influence of Layering Order on Stability

Structural stability depends on the rigidity of the structure and the rigidity of the support conditions (i.e., the boundary supporting conditions). The structural stability of laminated plate is closely related to the layering order. Hence, it is necessary to consider the influence of layering order on stability in the design phase.

(1) Influence of layering order on buckling of laminated plate

The buckling load of laminated plate is related to layering order, loading environment, geometric dimensions, and boundary supporting conditions. Thus, there are no general rules for setting the best layering order of a laminated plate. Specific analyses are needed for specific loading situations, geometric dimensions, and boundary conditions.

To enhance the buckling load of a laminated plate, the following observations may help guide layering design:

- (1) Symmetrical and balanced laminated layering are adopted in most cases, except for situations with special requirements, such as requirements for aeroelastic tailoring. To avoid plate deflection caused by coupling of flexural tension and bending, let $B_{ij} = 0$, $D_{16} \approx 0$ and $D_{26} \approx 0$. This deflection is equal to the amount of initial deflection of a laminated plate and it will decrease the buckling load.
- (2) For a rectangular laminated plate that is under pressure along its length, a higher buckling load may be achieved when $\pm 45^\circ$ plies are layered on the surface of the laminated plate.
- (3) For a rectangular laminated plate that is under pressure along its width, a higher buckling load may be achieved when 0° plies are layered on the surface of the laminated plate.
- (4) The maximum buckling load of a laminated plate under a given shear stress is achieved when $\pm 45^\circ$ plies are layered on the surface of the laminated plate. The buckling load value of a plate under positive shear stress is lower, than that of a plate under negative shear stress, as shown in Fig. 4.56. This effect is attributed to the D_{16} and D_{26} values of the plate. The buckling loads of an orthotropic plate are the same no matter if the plate is under positive or negative shear stress.

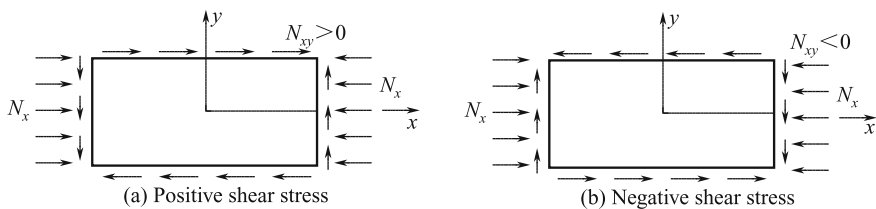


Fig. 4.56 Rules for shear plates under positive and negative shear stress

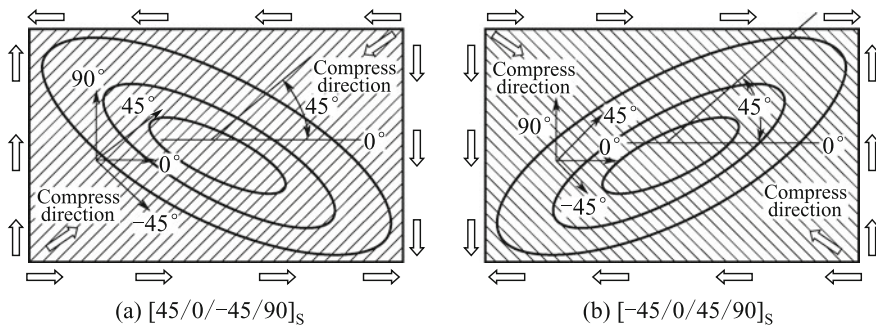


Fig. 4.57 Illustration of the 45°-surface fibers along the compression direction under combined shear stress

For symmetrical laminated plates, where $D_{16} \neq 0$ and $D_{26} \neq 0$, the fibers on the outer surfaces may allow for a higher buckling load when the plate is under a combination of shear stress in the pressure direction, as illustrated in Fig. 4.57.

- (5) The behavior of a laminated plate under combined stress from pressure and shear loading is an unusual situation because of the effects of D_{16} and D_{26} . In Sect. 4.1.1 of this chapter, a pressure and shear stress formula is presented for orthotropic laminated plates ($D_{16} = 0, D_{26} = 0$):

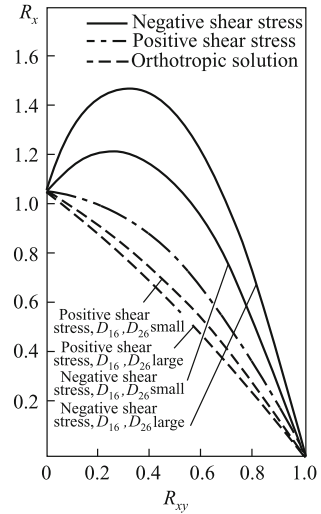
$$R_x + R_{xy}^2 = 1$$

Thus, a parabola may be defined in this the coordinate plane, to describe the pressure load-to-shear load ratio with R_x and R_{xy} as coordinates.

A related parabola for shear buckling of a symmetrical laminated plate under pressure and shear stress loading can also be defined. When $D_{16} \neq 0$ and $D_{26} \neq 0$, the parabola may be distorted becoming more prominent or concave according to the different direction of the shear stress (i.e., positive or negative shear stress). Figure 4.58 shows buckling curves of a symmetrical laminated plate, with $D_{16} > 0$ and $D_{26} > 0$, undergoing combined pressure and shear stress loading in the positive and negative directions. As shown in the figure:

- ① In the case of $D_{16} > 0$ and $D_{26} > 0$, a negative shear stress makes the parabola more prominent, indicating an enhancement of the buckling load under axial pressure. A positive shear stress makes the parabola concave and reduces the buckling load under axial pressure. Furthermore, higher values of D_{16} and D_{26} have a more prominent effect on the concaving of the parabola.
- ② In the case of $D_{16} < 0$ and $D_{26} < 0$, the influences of negative or positive shear stress on the buckling curves have the opposite effect. Thus, negative shear stress makes the parabola concave and decreases the buckling load under axial pressure; however, a

Fig. 4.58 Curves of pressure and shear stress buckling of symmetric laminated plate under negative/positive shear stress, with $D_{16} > 0$ and $D_{26} > 0$



positive shear stress makes the parabola more prominent and increases the buckling load under axial pressure.

According to results from experiments, the influence of this effect is related to the length-to-thickness ratio, boundary conditions, and the ratio of the lateral elasticity modulus to the transverse elasticity modulus (E_x/E_y). In the case of a laminated plate with four fixed supported edges, the effects of the shear stress direction (positive or negative) are stronger than the case of a laminated plate with four edges simply supported. A higher value of E_x/E_y indicates a stronger influence of the shear stress direction.

To increase the buckling load, the outer plies should have a fiber direction 45° to the compressive direction of the combined shear forces.

(2) Effects of layering order on partial buckling and crippling of stiffened stringer

Experimental data indicate that a 0° ply layer near the surface layer of a laminated plate element in a stiffened stringer will induce minimum values of partial buckling and crippling load of the reinforced stringer.

However, in terms of bending rigidity, the influence of the dimensions of the stiffened stringer is stronger than the influence of the layering order. For example, the Euler buckling load of an I-shaped reinforced stringer section depends on the cross-sectional dimensions of its flange and web plate. The influence of layering order is considerably reduced as the height of a middle I-shaped web plate is increased. Hence, the Euler buckling load has no relationship with layering order.

(3) The influence of layering order on stability of a stiffened stringer

The influence of layering order on the stability of a stiffened stringer is complicated and related to the instability failure modes of the reinforced stringer as well as the support conditions of the reinforced stringer with a cover.

- (1) Partial buckling or crippling of a stiffened stringer are unrelated to the layering order. However, the buckling load of a covered composite stiffened stringer, as well as post-buckling of the cover are affected by the layering order of the cover.
- (2) For the case of a stiffened panel with stronger stiffeners under an axial pressure, the buckling load of the axial pressure will decrease because the transverse distortion of the cover is restricted. Namely, the transverse distortion of the cover (free expansion) is restricted by the stiffened panel and additional transverse pressure is introduced because of the Poisson effect. Thus, the cover is under a two-way compression such that its buckling load in the axial pressure direction decreases. The level of this decrease is directly proportional to the Poisson ratio of the cover (ν_{yx}). The value of ν_{yx} can be calculated from the following formula:

$$\nu_{yx} = A_{12}/A_{11}$$

where A_{11} , A_{12} —in-plane stiffness coefficients of the skin.

In this situation, the design should aim to reduce the ν_{yx} value of the layering.

4.7.2 Overview of Post-buckling and Post-buckling Strength Analysis

The classic theory of linear buckling has been used to analyze the stability of structures in engineering. According to this theory, when a structure has achieved the critical state of initial buckling, its normal deformation (deflection) suddenly increases arbitrarily. This means that the structure loses its load-bearing capacity. In practice, when the skin of a thin-walled stiffened structure of a plane features local buckling, the structure generally maintains the ability to bear load, which is known as post-buckling strength. For structures designed according to their initial local buckling stress as the limiting allowable stress, the post-buckling strength of the structure is not used. Thus, the potential load-bearing capability of a structure is not fully accounted for [3, 16].

To explain the differences between the practical stabilities of structures and the stability calculated based on the theory of linear buckling, nonlinear large deflection buckling theory has been proposed. This theory is based on in-depth theoretical and experimental studies of post-buckling behavior of structures.

The structural stability analysis involves complicated elastic–plastic and mathematical theory. Analysis of a simple rectangular symmetric laminated panel by linear buckling theory requires the solution of high-order partial differential equations. However, nonlinear large deflection buckling theory requires even more complex calculations. Thus, although the foundations of this theory were laid in at the beginning of the twentieth century, it has not been widely applied in practice. In the 1960s, the emergence and rapid development of the FEM and advances in computing power provided the necessary tools to resolve the issues of a nonlinear field and enable practical application of the theory. Over the past three decades, post-buckling strength issues of structures have aroused considerable interest in the engineering sector.

The development and application of advanced composite materials has to on some extent depend on the discovery and use of this capability to determine the load a material can withstand beyond its initial buckling.

The analysis and solution of the large deflection theory of nonlinear buckling are complex and burdensome. The following sections introduce the basic concepts of nonlinear large deflection buckling theory and present a few examples of its application to analyzing post-buckling structural characteristics. The use of this theory in projects is also discussed.

4.7.2.1 Characteristics of Post-buckling Analysis

In this section, nonlinear large deflection buckling theory and linear buckling theory are compared in terms of analysis, processing, and the solutions derived. The basic concepts and features of post-buckling issues are introduced.

- (1) The post-buckling problem involves analysis of a structure from initial buckling to damage and failure.

Linear buckling theory analysis indicates that when a structure has achieved the critical state of initial buckling, its deformation (deflection) increases arbitrarily, and the load-bearing capacity is suddenly lost. It necessary to determine the load and buckling mode of the initial buckling of a structure.

Nonlinear post-buckling theory can be used to solve the deformation and forces acting on a structure from the initial buckling to damage to the failure. This approach involves both stability analysis and requires judgement of the failure related to the intensity of the damage. Thus, analysis of post-buckling unifies the analysis of the stability and the issue of strength. In the analysis, many factors that affect the stability and strength of the structure should be considered, including: the impact of damage, initial defects, temperature and humidity, and guidelines of material damage.

- (2) In the analysis of post-buckling of a structure, the impact of a large deformation needs to be considered to accurately describe the state and strength characteristics.

Linear buckling theory analysis establishes the equilibrium equations for the initial position and shape of the structure and, therefore, does not reflect the impact of structural deformation on the equilibrium state.

In practice, a structure under a load undergoes some deformation. After the initial post-buckling deformation, the structure will enter a buckled state. Analysis by theory of nonlinear buckling considers the structure and processes that might change the position and shape of the structure from their equilibrium values. This analysis allows for a more accurate description of the structure and the forces acting on it and can more truly reflect the characteristics of the system.

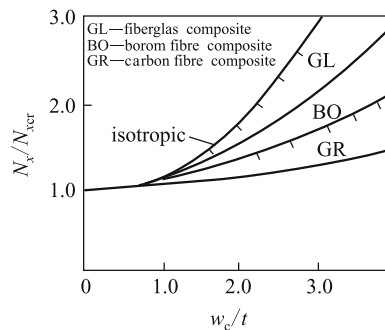
- (3) Post-buckling analysis of a structure is calculated from progressive data sets in the moment after a load is applied to the structure. The structure's stiffness after deformation as well as changes in its position and shape are recalculated in iterations. This analysis can determine whether a process will undermine the strength of a structure but requires an understanding of the structure and the acting forces.
- (4) The use of FEMs for linear buckling analysis of a structure can be reduced to solving a set of linear algebraic equations equal to zero for the determinant of a coefficient matrix of the eigenvalue problem.

The FEM and nonlinear buckling analysis require the solution of the nonlinear algebraic equations in repeated iterations. Accurate calculations and convergence are not always achieved. Thus, nonlinear analysis calculations are a specialized research field.

4.7.2.2 Reinforced Laminates and Post-buckling Laminate Properties

Recently, some practical post-buckling analysis procedures based on nonlinear buckling theory of structures have been introduced. These include ABAQUS, ADINA, ANSYS, ASKA, and MARC. For analysis of the buckling of composite structures and destruction post-buckling, a dedicated software, COMPOSS, has been developed in China.

Fig. 4.59 Axial load–deflection curves for laminated square plate simply supported on four sides by metal square plates



The following procedures may be followed for calculations of laminate composite materials, reinforced laminates with COMPOSS based on post-buckling analysis of a phase curve (path), to reveal the characteristics of subsequent buckling.

Figure 4.59 shows the axial load–deflection curve ($N_x/N_{xcr}-t$) for an isotropic laminated composite simply supported on four sides with metal side plates. N_x is the initial buckling load, w_c is the normal displacement of center point (deflection), and t is the thickness. For initial post-buckling as the deflection increased, the plates continued to show considerable load-bearing capacity.

Figure 4.60 shows the N_{xy} -deflection curve ($N_{xy}b^2/E_x t^3 - w_c/t$) of a laminated composite square plate simply supported on four sides with metal side panels, under a pure shear load.

With b as the width and t as the thickness, along the x direction for the plate, having a Young’s modulus w_c . The positive and negative shear loads of the laminates show different post-buckling performance.

Figure 4.61 shows axial damage path diagrams ($N_x/N_{xcr} - w_c/t$) of clamped laminated composite square plates in a post-buckling state. The solid lines in the figure represent a calculation, which does not consider an internal damage path,

Fig. 4.60 Shear load–deflection curves of, laminated square plate simply supported on four sides by metal side panels

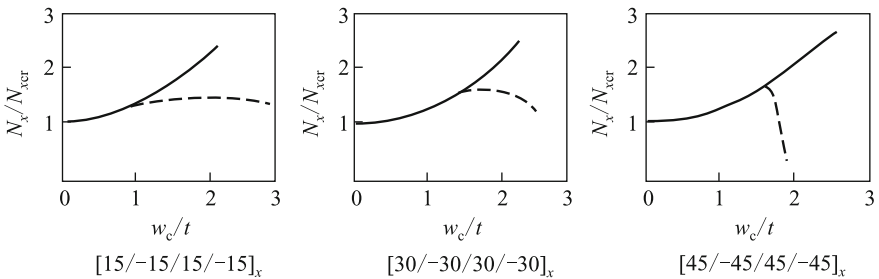
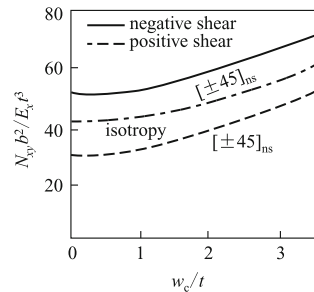
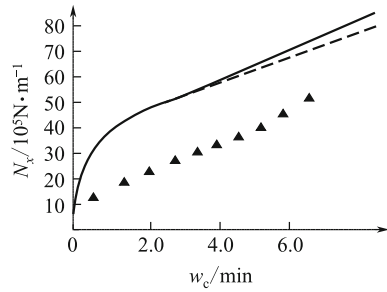


Fig. 4.61 Damage path in clamped laminated square plates composed of three layers with axis 15°, 45°, 30°

Fig. 4.62 Axial load–deflection curves of longitudinally reinforced laminates



while the dashed line shows a calculation considering the path of an internal damage. The laminate may undergo gradual failure indicated by the dashed line showing a gradual downward trend or a more sudden failure indicated by a sharp downward trend. Analysis of the former case suggests that failure occurred owing to tension caused by destruction of fibers. The latter case reflects tension (pressure) caused by the destruction of the matrix.

Figure 4.62 shows the load–deflection curve (N_x – w_c) of a vertical reinforced composite laminate material and skin layer, clamped at both ends under axial compression with two simply supported edges (taken from a NASA report). The focal points for deflection of the skin map, respectively, are given for a thin mesh (solid line), a dense grid (dashed lines), and theoretical calculations and experimental measurement points (triangles).

There is clearly a large difference between the theoretical values and the test results. In the theoretical analysis and experimental measurements of the reinforced laminates, the presence of geometric defects and internal damage, or improper handling of boundary conditions will cause errors in the results of theoretical calculations and experimental measurements.

4.7.2.3 Post-buckling Strength in a Project

Wing structures based on laminate composite materials and reinforced laminates have been the focus of most post-buckling analysis. It is desirable to evaluate the buckling load-bearing capacity to further reduce weight and increase efficiency.

FEMs are useful analytical procedures, but other factors that can affect the results must also be considered, such as initial flaws in the geometry and materials. Factors such as internal damage and the degree of damage require further evaluation by the user. Minimizing the number of iterations necessary for convergence of an analysis also requires the user to have sufficient professional knowledge and problem-solving experience. Furthermore, finite element analysis features a number

of common problems, including element selection, model simplification, mesh generation, and boundary condition treatment. These features bring considerable difficulties when used in engineering. Thus, it is necessary to adopt a consistent approach to experimental studies and projects as a whole.

Here, the subjects of axial compression of laminates and stiffened panel structures are discussed in terms of developing practical approaches to a project:

- (1) For the skin, the post-buckling laminate load-bearing capacity can be estimated by the effective width method;
- (2) For reinforcement of the post-buckling load-bearing capacity, tests can be used based on pressure loss curve estimates;
- (3) For a stiffened plate, the post-buckling load-bearing capacity can be estimated with the use of subtreatment and effective width methods.

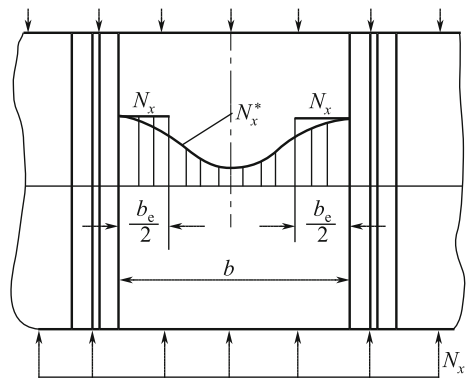
Test data are lacking for complex shear and pressure loading behavior. Therefore, the following considers a limited number of topics, including: axial load on laminated boards, reinforced laminates, and post-buckling load-bearing capacity.

- (1) Estimation of post-buckling laminate load-bearing capacity:

In the case of a reinforced laminate (skin) under uniform pressure at both ends and with both edges supported, the initial post-buckling and the distribution of compressive stress gradually become uneven. Before buckling occurs, as the pressure increases the middle part of the plate will feature alleviated stress. Test results show that the lateral distribution of stress takes the form shown in Fig. 4.63. With reference to treatments of metal plates, an effective width, or reduced width may be introduced. The width of the pressure effect may be reduced by multiplication by N_x to estimate the change in stress distribution over the board and the post-buckling load-bearing capacity. The effective width can be expressed as:

$$b_e = \varphi b \tag{4.49}$$

Fig. 4.63 Reinforced skin between the local buckling stress distribution



where b_e is the width and φ is the effective width coefficient, determined from experimental data.

A relationship for estimating the post-buckling load-bearing capacity of a stiffened plate of a given width is presented in subsection (3).

(2) Estimation of reinforced post-buckling load-bearing capacity:

A reinforced B_e in the buckling and pressure loss analysis may be divided into two types of stiffened plates. FEMs and experimental studies of the two types of plate elements have been used to study the buckling pressure loss after destruction in pressure loss curves. The B_e of components in a reinforced plate element under pressure loss can be considered to be a stress-weighted sum of estimates of the post-buckling load-bearing capacity.

(3) Estimation of stiffened panel post-buckling load-bearing capacity:

Here, two pilot projects based on this estimation method are introduced.

- ① The subsection approach used for metal plates can be applied to composites subject to axial compression. A long board is divided into shorter board panels based on the slenderness ratio (L'/ρ). Figure 4.64 illustrates three regimes for division of boards.

In a stiffened panel $L' = L/\sqrt{C}$ for an effective column length C , where the end of the stiffened plate support profile or ρ factor can take $C = 1-4$, although it is generally assumed that $C = 2.0$. The value of ρ for a stiffened plate radius of gyration can be determined by the following equation:

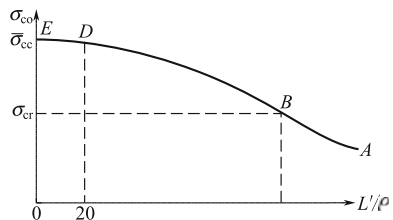
$$\rho = \sqrt{\frac{(EI)}{(EA)}}$$

where (EA) and (EI) are the stiffened plate tensile (compression) stiffness and bending stiffness, respectively, according to Eqs. 4.53 and 4.54.

In the pilot study and mechanical analysis:

- (a) In the $D-E$ section the short-board features pressure damage, where $0 < L'/\rho \leq 20$.
- (b) In the $B-A$ section a long board features damage leading to overall instability.

Fig. 4.64 Subprocessing curves of axial load-bearing capacity of longitudinally reinforced laminates



(c) In the *D-B* section of medium and long boards, before damage to the reinforcement between the skins local buckling occurs first. Thus, it is necessary to account for the post-buckling load-bearing capacity.

The *D-E* between each section, where $L/\rho = 20$, can be defined separately for the *D-B* sections and the *B-A* cutoff points between sections. For *B* the skin between the reinforced parts determines the initial buckling stress.

The actual structures of a stiffened panel include medium and long boards and stiffened plates. Thus, these are the focus of post-buckling load-bearing capacity analysis. Test results show that in the *D-B* section of a stiffened plate, the post-buckling load-bearing capacity and average failure stress can be fitted by a parabola. The vertex of the parabola is *D*, the other point is *B*. This allows estimation of the post-buckling load-bearing capacity of reinforced pressed plates from the equation:

$$\bar{\sigma}_{co} = \left[1 - \left(1 - \frac{\sigma_{cr}}{\bar{\sigma}_{cc}} \right) \frac{\sigma_{cr}}{\sigma_r} \right] \bar{\sigma}_{cc} \tag{4.50}$$

where

- $\bar{\sigma}_{co}$ stiffened panel average failure stress;
- $\bar{\sigma}_{cc}$ Type of short stiffened plate ($0 < L/\rho \leq 20$) average pressure loss of the failure stress;
- σ_{cr} reinforcement between the skin of the initial local buckling stress;
- σ_r A factor to discount the skin or b_e reinforcement after the effects of local buckling decreases the stiffness. In the calculation of the overall instability of stiffened plate stress, for b_e reinforcement of more than 4, the system can be considered a side support with the width determined by the Euler column formula.

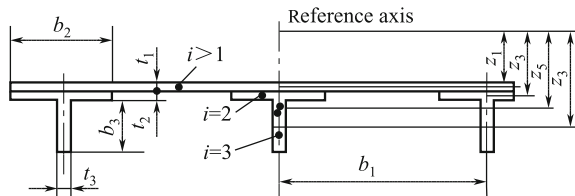
In preliminary design, the following simplified formula are used for preliminary estimates

$$\bar{\sigma}_{co} = \bar{\sigma}_{cc} - (\bar{\sigma}_{cc})^2 (L'/\rho)^2 / (4\pi^2 \bar{E}_x) \tag{4.51}$$

where

- \bar{E}_x stiffened plate *x* direction equivalent elastic modulus;
- ρ stiffened plate section radius of gyration;

Fig. 4.65 Schematic diagram of laminate reinforced vertical plate element



L' stiffened panel effective column length.

A stiffened plate can generally be divided into sections by symmetric laminates m yen (also known as a skin plate element. A calculation model (Fig. 4.65) can used based on the following equation A, (EA) and (EI) .

$$A = \sum_{i=1}^m b_i t_i \tag{4.52}$$

$$(EA) = \sum_{i=1}^m \left(A_{11i} - \frac{A_{12i}^2}{A_{22i}} \right) b_i \tag{4.53}$$

$$(EI) = \sum_{i=1}^m \left[\left(A_{11i} - \frac{A_{12i}^2}{A_{22i}} \right) b_i (z_i - z_c)^2 + \left(D_{11i} - \frac{D_{12i}^2}{D_{22i}} \right) b_i \right] \tag{4.54}$$

where

- b_i first plate element of width i ;
- t_i thickness of the i th plate element;
- $A_{11i}, A_{12i}, A_{22i}$ first plate element of the i th plane stiffness coefficient;
- $D_{11i}, D_{12i}, D_{22i}$ first plate element i of the bending stiffness coefficient;
- $(z_i - z_c)$ first section i of a plate element on the neutral axis from the center;
- Z_c stiffened plate section on the neutral axis position (from calculation of the distance between the reference axis).

$$z_c = \frac{\sum_{i=1}^m E_{xi} b_i t_i z_i}{\sum_{i=1}^m E_{xi} b_i t_i}$$

where

- E_{xi} first plate element i in x direction of the equivalent modulus of elasticity;
- z_i part i of a plate element calculation of the reference section of the center distance from the axis;

In general, Eq. (4.54) is used, when the second part is negligible compared with the first; see “Stability Analysis of Composite Structures Guide” in Appendix A.

- ② The effective width method for skin damage occurring prior to local buckling of a stiffened panel, can be used to estimate the post-buckling load-bearing capacity of the skin. For b_e reinforcement, the buckling

pressure loss or damage can be used to estimate the damage of the stiffened plate load.

The stiffened panel features skin n_1, n_2 arranged in a geometric space, such that the size and material properties of all reinforced features are the same for each article. The buckling load-bearing capacity can be calculated as:

$$P = (n_1 b_e t E_x^s + n_2 F E_x^{st}) \varepsilon_b \quad (4.55)$$

where

- P stiffened plate load damage;
 E_x^s direction of the skin equivalent elastic modulus;
 E_x^{st} reinforced b_e equivalent x direction modulus of elasticity,
 $E_x^s = \frac{1}{t} \left(A_{11} - \frac{A_{12}^2}{A_{22}} \right)$;
 t thickness of skin;
 F reinforced area profiles;
 ε_b reinforcement of the buckling pressure loss or strain;
 b_e effective width of skin.
 A_{11}, A_{12}, A_{22} skin stiffness coefficient of the plane.

When the computation can be divided into m articles reinforcing a symmetric laminated plate element, the following equations may be used:

$$E_x^{st} = \frac{1}{F} \sum_{i=1}^m \left(A_{11i} - \frac{A_{12i}^2}{A_{22i}} \right) b_i$$

$$F = \sum_{i=1}^m b_i t_i$$

where

- b_i reinforcement b_e of the first plate element of width i ;
 t_i reinforcement b_e of the first i of the thickness of a plate element;
 $A_{11i}, A_{12i}, A_{22i}$ reinforced articles in the first i -plane of the plate element stiffness coefficient.

The b_e reinforcement between the skin of the effective width can be determined by the following equations:

$$b_e = \varphi b$$

$$\varphi = \zeta + (1 - \zeta) \varepsilon_{cr}^s / \varepsilon_b$$

$$\xi = 1 - 2 / \left[3 + \eta \left(\frac{a}{b} \right)^4 \right] \quad (4.56)$$

where

- a, b b_e reinforcement between the length and width of skin;
 φ b_e reinforcement of a skin with the effective width coefficient;
 ε_{cr}^s local buckling of the strain skin;
 ε_b reinforcement of the buckling strain;
 η anisotropy degree of the skin, $\eta = A_{22}/A_{11}$.

In addition, the articles reinforcing the effective width between the skin can also be determined from the following equation:

$$b_e = \frac{b}{2} \left(1 + \frac{\sigma_{cr}^s}{\sigma_{cc}^f} \right) \quad (4.57)$$

where

- b_e reinforcement between the effective width of the skin;
 b reinforcement between the width of the skin;
 σ_{cr}^s local buckling stress of the skin;
 σ_{cc}^f pressure loss stress of skin attached to the end of the reinforced section.

If Eq. (4.57) is used, to estimate the damage to a stiffened plate, b_e can be determined from ε_b of the load P , with Eq. (4.55) where the response of the pressure loss is given by:

$$\sigma_b = \varepsilon_{cc}^{st} = \sigma_{cc}^{st} / E_x \quad (4.58)$$

where σ_{cc}^{st} is described in Sect. 4.7.1.2 of the method [Eq. (4.45)].

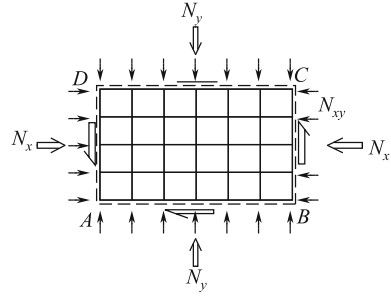
4.7.3 Buckling Analysis of Sandwich Structures

(1) Overall buckling analysis of sandwich structure

A large number of calculated and experimental results show that the FEM for overall buckling analysis of sandwich structures is well suited to their complexities. In buckling finite element analysis, note the following issues [2, 14]:

- ① Model grid segmentation: Grid partitions should maintain the principle of the instability mode, and the core thickness direction should be selected as a monolayer element. The rest of the other analysis is same as that for stress analysis;

Fig. 4.66 Finite element analysis grid



② For simulation of the supported edges, refer to Fig. 4.66.

In the case of all sides simply supported, the points of all sides AB, BC, CD, DA $w_i = 0$.

Corner points $u_A = v_A = 0, v_B = 0$ (or $u_A = v_A = 0, u_D = 0$).

All sides fixed: the points of all sides $AB, BC, CD, DA, w_i = 0, \theta_{xi} = \theta_{yi} = 0$

$$u_A = v_A = 0, v_B = 0 \text{ (or } u_D = 0).$$

Other supported boundary conditions can be used with this method. In the case of a support for an elastic boundary, the corresponding w and θ_{xi}, θ_{yi} values are given by the stiffness of the elastic support. For the sides of a fixed supported plate, θ_{xi} or θ_{yi} is 0; for the sides of simply supported plate $w_i = 0$ or replaced by the stiffness of the elastic support.

③ Loading, as shown in Fig. 4.66. Put in-plane load N_x, N_y, N_{xy} to the nodes of each side, with upper and lower points corresponding to the same node. If the load changes along the edge, the load of each node can be not same.

④ Critical buckling load: $N_{icr} = \lambda_{\min} N_i$

where λ_{\min} —minimum eigenvalue;

N_i —stress of analysis with design load.

(2) Local buckling analysis of laminate

In the local buckling analysis of laminates, the panel can be considered to be a beam support for the core, or flexibility base. The flexibility base has the bending stiffness and shear stiffness of the core.

Local buckling failure modes of laminates can be divided into three types: damage to laminated panels, damage to the core, and damage to the interface.

Failure modes of laminated panels include: single-layer instability, folding of the intergrid, laminated panel buckling.

Failure modes of the core: sandwich core crush, shear failure of sandwich core; interface damage of the sandwich core and panel debonding from the core.

The calculation methods of various failure modes are introduced as follows:

① Single-layer instability

$$\frac{\sigma_{jcr}}{G_z} = \begin{cases} \xi_j(2 - \xi_j) & \xi_j < 1 \\ 1 & \xi_j > 1 \end{cases} \quad j = x, y, xy \quad (4.59)$$

where

σ_{jcr} buckling stress of single-layer, $j = x, y, xy$, compressive buckling stress and shear buckling stress along the x- and y-axis. respectively;

G_z interlaminar shear modulus;

ξ_j stiffness parameter, $\xi_j = \frac{\sqrt{DB_j}}{S_j}$, $j = x, y, xy$;

B_j base stiffness, $B_j = \frac{LbE_f}{r}$, $j = x, y, xy$;

D bending stiffness, $D = \frac{\pi d_f^3 E_f b}{64W_f}$;

S_j shear stiffness, $S_j = \frac{bt'G_z}{L_j}$, $j = x, y, xy$.

Carbon fiber material:

d_f fiber diameter, recommended value is 0.007 mm;

W_f fiber spacing, recommended value is 0.005842 mm;

E_f fiber modulus, recommended value is 255,162 MPa;

E_z normal tensile modulus of composite panel, recommended value is $E_z = 0.5 \times (E_{22T} + E_{22C})$;

L_j effective layup percent along loading direction $j = x, y, xy$, calculation formula is:

$$L_x = SPL0 + SPL9 \times \frac{E_{22C}}{E_{11C}} + 0.5 \times SPL45 \\ \times \left(1 + 2.5 \times \frac{E_{22C}}{E_{11C}} \right)$$

$$L_y = SPL9 + SPL0 \times \frac{E_{22C}}{E_{11C}} + 0.5 \times SPL45 \\ \times \left(1 + 2.5 \times \frac{E_{22C}}{E_{11C}} \right)$$

$$L_{xy} = SPL45 \times \left(1 + \frac{E_{22C}}{E_{11C}} \right) + 0.25 \\ \times (SPL0 + SPL9) \times \left(1 + 2.5 \times \frac{E_{22C}}{E_{11C}} \right)$$

where

SPL0 percent of fiber in 0° direction;
SPL9 percent of fiber in 90° direction;
SPL45 percent of fiber in 45° direction:

$$SPL45 = 0.5 \times (1 - SPL0 - SPL9)$$

- ② Panel buckling: Panel instability refers to local panel buckling when a surface is under a compressive or shear load. The following formula applies to local buckling analysis of the compressive surface of an anti-symmetric sandwich structure (for example, a full-size wing).

The panel instability can be calculated by Eq. (4.59), the calculation of parameters *D*, *S*, and *B* require the following changes:

Base stiffness *B*

$$B = \frac{2E_c}{t_c} \quad (4.60)$$

Bending stiffness of panel *D_j*, *j* = *x*, *y*, *xy*

$$D_{ij} = \int_{-0.5t_f}^{0.5t_f} Q_{ij}^{(K)} z^2 dz \quad i, j = 1, 2, 6 \quad (4.61)$$

$$D_x = D_{11}$$

$$D_y = D_{22}$$

$$D_{xy} = 0.25 \times (D_{11} + D_{22}) + 0.5 \times (D_{12} + 2D_{66})$$

Shear stiffness *S_j*, *j* = *x*, *y*, *xy*

$$S_x = \frac{D_{11}^2}{DEN1}$$

$$S_y = \frac{D_{22}^2}{DEN2} \quad (4.62)$$

$$S_{xy} = \frac{D_{xy}^2}{\sqrt{DEN1 \times DEN2}}$$

where

$$DEN1 = \sum_1^N CA(i) \times t(i)/G_{13}$$

$$DEN2 = \sum_1^N CB(i) \times t(i)/G_{13}$$

$$CA(i) = \sum_1^i Q_{11}(k) \times AB2(k) \times t(k)$$

$$i_{\max} = N; k = 1, 2, \dots, i$$

$$CB(i) = \sum_1^i Q_{22}(k) \times AB2(k) \times t(k)$$

$$i_{\max} = N; k = 1, 2, \dots, i$$

$$AB2(k) = 0.5 \times h + (t_f - \sum_1^{k-1} t(i) - 0.5 \times t(k))$$

$$k = 1, 2, \dots, N$$

$$Q_{11}(k) = m(k) \times E_L(k)$$

$$Q_{22}(k) = m(k) \times E_T(k)$$

$$m(k) = (1 - \nu_{LT}(k) \times \nu_{TL}(k))^{-1}$$

② Folding of intergrid can be calculated as follows:

$$\sigma_{cr} = 2 \frac{E'_f}{\lambda} \left(\frac{t_f}{S_c} \right)^2 \quad (4.63)$$

where $E'_f = \sqrt{E_{1f} E_{2f}}$

$$\lambda = 1 - \nu_{12} \nu_{21}$$

E_{1f}, E_{2f} moduli of orthogonal axis of panel;

t_f thickness of panel;

S_c dimensions of a core-wise sandwich structure (diameter of inscribed circle for core-wise structure).

③ Shear failure of sandwich core

$$\sigma_{xcr} = \frac{V_x}{1 + \frac{\delta_0 \times B_7 \times \sqrt{4B/D_{11}}}{h \times \tau_{13b}}} \tag{4.64}$$

$$\sigma_{ycr} = \frac{V_y}{1 + \frac{\delta_0 \times B_8 \times \sqrt{4B/D_{22}}}{h \times \tau_{23b}}} \tag{4.65}$$

$$\sigma_{xycr} = \frac{V_{xy}}{1 + \frac{\delta_0 \times \sqrt{B_7 \times B_8} \times \sqrt{4B/D_{xy}}}{h \times \sqrt{\tau_{13b} \times \tau_{23b}}}} \tag{4.66}$$

$$B_7 = DD_{11}^2 / DDEN1$$

$$B_8 = DD_{22}^2 / DDEN2$$

where DD_{11} and DD_{22} are equivalent conversion bending stiffness of the composite panel, the equivalent conversion formula is:

$$[DD] = [D] - [B][A]^{-1}[B]$$

$$B_{ij} = \int_{-0.5t_f}^{0.5t_f} Q_{ij}^{(K)} z dz \quad i, j = 1, 2, 6$$

$$A_{ij} = \int_{-0.5t_f}^{0.5t_f} Q_{ij}^{(K)} dz \quad i, j = 1, 2, 6$$

where

$$DDEN1 = 2 \times DEN1 + CA(N)^2 \times \frac{h}{G_{C13}}$$

$$DDEN2 = 2 \times DEN2 + CB(N)^2 \times \frac{h}{G_{C23}}$$

- δ_0 initial wave range of panel;
- τ_{13b} normal shear strength of sandwich core;
- τ_{23b} normal shear strength of sandwich core;
- V_x, V_y compression along x - and y -axis; (i.e., the lowest value of the following: overall critical buckling stress of panel, critical buckling stress of layer, critical core-wise buckling stress of panel);

V_{xy} — shear; (i.e., the lowest value of the following: overall critical buckling stress of panel, critical buckling stress of layer, critical core-wise buckling stress of panel);

④ Sandwich core crush

$$\sigma_{jcr} = \frac{V_j}{1 + B \frac{\delta_0}{\sigma_{cc}}}, \quad j = x, y, xy \quad (4.67)$$

where

σ_{cc} compressive strength of sandwich core;
 $\delta_0, B, V_j, j = x, y, xy$ see definition above.

⑤ Interface failure of sandwich core and panel

$$\sigma_{jcr} = \frac{V_j}{1 + B \frac{\delta_0}{\sigma_{bt}}}, \quad j = x, y, xy \quad (4.68)$$

where

σ_{bt} bonding strength of sandwich structure panel;
 $\delta_0, B, V_j, j = x, y, xy$ definition see above.

The local buckling analysis described above is compiled in the calculation software BUCKLSCP.

4.8 Joint Design and Analysis

Advanced composites have an important advantage over metals in terms of structural integrity. However, technological limitations and the need for maintenance require some separate components to be connected. Proper analytical techniques are necessary to solve the problem of load transmission at joints. Thus, joint design is an important aspect of composite structure design.

Joints represent one of the greatest challenges in the design of structures in general, particularly for anisotropic composite structures. Joints represent potential weak points in a structure; thus, the design of the overall structure tends to follow from, and be limited by, the features of joints in the structure. Failure of the entire structure often originates at the joints. The reason for this is that joints involve interruptions of the geometry of the structure and discontinuities in materials, which

almost always produce local highly stressed areas. Stress concentration in composites is not only more severe but also more complex than that in metals. Stress concentration in metals depends only on geometry; however, composites are affected by the layering pattern as well as geometric parameters. Well-established joining technologies for metallic structures are not directly applicable to composites.

Stress concentration in mechanically fastened joints is particularly severe because the load transfer between the elements of the joint has to take place over a fraction of the available area.

Composite joint strength is closely related to the layering pattern, load direction, and environment. There are more failure modes of composite joints, and moreover, strength prediction is more difficult. These complicating factors require careful consideration.

This section deals with the joining of advanced fiber composites, mainly focusing on mechanically fastened and adhesively bonded joints.

4.8.1 Characteristics of Composite Joints

There are two methods of advanced composite joining: adhesive bonded and mechanical fastening [2, 13, 17, 18].

4.8.1.1 Characteristics of Adhesively Bonded Joints

Adhesively bonded joints have the following advantages:

- (1) No stress concentration caused by drilled holes and strength of basic laminate does not decrease;
- (2) Lower number of parts, lightweight structure, and high joint efficiency;
- (3) Anti-fatigue, sealing, shock absorption, and good insulation performance;
- (4) Good damage tolerance and fail-safe performance;
- (5) Smooth surface contours;
- (6) No fretting problems created by dissimilar materials;
- (7) Non-corrosive, i.e., no galvanic atmosphere created by the presence of dissimilar materials.

Adhesive bonded joints have the following disadvantages:

- (1) Difficultly of inspection of bond quality, poor reliability;
- (2) Large dispersibility, low peel strength, difficultly of transferring large loads;
- (3) Sensitive to hygrothermal and corrosive environments, aging problems;
- (4) Requirements for high-quality surface preparation and strict processing, which can result in residual stress;
- (5) Strict fitting tolerance between adherends and difficultly of repair;

- (6) Permanent joint formed which cannot be disassembled.

4.8.1.2 Characteristics of Mechanically Fastened Joints

Mechanically fastened joints have the following positive attributes:

- (1) Ease of quality inspection, good reliability;
- (2) Ease of disassembly and reassembly in manufacture, replacement, and maintenance;
- (3) No special surface preparation requirements;
- (4) Residual stresses are generally not a problem;
- (5) Environmentally insensitive;

Mechanically fastened joints have the following drawbacks:

- (1) Require machining of holes in the members, thereby weakening the members;
- (2) Require local reinforcement, resulting in increased weight and considerable stress concentration;
- (3) Cost can increase because of increased manufacture capacity;
- (4) Galvanic corrosion may occur when metallic fasteners are in direct contact with composite materials, thus fasteners should be composed of a material that has a small potential difference with the composite.

4.8.1.3 Characteristics of Combined Bonded-and-Bolted (or Riveted) Joints

Bonded-riveted (bolted) combined joints are used based on considerations of fail-safety and the need for additional assurance of joint safety and integrity over a bonded or bolted joint design alone.

Basic principles for use of combined bonded-and-bolted (or riveted) joints are as follows:

1. Select a ductile adhesive;
2. Improve the fit precision of the pin in the hole.

The following points should be noted for use of combined joints:

- (1) The use of fastener strengthening in a bonded structure is a complex question. On the one hand, the addition of fasteners may arrest and relax damage progression and improve anti-impact, anti-fatigue, and anti-creep performances. On the other hand, the fasteners may have an adverse effect on stress concentration and should be carefully considered in different situations;
- (2) Deformation of mechanically fastened joints is generally greater than that of adhesively bonded joints. Deformation behavior of combined bonds shows more similarities to the deformation of mechanically fastened joints;

- (3) The precision of the fastener fit with the hole is important. A poor fit will increase the shear deformation of the joint, resulting in shear failure of the bond-line, and induce shear failure of the fasteners and bearing failure of holes. Hence, there may be no net benefit to the use of fasteners and bonding.

4.8.1.4 Principles for Selecting Composite Joint Methods

The selection of the joining methods should seek to take advantage of the respective features of joint types. In general, some basic principles should be followed:

- (1) Bonded joints are generally suitable for thin structures with low running loads (load per unit width, i.e., stress \times element thickness) or structures carrying shear load. The main advantages of bonded joints are their lightweight nature and high joint efficiency. Thus, bonded construction tends to be more prevalent in small light aircraft and secondary aircraft structures. Well-designed, bonded joints can also transmit large loads;
- (2) Mechanically fastened joints are mainly used in structures where concentrated loads occur or an emphasis on high reliability is required. Bolted joints can transfer greater loads than riveted joints. Thus, bolted joints are mainly used in primary aircraft structural components. The main disadvantage of mechanically fastened joints is the decrease in the strength of the basic laminate owing to the fastener holes;
- (3) Combined joints are generally suitable for jointing places requiring greater margins and for medium thickness laminates.

4.8.2 Adhesively Bonded Joints

Bonded joints have advantages in terms of their lightweight and high joint efficiency; thus, their use in aircraft structural components has grown. For example, the spar of the B-737 horizontal stabilizers; the root-stepped joints of the F-14 all-movable horizontal stabilizers; the joints of wing panel-to-root rib of the F-15 aircraft; Joints of fuselage panels to frame and joints of skin-to-skin for the Lear Fan 2100 all composite plane; joints of the skin of the pelvic fin of the clapboard for the Y7-200B; the skin-stringer joint of the Y7-FC vertical stabilizer; joints of the π -stringer to panels, and the π -stringer to web for the DC-10 vertical stabilizer wall. Bonded step lap joints are used in the attachments for the F-14 and F-15 horizontal stabilizers as well as the F-18 wing root fitting, and the majority of the airframe components in the Lear Fan and the Beech Starship [2, 17–24].

4.8.2.1 Characteristics of Bonded Joint Design

The following points should be noted for bonded joint design:

- (1) The difference in the thermal expansion coefficient of carbon fiber composites and metals is relatively large. Elevated temperature bonding of composites to metallic components will generate considerable internal stress and deformation. Therefore, whenever possible, structural adhesive bonding of composites to metallic components in design, particularly aluminum, should be avoided. If necessary, titanium components with lower thermal expansion coefficients can be used.
- (2) Adhesive joints work best in shear and are poor in peel. Thus, the adhesive layer should carry the load in the maximum strength direction. Whenever possible, normal and peeling forces should be avoided. The interlaminar tension strength of carbon fiber-reinforced polymers is very low, and composites are prone to interlaminar tension failure, whereas metals tend to show peeling failure at bond-lines. Therefore, thick adherends are suitable for stepped and tapered joints.

It is vital to avoid letting the adhesive layer be the weak link in the joint; this means that, whenever possible, the joint should be designed to ensure that the adherends fail before the bond layer.

4.8.2.2 Main Factors Affecting Adhesive Joints Strength

The main factors affecting adhesive joints strength include: material of the adherends, stiffness ratio and thermal expansion coefficients of the adherends, joint configuration and geometry, fiber orientation of the bond-line, temperature and moisture, adhesive, and manufacturing procedure.

- (1) Effects of unbalanced adherend stiffness: All types of joint geometry are adversely affected by unequal adherend stiffness, where the stiffness is defined as the axial or in-plane shear modulus multiplied by the adherend thickness. As an example, for single-lap joints, if the stiffness of the adherends is balanced, the bending moments at two ends of the joint will be the same and the deformation of the adherends will be equal. If the stiffness of the adherends is unequal, the bending moment at two ends of the joint will be different and a higher deformation will generally occur at the loaded end of the more flexible adherend.

Where possible, the stiffness of adherends should be kept approximately equal. For example, for step lap and scarf joints between quasi-isotropic carbon/epoxy and titanium (Young's moduli: 55 and 110 GPa, respectively) ideally, the ratio of the maximum thickness (the thickness just beyond the end of the joint) of the composite adherend to that of the titanium should be $110/55 = 2.0$.

- (2) Thermal mismatch of adherends: Adherent thermal mismatch relates to dissimilar thermal expansion coefficients, which can induce initial curvatures in single-lap joints. These curvatures may influence the already eccentric load path and thereby change the bending moments at the ends of the joint. This effect can in turn change the adhesive shear and peel stress distribution. In general, the joint load capacity is usually decreased because one end of the joint is more critical than other.
- (3) Effects of ductile adhesive response: Adhesive ductility is an important factor in minimizing the adverse effects of shear and peel stress peaks in the bond layer. Ductility has a pronounced influence on the mechanical response of bonded joints. The elastic response may prevent applications in situations where a considerable amount of additional structural capability is required.
- (4) Temperature and humidity: Temperature and humidity have a pronounced influence on the performance of composite components and these environment variables must be considered. When a composite with a polymeric matrix is placed in a wet environment, the matrix will absorb moisture, which may cause material swelling. Particularly at higher temperatures, the material may soften and weaken the matrix and matrix/fiber interface. Absorbed moisture lowers the glass transition temperature and maximum operating temperature of the material. If the adhesive can be used over a range of operating temperatures, the influence of temperature is not important. However, combinations of temperature and humidity conditions should be considered. At high temperatures, the ability of moisture to absorb and diffuse in the material may increase, which could severely degrade the strength of the material.

Long-term environmental effects will obviously decrease bonded joint strength. In engineering design and analysis, these situations should be fully considered. To avoid any adverse effects from temperature and humidity, consider the following points:

- ① Bond-lines are sealed with an adhesive, which is effective against moisture;
 - ② The most severe potential environmental conditions should be precisely determined;
 - ③ The temperature and humidity range of the bonded joint should be precisely defined;
 - ④ The most effective adhesive should be selected considering the aforementioned points;
- (5) Effects of bond defects: Defects in adhesive joints, which are of concern include: debonding, flaws, cracking, cure imperfections, surface preparation deficiencies, voids and porosity, and thickness variations in the bond layer. Of the various defects that are of interest, debonding, cracking, and surface preparation deficiencies are likely of the greatest concern.

Any bond defects will result in load redistribution along the entire bond-line and stress from discontinuity of the bond-line will increase. When the defect size of debonding and cracks is small compared with the length of the bond-line, any increase in stress will not be obvious. The stress will increase markedly as the defect size increases. Thus, it is necessary to establish standards for bond quality.

4.8.2.3 Adhesives

(1) General requirements of adhesives

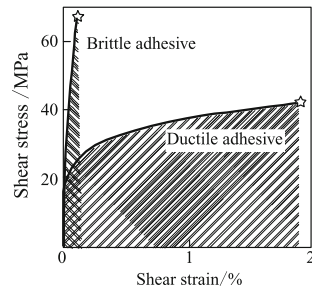
Adhesives should have the following features:

- (1) Compatibility with the adherends and high bonded strength, such that bond-interface failures will not occur;
- (2) The curing temperature should be as low as possible;
- (3) The thermal expansion coefficient of the adhesive should be nearly identical to that of the adherends;
- (4) Temperature effects should be minimal;
- (5) Good mechanical properties;
- (6) Simple processing;
- (7) The durability of the bond should be greater than the anticipated life of the structure.

(2) Types of adhesive and their selection

Adhesives can be broadly classified into two major groups on the basis of their stress–strain curve, i.e., ductile and brittle adhesives (Fig. 4.67). The limit of shear strain of a ductile adhesive is greater than 0.05, whereas that of brittle adhesive is typically far less than 0.05.

Fig. 4.67 Ductile and brittle adhesives



As shown in Fig. 4.67, the shear strength of a brittle adhesive is higher than that of a ductile adhesive. However, peel stresses can be eliminated from consideration by approaches such as adherend tapering. The static shear strength of the bonded joint does not depend only on a single parameter and is determined by the strain energy to failure of the adhesive under a shear load (i.e., the area under the curve). Therefore, joints based on ductile adhesives have greater strength. From the viewpoint of fatigue performance, a brittle adhesive will rupture near the inflexion and its fatigue life is lower. The ultimate strain of a ductile adhesive is also greater. Ductility in aerospace adhesives is beneficial in reducing stress peaks in the adhesive, i.e., lowering the stress concentration. If higher fatigue stresses can be withstood, the fatigue life will be longer. When the environment temperature does not exceed 70 °C, ductile adhesives should be used as far as possible.

Near the engine or in ultrasonic airplanes, high operating temperatures necessitate that the brittle adhesives are used despite the loss of strength.

It is necessary to consider the effects of temperature. If the temperature remains below the glass transition temperature of the adhesive, the bond strength will not be sensitive to temperature effects. However, the strength will be reduced at low temperature.

Materials commonly used in structural adhesive bonding of composite structures are thermosetting resins, which can be subdivided into four basic chemical classes: epoxy, polyimide, phenolic, and silicone.

- (1) Epoxy: The advantages of epoxy resins include its high strength and modulus, low levels of volatiles, excellent adhesion, low shrinkage, low moisture absorption, good adhesion, good chemical resistance, and ease of processing. Therefore, epoxy resins are the most widely used structural adhesives. Forms are packed with resin and curing agents, which are mixed and cured with heat. The major disadvantages of epoxy resins include brittleness, generic hardness, low thermal strength, and poor wear characteristics. The curing is usually accomplished by the application of heat under pressure. For example, a cure will typically be performed at 145 °C and 0.7 MPa and be complete within 20 min. Some cures will also be completed at room temperature.
- (2) Epoxy–Phenolic: This class of adhesives are a modified epoxy, which can be completed within 60 min at 250–350 °C. Its advantages include high strength and good performance at low temperatures; its major disadvantages are the need to heat during curing, porosity of the bond, and poor electrical performance.
- (3) Polyimides: This class of adhesives requires high temperature curing, usually between 250–400 °C. A post-cure is also required to attain maximum strength. The highest operating temperatures of these adhesives are in the range of 250–400 °C. Advantages of this class of adhesives include their resistance to temperature, moisture, fire, and corrosion as well as their low coefficient of thermal expansion. Disadvantages of polyimides include their high cost, porosity, and corrosiveness.

- (4) Phenolic: Mixed resin adhesives are usually composed of a phenolic resin mixed with another resin. The advantages of such mixtures include high thermal strength, acid resistance, low cost, and good electric performance. Their major disadvantages are the need for high curing temperatures, high shrinkage, and corrosiveness. Common used resins include:
- ① Phenolic polyamide: Shear strength can be as high as 36 MPa and maintains excellent strength at high temperature.
 - ② Phenolic ethylene: Shear strength can be as high as 30 MPa and can operate at very low temperatures. Performance is rapidly degraded above 100 °C.
- (5) Silicone has good resistance to heat, cold, radiation, and good isolation; however, its strength is low. Therefore, joints requiring high stability and the high mechanical strength may be achieved with the use of this resin in combination with others. Epoxy–silicone can be used continuously at temperatures as high as 340 °C and discontinuously at temperatures up to 510 °C.

(3) Adhesives suitable for bonding different materials

Adhesives for bonding different materials may be selected as outlined in Table 4.16. Blank entries for material/adhesive combinations in the tables indicate that it may be difficult to achieve bonding.

Adhesives suitable for aeronautic structures are listed in Table 4.17.

(4) Measurements of the mechanical properties of the bond-line

Stress–strain characterization of adhesive films and their mechanical performances form the basis of static strength design for adhesive bonded joints. Because the bond-line is very thin, the interface will have some influence and the specimens used for testing must have the same configuration as that of the actual part.

Measurement results show that the actual stress–strain curve (Fig. 4.68) is complicated and may be difficult to apply directly for joint analysis. Equivalent elastic–plastic and bilinear stress–strain curves are commonly used simplified models. The elastic–plastic curve is particularly useful and the simplification allows closed form analytical solutions to be obtained. The principles of this simplification are that any adhesive is defined by two straight lines having the same strain energy and failure stress and strain. The peak allowable shear stress should be multiplied by a factor of 0.8 to account for both bonding defects and the differences between laboratory and production fabrication. The peel strength and other data needed for design can be measured from related test standards.

Table 4.16 Adhesives suitable for the bonding different materials

	Metal	Polyamide	Silicone	Ceramics and glass	Polyflon	Polyurethane	Phenolic	Epoxy
Metal	E/T	E	S					
Polyamide	E	P	-	-				
Silicone	S	-	S	-	-			
Ceramics and glass	E	-	-	-	-	-		
Polyflon	E/T	-	-	-	E/T	-	-	
Polyurethane	E	-	S	-	-	E	-	-
Phenolic	E	-	-	E	-	-	E	-
Epoxy	E	-	-	-	E/T	-	E/T	E/T

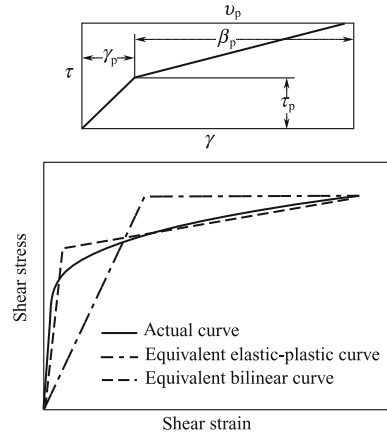
Note E epoxy; P polyamides; S silicone; T polysulfide rubber

Table 4.17 Properties of commonly used adhesives in aeronautical structures

Item	Trademarks of the adhesives							
	SY-24C (primer SY-D9)	SY-18 (primer SY-18)	J-47A (primer J-47B)	J-95 (primer J-96)	SY-14A (primer SY-D8)	J-99 (primer J-100)	J-116B [ⓐ] (primer J-117)	
Test standard	Q/6S928-93 Q/6S927-93	Q/6S348-83 (film) Q/6S347-83 (flour)	CB-SH-0037 -85	Q/HSY022-92 Q/HSY023-92	Q/6S104-88 Q/6S1234-95	Q/HSY039-92 Q/HSY026-92	Q/HSY043-93	
Basic components	Epoxy, dicyandiamide	Epoxy, nitrile rubber, curing agent, accelerator	Epoxy, nitrile rubber, amine, curing agent	Epoxy, nitrile rubber, epoxy amine	Epoxy, polysulfone, curing agent	Epoxy, polysulfone, curing agent	Epoxy, elastomeric, curing agent nylon carrier	
Shear strength MPa	55 °C	≥ 33		≥ 33	≥ 28	≥ 28	24.5	
	25 °C	≥ 33	≥ 30	≥ 33	≥ 30	≥ 28	24.5	
	80 °C	≥ 21(70 °C)		≥ 21 (70 °C)				
	100 °C		≥ 18	≥ 15				
	150 °C		≥ 10 (130 °C)		≥ 20	≥ 15	13.3	
175 °C					≥ 18			
90° peel strength/(kN/m)	≤ 55 °C	≥ 4.5 [ⓐ]		≥ 4.5 [ⓐ]				
	25 °C	≥ 6.0 [ⓐ]		≥ 6.0 [ⓐ]	≥ 5.9	≥ 7.0	7.5	
	150 °C				≥ 3.9		4.0	
Manufacturers	BIAM	BIAM	HIP	HIP	BIAM	HIP	HIP	
Overseas similar trademarks	Metland 1113.06 Metbond 6726			Metland 1113.06 Metbond 6726		Redux 319A Redux 119		
Overseas corresponding materials standard	DHS172-292 DHS186-211			DHS172-292 DHS186-211		DHS174-292 DHS186-231		

Note ①. All data of J-116B adhesives are B-basis; ②. Bell peel strength

Fig. 4.68 Shear stress–strain curves of adhesive layer



4.8.2.4 General Design Requirements for Adhesive Bonded Joints

(1) General principles for adhesive bonded joints

Effective bonded joints should be designed to ensure that the bonded strength is not less than that of the adherends. Otherwise, the adhesives will become weak links, resulting in the premature failure of the bonded structure.

From the standpoint of increasing strength and reducing costs, the basic principles for bonded joint design are as follows:

- (1) A rational joint configuration should be selected to ensure that the shear loads are carried by the bond-line in the maximum strength direction. Whenever possible, normal stress, cleavage, and peel forces should be avoided to prevent peeling failure;
- (2) Minimize joint eccentricities and stress concentration. Reduce peel stress. Interlaminar peel failure of end laminates should be avoided;
- (3) Balanced adherend stiffness is required to reduce peel stress;
- (4) Use adherends with similar coefficients of thermal expansion. The coefficient of thermal expansion of the adhesives should be close to that of the adherends to reduce residual stress;
- (5) Ductile adhesives are preferred over brittle ones;
- (6) Film adhesives are preferred over paste adhesives for large area bonds;
- (7) Ensure the bonded joint configuration can be visually inspected to improve reliability and confidence. It is important to emphasize the process control;
- (8) It should be recognized that slow cyclic loading is a major factor affecting the durability of adhesive joints. Avoid the worst effects of this type of loading by providing sufficient overlap to ensure that some of the adhesive is lightly loaded. Ensure that creep cannot occur at that position under the most severe potential humidity and temperature, to which the component will be exposed.

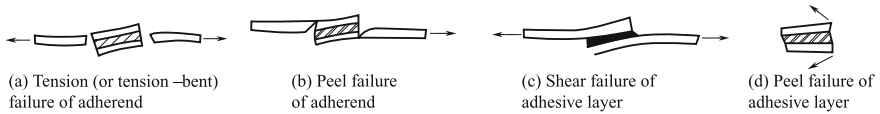
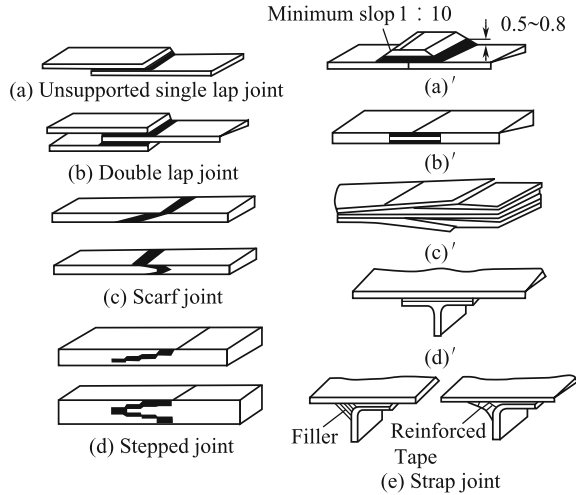


Fig. 4.69 Basic failure modes for bonded joints

Fig. 4.70 Basic configurations of bonded joints



The overall purpose of these principles is to ensure that the strength of the bonded layer is higher than or close to that of the adherends. Therefore, it is necessary to adopt measures to ensure that the configuration and geometric parameter satisfy these requirements.

(2) Failure modes of bonded joints

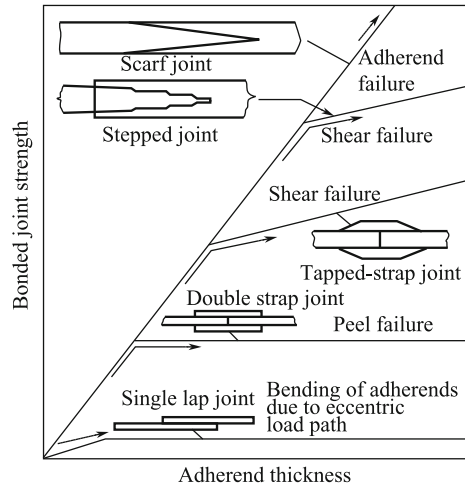
Basic failure modes for adhesively bonded composite joints are as follows (shown in Fig. 4.69):

- (1) Tension (or tension-bending) failure of adherend;
- (2) Shear failure of glue-line;
- (3) Peel failure of bond-line and adherends.

Alongside these three basic failure modes, combined modes may also occur. The failure modes of bonded joints will depend on the joint configuration, geometric parameters, fiber direction near the glue-line, and loading properties. The adherend thickness is the most important geometric parameter, as outlined for the following cases:

- (1) Tension (or tension-bending) failure of adherend will occur when adherends are very thin, and joint strength is sufficient;

Fig. 4.71 Influence of adherend thickness on selection of joint configuration



- (2) Shear failure of the glue-line will occur when the adherends are thick and the eccentric moment is small;
- (3) Peel failure will occur under eccentric moments when the adherend thickness reaches a certain value and the bond length is not long. The interlaminar tension strength of CFRP is very low; thus, composites are prone to interlaminar tension failure. Peel failure will reduce the load capability greatly and should be avoided.

(3) Selection of basic joint configuration for bonded joints

Figure 4.70 shows some basic joint configurations for panel components of aircraft.

The selection of a joint configuration is key for bonded joint design. Joints must be designed to transfer their maximum load in the shear direction with smaller loads in other directions. This will avoid the occurrence of large peel stress. Figure 4.71 illustrates the strengths of basic joint classifications as a function of the adherend thickness. Each curve shown represents the best strength that can possibly be obtained for each joint type.

- (1) Single-lap joints may be used when adherends are thin (≤ 1.8 mm). Note that additional bending moments, caused by eccentricity of the load path, will result in very high peel stress at both ends of the bonded joint, which will reduce the joint strength. Therefore, it is necessary to increase the overlap-to-thickness ratio. Bending moments may be alleviated through the use of a high ratio $L/t = 50\text{--}100$. When adherends feature an imbalance of stiffness, eccentricity effects will be greater. The use of single-lap joints should be avoided. However, in a single-lap joint supported against bending, eccentricity effects may be alleviated and deformations restricted. Such joints

Fig. 4.72 Geometric parameters of bonded joints

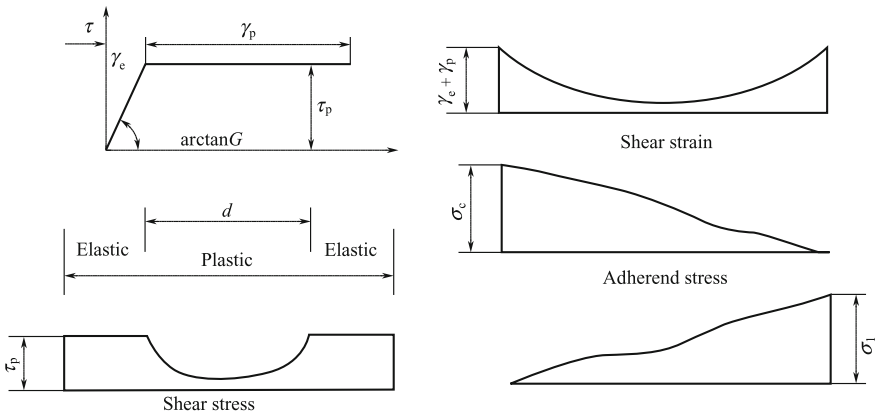
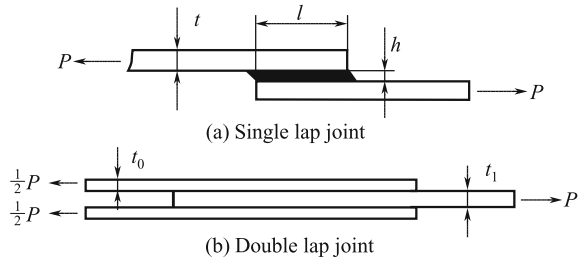


Fig. 4.73 Stress and strain distribution of balanced stiffness double-lap joint

may be treated as double-lap joints in analysis, by considering the single-lap joint as half of a double-lap joint. Secondary adhesive bonding is used extensively for thin, lightly loaded composite structures, to reduce the need for mechanical fastening.

- (2) Adherends of moderate thickness ($L/t \approx 30$) are suitable for double-lap joints.
- (3) Thick adherends are suitable for stepped and tapered joints, where stepped joints are most commonly used. Stepped-lap joints share some characteristics of both scarf and uniform lap joints. The pure shear state for every step can be closely attained and as the number of steps is increased a higher joint efficiency will result. As a rule, scarf joints are only used for repairs of thin structures.

(4) Selection of geometric parameters for bonded joints

As an example, the geometric parameters of single-lap joints under a tension load are: adherend thickness t , bond layer thickness h , and overlap length L (Fig. 4.72).

The adherend thickness is determined by the required transfer load P .

The thickness of an adhesive layer has an effect on joint strength. For most practical joints, adhesive layer thickness is maintained in the range 0.10–0.25 mm. Stress concentration can be reduced and joint strength can be improved by increasing the thickness of adhesive layer. However, thicker layers tend to have a high void content, and strength will be reduced. Furthermore, high-precision fitting

between adherends is required for thin adhesive layers such that a very thin glue-line may not be possible.

The design of simple, bonded splices of uniform thickness for near quasi-isotropic carbon/epoxy is simple. Use a $30t$ -overlap for double shear, $80t$ -overlap for single-lap joints, and a 1-in-50 slope for scarf joints. Overlapping ends should taper to 0.51 mm with a slope of 1/10.

Analysis and test results indicate that the shear stress distribution is not uniform throughout the bonded area under an applied load. Most of the load is transferred through two end zones which form a low stress elastic trough (Fig. 4.73).

Because of the presence of these elastic troughs, the load carrying capacity of the bonded joint increases gradually in the beginning. However, the width and depth of the elastic trough only increases continuously when the length of the overlap attains a certain value. Increases in overlap length above this value do not add to the joint's load carrying capacity. From the viewpoint of static strength, there is no need to increase the overlap length; however, service life and durability should also be considered and longer overlaps are often used. For very short overlap and transfer of large loads, the minimum shear stress and strain in the middle of the overlap area are nearly equal to that at both ends. Thus, the entire bond is in a plastic state. When the load is removed, the adhesive in the middle cannot recover, and the joint will fail soon. Analysis results demonstrate that at a minimum stress equal to 10% of the maximum stress the glue-line can recover its original state. For double-lap joints, an elastic trough width of $6/\lambda$ is sufficient to ensure a minimum adhesive shear stress distribution, which is no greater than 10% of the maximum stress.

(5) **Fiber orientation of the bond surface**

The surface fiber direction of the laminate should be in the primary load direction or 45° to the load direction, but not perpendicular to the load direction, to prevent adherend premature interlaminar tension (peel) failure.

(6) **Surface preparation of adherends**

The bonding of adhesive is a complicated activation process between the adherends and adhesives. It is important to prepare a quality adherend surface for good quality bonds in terms of static strength and durability. The bond should meet prescriptive technical specifications. Strict quality control and inspection should be performed in the bond processing. Nondestructive inspection should be performed for all important parts. Surface preparation deficiencies are particularly troublesome because there are currently no nondestructive evaluation techniques for detecting low interfacial strength between the bond and adherends.

For bonds between carbon-epoxy composites, solvents may be used to clean the surface together with mechanical abrasion of the surface. For bonds between composites and metal, in addition to the surface preparation the metal will require a surface treatment. Corrosion barriers (such as fiberglass and sealants) are placed at the interfaces between the composites and aluminum or steel to prevent galvanic corrosion.

Globally, surface treatment processes for metals include: stainless steel, no-treatment; titanium, phosphoric acid anodization or no-treatment; aluminum, chromic acid anodization.

Phosphoric acid anodization is a common surface treatment for aluminum in China. To prevent galvanic corrosion, a fiberglass or Kevlar insulated layer should be placed between the aluminum and composite.

4.8.2.5 Design of Thick Section Joints

Thin section joints can only transfer small loads; however, it is possible to transfer larger loads through thick section joints. Failure will occur preferentially in the adhesive for thick adherends in a simple joint configuration. Thick adherends cannot perform effectively and joint efficiency will be low. To ensure the glue-line is not a weak link in the joint and to make full use of the load-bearing capacity of the adherends and avoid premature failure, the bond surfaces should be increased and peel stress reduced. Complex stepped and tapped joints are typically used.

- (1) Selection of stepped and scarf joints: Thick adherends under a large load are suitable for stepped or tapped joints. The use of stepped or scarf joints is effective for reducing peel stress. The advantages of stepped joints over scarf joints are their ease of fit and high strength achievable by adjusting structural parameters. Therefore, higher joint efficiency may be attained. Composite-to-titanium stepped joints are used extensively throughout the aerospace industry for high load transfer.

Stepped and scarf joints are appropriate for highly loaded thick plate bonded joints. The use of scarf and stepped joints is effective for reducing peel stress. Unlike scarf lap joints, stepped joints have simple processing and can achieve high strength by adjusting structural parameters. Stepped-lap joints are commonly used for joining cover panels and titanium structures, see Fig. 4.74.

- (2) Strain-level requirements: In the design of strain levels for thick adherend structures, values should be properly lowered considering the need for future repair. It is impractical to repair thick structures by bonding because of the taper ratio requirement, i.e., 1:50. When there is no need for repairs such as one-shot

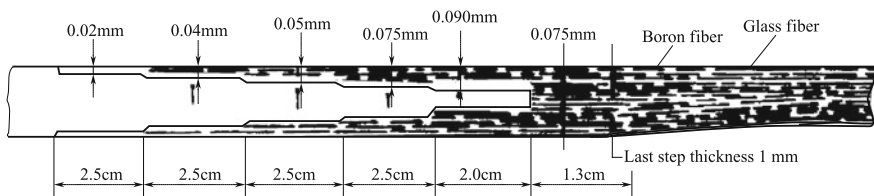


Fig. 4.74 Root-stepped joints of F-14 all-movable horizontal stabilizers

and throwaway structures, in missiles and unmanned aircraft, bonding permits extremely high structural efficiencies to be obtained, even on thick structures.

- (3) Geometric requirements of stepped-lap joints: Complex stepped joints are required to obtain sufficient joint efficiency in thick structures. Many steps are required to transfer load, and to ensure that the glue-line provides adherend strength. The thickness at the end step should be a minimum of 0.76 mm and the step length no longer than 9.5 mm, to prevent failure of the end step. Tapered ends of bonded overlaps should taper to a thickness of 0.51 mm with a 1-in-10 slope. This minimizes the induced peel stress that cause premature failure.
- (4) Layering requirements of stepped-lap joints: If possible, $\pm 45^\circ$ plies should be used on the first and last step of bonded step joints to reduce the peak inter-laminar shear stress at end steps.
If possible, do not end with more than two 0° plies, which have a thickness less than 0.36 mm, on any step surface. For 0° plies ending on the last step (longest 0° ply), serrated edges have been shown to reduce the stress concentration and reduced stress concentration at the end of the joint. 90° plies should butt up against the first step of a step joint.
- (5) The differences in thermal expansion coefficient between the adherends need to be minimized to reduce thermal stress for composite-to-metal joints. Bonding composites to titanium is preferred; steel is acceptable; aluminum is not recommended.
- (6) Technological considerations. Co-cured joints are preferred over pro-cured joints if there are fit-up problems. For pre-cured parts, machined scarfs are preferred over layered scarfs for improving the fit.

4.8.2.6 Detailed Design of Composite Bonded Structure

Detail design of composite bonded structures should not only consider the static strength of the bonded structure but also the durability, bonding technology, and cost of the bonded structure. In addition to the aforementioned basic principles, the following issues should be noted for detailed design of composite bonded structures.

- (1) Selection of bonded joint configuration: The configuration of a bonded joint is a critical design aspect. The load-bearing capabilities of bonded joints work best in the shear direction and have poor resistance to peeling. The maximum load should be transferred in the shear direction and minimum loading should be induced in other directions. The use of stepped-lap or scarf-lap joints is effective for reducing peel stress and ensuring the joint strength is not lower than that beyond the joint.

- (2) Procedures for reducing stress concentration and peel stress for adhesive joints: Whenever possible, the peel stress in the structure should be reduced by induction of eccentricities in the load path and asymmetry. For example, the use of a symmetric double-lap joint increases the bending stiffness of the outer adherend, and tapering of the edges of the overlap in single joints. Three procedures for decreasing stress concentration are illustrated in Fig. 4.75.

Fig. 4.75 Procedures for decreasing stress concentration

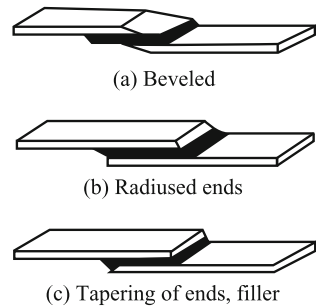


Fig. 4.76 Single-lap joint with transverse support

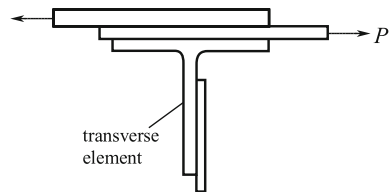


Fig. 4.77 Joint of corner reinforcement to skin

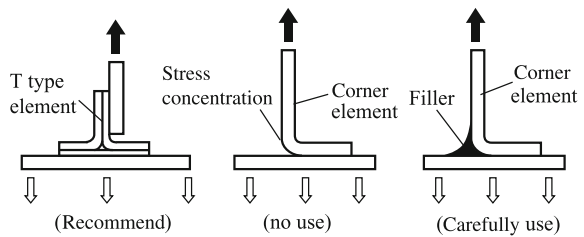
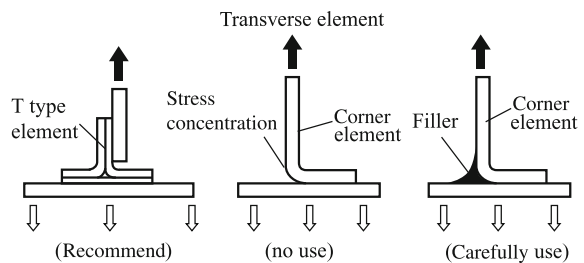


Fig. 4.78 Stress distribution of T-type reinforcement



A high stress concentration at both ends of the joint occurs owing to eccentricity in the load path for single joints. Thus, the peel stress can result in the premature failure of the adherends. The load-bearing capacity will be improved by supporting a joint with a transverse fully stiffened restraint (Fig. 4.76).

- (3) Skin (web) strengthening procedure: The use of T-type components rather than angled components is recommended. Peeling at the corner of the angle reinforcement can occur easily if there is a tension force. Premature peeling may be prevented with the use of filler at the corner (Fig. 4.77). When a T-type element is used, peeling can be prevented if there are tension forces. Peeling will be improved by edge tapering of the profile element and balancing the stiffness between the profile element and web. The stress distribution of T strengthened elements is shown in Fig. 4.78.
- (4) Thermal stress of bonded structures: In the bonding of carbon/epoxy, boron/epoxy composites to metals, such as titanium and steel, Thermal residual stress arises due to differences in thermal expansion coefficient of the materials. In particular, the thermal stress is proportional to the difference between the operating and cured temperature. Thermal stress can be reduced through the use of laminate layering design.
- (5) Avoidance of galvanic corrosion: In the bonding of composites to metal, galvanic corrosion may occur owing to differences between the electrode potentials of materials. Surface treatment of metal elements should be performed. Whenever possible, direct bonding of carbon composites to aluminum should be avoided and an isolating layer should be placed between the materials.
Carbon fibers must be isolated from aluminum or steel through the use of an adhesive layer and/or a thin glass-fiber ply at such interfaces. The galvanic interaction between carbon and aluminum or steel will cause corrosion of the metal.
- (6) Prevention of moisture entering adhesive layer: Unlike metal adherends, composite adherends are subject to the effects of moisture diffusion. As a result, moisture is more likely to affect the whole component rather than be confined near the exposed edges of the joint in the case of metal adherends. The response of adhesives to moisture is an important issue for composite joints.
- (7) Tooling design and manufacture: The quality of bonded joints is influenced greatly by tooling. Therefore, careful attention is required for the design and processing of bonded joints to minimize thermal deformation and residual stress. Tools should be applied under uniform pressure to the adherends.
- (8) Quality control: Adhesive quality should be controlled based on allowable values for defects prescribed for different positions.

4.8.2.7 Durability Design of Bonded Structures

Durability of composites relates to their fatigue performance under cyclic loading and different environmental conditions. Like metals, it is difficult to reliably estimate the life of composite structures. Durability of composite structures is mostly assured by performing constant or variable amplitude cyclic loading tests.

Durability of bonded structures is based on adhesive performance, surface preparation, loading and environmental conditions, structural characteristics, and the detailed design.

The design of adhesive joints should be focused on joint durability rather than static strength and should meet certain conditions. Three major considerations for bonded joint durability, based on the design philosophy of Hart–Smith, are as follows:

① Either the adherent thickness should be limited, or more sophisticated joint configurations, such as scarf and step lap joints, should be used to ensure that adherend failure takes precedence over bond failure; ② The design should minimize peel stress, either by keeping the adherends sufficiently thin or by tapering the adherends for intermediate adherend thicknesses (see discussion of effects of adherend tapering); ③ It is essential that good surface treatment practices are maintained to ensure that the bond between the adhesive and adherends does not fail. When these conditions are met, reliable joint performance can be expected for the most part, except in environmental extremes (hot–wet conditions). The Hart–Smith approach focuses primarily on creep failure associated with slow cyclic loading (i.e., one cycle over several minutes to an hour) under hot–wet conditions.

In fact, the distribution of shear stresses of bonded joints is non-uniform. The maximum stress occurs at both ends of bonded joints and stress in the middle area is basically zero. The Hart–Smith criterion for avoidance of creep failure is that the minimum shear stress along the bond length should be no greater than one tenth the yield stress of the adhesive.

In addition to creep failures under hot–wet conditions, the joint may fail due to cracking in the bonding layer.

4.8.2.8 Summary of Bonded Joint Analysis

Stress analyses of adhesive joints range from very simplistic ‘P over A’ formulations in which only the average shear stress in the bond layer are considered, to extremely elegant elasticity approaches that consider fine details—for example, calculation of stress singularities by applications of fracture mechanics concepts. A compromise between these two extremes is desirable, because the adequacy of structural joints does not usually depend on knowledge of their details at the micromechanics level, but rather at the scale of the bond thickness. Practical considerations require bonded joints to incorporate adherends, which are thin relative to their dimensions in the load direction; hence, the stress variation through the thickness of the adherend and the adhesive layer tend to be moderate. Such variations do tend to have a great effect on polymer matrix composite adherends because of their relative softness with respect to transverse shear and thickness

normal stresses. However, design procedures have been developed by neglecting the thickness-wise adherend stress variation. Such approaches involve the use of 1D models in which only variations in the axial direction are accounted for.

FEMs are often used for investigating various features of bonded joint behavior. However, there are serious pitfalls, which the analyst must be aware of to avoid problems in such analyses. There is a tendency for the bond layer thickness to unbalance the finite element model. To achieve adequate accuracy, it is especially important to provide a high degree of mesh refinement around the ends of the overlap and the mesh should transition to a coarser representation away from the ends of the overlap to avoid unneeded computational costs. Without such approaches, the aspect ratios of elements may be limited and will force either a crude representation of the bond layer or an excessively over-refined mesh for the adherends.

Currently, the most useful analytic method is based on the simplified one-dimensional approaches characterized in the work of Hart–Smith. This method emphasizes principles, which have been determined from practical experiences in joint design, and has been successfully applied to aircraft components. Before analyses, a stress–strain diagram of the glue-line and other characteristic parameters, similar to those shown in Fig. 4.68, needs to be measured for the adherends and adhesives. The analytic methods for single-lap, double-lap, stepped, and scarf joints are presented in references [4–7]. It should be noted that design parameters based on these methods consider only static strength. Other factors should be considered separately—specifically, the influence of long-term loading in particular environments. The ultimate design parameters should be determined by the necessary tests.

4.8.3 Mechanically Fastened Joints

4.8.3.1 Design of Mechanically Fastened Joints

Characteristics of Mechanical Joint Design

The following points should be noted for mechanical joints [2, 13, 17]:

- (1) Owing to the brittle nature of composite materials, multiple fastener joint load distributions are non-uniform. The stress and strain of basic laminates will be lower when joints fail;
- (2) The bolted joint strength of laminates with a certain content of 0° -plies is less than the unnotched laminate strength;
- (3) The load-carrying capability of joints does not show a directly proportional increase with the end distance;
- (4) Bolted joints should be designed to carry a load such that the bolt is under a shear force rather than tension. Bolt bending in composites is more common than that in metals.

Main Factors Affecting Mechanical Joint Strength

There are many more factors that affect the mechanical joint strength of composites than those affecting metals. It is important to understand and consider all factors in design.

These factors can be classified into the following five types:

- (1) Material type and form: unidirectional tape or woven fabric fibers, resin type, fiber orientation of, fiber volume fraction, and laminate pattern;
- (2) Processing methods: prepreg, RFI, RTM, curing, and consolidation processes (vacuum bag molding and oven and autoclave curing);
- (3) Configuration: joint types (single or double lap), geometry (pitch, space, edge distance, side-end distance, thickness, hole diameter and tolerance, hole patterns, and washer size);
- (4) Fastener types (hexagonal head bolt, big foot bolt, blind fastener, protruding and countersunk head fastener), clamp-up force;
- (5) Load: static, dynamic, fatigue load, load direction, loading rate;
- (6) Environment: temperature and humidity.

(1) Laminate pattern

Laminates used in aerospace structures are generally composed of layers in the 0° , $\pm 45^\circ$ and 90° directions with respect to the axes of the laminate. The percentage of $\pm 45^\circ$ plies has an important effect on laminate bearing strength. Shear-out or cleavage failure can occur more readily when the $\pm 45^\circ$ -ply content is less than that of the 0° plies. Unlike metals, shear-out failure can only be prevented by increasing the end distance of holes. It is more important that a proper percentage of $\pm 45^\circ$ plies is maintained. Bearing strength increases with the percentage of $\pm 45^\circ$ plies. The recommended layering ranges to achieve maximum strength in joint areas are $\pm 45^\circ$ plies $\geq 40\%$, 0° plies $\geq 30\%$, 90° plies in the range 10–25%, with variations of 5% allowed. Bearing strength will decrease as the percentage of the $\pm 45^\circ$ layers is increased further.

Characteristics of $\pm 45^\circ$ layer content $\geq 50\%$ are as follows:

- (1) Joint strength is less sensitive to load direction;
- (2) Initial failure strength may occur earlier;
- (3) Shear load-bearing ability is stronger and tension load-bearing ability is lower.

Particular care should be given to the tension in multi-row fastener joint design.

(2) Ply stacking sequence

The stacking sequence is a special parameter effecting the mechanical nature of composites. Laminates of the same ply numbers and proportions can have various stacking sequences, which can change interlaminar stresses, and the mechanical natures of laminates may be affected. Whenever possible, maintain a well-dispersed stacking sequence and avoid grouping similar plies.

(3) Fastener torque

Bearing strength is sensitive to clamping forces, namely the force in the through-thickness direction caused by tightening the bolt. Bolt clamp-up improves the strength of composite joints. Test results have demonstrated that bearing strength increases with torque moment until a certain value, after which the bearing strength will not increase. Excessive bolt tightening could damage the laminate.

(4) Joint configuration

Joint configuration is one of the important factors affecting mechanical fastening strength. In comparison with double shear lap joints, lap joint strength decreases because of eccentricity in the load path. The magnitude of the single shear effect depends on plate thickness and has little effect on thin laminates; however, it has a clear effect on the initial bearing failure strength. Single shear effects will increase gradually with plate thickness.

(5) Width-to-diameter ratio

The width-to-diameter ratio mainly effects the net-tension failure strength of mechanical joints. Failure modes of joints will transform from tension to bearing with increasing plate width, when the end edge distance is sufficient. Because bearing failure is a local phenomenon, further increases in W/D do not affect the joint strength. However, joint efficiency can be reduced. The W/D ratios of failure mode transitions from net-tension to bearing are different for various laminates. It is recommended that laminate patterns in joint areas should have a minimum bearing failure of $W/D = 5$. For orthotropic ($0^\circ = 50\%$, $90^\circ = 50\%$) and $100\% \pm 45^\circ$ layers laminates, larger W/D values are needed for bearing failure to occur.

(6) End edge distance-to-diameter ratio

The end edge distance-to-diameter ratio mainly affects the shear-out failure strength. Failure modes of joints will change from shear to bearing with increasing e/D when the plate width is sufficient. It is recommended that patterns in the joint areas should have a minimum e/D not less than three. For laminates including a lower proportion of $\pm 45^\circ$ layers, a larger e/D value is needed. The transition ratios of e/D will differ among various laminates.

(7) Hole diameter-to-thickness ratio

When W/D , e/D , and D/t are constant, failure loads of mechanical joints will increase with hole diameter, but bearing strength will decrease. The joint strength will attain a maximum at approximately $D/t = 1.0$. The joint strength will decrease as D/t is increased further. The bearing strength will decrease about 13% when $D/t = 3$.

It should be noted that fastener failure will generally occur if the fastener diameter is smaller than the plate thickness. When the laminate capacity is calculated, the effective thickness $t_e = d$ should be used:

$$t_e = t \text{ for } t \leq d;$$

$$t_e = d \text{ for } t > d.$$

(8) Load direction

The angle between the fastener load and 0°-ply direction can affect joint strength owing to the anisotropic nature of the strength and stiffness of composite materials. Test results have indicated that the bearing strength decreases as the angle between the fastener load and 0°-ply direction increases. The more isotropic the layering, the less sensitive the laminate will be to load direction.

(9) Countersink holes

Countersinks will clearly decrease laminate bearing strength. This effect will decrease gradually with increasing plate thickness.

(10) Hygrothermal environment

Environmental conditions such as temperature, moisture, and corrosion have a significant effect on laminate bearing strength. The extent of these effects is outlined in Sect. 4.8.3.4 of this chapter.

Design Basic of Mechanical Joints

(1) General requirements of mechanical joints

The following basic principles should generally be followed in the design of mechanical joints:

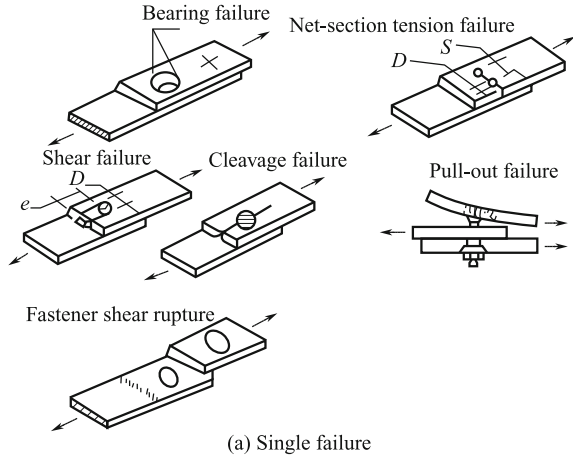
- (1) Strength requirement should be satisfied in terms of the design of joint geometry and laminates. Allowable bearing stress cannot be exceeded in design loads;
- (2) Future repair activities should be considered such that joints can accommodate the next largest fastener size;
- (3) Use double shear joint configurations;
- (4) Fasteners should bear load in shear direction and avoid tension and bending;
- (5) Requirements of galvanic corrosion resistance should be satisfied;
- (6) Consider the environmental effects of operating conditions and special requirements.

(2) Failure modes of mechanical joints

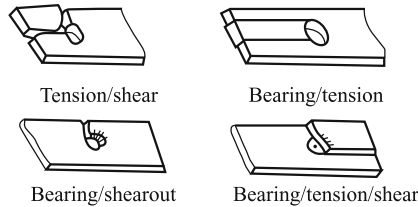
Composite mechanical joints mainly have the following failure modes:

Single failure modes: Bearing, tension, shear-out, and cleavage failure of laminates (Fig. 4.79a).

Fig. 4.79 Single and combined failure modes of mechanical joints



(a) Single failure



(b) Mixed failure

Mixed failure modes: bearing-tension, bearing-shear-out, tension-shear-out, bearing-tension- shear-out failure of laminates (Fig. 4.79b); Pull-through, fastener shear rupture, tension and bending failure of fastener modes.

Mechanical joint failure modes mainly depended on the joint geometry and the fiber pattern. Tension and shear-out failures occur when W/d and e/d are respectively too small. Note that increasing the end distance will have no benefit if shear and cleavage failure occur because the 0° -ply content is likely too high. Cleavage and shear failures are two kinds of low strength failure modes, which should be prevented. Bearing failures occur when both W/d and e/d are too large. Bearing damage is localized and is usually not associated with catastrophic failure of a composite structure. Fastener shear and bending failure may occur when the ratio of plate thickness to the fastener diameter is large. For single-row fastener joints, from the perspective of joint safety and efficiency, whenever possible, mixed modes associated with bearing failure should be designed. Tension failure generally occurs for multirow joints, because this failure mode is governed by bearing–bypass load interactions. Special care should be taken in the design of these joints.

(3) Configuration and selection of mechanical joints

Composite fastening joints can be classified as single and double shear lap joints. Each joint type has uniform and varying thickness conditions (Fig. 4.80).

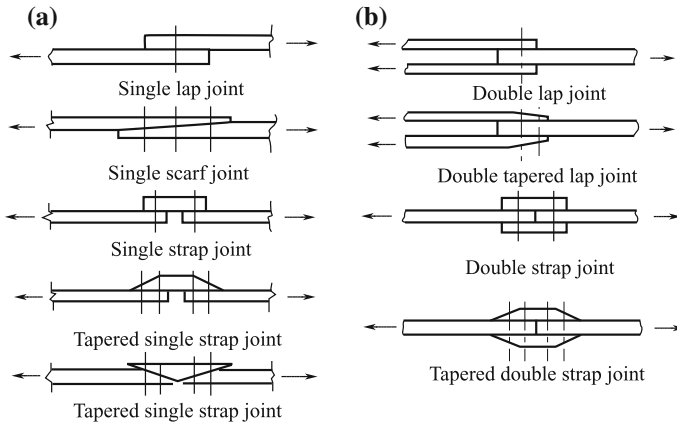


Fig. 4.80 Basic types of mechanical joints

The following principles are recommended for selection of composite fastening joints:

- (1) Joint design should be suitable for use in double shear lap joints. Whenever possible, unsymmetrical single shear lap joints with low efficiency should be avoided;
- (2) Multiple rows are recommended for unsymmetrical joints such as single shear lap joints. The back pitch should be as high as possible, to minimize bending induced by eccentric loading. Local reinforcement of unsymmetrical joints by arbitrarily increasing the laminate thickness should generally be avoided because the increased resulting eccentricity might increase bending stress. This effect will counteract or negate the increase in the material area;
- (3) Carbon fiber/resin matrix composites do not generally feature plastic deformation. This may result in a severe non-uniform load distribution in multirow fastener joints. Therefore, joints with more than two rows of fasteners should not be used, and hole patterns with parallel-row joints should be used whenever possible;
- (4) Tapered joints can improve the non-uniformity of load distribution in multirow fastener joints and increase the load-bearing capacity of joints. It is important to select tapered splice plate thickness and fastener diameters in the design.

(4) Ply-layering requirements in joint areas

To improve the strength and flexibility of mechanical joints, the following principles should be considered in addition to general ply-layering requirements:

- (1) The percentage of $\pm 45^\circ$, 0° , and 90° plies should not be less than 40%, 30%, and 10%, respectively. This is particularly important for mechanical joint design;
- (2) Extremely thin laminates should be reinforced locally at the attachment area to provide greater thickness. This reinforcement will avoid the reduced bearing allowables that result from a D/t ratio greater than four. The general rules $D/t \geq 1$ should be followed to avoid failure of the fastener;
- (3) In areas of load induction there should be equal numbers of $+45^\circ$ and -45° plies on each side of the mid-plane;
- (4) Butt-splined fibers should be avoided in join areas.

(5) Geometry requirements

To prevent low strength failure and ensure high strength of mechanical joints, geometric parameters of jointed plates should be selected according to Table 4.18. Definitions of the geometric parameters are shown in Fig. 4.81.

In addition, the geometric size of joints should consider future repair demands. The next largest size fastener should be useable after the repair.

(6) Fastener requirements

To prevent galvanic corrosion, fasteners made from titanium, titanium alloy, stainless steel, and Monel should be used because the electrode potentials of these alloys are close to those of the composites.

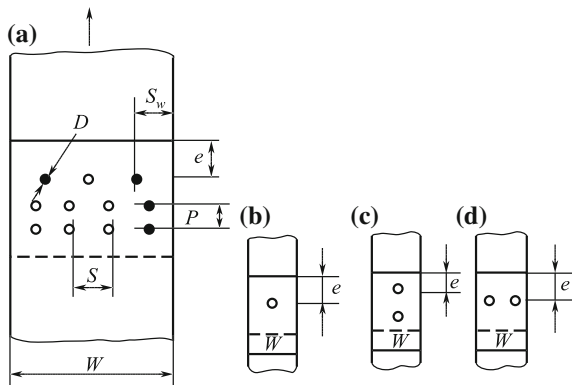
- (1) Principles for selecting fastener diameter: General guidance for selecting fastener diameters are as follows:

- ① Sufficient bearing strength of jointed component should be ensured.

Table 4.18 Select of geometric parameters of mechanical joints

S/D	p/D	S_w/D	e/D	D/t	H/mm
≥ 5	≥ 4	≥ 2.5	≥ 3	$1 \leq D/t \leq 2$	$H \leq 0.7t$

Fig. 4.81 Definition of geometric parameters of mechanical joints



The fastener diameter-to-thickness ratio should be properly considered to guarantee sufficient fastener strength. The rated shear strength of fasteners does not usually control the joint design. Bolt diameter is usually governed by the need to avoid exceeding the allowable bearing stress of the laminate.

- ② Fasteners should have sufficient stiffness to prevent any reduction of the laminate allowable bearing stress, owing to severe bending of the fastener.

Primary determination of fastener diameter is based on the occurrence of fastener shear failure and laminate bearing failure at same time, that is,

$$D/t = 4[\sigma_{br}]/\pi[\tau_b] \quad (4.69)$$

where

- D —fastener diameter, mm;
- t —laminate thickness, mm;
- σ_{br} —allowable laminate bearing strength, MPa;
- $[\tau_b]$ —allowable fastener shear strength, MPa.

(2) Selection principles for fastener type

- ① Bolts are used for structural joints transferring high load, which may require reassembly. Rivets are used for structures that are not intended to be disassembled. The laminate thickness range suitable for rivets is generally 1–3 mm;
- ② Carbon fiber laminates in direct contact with aluminum (without a coating), steel components with aluminum- or cadmium-plating should be avoided to prevent galvanic corrosion. If it is necessary to use such parts, insulating layers should be added. Measures to prevent galvanic corrosion may be adopted for carbon fiber laminates in contact with stainless steel. Titanium alloy and stainless steel fasteners are often installed wet with sealant;
- ③ Tension head fasteners are preferred for most applications. Shear head fasteners can lead to local hole bearing damage because of the size of their smaller heads, which can roll. Shear head fasteners may be used in special applications only where stress considerations allow;
- ④ In generic joints, it is recommend that the precision of the fastener-to-hole size is not lower than H9/h9. Precise ream holes are used for important joints. Interference fits should not currently be used because interference fit assembly technology has not yet been fully mastered.

(3) Requirements of bolt torque

Table 4.19 Bolt tightening torque /N·m

Screw diameter	Nut type		
	Thick type	Thin type	All types
	Countersunk head tension Hexagonal head	All types	Countersunk head share
M5	3–5	2.3–3.2	2.3–2.9
M6	5–8	2.9–4.9	3.1–3.9
M8	10–15	6.4– 10.8	10.2–11.3
M10	18–25	12.3–19.1	10.8–11.9
M12	25–30		

Proper tightening torque can increase bolt-joint strength. The torque moment should be selected based on the relational standard for various material, diameter, and the bolt type. If there are no special requirements, the tightened torque may be selected according to Table 4.19.

(7) Requirements of galvanic corrosion resistance for mechanical joints

The three conditions which lead to galvanic corrosion should be excluded in the design: potential differences between materials, presence of an electrolyte, and the electric connections. The following measures of corrosion prevention should be used:

- ① Material matching can prevent galvanic corrosion. Metals that have electrode potentials that match those of carbon/epoxy composites include: titanium alloy and stainless steel.
- ② Prevention of electrolyte accumulation should be considered in the design; sealing of joints should be performed to prevent infiltration of electrolyte and avoiding corrosion battery formation.
- ③ For materials unsuitable for direct contact, an insulating layer of glass/epoxy or aramid/epoxy should be used. At important joint sites which may be predisposed to corrosion, full sealing of the joints should be used to prevent corrosion.
- ④ Joints can be installed wet with sealant, in addition to insulation. In riveted joints, it is important to wet set with sealant, to prevent galvanic corrosion but also compensate for any manufacturing damage.
- ⑤ Fiber laminates in direct contact with aluminum and aluminum and cadmium plated steel components should be avoided to prevent galvanic corrosion. Otherwise, an insulating layer should be added. Carbon fiber

in direct contact with stainless steel should adopt some measures to prevent corrosion. Titanium may be used directly without any protection.

(8) **Gap filling requirements**

The gap between attached parts should not exceed 0.8 mm for non-structural shim. Large gaps cause excessive bolt bending, non-uniform load-bearing stress, and an eccentric load path. Any gap in excess of 0.13 mm should be shimmed to minimize interlaminar stress due to clamp-up.

Design of Riveted Joints

(1) **Design requirements for riveted joints**

Selection of geometric parameters of riveted joints should follow the parameters given in Table 4.18. Laminate design should follow the principle described in section “4.Design Basic of Mechanical Joints”.

(2) **Selection principles of rivets**

Principles for selecting rivets are as follows:

- (1) In addition to galvanic corrosion prevention and high strength, rivet materials should have good plasticity to satisfy the requirements of riveting assembly technologies. Titanium alloy, pure titanium and titanium–niobium alloy rivets are preferred to avoid galvanic corrosion. Aluminum and low-alloy-steel rivets are not suitable owing to the large difference between their electrode potential and that of the composites. A286 and Monel are less applicable because of their lower specific strength. Stainless steel fasteners in contact with carbon should be permanent and wet set with sealant.
- (2) Bimetallic and blind rivets should be preferred to avoid damage to the laminate.
- (3) The rivet diameter should generally not exceed 4 mm, to allow for easy formation and avoid damage to the laminates. Flush fastener and round head rivets should be used whenever possible where the structure requirements are satisfied.
- (4) To allow for disassembly and for non-stressed or secondary stressed inner components, a low number of aluminum rivets may be used from the view

point of reducing weight and cost. However, these must be wet set and strict measures taken to prevent galvanic corrosion prevention.

- (5) Avoid buck rivets in composite structures. Squeeze rivets can be used if washer is installed on the tail side.

(3) Measures to improve pull-out strength

For outer surface of structures, such as the rudder, a hole cap and countersink can be used to strengthen the structure with titanium alloy or stainless steel to improve the pull-out strength.

(4) Reliable measures for galvanic corrosion prevention

(5) Riveting processing requirements

- (1) Riveting should follow technology specifications. Strict quality control and inspection should be conducted during hole drilling, countersinking, and riveting. Nondestructive evaluation should be conducted for important parts;
- (2) Damage to the exit site of the drill should be prevented by coating the composite with a layer of film adhesive, glass-cloth, or a pad plate;
- (3) When composites come into direct contact with metallic components, under structure permissive conditions, snap the head of the rivet at the metallic surface whenever possible. If the snapped head of the rivet is on a composite surface, a pure titanium, titanium alloy, or stainless steel washers must be placed on the snap head;
- (4) Whenever possible, squeeze rivets should be used for parts requiring common solid rivets. Bull rivets may be considered where squeeze riveting cannot be conducted. Strong power rivets should be avoided.

Fatigue of Mechanical Joints

Mechanically fastened joints are the main joint type used in primary composite structures. To meet structural integrality requirements, in addition to meeting strength and stiffness requirements, fatigue, damage tolerance, and functional requirements must also be satisfied. Stress concentration in mechanical joints can create fatigue weak points in the primary composite structure. Fatigue strength is determined mainly by testing now, because methods for pre-estimating the life time of composite joints are not mature, and are complicated by environmental conditions.

Three fatigue failure criteria should be considered in the rational design of mechanical joints under wet-heat conditions and different load spectrums.

Tension, shear-out, and bearing failure of fasteners loaded hole; permanent elongation deformation of fastener holes exceeding allowables; residual strength of joints is lower than the design requirements. The joint life will fail when any one of aforementioned items occurs. Generally, permanent elongate deformation of loading holes is the first limiting value.

Limiting values of permanent elongation of fastener holes depend on the subsequent damage to structure integrity. Control of the deformation value is based on the critical degree of deformation of the specific joint structure. Permanent deformation of a loading hole should not exceed 5% of the hole diameter.

Experimental investigations have shown that symmetric mechanical joints are insensitive to tension–tension and compression–compression fatigue if $K < 0.67$ in both flight and gust spectrum action. In high-speed aircraft, the hygrothermal conditions spectrum, tension–compression fatigue with high K values, and unsymmetrical joint design should be considered in fatigue problems. Residual strength should not be lower than the inherent static strength. Fatigue is insensitive to processing defects, delamination, and damage growth resistance. For matrix-dominated laminates in a high loading cycle range and fiber-dominated laminates, signs of macrodamage are not obvious before rapid failure; thus, it is difficult to inspect damage in advance and prevent failure.

4.8.3.2 Design of Main Load Carrying Joints

Characteristics of Multirow Fastener Joint Design

One major difference in the mechanical behavior of composite materials and metals is that composites are brittle and anisotropic; while metals are plastic. Metal has the capability to redistribute load, thus allowing each of the fastener holes of a multirow joint to uniformly carry the load distribution. However, for brittle composite materials this is not the case [26–31].

Composite (fiber-dominated) laminates generally show linear behavior up until failure. The material will not yield locally and redistribute stress. Effective joint design should adopt measures to reduce the bolt bearing stress in the most critically loaded locations. Even if at ultimate load non-uniformity of the fastener load distribution shows little improvement in comparison with the initial load for steel or titanium fasteners. Effective joint design requires that the greatest load-bearing fastener row should be reduced.

The strength of multirow bolted joints in composite structures is governed by associated bearing–bypass load interactions under tensile or compressive loads. The key to obtaining high operating strain in bolted joints in fibrous composite laminates is to restrict the bolt bearing stress in the most critically loaded locations. By tailoring the joint geometry, a bolt load distribution can be generated which maintains low bearing high bypass conditions in the first or outermost row of fasteners. With efficient joint design, cross-section strain in basic skin laminates can reach 0.005 in room-temperature tests.

The laminate fiber pattern is a design variable and optimizing the joint for maximum strain does not guarantee the highest strength or the most weight-efficient design. The principle design parameter governing the design of composite joints is the amount of load that must be transferred rather than the operating strain level of the adjacent structure.

General Principles of Joint Area Design

Design principles for multirow fastener joints include:

- (1) The joint area should be designed first and the basic structure filled later. Optimization of the laminate fiber pattern should be performed considering the amount of load that must be transferred rather than the operating strain level of adjacent structures.
- (2) The load distribution of multirow joints mainly depends on the relative stiffness of jointed members. To obtain even load sharing, joined components need to have similar stiffness. Fastener stiffness also has a slight effect.
- (3) The geometry of joints should be optimized to improve the load-bearing capacity of multirow joints. The bearing stress of load holes can be reduced through the use of variable fastener diameters and thickness. Skins of uniform thickness in combination with tapered splice plates should be used for joints. The use of tapered splice plates can optimize fastener load distribution and reduce the bearing of the most severely affected fastener row. Both analysis and test results have shown these joint geometries are more efficient than other joint geometries. Notably composite tapered splice plates that have tapered washers should be used on spot faces milled at locations that may not be able to accommodate fasteners and nuts, because machining may induce small cracks on the surface.
- (4) Total thickness of the top and bottom splice should be slightly greater than that of the center cover even for the same material and fiber pattern. The reason for this requirement is that stress in the splice plate should be lower than that in the skin to prevent splice delamination. Otherwise, failure will occur at the splice plates. This is because, regardless of whether the applied loads are tensile or compressive, there is also a strong influence from the presence or absence of the through-thickness clamp-up. External splice plates have a relatively small amount of clamp-up provided by fastener bolts and nuts compared with the clamp-up of the center plate sandwiched between two splice members. Therefore, the bearing strength of the center cover is larger than that of the external splice plates.
- (5) Avoid skin reinforcement: As a basic philosophy, skin reinforcements should be avoided wherever possible from the perspective of both cost and basic skin reparability. A skin pad-up is a bolted splice area where the joint operates to its maximum efficiency implying that repairs to bolted joints or bolted repairs will occur in other regions. The pad-up cannot restore the ultimate strength of structure. Thus, pad-ups are allowed if warranted by other design considerations, but the joint itself must not be loaded to the point that the surrounding maximum load on the structure would be unreparable.
- (6) Joint strength is sensitive to the joint geometry as well as the type of fiber and resin used. However, joint strength is insensitive to minor changes in the

fiber pattern for optimal layer compositions. For carbon–epoxy laminates, the optimum w/d is likely to be in the range 4–5 for multirow joints.

- (7) Adequate consideration of the bolt diameter-to-laminate thickness ratio (or more appropriately, bolt bending stiffness-to-laminate thickness ratio) is warranted in joint design to assure that fasteners are the weak link. Fastener bending elastic deformation may decrease the clamp force and allowable bearing stress and should thus be avoided. Therefore, selection of fastener sizes should not be based only on the rated shear strength of the fasteners but should also consider the fastener stiffness.
- (8) Interference fit systems with a sleeve of fasteners having the same outer diameter as the sleeve, generally do not feature increased strength (strength may actually decrease slightly). This is because any potential benefits are negated by recurrent bolt bending failures.
- (9) Materials should be selected to take advantage of their strengths while avoiding their weakness. Metals should be used in parts for which composite materials are unsuitable.

Metal materials are selected for splice plate members for several reasons.

If protruding head fasteners are used in the subcomponent tension joints of tapered composite splice plates, tapered members require either spot-facing of the splice plate surface or the use of tapered washers under the fastener heads and nuts. These features may cause premature failure owing to the high peel stress and interlaminar forces. The use of tapered washers also increases the cost and complexity of the assembly procedure. Thus, metallic splice plates with spot-facing on tapered surfaces are used to accommodate the fastener seating. The use of metallic splice plates is the simplest and most cost-effective way of avoiding these potential failure modes.

Composite materials are not well-suited to applications where high out of plane forces are present. The T-splice members are likely to encounter such forces, and the magnitude of the forces is very difficult to predict analytically or measure experimentally. The fabrication of the corner fittings based on composite materials would be impractical for similar reasons and cost-prohibitive compared with the use of aluminum parts.

The splice plates may be slightly heavier, owing to the use of metals; however, any small extra weight in the splices (or fasteners) is compensated by maximizing the efficiency of the large heavy skins. For a large airplane, the weight of the splicing elements as a percentage of the total wing weight is small, and splice efficiencies should be evaluated solely on the basis of the minimum splice and fastener weight.

- (10) Joint strength is typically greater under compression than under tension loading. An example of the application of these principles is presented in Fig. 4.82. An optimum splice structure is represented, including a cover of uniform thickness, tapered splice plates and varying diameter fasteners. The bolt diameter of the inner most row near the cover butt is largest, $S/D = 3$. There are no bypass loads on the skin. The combination of maximum bearing

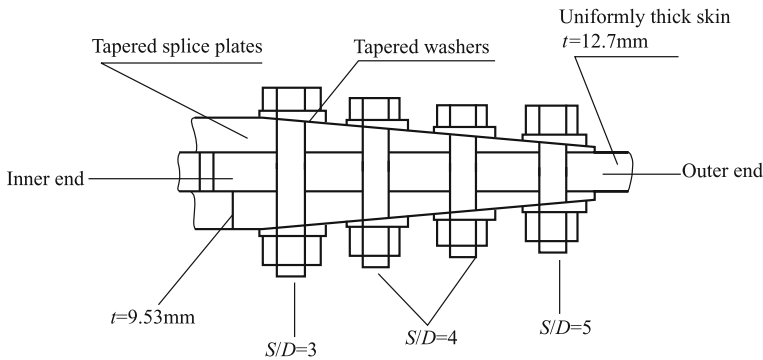


Fig. 4.82 Optimum proportions for multirow bolted composite joints

and bypass loads act on the splice plate of the innermost skin such that the splice plate thickness must be properly increased. Research results indicated that the optimum splice plate thickness is 1.5 times the basic plate thickness. In the example, the basic plate thickness is 12.7 mm, and the total plate thickness of the taped splice is 19.1 mm, including the thickness of both the top and down taped splice (9.5 mm each). The diameter of the middle two row bolts has an intermediate S/D value of 4. The diameter of the outermost row of bolts is smallest with $S/D = 5$. A low thickness of the splice plate outer end may result in shear failure of laminates under a large load, which should be avoided.

4.8.3.3 Static Analysis of Mechanical Joints

Static analyses of mechanical joints generally include the following three aspects [2, 17, 25–31]:

- (1) Exterior forces acting on the mechanical joint are determined from overall structural analysis of the whole joint.
- (2) These forces are then used to determine individual fastener loads and bypass forces acting at each fastener hole of the joint.
- (3) Joint strength can be assessed by applying two methods: one is the semiempirical failure envelope method; another is to use material failure criteria and characteristic curves.

Finite Element Analysis of Fastener Load Distribution in Mechanical Joints

Methods of determining the fastener load distribution of mechanical joints can be separated into three classes: classical stiffness methods, elastic mechanics, and FEMs. This section considers the application of FEMs, which also have broader applicability to analysis of other components. FEMs are suitable for both regular multi-row fastener arrangements and complex shaped joints. More information on the other two methods can be found in Ref. [1].

There are two major differences that should be considered when dealing with composite materials: First, composite laminate stiffness is dependent on the direction of the applied force; second, most composite materials tend to exhibit nearly linear stress–strain behavior up until failure and have little load redistribution capability.

The MSC/NASTRAN program has become widely applied in aeronautic design. Therefore, we introduce issues affecting calculations of fastener load sharing with MSC/NASTRAN.

(1) Element modes

One important point to consider for solving fastener load distribution is that fasteners are regarded as fastener elements. Two end points of the fastener elements are placed at finite element net nodes of the joining members.

- (1) Fastener modes: Fasteners can be modeled with shear fastener type elements (CELAS2 spring element) and beam elements (BAR element). However, beam elements are used more frequently because bending effects can be considered. Beam elements are suitable for both single and double shear joints, but spring elements are only suitable for double shear joints.
- (2) Joined plate modes: Joined plates are modeled with QUAD4 elements, which have membrane and bending type elements. Bending plate elements are used generally when the fasteners are modeled with beam elements. The use of bending plate elements has no meaning if the fasteners are modeled as spring elements. For commonly used geometric sizes of multi-fastener joints, it is suggested that the node numbers placed along the plate width are no less than five, and those placed between fasteners are no less than one.

(2) Fastener flexibility

The distribution of internal loads within a complex redundant mechanical joint depends upon the plate members and the fasteners connecting them. Each fastener's contribution to joint flexibility is dependent upon fastener stiffness, joint member stiffness, and load eccentricity.

- (1) Linear analysis: In normal practice, the fastener load/deflection behavior is assumed to be linear throughout the loading range. Friction and clearance between the fastener and hole effects are usually ignored. For preliminary

design purposes, the following relation of bolt flexibility can be used, which is simple and satisfies engineering precision requirements.

$$\alpha = L/K_s = L/A_s G \tag{4.70}$$

where

- K_s —shear stiffness of the fastener;
- A_s —shear area of the fastener;
- G —shear modulus of the fastener;
- L —effective length of the fastener.

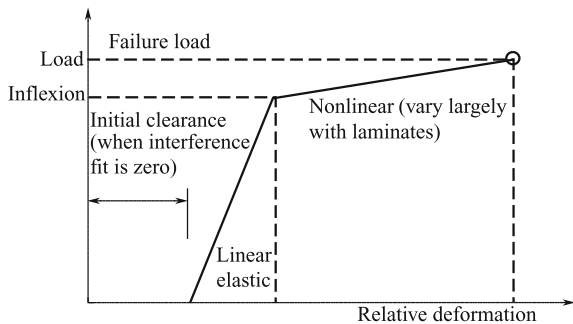
For single shear, the effective length l can be assumed to be one-fourth the combined thicknesses of the attached sheets. The effective length in double shear can be approximated as half the single shear value. Equation 4.8.2 is used for fasteners where only shear is accounted for; fastener bending and rigid body rotation (in a single-lap joint) are not considered. The fastener load distribution derived from these relations will be slight conservative.

- (2) Nonlinear analysis: Load-deflection ($P-\delta$) curves from single fastener joint tests can be modeled as bilinear curves, as shown in Fig. 4.83. The nonlinear strength analysis should permit some bolts to fail while the structure should still be able to carry loads. Nonlinear analysis can provide more exact load-sharing analysis and ultimate strength predictions.

Detailed Stress Analysis Methods

Stress analysis methods of single fastener joints are described in detail in Ref. [1].

Fig. 4.83 Bilinear load-deflection ($P-\delta$) curves



After the load distribution is determined (i.e., the bearing and bypass loads of fastener holes) analytical methods for single fastener joints can be used to calculate the detailed stress and strain near the fastener hole. Finally, joint strength and failure modes can be assessed by applying material failure criteria or characteristic curves.

Theoretical analytical methods of single fastener joints mainly depend on analytical and FEMs. In finite element analysis a fine mesh must be used in regions of high stress gradients, such as around the cutouts and at ply and stiffener drop-offs. Joint analysis should include the effects of shimming to the limits permitted by drawings. The effects of shimming may reduce joint strength. The effects of permissible manufacturing parameters should be considered, for example, hole perpendicularity ($\pm 10^\circ$), shimming, and loose holes.

Semiempirical Methods

Analyses of mechanical joints in composite structures typically follow the procedures: First, load-sharing analysis is performed; second, detailed analyses are conducted for individual severely loaded holes to determine the stress distribution; finally, failure hypothesis and material failure criteria are used to assess whether a joint will fail or not.

The disadvantages of detailed analysis include the requirements of manpower and material resources and the use of failure criteria. Currently, no single material failure criteria are uniformly endorsed, and moreover, some failure criteria have an empirical nature. Generally, analysis of fastener load distribution is more exact and errors of estimates of the strength derive mainly from the failure criteria. A failure envelope is used by the test judge to determine whether failure will occur, and complicated detailed analysis and disputed failure criteria may be avoided.

Having determined the bearing and bypass load of individual fastener holes by finite element or other methods, joint strengths are pre-estimated by empirical methods. Thus, a failure envelope is determined from test specimens and used to judge the likelihood of joint failure.

(1) Tensile load conditions

Under the combined action of bearing and bypass loads, assume that the joint tensile failure will occur when Eq. (4.71) is satisfied:

$$K_{bc}\sigma_{br} + K_{tc}\sigma_{net} = \sigma_b, \quad (4.71)$$

where

- σ_b —unnotched laminate tensile strength;
- σ_{br} —loaded hole bearing stress;
- σ_{net} —laminate net-tension stress caused by bypass loads;
- K_{bc} —composite bearing stress concentration factor, with respect to bearing stress;

K_{tc} —composite stress concentration factor, with respect to net-section tension stress;

$$K_{tc} = 1 + C(K_{te} - 1) \tag{4.72}$$

$$K_{te} = 2 + (1 - D/W)^3 \tag{4.73}$$

$$K_{bc} = \left\{ 1 + C \left[1 + (W/D - 1) - 1.5 \times \frac{W/D - 1}{W/D + 1} \times \theta \right] \right\} / (W/D - 1) \tag{4.74}$$

K_{te} —elastic isotropic stress concentration factor, with respect to net-section tension stress;

W —width;

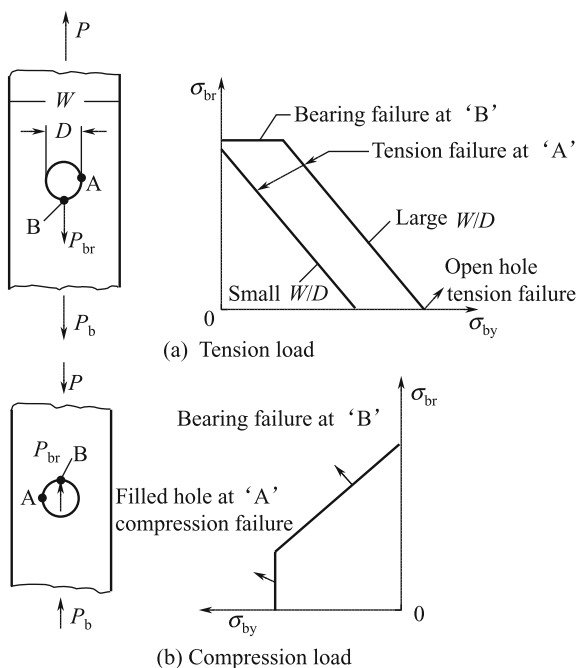
D —hole diameter;

θ —may be considered as 1.0;

C —stress concentration correlation coefficient, as seen in Fig. 4.85.

The left side of Eq. (4.71) can be regarded as the sum of contributions from the combination of bearing and bypass loads to tensile stress. Failure will occur when it exceeds the laminate tensile strength.

Fig. 4.84 Failure envelope



Otherwise, joint-bearing failure will occur when the bearing stress achieves the bearing strength:

$$\sigma_{br} = \sigma_{bru} \tag{4.75}$$

where σ_{bru} —is bearing strength.

A typical failure envelope is shown in Fig. 4.84a. The inclined line AB represents the tensile failure satisfying Eq. (4.71). The flat line BC represents the bearing failure satisfying Eq. (4.75).

(2) Compressive load conditions

Under the combined action of bearing and bypass loads, assume that the joint-bearing failure will occurred when Eq. (4.76) is satisfied:

$$\sigma_{br} + \sigma_{net} = \sigma_{bru} \tag{4.76}$$

Compressive failure will occur when Eq. (4.77) is satisfied:

$$K_{tc}\sigma_{net} = \sigma_c, \tag{4.77}$$

where σ_c —unnotched laminate compressive strength.

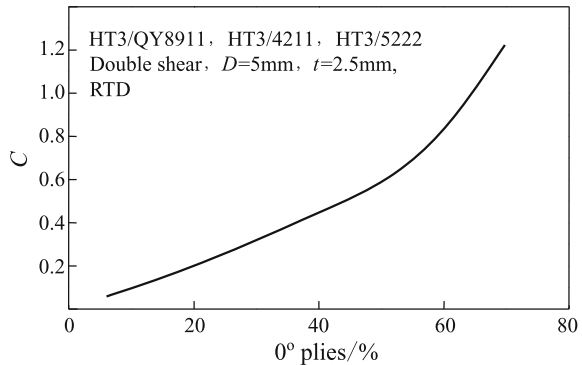
In the absence of a filled hole K_{tc} value, the mean open hole K_{tc} value of 1 can be used.

This failure envelope is shown in Fig. 4.84b, where the inclined line represents the bearing failure satisfying Eq. (4.76). The vertical line represents compressive failure satisfying Eq. (4.77).

(3) Stress concentration correlation coefficient C

The stress concentration correlation coefficient considers the effects of anisotropy, non-homogeneity, nonlinearity, and damage to the composite material. Test results of composite specimens are used to measure C.

Fig. 4.85 C curves as a function of ply proportions



The stress concentration correlation coefficient C is key to applying empirical methods. Because stress concentration factors of open holes and loaded holes for isotropic materials are known. If the C value is determined, stress concentration factors for composites can be determined by linear relations. Thus, joint strengths can be simply estimated.

Figure 4.85 shows C curves as a function of ply proportions. The curves are based on test results of HT3/QY8911, HT3/5222, and HT3/4211.

In general, C takes values between 0 and 1.0. If the proportion of 0° -plies of laminate is too high and that of $\pm 45^\circ$ -plies is too low, C may be greater than 1, and loses its meaning as a stress concentration correlation coefficient. Nevertheless, the same, single fastener joint strength can be pre-estimated from the C value.

In the absence of test data, within the recommended range of layering conditions in joint areas, C may be considered to be:

$$C = (\%0^\circ \text{ plies})/100$$

(4) Failure envelopes

Failure envelopes provide failure criteria for multirow joint analysis. The failure envelope is the foundation for estimating joint strength by empirical approaches. Failure envelopes can be determined for single fastener and unloaded hole specimens by the following methods:

- (1) The bypass stress point at the abscissa can be determined from the tensile and compressive strength of unloaded hole (fill-hole) specimens.
- (2) The cutoff can be determined from the bearing strength of a wide plate ($W/D = 6-8$).
- (3) The inclined line represents the tensile failure, which may be determined from the stress concentration correlation coefficient C and joint geometry.

4.8.3.4 Checking Mechanical Joint Strength

Allowable Bearing Stress of Full Carbon Fiber Composites

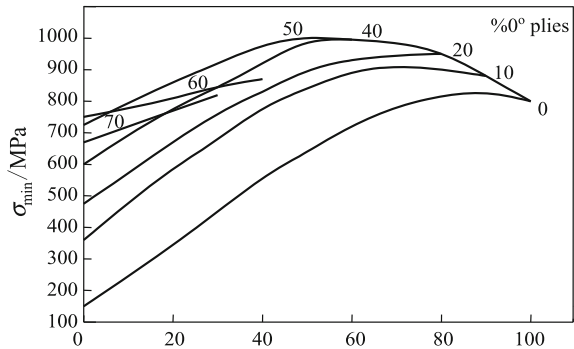
The information presented here is not only applicable to single fastener joints, but also useful for determination of multirow joint strength. All joint strength data are developed from tensile test results, and the results will be conservative for use in compression loads [2, 17].

- (1) **Allowable bearing stress**

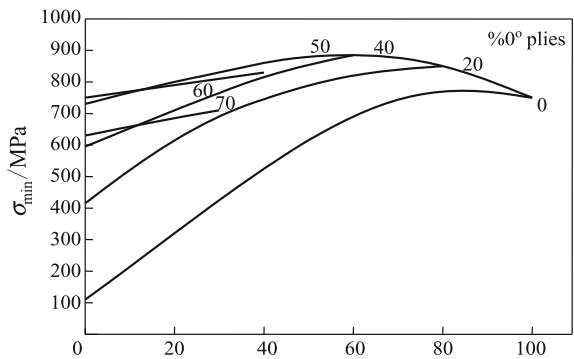
To ensure structure integrity the loading should generally not be greater than the initial bearing failure stress. Therefore, selection of an allowable bearing stress strongly depends on the failure criteria. The initial bearing stress is very different to the definition of failure. Failure criteria can be classified in different ways: One approach is to base failure on stress, which guarantees that structures have sufficient strength; another is based on deflection of the loaded hole, which guarantees that structure have sufficient stiffness. One frequently used approach is based on the degree of hole deformation. However, the failure deflection limits of loaded holes selected by various countries and departments are very different, ranging from 0.5 to 6%.

The following are recommended criteria for determining the initial bearing failure stress of a loaded hole: the lowest value between the first slope inflexion point and bearing deformation of 4% in the load deformation curve. Experience indicates that the minimum initial bearing failure stress can be considered to be half of the ultimate bearing strength σ_{bru} .

Fig. 4.86 Bearing strengths of three composite systems



(a) HT3/QY8911 and HT3/5222 $\% \pm 45^\circ$ plies



(b) HT3/4211 $\% \pm 45^\circ$ plies

The ratio of the initial bearing failure stress to the ultimate bearing strength depends on the material system and laminate pattern. Generally, the ratio decreases as the proportion of $\pm 45^\circ$ plies is increased. For laminate frequently used in joint areas, the ratio is in the range 0.55–0.66. Selection of allowable bearing stress should also consider joint importance, structural characteristics, load type, durability and service life and environmental effects.

Allowable bearing stress can be determined from the following:

$$[\sigma_{br}] = C_w C_e C_p C_d C_s C_{en} K \sigma_{bru} \quad (4.78)$$

where

- C_w correlation factor for width;
- C_e correlation factor for end distance;
- C_p correlation factor for load direction;
- C_d correlation factor for hole diameter;
- C_s correlation factor for single shear;
- C_{en} correlation factor for environment;
- K factor considering initial failure, durability, aging, and technological quality. The value of K is typically in the range 0.50–0.66;
- σ_{bru} bearing strength, MPa.

The bearing strengths of several composite laminates are illustrated in Fig. 4.86. Various correlation factors are shown in Fig. 4.86 for $W/D \geq 6$, $e/D \geq 4$, $D/t = 1.0$ – 2.0 , $D = 5$ mm, double shear, torque 4 N·m, at room temperature, in dry conditions.

For laminates typically used in joint areas (i.e., 0° -plies = 25–50%, $\pm 45^\circ$ -plies $\geq 40\%$, 90° -plies = 10–25%), the allowable bearing stress for HT3/QY891 and HT3/4211 can be taken as 600 and 500 MPa, respectively.

Hence, the formula (4.78) is a concise, convenience, and effective model. The effects of many parameters have been considered in various correlation factors, and therefore, numerous procedures can be avoided. Traditionally, both the bearing strength and tension strength as well as shear strength would require checking. This method has been successfully used in joint design for many aircraft structures.

(2) Bearing strength

To fully develop the bearing capability, joint geometry selection requires that bearing failure or combined failure modes depending on bearing failure are considered. Full load-bearing failure strengths are the foundation of joint design. Failure modes are dependent not only on geometric parameters but also the fiber pattern. Full bearing failures typically occur when $W/D = 6$ and $e/D = 4$ in the laminate pattern range of joint areas. The bearing strengths given in this paragraph are equal to the ultimate load divided by the bearing area Dt .

The bearing strengths of laminates of HT3/QY8911 and HT3/5222 composites are shown in Fig. 4.86a. The laminate bearing strengths of HT3/4211 composite are given in Fig. 4.86b. The test parameters are as follows: double shear, hole diameter 5 mm, $W/D \geq 6$, $e/D \geq 4$, $D/t = 2$, load direction was consistent with the 0° fiber orientation. The fixture was made of steel with a stiffness approximately 8 times as high as that of the specimen. Loading bolts were made of 30CrMnSiA steel. The fit precision of the bolt in the hole was H8/h8, and the bolt tightened torque was 4 N·m. The interior and exterior diameters of the washers were 5.5 and 10 mm, respectively. The environmental conditions were room temperature and a dry atmosphere.

The double shear method is a basic procedure and preferable to single shear joint tests. For double shear joints, the test specimen size is smaller and test fixture is simpler. These features not only can save costs and time, but also give a smaller data dispersion. Moreover, actual aircraft single shear joints with supported structures differ considerably from tests of single shear joints. Therefore, test results of single shear joints may be considered conservative.

(3) Correlation factors of bearing strength

When the actual applied parameters are different from those in Fig. 4.86, it is necessary to correct the bearing strength in Fig. 4.86. The bearing strength correlation factors are mainly based on HT3/QY8911, HT3/5222, and HT3/4211 laminate test results. Laminate codes names used in this paragraph are described in Table 4.20.

- (1) Width correlation factors C_w : The width correlation factors C_w are shown in Fig. 4.87a for several representative laminates.
- (2) Edge distance correlation factor C_e is shown in Fig. 4.87b for several representative laminates.
- (3) Load orientation correlation factors C_p are shown in Fig. 4.87c. Generally, the more 0° plies, the greater the load orientation effect, i.e., more $\pm 45^\circ$ -plies will give a smaller load orientation effect.
- (4) The hole diameter correlation factor C_d : When geometric sizes (W/D , e/D , and D/t) of mechanical joints are all the same, a larger hole diameter will lower strength. Hole diameter correlation factors C_d are shown in Fig. 4.87d.
- (5) Single shear correlation factor C_s : The single shear correlation factor C_s is given in Fig. 4.87e. Note that for single shear joints in actual aircraft

Table 4.20 Laminate codes

Laminate codes	Percentage ($0^\circ/\pm 45^\circ/90^\circ$)	Stacking sequence
2	70/20/10	[45/0/0/-45/0/0/0/90/0/0] _S
4	50/40/10	[45/0/-45/0/90/0/45/0/-45/0] _S
6	30/60/10	[45/0/-45/0/45/90/-45/0/45/-45] _S
8	0/100/0	[±45] _{SS}
9	50/0/50	[0/90] _{SS}
10	25/50/25	[45/0/-45/90] _{2S}

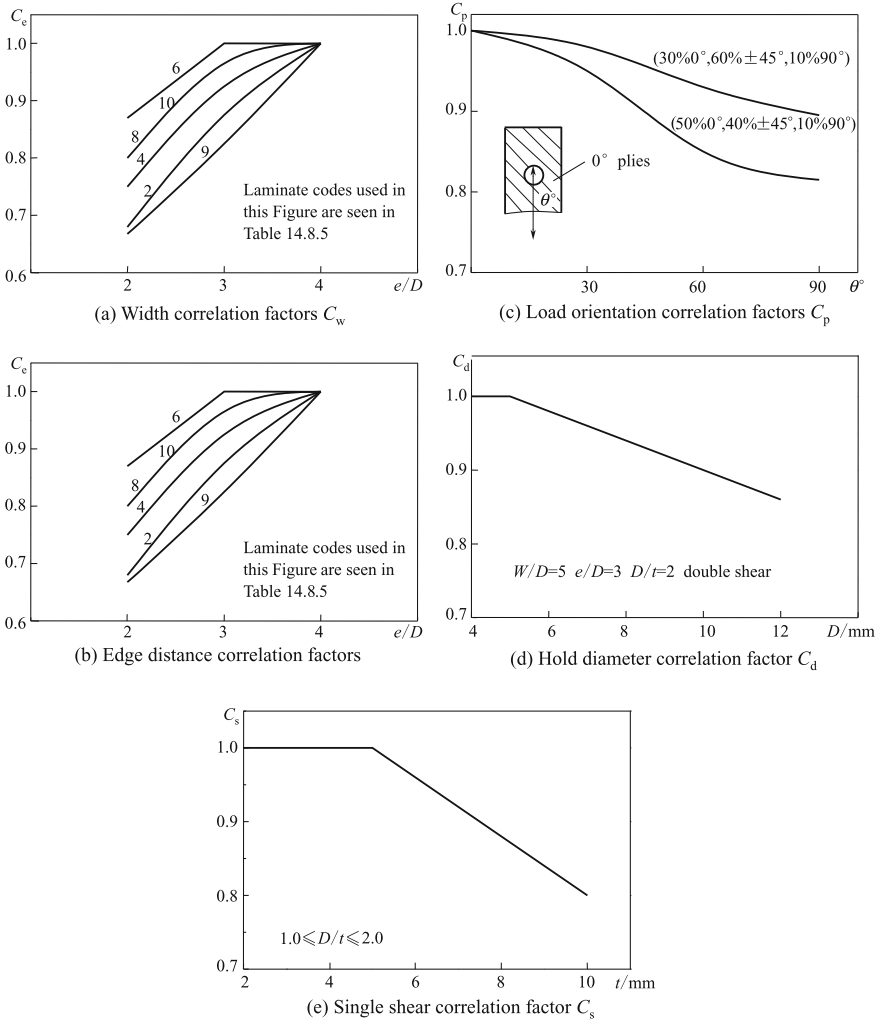


Fig. 4.87 Correlation factors of bearing strength

Table 4.21 Environmental correlation factor C_{en}

Materials	Environmental condition	C_{en}	Materials	Environmental condition	C_{en}
T300/QY8911	100° moisture content 1%	0.75	T300/4211	82° moisture content 1%	0.83
	130° moisture content 1%	0.67		100° moisture content 1%	0.75

structures, owing to support by surrounding components, practical bending effects will far less than those in test cases. Consequently, C_s is used to reflect an actual aircraft structure.

- (6) Environmental correlation factor C_{en} : Environment has strong effects on bearing strength of laminates. In the laminate pattern range recommended for joint areas, the environmental correlation factors C_{en} of T300/QY8911 and T300/4211 laminates are given in Table 4.21.

Strength Checking of Single Fastener Joints

- (1) Strength checking of joined plates: Bearing strength checking is performed as follows:

$$\sigma_{br} = P_{br}/Dt_e \leq [\sigma_{br}] \tag{4.79}$$

where

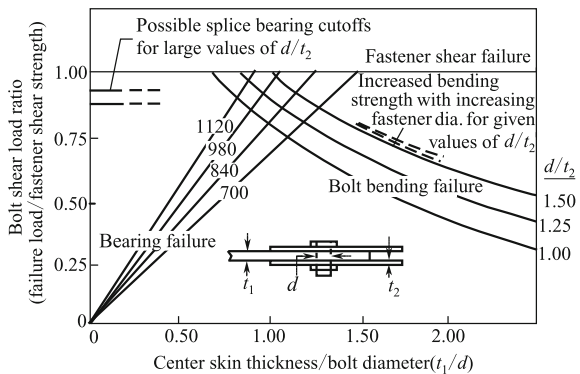
- P_{br} —fastener load, N;
- D —hole diameter, mm;
- t_e —plate effective thickness, defined as:
 $t_e = t$, when $t \leq D$,
 $t_e = D$, when $t > D$;
- $[\sigma_{br}]$ —allowable bearing value, MPa.

Note that tension and shear strength will be satisfied automatically without checking because the effects of width and edge distance have been considered in the allowable bearing strength value.

- (2) Checking of fastener strength: The shear strengths of single fastener joints can be checked as follows:

$$\tau = 4P_{br}/Dt_e \leq [\tau] \tag{4.80}$$

Fig. 4.88 Approximate single-row allowables



where $[\tau]$ —allowable shear strength of fastener.

- (3) Bolt bending failure curves: Design guidelines for the selection of fastener were sizes traditionally based on the fastener shear strength and limitations of the allowable d/t ratio. However, such a broad criterion can sometimes be either unconservative or overly conservative, depending on the relative dimensions of the members to be joined or the splicing material through which the load is transferred. The chart shown in Fig. 4.88 was developed to provide a more comprehensive method for selecting fastener sizes, with consideration given to the bearing strengths of the materials to be joined, the fastener shear strength, and the potential for bolt bending failures. The bolt bending failure curves were derived from limited test results and assume that the bending failure is a function of the d/t ratio for both the skin and splice members.

Figure 4.88 was developed for double shear and is nondimensionalized, except for the center skin bearing stress allowables, which are plotted in units of ksi. The chart shows that when the value of d/t_2 (t_2 is the thickness of one splice plate) is low, and the value of d/t_1 (for the central skin) is about 1.0, the bearing stress allowables of composite joints reach maximum. The bending failure curves show that at low d/t ratios for both the skin and splice plates, bending failure can occur at low percentages of the joint member bearing strength and fastener shear strength. As the d/t_2 ratio increases, the propensity for bolt bending failure decreases owing to the lower eccentricity, and fastener shear strength becomes the limiting factor. Eventually, as the d/t_2 ratio becomes large, the splice plate bearing strength approaches the strength cutoff, as indicated by the dashed lines in the upper left of Fig. 4.88. It should be noted that the bolt bending curves on this chart are approximate, and will likely require modification as more test data are obtained. All potential failure modes can be included on this chart except for net-section failure, which must be calculated separately.

Strength Checking of Multirow Fastener Joints

(1) Tensile load

- (1) Bearing strength checking: With knowledge of fastener loads, bearing strength checking is the same as that of single fastener joints according to formula (4.78). For joints of uniform plate thickness and equal fastener diameter, only the fastener holes of maximum load-carrying capability need to be checked.

- (2) Tensile strength checking: For strength checking, the tensile loading of a multirow joint, σ_b , of the right side of Eq. (4.71) can be replaced by the allowable tension stress of the laminate, i.e.,

$$K_{bc}\sigma_{br} + K_{tc}\sigma_{net} = [\sigma] \quad (4.81)$$

where

- $[\sigma]$ —allowable tension stress of laminate, MPa, $[\sigma] = E_{xt}[\varepsilon]$;
 E_{xt} —longitudinal tensile elasticity modulus of laminate, MPa;
 $[\varepsilon]$ —allowable tensile strain of laminate.

Design allowable strains can be classified on A-basis and B-basis. The use of either basis depends on the structure design criteria of the practical engineering project. Generally, for components without a structure test or single path transfer component, A-basis is used; B-basis is used for multi-path transfer or fail-safe components. For carbon fiber resin matrices composites, allowable tension strains are $[\varepsilon_A] = 0.0082$ for A-basis and $[\varepsilon_B] = 0.0090$ for B-basis. Shear failure will not occur within the ply range recommend for joint areas when the pitch is not less than 4D and the edge distance is not less than 3D.

(2) **Compressive load**

For strength checking of multirow joints under a compressive load, σ_{bru} on the right side of Eq. (4.71) may be replaced by the allowable bearing stress of the laminate, $[\sigma_{br}]$, i.e.,

$$\sigma_{br} + \sigma_{net} = [\sigma_{br}] \quad (4.82)$$

4.9 Damage Tolerance and Durability

4.9.1 Overview

4.9.1.1 General Concepts

Inspection plans should be combined with knowledge of damage threats, including damage growth rates and residual strength. This concept is referred to as damage tolerance. Specifically, damage tolerance is the ability of a structure to sustain design loads in the presence of damage caused by fatigue, corrosion, environmental effects, accidental events, and other sources until such damage is detected, through inspections or malfunctions, and then repaired. Thus, safety is the primary goal of damage tolerance.

Durability considerations are typically combined with damage tolerance to meet economic and functionality objectives. Specifically, durability is the ability of a structural application to retain adequate strength and stiffness to resist fatigue cracking, corrosion, thermal deterioration, peeling, delamination, wear-off, and external impact damage over the designed operation life time. Structures should have a certain durability under expected loads and environmental conditions to avoid high costs caused by frequent maintenance, repair, and replacement of parts over the designed operation life time. Thus, economics is the primary motivating factor for durability.

4.9.1.2 Composite Damage Tolerance and Durability

All structural applications should be designed to be damage tolerant and durable. In the use of composite materials, typical design objectives involve meeting or exceeding the design service and reliability objectives for the same structure made of other materials. Generally, the good fatigue and corrosion resistance of composites can help to achieve these objectives. However, the unique characteristics of composite materials also present some challenges for developing safe and durable structures.

The new problems of composites relate to their impact resistance, and residual load-bearing ability after an external impact and before damage is inspected. Damage resistance has become an important topic in composite research in recent years. Although composites offer excellent anti-fatigue and corrosion resistance, they are very sensitive to impact. In particular, thin skin structures or thin skin surface panel sandwich structures are susceptible to small external impacts encountered in manufacture or operation, which can necessitate considerable maintenance and repair. Studies on damage resistance of composites typically focus on two aspects: characterization of the impact resistance of composite systems, and the durability design requirements of composite structures. The feature of composite damage tolerance is that barely visible impact damage (BVID) can decrease compression strength by up to 40%, and the regular inspection and maintenance of composite structures cannot use special NDT equipment. Only visible inspection of dent depth is specified as standard in design. Similarly, studies on composite damage tolerance involve two aspects: characterization of damage resistance of the

composite system and the damage tolerance design requirements of composite structures. The damage resistance and damage tolerance design requirements of composite structures are discussed in Sect. 4.9.2.

The optimum balance of damage resistance and damage tolerance for specific composite applications involves a number of technical and economic issues early in the design process. Damage resistance often competes with damage tolerance during the design process, both at the material and structural level. In addition, materials and fabrication costs, as well as operational costs associated with inspection, repair, and structural weight, are strongly influenced by the selected material and structural configuration. For example, toughened resin material systems typically show improved damage resistance compared with untoughened systems, which results in reduced maintenance costs associated with damage from low-severity impact events. However, these cost savings compete with the higher material costs per unit weight of the toughened systems. In addition, these materials can also result in lower tensile capabilities of the structures with large damage or notches, which might require the additional material to satisfy structural capability requirements at the limiting load. This extra material and increased weight will result in higher material and fuel costs, respectively.

4.9.2 Evaluation of the Effects of Defects/Damage on Strength

Damage can be divided into two types according to its source: manufacturing defects, which cover structural abnormalities caused by production, and operational damage, which covers structural abnormalities caused in service [1, 2].

4.9.2.1 Manufacturing Defects

Manufacturing defects can usually be divided into two categories: First, lamination and part curing processes may create defects such as voids, delamination, debonding, inclusions, resin-rich or resin-poor areas, improperly cured resin, deviation of fiber orientation (fiber bending), layering sequence errors, and gaps between fibers. Second, defects may be produced in machining, packing and delivery such as scratches, abrasion, improper hole drilling, and torque and impact damage.

4.9.2.2 Operational Damage

Operational damage mainly concerns impact damage occurring in service. Impacts can be classified by the type of external impact energies. The impact caused by

external bodies such as bullets, non-inclusive engine fragments and bird-strikes are classed as high-energy impacts. These events are also known as high-speed impacts and can produce penetrating damage with a certain amount of delamination. Lightning can also break through the structure of the skin and produce deep delamination and burning. This type of damage is visibly inspectable and can be detected, allowing the part to be replaced or repaired. During production and maintenance, low-energy impacts include events such as: tool dropping; impact with maintenance facilities such as forklifts, trucks, and work platforms; damage by personnel standing on structures; impacts caused by stones, screws, and tire fragments during taking off or landing; impact of hail stones.

In fact, impact damage modes depend not only on external impact energy, but also the laminate thickness. For thin skins or thin surface panels, impact damage mainly results in fiber fracture, or penetration, resulting in decreased compressive and shear strength. Furthermore, after such damage water may diffuse into the sandwich core and causing durability issues. For medium thickness laminated structures (less than 6 mm), impact damage may not be visible from the surface. However, damage may be induced inside the laminate in the form of delamination or matrix cracking. Such damage will greatly reduce the compression strength of the component and presents damage tolerance safety issues.

4.9.2.3 Evaluation on the Effects of Defects/Damage on Strength

Great attention has been paid to the effects of defects/damage on the strength of composites. Since their initial use in aircraft primary structures in the 1970s, many tests and investigations have been performed on the effects of damage on composites. On the basis of test data derived from various composite material systems (mainly carbon/epoxy, and carbon/BMI systems), and studies on the effects of defects/damages on the static strength and fatigue strength of specimens under different ambient conditions (room temperature/dry, hot/wet, cold/dry), the effects of defects/damage on composite strength have been established as follows:

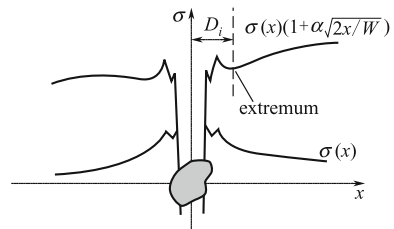
- (1) Tensile loading: Many dangerous defects, such as cuts and slots, are inspectable to some extent. The residual strength of laminates containing cuts will mainly depend on the width, and is basically independent of the cut shape. Test results for an open hole (typically 6.35 mm in diameter) can be used to consider the strength reduction associated with an edge cut of similar size, when the structure design allowable values are to be determined.
- (2) Compression loading

Table 4.22 Notch sensitivity and applicable failure criterion

Laminate type	Load type	Defect type	Notch sensitivity	Applicable failure criterion
0° unidirectional	Tensile	Penetration	No	Net cross-section failure criterion
[±45]nS	Tensile	Penetration	No	Net cross-section failure criterion
Multi-directional laminates	Tensile	Penetration	Yes	DI criterion, FD criterion, AS criterion, PS criterion
	Compression	Penetration	Yes	FD criterion
		Delamination		DI criterion
		Impact damage		DI criterion, FD criterion

Note The failure criterion under compression load can only suit the case of no buckling before failure

Fig. 4.89 DI criterion schematics



- ① Compared with many defects caused in production and operation (including delamination up to 50 mm in diameter, hole making defects, scratches, and void content up to 2%), the low-speed impact damage caused by an impactor 12.7–25.4 mm in diameter will induce more critical damage.
- ② Compression strength reduction caused by filled and load-free hole 6.35 mm in diameter can be used to as a model for the effects of all other defects including: delamination up 38.1 mm in diameter, hole making defects, scratches, and void content up to 2%.
- ③ BVID of the front surface may cause a static compression strength reduction up to 60%.
- ④ The compression fatigue $S-N$ curve is quite flat and smooth, and the conditional fatigue ultimate strength (the fatigue strength corresponding to 10^6 testing cycles) will be 60% of the static residual strength of a specimen containing a defect of the same size. The fatigue threshold value may be higher when structures are load bearing in aircraft with a random fatigue load spectrum.
- ⑤ No clear regularity of damage growth can be found in specimens with impact damage under fatigue loading conditions.

4.9.3 Analysis of Durability and Damage Tolerance

4.9.3.1 Analytical Methods Applied to Damage Tolerance

(1) **Notch sensitivity and applicable failure criterion**

The different ply stacking of laminates will result in different notch sensitivities as well as different failure criteria. In Table 4.22, the notch sensitivities of different laminates and their applicable failure criteria are listed. In addition, failure criterion is also related to failure modes, and the criteria listed in the table are applicable for laminates with fiber-dominated failure modes [1, 2, 32–37].

(2) **Introduction to applicable failure criterion**

(1) Damage influence (DI) criterion can be expressed as: the point where weighted normal stress at a characteristic point near the notch (damage) reaches laminate failure strength, at which point the damaged laminate will fail (see Fig. 4.89). The expression for DI is given as:

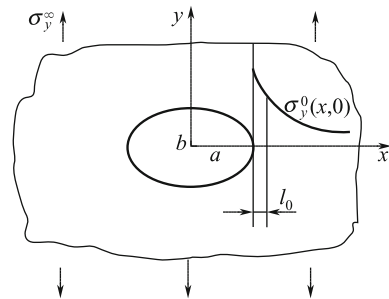
$$\sigma_y(x, 0)(1 + \alpha\sqrt{2x/W}) \Big|_{x=D_i=\sigma_b} \tag{4.83}$$

where D_i is equal to the x value,

$$\frac{d}{dx} \left(\sigma_y(x, 0) \left(1 + \alpha\sqrt{2x/W} \right) \right) = 0 \tag{4.84}$$

Where

Fig. 4.90 Stress distribution of 0° plies near the notch of laminate with a hole



- σ_b — laminate damage-free strength;
- $\sigma_y(x, 0)$ — normal stress distribution near damage;
- W — specimen width;
- α — constant related to the damage types (hole, crack, delamination, impact damage), loading condition and performance. For open hole tensile loading:

$$\alpha = \left| \frac{A_{11} + A_{12}}{2A_{22}(1 + (K_T^\infty - 3)^2)} - \nu \right| + K_T^\infty \left(\sqrt{\left(\frac{2R}{W}\right)^3} - \left(\frac{2R}{W}\right)^2 \right) \quad (4.85)$$

where

- A_{ij} — laminate in-plane stiffness coefficient;
- ν — laminate Poisson’s ratio;
- K_T^∞ — laminate hole edge stress concentration coefficient.

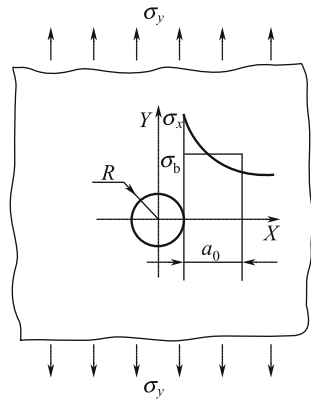
- (2) Failure criterion for fiber breakage in damage zone can be expressed as: the point when average normal stress of 0° plies within the characteristic distance l_0 near the notch (or damage) reach the ultimate strength of a unidirectional laminate (see Fig. 4.90). At this point, the damaged laminate will behave according to the expression:

$$\frac{1}{l_0} \int_a^{a+l_0} \sigma_y^0(x, 0) dx = X_t \quad (4.86)$$

where

- $\sigma_y^0(x, 0)$ —the normal stress distribution of 0° plies on the notch cross section without considering damage zone influence;

Fig. 4.91 Average stress criterion



- l_0 —material system constants independent of ply orientation and notch shape and dimensions;
- a —half the length of a notch in the x -axis direction;
- X_t —longitudinal tensile or compression strength of unidirectional laminates.

(3) Average stress criterion (AS) and point stress criterion (PS)

- ① Average stress criterion: This criterion considers the average stress within a characteristic distance a_0 from the hole edge, which achieves the ultimate strength of a notch-free laminate. Failure will occur in laminates as shown in Fig. 4.91, according to:

$$\frac{1}{a_0} \int_R^{R+a_0} \sigma_y(x, 0) dx = \sigma_b \tag{4.87}$$

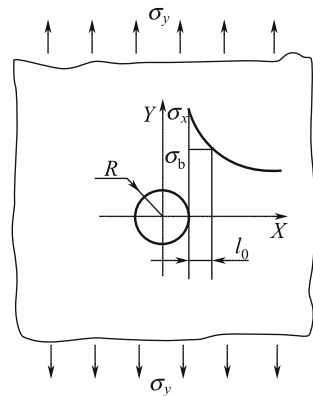
where

- $\sigma_y(x, 0)$ —stress distribution in Y direction of the minimum cross section with a hole;
- R —hole radius, and half length of the central crack;
- a_0 —characteristic length determined by testing.

For orthotropic infinite laminates with a tensile hole, the hole edge stress distribution is substituted into the average stress criterion Eq. (4.87), and the equation for residual stress calculation can be derived as:

$$\sigma_c^\infty = \frac{2\sigma_b(1 - \xi_2)}{2 - \xi_2^2 - \xi_2^4 + (K_T^\infty - 3)(\xi_2^6 - \xi_2^8)}, \tag{4.88}$$

Fig. 4.92 Point stress criterion



where $\xi_2 = \frac{R}{R+a_0}$.

- ② Point stress criterion (PS): This criterion assumes that failure of the laminate will occur if the stress σ_y at a point d_0 , a characteristic distance, reaches the ultimate strength σ_b of a notch-free laminate (Fig. 4.92), that is:

$$\sigma_y(x, 0)|_{R+d_0} = \sigma_b \quad (4.89)$$

For an orthotropic infinite laminate with tensile holes, the hole edge stress distribution is substituted into the point stress criterion expression (4.89), and an equation for residual stress calculation can be derived as:

$$\sigma_c^\infty = \frac{2\sigma_b}{2 + \xi_4^2 + 3\xi_4^4 - (K_T^\infty - 3)(5\xi_4^6 - 7\xi_4^8)} \quad (4.90)$$

where $\xi_4 = \frac{R}{R+d_0}$.

- ③ Characteristic length a_0 and d_0 : The characteristic length a_0 and d_0 in average stress criterion and point stress criterion are determined by testing. A number of specimens with different hole sizes and crack lengths are used for tensile failure testing to obtain a set of residual strength data $(\sigma_c^\infty)_T$. These data are substituted into the residual calculations by Eqs. (4.88) and (4.90) based on the average stress criterion and point stress criterion. The finite width correction and notch-free specimen tensile strength σ_0 , and a set of a_0 and d_0 values corresponding to hole diameter, and crack length can be derived. Their average values will be the characteristic lengths a_0 and d_0 .
- ④ Finite width correction: The above-mentioned open hole laminate or cracked laminate residual strength σ_c^∞ is the stress of a laminate with an infinite width. Thus, corrections should be performed for finite width laminates. Let σ_c be the residual strength of a finite width laminate, such that:

$$\sigma_c^\infty = \eta\sigma_c \quad (4.91)$$

where η is the correction coefficient for a finite width laminate, when the ratio between the defect width and laminate width is equal to or less than 1/3 (laminate width is W). For a laminate with a central hole radius R :

$$\eta_1 = \frac{2 + (1 - 2R/W)^3}{3(1 - 2R/W)} \quad (4.92)$$

For laminates with an ellipse hole (long axis is $2a$, short axis is $2b$):

$$\eta_2 = \frac{\lambda^2}{(1 - \lambda)^2} + \frac{1 - 2\lambda}{(1 - \lambda)^2} \sqrt{1 + (\lambda^2 - 1) \left(\frac{2a}{W} M\right)^2} - \frac{\lambda^2}{1 - \lambda} \left(\frac{2a}{W} M\right)^2 \left[1 + (\lambda^2 - 1) \left(\frac{2a}{W} M\right)^2\right]^{-1/2} \quad (4.93)$$

where

$$M^2 = \left(\sqrt{1 - 8 \left[\frac{3(1 - 2a/w)}{2 + (1 - 2a/w)^3} - 1 \right]} - 1 \right) / 2(2a/w)^2, \lambda = \frac{b}{a}.$$

For laminates with a central crack length $2a$:

$$\eta_3 = \sqrt{(W/\pi a) \tan(\pi a/W)} \quad (4.94)$$

(3) Estimation of residual strength of laminate with penetrating defect

- (1) Tensile loading: The above-mentioned four failure criteria can be used to perform residual strength estimation. The defect shape has no effect and can be simplified as a hole with a diameter equal to the defect width. Because no tests are needed for determination of material constants, DI criterion will become the first selected method.
- (2) Compression loading: Fiber breakage damage failure criterion (FD) can be used for the estimation, as given in Eq. (4.86), where X_t in the equation is changed into a unidirectional laminate compression strength X_c , and the characteristic length l_0 should use the value given in the compression load case.

(4) Estimation of residual compression strength of laminate with impact damage

The estimation of residual compression strength of laminates with impact damage consists of two parts, namely the estimation of impact damage and the estimation of the residual compression strength of the laminate with impact damage.

- (1) Estimation of impact damage: To analyze the residual characteristics of composite laminates after impact, it is necessary to know characteristics of

the impact damage, such as shape, size, and distribution along the thickness. This information can be derived from testing and inspection (such as nondestructive CT-scans and X-ray methods), or from quantitative analytical estimations. The analytical estimation of composite laminate impact damage includes two parts: a) analysis of the impact transient response of laminates, b) the use of appropriate failure criteria to calculate the impact zone, which will be mainly discussed in this section.

Impact damage of composite laminates includes matrix cracking, fiber rupture, and delamination. In the following section, methods for calculating impact damage size will be discussed based on delamination failure criterion, which can be used in composite structural design.

- ① Delamination failure criterion: In terms of bending strain energy density delamination failure criterion, If impact delamination of composite laminates is dominated by matrix strength and interlaminar strength, initial delamination can be derived from the criterion:

$$R = (y_S/Y_S^*)^2 + (y_M/Y_M^*)^2 \geq 1 \quad (4.95)$$

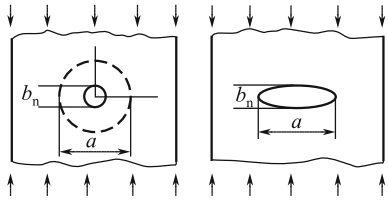
where $Y_S^* = (9/50)(S_i^2/E_f)$ is the average transverse shear strain energy density, while S_i is interlaminar shear strength, E_f is the corresponding bending modulus, $Y_M^* = (1/2)(S_y^2/E_y)$ is the strain energy density reflecting matrix failure, while S_y is the tensile strength or compression strength vertical to fiber direction (depending on stress conditions), E_y is the tensile modulus or compression modulus vertical to fiber direction; $y_S = (1/2)\tau_{xz}\gamma_{xz,\max}$, while τ_{xz} is interlaminar shear stress, $\gamma_{xz,\max}$ is the maximum shear strain; $y_M = (1/2)\sigma_y\varepsilon_y f$, while σ_y , ε_y are the stress and strain vertical to fiber direction, respectively. Here, f is an empirical coefficient reflecting stiffness inconsistencies as well as the thickness difference between two adjacent plies, and has the following form:

$$f = (t^L/t^U) / \left[1 + \left(\frac{Q_{11}^L - Q_{11}^U}{Q_{11}^L - Q_{22}^U} \right) \right] \quad (4.96)$$

where superscripts L and U indicate the lower and upper plies, respectively. This means that the stiffness should be converted according to the following lower ply fiber direction.

- ② Shear strain energy density delamination failure criterion: This is a new delamination failure criterion from consideration of the effects of transverse strength on delamination failure based on the bending strain energy density delamination failure criterion:

Fig. 4.93 Analytical model of impact damage



$$e_D = f_1 \left(\frac{\sigma_2^L}{Y^L} \right)^2 + f_2 \left(\frac{\tau_{23}^U}{S_{23}^U} \right)^2 + f_3 \left(\frac{\tau_{31}^L}{S_i} \right)^2 \geq 1 \quad (4.97)$$

where f_1 is the influence coefficient reflecting the stiffness inconsistency between two adjacent plies:

$$f_1 = \left(\frac{t^L}{t^U} \right) \left(\frac{Q_{11}^L - Q_{11}^{nU}}{Q_{11}^L - Q_{22}^U} \right) \quad (4.98)$$

where t^L, t^U are the upper and lower ply group thickness, respectively. Q_{11}^L is the stiffness coefficient along fiber direction of lower ply, Q_{22}^U is the stiffness coefficient vertical to fiber direction of the upper ply, Q_{11}^{nU} is the off-axis stiffness coefficient of the top ply along the lower ply fiber direction.

$$f_2 = \frac{1}{2} \left(1 + \frac{G_{23}^U}{G_{23}^L} \cos^2(\Delta\theta) + \frac{G_{23}^U}{G_{31}^L} \sin^2(\Delta\theta) \right) \quad (4.99)$$

$$f_3 = \frac{15}{16} \left(1 + \frac{G_{31}^U}{G_{31}^L} \cos^2(\Delta\theta) + \frac{G_{31}^U}{G_{23}^L} \sin^2(\Delta\theta) \right) \quad (4.100)$$

This model not only allows determination of bending strain energy density delamination failure criterion, but also reflects the characteristics of impact delamination along the thickness direction.

(2) Estimation of residual strength: In this section, two methods for estimating residual strength of laminates containing impact damages will be discussed.

① Estimations based on the FD criterion have the main steps given below (as shown in Fig. 4.93):

- (a) Testing, determination, or estimation of impact damage;
- (b) Simplify impact damage as an ellipse with its long axis equal to the projected width of delamination, the projected delamination can be determined by NDT or calculated by the following the procedures mentioned above. The short axis is equal to the width of a surface dent that can be measured directly, or is assumed to be 0.3 on the long axis;

Fig. 4.94 Cross section of damaged zone

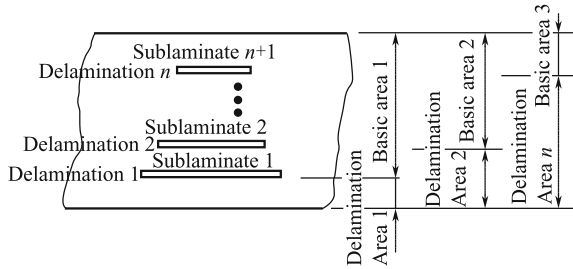
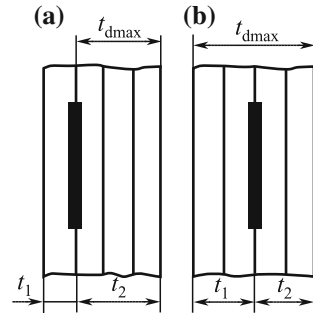


Fig. 4.95 Calculation method of t_{dmax}



- (c) A complex stress functional method or FEM is used to calculate the normal stress distribution of 0° -plies near the elliptic notch;
 - (d) FD criterion are used [as given in Eq. (4.88)] and the characteristic length l_0 determined by open-hole laminate compression tests.
- ② Estimation based on DI criterion: Estimating methods based on DI criterion can be used to calculate residual compression strength after impact, the main steps are:
- (a) Determine the impact damage conditions (such as delamination, matrix crack, and fiber rupture) by the above-mentioned methods, or by NDT inspection. Store the damage information as a data damage structure (DDS).
 - (b) Assume that the impact causes delamination in the sublaminate with a certain thickness, and perform multi-sublaminate buckling analysis.
 - (c) Use the analytical results to calculate the stiffness reduction of delaminated zone. If fiber rupture or matrix cracks are included in DDS, it is necessary to perform stiffness degradation for the corresponding damaged units, letting the damaged zone be a softened ply. The delamination and delamination zone are defined as represented in Fig. 4.94.

- (d) Use FEM to calculate the stress distribution of the laminate with a softened ply;
- (e) Use DI failure criterion [Eq. (4.82)] to estimate the compression strength. The damage effect distance D_i is defined in Fig. 4.88. For an impact damaged laminate, α is the influence factor involving the delamination distribution along the laminate thickness direction, and defined as:

$$\alpha = \left(2 \left(1 - \frac{t_{d\max}}{h} \right) \right)^{\left(1 - \frac{t_{d\max}}{h} \right)} \quad (4.101)$$

where $t_{d\max}$ is the total thickness of plies (ply group) in a continuous arrangement with the same stiffness degradation coefficients (as shown in Fig. 4.95), and h is laminate thickness.

(5) Estimation of residual strength of laminate containing delamination

The calculation steps are the same as mentioned in the above section on estimations based on DI criterion.

(6) Estimation of stiffened laminates containing defects/damage

- (1) Estimation of stiffened laminate with impact damage: As for the estimation of impact damage of laminates, to analyze the residual strength of a stiffened laminate after impact, characteristics of the impact damage shape, size and distribution along the thickness should be derived from NDT inspection or analytical estimations.
- (2) Estimation of stiffened laminates containing damage: The analysis may be divided into two cases: the estimation of residual strength of stiffened laminate containing penetrating defects (hole or cracks) under a tensile load; and the estimation of the residual strength of stiffened laminates containing holes or impact damage under a compression load. In this calculation software, a force calculation of the crack tip stress strength factor, similar to that of a stiffened metal plate, is used, and the stress distribution in the area adjacent to the notch (including crack and ellipse hole) of an anisotropic stiffened laminate can be determined. In this case, both the simplification of the impact damage as an ellipse hole and the DI failure criterion are used simultaneously.

4.9.3.2 Analysis of Durability

Composite laminated structures can offer excellent fatigue performance. For common fiber-dominated multi-direction laminates (including specimens with holes), the tensile-tensile fatigue life is 10^6 cycles under a maximum stress equal to 80% of the ultimate tensile strength. In the case of tensile-compression fatigue, the fatigue strength will be slightly

lower, with the fatigue strength equal to 50% of the corresponding static strength after 10^6 cycles. In particular, for specimens with impact damage, the fatigue strength will not be lower than 60% of the corresponding static strength after 10^6 cycles. In thermoplastic composites, values may reach up to 65% under the same conditions. Currently used allowables in composite structure design mainly depend on damage tolerance allowables. Under such strain levels, composite structures can have infinite service life, which is so-called static cover fatigue. Special attention should be paid to adhesive structures because fatigue failure may occur if the design is performed incorrectly. Currently, fatigue failure is not a critical problem in design; however, no mature analytical methods for durability are currently available.

4.9.4 Measures to Improve Durability and Damage Tolerance

(1) Softened-zone design

With softened-zone design, the damage tolerance of structures can be effectively improved while maintaining low weight and costs. This is a potentially effective design approach, which has a wide range of applications [1, 2]:

- (1) Tension panels: In this design method, high failure strain fibers (such as a glass-fiber) or prepreg tape (such as $\pm 45^\circ$ with a high failure strain and low modulus) are spread at intervals in a high modulus fiber that bears main structural load. These constituents can inhibit damage growth and improve damage tolerance. This design method may become an important approach for damage growth inhibition. For example, a number of strips can be selected in the panel and constructed into a glass/carbon fiber hybrid softened zone, arranged at intervals in a high modulus panel parallel to the load direction. This design can inhibit damage growth and direct damage growth along the softened-zone edge, so that the residual tensile strength will be increased. This design approach can be used for the design of carbon/epoxy composite wing skin and fuselage integral stiffened or sandwich panels.
- (2) Mechanical joint zone: Mechanical joining is suitable for high and complex load-bearing situations, and has become a commonly used composite structure joining method. Holes can cause more serious problems in composites than in metals, and will influence the joint strength. In a softened design, low modulus ply or prepreg tape is placed in the mechanical joining zone to improve the connection strength.

(2) Soft skin design approach

The basic concept in soft skin design is to place ply groups with different ply angles into skin or stiffener to enhance the structural damage tolerance and the allowable strain in the damage tolerance design. The so-called soft skin is a designed low stiffness wing skin with a low thickness. Soft skin mainly uses

low modulus $\pm 45^\circ$ plies (at a percentage of 70–80%), and contains a certain amount of glass-fibers in some local zones, which can bear shear load and the internal pressure of an oil tank for example. Laminates with a small ratio of 0° , 90° plies, such as a (10/80/10) ply ratio, can also be used to ensure local strength and structural stability. Stiffeners mainly use 0° plies that are orientated along the wing span direction and can be used to withstand tensile and compression loading in wing panels. The skin and stiffeners are mechanically joined or co-cured to form the wing panel. In some design programs (such as for body panels), a certain proportion of 0° plies are embedded into the soft skin at certain intervals as additional reinforcing elements (crack-blocking zones). This approach is mainly used in shear-bearing transportation aircraft wings.

(3) **Film enclosure**

A layer of adhesive film may be introduced in between laminate plies to increase the interlaminar damage resistance or to reduce the interlaminar stress concentration for easily impacted structures. Epoxy films (such as FM series films) or thermoplastic films (such as HXT series films and PEEK film) can be inserted between the carbon fiber plies to increase damage resistance. A new generation of interlaminar enclosed films can be made by spraying toughened particles on prepreg tapes, which can largely increase the interlaminar toughness and compression strength after impact without increasing the thickness between plies.

(4) **3D reinforcing (Z-axis reinforcing)**

3D reinforcing is mainly used to inhibit the delamination growth caused by impacts and to increase the composite structural damage tolerance. Approaches include reinforcement braiding in the thickness direction (such as 3D braiding and Z-axis knitting performed in combined RFI and RTM processing), as well as fasteners and Z-axial pin joining. Among these methods, dry/knitting and 3D braiding/RTM show great potential for applications in improving damage tolerance.

Z-pin joining is another mechanical joint for Z-axial reinforcement, other than the use of metal fasteners. A foam preform (made of FM) containing small strong carbon/epoxy pins is placed on a laminate structure. These preforms will be pressed into laminates during hot pressing. This approach can be used for reinforcement, locally or over the entire component. This approach can also be used to replace metal fasteners used to fix frame construction. Test results indicate that it may be possible to reduce delamination size and increase damage tolerance with this method.

(5) **Other approaches for durability/damage tolerance improvement**

Three approaches can be used for durability/damage tolerance improvements: use of special designs methods to inhibit damage growth and increase residual strength. On the basis of the analysis of failure mechanisms of laminated structures containing damage (including impact damage), the composite performances can be improved to increase their damage tolerance. Namely, the residual strength can be improved when laminates contain damage of the same

size. On the basis of statistical analysis of external impact energies, and improved production and maintenance conditions (increased supportability), the current damage tolerance requirements may be revised. The initial defect sizes are changed from the current BVID to the external impact energy probability distribution at different locations.

(6) Special issues

- (1) Owing to the variety of damage patterns with different formation and expansion mechanisms, proper design approaches should be used for different damage types, such that damage tolerance can be effectively improved.
- (2) In this section, improvements of impact damage tolerance are discussed. Attention should be paid to other possible damages caused under different loading conditions, for example, holes or other penetrating damage may cause potential dangers under tensile or tensile–shear loads. To improve the structural efficiency and design strain level, special design approaches should be used based on the different load conditions and the potential damage modes.
- (3) In practice, no single approach can be used to improve composite structural damage tolerance. Good results can be achieved only through consideration and use of a combination of design concepts.
- (4) It should be noted that damage tolerance is critical, for example, if damage tolerance contributes only a small part to the whole structure (20% for example), the weight may be increased by approximately 4% by increasing the thickness to reduce the strain level. However, the design approaches used for improving damage tolerance can be costly. In practice, a combination of considerations should be taken, including structural strength, stiffness durability, damage tolerance, weight and cost, so that the structure is optimized in terms of cost effectiveness, while balanced performance is achieved.

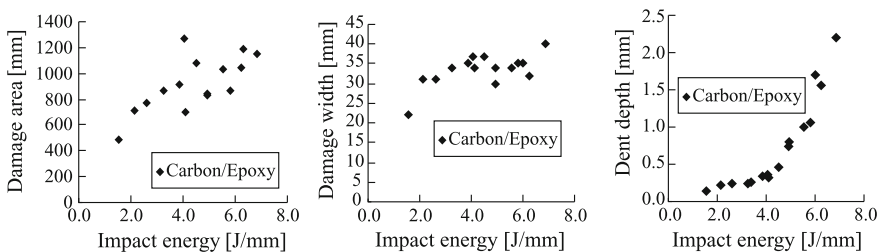


Fig. 4.96 Typical relationship of damage size and impact energies

4.9.5 Characterization of Composite Damage Resistance and Damage Tolerance

4.9.5.1 Review

In fact, the most effective approach to increase composite structure damage tolerance and damage resistance is to develop new material systems with high damage tolerance and high damage resistance. The traditional method to evaluate the composite damage tolerance is use of compression strength after impact (CAI) as detained in NASA RP1142 and SACMA SRM 2R-94; in the recent studies, it has been indicated that CAI obtained in such approaches can only evaluate damage

Fig. 4.97 Typical relationship of compressive failure strain and damage size

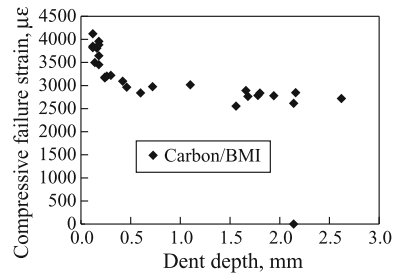


Fig. 4.98 Typical knee point phenomenon for damage tolerance and damage resistance properties of composite systems

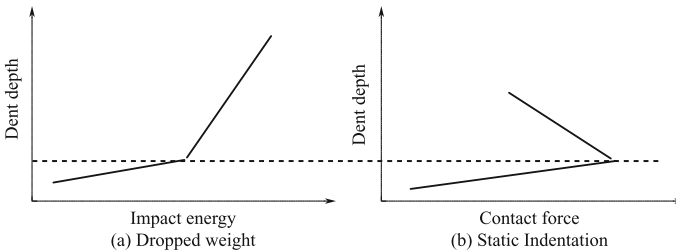
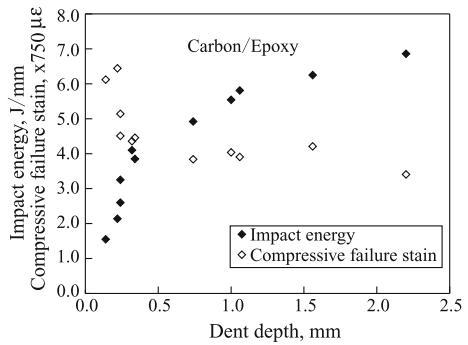
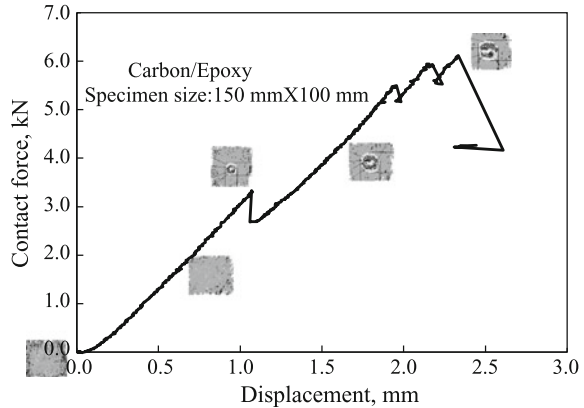


Fig. 4.99 Comparison of damage resistance behavior obtained by two methods

Fig. 4.100 Typical contact–displacement curve of composite laminates and corresponding internal damage state



resistance, rather than damage tolerance, which needs a proper evaluation approach [38–45].

In ASTM D 3878–07 Standard Terminology for Composite Materials, definitions on damage resistance and damage tolerance are given, and their differences are also discussed.

4.9.5.2 Complete Description of Damage Resistance, Tolerance and Knee Point

As discussed above, a main parameter describing composite damage resistance is the damage size, which is a function of the impact event. Other parameters describing composite damage tolerance, including the compression load-bearing capacity, are a function of damage size. Usually, impact energy is used as a parameter to describe an impact event. As shown in Fig. 4.96, testing data have indicated that, among the commonly used damage size parameters (such as damage area, damage width and surface dent depth), surface dent depth measured immediately after impact shows a good linear relationship with the impact energy. This measurable is also consistent with the damage parameters required in aircraft structural design. Compression load-bearing capacity is usually expressed by compressive strength or compression failure strain. A comprehensive description of composite damage resistance and tolerance is illustrated in Figs. 4.96 and 4.97. Testing data have indicated that there will be a visible knee point for composite damage resistance and damage tolerance, occurring at the same damage size for a dent depth of approximately 0.5 mm, as shown in Fig. 4.98. It has been verified by theory and experiments, that quasi-static indentation forces can be used to replace hammer dropping to induce damage. The same conclusion is derived as shown in Fig. 4.99. In some studies, supersonic C-scans have been used to study damage propagation with increasing indentation force under quasi-static pressing conditions. The change of damage size was the same as that found for impact energy, as shown in Fig. 4.100. From these studies, we may conclude that when the

indentation force reaches a lower threshold (corresponding to a certain impact energy), apparent delamination occurs inside the specimen, while no dent can be found on the surface. As the indentation force increases (also corresponding to an increase of impact energy), the degree of inner delamination increases gradually as the surface dent depth increases to a depth not larger than 0.3 mm. When the indentation force reaches the ultimate value it drops down quickly and the dent depth will rapidly increase. This is analogous to the impact energy reaching a threshold, such that the dent depth increases markedly, as shown in Figs. 4.99 and 4.100, where the dent depth will not exceed 0.5 mm. Further increases of indentation force or impact energy will not increase the internal damage size further although the dent depth will increase continuously.

In some studies, the two methods described above have been used to induce damage in specimens; damaged specimens from before and after the knee point were soaked with gold chloride ether solution, and ply peeling of the internal damage states was observed. These results have indicated that impact damage prior to the knee point involves matrix cracking and internal delamination. After the knee point, fiber breakage can be found on the front surface of the specimen. Thus, the knee point marks the onset of fiber breakage at the impact point on the front surface. Knee point phenomenon indicates a sudden change of impact (or contact force) resistance in composite laminates. Before the knee point, the impact resistance of a composite derives from both resin and fibers. Damage is induced to the matrix in the form of cracking and delamination; however, the ply, as the basic unit of a composite and, particularly, plies on the surface (including their matrix and inter-laminar structure) are undamaged before the knee point. After that the knee point fiber breakages occur, and damage becomes visible on the surface plies. This indicates that the laminates cannot provide further impact resistance. The damage growth will cause fiber ruptures from the front and back surfaces extending to the center, and internal delamination will also increase. Internal delamination is the main factor contributing to the reduction of the composite laminate compression strength, and the size of delamination will not change greatly after the knee point. Thus, the compression strength will remain unchanged.

For composite laminates, a knee point on the impact energy versus dent depth curve will also be a knee point on the impact energy (dent depth) versus compression failure strength (strain) curve. The former relates to the damage resistance characteristics of a composite laminate, while the latter relates to the damage tolerance characteristics of the laminate. The former denotes a sudden change of damage resistance in composite laminates after an impact event. Before such an event, external impacts are resisted by the combination of matrix and fibers. Damage is caused mainly in the form of internal delamination and small matrix cracking. The same increase in impact energy can result in a small increase in the dent depth, while a larger increase in the damage area and damage width can be expected with good regularity. The presence of a knee point indicates fiber breakage on the surface, and further increases in impact energy will not produce greater delamination beyond that which exists in the damage width. Instead, further increases in the impact energy will produce more fiber breakages from the surface to the inside. Thus, increasing impact energy will increase the dent depth, and

have a smaller effect on the damage area and damage width. The residual compression strength is directly related to the damage width (damage area); thus, a knee point on the impact energy (dent depth) versus compression failure strength (strain) curve will result. Before the knee point, the compression failure strength (strain) will rapidly decrease as the impact energy (dent depth) increases. After the knee point, the compression failure strength (strain) will not change any further or only show a small change.

On the basis of the physical consequences of a knee point, typical values taken from areas adjacent to the knee point can be used to characterize the damage resistance and damage tolerance of composite laminates.

4.9.5.3 Characterization of Composite Damage Tolerance and Damage Resistance

It is recommended that the following physical parameters are used to characterize the damage resistance and damage tolerance of composite systems.

- For quasi-isotropic laminates, the maximum indentation force F_{max} on the indentation force versus displacement curve obtained by static indentation testing can be used to characterize the damage resistance of a composite system.

Fig. 4.101 Comparison of damage tolerance behavior for two composites with different CAI

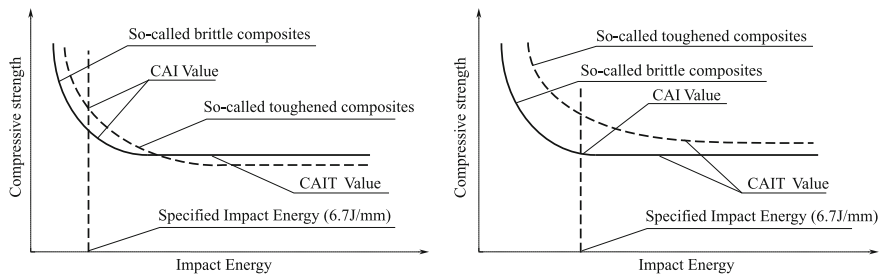
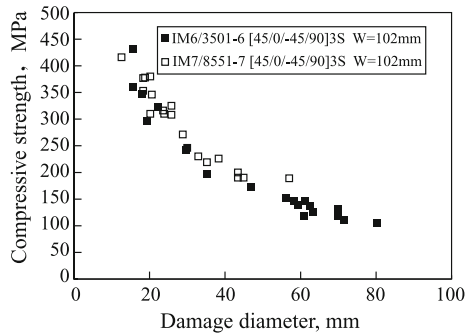


Fig. 4.102 Comparison of CAI and CAIT values

Table 4.23 Damage properties for four composite systems

Composite system	CAI (MPa)	CAIT	
		Strength (MPa)	Failure stain
T300/Epoxy A	136	136	2910
T700S/Epoxy B	167	127	2593
CCF300/BMI A	149	142	2730
CCF300/BMI B	194	177	3419

This represents the maximum capacity of a composite system to resist an external impactor.

For quasi-isotropic laminates, the dent depth (or impact energy) versus compression failure strain curve threshold (CAIT), or the compression strength (or failure curve) (CAI) at a dent depth of 1.0 mm (measured immediately after impact) can be used to characterize the damage tolerance of a composite system.

On the basis of these characterizations, composite systems, which are shown to have good damage resistance, will also give aircraft structures with good damage resistance. Similarly, if composite systems have very good damage tolerance behavior, aircraft structures made of these composite systems will also show good damage tolerance.

4.9.5.4 Comparison Between the Recommended Method and the Traditional CAI Evaluation

For a long time, CAI values obtained from NASA RP 1142 or SACMA SRM 2R-94 have been considered to be the main specifications for characterizing damage tolerance. In the NASA standard, an impactor 12.7 mm in diameter with an impact energy of 27 J (about 4.45 J/mm) is used. In the SACMA standard, an impactor 16 mm in diameter with an impact energy of 6.67 J/mm is used.

Here, the obtained damage tolerance values represent the corresponding compression failure strength obtained under testing conditions of 27 J (NASA standard) or 6.67 J/mm (SACMA standard). In fact, the impact energy cannot reflect damage parameters, such that values derived from these methods cannot be used to evaluate the damage tolerance behavior of composite systems perfectly. In Fig. 4.101, the relationship between the damage width versus compression failure strain of two different toughened composite systems is shown. In terms of damage tolerance, the composite systems IM6/3501-6 (brittle epoxy) and IM7/8552-1 (toughened epoxy) have similar damage tolerance behavior, but their CAI values are quite different [15]. According to the above analysis, the composite systems with the higher CAI value at knee point may produce a larger maximum damage area (or diameter) than composite systems with a lower CAI values. Composite systems with higher CAI values may show lower CAIT as given in Fig. 4.102. In Table 4.23, some test results are listed.

4.10 Environmental Effects and Protection

4.10.1 Introduction

Aircraft composite structures in service may be subjected to maneuver and gust loading environments. External environmental conditions, such as temperature, humidity, lightning strikes, sand, hail, rain, snow, ultraviolet light, and atmospheric pollution may influence the structural integrity of composites. The local environment, including fuel, hydraulic fluid, and cleaning solvents can also affect composites. Thus, environmental effects should be considered at the stage of material and configuration selection in the detailed design phase of composite structure design. Environmental design criteria and effective environmental protection methodologies must be established. The influences of hygrothermal and aging environments on airplane composite structures should be considered in structural design and these aspects are discussed in this chapter.

4.10.2 Environmental Design Criterion

Environmental design criteria for aircraft composite structures should be determined based on the service area, flight scope, material systems, mission purpose, and structural status [1, 2, 13].

4.10.2.1 Hygrothermal Environment

For composite structures, the hygrothermal environment must be considered as part of the overall environment. Two aspects should be carefully considered: first, the degradation of mechanical properties caused by the most extreme potential hygrothermal environments, and second the effects of long-term hygrothermal aging on mechanical behaviors. These aspects should be qualified through analysis and testing of composite structures within the designated service life duration. Structures should maintain sufficient integrity under the individual or combined actions of temperature, humidity, and loading environments. In certain special structural positions, the combined effects of local and overall environments should also be qualified. Detailed requirements are as follows:

- (1) Rigorous structural use environments can be determined based on flight missions, the structural configuration, and the ground rest environment. Thermal spiking effects caused by aerodynamic heating in flight at speeds greater than Mach 2 should also be considered.
- (2) Moisture diffusion behaviors of a chosen material system under a specific hygrothermal environment and the effects of this environment on the physical and mechanical properties of the system should be determined.

- (3) The service moisture absorption content, final moisture content, steady conditions, and hygrothermal allowables of chosen materials and configurations should be determined.

4.10.2.2 Physical Impacts

Aircraft composite structures are susceptible to impact damage from tool dropping, runway detritus, hail stones, and ground service vehicles. Other considerations include lighting strikes, bird-strikes, and bullet damage. In general, lightning strikes will result in visible damage and local ablation of the composite structures,

Table 4.24 Typical airplane service environmental areas in China

Type	Typical area	Main characteristics	Representative regions
1	Dry-cold	Low air-temperature; annual average air-temperature lower than 10 °C; low rainfall; not more than 500 h of relative humidity more than 80% on average; low levels of industrial pollution and corrosive media in air	Tibet, Qinghai, Ningxia, Jilin and most of the Heilongjiang region
2	Basic warm	Moderate air-temperature; annual average air-temperature lower than 15 °C; moderate rainfall, relatively dry; not more than 3000 h of relative humidity more than 80% on average; moderately serious industrial pollution	Xi'an, Zhengzhou, Beijing, and Shenyang
3	Hot-wet inland	High air-temperature; annual average air-temperature of 15–20 °C; high levels of rainfall, dew, and fog; high air humidity; more than 4000 h hours of relative humidity more than 80% on average; serious industrial pollution and high levels of corrosive media in air; semitropical humid climate	Chongqing, Wuhan, Changsha, Guangzhou, and Nanjing
4	Warm coastal	Moderate air-temperature, annual average air-temperature lower than 15 °C, high levels of rainfall, high air humidity, strong winds, high salt content in air, high salt-fog sedimentation, serious industrial pollution	Qingdao, Xiamen, and coastal regions
5	Hot-wet coastal	High air-temperature, annual average air-temperature more than 20 °C, other characteristics resemble those of the warm coastal region	Hainan coast

introducing through-thickness holes or local delamination. Bird and bullet strikes will produce through-thickness holes.

For composite structures, the requirements of strength and service life after low-energy impacts must still be satisfied, and damage caused by high-energy strikes should not grow further.

4.10.2.3 Aging Environment

Here, the aging environments used to study composite structures are discussed, including corrosive liquids (fuel, hydraulic fluid, and antifreeze), ultraviolet radiation, weathering, and sand and rain erosion.

Table 4.25 Maximum and minimum air-temperature of every month in typical areas °C

Area	1		2		3		4		5	
Month	Dry-cold		Basic warm		Hot-wet inland		Warm coast		Wet-hot coast	
	T_{max}	T_{min}	T_{max}	T_{min}	T_{max}	T_{min}	T_{max}	T_{min}	T_{max}	T_{min}
1	-7.4	-21.8	1.4	-9.9	9.6	3.2	3.5	-2.6	20.0	12.0
2	-4.0	-18.4	2.5	-8.5	9.8	3.9	4.4	-0.2	20.0	12.0
3	4.0	-10.4	10.5	-0.5	15.7	6.8	8.1	1.4	24.0	16.0
4	12.6	-0.8	18.6	6.0	20.2	12.8	11.6	5.7	30.0	22.0
5	18.9	5.5	27.0	15.0	26.7	18.8	18.2	11.2	31.0	23.0
6	23.5	10.1	30.0	19.0	28.3	20.5	22.1	16.7	32.0	24.0
7	25.5	12.6	30.8	21.5	31.9	23.5	25.5	21.3	33.0	24.0
8	23.8	11.6	29.5	20.5	31.1	22.5	28.2	23.7	34.0	24.0
9	18.2	5.4	23.5	4.5	29.3	19.5	25.1	19.7	32.0	22.0
10	13.2	-2.4	18.0	6.0	21.4	4.1	20.2	15.4	28.0	22.0
11	1.6	-13.2	9.30	-3.0	16.4	9.3	13.0	6.2	24.0	18.0
12	0.2	-20.2	2.0	-10.0	11.5	3.5	6.9	0.5	21.0	13.0

Table 4.26 Statistical results of relative humidity in basic warm and dry-cold areas

Area	Relative humidity/%			
	Average monthly maximum	Average monthly minimum	Monthly maximum	Monthly minimum
Basic warm	85	30	100	0
Dry-cold	78	25	100	0

4.10.3 *Hygrothermal Environment Effect*

One important key point for composite structure design is to consider the influence of the hygrothermal environment on structural performance. The resin matrix has the ability to absorb moisture, and moisture diffusion can result in a distribution of moisture content in the structure. Thus, both the anti-corrosion resistance of fibers and the glass transition temperature T_g might decrease. The structural stiffness and strength of the composites might also be reduced through these effects. At all stages of material and configuration selection, detailed design and testing of the composite structure should account for environmental response of the system [1, 2, 13].

4.10.3.1 **Aircraft Service Environment in China**

The long-term environmental conditions to which an aircraft will be exposed should be determined as the use environment. The most extreme environmental conditions and use environment can be confirmed by a statistical process based on a large volume of measured data. Typical airplane service areas in China are represented in Table 4.24. The average maximum and minimum air-temperature and average relative humidity (RH) each month in typical areas are listed in Tables 4.25 and 4.26.

4.10.3.2 **Prediction of Moisture Absorption Diffusion Behaviors**

To use composites in structures, first issues related to changes of mechanical performance after moisture absorption by the resin matrix should be addressed. The change of mechanical performance depending on moisture content should be qualified. The composite moisture content in a specific environmental and the time taken for that moisture content to be attained under specified environmental conditions should be determined by theoretical analysis and moisture absorption experiments.

Theoretic Predictions

Characteristics of moisture absorption and diffusion can be predicted by the following two models at the initial stages of composite structure design. Moisture diffusion in composites at low relative humidity can be described by the *Fickian* diffusion model, while moisture diffusion processes at high relative humidity are preferably described by the vapor boundary model.

(1) **Fickian model**

Analysis of the moisture diffusion in resin matrix composites can be accomplished with this simple model. The main characteristics of this model are its initial linear moisture absorption curve leading over the long term to a steady moisture level. The model is equivalent to that for moisture absorption of a material immersed in water. The moisture diffusion of bismaleimide (BMI) matrix composites can be described perfectly by this model. In one dimension the model is:

$$\frac{\partial C}{\partial t} = D_z \frac{\partial^2 C}{\partial z^2} \quad t > 0, z \in [-h/2, h/2] \quad (4.102)$$

The boundary conditions are:

$$C(z, 0) = C_0$$

$$C(-h/2, t) = C(h/2, t) = C_\infty \quad t > 0$$

where

- C moisture concentration;
- C_0, C_∞ initial concentration and equilibrium concentration;
- D_z moisture diffusivity through the thickness direction;
- t time;
- h laminate thickness;
- z coordinate in the thickness direction.

The total moisture content is:

$$M(t) = M_\infty - (M_\infty - M_0) \frac{8}{\pi^2} \sum_{n=0}^{\infty} \left\{ \frac{1}{(2n+1)^2} \times \exp(-\lambda_n^2 D t / h^2) \right\} \quad (4.103)$$

where

- $M(t)$ moisture of laminate;
- M_0, M_∞ initial moisture content and equilibrium moisture content

$$\lambda_n = 2\pi + n, \quad n = 0, 1, 2, \dots$$

For long-term moisture absorption, the $n = 0$ term is unchanging. When diffusivity of the material system and equilibrium moisture content are known the moisture content at any time point can be calculated. Diffusivity can also be calculated from knowledge of the moisture content at two different times.

$$D = \pi \left(\frac{h^2}{4(M_\infty - M_0)} \right)^2 \left(\frac{M(t_1) - M(t_2)}{\sqrt{t_1} - \sqrt{t_2}} \right)^2 \tag{4.104}$$

The disadvantage of this model is the use of fixed boundary conditions, and the shape of the moisture curve at the initial stage are not accurately described. Therefore, the initial moisture absorption is greatly over estimated and the diffusivity is under estimated.

(2) Vapor boundary model

When a solid absorbs or desorbs water vapor from the atmospheric environment, the *Fickian* model produces large deviations. A proportionality constant F may be introduced. Hence, F is defined as the moisture absorption gradient and is proportion to the difference between the actual surface concentration and equilibrium concentration. The diffusion equation is unchanged from that given in (4.102); however, the boundary conditions are modified as:

$$C(z, 0) = C_0 \tag{4.105}$$

$$C(\pm h/2, t) = C_\infty + \frac{D}{F} \times \frac{\partial C}{\partial z} (\pm h/2, t)$$

Thus, in the limit $F \rightarrow \infty$, the vapor boundary model degrades to the *Fickian* model.

The moisture content is:

$$M(t) = M_\infty - (M_\infty - M_0) \sum_{n=0}^{\infty} \left\{ \frac{2 \sin^2 \beta_n}{\beta_n (\sin \beta_n \cos \beta_n + \beta_n)^2} \times \exp(-4\beta_n^2 D t / h^2) \right\} \tag{4.106}$$

$$\beta_n : \beta \tan \beta = hF / 2D \quad n = 0, 1, 2, \dots$$

$$\beta_n \in \left\{ n\pi, \frac{\pi}{2} + n\pi \right\}$$

as $\frac{F}{D} \rightarrow 0, \beta_n \rightarrow n\pi,$

as $\frac{F}{D} \rightarrow \infty, \beta_n \rightarrow \frac{\pi}{2} + n\pi,$

An iteration of the following form can be adopted.

$$\beta^{i+1} = \beta^i - \frac{(\beta^i \tan \beta^i - hF / 2D) \cos^2(\beta^i)}{\sin \beta^i \cos \beta^i + \beta^i} \quad I = 0, 1, 2, \dots$$

The value of F can be determined from measurements of moisture content at times t_1 and t_2 .

Table 4.27 Equilibrium moisture content and diffusivity of materials in specified environment

Material	D	D	m_e
	30 °C, 95%RH	50 °C, 95%RH	50 °C, 95%RH
T300/5405	$1.15 \times 10^{-7} \text{ mm}^2/\text{s}$	$3.788 \times 10^{-7} \text{ mm}^2/\text{s}$	0.85%
T300/QY8911	$3.50 \times 10^{-7} \text{ mm}^2/\text{s}$	$7.043 \times 10^{-7} \text{ mm}^2/\text{s}$	1.35%

$$F = \frac{1}{2(C_\infty - C_0)} \left(-\frac{2M_0}{t_2} - \frac{M_0(t_2 - t_1)}{t_1 t_2} + \frac{M(t_1)}{t_1} + \frac{M(t_1)}{t_2 - t_1} - \frac{M(t_2)t_1}{t_2(t_2 - t_1)} \right) \quad (4.107)$$

This model corresponds to a situation in which moisture enters the material from the ambient environment. The initial rate parameters can be obtained easily and have clear physical meanings. Results predicted by this model for high relative humidity are consistent with experimental findings, and at low relative humidity the predictions can satisfy engineering requirements.

In conclusion, for environments with low relative humidity, the moisture absorption diffusion process in composite laminate can be described by the *Fickian* model; however, under environments of high relative humidity, the moisture absorption diffusion process is better described by the vapor boundary model owing to swelling of the composite laminate.

Moisture Absorption Experiments

Composite material systems require experimental confirmation of moisture absorption and testing should be performed. The purpose of moisture absorption tests is to determine the moisture diffusivity at different temperatures and the equilibrium moisture content at different relative humidity. The test must be performed according to the aviation industry standard *Environmental Moisture Absorption Test Method (HB-7401-96)*. The moisture absorption and desorption behaviors of resin matrix composites are controlled mainly by two parameters; the equilibrium moisture content of the material, which depends on the environmental relative humidity; and the moisture diffusivity, which correlates with the environmental temperature (Table 4.27). The moisture absorption content within a specified time may be determined from these two parameters. Moisture absorption tests should be performed at three different combinations of temperature and humidity for every type material. Two sets of conditions will have the same relative humidity, and two sets of conditions will have the same temperature. Hence, these basic parameters will allow the moisture absorption content to be calculated under a specified environment at different time intervals. Furthermore, the required time to achieve a certain moisture absorption level in a specified environment can be estimated.

4.10.3.3 Principle and Methodology of Accelerated Moisture Absorption

The mechanical, thermodynamic, and chemical properties of resin matrix composites will change on exposure to certain hygrothermal environments over a long time. This is a slow accumulative process, and hygrothermal experiments are time consuming and costly. Therefore, accelerated hygrothermal experiments are a necessary part of such studies.

A large volume of experimental results has indicated that there is a direct relationship between the moisture content and the mechanical performances of composite laminates after moisture absorption. Moreover, this relationship is not affected by the hygrothermal history of the composite. This is the basis for accelerated laboratory moisture absorption testing for prediction of mechanical properties after moisture absorption. Additional material degradation should not be induced. The use of high temperatures for accelerated moisture absorption is not generally appropriate.

Two methods for calculating accelerated moisture absorption are given as follows:

- (1) **The accelerated time coefficient K can be estimated according to following equation:**

$$k = \frac{t_1}{t_2} = \frac{e^{-C/T_2\phi_2}}{e^{-C/T_1\phi_1}} \quad (4.108)$$

where

- K accelerated time coefficient;
 t_1 actual exposed time;
 t_2 time after acceleration;
 $T_1\phi_1$ temperature ($^{\circ}\text{C}$) and relative humidity of actual exposure environment;
 $T_2\phi_2$ temperature ($^{\circ}\text{C}$) and relative humidity of accelerated environment.

- (2) **The accelerated time coefficient K can be estimated from the ratio of diffusivity in the different environments:**

$$K = \frac{t_1}{t_2} = \frac{D_2}{D_1}$$

$$D = D_0 \exp(-C/T) \quad (4.109)$$

where

Table 4.28 Diffusion constants of different materials under different environments at room temperature

Material Constant	T300/1034		AS/3501-5		T300/5208		934		3501-5		5208	
	D_0	C	D_0	C	D_0	C	D_0	C	D_0	C	D_0	C
Distilled water	16.3	6211	768	7218	132	6750						
Saturated brine	5.85	6020	5.38	6472	6.23	5912						
Moist air	2.28	5554	6.5	5722	0.57	4993	4.85	5113	16.1	5690	4.19	5448

D_0, C —two diffusion constants under different moisture environments at room temperature;

T —absolute temperature.

The diffusion constants of different materials under different moisture environments are shown in Table 4.28.

The results estimated from these two methods are often inconsistent and the more conservative result should be adopted. For example, suppose that T300/5208 laminate is exposed to an environment at 25 °C and 60% relative humidity for 100 days. For accelerated moisture absorption at 60 °C and 95% relative humidity, the accelerated time required is $t_2 = 10.4$ days according to Eq. (4.108), and $t_2 = 17.2$ days according to Eq. (4.109). The differences may be caused by the experimental and material constants used. To obtain the most conservative result, both methods should be used and the longer accelerated time selected.

4.10.3.4 Influence of Hygrothermal Environment on Composite Performance

Composites are sensitive to their hygrothermal environment. Moreover, the combination of temperature and humidity has a synergic effect. The influence of hygrothermal environment on the physical and mechanical properties can be predicted based on empirical equations or interpolation of experimental results. Alternatively, the influence could be numerically calculated at a structural level. Namely, the initial strains caused by temperature and humidity could be calculated based on the structural temperature and humidity distribution. The initial strains are transformed to the initial load and the initial load can be superposed with a mechanical load. Finally, the structural stress analysis and strength could be checked by FEMs [46].

Influence of Hygrothermal Environment on Physical Properties of Composites

(1) Glass transition temperature

Changes in the physical behavior of composites occur after moisture absorption. The glass transition temperature T_g will decline with increasing moisture content. The extent of this influence can be predicted by the following equation:

$$T_g = \frac{[\beta_m(1 - v_f)T_{gm} + \beta_f v_f T_{gf}]}{[\beta_m(1 - v_f) + \beta_f v_f]} \quad (4.110)$$

where

- T_g glass transition temperature of matrix under certain moisture content;
- β_m wet swelling coefficient of matrix under certain moisture content;
- β_f wet swelling coefficient of fiber under certain moisture content, usually equal to zero;
- V_f fiber volume content under certain moisture content;
- T_{gm} glass transition temperature of matrix under certain moisture content;
- T_{gf} glass transition temperature of fiber under certain moisture content.
- T_{gf} —glass transition temperature of fiber under certain moisture content.

The changes of glass transition temperature with moisture content for some composite material systems are given in Table 4.29. The experimentally determined variation of the glass transition temperatures of three material systems is presented in Fig. 4.103. This figure shows that for polymer matrix systems the T_g declines by approximately 25 °C for at a moisture content of 0.5%. For further increases in the moisture content over 1.2% there is only a slight decrease of T_g . For cyanate esters matrix composites, T_g declines by approximately 20 °C when the moisture content is greater than 0.3%. For a BMI matrix composite, moisture content has hardly any effect on T_g .

(2) Wet swelling coefficient and thermal expansion coefficient

The wet swelling and thermal expansion coefficients for some materials are shown in Table 4.30. The change of the thermal expansion coefficient with moisture content can be predicted by the following equation:

$$\alpha(T) = \alpha(RT) \left(\frac{T_{gw} - T}{T_{gd} - T_{RT}} \right)^{-\frac{1}{2}} \quad (4.111)$$

where

- $\alpha(T)$ thermal expansion coefficient at temperature T under a certain moisture content;
- $\alpha(RT)$ thermal expansion coefficient at room temperature;
- T_{gw} glass transition temperature at certain moisture content;

Table 4.29 The change of glass transition temperature with moisture content for some materials

Material	914						T300/914C						T300/5222						T300/4211						4211					
	Moisture content/%		$T_g/^\circ\text{C}$		Moisture content/%		$T_g/^\circ\text{C}$		Moisture content/%		$T_g/^\circ\text{C}$		Moisture content/%		$T_g/^\circ\text{C}$		Moisture content/%		$T_g/^\circ\text{C}$		Moisture content/%		$T_g/^\circ\text{C}$							
	0	0.9	0.6	2.9	4.7	0	0.9	1.6	0	1.0	0	1.0	0	1.0	0	1.0	0	1.0	0	1.0	0	1.0	0	1.02						
	208	188	178	160	137	219	169	153	245	195	99	84	156	132																

Fig. 4.103 Change of T_g with moisture content for three material systems

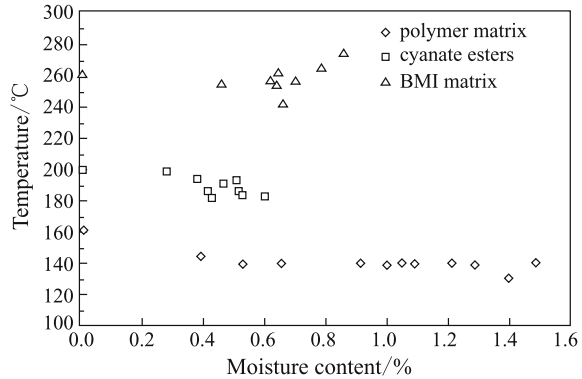


Table 4.30 Wet swelling and thermal expansion coefficients of some materials

	T300/5208	B/5505	AS/3501	Scotch/1002	Kevlar/epoxy
$\alpha_L/10^{-6}K^{-1}$	0.02	6.1	-0.3	8.6	-0.4
$\alpha_T/10^{-6}K^{-1}$	22.5	30.3	28.1	22.1	79.0
β_L	0.0	0.0	0.0	0.0	0.0
β_T	0.6	0.6	0.44	0.6	0.6

T_{gd} the glass transition temperature in dry state;

T_{RT} room temperature.

The changes of the thermal expansion coefficients for 914C pure resin and T300/914C unidirectional laminate with temperature are shown in Table 4.31 and Fig. 4.104. Equation (4.111) is used and has already been validated. The wet swelling coefficient is shown in Fig. 4.105, and the change of wet swelling strain with moisture content is shown in Fig. 4.106. These results indicate that the change of lengthways wet swelling coefficient β_L is small, while the transverse wet swelling coefficient varies linearly with moisture content.

Influence of Hygrothermal Environment on Mechanical Properties of Composites

Composite mechanical performances, particularly the mechanical performances related to the matrix, are strongly influenced by the hygrothermal environment. Test results have highlighted the importance of considering the influence of hygrothermal environment on the compression, interlaminar shear, compression after impact, and tension and compression strength with an open hole in composite structure design. The non-dimensional parameter T^* may be introduced.

Table 4.31 Change of thermal expansion coefficient with temperature

$T/^\circ\text{C}$	$\alpha_T/10^{-6}\text{K}^{-1}$	$\alpha_L/10^{-6}\text{K}^{-1}$
120	38.4	
80	36.0	
40	34.4	-0.8
23	32.8	
0	32.0	
-55	29.6	

Fig. 4.104 Change of thermal expansion coefficient for 914C pure resin and T300/914C unidirectional laminate with temperature

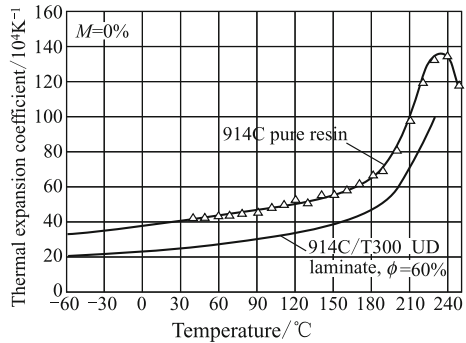


Fig. 4.105 Change of wet swelling coefficient for 914C pure resin and T300/914C unidirectional laminate with fiber volume content

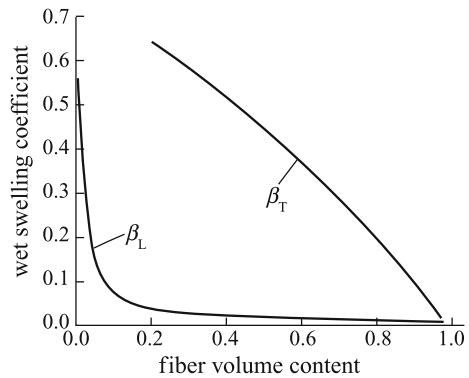
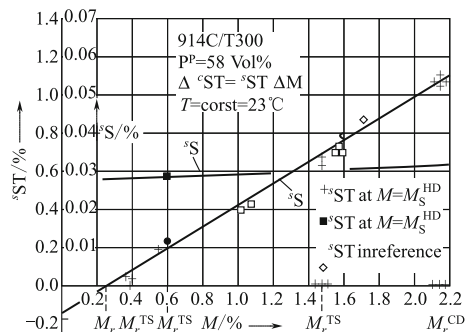


Fig. 4.106 Change of swelling strain with moisture content for 914C pure resin and T300/914C unidirectional laminate



$$T^* = (T_g - T)/(T_g - T_r) \quad (4.112)$$

where

T operation temperature;

T_g glass transition temperature;

T_r reference temperature or room temperature.

When experimental results on the influence of hygrothermal environment on composite mechanical performance are lacking, the following equations may be used to make predictions:

$$\begin{aligned} X_f/X_f^0 &= (V_f/V_f^0)(T^*)^{0.04} \\ E_1/E_1^0 &= (V_f/V_f^0)(T^*)^{0.04} \\ X_C/X_C^0 &= (V_f/V_f^0)(T^*)^{0.04}(T^*)^{0.05} \\ E_2/E_2^0 &= \left[(T_g - T)/(T_g^0 - T_r) \right]^{0.5} \\ G_{12}/G_{12}^0 &= \left[(T_g - T)/(T_g^0 - T_r) \right]^{0.5} \\ S/S_0 &= (T^*)^{0.2} \\ \nu/\nu^0 &= \alpha \left[(T_g - T)/(T_g^0 - T_r) \right]^{0.5} \end{aligned} \quad (4.113)$$

where

the superscript 0—represents the dry state;

α —parameter related to moisture content, for carbon fiber-reinforced composite (when moisture is not more than 1.0%, $\alpha \approx 1.0$);

V_f —fiber volume content.

Tension and compression tests have been performed on different multi-laminate T700S/5405 material systems of different thicknesses immersed in 70 °C distilled water for 3 weeks. The ply ratio of these laminates was 0°-plies 40%, 45°-plies 50%, and 90°-plies 10%. The test results are shown in Table 4.32. The following conclusions could be drawn:

- ① Moisture absorption alone has little influence on the tension strength and modulus.
- ② Moisture absorption alone has little influence on the compression modulus; however, the compression strength of 1.5-, 2.5-, and 3.0-mm-thick laminates dropped 2.2%, 8.6%, and 5.0%, respectively.

Table 4.32 Tension and compression properties of T700S/5405 system laminate at different thickness

Properties		Nominal thickness of specimen					
		1.5 mm	$C_v / \%$	2.5 mm	$C_v / \%$	3.0 mm	$C_v / \%$
Tension strength/MPa	Dry	1410.0	3.1	1151.8	7.5	1291.1	6.0
	Wet	1326.0	6.6	124.8	3.9	1308.5	6.3
Tension modulus/GPa	Dry	81.77	3.5	64.71	3.3	71.92	3.3
	Wet	81.72	4.6	66.31	1.5	75.56	6.2
Tension Poisson's ratio	Dry	0.34	5.6	0.52	3.5	0.52	5.9
	Wet	0.36	6.7	0.53	2.8	0.53	3.3
Tension extensibility/ %	Dry	2.03	5.0	2.09	6.6	2.11	5.1
	Wet	1.90	8.8	2.17	3.6	2.01	5.9
Compression strength/MPa	Dry	560.28	7.9	716.81	7.1	752.66	6.9
	Wet	548.07	6.8	654.99	4.1	715.10	6.6
Compression modulus/GPa	Dry	79.19	8.7	61.32	2.7	67.71	5.1
	Wet	80.97	10.3	64.00	9.6	73.79	5.2
Compression Poisson's ratio	Dry	0.31	8.5	0.48	8.3	0.49	4.1
	Wet	0.32	9.4	0.48	13.4	0.50	10.6

- ③ The change of the compression strength was more pronounced in thicker laminates.

Mechanical performances tests have been performed on a stitched multi-laminate T300/QY 8911-III material system of different thicknesses immersed in 70 °C distilled water for three weeks. The specimens were divided into types A and B. The ply proportions of the type A laminate were 0°-plies 50%, 45°-plies 40%, and 90°-plies 10%. The ply proportions of the type B laminate were 0° lamina 45%, 45° lamina 40%, and 90° lamina 15%. The test results are shown in Table 4.33, and the following conclusions may be drawn:

- ① The moisture content of stitched T300/QY 8911-III laminate was approximately 1.5 times as large as that of the unstitched laminate.
- ② Moisture absorption only had little influence on the tension strength, modulus, and Poisson ratio of the stitched T300/QY8911-III laminate.
- ③ Moisture absorption alone had little influence on the compression modulus of stitched T300/QY 8911-III laminate. However, the compression strength of the 3.0-, 4.0-, and 4.5-mm-thick laminates dropped 15.3%, 3.3%, and 8.6%, respectively.
- ④ Moisture absorption alone had little influence on the in-plane shear strength of stitched T300/QY
For 8911-III laminate, however, the in-plane shear strength of 3.0-mm-thick laminates dropped by 11.3%.

Table 4.33 Mechanical properties of T300/QY8911-III system stitched laminate under different thickness

Properties		Layering and nominal thickness of specimen					
		Type A			Type B		
		3.0 mm	4.0 mm	4.5 mm	3.0 mm	4.0 mm	4.5 mm
Tension strength/MPa	Dry	631.03	565.16	601.80	498.55	671.29	707.15
	Wet	672.38	573.61	609.30	–	–	–
Tension modulus/GPa	Dry	63.21	58.59	56.88	54.97	68.11	69.85
	Wet	64.03	64.92	62.86	–	–	–
Tension Poisson ratio	Dry	0.41	0.49	0.42	0.42	0.54	0.38
	Wet	0.42	0.52	0.45	–	–	–
Tension extensibility/%	Dry	1.22	1.15	1.25	1.08	1.16	1.21
	Wet	1.20	1.05	1.16			
Compression strength/MPa	Dry	613.41	659.89	610.26	435.86	648.97	693.03
	Wet	519.59	637.94	557.81	–	–	–
Compression modulus/GPa	Dry	51.81	52.99	51.42	48.20	65.31	66.57
	Wet	54.38	54.07	52.48	–	–	–
In-plane shear strength/MPa	Dry	247.92	276.32	289.41			
	Wet	219.92	271.09	294.88			
In-plane shear modulus/GPa	Dry	13.13	16.77	17.47			
	Wet	15.37	18.11	18.25			
Flexural strength/MPa	Dry	713.33	699.77	74.61	783.13	801.58	765.60
	Wet	–	700.75	–	793.79	–	771.36
Flexural modulus/GPa	Dry	47.93	40.66	48.30	52.60	44.18	52.03
	Wet	–	40.58	–	53.41	–	51.99
Flexural failure deformation/mm	Dry	10.20	10.70	7.38	10.55	10.58	7.86
	Wet	–	10.73	–	10.45	–	8.00
Interlaminar shear strength/MPa	Dry	53.61	64.28	60.69	57.03	66.23	67.37
	Wet	53.19	62.74	58.48	–	–	–

- ⑤ Moisture absorption had little influence on the flexural performances of stitched T300/QY 8911-III laminate.
- ⑥ The interlaminar shear strength of stitched T300/QY 8911-III laminate decreased appreciably after moisture absorption.

Mechanical performances tests have been performed on nine material systems (T700S/5428, T700S/5429, T700S/5405, T700S/5228, T300/5405, T800/QY9511, T700S/QY 9511, T300/QY8911, and stitched T300/QY9512) immersed in 70 °C distilled water for 3 weeks in six different environments (-55 ± 2 °C, 23 ± 2 °C and $(50 \pm 5)\%RH$, 80 ± 2 °C and $(50 \pm 5)\%RH$, 125 ± 2 °C, 150 ± 2 °C, 170 ± 2 °C). The ply ratio in the eight unstitched laminates was 0°-plies 33%, 45°-plies 57%, and 90°-plies 10%. The ply ratio in the stitched laminate was 0°-plies 35%, 45°-plies 53%, and 90°-plies 12%.

Table 4.34 Moisture contents of nine materials systems after immersion in 70 °C distilled water for three weeks

Material	Moisture content/%	Material	Moisture content/%
T700S/5428	0.58	T800/QY9511	0.95
T700S/5429	0.46	T700S/QY9511	0.58
T700S/5405	0.67	T300/QY8911	1.11
T700S/5228	1.00	Stitched T300/QY9512	1.45
T300/5405	0.66		

The moisture contents of the nine materials systems after immersion in 70 °C distilled water for three weeks are shown in Table 4.34. The moisture content of the T700S/5429 system was lowest. The moisture content of the stitched T300/QY9512 system was highest, and approximately 3.2 times as large as that of the T700S/5429 system.

Results of testing tension and compression, and tension and compression with an open hole for nine material systems are shown in Table 4.35 and Figs. 4.107, 4.108, 4.109, 4.110.

- ① The tension strengths of the nine wet open hole specimens were very similar under the six hygrothermal environments. The tension strength of the open-hole specimen of the T700S/5405 system was slightly higher than that of other systems.
- ② The tension strength gradually declined as temperature was elevated. The tension strength of the specimens at -55 °C was basically equivalent to that room temperature. The material most sensitive to elevated temperature was T700S/5405, which at 170 °C featured a tension strength drop of 25.7%. The material most sensitive to cryogenic temperatures was T700S/5429; the tension strength at -55 °C dropped by 8.1% compared with that at room temperature. Among the nine materials, the tension strength of the T700S/5405 system was highest. The tension modulus fluctuated within a range of 20% at the six temperatures.
- ③ The Poisson's ratio at high temperature was elevated increased except for the T700S/5228 system.
- ④ The tension and the tension performance of the open-hole specimen of the stitched laminate gradually declined at elevated temperature. The corresponding strengths decreased by 17.0% and 4.9%, compared with room temperature.
- ⑤ Hygrothermal environment had a strong influence on the compression performance of the open-hole specimens for all the material systems. The residual performances of the various materials are shown in Table 4.36. The compression strength of the open-hole specimens at 170 °C decreased by more than 50%. The residual compression strength of the stitched T300/QY9512 system was only 16.6%.

Table 4.35 Test results of tension and compression and tension and compression with open hole specimens for nine material systems

Material	Test environment	Test type						
		Tension with an open hole	Tension			Compression with an open hole	Compression	
			σ_{kt} /MPa	σ_t /MPa	E_t /GPa		ν_t	σ_c /MPa
T700S/5428	-55 °C	628.3	991.5	63.36	0.46	347.2	574.5	53.50
	23 °C, 50% RH	675.5	1071.4	59.58	0.51	332.2	549.4	59.39
	80 °C, 50% RH	694.8	1045.6	3.48	0.54	283.8	466.3	54.04
	125 °C	709.4	908.4	72.12	0.55	248.0	419.2	54.54
	150 °C	717.5	934.0	68.29	0.48	204.1	358.4	54.98
	170 °C	728.5	870.1	69.32	0.53	146.0	260.1	55.31
T700S/5429	-55 °C	622.0	1037.2	59.78	0.48	348.4	543.1	50.31
	23 °C, 50% RH	636.9	1129.1	58.51	0.49	304.1	491.3	50.06
	80 °C, 50% RH	626.9	1047.8	57.03	0.53	276.6	495.8	50.73
	125 °C	654.3	990.5	68.54	0.60	263.3	433.4	47.63
	150 °C	637.1	900.0	68.66	0.59	165.3	360.0	53.55
	170 °C	636.4	863.0	68.27	0.53	135.4	234.7	44.57
T700S/5405	-55 °C	706.8	1261.2	65.60	0.50	411.8	525.9	54.84
	23 °C, 50% RH	732.5	1268.7	68.48	0.53	355.4	493.3	51.08
	80 °C, 50% RH	874.0	1151.4	63.46	0.56	306.8	485.9	52.78
T700S/5405	125 °C	722.1	1045.8	69.81	0.60	239.0	411.5	50.69
	150 °C	683.2	1004.3	64.55	0.54	120.8	409.6	52.42
	170 °C	668.9	942.3	50.69	0.45	92.0	250.7	51.04
T700S/5228	-55 °C	522.9	905.7	56.36	0.53	363.0	528.4	45.44
	23 °C, 50% RH	573.5	832.6	49.99	0.51	319.3	497.6	44.15
	80 °C, 50% RH	577.7	899.3	52.65	0.54	258.1	500.5	44.58
	125 °C	532.5	843.6	69.08	0.52	180.2	436.3	44.32
	150 °C	507.7	754.2	59.76	0.50	108.2	315.1	47.22
	170 °C	533.9	685.5	59.70	0.52	81.3	215.4	48.60
T300/5405	-55 °C	355.2	768.2	64.28	0.49	449.9	644.4	61.37
	23 °C, 50% RH	340.3	702.4	69.01	0.50	356.1	570.9	56.12
	80 °C, 50% RH	352.3	688.8	61.60	0.52	299.3	487.7	54.14

(continued)

Table 4.35 (continued)

Material	Test environment	Test type						
		Tension with an open hole	Tension			Compression with an open hole	Compression	
			σ_{kt} /MPa	σ_t /MPa	E_t /GPa		ν_t	σ_c /MPa
T800/QY9511	125 °C	331.6	650.0			233.5		55.42
	150 °C	339.0	556.6	75.70	0.53	125.1	281.1	55.32
	170 °C	331.2	476.1	70.32	0.46	91.1	210.4	58.46
	-55 °C	470.3	893.7	65.27	0.51	373.33	646.4	70.82
	23 °C, 50% RH	479.9	949.0	61.01	0.52	336.51	628.3	76.89
	80 °C, 50% RH	469.9	901.6	59.36	0.54	311.71	530.7	68.64
	125 °C	505.6	927.9	67.71	0.59	238.05	515.6	70.65
T700S/QY9511	150 °C	518.1	802.0	53.23	0.51	200.77	383.5	74.32
	170 °C	499.1	746.7	60.47	0.53	168.45	321.9	65.77
	-55 °C	591.8	968.9	54.32	0.50	404.7	651.3	62.92
	23 °C, 50% RH	584.2	956.3	55.51	0.51	338.6	636.0	71.16
	80 °C, 50% RH	608.9	956.1	59.58	0.53	317.4	476.8	60.67
	125 °C	586.2	877.4	58.72	0.53	247.8	485.4	56.09
	150 °C	640.1	870.1	51.08	0.53	216.6	413.7	53.25
T300/QY8911	170 °C	613.0	830.9	56.21	0.50	147.3	280.9	58.37
	-55 °C	312.9	743.2	60.33	0.47	378.0	649.1	52.48
	23 °C, 50% RH	329.4	673.8	63.40	0.49	380.2	675.5	59.49
	80 °C, 50% RH	329.7	672.7	58.31	0.53	353.2	605.3	56.76
	125 °C	327.0	591.7	63.93	0.51	249.5	457.7	58.97
	150 °C	317.8	556.3	71.63	0.51	168.4	255.1	60.18
	170 °C	306.9	523.9	64.05	0.52	128.3	200.4	59.29
Stitched T300/QY9512	-55 °C	299.8	577.7	56.30	0.42	376.6	576.5	49.96
	23 °C, 50% RH	323.2	536.1	57.76	0.44	341.3	550.4	46.75
	80 °C, 50% RH	334.2	506.0	61.32	0.54	249.1	432.6	44.46
	125 °C	301.7	498.5	54.72	0.43	127.1	227.8	43.72
	150 °C	291.8	396.9	58.34	0.42	76.5	139.2	47.36
	170 °C	307.4	445.2	53.79	0.46	56.8	80.4	42.13

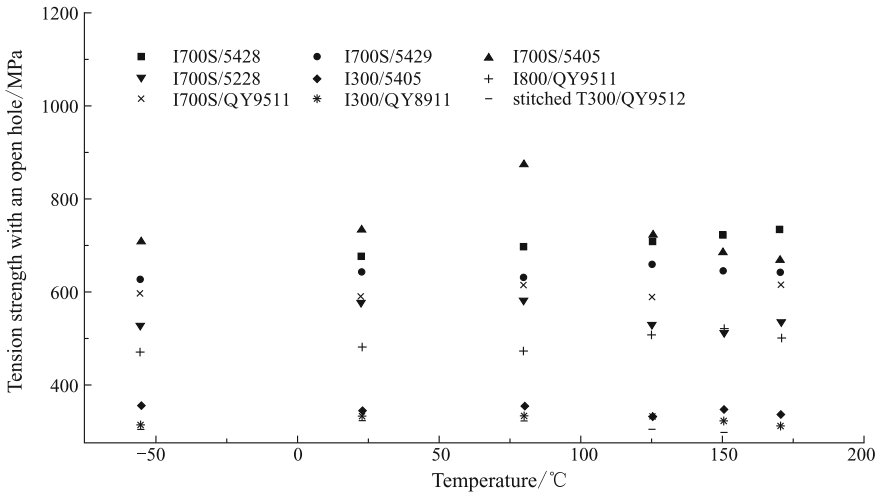


Fig. 4.107 Influence of temperature on tension strength with an open hole for nine material systems

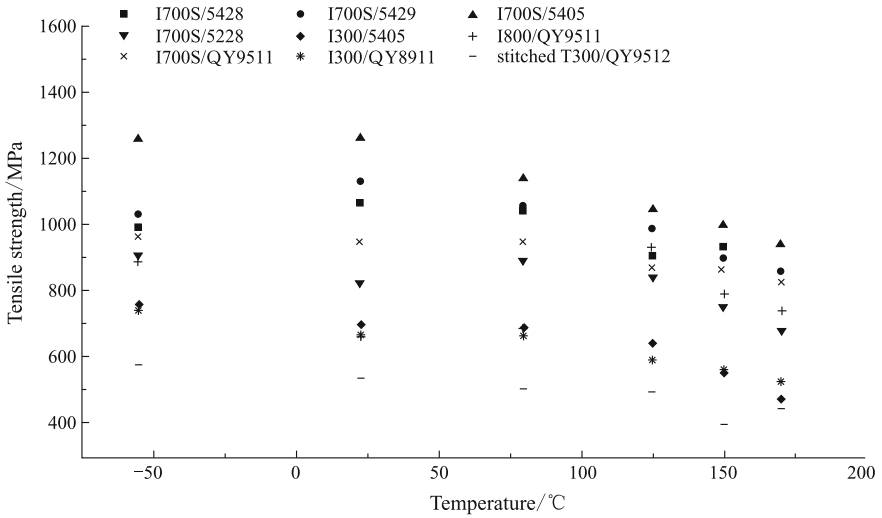


Fig. 4.108 Influence of temperature on tension strength for nine material systems

- ⑥ The hygrothermal environment also strongly affected the compression strength of the nine material systems. The compression strength at 170 °C dropped to 50% or less, and the residual compression strength of the stitched T300/QY9512 system was only 4.6%. The modulus dropped

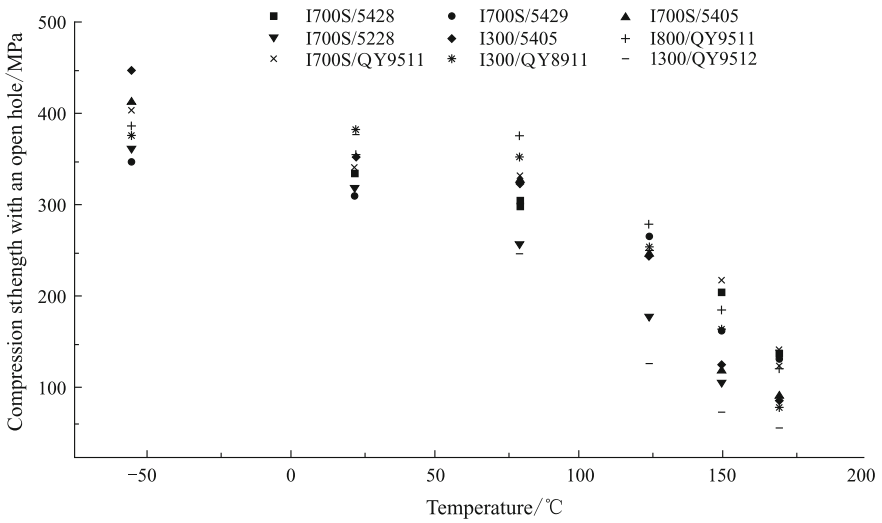


Fig. 4.109 Influence of temperature on compression strength with an open hole for nine material systems

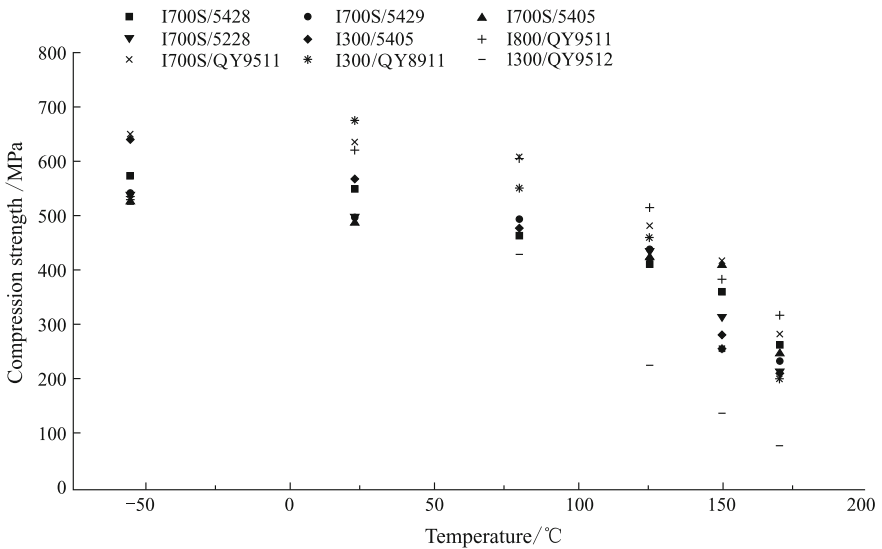


Fig. 4.110 Influence of temperature on compression strength for nine material systems

approximately 10% on average. The modulus of the T700S/QY9511 system dropped 18%.

- ⑦ The compression strength at $-55\text{ }^{\circ}\text{C}$ was equivalent to that at room temperature. The most sensitive material to cryogenic temperatures was

Table 4.36 Strength and modulus survivability of compression and compression with an open hole

Residual performance	T700S/5428					T700S/5429						
	-55 °C	23 °C, C, 50% RH	80 °C, C, 50% RH	125 °C	150 °C	170 °C	-55 °C	23 °C, 50% RH	80 °C, 50% RH	125 °C	150 °C	170 °C
$\sigma_{kc}/\%$	104.5	100	85.4	74.7	61.4	43.9	14.6	100	91.0	86.6	54.4	44.5
$\sigma_c/\%$	104.6	100	84.9	76.3	65.2	47.3	110.5	100	101	88.2	73.2	47.8
$E_c/\%$	90.1	100	91.0	91.8	92.6	93.1	100.5	100	101.3	95.1	107	89.0
Residual performance	T700S/5405					T700S/5228						
	-55 °C	23 °C, C, 50% RH	80 °C, C, 50% RH	125 °C	150 °C	170 °C	-55 °C	23 °C, 50% RH	80 °C, 50% RH	125 °C	150 °C	170 °C
$\sigma_{kc}/\%$	115.9	100	86.3	67.2	34.0	25.9	113.7	100	80.8	56.4	33.9	25.5
$\sigma_c/\%$	106.6	100	98.5	83.4	83.0	50.8	106.2	100	100.6	87.7	63.3	43.3
$E_c/\%$	107.4	100	103.3	99.2	102.6	99.9	102.9	100	101	100.4	107	110.1
Residual performance	T3000/5405					T800/QY9511						
	-55 °C	23 °C, C, 50% RH	80 °C, C, 50% RH	125 °C	150 °C	170 °C	-55 °C	23 °C, 50% RH	80 °C, 50% RH	125 °C	150 °C	170 °C
$\sigma_{kc}/\%$	126.3	100	84.0	65.6	35.1	25.6	110.9	100	92.6	70.7	59.7	50.1
$\sigma_c/\%$	112.9	100	85.4	73.3	49.2	36.9	102.9	100	84.5	82.1	61.0	51.2
$E_c/\%$	109.3	100	96.5	98.8	98.6	104.2	92.1	100	89.3	91.9	96.7	85.5

(continued)

Table 4.36 (continued)

Residual performance	T700S/5428					T700S/5429						
	-55 °C	23 °C, C, 50% RH	80 °C, C, 50% RH	125 °C	150 °C	170 °C	-55 °C	23 °C, 50% RH	80 °C, 50% RH	125 °C	150 °C	170 °C
$\sigma_{kc}/\%$	119.5	100	93.7	73.2	64.0	43.5	99.4	100	92.9	65.6	44.3	33.7
$\sigma_c/\%$	102.4	100	75.0	76.3	65.0	44.1	96.1	100	89.6	67.8	37.8	29.7
$E_c/\%$	88.4	100	85.3	78.8	74.8	82.0	88.2	100	95.4	99.1	101.2	99.7
Residual performance	T300/QY9511											
	Stitched T300/QY9512											
$\sigma_{kc}/\%$	110.3	100	73.0	37.2	22.4	16.6	-55 °C	23 °C, C, 50% RH	80 °C, 50% RH	125 °C	150 °C	170 °C
$\sigma_c/\%$	104.8	100	78.6	41.4	25.3	4.6						
$E_c/\%$	106.9	100	95.1	93.5	101.3	90.1						

T300/QY8911; the compression strength and modulus at $-55\text{ }^{\circ}\text{C}$ dropped 4.9% and 11.8%, respectively, compared with room-temperature values.

Influence of Hygrothermal Environment on Composite Failure Mode

The hygrothermal environment not only affects the physical and mechanical properties of composite laminate, but also affects failure modes. The failure modes at low temperatures and in the dry state are related to basic failure of the matrix itself. The failure modes of wet composites at room temperature involve hybrid failure of a matrix/interphase. The failure modes of wet composites at elevated temperature involve failure of the fiber/matrix interface.

Hygrothermal Stress Analysis

The hygrothermal environment seriously affects the stress distribution of composite structure and composite/metal hybrid structures. The response of the steady or quasi-steady hygrothermal field in structural stress analysis should be dealt with by linear superposition, neglecting coupling. Thermal strain and wet strain can be considered as the initial strain, and the equivalent hygrothermal initial load can be created. The hygrothermal initial load should then be superposed on the mechanical load. The displacement and total strain can be resolved by FEMs and the stress distribution of the structure can be resolved by subtracting the initial strain from the total strain.

The initial strain and the equivalent hygrothermal initial load caused by the hygrothermal environment can be calculated from the following equations.

- ① For an isotropic material:

$$\begin{aligned}\varepsilon_T &= \alpha\Delta T \\ \varepsilon_C &= 0\end{aligned}\tag{4.114}$$

$$\{R_T\}^e = \Delta t \iint [B]^T [D] \{\varepsilon_T\} dx dy$$

- ② For an anisotropic material:

$$\begin{aligned} \begin{pmatrix} \varepsilon_{1T} \\ \varepsilon_{2T} \\ 0 \end{pmatrix} &= \begin{pmatrix} \alpha_1 \Delta T \\ \alpha_2 \Delta T \\ 0 \end{pmatrix} \\ \begin{pmatrix} \varepsilon_{1C} \\ \varepsilon_{2C} \\ 0 \end{pmatrix} &= \begin{pmatrix} \beta_1 \Delta C \\ \beta_2 \Delta C \\ 0 \end{pmatrix} \\ \{R_T\}^e &= \Delta t \iint_e [B]^T [T]^T [Q] \{\varepsilon_T\} dx dy \\ \{R_T\}^e &= \Delta t \iint_e [B]^T [T]^T [Q] \{\varepsilon_T\} dx dy \\ \{R_C\}^e &= \Delta t \iint_e [B]^T [T]^T [Q] \{\varepsilon_C\} dx dy \end{aligned} \quad (4.115)$$

where

- α —thermal expansion coefficient of material, $1/^\circ\text{C}$;
- ΔT —increment of temperature, $^\circ\text{C}$;
- ΔC —increment of moisture content;
- α_1 —longitudinal thermal expansion coefficient of laminate, $1/^\circ\text{C}$;
- α_2 —transverse thermal expansion coefficient of laminate, $1/^\circ\text{C}$;
- β_1 —longitudinal wet swelling coefficient of laminate;
- β_2 —transverse wet swelling coefficient of laminate;
- ε_T —initial strain caused by temperature;
- ε_C —initial strain caused by moisture absorption;
- $\{R_T\}^e$ —equivalent thermal load at element node;
- $\{R_C\}^e$ —equivalent wet swelling load at element node.

4.10.4 Hygrothermal Aging Response

The strength and stiffness performance of resin matrix composites will vary considerably with extended usage-time, especially in certain hygrothermal environments. Hygrothermal aging of fiber-reinforced composites is a gradual degradation process caused by the combined action of moisture uptake, temperature, and stress. Fibers and the fiber/matrix interface are degraded by physical/chemical reactions. During the moisture absorption process, a swelling stress will be introduced to the interior of composites. A greater swelling stress might be introduced owing to rapid desorption of the surface layer of wet structures under thermal spiking. Under this repeated interior stress, at a certain threshold stress, cracking will occur followed by crazing. The moisture re-absorption and re-desorption rates will be affected by the

crazing, and finally, macroscale cracks will form. Therefore, the hygrothermal aging response of any selected composite material system should be investigated at the design stage. However, this theoretical analysis is difficult owing to uncertainties of the environmental and the coupling effect between hygrothermal stress and exterior loading. In general, experimental methods are used to study these factors based on ground environmental aging, accelerated laboratory aging and aging in actual flights. The experimental data are globally analyzed to obtain design criterion for hygrothermal aging [1, 2, 13].

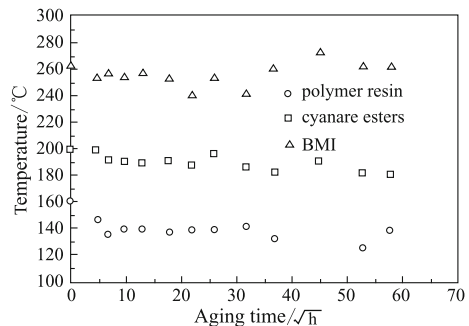
4.10.4.1 Influence of Hygrothermal Aging on Composite Physical Properties

In certain hygrothermal environments over a long period, matrix constituents will undergo chemical reactions, particularly at elevated temperatures. The rate of these reactions will be affected by many factors, including the chemical components of the materials, the aging temperature, fiber volume fraction, and ply stacking sequence of the laminate. For any composite system, the main factors are aging time and temperature.

There have been few investigations on the effect of hygrothermal aging on the physical properties of composites. The changes of T_g with aging time for three material systems under a 70–85%RH aging environment are shown in Fig. 4.111. The T_g of the polymer matrix composite was considerably affected by aging. From the start of aging to 50 h, T_g declined lineally; a maximum decrease of 25 °C was found, after which the T_g stabilized. Aging up to 900 h, the T_g underwent a second drop of approximately 10 °C which remained stable with aging for 2700 h. For a cyanate ester matrix composite, the T_g showed a slow reduction with increasing aging time. After about 1400 h of aging, the T_g dropped by 20 °C and then stabilized. For BMI composite, aging time had hardly any effect on T_g .

The influences of hygrothermal aging on the thermal expansion coefficients of a composite matrix can be determined as follows:

Fig. 4.111 Change of T_g with aging time under 70 °C/85% RH environment



$$\alpha'_m = \alpha_m [1 + \Delta\alpha_{a1} (a_1)^{n_{\alpha a1}}] [1 + \Delta\alpha_{a2} (a_2)^{n_{\alpha a2}}] \quad (4.116)$$

$$\alpha_1 = \frac{T_{gd} - T_g^0}{T_{gf} - T_g^0}$$

$$\alpha_2 = \frac{m_0 - m}{m_0 - m_f}$$

where

α'_m	matrix thermal expansion coefficient after accounting for aging effects;
α_m	matrix thermal expansion coefficient at room temperature in dry state;
α_1	degradation parameter of the crosslinking mechanism;
α_2	parameter of matrix mass change;
T_{gd}	measured glass transition temperature at room temperature in dry state;
T_g^0	measured glass transition temperature at initial aged state;
T_{gf}	measured glass transition temperature at final aged state;
m_0	mass of a small neat matrix specimen at initial aged state;
m	mass of a small neat matrix specimen at room temperature and dry state;
m_f	mass of a small neat matrix specimen at final aged state.
$\Delta\alpha_{a1}, \Delta\alpha_{a2}, n_{\alpha a1}, n_{\alpha a2}$	fitting parameters based on the change of a_1 and a_2 data.

The matrix wet expansion coefficient can also be modified by an analogous methodology.

4.10.4.2 Influence of Hygrothermal Aging on Mechanical Properties of Laminates

The aging of resin matrix composites involves degradation (degeneration) processes. During this process, mechanical properties, in particular matrix controlled properties, such as shear and transverse behavior, are markedly affected.

The thermal aging properties of HT3/QY8911 and HT3/5405 unidirectional laminates are shown in Tables 4.37 and 4.38. Test results of the interlaminar shear strength for a polymer matrix composite at different temperatures after 70–85% RH environmental aging are shown in Figs. 4.112 and 4.113. The influence of aging time and moisture content on interlaminar shear strength at room temperature was slight; however, the interlaminar shear strength at 100 °C decreased linearly with increasing moisture content. For every 1% increase in moisture content, the interlaminar shear strength dropped by approximately 7.9 MPa. The hygrothermal aging

Table 4.37 Thermal aging properties of T300/QY8911 unidirectional laminate

Aging time	τ_b^i /MPa		σ_b^f /MPa	
	25 °C	150 °C	25 °C	150 °C
0	14.1	77.0	1916	1752
100	118.1	94.4	1925	1748
240	113.2	84.1	1876	1759
400	14.8	92.2	1819	1700
710	117.5	89.1	1914	1684
1000	14.7	88.0	1941	1684

Table 4.38 Thermal aging properties of T300/5405 unidirectional laminate

		Aging time /h			
		0	310	607	1000
s_b^i (RT)	Average value/MPa	96.8	90.0	88.4	93.1
	Standard deviation/MPa	5.9	3.8	3.6	3.9
	C_v /%	6.1	4.2	4.0	5.2
t_b^i (130 °C)	Average value/MPa	81.2	82.2	81.5	84.9
	Standard deviation/MPa	1.1	1.8	4.9	1.8
	C_v /%	1.4	2.3	6.1	2.1
s_b^f (RT)	Average value/MPa	1770	1764	1876	1865
	Standard deviation/MPa	56.0	29.9	75.4	35.4
	C_v /%	3.2	1.7	4.0	1.9
s_b^f (130 °C)	Average value/MPa	1300	1323	1396	1437
	Standard deviation/MPa	58.7	56.6	86.6	76.2
	C_v /%	2.6	2.4	3.5	3.0
S (RT)	Average value/MPa	113.6	108.2	104.5	97.2
	Standard deviation/MPa	1.3	1.6	6.7	2.3
	C_v /%	1.2	1.5	6.4	2.4
S (130 °C)	Average value/MPa	96.3	102.6	103	99
	Standard deviation/MPa	0.2	1.0	2.6	1.3
	C_v /%	4.3	1.1	1.5	1.4
G_{12} (RT)	Average value/GPa	1.75	4.51	4.60	4.57
	Standard deviation/GPa	0.06	0.08	0.09	0.05
	C_v /%	1.4	1.7	2.0	1.1
G_{12} (130 °C)	Average value/GPa	3.1	3.8	4.0	4.1
	Standard deviation/GPa	0.2	0.6	0.1	0.1
	C_v /%	5.1	1.6	2.7	2.7

responses of BMI matrix composite are shown in Figs. 4.114 and 4.115. When the moisture content was less than 0.6% (corresponding to 70 h of aging), there was little change in the interlaminar shear strength; however, for a moisture content greater than 0.6%, the interlaminar shear strength showed a marked decrease. The interlaminar shear strength of the moisture saturation state dropped by approximately 50% compared with that of the dry state.

Fig. 4.112 Change of interlaminar shear strength with aging time for polymer matrix composite after 70–85% RH environmental aging at different temperatures

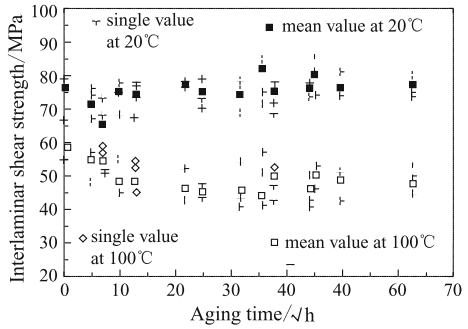


Fig. 4.113 Change of interlaminar shear strength with moisture content for polymer matrix composite after 70–85% RH environmental aging at different temperatures

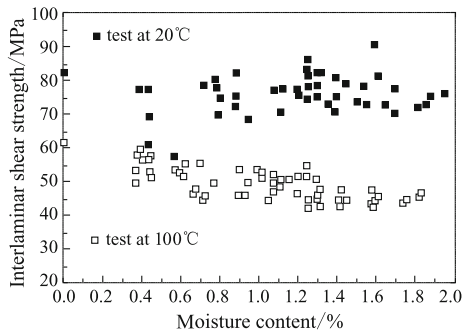


Fig. 4.114 Change of interlaminar shear strength with aging time for BMI matrix composite after 70–85% RH environmental aging at different temperatures

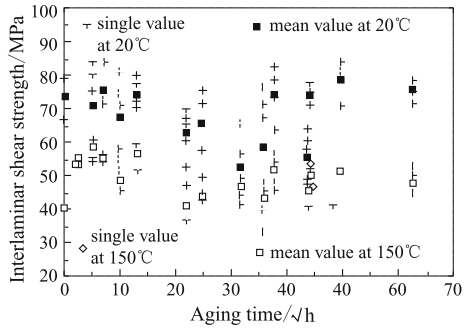
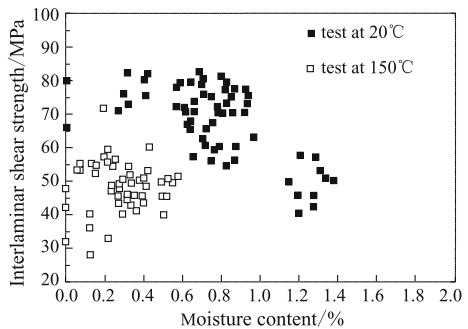


Fig. 4.115 Change of interlaminar shear strength with moisture content for BMI matrix composite after 70–85% RH environmental aging at different temperatures



This may be explained by the reaction between the water and matrix requiring a certain time. Thus, controlling moisture content is a design criterion for application of MBI matrix composites in structures.

4.10.4.3 Prediction of Composite Aging Effects

Physical Aging

When a polymeric matrix material is used below its glass transition temperature for a long time, the mechanical properties will change markedly. This change is termed physical aging. During the physical aging process, the material becomes stiffer, with decreased compliance and an increased modulus. The physical aging responses of resin matrix composites have received considerable research attention. The results of various investigations have shown that the matrix-dominated properties of continuous fiber-reinforced composite (e.g., the shear and transverse responses) are most seriously affected by physical aging in a similar manner to that of a pure polymer.

Physical Aging of Polymers

(1) Influence of aging time

The polymeric compliance varies with aging time according to:

$$S(t) = S_0 e^{(t/t_e)^\beta}$$

$$\tau(t_e) = \tau(t_{\text{ref}})/a_{t_e} \quad (4.117)$$

$$a_{t_e} = \left(\frac{t_{\text{ref}}}{t_e}\right)^\mu$$

$$\mu = -\frac{d \lg a_{t_e}}{d \lg t_e}$$

where

- $S(t)$ compliance at time t ;
- S_0 initial compliance;
- t_e aging time;
- τ relaxation time;
- T time;
- t_{ref} reference aging time;
- a_{t_e} aging time shift factor at aging time;
- β shape parameter;
- μ shift rate.

Note from Eq. (4.117) that if the initial compliance S_0 , shape parameter β , shift rate μ and relaxation time τ at reference aging time t_{eref} of the polymer are known, then the compliance at any time may be determined. If $t_e > t_{\text{eref}}$, then $a_{t_e} < 1$; otherwise, $a_{t_e} > 1$. In the case of $t_e > t_{\text{eref}}$, the relaxation time at t_e is also greater than that at the reference aging time [$\tau(t_e) > \tau(t_{\text{eref}})$]. This relation shows that at a given time the modulus of the material is higher and the compliance is lower [$S(t; t_e) < S(t; t_{\text{eref}})$].

For most polymers, if the material is being used at temperatures close to its T_g , the material changes into an equilibrium state in a relative short time. The time required to achieve the equilibrium state is known as the equilibrium aging time.

The shift factor, μ characterizes the influence of aging on material properties. For the same aging time a larger value of μ indicates a smaller compliance change. Thus, the shift factor μ can be used as a screening parameter for selection of materials. Materials with larger μ values should be chosen. In general, experimental results have shown that before the aging equilibrium $\mu \approx 1$ and after the aging equilibrium $\mu \approx 0.1$. These results indicate the dramatic change of materials in the aging equilibrium state. Thus, in the design stage of polymer matrix composite structures, materials with larger μ value should be selected, while avoiding aging to an equilibrium state during the full life period, particularly in structures for use in high temperature applications.

(2) Influence of aging temperature

Although the shift factor μ over a large temperature range is constant, in fact, both μ and a_{t_e} are functions of temperature. In general, the relationship of the time temperature-aging time shift factor can be expressed as:

$$\lg a = \lg a_{t_e} + \lg \bar{a}_T \quad (4.118)$$

where \bar{a}_T is a time temperature shift factor, i.e., a function of temperature and aging time at temperatures below T_g .

The relationship between \bar{a}_T and $\mu(T)$ can be expressed as:

$$\frac{\bar{a}_{T_1/T_2}^{t_{e2}}}{\bar{a}_{T_1/T_2}^{t_{e1}}} = \left(\frac{t_{e2}}{t_{e1}} \right)^{\mu(T_2) - \mu(T_1)} \quad (4.119)$$

where $\bar{a}_{T_1/T_2}^{t_{e1}}$ —time temperature shift factor between temperature T_1 and T_2 at aging time t_{e1} .

Thus, if the $\mu(T)$ value or its expression and the time temperature shift factor at a single aging time are given, then \bar{a}_T at any aging time can be calculated. Therefore, the shift factor, μ , and the time temperature shift factor, \bar{a}_T , have an effect on aging time.

Aging Response of Unidirectional Laminate

The effective compliance matrix of a unidirectional laminate under plane stress condition can be described as:

$$[\bar{S}] = [T]^{-1}[S][T] \quad (4.120)$$

where

$[\bar{S}]$ —effective compliance matrix;

$[S]$ —compliance matrix with respect to the fiber coordinate system;

$[T]$ —transformation matrix.

The elastic stress–strain relation under in-plane loading is given by:

$$\begin{bmatrix} \varepsilon_{xx} \\ \varepsilon_{yy} \\ \varepsilon_{xy} \end{bmatrix} = [\bar{S}] \times \begin{bmatrix} \sigma_{xx} \\ \sigma_{yy} \\ \sigma_{xy} \end{bmatrix} \quad (4.121)$$

Experimental studies of polymer matrix composites have shown that the transverse compliance S_{22} and the shear compliance S_{66} are related to time temperature and subject to physical aging. Their values can be determined by Eq. (4.122), such that in a functional form:

$$\begin{aligned} S_{22}(t) &= f(S_{22}^0, \beta_{22}, \tau_{22}(t_{\text{ref}}), \mu_{22}, t) \\ S_{66}(t) &= f(S_{66}^0, \beta_{66}, \tau_{66}(t_{\text{ref}}), \mu_{66}, t) \end{aligned} \quad (4.122)$$

Note from Eq. (4.122), the transverse and shear compliance of composite unidirectional laminates are independently described by four viscoelastic parameters, namely the initial compliance, shape parameter, relaxation time at a given reference aging time, and shift factor. For any given material the four independent parameters may be determined by short-term aging tests in the laboratory.

Equation (4.121) is rewritten, accounting for time relativity as:

$$\begin{bmatrix} \varepsilon_{xx}(t) \\ \varepsilon_{yy}(t) \\ \varepsilon_{xy}(t) \end{bmatrix} = [\bar{S}(t)] \begin{bmatrix} \sigma_{xx} \\ \sigma_{yy} \\ \sigma_{xy} \end{bmatrix}, \quad (4.123)$$

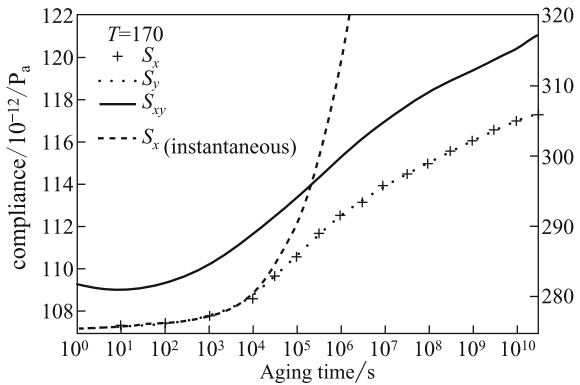
$$\bar{S}_{ij}(t) = f(\theta, S_{ij})$$

Investigations have shown that the compliance of 0° -ply laminates shows essentially no change with aging time, and that the response of other angle plies shows an increasing trend with angle. The compliance change is highest for 90° -ply laminates.

Table 4.39 Viscoelastic parameters, transverse and shear compliance of IM7/8320 material system

Viscoelastic parameter	S_{22}	S_{66}
μ	0.77	0.93
β	0.416	0.456
τ	1.19×10^6 s	4.31×10^5 s
S_0	750×10^{-9} Pa ⁻¹	1364×10^9 Pa ⁻¹
t_{eref}	3.24×10^4 s	3.24×10^4 s
Elastic parameters:	$S_{11} = 5.75 \times 10^{-91}$ /psi	$\nu_{12} = 0.348$

Fig. 4.116 Predicted aging response of IM7/8320 system



Aging Response of Laminate

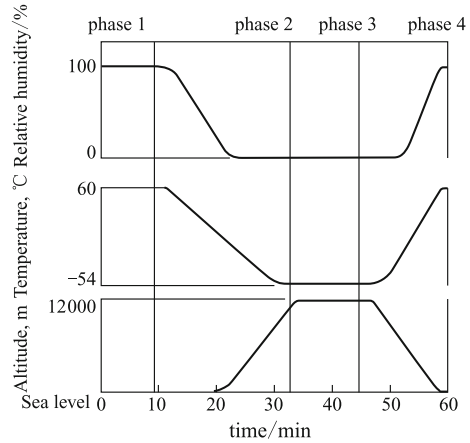
To determine the influence of physical aging on composite properties, first, the transverse and shear compliance in each lamina self-coordinate system under a specific aging environmental condition is determined. These values are transformed in the laminate coordinate system, and finally the laminate response is resolved by laminate theory.

The viscoelastic parameters, transverse and shear compliance of IM7/8320 composite lamina, are listed in Table 4.39. The estimated aging response for a quasi-isotropic laminate $[0/\pm 45/90]_s$ IM7/8320 is illustrated in Fig. 4.116. The figure shows that although the quasi-isotropic laminate is fiber-dominated, the compliance changes by 8–10% over a 10-year aging period. This type of change must be considered in the composite structure design stage.

4.10.4.4 Aging Test Results of Boeing Commercial Group

The influence of environmental exposure on the performance of three composite material systems is experimentally investigated. More than 8000 standard specimens made from T300/5208, T300/5209, T300/934, machined according to the

Fig. 4.117 Laboratory accelerated aging scheme of Boeing Commercial Group



required test methods, were exposed for approximately 13 years. The exposure tests included ground exposure, flight travel exposure, and accelerated laboratory aging, which simulated the change of temperature, humidity, and pressure during aircraft flight. The ground-based exposure tests were performed at Dallas, NASA Dryden, Honolulu, and Wellington. Aloha Airlines, Air New Zealand Ltd., and Southwest Airlines were selected for flight exposure studies. The laboratory accelerated aging results are shown in Fig. 4.117.

On the basis of global analysis of the test results, the following recommendations for composite structural design were proposed:

- ① The tension and flexure strength at room temperature after aging for the three materials showed a slight overall increase. At elevated temperatures, the results were mixed. For the T300/5209 and T300/934 systems the flexure and tension strength decreased slightly. For the T300/5208 system, both these properties were greater their baseline strength. The T300/934 tension strength also increased. However, in all cases, the differences were relatively small.
- ② Room-temperature compression strength dropped in general. At the end of 10 years' exposure, all three materials showed decreases of approximately 30%. The elevated temperature residual strength was likely seriously decreased; however, the exact test data could not be determined owing to the grab-tab failure.
- ③ The short-beam shear displayed a peculiar pattern for residual strength in both room and elevated temperature tests on all three material systems. The drop of the shear strength was largest after 1, 2, and 3 years of exposure; lesser degradation was found after 5 years exposure; however, the room-temperature residual strength increased slightly, and strength at elevated temperatures remained at or near their baseline levels after 10 years of exposure.

- ④ Accelerated laboratory aging can be useful for predicting the relative durability of composite materials. Accelerated aging over a 6-month aging period was sufficient to predict changes in the properties of all three materials systems.
- ⑤ Strength tests after aging at both room and elevated temperatures should be performed.

4.10.4.5 Accelerated Hygrothermal Aging Scheme for Fighter Aircraft and Test Results

In general, the designed life of fighter aircraft is 5000 flight hours, or 20–30 years. Complete simulation of both the mechanical and environmental loading history is the most credible evaluation; however, this would be impractical. Acceleration of the actual temperature/humidity time history can be used to obtain the accelerated hygrothermal aging results. Therefore, a large amount of comparable data can be accumulated and the development period for structures can be shortened and the test costs reduced. Furthermore, individual test results can be very easily interpreted and estimated.

In this section, based on the flight environment and service mission of aircraft in China, accelerated hygrothermal aging and test results for composite components of certain fighter aircraft are introduced.

(1). Basis for Establishing Scheme

On the basis of a typical mission profile, involving 5000 flight hours over 20 years, an accelerated aging program is developed.

(2). Developing Requirements and Basic Rules

- ① Accelerated tests should yield the same results for composite degradation and residual strength compared with that resulting from the real-time history, or give more conservative results than those from experiments.
- ② The actual aircraft usage environment should be reflected reasonably.
- ③ For accelerated aging, the response of thermal spiking caused by aerodynamic heating should be considered because an elevated temperature environment will have a considerable influence on composite properties over the long term.
- ④ The greatest test acceleration may be achieved by compressing the simulated ground standing time as much as possible. The ambient environmental exposure over 20 years may be simulated by accelerated tests over one year.
- ⑤ The selected accelerated conditions should not have any additional effects on composites. For BMI matrix systems, an accelerated temperature of 70 °C is appropriate.

(3). Flight Temperature and Humidity Profiles and Their Simulation

In the accelerated spectrum, the temperature profile of composite structures subjected to high loads and sites that experience elevated temperatures should be considered. Elevated temperatures may approach the glass transition temperature of the resin. Elevated temperatures below the glass transition temperature will also diminish the ability of the resin matrix to support fibers against compression buckling and load transfer from fiber to fiber.

Testing should include low-temperature environments; however, these effects are smaller and may be neglected to reduce test time and cost.

The time of flight missions can be described by four stages, namely, ground running, climbing, cruising, gliding and landing. Representative extreme temperature and humidity profiles may be chosen for each of these stages. The detailed conditions are as follows:

- ① Slide running: $M = 0.6$, $T = 20\text{--}30\text{ }^{\circ}\text{C}$; $M = 0.6\text{--}0.95$, $T = 60\text{ }^{\circ}\text{C}$; $M = 1.8$, $T = 110\text{ }^{\circ}\text{C}$; $M \geq 2.0$, $T = 125\text{ }^{\circ}\text{C}$;
- ② On the ground: $M < 0.6$, environmental humidity is 95%; $M = 0.6\text{--}0.8$ (flight altitude $H = 0\text{--}5\text{ km}$), 50% RH; $M = 0.8\text{--}1.8$ ($H = 11\text{--}15\text{ km}$), 0% RH;
- ③ Change of air pressure can be neglected and pressure was not simulated in the accelerated aging scheme;
- ④ One symmetrical axis may be used to describe sliding/take-off/climbing/cruising/gliding/landing processes, as shown in Fig. 4.118.
- ⑤ The overall flight time should be determined based on Fig. 4.119. According to flight numbers the flight characteristics (M number, temperature, humidity) may be cycled at the same amplitude. This accelerated model closely replicates the situation of a real flight in terms of the elevated temperatures and the time of the temperature changes.
- ⑥ The test time may be shortened by acceleration for $M = 0\text{--}0.6$, as for the case of ground standing.

Fig. 4.118 Symmetrical assumption

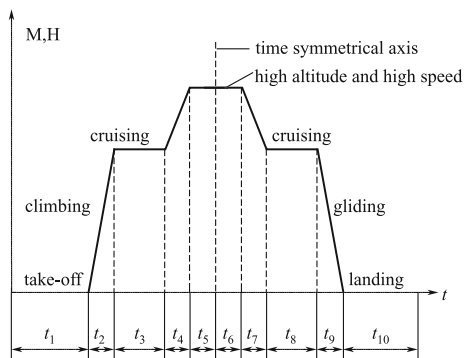
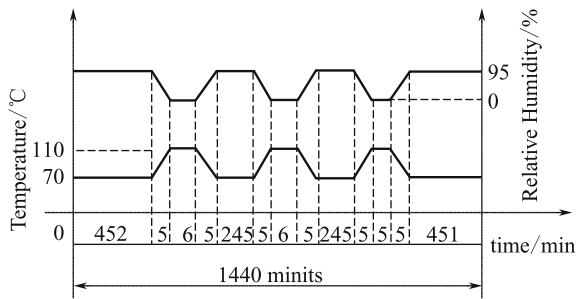


Fig. 4.119 Accelerated hydrothermal scheme



(4). Accelerated Aging Methods for Aircraft at Rest on the Ground

It may be assumed that aircraft are exposed to open air on the ground, which should result in more conservative test results. The effects of ambient temperature, humidity, and solar radiation heating should be considered for outdoor standing conditions.

The airfield temperature and humidity from Guangzhou and Beijing airfield over half a year were adopted, respectively. Thus, conditions of 70 °C/95%RH were chosen for the accelerated testing environment. A ground standing time of one year was simulated by accelerated hydrothermal aging over 14 days.

(5). Developed Accelerated Hydrothermal Aging Testing Scheme

The flight life only accounts for about 3% of the total life of a fighter aircraft. In the accelerated testing the moisture recovery between flight intervals and maximum acceleration from rest on the ground are considered adequately. For climbing, high-speed cruising, and gliding, a real simulation may be adopted.

The developed accelerated testing scheme is illustrated in Tables 4.40 and 4.41 and Fig. 4.119. One cycle covers 1 day, and an accelerated laboratory aging of 268 days can be used to simulate the hydrothermal history of a fighter composite structure with a service life of 20 years and 5000 flight hours.

(6). Test Results

Tests of the mechanical properties of 312 specimens made from the HT3/QY8911 material system subjected to the hydrothermal aging testing procedures described above were performed. The tests included tension, compression, bend, shear, bond-joint, interlaminar tension–shear, single bolt-joint measurements for multi-laminates and tension, compression, bend, shear measurements for sandwich constructions.

The test results showed:

- (1) Tension strength after hydrothermal aging did not decrease, in fact a slight increase was found.
- (2) Compression strength after aging was markedly decreased.
- (3) Interlaminar shear strength after aging showed the most serious decrease.
- (4) Bearing strength of bolt joints after aging showed a large decrease of approximately 15%.

Table 4.40 Accelerated hygrothermal aging spectrum

t_i	Temperature spectrum		Humidity spectrum		Remarks:
	Durative time/min	Temperature /°C	Durative time/min	Relative humidity /%(RH)	
t_1	452	70	450	95	① “2 + 5” represents humidity decrease from 95%RH to 50%RH within 2 min, then from 50%RH to 0% within 5 min. ② Highest temperature: +110 °C. ③ Lowest temperature: +70 °C ④ Maximum humidity: 95% RH ⑤ Minimum humidity: 0% RH ⑥ Rate of temperature increase/decrease: 8.0 °C/min
T_2	5	70–110	2 + 5	95–50–0	
t_3	6	110	6	0	
t_4	5	110–70	5	0–95	
t_5	245	70	243	95	
t_6	5	70–110	2 + 5	95–50–0	
t_7	6	110	6	0	
t_8	5	110–70	5	0–95	
t_9	245	70	243	95	
t_{10}	5	70–110	2 + 5	95–50–0	
t_{11}	5	110	5	0	
t_{12}	5	110–70	5	0–95	
t_{13}	451	70	451	95	

Table 4.41 Accelerated hot–wet spectrum aging results of laminates and sandwich construction

Strength properties	Baseline value	Accelerated hot–wet spectrum aging
Compression/MPa	525.3	500.4
Tension/MPa	606.7	660.1
SBS/MPa	68.2	46.7
Interlaminar shear/MPa	4.3	13.3
Bearing/MPa	104.1	851.1
Flatwise tension/MPa	2.1	2.1
Core shear/MPa	1.1	1.0
Core shear modulus/MPa	39.6	38.7

(5) Properties of the sandwich construction after aging were unchanged with the exception of the facing modulus.

4.10.4.6 Accelerated Hygrothermal Aging Spectrum for Transport Airplane and Test Results

Aerodynamic heating effects can be neglected for investigations of hygrothermal aging response of composite structures used in transport airplanes. The accelerated aging spectrum may be developed based on the ground standing environment. A coastal tropical environment was simulated, and 80%RH adopted as the average humidity. The accelerated environment was 70 °C/100%RH (distilled water

immersion). On the basis of the acceleration principle, 1 year of the natural environment could be simulated by 28 days of in the accelerated environment. The effects of midday solar radiation in June, July, August, and September were considered. If the irradiation time each day is 2 h, and the irradiation temperature is 50 °C, and then the total irradiation time of each month is 60 h, or 240 h in 4 months. Therefore, 1 year of ambient environmental aging could be simulated using our accelerated testing method for 38 days. This scheme involved the following steps:

$$4 + \textcircled{1} + 4 + \textcircled{1} + 4 + \textcircled{2} + 4 + \textcircled{2} + 4 + \textcircled{2} + 4 + \textcircled{1} + 4 + \textcircled{1} \quad (4.124)$$

where

- 4—Immersion in 70 °C/100% RH (70 °C distilled water immersion) for 4 days;
- —50 °C heating for 1 day;
- ②—50 °C heating for 2 days.

For an aging duration of 3 years, the above spectrum may be repeated three times.

Ambient environmental aging for 1 and 3 years was performed at an environmental experiment field in Hainan Province in China. The corresponding accelerated aging was performed in a laboratory of the Aircraft Strength Research Institute. The test results are shown in Tables 4.42 and 4.43. The test results indicated:

- ① Ambient aging has no measurable influence on tensile and compressive strength.
- ② Ambient aging has a large influence on short-beam shear (SBS) strength. The SBS strength after 1 and 3 years of ambient aging decreased by 26.5% and 37.0%, respectively. The shear strength of single- and double-lag bonds after 1 and 3 years of ambient aging decreased by 45.1% and 12.7%, and 51% and 30.2%, respectively. The tension–shear strength after 1 and 3 years of ambient aging decreased by 9.8% and 30.2%, respectively.

Table 4.42 Ambient aging and accelerated laboratory aging results of laminates

Strength properties	Baseline value	1 year ambient aging	3 years ambient aging (unpainted)	3 years ambient aging (painted)	1 year accelerated aging	3 years accelerated aging
Compression/MPa	525.3	533.3	659.7	695.6		482.8
Tension/MPa	606.7		662.4	682.6		
SBS/MPa	68.2	50.1	43.0		65.9	55.1
Bonded I/MPa	37.7	20.7	18.5			
Bonded II/MPa		32.9	26.3			
Tension–shear/MPa	4.3	12.9	11.8			

Table 4.43 Ambient aging and accelerated laboratory aging results of sandwich construction

Strength properties	Baseline value	1 year ambient aging	3 years ambient aging (unpainted)	3 years ambient aging (painted)	1 year accelerated aging	3 years accelerated aging
Flatwise compression ($H = 19$)/MPa	3.62	3.49	2.96			
Flatwise compression ($H = 44$)/MPa	2.88	3.03	2.97			
Core shear ($H = 19$)/MPa	1.21	1.23	0.77	0.76		
Core shear ($H = 44$)/MPa	1.11	1.04	1.03	1.06		
Core shear modulus ($H = 19$)/MPa	39.2	33.7	45.0	44.4		

- ③ Ambient aging had little influence on the properties of the sandwich construction. The residual strength after accelerated ambient aging was higher than that of ambient aging. This indicates that the above-mentioned accelerated ambient aging scheme is less conservative than ambient conditions. It is recommended that to simulate the aging effects of 1 year, the testing method described in this section may be repeated 2 or 3 times.

4.10.5 *Protection of Composite Structures in Corrosive Environments*

Aircraft composite structures in service may encounter a range of environmental conditions, including temperature, humidity, rain and snow, sun light, lightning strikes, wind borne sand, dust, salt-fog, noise, and industrial pollution. These conditions may degrade composite structures [1, 2, 13].

This process may be considered to be a corrosive process. However, there are no satisfactory explanations of the corrosive mechanisms of composites because of their complexity. The relationship between corrosion–strength–time is difficult to predict. In service, aircraft structures may be affected by the exterior environments, and interior fuel, hydraulic fluid, refrigerants, and sealants. Acidic and alkali substances may be introduced in fabrication and service processes. Furthermore, composites are considered to be high electrode potential materials; thus, in connection with a low electrode potential materials galvanic erosion may occur. Corresponding protection methodologies should be considered during the

composite structure design. These protective measured should also be tested to ensure the integrity of the composite structure.

4.10.5.1 Control of Corrosion in Composites

(1) Corrosive Effects of Environment on the Constituents of Composites

The following effects may occur to constituents of composites exposed to corrosive environments: corrosion of the resin matrix, reinforced fiber, interface, and corrosive fatigue. The chemical erosion behaviors of general thermoset resins are given in Table 4.44. Epoxy resin matrices used for aircraft structures appear to have good corrosion resistance against acid and alkali.

(2) Influence of Environmental Media on Mechanical Performance of Composites

The influence of hygrothermal aging on composite performance have been discussed in detail in 4.10.4. On the basis of experiments and usage experiences, the influences of other corrosive agents in the aging environment can be summarized as follows:

- ① Composites are not susceptible to corrosive liquids, such as interior fuel, hydraulic fluid, and antifreeze. Hence, the influence of these liquids can be neglected.
- ② Damage caused by ultraviolet radiation is a slow cumulate process. This type damage can be neglected if the protective coating of the structural surface is in good condition. If the surface coating brushes off, a new layer of coating should be applied to the surface. The most feasible method is to spray paint an acrylate paint. If a varnish is adopted an appropriate ultraviolet absorber should be applied. Light colored paints are more effective. If no protecting coat is applied, ultraviolet radiation

Table 4.44 Anti-chemical erosion behaviors of typical thermoset resins

Medium	Phenol ether	Polyester	Epoxy (amine cure)	Epoxy (acid anhydride cure)
Thin acid	Slight corroded	Slight corroded	Uncorroded	Uncorroded
Strong acid	Eroded	Eroded	Eroded	Slight corroded
Thin alkali	Slight corroded	Slight corroded	Uncorroded	Slight corroded
Strong alkali	Decomposed	Decomposed	Slight corroded	Eroded
Solvent	Decomposed by some solvent	Eroded	Anti-erosion	Anti-erosion

might have an effect on laminate performance. The effects of ultraviolet radiation on the modulus of unidirectional laminate have been investigated by MBB Company.

The results showed that under 12260–40866 equivalent hours of solar irradiation the specimen tensile stiffness dropped approximately 6–10% (see Fig. 4.120), under 17,800 and 22,800 equivalent hours' sun irradiation the bending modulus dropped 12.5% and 28.0%, respectively (see Fig. 4.121).

- ③ Damage caused by wind, sand, and rain erosion is a slow cumulative process. This type of damage can be prevented provided that an anti-rain erosion protective paint is sprayed on structural surfaces. If the surface coat brushes off, applying a new layer of the coat to surface will give sufficient protection. The mechanism of rain erosion and respective anti-rain erosion measures has been widely investigated. It has been shown that the pressure impulse and fluid of rainwater impacts are physical factors of rain erosion. The main factors influencing rain erosion are the angle of incidence of the raindrop and raindrop parameters,

Fig. 4.120 Effects of ultraviolet radiation on tensile stiffness of unidirectional laminate

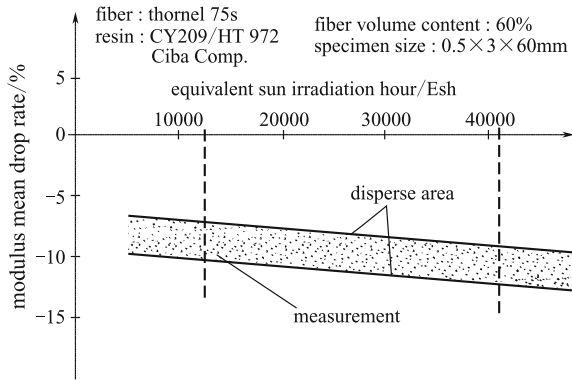
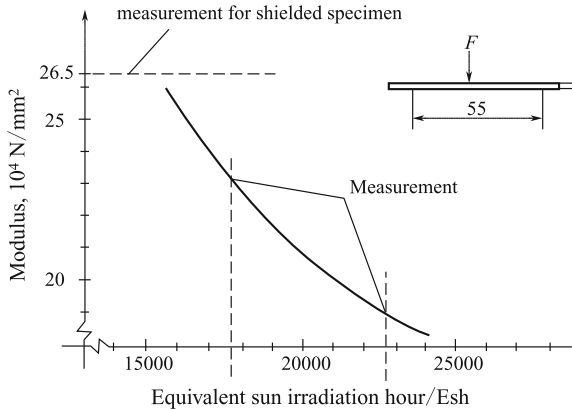


Fig. 4.121 Effects of ultraviolet radiation on flexural modulus of unidirectional laminate



such as its size and velocity. When the angle of incidence of a raindrop is 90° and the raindrop velocity is more than 200 m/s an anti-rain erosion protective coat should be applied to the surface of the composite structure. At the design stage, the layout of components should attempt to minimize the area of impacted surfaces and lower the angle of rain drop incidence in addition to protective coatings. Anti-erosion paint and metal or ceramic protective coatings may be adopted as anti-rain water erosion measures.

(3) **Corrosive Control**

There are two main principles for controlling composite corrosion caused by environmental media.

- (1) Enhance innate material corrosion resistance: In some cases it is possible to improve the crystallinity, tropism grade, or crosslinking density of composites. The matrix compactness can also be enhanced to reduce the diffusion coefficient and penetrative coefficient of the medium. A surface cleanup solvent may be used to enforce the adherence strength between the reinforced fiber and matrix, reduce the interface clearance, and enhance impermeability.
- 2) Use of protective coatings: A protecting coat is sprayed on the composite surface to avoid direct corrosion of the composite by environmental media.

(4) **Biological Corrosion and its Control**

Biological corrosion occurs mainly at the fuel box position of aircraft structures. The combination of moisture and other impurities in fuel can provide appropriate conditions for biological organisms to grow. The main microorganisms that might affect composites are germs, epiphyte, and mildew. Such microorganisms may reproduce and excrete acidic substances, such as lactic acid and grass fungus. These acidic substances might react with composites. Biological corrosion of composite structures used in a sea environment can pose a threat. Composite destruction caused by oceanic organisms can occur. The composite might be bitten away by hexapods and chisel-ship worms, and the above-mentioned microbe encroachment can become more serious. The following steps should be taken to control biological corrosion:

- ① Fuel quality should be controlled. The content of moisture and impurities in fuel and possible pollution during the fuel transport process should be minimized to remove the conditions necessary for microbial growth.
- ② An effective drainage system should be designed in the fuel tank. A fluent-fuel mouth should be installed at the lowermost position and water should be drained at intervals.
- ③ Anti-bioerosion protective coatings may be applied. A coating in common use is SF-9 epoxy, which can effectively prevent biological growth.

- ④ Additives made be added to fuel. Typical additives include: chromic acid, strontium glycol ether and organic borides. These additives can kill microorganisms and effectively limit bioerosion.

4.10.5.2 Galvanic Erosion Between Composites and Metals

When two types of materials with different electrode potentials are directly connected or in contacted through an electrolyte, accelerated corrosion might be caused in the lower potential material. This is known as galvanic or electrical dipolar erosion. Carbon has good electrical conductivity and a relatively high electrode potential. Carbon fiber-reinforced composites under general environmental conditions show inert behavior similar to that of noble metals with high electrode potentials. Thus, when carbon fiber-reinforced composites are joined with metal the cathode-like behavior could accelerate corrosion of the metal. The electrode potential difference between carbon fiber-reinforced composite and most metals is 0.5–1.0 V, and in some cases, may reach as high as 1–2 V. Therefore, anti-electrical dipolar erosion steps must be adopted in areas of connected metals and composites. The generation of electrical dipolar erosion requires three conditions: an electrode potential difference, electrolyte, and an electrical conductive connection. Protective measures against galvanic erosion should consider these three aspects.

(1) Structural Design

The accumulation of electrolyte can be prevented to a large extent by careful structural design to avoid formation of corrosion batteries.

- ① Attention should be paid to structural seals, to avoid infiltration of rainwater, fog, and seawater. Holes and places where contamination may accumulate should be reduced. Countermeasures should be mounted at positions subject to seepage.
- ② Small metallic elements surrounded by a large area of composite should be avoided. Strict protecting steps should be adopted for mechanical fastener joints.
- ③ The lumen and blind holes should be designed with perforation to prevent condensation water cohesion.

(2) Selection of Materials

Consistent materials should be selected to prevent galvanic erosion.

- ① Anticorrosive materials and materials with a low potential difference compared with that of the composite should be chosen. Pay special attention to small parts such as fasteners.
- ② Insulated and closed down materials should be non-hygroscopic and should not contain any corrosive components. When a single layer of

co-cured glass-cloth on a surface is used as an insulating coat, the edge must be sealed. Otherwise, counterproductive effects may be caused.

(3) Protective Methodologies

Effective protective measures must be adopted for metals, which show corrosion in direct contact with composites and the contact is otherwise unavoidable.

- ① An appropriate overlay coating for the metal or a non-metal may be used as a transition layer or adjustment. For example, anodization, chemical oxygenation, passivation, and phosphorization are commonly used treatments. The contact resistance is increased and the electrical dipolar erosion can be reduced providing that the covering coat is perfect. Selection principles for the thickness of an over coat and its applicable range can be found in the standard HB5033.
- ② Efforts to insulate the component should be made; however, steps to reduce the electrode area should also be taken through the use of appropriate coatings on the surfaces. Protective coats should be applied to both the metal and composite to avoid forming large cathode and small anode areas in case electrolyte in-leakage occurs via microholes or local damage of the protecting coats. Furthermore, the protective coats should be resistant to alkali because alkaline substances are generated at the cathode by electrical dipolar erosion.
- ③ Gaskets, cannula, and adhesive tapes made from inert materials should be used between metals and composites to form an insulated coating.
- ④ Appropriate hermetic sealing materials should be used to form gapless seals that insulate against electrolyte formation. Such sealants are effective at slowing corrosion.

(4). Protection of Metals Against Galvanic Erosion of Carbon Fiber-Reinforced Composite

- ① The composite should not be connected with magnesium or magnesium alloy.
- ② Aluminum and its alloys should be treated as follows: The metal may be placed in a recycling hot water or chromate solution after an anodization process. Typical coatings include chromate +H06-2 zinc yellow epoxy resin priming and chromate +SF-9 for fuel tank dope (used interior of fuel tank).
- ③ Steel and low-carbon steel should be treated by any of the following: coating by galvanization and H06-2 zinc yellow epoxy resin priming; phosphorized and coated with X04-1 acetal phosphoric paint and X04-1 varnish (oil proof); phosphorized and coated with H06-2 iron red epoxy resin priming and X04-2 epoxy nitril magnetism paint (available in various colors); phosphorized and two-layer zinc yellow epoxy resin priming (add FLU_{1-4} aluminum powder) and H61-2 steel gray organic silicon epoxy polyamide magnetism paint applied.

- ④ Stainless steel should be treated as follows: The unmodified surface may be used or one of the passivation process described above.
- ⑤ Titanium alloy should be treated as follows: The unmodified surface may be used; an anodized process; souring or sand blasting and H06-2 zinc yellow epoxy resin priming and 13-2 propenoic acid polyurethane magnetism paint; souring or sand blasting and F06-9 zinc yellow phenolic priming and 13-2 propenoic acid polyurethane magnetism paint.

The above-mentioned methodologies may be selected based on the service environment and structural conditions. Under poor environmental condition metals should also be sealed, with sealants such as XM 22, XM 23, XM30, and XM 34.

4.10.5.3 Protective Coatings for Composites

Protective coatings for composite components can not only improve the appearance of faces but are also important for slowing moisture absorption and aging processes of the material. The application of an anti-friction dope on the front structural features can improve resistance to sand and rain erosion. Application of anti-friction dope on interior surfaces can prevent direct contact of composites with metal and avoid electrical dipolar erosion.

(1) Cover Coatings and their Effects

Different cover coat materials are used at different positions and fall mainly into the following types:

- ① For interior surfaces and end faces a protective coat formed by priming should be applied.
- ② For general exterior surfaces with ornamental protective coatings, priming, sealants, transition priming, and surface paint may be applied.
- ③ For front structural features, an anti-friction and anticouling protective coating system formed by priming, an elastic anti-friction dope, and surface paint should be applied.
- ④ For upright surfaces or other surfaces requiring anti-static protection, anti-static protective coatings system formed by priming, and anti-static or elastic anti-static dopes should be applied.
- ⑤ For the interior surfaces of the fuel tank an anti-static protective coat system formed by priming, and anti-static and oil proof dopes should be applied.
- ⑥ For exterior surfaces of the fuel tank, an electrical protective coating system formed by priming, an electrical layer, and painting of the surfaces should be applied.

(2) Surface Dopes and Coating Systems

Currently, the most widely used dopes are epoxy- and polyurethane-based. Epoxy dopes are strongly adherent, show low contraction, and good toughness.

Epoxy dopes are versatile and can be applied with many types of surface paint. However, because this dope has poor gloss retention after film formation and it is prone to pulverization, it is mainly applied in priming coats.

A large variety of polyurethane dopes are available, which shows excellent performance, strong adherence, and high rigidity. Polyurethane dopes form bright films with excellent oil and moisture proofing, heat endurance, and wear and chemical resistance. Therefore, these dopes are widely applied in the aviation industry.

Dopes and coating systems in common use for aircraft composite structures are shown in Tables 4.45 and 4.46.

4.10.6 Relationships Between Atmospheric Aging, Accelerated Atmosphere Aging, and Hygrothermal Aging and Recommendations

The relationships between three different types of aging methods are investigated to determine an optimal method for studying aging response. It is important for the method to not only reflect the real history of an aircraft but also to be convenient and simple. On the basis of real investigations, the following recommendations are given.

- ① For the composite structures of military aircraft, the accelerated testing scheme shown in Fig. 4.119 may be considered to be a standard accelerated hygrothermal scheme. An actual history of 5000 flight hours and 20-year service life can be simulated in approximately 1 year. The highest temperature of thermal spiking can be determined based on the type of fighter plane ($M = 2.0$, $T = 110$ °C; $M = 2.2$, $T = 125$ °C).
- ② In general, the compression, interlaminar shear and compression after impact strength are sensitive to hygrothermal aging. Thus, the aforementioned properties must be tested for all material selected during the structural design phase.
In particular, the residual strength should be tested at the operating temperatures.
- ③ Hygrothermal aging has an influence on the facing properties of sandwich constructions, but it has no obvious influence on other properties providing that the facing is undamaged and sealed.
- ④ Ultraviolet radiation and rain erosion have no obvious effects on composite properties providing that a protective coating is maintained.
- ⑤ Cryogenic temperatures and changes of air pressure have little effect on the properties of composites and may be neglected to reduce the test costs.

Table 4.45 Paint and coatings commonly used for composites

Number	Title	Sign Standard	Main constituent	Elasticity /mm	Impact /N·cm	Grade of adherent force	Properties	Dry criterion	
								77°C	t/h
1	Epoxy polyamide varnish	H01-101H Q/6s72-80	E-20 epoxy and polyamide resin	1	490	1	Paint film tenacity, good adhesiveness with composites, liquid proof, waterproof, low air permeability	18-25 50-60 110-120	24-26 6-8 1-2
2	Epoxy polyamide priming	H01-102H Q/6s455-85	E-20 epoxy and polyamide resin, strontium yellow	1	490	1	Liquid proof, matches with many other surface paints, high interlaminar adhesion force, good adaptability	18-25 50-60 110-120	24-26 6-8 1-2
3	Polyurethane surface paint	13-2	Acrylic resin, HOI, paint, padding	1	490	1	Good adhesiveness, waterproof, hygrothermal resistance, excellent resistance to radiation and weatherability	18-25 50-60 110-120	24-26 6-8 1-2
4	Elastic polyurethane magnetism paint	HTY/B-80-15(1)	TDI mixed polyamine prepolymer, MOCA curing agent, paint padding	1	490	180° peel off ≥ 39.2 N/cm	Paint film tenacity and good elastic behavior, good wear, rain, and scouring resistance, good adhesiveness to priming	18-25 50-60	24-26 8-12

(continued)

Table 4.45 (continued)

Number	Title	Sign Standard	Main constituent	Elasticity /mm	Impact /N·cm	Grade of adherent force	Properties	Dry criterion	
								77°C	∇/h
5	Epoxy polyamide sealant	Q/6sz358-83	Epoxy polyamide varnish, talcum powder				Good adhesiveness to fundus varnish and transition priming, easily scraped, easily polished, low contraction	18-25 50-60	36-48 6-8
6	Thinner	X-7 X-10	Xylene, positive butyl alcohol, butyl-resin, cyclohexanone				Use to dilute epoxy type paints Use to dilute polyurethane type paints		
7	Epoxy black polysulfide electric dope	HL04-1019 H.D Q/6s530-90	Epoxy resin, Thiokol, electriccarbon black	1	490	1	Good electrical properties (0.5-15 MΩ/m), oil proof, good adhesiveness to sealant, apply as a thin glue in the interior surface of the fuel tank	70	24
8	Epoxy polyamide electric dope	H06-1020 H.D Q/6s530-90	Epoxy and polyamideresin, ST-3 electric powder	1	490	1	Good electric properties (0.5-15 MΩ/m), oil proof, apply to the bottom priming in the interior surface of the fuel tank	90 - 100 100- 120	4 2

Table 4.46 Dopes in common use for composites

Number	Coating system	Dry criterion		Coat thickness		Coating property	Location of use
		T/°C	t/h	Monolayer /μm	Total/μm		
1	First or second epoxy polyamide varnish (lower varnish)	18–50–110–120	24–36–6–8–1–2	First 15–20 Second 25–35	15–20 25–35	Low air permeability, good adhesiveness, and waterproof as a sealant	Interior and exterior surfaces, end faces and walls of holes
2	First epoxy polyamide varnish	18–25	24–36	First 15–20	80–100 100–120	Good interlaminar adhesion force, waterproof, hydrothermal proof	Exterior surfaces of components
	Smearred locally polyamide sealant	18–25 50–60	24–36 6–8				
	First polyamide priming (filtration priming)	18–25 50–60	24–36 6–8	15–20			
	Second polyurethane surface paint	18–25 50–60	36–48 6–8	50–60			
3	First epoxy polyamide varnish	18–25	24–36	15–20	240–260	Good interlaminar adhesiveness, excellent wearability, anti-scourability; Facing- paint is hydrothermal proof and has good weatherability	Front facing surfaces and those requiring anti-friction coatings
	Eight elastic polyurethane magnetism paint	18–25 50–60	24–36 8–12	180–200			
	Second polyurethane surface paint	18–25 50–60	36–48 6–8	40–50			
4	Epoxy polyamide varnish, epoxy polysulfide electric dope	18–25 50–60 70	18–25 6–8 24	15–20 50–60	80–100	Good electrical properties, oil proof, and good interlaminar adhesion force	Fuel tank, up panels and other position requiring oil proofing
5	Epoxy polyamide varnish, epoxy polyamide electric dope, XM-electric thin glue, epoxy black polysulfide electric dope	18–25 50–60 70 70 70	24–36 6–8 24 24 24	25–30 40–50 50–60	200–400	Good electrical properties, oil proof, and good interlaminar adhesion force	Fuel tank, erect gaps, horizontal gaps, down panels and edges

4.11 Impact Damage Tolerance Reliability of Composite Structures

4.11.1 Introduction of Structural Reliability Design and Analysis

4.11.1.1 General

Composite materials are widely used in modern structures for their high performance and reliability. However, because these structures usually operate in hostile and variable service environments, it is difficult to predict their structural performance. In addition, experiments show that composite structural behavior exhibits a wide scatter as a result of the inherent uncertainties in design variables.

Design variables, known as primitive variables, include: the fiber and matrix material properties at the constituent level; fiber and void volume ratios; ply misalignment and ply thickness; the fabrication process; size of random structures; boundary conditions; loadings; and the operating environment.

The full range of structural behavior cannot be computationally simulated by traditional deterministic methods, which use a safety factor to account for uncertain structural behavior. Thus, the true structural reliability cannot be discerned. A probabilistic design methodology is needed to accurately determine the structural reliability of composite structures.

For the purposes of structural reliability analysis, it is necessary to distinguish between at least three types of uncertainty: physical uncertainty, statistical uncertainty, and model uncertainty.

4.11.1.2 Reliability Function

The probability of failure $F(t)$

$$F(t) = P\{T \leq t\} \quad (4.125)$$

The probability density function $f(t)$

$$f(t) = \frac{dF(t)}{dt} \quad (4.126)$$

The reliability function $R(t)$, which is the probability that the system will still be operational at time t is given by

$$R(t) = P\{T > t\} = 1 - F(t) \quad (4.127)$$

4.11.1.3 Structural Reliability

According to Chinese standard GB/T 3187 (Reliability and maintainability terms), the reliability of a structure is its ability to fulfill its design purpose for some specified time.

4.11.2 Types of In-Service Damage

To analyze the rate of occurrence of in-service damage to composite structures, potential mechanical impact and types of in-service damage should be categorized. Depending on the projectile speed (V), mechanical impacts causing damage in composites may be subdivided into low-speed ($V < 6\text{--}8$ m/s) and mid-speed ($V < 30\text{--}200$ m/s) phenomena.

Unlike metals, where impacts may be absorbed by plastic deformation, polymer composites fail as brittle materials. Therefore, low- and mid-speed impacts cause damage to a composite skin which may be categorized as follows:

- ① Surface damage, scratches, and fracture notches. Such damage has a negligible effect on the load-bearing capabilities of a structure and may be neglected in analyses.
- ② Delamination followed by matrix cracking and fiber failure. This damage occurs inside the composite layer. The external skin surface may feature indentation. Delamination may be categorized as: internal delamination, visually undetectable at both skin surfaces, which may be followed by matrix cracking at the face opposite to the impacted surface; delamination visually detectable at the external skin surface, with respect to the impact surface.
- ③ Through damage cracks and punctures. In this case, the damaged area will feature failure of layers through the thickness of the composite. Through damage may be characterized as either clean holes or other damaged material. Puncture edges usually show delamination and cracking.

Damage types 2 and 3 may considerably reduce the load-bearing capability of a structure and must be accounted for in analyses.

4.11.3 Random Variables

Variables that need to be considered in the stiffness reduction model can be classified into three categories:

- ① Material parameters, which include strength of the undamaged laminate, fracture toughness of the material system, laminate thickness, and laminate layer pattern.
- ② Structural parameters, which include boundary conditions and sub-structural configurations.
- ③ Impact threat parameters, which include impact energy and impactor size. The model assumes that the severity of stiffness reduction, for a given material system and impact condition, depend on the impact energy.

In considering the structural integrity of a structural component containing damage, potential random variables should be accounted for including the number of damage sites, damage size, time to detection/repair of damage, load, and strength properties. The effectiveness of inspections is another potential random variable. The effectiveness of an inspection can be characterized by the probability of damage detection distribution. In total, nine random variables are considered:

- ① Number of damages sites per life, for each type of damage;
- ② Time of damage initiation;
- ③ Damage size, for each type of damage;
- ④ Time from damage initiation to repair, i.e., a random function of damage size and damage initiation;
- ⑤ Initial failure load, for each load case;
- ⑥ Residual strength of damaged structure for each type of damage and each load case;
- ⑦ Failure load of repaired structure, for each type of damage;
- ⑧ Structural load for each load case;
- ⑨ Structural temperatures at the sites when maximum external loads occur.

4.11.4 Impact Threat Distribution

At the beginning of advanced certification methodology for composite structures, no detailed data existed on the actual impact threat encountered by in-service composite structures. Consequently, some scenarios for impact threat distributions were developed. The impact threat scenarios clearly depend on the location of the structure and its structural configuration. To establish realistic impact damage requirements, a structural zoning procedure is used to categorize the structure. On the basis of available data, the impact threat can be tentatively divided into three levels — high, medium, and low. The probabilistic distributions of these impact threats are discussed below [3, 47–52].

To quantify the different levels of impact threat, it is assumed that the probability of a structure being exposed to a given impact can be described by a two-parameter Weibull distribution in terms of the impact energy. Instead of expressing the

distribution by the usual scale (β) and shape (α) parameters, the threat is characterized by two impact energy levels. These are the model energy level associated with a high possibility of occurrence (X_m), and the high energy level associated with a low probability of occurrence (X_p). The relationships between the energy parameters and the Weibull scale and shape parameters can be expressed by the following two equations.

$$X_m = \left(\frac{\alpha - 1}{\alpha} \right)^{1/\alpha} \beta \quad (4.128)$$

and

$$X_p = \beta [-\ln(P)]^{1/\alpha} \quad (4.129)$$

where P is the probability of occurrence of the impact energy $P(X > X_p)$.

Combining Eqs. (4.128) and (4.129) gives:

$$\frac{X_m}{X_p} = \left[\frac{\alpha - 1}{-\alpha \ln(P)} \right]^{1/\alpha} \quad (4.130)$$

Equation (4.130) is solved for α by iteration and β is then obtained from Eq. (4.128). The Weibull distribution for the impact threat to a structure is then defined from the obtained values of α and β .

The three scenarios of impact threats, denoted as high, medium and low, are defined as shown in Table 4.47. The high threat distribution is considered to be a conservative estimate of the impact threat to a structure. The medium threat is a more realistic estimate of the impact damage threat for composite structures. The table shows the computed Weibull parameters corresponding to these threats. Figure 4.122 shows that all three assumed threat scenarios are conservative compared with the MCAIR in-service survey results.

Table 4.47 Impact threat scenarios

	High threat	Medium threat	Low threat	MCAIR Data fitting
Modal energy $X_m(\times 1.36 \text{ J})$	15	6	4	1
$X_p(\times 1.36 \text{ J})$	100	100	100	35
$P(X > X_p)$	0.1	0.01	0.0001	0.00005
α	1.264	1.192	1.221	1.177
β	57.7	27.8	16.2	4.992

4.11.5 Cases and Solution Steps

In this section, four cases will be introduced as follows:

(1) **Case one**

Calculate the structure reliability R at a given applied stress and impact energy as shown in Fig. 4.123.

(2) **Case two**

Establish the relation between the reliability R and impact energy E as shown in Fig. 4.124.

(3) **Case three**

Calculate the cumulative damage tolerance strength reliability \bar{R} at a given stress and impact threat as shown in Fig. 4.125.

(4) **Case Four**

Establish the relationship between stress and cumulative damage tolerance strength reliability as shown in Fig. 4.126.

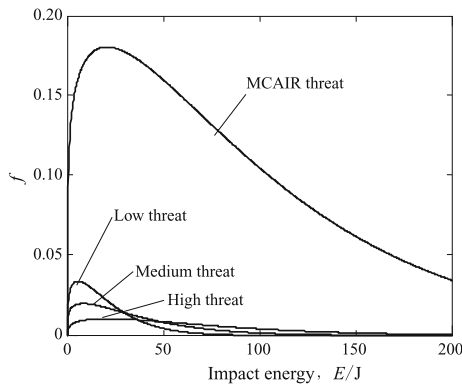


Fig. 4.122 Impact threat distributions

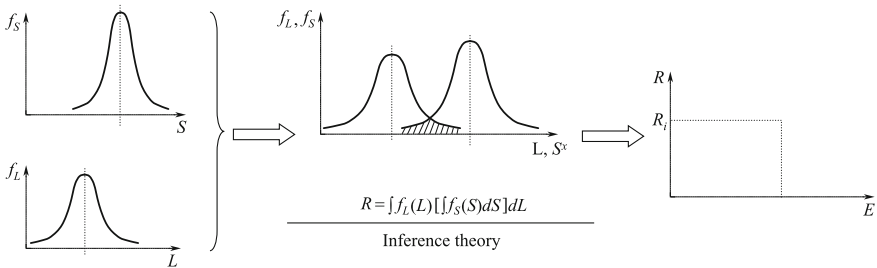


Fig. 4.123 Inference theory

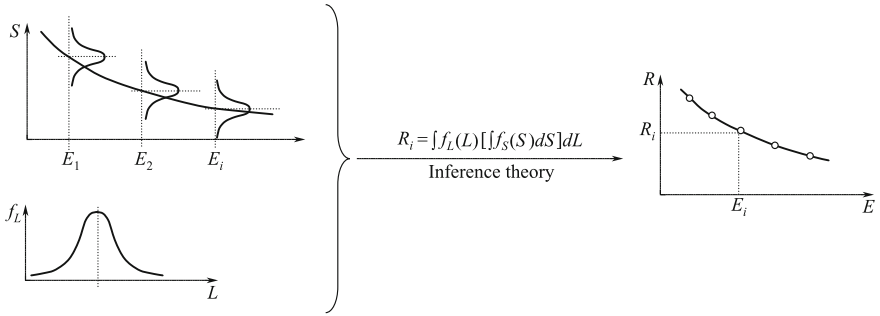


Fig. 4.124 Relation between the reliability R and impact energy E

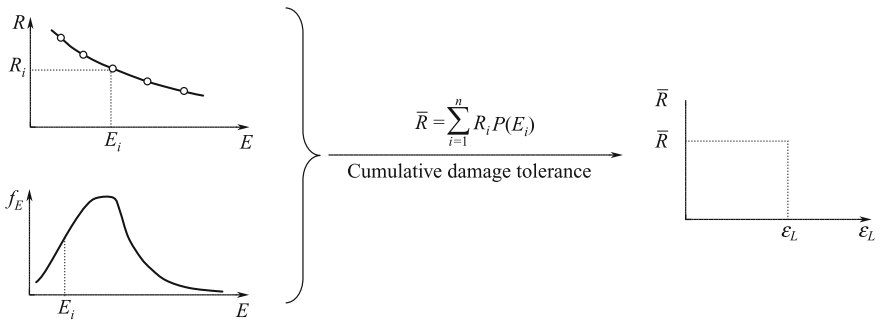


Fig. 4.125 Cumulative damage tolerance strength reliability \bar{R}

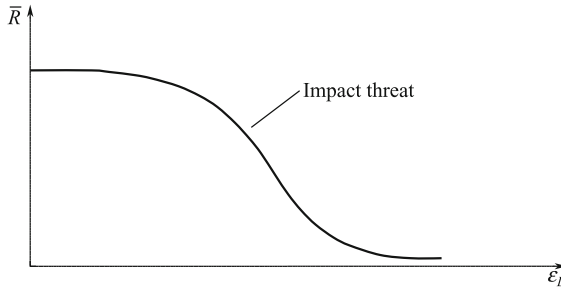


Fig. 4.126 Relation between Stress and Cumulative Damage Tolerance Strength Reliability

(In the Chapter, 4.1–4.6 and 4.9 were translated by Jianmao Tang; 4.7 was translated by Jiahui Xie.)

(4.1–4.6 and 4.9 were translated by Jianmao Tang, 4.7 was translated by Jiahui Xie.)

References

1. Shen Z (1995) design guideline of durability/damage tolerance for composite aircraft structures. Aviation Industry Publisher, Beijing
2. Shen Z (2001) Design Handbook for Composite Structures. Aviation Industry Publisher, Beijing
3. U.S. Department of Defense (2002) MIL-HDBK-17F. Composite material handbook, vol 3. Polymer matrix composites materials usage, design, and analysis
4. Briston JW (1986) Airworthiness of composite structures—some experiences from civil certification. In: Proceedings of the 2nd international conference on fiber reinforced composites
5. Soderquist JR (1987) Design/certification considerations in civil composite aircraft structure. SAE 871846
6. Brandecker B, Hilgert RS (1988) A320 full scale structural testing for fatigue and damage tolerance certification of metallic and composite structure. In: Proceedings of the 16th ICAS
7. Shen Z (1988) The design allowables of composite aircraft structures and their determination principle. *Acta Aeronautica Et Astronautica Sinica* 19(4):385–392
8. Jones RM (1981) (trans: Zhu YL) Mechanics of composite materials. Science and Technology of Shanghai Publisher, Shanghai
9. Zhou L, Fan FQ (1991) Mechanics of composite materials. Higher Education Press, Beijing
10. Zhu YL (1979) Review on mechanical properties of advanced composites. glass-fiber reinforced plastics. GFRP Structures Research Institute of Shanghai
11. Yang NB, Zhang YN (2002) Composite aircraft structure design. Aviation Industry Publisher, Beijing
12. Jiang YQ, Lu FS, Gu ZS (1990) Mechanics of composite materials. Xi'an Jiaotong University Press, Xi'an
13. Chen SJ (1990) Design handbook of composite materials. Aviation Industry Publisher, Beijing
14. Tong XX (2002) Guideline of stability analysis for composite structures. Aviation Industry Press, Beijing
15. Niu MC (1992) Composite aircraft structures. Cinmilit Press Ltd, Hong Kong
16. Zhu JF, Wang H (1996). Analysis code of post-buckling strength and failure for composite stiffened panel and shell structures (COMPOSS). *Comput Struct Mech Its Appl* 13(4)
17. Xie MJ (1995) Handbook for composite joints. Aviation Industry Press, Beijing
18. ASM International Handbook Committee (1987) Engineered materials handbook, vol 1. Composites
19. Hart-Smith LJ (1973) Adhesive bonded single lap joints. NASA CR-112236
20. Hart-Smith LJ (1973) Adhesive bonded double lap joints. NASA-CR-112235
21. Hart-Smith LJ (1973) Adhesive bonded scarf and stepped lap joints. NASA CR-112237
22. Hart-Smith LJ (1982) Design methodology for bonded-bolted composite joints. AD-A117342 (AFWAL TR 81-3154)
23. Collings TA (1977) The strength of bolted joints in multidirectional CFRP laminates. ARC CP 1380
24. Garbo SP, Ogonowski JM (1981) Effect of variance and manufacturing tolerances on the design strength and life of mechanically fastened composite joints. AD- A101657
25. Chi J, Xie MJ (1988) FE analysis investigation on bolt-load distribution in composite laminate joints. *Acta Aeronautica Et Astro- Nautica Sinica* 19(7) (in Chinese)
26. Hart-Smith LJ (1976) Bolted joints in graphite composites. NASA-TR-144899
27. Hart-Smith LJ (1978) Mechanically fastened joints for advanced composite-phenomenological consideration and simple analysis. In: Presented to the conference on fibrous composites in structure design
28. Bunin BL (1985) Critical joints in large composite primary aircraft structures. NASA-CR-3914 Vol. I — Technical summary

29. Bunin BL (1985) Critical joints in large composite primary aircraft structures vol II — Technology demonstration test report. NASA-CR-172587
30. Bunin BL, Sagui RL (1985) Critical joints in large composite primary aircraft structures vol III—Ancillary data test results. NASA-CR-172588
31. Nelson WD, Bunin BL, Hart-Smith LJ (1983) Critical joints in large composite primary aircraft structures. NASA-CR-3710
32. Hortin RE, McCarty JE (1987) Damage tolerance of composites. In: Engineered materials handbook Vol.1 Composites. ASM International, Ohio, USA, pp 259–267
33. Tang XD, Shen Z, Chen PH, Gaedke M (1997). A methodology for residual strength of damaged laminated composites. AIAA Paper 97–1220
34. Chen PH (1999). Damage tolerance analysis for composite laminates and stiffened panel. PhD thesis of Nanjing Aeronautical and Astronautical University
35. Chen PH, Shen Z, Wang JY (2001) Damage tolerance analysis of cracked stiffened composite panels. *J Compos Mater* 35(20)
36. Chen PH, Shen Z, Wang JY (2001). Impact damage tolerance analysis of stiffened composite panels. *J Compos Mater* 35(20)
37. Chen PH, Shen Z, Wang JY (2001) Prediction of the strength of notched composite laminates. *Compos Sci Technol* 61(10)
38. Chen PH, Shen Z, Wang JY (2002) A new method for compression after impact strength prediction of composite laminates. *J Compos Mater* 36(5)
39. ASTM D 3878-07 (2004) Standard terminology for composite materials
40. ACEE Composites Project Office (1985) NASA/Aircraft industry standard specification for graphite fiber/toughened thermoset resin composite material. NASA RP 1142
41. SACMA 2R-94 (1994) SACMA recommended test method for compression after impact of oriented fiber-resin composites
42. Dost EF, Avery WB, Finn LB, Ilciewicz LB, Scholz DB, Wishart RE (1993) Impact damage resistance of composite fuselage structure, Part 3. In: Paper presented at fourth ACT conference
43. Shen Z, Zhang ZL, Wang J, Yang SC, Ye L (2004) Characterization on damage resistance and damage tolerance behavior of composite laminates. *Acta Materiae Composite Sinica* 21(5):140–145 (in Chinese)
44. Chen PH, Shen Z et al (2006) Failure mechanisms of laminated composites subjected to static indentation. *J Compos Struct* 75(1–4):486–495
45. Shen Z, Yang SC, Chen PH (2008) Experimental study on the behavior and characterization methods of composite laminates to withstand impact. *Acta Materiae Composite Sinica* 25(5):125–133 (in Chinese)
46. Li Y (1998). Effect of hygrothermal spectrum aging on composite laminates. NCCM-10. Hunan Science and Technology Press, Changsha, pp 143–146
47. Kan HP, Whitehead RS, Kauts E (1992). Damage tolerance certification methodology for composite structures, N92-32579
48. Bai G (1997). Reliability evaluation of composite laminates under impact threat. MSC thesis of Northwestern Polytechnical University
49. Ma ZK, Yang L (1998) Analysis method of cumulative damage tolerance reliability for composite laminated structures. Design and Research of Commercial Aircraft
50. Chen PH, Shen Z (2004). Statistical analysis and reliability evaluation of post- impact compressive residual strength. *Acta Aeronautica Et Astronautica Sinica* 25(6)
51. Tong MB, Chen P H, Shen Z (2004). Reliability analysis of impact damage tolerance for composite materials. *Acta Materiae Composite Sinica*, 21(6)
52. JSSG-2006 (1998) Joint service specification guide—Aircraft structures

Chapter 5

Composite Property Testing, Characterization, and Quality Control

Zuoguang Zhang, Zilong Zhang, Zhen Shen, Shuangqi He, Yubin Li
and Ming Chao

Property testing, characterization, and quality control are three major issues in advanced composite research, development, and applications. These also are common concerns for material scientists, structural designers, and users of composite materials. To extend the application of advanced composites, especially in high-tech areas, the performance stability of composites should be characterized to justify the use of composites in a design. To fulfill these requirements, advanced composite testing, characterization, and quality control are required.

Composites are multiple material systems composed of two or more different materials fabricated with the use of physical and chemical processing techniques. Composites must be considered in terms of their various constituents, combinations of materials, and their structural processing and multilayer construction. Each of these factors presents difficulties for achieving high standards for composite property testing, characterization, and quality control.

In terms of materials and processing, the stability of a given property is an important factor, which affects advanced composite quality. Factors that can influence composite stability are summarized as follows:

Editors for this chapter: *Zuoguang Zhang, Zilong Zhang.*

Z. Zhang (✉) · Y. Li · M. Chao
Beihang University, Beijing 100191, China
e-mail: zgzhang@public.bta.net.cn

Z. Zhang
Beijing Institute of Aeronautical Materials, Beijing 100095, China

Z. Shen
Aircraft Strength Research Institute of China, Xi'an, Shaanxi 710065, China

S. He
Beijing Research Institute of Aerospace Materials & Technology, Beijing 100076, China

- ① Lack of knowledge about materials characteristics: For many features of composites, there are currently no perfect theories available to explain and predict their properties. In many cases, empirical approaches are the main tool for evaluating composite performance. Owing to the lack of a systemic understanding of composite features, it is very difficult to accurately evaluate the stability of composite properties.
- ② Variation of constituent properties: The non-uniformity of constituent materials results in a certain scatter of their performance. The performances of composites not only depend on their constituent materials, but also the combination of constituents.
- ③ Instability of processing techniques: Knowledge is limited on the physical and chemical mechanisms currently used to prepare composite materials. This results in poor reproducibility of processing and a large scatter in the performance of materials.
- ④ Imperfectness of testing methods: As a relatively new kind of material, currently there are no suitable methods and standards to test and inspect certain properties of composites. In the established standards, specimens cannot perfectly reflect the real-world performance of composite structures. There is much work required on evaluating composite stability by nondestructive testing.
- ⑤ Lack of statistical data: Compared with traditional materials, data on composite performances are severely limited. In many databases, typical values are given with insufficient statistical data.
- ⑥ Lack of knowledge about the regularity of changes in composite material properties over time: Composite matrices are very sensitive to time- and temperature-dependent effects and their performances will change with time. Current accumulated data still does not reflect the behavior of composites over a full range of ambient conditions and different time periods.

This chapter is divided into six sections focusing on issues surrounding testing of composite properties, characterization, and quality control. In Sects. 5.1 and 5.2, methods for testing composite properties, developing test plans, processing test data, and matrix testing, are discussed. In Sect. 5.3, prepreg performance characterization and characterization technologies, physical parameters, and processing ability characterization are introduced. In Sect. 5.4, laminate property testing is discussed, including test methods for basic physical and mechanical properties, fracture toughness, and damage resistance. In Sect. 5.5, composite quality evaluation and control are examined together with a discussion on the complexity of quality evaluation and existing problems. Two quality evaluation approaches are first proposed to address the quality control of composites. Three processing quality control methods are also introduced. The final section concerns composite failure analysis.

5.1 Guidelines for Composite Property Testing

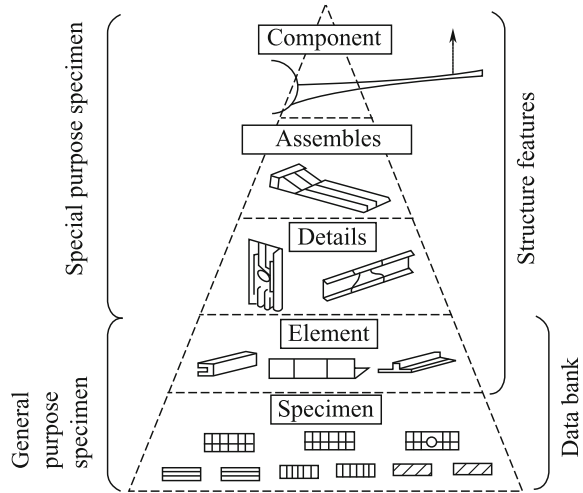
Composite property testing is of great importance in composite design selection, processing quality control, product quality inspection, assembly, and repairs. The properties of composites have implications for the overall course of material development, structure design, processing, manufacture, quality evaluation, and service and maintenance. Much attention has been paid to these aspects and many test methods and related techniques have been developed. Some of these methods have now become standards, and most are based on test methods for traditional metal materials. However, compared with traditional metallic materials, composites have several unique features to consider such as small rates of extension, anisotropic properties, internal structure complexity, and sensitivity to applied load. These features can cause problems for traditional test methods, including: ① Currently, most test methods only give apparent test results rather than the intrinsic characteristics. ② Testing results depend strongly on the specimen dimensions with a large size effect. This makes it difficult to evaluate the equivalence between specimens of different sizes. ③ There are many methods available for testing the same material property, which makes it difficult to select more suitable and reliable methods. ④ Test results are often not compatible with the practical effectiveness. ⑤ Many methods are complex, time-consuming, and difficult to implement. Thus, the development of more rigorous and effective test methods requires the establishment of more reasonable test systems and standardization of test data from composite materials.

5.1.1 Features of Property Characterization of Composites

Property characterization is an important topic in materials research and structural applications. For polymer matrix composites, the property characterization has special importance as outlined below:

- (1) Unlike isotropic metals, composites are composed of two or more constituents. Thus, the characterization should start by examining the constituents.
- (2) The failure mechanisms are different from those of traditional metals and test methods developed for metals are not suitable for composites. Hence, the development of new test methods is needed.
- (3) Owing to some unique features, many new requirements have been proposed for composite property characterization, in particular the hot–wet characteristics and impact resistance.
- (4) Composites are highly designable. The structural laminates are composed of plies with different fiber ratios and orientations, which contribute to the characteristic complexities of laminates—the basic structure element.

Fig. 5.1 Building block approach for composite verification



- (5) Composite materials and their structure are simultaneously determined during manufacture. Thus, variations of materials and processing will affect the material and structure.
- (6) Owing to a lack of experience with composite materials, structure design, and applications, the building block approach is an important approach for verification of composites (Fig. 5.1). Property characterizations may be divided into five levels: constituent, lamina, laminate, structural element, assembled component, and higher levels. Thus, more levels are involved for composites materials than for metals in terms of the categories and numbers of samples.
- (7) Property characterization is important for structure development based on composite materials. On the basis of the application of the data, the characterization testing can be divided into the following types: material screening, material verification, material acceptance, material equivalent evaluation, and structural certification.

Owing to the importance of property characterization in the development and production of composites characterization and the standardization are important aspects in the field of composite materials. Standardization encompasses two key aspects: the scope and method of property characterization (including test standards, sample quantity, and data processing), and the recommended test matrices for different applications.

As applications of composite materials have been extended, methods for their standardization have also progressed. For example, the MIL-HDBK-17 (Handbook of Composites) and ASTM D30 composite division are being continuously revised and updated.

5.1.2 Test Design and Classification

Test activities can be defined into two basic approaches, the structural complexity level and the data application category. The classes within each are discussed in more detail in the following sections and can be used to set out large-scale testing programs to guide test planning.

(1) Structure complexity levels

The five structural complexity levels¹ are each based on geometry or form: constituent, lamina, laminate, structural element, and structural subcomponents. The five structural complexity levels cover the following areas:

- (1) Constituent testing: This evaluates the individual properties of fibers, fiber forms, matrix materials, and fiber-matrix preforms. Key properties, for example, include fiber and matrix density, fiber tensile strength and tensile modulus, and fracture elongation.
- (2) Lamina testing: This level evaluates the properties of the fiber and matrix together in the composite material. For the purposes of this discussion prepreg properties are included in this level, although they are sometimes broken down into a separate level. Key properties include fiber area weight, matrix content, void content, cured ply thickness, lamina tensile strengths and moduli, lamina compressive strengths and moduli, and lamina shear strengths and moduli.
- (3) Laminate testing: Laminate testing characterizes the response of the composite material in a particular laminate design. Key properties include tensile strengths and moduli, compressive strengths and moduli, shear strengths and moduli, interlaminar fracture toughness, and fatigue resistance.
- (4) Structure element testing: At this level, the ability of a material to tolerate common laminate discontinuities is evaluated. Key properties include open- and filled-hole tensile strengths, open- and filled-hole compressive strengths, compression after impact strength, and joint bearing and bearing bypass strengths.
- (5) Structural subcomponent (or higher level) testing: This testing level evaluates the behavior and failure modes of more complex structural assemblies, which are usually used in verification tests based on lower-level testing.

The material form(s) to be tested, and the relative emphasis placed on each level, should be determined early in the material data development planning process. The selection of test forms will likely depend upon many factors, including: the

¹Owing to the popularity of lamina level testing and analysis, discussions in this handbook emphasize development of a lamina level database; however, this is not intended to inhibit the use of any of the other structural complexity level, either singly or in combination. This handbook does not emphasize the structural subcomponent category because it is so strongly application dependent; however, the concepts related to test planning and data documentation for coupon testing contained herein can be extended to structural subcomponent (or higher level) testing.

manufacturing process, structural application, corporate/organizational practices, and the procurement and/or certification agency. While a single level may suffice in rare instances, most applications will require at least two levels, and it is common to use all five in the complete implementation of the building block approach. Regardless of the selected structural complexity level, physical or chemical characterization of the prepreg properties (or matrix, if it is included as part of the process, as for resin transfer molding) is necessary to support the physical and mechanical property test results. Each procurement or certification agency has specific minimum requirements and guidelines for use of data. It is advisable to coordinate with the procuring or certifying agency before planning to ensure testing is conducted, which supports these structural qualification or certification.

(2) Data application categories

Other than classifications based on structural complexity, material property testing can also be grouped in terms of the data application into one or more of the following five categories: screening,² qualification, acceptance, equivalence, and structural substantiation. The starting point for testing most material systems is usually material screening. Material systems intended for use in engineering hardware are subjected to further testing to obtain additional data. The five data application categories cover the following areas:

- (1) Screening testing: This is the assessment of material candidates for a given application, often with a particular application in mind. The purpose of screening testing is initial evaluation of new material systems under worst-case environmental and loading test conditions. This handbook provides guidelines for screening new material systems based on key properties for aerospace structural applications. The MIL-HDBK-17 screening test matrix provides average values for various strength, moduli, and physical properties, including both lamina and laminate level testing, and is designed both to eliminate deficient material systems.
- (2) Material qualification testing: This step proves the ability of a given material/process to meet the requirements of a material specification. This step is also the process for establishing the original specification requirement values. Rigorous material qualification testing considers the statistics of the data and is ideally a subset of, or directly related to the design allowable testing, performed to satisfy structural substantiation requirements. However, while a material may be qualified to a given specification, it must still be approved for use in each specific application. The objective is quantitative assessment of the variability of key material properties, leading to statistical data that are used to

²A more limited form of screening testing for the characteristic response of a limited number of specific properties (often only one property) is not explicitly named as a testing category, but is commonly performed. Such limited testing consists of small test populations of three to six specimens, usually from a single material batch, and often focuses on specific environmental conditions.

establish material acceptance, equivalence, quality control, and design basis values. Because there are various sampling and statistical approaches used within the industry, the approach used must be explicitly defined. A generic basis value can be obtained in many ways: Each user’s basis value carries with it well-defined sampling requirements and a specific statistical determination process. There is also an emphasis on additional considerations such as test methodology, failure modes, and data documentation.

- (3) Acceptance testing: This is the task of verifying a material’s consistency through periodic sampling of the product and evaluation of key material properties. Test results from small sample sizes are statistically compared with control values established from prior testing to determine whether or not the material production process has changed significantly.
- (4) Equivalence testing: This task assesses the equivalence of an alternate material to a previously characterized material, often for the purpose of using an existing material property database. The objective is to evaluate key properties of test populations large enough to provide a definitive conclusion, but small enough to avoid the costs of generating an entirely new database. A common application includes evaluation of potential secondary sources for a previously qualified material, and for evaluation of minor changes to constituents, constituent processing, or fabrication processing from a qualified material system. The testing aims to substantiate the replacement material based on previously established basis values.
- (5) Structural substantiation testing: This is the process of assessing the ability of a given structure to meet the requirements of a specific application. The development of design allowables is considered a part of this step. The allowables should ideally be derived or related to material basis values obtained during materials qualification.

A matrix is shown in Table 5.1, which illustrates a common testing sequence in the substantiation of a composite-based aerospace structural application. The material property tests from the structural complexity levels and data application categories are listed on the axes of an array, with each intersecting cell describing a

Table 5.1 Test program definition

Structural complexity level	Data application categories				
	Material screening	Material qualification	Material acceptance	Material equivalence	Structural substantiation
Constituent	1				
Lamina	2	4			
Laminate		5			7
Structural element	3	6			8
Structural subcomponent					9

distinct testing activity. Groups of cells can be used to summarize the scope of unique test programs. The sequence begins with the hatched cells at the upper left of the array and proceeds, with time, toward the cells at the lower right, with the numbered notes indicating the approximate order of the test sequence.

5.1.3 Test Program Planning

All major testing programs should begin with the preparation of a detailed test plan document. Characterization of composite material properties is distinctly different for that of metals and unreinforced plastics. There are many critical factors that affect testing and test planning. In addition to the material properties to be tested, the method of testing and the preparation of the specimens should be specified in the testing program. Other factors such as the testing acceptance and requirements for nondestructive evaluation, data processing, and specimen moisture absorption, which can affect the test results, should be considered in the testing program. A full discussion of these issues will be the focus of this section. In addition, consideration will be given to material operation limits and property testing under ambient and non-ambient conditions, because of their importance in testing of composite structural properties.

5.1.3.1 Test Property Selection

Composites are produced from two or more different materials. The multiple raw materials and complexity of the composition, including anisotropic properties and “dimensional effects” in hot-wet conditions, mean that it is uneconomical to evaluate and test all properties. In practice, only those properties that are critical to the composite application will be selected and evaluated. The main factors will be the critical test method and test conditions. Special applications may involve some other factors.

In lamina level tests, the material strength and stiffness are selected including the tensile, compression and shear strength, and moduli. Measurements of the 0° tensile and compression in the longitudinal direction can provide the static strength and stiffness. The ±45° tensile strength is used to determine the shear modulus and the effective strength. Laminate testing also aims to test features of discontinuous stress, such as fastener element holes, bolt by-passing bearing, and impact damage. These tests are usually performed at room temperature. The effects of environment can be evaluated by lamina tensile and open-hole compression testing. Finally, the compression after impact (CAI) is used to evaluate the damage resistance.

For composite materials to be used at high temperature or in special liquid environments, further high-temperature resistance and liquid sensitivity tests should be performed. High-temperature performance typically involves dry-wet high-temperature static mechanical tests, thermal-oxidation stability, and thermal cycle

fatigue tests. The highest exposure temperature for thermal-oxidation stability and thermal cycle fatigue tests should be selected between the wet and dry glass transition temperatures. The thermal oxidative stability (TOS) test should be performed for a minimum of 1000 h. Weight loss should be measured during testing at specified intervals of 100, 250, 500, 750, and 1000 h. This test is a measure of the oxidation rate of a material. Thermal cycle fatigue tests should be performed for a minimum of 500 thermal cycles at a specified temperature. Over the course of the test, crack generation and crack growth rates should be determined to characterize the thermal fatigue resistance of the composite.

The liquid sensitivity test is mainly used to evaluate the possibility of property changes caused by long-term contact with chemical agents, such as fuel oil, hydraulic fluid, detergent, and ice removing agents. For example, epoxy resin exposed to strongly acidic media can undergo degradation and high-temperature BMI and polyimide resins are easily degraded by strong alkali conditions. Liquid sensitivity tests can be also used to evaluate the resistance of the composite to liquids, which are likely to come into contact with the part. In some cases, additional modifiers may change the resin resistance to solvents. For example, poly-sulfone thermoplastic composite structures have lower resistance to hydraulic fluid; however, some other thermoplastic materials give good resistance to moisture and hydraulic fluid, but poor fuel oil resistance.

5.1.3.2 Test Method Selection

Although the basic physics of test methods for composite materials are similar to those for testing metals or plastics, the heterogeneity, orthotropic, moisture sensitivity, and low ductility of typical composites often lead to major differences in test requirements, particularly for mechanical tests. These differences include:

- (1) The strong influence of constituent content on material response necessitates measurements of the material response of every specimen.
- (2) Properties should be evaluated in multiple directions.
- (3) Specimens should be conditioned to quantify and control moisture absorption and adsorption.
- (4) The methods of specimen alignment and load induction have increased importance for composites.
- (5) The consistency of failure modes requires some assumptions to be made.

Thus, many historical test methods which have been developed for metals or plastics cannot be directly applied to advanced composite materials in most cases. Other distinguishing characteristics of many composite materials also contribute to differences in testing. For example, compressive strength is often lower than tensile strength, operating temperatures are closer to the material's transition temperatures, the shear stress response is uncoupled from the normal stress response, and specimens are highly sensitive to the preparation methods.

Therefore, to properly evaluate the properties of composites, suitable testing methods should be developed. Many investigations on different test methods have been performed and standards have been established. However, current testing methods remain inadequate.

One measure of a test method is the ability of a perfect test to reproduce a desired behavior, such as the uniform uniaxial stress state. However, the above factors tend to increase the sensitivity of composites to a wider variety of testing parameters than those affecting traditional materials. Therefore, the robustness of a test method, or its relative insensitivity to minor variations in the specimen and test procedure, is just as important as theoretical perfection. Robustness, or lack thereof, is assessed by interlaboratory testing, and is measured by precision (variation in the sample population) and bias (variation of the sample mean from the true mean).³ The precision and bias of test methods are evaluated by comparison testing (often called “round-robin” testing) both within-the same and between external laboratories. An ideal method should have high precision (low variation) and low bias (sample mean close to true average) both within-laboratory and between laboratories. Such a test method would repeatedly give reproducible results regardless of the material, operator, or test laboratory. However, quantification of bias requires a material standard for each test. Such standards are not currently available for composites. As a result, bias of composite test methods can currently only be qualitatively assessed.

Other separate issues from the precision and bias of a test method (for a given specimen) are the effects of test specimen size and geometry on precision and bias. For heterogeneous materials, physically larger specimens can be expected to contain a more representative sample of the material microstructure. Although this is desirable, a larger specimen is more likely to contain more micro- or macro-structural defects than a smaller specimen and can be expected to produce somewhat lower strengths. Variations in specimen geometry can also create differing results. Size and geometry effects can produce statistical differences in results independent of the “degree of perfection” of the remaining aspects of a test method. Therefore, an “ideal” test method will use a specimen geometry that can be consistently correlated with its structural response.

The criticality of various test parameters is not yet well understood and the subject of current research. Furthermore standard practices, may vary from laboratory to laboratory upon close examination. Hence, methods should be selected that are commonly used, easily controlled, and meet the user’s requirements. For example, mechanical testing using a unidirectional specimen will generally not enable effective or reproducible results. Therefore, alternate approaches are often used. For example, $[90/0]_{ns}$ cross-ply laminates are often used for static mechanical testing, and the equivalent unidirectional strength and stiffness can be calculated based on laminate theory. Cross-ply laminates have been shown to have a large

³The term “accuracy” is often used as a generic combination of aspects of both precision and bias. The terms “precision” and “bias”, being more specific, are preferred for use where appropriate.

tolerance to secondary deviations in specimen preparation and testing implementation, which can often give high average strength measurements and low scatter of data. In terms of practical applications, it is commonly thought that cross-ply laminates are more representative of the material response of structural laminates.

In addition, the testing methods and parameters used should be detailed in specifications to reduce the variation caused by some occasional factors.

5.1.3.3 Population Sampling

In material property testing, results may be different from each other even if the materials, testing methods and conditions are maintained, and the data may show considerable scatter. In general, the properties of composites will change between different batches. Furthermore, data should not be acquired from a single testing condition. Instead, a testing population should be used based on many factors such as temperature, moisture, and ply layer sequence. To obtain results with high reliability, data from enough specimens are needed to ensure that the testing results are sufficiently reproducible to meet engineering accuracy requirements. The level of data deemed to be sufficient depends on many factors including: statistical models for population sampling, the necessary replicates of a desired result (i.e., the selection of A-basis and B-basis values), the deviation of the measured properties from those under practical conditions, and the deviation of the measured properties caused by testing methods.

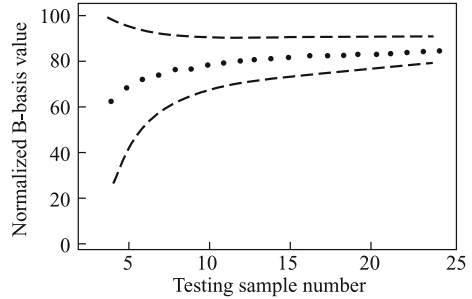
Owing to the reasons mentioned above, the sample size cannot be strictly defined; instead, only general guidelines can be given according to the application requirements. According to the statistical model applied, a larger sample number will be needed for a Weibull distribution model than that required for a normal distribution model. The A-basis value is a 95% lower confidence bound of the first percentile of a specified population of measurements, while the B-basis is a 95% lower confidence bound on the tenth percentile of a specified population of measurements. Thus, the A-basis requires much more data than B-basis for a given replicate.

Population sample sizes include the selection of sample size of each batch and the selection of batch numbers. For general data development, sampling techniques and sample sizes will depend on the application or qualification/certification agency. Any sampling scheme should have multiple batches composed of uniformly sized subpopulations. These two aspects will be discussed in the following:

(1) Sample size selection

Regardless of the sampling scheme, for small sample populations, the results of any basis value calculation depend strongly on the sample size. Smaller sample populations are clearly less costly to test; however, as the population size decreases, so does the value of the calculated basis. Figure 5.2 shows, a hypothetical example, the effect of sample size on the calculated B-basis value for samples of various sizes

Fig. 5.2 Normalized B-basis of $1-\sigma$ limits



drawn from a given infinite normally distributed population. In the limit, for very large sample sizes, the B-basis (tenth percentile) value for this example would be 87.2. The dotted line in the figure is the mean of all possible B-basis values for each sample size; this line can also be interpreted as the estimated B-basis value as a function of population size for a fixed sample coefficient of variation (CV) of 10%. The dashed lines represent the $1-\sigma$ limits for any given sample size (a $2-\sigma$ limit would approximately bound the 95% confidence interval).

It can be seen from this figure, not only does the estimated B-basis value increase with larger sample sizes, but, as the $1-\sigma$ limits illustrate, the expected variation in the estimated B-basis value significantly decreases. The lower $1-\sigma$ limit is farther from the mean B-basis value than the upper $1-\sigma$ limits, illustrating a skewing of the calculated B-basis value, which is particularly strong for small sample sizes. As a result of this skew, for small populations the calculated B-basis value is much more likely to be over-conservative than under-conservative. This result increases the penalty paid for B-basis values determined from the use of small populations. While similar examples for non-normal distributions show different quantitative results, the trends with sample size can be expected to be similar.

(2) Batch quantity selection

If the data variation between samples is caused by occasional factors in the same batch, the property data between different batches will show a much more complex deviation. For example, many factors such as raw materials, processing history, and the state of equipment can cause large variations of properties between batches. If testing is performed only on samples from a single batch, and the average result approaches a constant value, this constant will be different from that obtained from testing of different batches. The former reflects convergence to a certain value of a specific population batch, while the latter is the real convergence to the total population average value (full average value). The differences of the average values between the total population and a special single population are the second variance of the measured material property values. This variation is a random measurement and will change from batch to batch. Therefore, statistical approaches should be used to determine the variation between batches, and the batch quantity should be determined according to the needs of a specific property test.

If the resulting statistical analysis indicates excessive batch-to-batch variation, the data are not conventionally pooled but should instead be evaluated using Analysis of Variance (ANOVA). It is often necessary to add batches to generate more statistical data. When the statistical analysis shows no clear variation between batches compared with that within a single batch, the data obtained from different batches can be merged and a smaller number of batches can be used to perform testing.

Small numbers of batches can cause ANOVA to produce extremely conservative basis values, because it essentially treats the average of each batch as a single data point for input into a conventional normal distribution technique for basis value determination. This statistical method assumes that the test variation is negligible, and that variation caused by testing, either within or between batches, is treated as real material/process variation, which can result in unrealistically low basis values. Also, the between-batch variation test becomes progressively weaker as the number of batches decreases or as the variation between batches decreases, or both. For example, when only a small number of batches are sampled, a batch variation test result that indicates no significant batch variation may not be reliable. Testing of additional batch samples may indicate that the batch variation exists, but was masked by the original small number of batches. Attention should be paid to this issue when batch variation exists and the ANOVA basis values are calculated based on less than five batches.

5.1.3.4 Material and Processing Variation

The majority of fibers, resins, and composite material forms and structural elements are the products of complex multistep materials processes. Figure 5.3 illustrates the nature of processing from raw materials to a finished composite product. These processes may involve elevated temperatures, stress, and pressure. The procedures often involve evolution of volatiles, resin flow and consolidation, and readjustment of the reinforcing fibers. As shown in Fig. 5.4, each rectangle represents a process during which additional variability may be introduced into the material. In Fig. 5.3, each obtained product will become the raw material for the next processing step. The variations of materials and processing in this processing are often superimposed. If the measured properties of composite materials are to be interpreted correctly and used appropriately, the variability of the properties of the materials must be understood. This variability arises during routine processing and may be increased by the various anomalies that may occur during processing.

Currently, polymer matrix composites are most widely used. These composites feature organic matrices (either thermosetting or thermoplastic) and organic or inorganic reinforcing fibers. Variation of the mechanical properties of the reinforcing fibers can arise from many sources, such as flaws in the fiber microstructure,

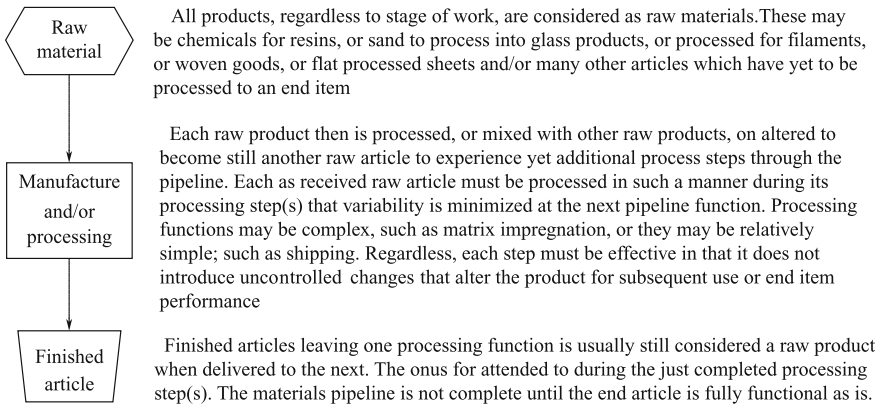


Fig. 5.3 Basic flow chart of composite processing

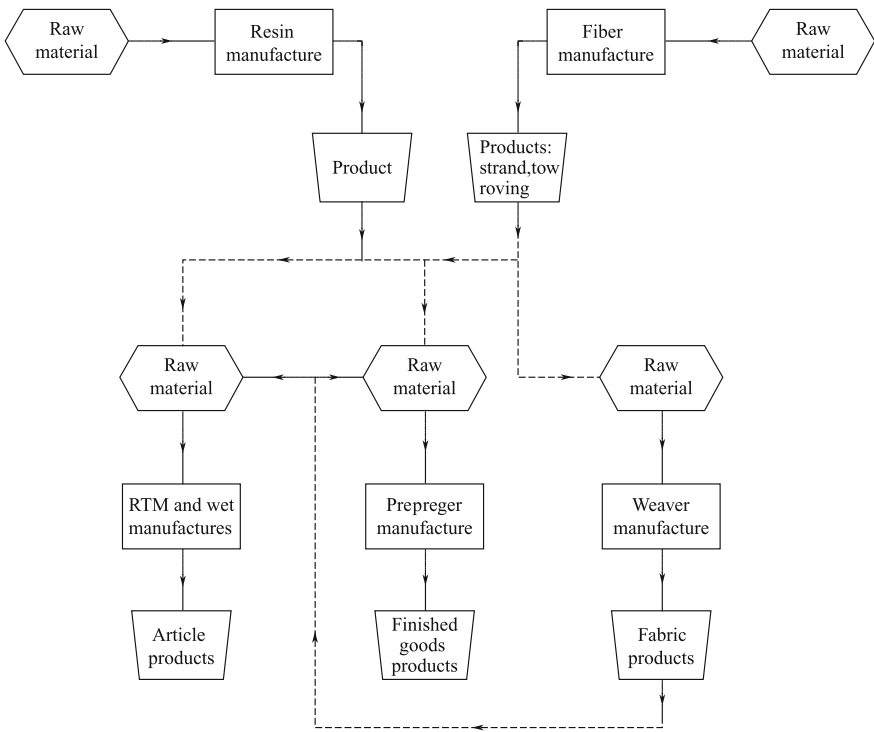


Fig. 5.4 Raw material flow chart of composite processing

or variation in the degree of orientation of the polymer chains in the organic fibers. Damage can also be induced during filament merging and product delivery; hence, a layer of protective coating is usually applied to the fiber surface.

Thermoplastic matrices can exhibit variations in the molecular weight and molecular weight distribution of the polymer as a result of processing. The melt viscosity and resulting processability of a thermoplastic matrix can be strongly affected by such variability. Thermosetting resins are often applied to fibers in a prepregging operation and in some forms, are partially cured to a so-called B-stage. Other methods for stabilizing thermosetting resin systems may also be used before the prepregging operation. Stability of these materials is important because there are many potential sources of variability during packaging, shipping and storage of improperly, and even properly, stabilized intermediate forms such as prepreg tape, fabrics, and roving.

Compared with handling of raw materials, property variation is more often encountered during the composite processing step. For example, the placement of reinforcing fibers or prepreg tapes may be accomplished through manual or automated processes with high precision. Lack of precision in fiber placement or subsequent shifting of the reinforcing fibers during the matrix flow and consolidation can introduce variability. Depending on the curing process, consolidation can occur simultaneously with the fiber placement, or after the fiber placement. This step in the process is especially vulnerable to the introduction of variability. For example, consider the curing of a composite part from a B-staged prepreg tape in an autoclave, a press, or an integrally heated tool. When the resin is heated and has begun to flow, the material consists of a gas phase (volatiles or trapped air), a liquid phase (resin), and a solid (reinforcement) phase. To avoid variability in material properties due to excessive void volume, the void producing gas phase material must be either removed or absorbed by the liquid phase. To avoid variability caused by variations in the fiber volume fraction, the resin must be uniformly distributed throughout the part. The fiber must maintain its selected orientation to avoid variability or loss of properties due to fiber misalignment.

In general, during the selection of raw materials and processing implementation, pertinent processing parameters and material effects should always be documented to support process control and troubleshooting. If potential processing and manufacturing pitfalls are not identified and avoided in this way, resources may be wasted in testing materials, which are not representative of those that occur in the actual part or application. Furthermore, heavy weight penalties might be paid to allow for avoidable material variability. A better understanding of these processing parameters and their potential effects on material properties will also allow a composites supplier or manufacturer to avoid the considerable expenses involved in the production of materials, parts, or end items, which have unacceptable properties.

5.1.3.5 Sample Preparation and Inspection

(1) Sample preparation

The validity of material properties used in design of a structure depends on the quality of the tested specimens. If the objective of the testing is to provide comparative information of different materials, it is crucial that variability due to specimen preparation be minimized. If the data being generated are intended for the generation of an allowable, the aim should be to reflect the interaction of the base material and processing, which may be expected to occur in production. In either case, care must be taken in the specimen preparation process to minimize the variation, which naturally occurs during the process. Issues to consider in specimen fabrication include specimen traceability, test article⁴ fabrication, specimen location, configuration, and machining.

- (1) Traceability: all specimens should be traceable to the material batch number, lot number, and roll number. Each specimen should be traceable to its location within the test article and processing information, should be included in the specification to enable full traceability. When uncured materials are purchased all available traceability information, including vendor certifications, and material inspection data of acceptance test results, should be delivered with the material. All prepreg materials that are stored before fabrication should have a storage history record. Information such as accumulated time in and out of refrigeration should be recorded.
- (2) Test article fabrication: the following is a list of important items that should be considered when fabricating test articles:
 - ① Test articles should be built according to engineering drawing requirements or sketches. The drawing requirements or sketches should specify: ply materials, test article reference orientation, ply orientation, material and process specifications or equivalent process documents, and inspection requirements.
 - ② Important material and process identification, such as prepreg batch number, lot number, roll number, autoclave run, pressing or other consolidation method, and layer stacking sequence should be recorded. This information should be stored to maintain the traceability of the test articles. This same traceability should be maintained for any excess material left after the specimens have been removed.
 - ③ The test article identification code and witness line should be permanently identified on each test article. A witness line should be established on the fabrication tool to act as a reference to the fiber orientation of the test article.

⁴A test article is any construction from which individual specimens are extracted. Such a test article may be a flat panel fabricated specifically to develop material properties, or it may be a production part set aside for test purposes.

For hand-laying methods, a witness line should be maintained during the layup and curing process and identified as a reference for the orientation.

The angular tolerance between the plies depends on the processing specifications applied to the material. For automated processes, some other method of establishing the reference orientation must be established. Once established, the witness line should be transferred to the test article and maintained throughout the specimen extraction.

- ④ It is generally recommended that for cured test articles at least 1 in. (25 mm) of material be trimmed from the edges. One of the machined edges of the test article may be used to permanently maintain the reference orientation on the article.
 - ⑤ The requesting organization (or if required, the appropriate quality assurance organization) should inspect test articles. This inspection should be performed before the specimens are fabricated to ensure that all requirements are met in the control process specification or appropriate equivalent document.
- (3) Specimen fabrication: The following is a list of important points that should be considered when fabricating specimens.
- ① Specimens should be extracted from test articles in the region that meets all process, engineering drawing, and specimen drawing requirements.
 - ② Specimens should be located on the test article according to the cutting diagram provided by the requesting organization. If a test article does not pass the inspection criteria, the requesting organization may choose to cut specimens relative to the identified test article defects to ensure that effects of the defects on the specimen response are representative of the full-scale item.
 - ③ A specimen identification code should be defined in the test plan, referenced in the test instructions, and recorded in the data sheets. The specimen identification code should be permanently marked on each specimen. Care should be taken to mark the code outside the failure area of the specimen.
 - ④ For specimens too small to allow marking with the complete code, a unique serial number may be marked on the specimen. It is recommended that care is taken to place small specimens in bags properly labeled with full identifying information.
 - ⑤ If it is required that the location of the specimen on the test article be known, specimens should be labeled before being extracted. This labeling method should allow all specimen and excess material locations to be known after cutting.
 - ⑥ The reference edge of the specimen should be aligned with the specified orientation by the witness line. In instances where a smaller subtest article is machined and used to make several specimens at once, a reference line or edge should be transferred to the subtest articles from the witness line. This transfer line should be orientated within $\pm 0.25^\circ$ with respect to the witness line.

- ⑦ Specimens should be extracted from the fabricated test articles according to the appropriate machining procedure as specified. Specimens may be machined with a variety of machining tools. In general, the final cutting tool should have a fine grit, be hardened, and run at a high tool speed without wobble. The cut itself should be executed to minimize excess heating of the laminate.
- ⑧ The added cost and manufacturing associated with tabbed specimens should be considered when selecting specimen type. The limitations and problems associated with tabbing of specimens are stated in each individual test method. If bonded tabs are required, the cure of the adhesive should be evaluated to determine if it is compatible with the composite system and tab material (if different). If the tab configuration produced in the bonding process is not within the geometry requirements of the specimen configuration, further machining of the tabs may be required.
- ⑨ Holes in specimens should be drilled in accordance with the applicable process specifications.
- ⑩ Any fasteners that are required should be installed in accordance with the applicable process specifications.

Completed specimens should be inspected prior to testing to ensure conformance with the standards being used. Variation in individual specimen thickness should be within the applicable test method tolerances. Larger variations may cause improper loading when used with close tolerance test fixtures. These variations may indicate that the specimen was fabricated improperly (e.g., ply drop-off or resin bleeding).

(2) **Nondestructive evaluation**

In specimen preparation, composites will be subject to mechanical machining, which may cause damage to specimens. To acquire correct test results, a nondestructive examination (NDE) report should be submitted together with the specimens by the manufacturer. If necessary, the test operator should conduct a nondestructive testing (NDT) inspection when accepting a specimen to verify the inspection report submitted by the manufacturer. If a specimen contains defects from the preparation, such defects should be verified and the location and dimensions indicated by the user.

Commonly used NDT inspection methods include visible inspection, tapping, supersonic inspection, and acoustic emission and infrared thermal imaging. In general, no single method can be applied to all types of defect/damage in a composite structure, and two or more methods may be required for real applications.

5.1.3.6 Moisture Absorption and Conditioning Factors

Most polymeric materials, whether in the form of a composite matrix or a polymeric fiber, are capable of absorbing relatively small amounts of moisture from the

surrounding environment.⁵ This absorbed water may produce dimensional changes (swelling), lower the glass transition temperature of the polymer, and reduce the matrix and matrix/fiber interface dependent mechanical properties of the composite, effectively lowering the maximum use temperature of the material. Because absorbed moisture is a potential design concern for many applications, material testing should include evaluations of properties after representative moisture exposure.

(1) Description of moisture absorption

Assuming there are no cracks or other wicking paths, the physical mechanism for moisture gain is generally assumed to be mass diffusion following Fick's law.

While material surfaces in direct contact with the environment absorb or desorb moisture almost immediately, moisture flow into or out of the interior occurs relatively slowly. The moisture diffusion rate is many orders of magnitude slower than heat flow in thermal diffusion. Nevertheless, after a few weeks or months of exposure to a humid environment, a considerable amount of water will eventually be absorbed by the material. The amount of moisture absorbed by a material depends on its thickness and the exposure time. The moisture properties of a material can be expressed by two parameters: moisture diffusivity and moisture equilibrium content (weight percent moisture). These properties are commonly determined by gravimetric testing methods.

The rate of moisture absorption is controlled by a material property, moisture diffusivity. Moisture diffusivity is usually only weakly related to relative humidity and is often assumed to be a function only of temperature, following an Arrhenius-type exponential relation with an inverse absolute temperature. This strong temperature dependence is illustrated in Fig. 5.5, which shows moisture diffusivity versus temperature for a particular type of carbon/toughened epoxy.

Moisture equilibrium content is only weakly related to temperature and is usually assumed to be a function only of relative humidity. The largest value of moisture equilibrium content for a given material under humid conditions occurs at 100% relative humidity and is also often called the saturation content. The moisture equilibrium content at a given relative humidity has been found to be approximately equal to the relative humidity multiplied by the material saturation content; however, as illustrated by Fig. 5.6, this linear approximation does not necessarily hold well for all material systems. Regardless, if a material does not reach the moisture equilibrium content for a given relative humidity, then the local moisture content will not be uniform through the specimen thickness. Furthermore, moisture absorption properties under atmospheric humid conditions are generally not equivalent to liquid immersion or exposure to pressurized steam. These latter environments alter the material diffusion characteristics, producing higher moisture

⁵Certain polymers, like polybutadiene, resist moisture absorption to the point that moisture conditioning may not be required, these materials are considered rare exceptions. However, many reinforcing materials, including those of carbon, glass, metallic, and ceramic fiber families, are not hygroscopic. As a result, except for polymeric fibers such as aramid, it is usually assumed that any moisture absorption is limited to the polymer matrix.

Fig. 5.5 Moisture diffusivity as a function of temperature

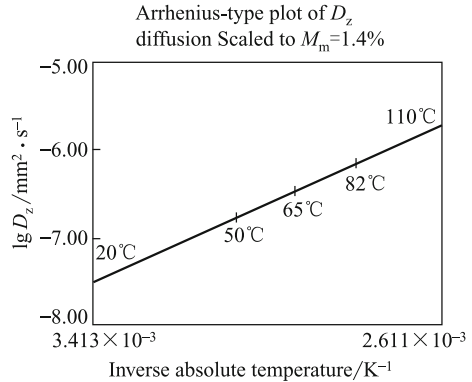
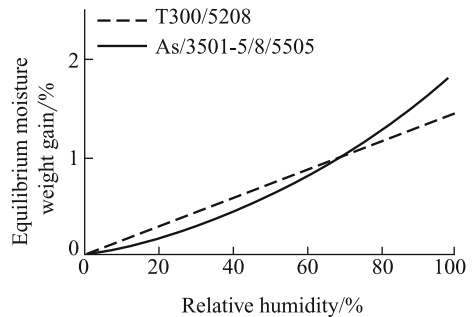


Fig. 5.6 Equilibrium moisture content versus relative humidity



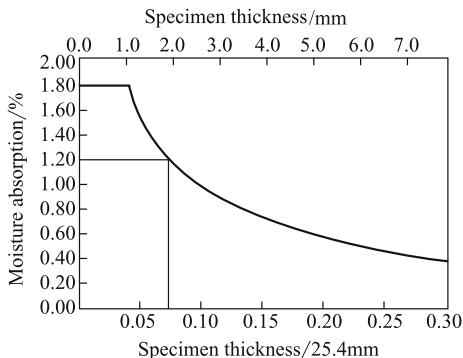
equilibrium content, and should not be used unless they simulate the relevant application environment.

(2) Sample immersion process

There are two methods for sample immersion treatment: One is fixed-time immersion, in which the sample is exposed to a moisture environment for a specified time period. Another method is equilibrium immersion, in which the sample exposure is terminated when the equilibrium between the sample and moisture environment is reached. Although fixed-time immersion is still commonly used in materials screening, this approach results in non-uniformity of the moisture absorption along the sample thickness direction. Thus, fixed-time immersion is not sufficiently representative and is only used for some screening-level purposes or as part of a structure application-level testing program. Instead, a conditioning procedure should be followed that accounts for the diffusion process and terminates with a nearly uniform moisture content through the thickness.

When absorbed moisture is included in the design, the evaluation of material moisture absorption characteristics (diffusion rate and equilibrium content) should be included in the material testing program. The effects of moisture on some key design properties after environmental exposure should also be considered.

Fig. 5.7 Two-sided moisture absorption of carbon/epoxy laminate after 30 days exposure at 60 °C/95% RH



- (1) Fixed-time immersion: As stated earlier, fixed-time conditioning has only limited usefulness and cannot generally provide the desired uniform moisture conditions through the thickness of the material. The shortcomings of the fixed-time approach are illustrated in Fig. 5.7 for a simulated 30-day exposure of IM6/3501-6 carbon/epoxy at 60 °C and 95% relative humidity (RH). With the use of known values for moisture diffusivity and moisture equilibrium content, the calculated average moisture content of various laminate thicknesses can be plotted as a smooth curve. From this curve, the maximum laminate thickness that can reach equilibrium at this temperature during this fixed conditioning exposure is 0.89 mm. For greater thicknesses, the moisture distribution through the thickness will not be uniform, as the interior moisture levels will be below the equilibrium moisture content.

As seen from the examples above, total moisture content resulting from fixed-time conditioning is thickness dependent. However, because fluids diffuse through different materials at different rates, fixed-time conditioning cannot produce uniform conditions for all materials,⁶ even if the thickness is constant. Therefore, test results based on fixed-time conditioning should not be used for design values, and generally should not even be used in qualitative comparisons between different materials.

- (2) Equilibrium immersion: To evaluate worst-case effects of moisture content on material properties, tests are performed with specimens preconditioned to the design service (end-of-life) moisture content. The preferred conditioning methodology should include procedures for the conditioning, as well as the determination of moisture diffusivity and moisture equilibrium content.

⁶Including specific material systems produced with different resin contents.

ASTM D5229/D5229 M is a gravimetric test method that exposes a specimen to a moisture environment and plots moisture mass gain versus the square root of elapsed time, as shown in Fig. 5.8. The early portion of the mass/square root time relationship is linear, the slope of which is related to the moisture diffusivity. As the moisture content of the material near the surface begins to approach equilibrium, the gradient of this curve becomes increasingly small. Eventually, as the interior of the material approaches equilibrium, the difference between subsequent weighing steps will be very small and the slope will be nearly zero. At this point, the material is said to be at equilibrium moisture content. This process is illustrated in Fig. 5.8, where the different curves show the difference in response at different temperatures. At 66 °C condition (diamonds in Fig. 5.8), the moisture profile through the thickness of the specimen, as shown in Fig. 5.9, illustrates the rapid moisture uptake near the surface at soon after exposure and the relatively slow uptake of moisture in the middle of the specimen.

Fig. 5.8 Typical moisture absorption response

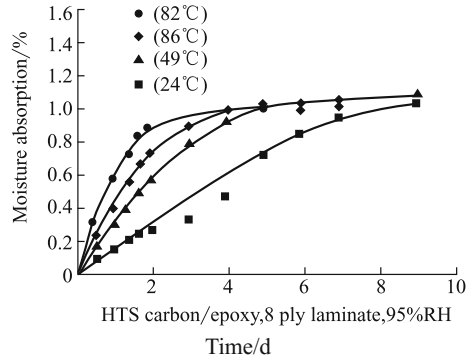
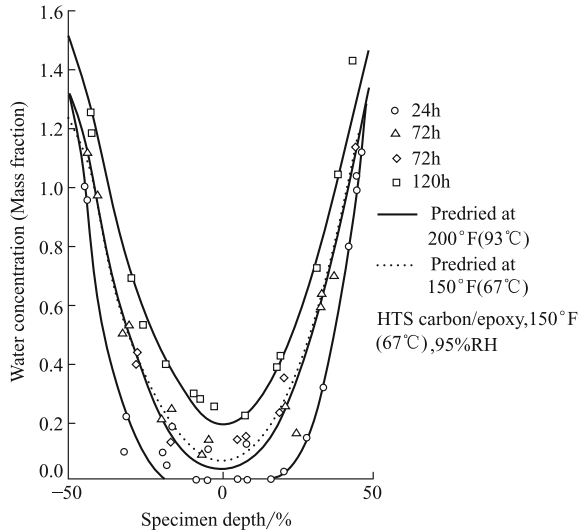


Fig. 5.9 Through thickness moisture profile versus time



- (3) Accelerated immersion conditioning: Because equilibrium moisture conditioning can take a very long time, it is desirable to accelerate the process. Certain two-step, accelerated conditioning cycles are considered acceptable, such as use of an initial high-humidity step (95% RH) to speed up moisture gain, followed by a stage at a lower final humidity level (85% RH) before equilibrium is reached. However, the selection of an accelerating environment should not change the material or alter the physics of diffusion. Because the moisture diffusion rate is so strongly dependent on temperature, it is tempting to accelerate the process by increasing the conditioning temperature. However, long-term exposure to high temperatures and moisture may alter the chemistry of the material. Cure epoxy-based materials are typically not conditioned above 82 °C to avoid these problems; materials that cure at lower temperatures may need to be conditioned below 82 °C. While an initial high relative humidity step is acceptable, extreme cases of exposure to pressurized steam or immersion in hot/boiling water are not accepted methods of accelerating humidity absorption, as these methods have been found to produce different results from those measured at 100% humidity.⁷
- (4) General procedures for immersion: The procedural descriptions and requirements are fairly complete for some standards; however, the following points should be emphasized:
- ① It is highly recommended that before performing conditioning some knowledge of the material moisture response be obtained, either from the literature or from prior testing.
 - ② In moisture property measurements the actual specimen must be initially dry, and the precision and timing of early mass measurements is critical. For the purposes of material conditioning, knowledge of the initial moisture content may not be important, or may be separately determined from other specimens in parallel. Therefore, moisture conditioning is not normally performed with a material dry out step. Moisture conditioning also does not require repetitive, precise weighing early in the exposure process that is necessary to determine the moisture diffusivity. Thus, conditioning without simultaneous determination of the moisture absorption properties is faster and less labor intensive.
 - ③ If the moisture properties are desired, it is faster and less labor intensive to create two other sets of specialized moisture property specimens, including a thin set that will reach equilibrium quickly, and a thick set, from which a stable slope to the moisture weight gain versus square root time curve can be reliably obtained with minimum test sensitivity.

⁷The differences reported in the literature are probably caused in part by excessively-high conditioning temperatures; however, even at moderate temperatures water immersion appears to produce a different response in many polymers than that from water vapor exposure. In some cases, matrix components have been known to dissolve into the water.

Moisture content measurements should be performed by either weighing the actual specimens, or by weighing “travelers,” in their place. The travelers are material conditioned specimens cut from the same panel and conditioned at the same time as the specimens. Travelers are required when the specimen is either too small, too large, or includes other materials, such as specimens with tabs or sandwich specimens. A traveler accompanies the specimen or group of related specimens, throughout the conditioning process. Because the weight gain of typical polymeric composites is relatively small (on the order of 1%), mass measurement equipment must be selected accordingly. For larger specimens (>50 g), a balance accurate to 0.001 g is generally adequate. For smaller specimens with a mass of the order of 5 g, a precision analytical balance capable of reading to 0.0001 g is required. Direct moisture mass monitoring of coupons weighing less than 5 g is not recommended; a traveler should be used instead.

Near the end of conditioning, minor weighing errors or small relative humidity excursions of the environmental chamber, particularly slight depressions in the relative humidity, may artificially cause the material to appear to have reached equilibrium, when, in fact, the material is still absorbing moisture. At lower temperature (lower diffusion rates), these errors become more important. In view of the possibility of these experimental errors, a prudent engineer should consider the following measures.

- ① Even after the material appears to satisfied the definition of equilibrium, review the chamber records to ensure that a depression in chamber relative humidity did not occur during the reference time period (weighing time interval). If such a depression is found to have occurred, continue the exposure until the chamber has stabilized, then processed to point ②.
- ② Even after the material satisfies the definition of equilibrium, maintain the exposure, and ensure satisfaction of the criteria for several consecutive reference time periods.

If a drying step is included, either as an initial step prior to moisture conditioning, or as part of an oven-drying experiment, care should be taken to avoid excessively high drying temperatures and high thermal excursions that may induce thermal cracking of the material.

For a specific material and relative humidity, a variant of equilibrium conditioning uses equilibrium conditioning test data to establish a relationship between the minimum exposure times required to achieve equilibrium versus laminate thickness. This approach eliminates many repetitive weighing steps.

(3) Conditioning and test environment

In immersion processes, the required equilibrium RH depends on the practical application. The designed service moisture content is only a semi-empirical calculated value, and for aircraft structural composites, this value is between 80% and 85% RH

based on different calculations. Thus, 85% RH is used as the test condition for equilibrium moisture content, if no other particular need is specified.

Hot-wet testing should use specimens conditioned to equilibrium moisture content and tested at the material operational limit (MOL) temperature or below. The effects of environment are generally small for matrix-dependent properties at temperatures below room temperature. Owing to these factors, qualification/certification testing programs typically do not require moisture conditioning below room temperature. Because there is generally no need to determine a cold MOL, specimens are simply tested at the coldest design service temperature (often $-55\text{ }^{\circ}\text{C}$).

5.1.3.7 Non-ambient Testing Environments

Composite materials can be affected by exposure to non-laboratory ambient environmental conditions and must be tested to determine those effects. Temperatures above and below ambient laboratory temperatures must be included in the test matrix to determine the effects of these environments. Many different regimes of testing may be appropriate depending on the usage of the materials. Normal environmental conditions for terrestrial applications can range from temperatures of $-55\text{ }^{\circ}\text{C}$ up to $180\text{ }^{\circ}\text{C}$. Conditions in space widen the range of performance temperatures from $-160\text{ }^{\circ}\text{C}$ to $230\text{ }^{\circ}\text{C}$. Cryogenic conditions less than $-160\text{ }^{\circ}\text{C}$ may also be of interest for storage tank applications. Special conditions may dictate the use of composite materials up to and beyond $315\text{ }^{\circ}\text{C}$ around leading edges or engine components. Composites used in space applications will also be subjected to ultraviolet radiation, atomic oxygen, micrometeoroid debris, and a charged particle environment. Thus, it is necessary to specify the application of materials to identify the required non-ambient test environmental conditions. The following discussion will examine high- and low-temperature testing conditions.

(1) Subambient testing

Testing performed below laboratory ambient test temperatures should use special fixtures or lubrication to ensure that the properties measured are related to material behavior and not due to freezing or sticking of sliding surfaces. Further challenges will be encountered in most cases. Materials can become more brittle and change their failure modes. Special instrumentation may be necessary to record material properties at cold temperatures. Adhesives used for tabbing or strain gaging should retain their elongation properties at cold temperatures.

Test temperatures as cold as $-55\text{ }^{\circ}\text{C}$ are common and considered to be representative. The cooling medium may be liquid nitrogen (LN_2), liquid carbon dioxide (LCO_2), or a refrigerated chamber. Temperature measurements are commonly made with J, K or T type thermocouples (T/C). The test setup in a test chamber must be precooled until stabilization at the test temperature. A dummy test specimen should be used to determine the soak times prior to actual testing. The dummy specimen should be fabricated from the same material and with the same ply orientation as

those of the test specimen. To determine the soak time, a T/C should be inserted into a hole drilled at the centerline of the dummy specimen. The time taken to reach the desired test temperature should be recorded and this time should be used when testing to ensure the test specimens are at the appropriate test temperature. Cool down rates should be controlled to minimize thermal shock and the possibility of damage and/or microcracking.

Freezing of test fixtures can cause anomalous test results. Fixture clearances must be checked to ensure free sliding surfaces. Proper lubrication or no lubricants should be used at the cold temperatures to prevent any fixture related effects on the test results. A thermocouple (T/C) should be placed in contact with the surface of the test specimen at the time of test. A typical soak time of 5–10 min, or the time determined from actual experimentation, should be used, after reaching the test temperature. Appropriate safety equipment should always be worn to prevent cold burns. Care must be taken if using liquid N₂ or dry ice (CO₂) when cooling the chamber to ensure that room oxygen is not depleted.

(2) Above ambient testing

Testing above ambient temperatures must be performed with consideration for the temperature and moisture content of the test sample. Special fixtures may be needed to accommodate the high temperatures. The possibility of adhesive failure and drying of test specimens should be evaluated before proceeding with a test program. Special lubricants may be required to prevent fixtures from sticking or binding. Instrumentation made especially for the required temperatures must be used to ensure valid data is recorded. Strain gauges, extensometers, and adhesives with the correct temperature rating must be identified and used. Special strain gauge foils or backing materials may be required to withstand elevated temperatures during testing. Instrumentation may require additional calibration at the test temperatures.

Above ambient test temperatures can typically reach temperatures as high as 180 °C. As for the case of subambient testing, the test setup in a test chamber must be heated until stabilization at the test temperature. Fixtures should be allowed to stabilize prior to testing. Heating of the test fixture with specimens, or the specimen only, is usually accomplished with an electrically heated chamber. To determine the soak time, a T/C should be inserted into a hole drilled at the centerline of the dummy specimen. The time taken to reach the desired test temperature should be recorded. This time should be used when testing to regulate the appropriate test temperature for the specimens. Heat up rates should be controlled to minimize thermal shock and the possibility of damage and/or microcracking. Excessive heat up rates may cause charring or melting of test specimens or adhesives. An appropriate lubricant, such as molybdenum disulfide, should be used on sliding surfaces to ensure freedom of movement of test fixtures.

For moderate test conditions, i.e., less than 93 °C, a humidity controlled test chamber is optional for short duration tests. When testing above 93 °C, then precise

humidity control is impractical and specimen dry out is a concern, especially for fatigue testing. A standard soak time is 5–10 min, after reaching the test temperature, if the test conditions are dry. If the test conditions are wet, soak times prior to the test should be kept short (<3 min) to minimize dry out.

Testing performed at temperatures above 180 °C must use special strain gauges and strain gauge adhesives, extensometers, and fixtures designed for the elevated temperatures. Special high-temperature-capable tab materials and tab adhesives are needed to prevent tab failures.

5.1.4 Data Reduction

5.1.4.1 Data Outlier Screening and Processing

An outlier is a data point that is much lower or much higher than the majority of other observations in a data set. Outliers are often erroneous values, perhaps caused by clerical errors, incorrect setting of environmental conditions during testing, or a defective test specimen. Data should routinely be screened for outliers, because these values can have a substantial influence on the statistical analysis. The maximum normed residual (MNR) method is used for quantitative screening for outliers.

(1) The maximum normed residual

The MNR test is a screening procedure for identifying an outlier in an unstructured set of data. A value is declared to be an outlier by this method if it has an absolute deviation from the sample mean which, when compared to the sample standard deviation, is too large to occur by chance. The MNR method can only detect one outlier at a time; hence, the significance level pertains to a single decision.

Let x_1, x_2, \dots, x_n denote the data values in a sample of size n , and let \bar{x} and s be the sample mean and sample deviation, respectively. The MNR statistic is the maximum absolute deviation from the sample mean divided by the sample standard deviation:

$$\text{MNR} = \frac{\max |x_i - \bar{x}|}{s} \quad (i = 1, 2, \dots, n) \quad (5.1)$$

The MNR value is compared with the critical value for the sample size n from Eq. (5.1). If the MNR is smaller than the critical value, then no outliers are detected in the sample; otherwise, the data value associated with the largest value of $|x_i - \bar{x}|$ is declared to be an outlier.

$$C = \frac{n-1}{\sqrt{n}} \sqrt{\frac{t^2}{n-2+t^2}} \quad (5.2)$$

where t is the $[1 - \alpha/(2n)]$ quantile of the t -distribution with $n-2$ degrees of freedom and α is the significance level. The recommended significance level for this test is $\alpha = 0.05$.

If an outlier is detected, this value is omitted from the calculations and the MNR procedure is applied again. This process is repeated until no outliers are detected. Note that the j th time that a sample is screened for an outlier, the mean, standard deviation, and critical value are computed based on a sample size of $n - j - 1$. It should be noted that for small samples, for example a batch containing five or six data, this procedure may identify most of the data as outliers, particularly if two or more of the values are identical. In this case, observational methods can be used to identify outliers.

(2) Disposition of outlier data

When outlier data are detected, the first action should be to identify evidence of a physical cause. The following list gives some examples of conditions that could be used as the basis for discarding outlier data.

- (1) The material (or a constituent) was out of specifications.
- (2) One or more panel or specimen fabrication parameters were outside the specified tolerance range.
- (3) The test specimen dimensions or orientation were outside the specified tolerance range.
- (4) A defect (not under study) was present in the test specimen.
- (5) An error was made in the specimen preconditioning (or conditioning parameters were out of the specified tolerance ranges).
- (6) The test machine and/or test fixture was improperly set up in a specific and identifiable manner.
- (7) The test specimen was improperly installed in the test fixture in a specific and identifiable manner.
- (8) Test parameters (e.g., speed, test temperature) were outside of the specified range.
- (9) The test specimen slipped in the grips during test.
- (10) The test specimen failed in a mode other than the tested mode (e.g., loss of tabs, unintended bending, failure outside the gauge section).
- (11) A test was purposely run to verify conditions suspected to have produced the outlier data.
- (12) Data were improperly normalized.

When an outlier is detected, it may or may not be a cause of concern. If its inclusion in the data does not significantly affect the calculated basis values and does not raise other engineering issues, it may simply be retained without further consideration.

In the case of a single data set outlier where additional data sets are available, the first consideration is to determine if the outlier in question is within the range of the non-outliers of the other data set(s). If it is within the non-outlier range of the other data, it is recommended that the outlier be retained.

If a single data set outlier is outside of the non-outlier range of other data, the next option is to retest with specimens from the same part or panel used to obtain the original data, which contained the outlier. If the retest data refute the outlier data, the retest data set may be used in place of the entire original data set. The replacement data set is then combined with the other data sets. If outliers still exist in the retest data, the original data can be retained and combined with the other data sets. The retest data set may also be added to the body of data. Regardless of whether the original data were replaced or not, the combined set is then tested for outliers. If no outliers are detected in the combined set of data, no deletions from the combined set are made.

5.1.4.2 Data Normalization

Most composite properties depend on the relative ratio between the reinforcement and matrix. In the characterization of continuous fiber-reinforced composite properties, calculations or direct comparisons may not be valid if test specimens have different fiber volume contents. Normalization is used to adjust raw test values to single (specified) fiber volume content. For many composites measured along the fiber direction,⁸ the relationships between properties and fiber volume content are basically linear. This relationship offers the possibility of adjusting some measured properties to a single specified fiber volume content, which allows normalized values to be obtained. In the following sections, normalization theory, methodology, and application will be discussed.

(1) Normalization theory

Mechanical properties that are dominated by the properties of the reinforcing fiber depend on the volume fraction of fiber in the laminate. In the commonly used “rule of mixtures” model, the 0° tensile strength of a unidirectional laminate, for example, is assumed to be equal to the matrix tensile strength at 0% fiber volume, and equal to the fiber strand tensile strength at 100% fiber volume. Thus, neglecting the effects of resin starvation at high fiber contents, the relationship between fiber volume fraction and ultimate laminate strength is linear over the entire range of fiber/resin ratios. This follows from the fact that the volume percent of fiber is the same as the area percent of the fiber in the specimen cross section. Tensile modulus can be expected to follow the same behavior. Thus, test specimens having different fiber volume contents have fiber-dominated properties that vary linearly with the fiber volume fraction.

⁸Refers to the fiber-dominated properties.

Two factors can cause the laminate fiber volume fraction to vary: the amount of matrix resin present relative to the amount of fiber (resin content) and the porosity (void volume). These factors give rise to differences in the fiber volume fraction from material to material, batch to batch, panel to panel, and even between specimens from within a panel. To perform data analysis that compares materials, batches, panels, or specimens, data for fiber-dominated properties must be adjusted to a common fiber volume fraction. If this correction is not applied, an additional source of variability will be included in the data, which might lead to erroneous conclusions. The process of data normalization attempts to remove or reduce this source of variability in fiber-dominated properties.

(2) Normalization methodology

In theory, fiber-dominated strength and stiffness properties vary linearly with fiber volume fraction. Thus, an obvious first approach would be to determine the actual fiber volume fractions of the test specimens by an appropriate method such as matrix digestion, ignition, or optical techniques. The raw data values may be adjusted according to the ratio of a common fiber volume fraction (chosen or specified) as represented in Eq. (5.3).

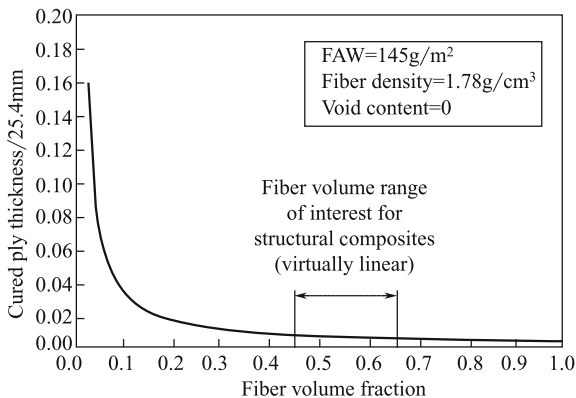
$$\text{Normalized value} = \text{Test value} \times \frac{FV_{\text{normalizing}}}{FV_{\text{specimen}}} \quad (5.3)$$

where $FV_{\text{normalizing}}$ is the chosen common fiber content (volume fraction or %); FV_{specimen} is the actual specimen fiber content (volume fraction or %).

Although this would appear to be the most direct approach, it has some limitations. The most serious deficiency is that fiber volume is not commonly measured for each individual test specimen. At best, representative pieces from each test panel are used to estimate the average panel fiber volume fraction. However, resin content might vary significantly within a panel owing to movement of resin during processing and other factors. Hence, the fiber volume fraction might not be the same for all specimens cut from the panel. As a result, accurate normalization of each individual specimen is not possible.

A preferred method of data normalization uses an approach that accounts for the fiber volume variation between individual test specimens. The basis of this method is the relationship between the fiber volume fraction and laminate cured ply thickness. As stated earlier, the laminate fiber volume fraction is a function of resin content and void content. At a given void content, the laminate fiber volume fraction is entirely dependent upon the resin content. Furthermore, for a given void content and fiber area per unit weight, the panel thickness is also dependent only upon the resin content. This relationship permits normalization of each individual test specimen by its ply thickness (total thickness divided by number of plies). An

Fig. 5.10 Example of correlation of cured ply thickness with fiber volume fraction



example of the relationship between cured ply thickness and fiber volume fraction is shown in Fig. 5.10.

A near linear trend is found within the 0.45–0.65 fiber volume fraction range of usual interest for structural composites. By calculation, the new normalized value can be expressed as:

$$\text{Normalized value} = \text{Test value} \times \frac{1000 FV_{\text{normalizing}} CPT_{\text{specimen}} \rho_f}{FAW_{\text{batch}}} \quad (5.4)$$

where $FV_{\text{normalizing}}$ is the fiber volume fraction specified or chosen for normalizing; CPT_{specimen} is the actual specimen ply thickness (specimen thickness divided by number of plies), mm; ρ_f is the fiber density, g/cm^3 ; FAW_{batch} is the batch average fiber area weight, g/m^2 .

Another hybrid method uses both individual specimen thickness and fiber volume data obtained by experimental methods, given by Eq. (5.5):

$$\text{Normalized value} = \text{Test value} \times \frac{CPT_{\text{specimen}} FV_{\text{normalizing}}}{CPT_{\text{batch average}} FV_{\text{batch average}}} \quad (5.5)$$

where CPT_{specimen} is the actual specimen ply thickness (specimen thickness divided by number of plies), mm; $CPT_{\text{batch average}}$ is the batch average cured ply thickness calculated from a number of panels or specimen thickness measurements, mm; $FV_{\text{normalizing}}$ is the fiber volume fraction specified or chosen for normalization; $FV_{\text{batch average}}$ is the batch average fiber volume fraction calculated from a number of experimental fiber volume determinations from panels within the batch.

In Eq. (5.5), the test value is first adjusted by specimen ply thickness to an average batch ply thickness. This operation essentially normalizes the data to a common fiber volume fraction, presumably the batch average fiber volume fraction. The second ratio in Eq. (5.5) then makes a further adjustment from the batch

average fiber volume fraction to the normalized fiber volume fraction. This method can be useful when fiber area weights are not available. However, this approach requires another assumption that the specimens used to experimentally determine the batch average fiber volume fraction had an average ply thickness equal to $CPT_{\text{batch average}}$. This is not generally the case, because the batch average cured ply thickness may be determined from many measurements over a number of panels, while the batch average fiber volume fraction may be obtained from comparatively few specimens. If fiber volume specimens are selected carefully to be representative of batch ply thickness, this method may be used successfully.

5.1.4.3 Data Equivalence and Pooling

Evaluation of data equivalence includes evaluations of data pooling and evaluations of material equivalence. The ability to pool different subpopulations of test data is highly desirable, to obtain larger populations that are more representative of the whole system. Equally desirable is the ability to relate one material, without basis values, to another equivalent material that already has established basis values. Hence, the properties of materials having basis values can be used to replace property data of candidate materials in design, avoiding the need for repeat testing. In the former case, the similarity of data from two possibly different subpopulations is assessed for the possibility of combination. The latter case requires evaluation of materials with common characteristics to determine if they are sufficiently alike to use the data interchangeably for design. Both require statistical procedures to assess the similarities and differences between two subpopulations of data.

Before determining the statistical degree of equivalence, basic engineering considerations should be satisfied; the two materials should have the same chemical composition, microstructure, and material and form families. To some extent, the criteria for this may be application dependent. For example, property data from two composite systems with the same matrix and similar fibers may not warrant pooling if the fiber/matrix interface is distinctly different, even if the fibers have similar modulus and tensile strength. Usually, data equivalence is typically evaluated for data sets that differ in terms of relatively minor changes in precursor manufacturing or material processing. Such minor changes could include variation of the constituents or constituent manufacturing processes, use of identical materials processed by different component manufacturers, identical materials processed at different locations of the same manufacturer, slight changes in the processing parameters, or any combination of the above.

Statistical data equivalence methods currently assume that between- and within-laboratory test method variation is negligible. When this assumption does not hold, test method-induced artificial variation will severely weaken the ability of the statistical methods to meaningfully compare two different data sets.

After evaluation of data equivalence, similar but not equivalent property data of different materials from different component manufacturers, different locations of

the same manufacturer, or slight changes in processing parameters of the same manufacturer, can be pooled to establish more basis values.

5.1.5 Requirements of Test Reports

A test report should include the following contents:

- (1) Name of test item;
- (2) Specimen manufacturer and preparation, material class and specification;
- (3) Specimen lot number, shape, dimensions, appearance and quantity;
- (4) Testing temperature, RH, and condition adjustment;
- (5) Testing equipment and instrument including models, measuring range and service state;
- (6) Test results: property values, mathematical mean value, standard deviation and variation coefficient, as well as the failure mode of each specimen, if required;
- (7) Testing personnel, date, etc.

5.2 Characterization of Mechanical Properties and Recommended Testing Matrices

The lowest level of the building block design and verification approach involves mechanical tests at a specimen level. This step features three essential tasks: material screening, material specification development, and material allowable determination. In practical applications, as alterations or changes of materials and processing techniques take place more frequently, equivalent material evaluations will become more common. In this chapter, the characterization of mechanical properties and recommended testing matrices for the aforementioned concerns will be presented.

5.2.1 Expression of Mechanical Properties for Material Screening

At the initial phase of a composite material system development, the necessary material screenings should be performed. The objective of the screening process is to identify key mechanical property attributes and/or inadequacies of new candidate material systems, while limiting the amount of required testing to a minimum. The specifications established for these key properties are finally used to evaluate the

suitability of a composite material system to meet the structural integrity requirements of aircraft structures.

The integrity of aircraft structures can be defined as: the general terms of aircraft structure performances such as structural strength, stiffness, damage tolerance, durability, and other functions that can affect aircraft service safety, cost, and expense. Considering the characteristics of composites, the particular requirements for structural integrity include:

- (a) Determination of design allowables based on recognition of the effects of initial defect/damage on static structural strength.
- (b) Static strength design and verification of hot–wet environmental effects.
- (c) Durability design and verification of static cover fatigue and consideration of impact damage resistance.
- (d) Damage tolerance design approach based on impact damage and no-growth of damage.

On the basis of these considerations, recommended testing matrices are given in Table 5.2. The maximum testing temperature is equivalent to the maximum service temperature of the materials in service.

For polymer matrix composites applied at high temperatures (greater than 250 °C), TOS testing should be performed for a minimum of 1000 h to determine the weight loss. Thermal cycling tests should be performed for a minimum of 500 thermal cycles to determine if microcracking occurs and the rate of microcrack growth. An example test matrix is given in Table 5.3, although the actual test

Table 5.2 Recommended test matrices for material system screening

Testing		Test condition/ specimen number			Evaluation emphasis
		CTD	RTD	ETW	
Laminar	0° tensile	5	5	–	Fiber governing properties
	0° compression	–	5	5	Fiber/matrix inter-reaction
	±45° tensile	–	5	5	Fiber/matrix inter-reaction
Laminate ([45/0/ –45/90] _{ns})	Open-hole compression	–	5	5	Stress concentration
	Open-hole tensile	5	5	–	Stress concentration
	Bolt double-shear bearing	–	5	5	Bearing
	Compression after impact	–	5	–	Damage tolerance
	Static indentation	–	5	–	Damage resistance

Note CTA-cold temperature ambient, RTA-room temperature ambient, ETW-elevated temperature wet

Table 5.3 Test matrix for high-temperature PMC

Mechanical property	Test condition/specimen number					
	Dry test temperature			Wet	TOS	Thermal cycling
	-55 °C	23 °C	ET1	ET1	ET2	ET2
0° (longitudinal) tensile	5	5	5	–	5	–
0° (longitudinal) compression or open-hole compression (OHC)	–	5	5	5	5	5
In-plane shear	–	5	5	5	–	5

matrix may vary depending on the purpose of the investigation. It is important that all exposure conditions should be evaluated. The elevated test temperature (ET1) should be less than the wet glass transition temperature of the material. The elevated test temperature (ET2) used for TOS or thermal cycling should be higher than ET1 but lower than the dry T_g .

For composite systems that may be exposed to harmful fluid environments, the polymer resin serviceability should be evaluated. Different fluid exposure levels should be considered for composites exposed to fluids, with the exposure levels categorized as:

- (a) Group I: fluids that have the potential for pooling or will come into contact with the material for an extended period of time, such as jet fuel, hydraulic fluid, cooling fluid, and engine lubricating oil.
- (b) Group II: fluids that are wiped on and off parts (or evaporate) but will not be in contact with the material for an extended period of time, such as cleaning solvents, washing liquid, and ice removal agents.

The weight loss of material in a fluid should be evaluated by specimen immersion and the following evaluation procedures are recommended:

For Group I, immerse the material in fluid until the equilibrium weight gain is reached, unless test involves sump water immersion and corrosion testing.

For Group II, immerse the material in fluid for 15 days to determine the worst-case effects.

Both mechanical and physical testing should be performed after immersing the material. Mechanical testing should include open-hole compression testing (OHC) and in-plane shear testing on quasi-isotropic laminates at room temperature and the maximum service temperature. If a 20–40% loss in the in-plane shear modulus results after immersion, further investigations should be performed with a minimum of five specimens. In-plane shear testing or short-beam shear (SBS) testing can also be used for the evaluation. The physical property tests should include inspection of the mass change, microcrack observation by microscope imaging, and if necessary surface craze inspection by scanning electronic microscopy. New resin systems should be subjected to long-term exposure testing in crucial fluids (Group I), and the testing should be performed at an early phase of the evaluation.

If water or moisture is verified as fluids causing the worst property degradation, other fluid exposure tests can be eliminated in the following design testing.

For Group II fluids, resin matrix composites with a service history are recommended for use as reference materials.

5.2.2 Expression of Mechanical Properties for Material Specification

Composite specifications indicate the outgoing standards of prepreg products. These standards also act as the user's acceptance criteria. Composite specifications involve many requirements; the requirements on mechanical properties of cured prepregs should, at a minimum, include:

- (a) Longitudinal (0° or wrap) and transverse (90° or fill) tensile strength and modulus;
- (b) Longitudinal (0° or wrap) and transverse (90° or fill) compression strength and modulus;
- (c) In-plane shear strength and modulus;
- (d) Short-beam shear strength;
- (e) Open-hole tensile strength;
- (f) Open-hole compression strength;
- (g) Bolt double-shear bearing strength.

In the above properties, the strength is usually given as the minimum mean value and the minimum individual value. The modulus is given as a mean value or range.

For thin skins or the thin surface of a sandwich construction, which are easily damaged by external impact, the maximum contact forces causing static indentation should be included with the composite system. The minimum mean and the minimum individual values should be identified.

For primary structural composite systems, the compression strength after impact should be included and the minimum mean and the minimum individual values should be identified.

To establish mechanical property standards in material specifications, a recommended number of test specimens and environmental conditions are given in Table 5.4.

According to the user's requirements, the following mechanical properties can also be included in the material specification:

- (a) Typical laminate non-notched tensile and compression strength;
- (b) Typical laminate open-hole tensile and compression strength;
- (c) Typical laminate filled-hole tensile and compression strength;
- (d) Typical laminate single shear bearing ultimate strength;
- (e) Typical laminate compression strength after impact (a number of impact energy levels);

Table 5.4 Mechanical property test matrix for establishing composite specifications

Test content		Test conditions/specimen number			
		CTD	RTD	ETD	ETW
Laminar	Longitudinal (0° or wrap) tensile strength and modulus	3×2×3	3×2×3	3×2×3	–
	Longitudinal (0° or wrap) compression strength and modulus	3×2×3	3×2×3	3×2×3	3×2×3
	Transverse (90° or fill) tensile strength and modulus	–	3×2×3	1×2×3	3×2×3
	Transverse (90° or fill) compression strength and modulus	–	3×2×3	1×2×3	3×2×3
	In-plane shear strength and modulus	3×2×3	3×2×3	3×2×3	3×2×3
	Short-beam shear strength	–	3×2×3	–	–
Laminate ([45/0/–45/90] _{ns})	Open-hole tensile strength	3×2×3	3×2×3	–	1×2×3
	Open-hole compression strength	–	3×2×3	–	3×2×3
	Bolt double-shear bearing strength	–	3×2×3	–	3×2×3
	Compression strength after impacting	–	3×2×3	–	–
	Maximum contact forces for static indentation	–	3×2×3	–	–

- (f) Model I interlaminar fracture toughness;
- (g) Model II interlaminar fracture toughness;
- (h) Typical laminate open-hole tensile/compression ($R = -1$) $S-N$ curve;
- (i) Thickness direction tensile and compression strength.

Table 5.5 Definition of typical laminate

Typical laminate name	Laminate ratio [0/±45/90]	Recommended laying sequence	Remarks
Typical skin laminate I	(50/40/10)	[45/0/–45/90/0/45/0/–45/0] _{ns}	Typical structural laminating
Typical skin laminate II	Unidirectional tape: (40/40/20) Fabric: (40/20/40)	Unidirectional tape: [45/0/–45/90/0] _{ns} Fabric: [0 _f /90 _f /0 _f /90 _f /45 _f /–45 _f /90 _f /0 _f /90 _f /0 _f] _{ns}	Structural laminating upper limitation
Quasi-isotropic laminate	(25/50/25)	[45/0/–45/90] _{ns}	–
Typical skin laminate III	(10/80/10)	[45/–45/90/45/–45/0/45/–45] _{ns}	Structural laminating lower limitation

For the properties listed above, the data collection should be adapted to the user's requirements.

The definition of typical laminates is given in Table 5.5, in which typical values and upper and lower limitations of a laminating ratio can be selected and used for structures. The definitions given in this table are mainly used for transportation aircraft wing skins; however, other definitions for other vehicle structures may be determined according to their structural requirements.

5.2.3 Determination of Material Allowables and Recommended Test Matrices

Material allowables are used to characterize composite systems. For structural design and analysis, all test specimen should be prepared by following authorized material specifications and processing specifications, so that the obtained testing data can describe the performance of the materials to be used in the structure. Materials and processing alternatives should be considered in the determination of material allowables. The service safety of structures manufactured from a specific material system can be guaranteed if the data are used for structure design.

Material allowables consist of two types of property data:

- (a) Lamina level material allowables and quasi-isotropic laminate mechanical properties indicating structural application. The latter of these is mainly used to characterize a material system and provides the basic mechanical property data for structural design.
- (b) Material allowables are related to the structural design, which is the basis for establishing structural design allowables, and can be used for all structure designs based on a material system within the same manufacturer.

5.2.3.1 Lamina Level Material Allowables and Quasi-isotropic Laminate Mechanical Properties Required by Structural Applications

(1) Lamina Level Material Allowables Include:

- (a) Longitudinal (0° or wrap) and transverse (90° or fill) tensile strength and modulus;
- (b) Longitudinal (0° or wrap) and transverse (90° or fill) compression strength and modulus;
- (c) Main Poisson's ratio;
- (d) In-plane shear strength and modulus.

Among these properties, the 0° (or wrap) and 90° (or fill) tensile and compression strength, in-plane shear strength are usually taken as B-allowables, the modulus and main ratio are taken as mean values.

The mechanical properties of a quasi-isotropic laminates are related to their structural application and include:

- (a) Open-hole tensile strength.
- (b) Open-hole compression strength.
- (c) Bolt double-shear bearing strength.
- (d) Compression after impact.
- (e) The maximum contact force for static indentation.

These properties are usually taken as B-allowables.

For structures subjected to high frequency fatigue loads (usually higher than 1×10^7 fatigue cycles), fatigue should be regarded as an important factor. The effects of fatigue should be handled by following the principles below according to the structure loading conditions:

- (a) Basic material property screening—mainly used for material selection.
- (b) Design allowables—mainly used for the characterization of the selected materials to guarantee that the selected material can meet the design requirements. Can also be used as the fatigue magnifying coefficient to determine the testing conditions for high-level (more complex) components and structures.

(2) Recommended Testing Matrices and Expression Criteria

- (1) Laminar Level Material Allowables: general requirements of a mechanical property testing matrices include:
 - (a) The recommended mechanical property testing matrices are given in Table 5.3.
 - (b) A minimum of 30 test specimens per condition per property (at least six replicates for each of at least five batches) will be needed to perform the statistical analysis for determination of B-basis properties. Fewer replicates or batches may be acceptable if an agreement is reached between the contractor and the procuring or certifying agency; however, a minimum of three batches should be tested.

Table 5.6 Laminar level mechanical test matrix

Mechanical property	Test conditions/specimen number			Specimen subtotal
	CTD	RTD	ETW	
0°-tensile (wrap)	5×2×3	5×2×3	5×2×3	90
90°-tensile (fill)	5×2×3	5×2×3	5×2×3	90
0°-compression (wrap)	5×2×3	5×2×3	5×2×3	90
90°-compression (fill)	5×2×3	5×2×3	5×2×3	90
In-plane shear	5×2×3	5×2×3	5×2×3	90
Total specimens				450

Table 5.7 Laminar level mechanical property test matrix for regression analysis

Mechanical property	Test conditions/specimen number per batch					Specimen subtotal
	CTD	RTD	ET1	ET2	ET3	
0°-tensile (wrap)	5×1×3	5×1×4	5×1×3	5×1×4	5×1×4	90
90°-(or fill) tensile	5×1×3	5×1×4	5×1×3	5×1×4	5×1×4	90
0°-(or wrap) compression	5×1×3	5×1×4	5×1×3	5×1×4	5×1×4	90
90°-(or fill) compression	5×1×3	5×1×4	5×1×3	5×1×4	5×1×4	90
Transverse (in-plane) shear	5×1×3	5×1×4	5×1×3	5×1×4	5×1×4	90
Total specimens						450

Note ET2 represents the given maximum operation temperature; ET1 represents an intermediate temperature higher than R.T. but lower than ET2; ET3 represents the maximum operating temperature of the material system

- (c) In Table 5.6, the CTD is $-55\text{ }^{\circ}\text{C}$ cited for all types of aeronautical structures. The ETW high temperature is the maximum material operational capabilities (MOL).
- (d) In this chapter, the formula of $a \times b \times c$ is used to represent numbers of specimens, wherein a represents the test groups and b is the number of laminates tested in each group. At least two laminates should be produced from different batches. The specimen numbers of each tested laminate are reflected by c .
- (e) Except for in specific cases, the wet specimen should be exposed to 85% relative humidity until the equilibrium moisture absorption is reached. To accelerate moisture absorbing, the immersing can be performed at high temperature; however, for epoxy resin matrix composites, the maximum temperature should not exceed $80\text{ }^{\circ}\text{C}$. Usually, the conditions of $70\text{ }^{\circ}\text{C}/85\%$ RH are used to accelerate a specimen toward its equilibrium moisture absorption.

The test matrix in Table 5.6 can be replaced by that given in Table 5.7, the repressive analysis principles used in a laminar level mechanical test matrix are as follows:

Table 5.8 Recommended test temperatures for different composites ($^{\circ}\text{C}$)

Composite system	CTD	RTD	ET1	ET2	ET3
120 $^{\circ}\text{C}$ cured epoxy resin	-55	23	80	-	-
180 $^{\circ}\text{C}$ cured epoxy resin	-55	23	80	100	120
200 $^{\circ}\text{C}$ cured BMI	-55	23	100	130	150
230 $^{\circ}\text{C}$ cured BMI	-55	23	120	180	200
315 $^{\circ}\text{C}$ cured polyimide	-55	23	180	230	290

Note ET2 represents the given maximum operation temperature; ET1 represents an intermediate temperature higher than R.T. but lower than ET2; ET3 represents the maximum operating temperature of the material system

Table 5.9 Test matrix for filament winding structures

Mechanical property	Test conditions/specimen number per prepreg batch			Specimen subtotal
	CTD	RTD	ETW	
0°-tensile	5×2×3	5×2×3	5×2×3	90
90°-tensile	5×2×3	5×2×3	5×2×3	90
0°-compression	5×2×3	5×2×3	5×2×3	90
90°-compression	5×2×3	5×2×3	5×2×3	90
In-plane shear	5×2×3	5×2×3	5×2×3	90
Total specimens				450

Table 5.10 Mechanical test matrix of quasi-isotropic laminates related to their structures

Mechanical properties	Testing condition/specimen number		
	CTD	RTD	ETW
Open-hole tensile strength	3×2×3	3×2×3	–
Open-hole compression strength	–	3×2×3	3×2×3
Bolt double-shear bearing strength	–	3×2×3	3×2×3
Compression strength after impacting	–	3×2×3	–
Maximum contact force (QSI)	–	3×2×3	–

- (a) Regression analysis allows sharing of data obtained under different environmental conditions such as temperature and absorbed moisture content. For materials from different batches, the baseline generated from “as-fabricated” specimens can be used to determine the B-basis or A-basis allowables per property per condition.
- (b) Three high temperatures may be used to replace the maximum temperature condition. A proper combination of different temperatures and specimen conditions (dried or wet) can be used according to the operating requirements. All the selected temperatures at dried condition should be below the dry T_g , and lower than wet T_g if testing is performed under wet conditions.
- (c) Recommended test temperature distributions for different composites are given in Table 5.8.

The recommended mechanical property tests for filament winding structures are given in Table 5.9. It is recommended to use test panels that can simulate the processing technique of the end products and to perform the tests by standard test methods approved by the relevant certifying agency. Some standards are available in Appendix B.

- (2) Mechanical Property Testing Matrix of Quasi-isotropic Laminates Related to their Structures: A mechanical property testing matrix of quasi-isotropic laminates related to their structure application is given in Table 5.10, wherein the

ETW temperature is the maximum service temperature of the composite system.

5.2.3.2 Material Allowables Related to Structural Design

(1) Characteristics of Mechanical Properties

The mechanical properties of non-notched typical layered laminates are commonly used to verify and determine laminate failure criteria of a material system. On the basis of test data and classical laminate theory, testing can verify failure criteria, and carpet plots of the laminates with all the possible laminating ratios used in structure design can be calculated and determined. The required properties are given below:

- (a) Typical layered laminate x axis tensile strength and modulus;
- (b) Typical layered laminate y axis tensile strength and modulus;
- (c) Typical layered laminate x axis compression strength and modulus;
- (d) Typical layered laminate y axis compression strength and modulus;
- (e) Typical layered laminate x - y plane in-plane shear strength and modulus;
- (f) Typical layered laminate major Poisson's ratio.

The x - y coordinate system refers to the typical layered laminate reference coordinate system. Among the properties listed above, strength takes a B-basis value, while the modulus and Poisson's ratio take mean values.

The notched tensile and compression strength of typical layered laminates can reflect the effects of allowable defects on the tensile and compression strength of the composite system. The test-verified failure criteria and calculations can be used to establish carpet plots for open-hole tensile and compression strength, including:

- (a) Typical layered laminate open-hole tensile strength;
- (b) Typical layered laminate open-hole compression strength.

The above properties take B-base values.

The compression strength after impact of a typical layered laminate represents the effects of impact damage on the compression strength of the composite system. The test-verified failure criteria and calculations can be used to establish carpet plots of the compression strength after impact. The selection of impacting energy depends on the selected requirements for initial impact damage in the design criteria. The compression strength after impact takes B-basis values. Although a small number of specimen test results cannot reflect the performance of impact-damaged structures, these tests are generally conservative and can be used for in the preliminary design phase.

Table 5.11 Unnotched laminate strength testing matrix

Typical laminate	Thickness ^①	Angle to loading direction ϕ	Specimen number			
			Compression RTD	Compression ETW	Tensile CTD	Tensile RTD
Typical skin laminate I	T1	0	3×2×3	3×2×3	3×2×3	3×2×3
	T2	0	3×2×3	3×2×3	3×2×3	3×2×3
	T1	22.5	–	1×2×3	1×2×3	–
Typical skin laminate II	T1	0	3×2×3	3×2×3	3×2×3	3×2×3
	T2	0	3×2×3	3×2×3	3×2×3	3×2×3
	T1	22.5	–	1×2×3	1×2×3	–
Quasi-isotropic laminate	T1	0	–	1×2×3	1×2×3	–
Typical skin laminate III	T1	0	–	1×2×3	1×2×3	–
Subtotal	–	–	72	96	96	72
Total specimens	336					

① T1 represents a laminate thickness 2–6 mm; T2 represents a second laminate with thickness selected based on the upper limit of the structural laminate. In some cases, 1×2×3 specimens should be used for the statistical analysis necessary to establish the minimized B-base value. The derived decreasing coefficient can be used in other cases

The bearing strength of a typical layered laminate reflects the mechanical joining properties of the composite system, and takes B-basis values, which can be used to determine the allowables in mechanical joint design.

(2) Mechanical Property Testing Matrix

The recommended testing matrix for unnotched laminates is given in Table 5.11. If the structure thickness range significantly exceeds the basic T1 thickness range (2–6 mm), a second three-batch series of T2 laminate thickness tests is required for all test conditions. However, if the application range of the structure and laminate thickness vary within 4 mm, only one thickness test matrix is required. A recommended test matrix for typical layered laminates containing holes (including filled holes) is given in Table 5.12. A recommended CAI test matrix for typical layered laminates is given in Table 5.13.

The bolt bearing strength test matrices are specified as following:

- (a) The bearing strength tests reveal the mechanical joint properties of a material system. If the thickness variation of a structural laminate is within 4 mm, one thickness can be selected for testing (usually $t = 3.0\text{--}5.0$ mm). Other thicknesses should also be taken into account, and for a typical bolt diameter D (usually 5 mm for aircraft structures) three thicknesses of the most commonly used laminates (usually 0/±45/90 with the laying-up ratio of 30/60/10) should be selected to determine the $t/D \sim \sigma_{\text{bru}}$ curves.

Table 5.12 Open-hole (filled hole) laminate strength testing matrix

Typical laminate	Hole diameter <i>D</i> / mm	Width W/mm	W/D	Tensile (CTD)	Tensile (RTD)	Compression (RTD)		Compression (ETW)		Specimens
						Open hole	Filled hole	Open hole	Filled hole	
Typical skin laminate I	4.0	24	6.0	–	1×2×3	1×2×3	–	–	–	12
		32	8.0	–	1×2×3	1×2×3	–	–	–	12
	5.0	30	6.0	–	1×2×3	1×2×3	–	–	–	12
		30	5.0	–	1×2×3	1×2×3	–	–	–	12
Typical skin laminate II	6.0	36	6.0	1×2×3	3×2×3	3×2×3	1×2×3	1×2×3	1×2×3	60
		36	6.0	1×2×3	3×2×3	3×2×3	1×2×3	1×2×3	1×2×3	60
Quasi-isotropic laminate	6.0	36	6.0	1×2×3	3×2×3	3×2×3	1×2×3	1×2×3	1×2×3	60
Typical skin laminate III	6.0	36	6.0	1×2×3	3×2×3	3×2×3	1×2×3	1×2×3	1×2×3	60
Total specimens	–			18	66	66	18	18	18	288

Note 1. Tensile specimen thickness range 2.0–4.0 mm, compression specimen thickness range 3.0–5.0 mm; 2. In some cases, 3×2×3 specimens are used to establish the minimized B-basis value, and the derived decreasing coefficient can be used in other cases

Table 5.13 Impact-damaged laminate compression strength testing matrix (RTD)

Typical laminate	Specimen number
Typical skin laminate I	3×2×3
Typical skin laminate II	1×2×3
Quasi-isotropic laminate	1×2×3
Typical skin laminate III	1×2×3
Total	36

Note 1. Tensile specimen thickness range 4.0–6.0 mm; 2. In some cases, 3×2×3 specimens are used to establish the minimized B-basis value, and the derived decreasing coefficient can be used in other cases

- (b) The bearing strength has been shown to be basically constant if laminates with both 20–40% 0°-plies and 40–60% ± 45°-plies are used for testing. Hence, two laminate ply ratios should be sufficient in this case, i.e., the typical structural laminate ply ratios of 30/60/10 and 40/50/10.
- (c) A single shear testing configuration should be able to stimulate real cases of the most aircraft bolt connections more effectively than double-shear testing. Thus, single shear/single bolts should be initially selected for evaluation in the testing matrix. Furthermore, the effects of single shear/double bolt, double shear, and liquid gaskets should be taken into account.
- (d) The hygrothermal effects on composite static strength should be considered, including two environmental conditions (dry and wet or equilibrium moisture content absorbed at 85% RH) at room temperature and elevated temperatures (70 °C and the maximum operation temperature).
- (e) Data processing should be performed on the test results obtained under the test conditions used to establish B-base values, to confirm that a decreased coefficient induced by one condition is applicable to other conditions.
- (f) Test philosophy of a test matrix: for joints between composites and joints between composites and metals, the bearing strength of a single bolt/shear specimen of a typical laminate (thickness about 4 mm) with a bolt hole diameter $D = 5$ mm is used to determine mechanical joint design allowables. This test matrix should account for the effects of single shear and double shear, multibolts, laminate thickness, laminating ratio, gasket, hygrothermal conditions, bolt hole size, and data scatter to generate correction coefficients for different cases.
- (g) On the basis of the $t/D-\sigma_{\text{bru}}$ test curves and the real laminate and t/D ratio, the incorporation of correction coefficients in different cases, can permit design allowables for joint bearing strength to be derived for different laminates.

A recommended test matrix for typical laminate bearing strength is given in Table 5.14. The testing items and numbers given in the table present the general requirements, which can be modified to suit specific structural applications, material types, environmental conditions, and processing techniques.

Table 5.14 Test matrix for mechanical joint bearing strength

Material	Laminating ratio	Thickness/mm	Hole diameter/mm	Environmental conditions	Single/double shear	Single/double bolt	Fasten end shape	Gasket	Testing number		
Composite/composite	30/60/10	T1 (~4)	5	RTD	Single shear	S. bolt	Rising head	Yes	1×2×3		
							Embedded head	No	3×2×3		
								D. bolt	S. bolt	3×2×3	
		ETW		Double shear	1×2×3						
					RTD	1×2×3					
						ETW	1×2×3				
		RTD		Single shear			1×2×3				
					ETW		1×2×3				
						RTD	1×2×3				
	40/50/10	T2 (~3)	4	ETW			Single shear	S. bolt	Embedded head	No	3×2×3
					RTD						
						ETW					
		RTD		1×2×3							
					ETW		1×2×3				
						RTD		1×2×3			
		ETW		1×2×3							
					RTD		1×2×3				
						T3 (~2)		5	ETW	Single shear	S. bolt
RTD	1×2×3										
		ETW	1×2×3								
				RTD	1×2×3						
ETW	1×2×3										
		RTD	1×2×3								
				ETW	1×2×3						
RTD	1×2×3										
		T1 (~4)	4			ETW	Single shear		S. bolt	Embedded head	No
				RTD	1×2×3						
ETW	1×2×3										
		RTD				1×2×3					
				ETW	1×2×3						
RTD	1×2×3										
		ETW				1×2×3					
				RTD	1×2×3						
T1 (~4)	5						ETW	Single shear	S. bolt	Embedded head	No
		RTD	1×2×3								
				ETW	1×2×3						
RTD						1×2×3					
		ETW	1×2×3								
				RTD	1×2×3						
ETW						1×2×3					
		RTD	1×2×3								
				T1 (~4)	6		ETW	Single shear	S. bolt	Embedded head	No
RTD	1×2×3										
		ETW	1×2×3								
				RTD		1×2×3					
ETW	1×2×3										
		RTD	1×2×3								
				ETW		1×2×3					
RTD	1×2×3										

(continued)

Table 5.14 (continued)

Material	Laminating ratio	Thickness/mm	Hole diameter/mm	Environmental conditions	Single/double shear	Single/double bolt	Fasten end shape	Gasket	Testing number			
Composite/metal	30/60/10	T1 (~4)	5	RTD	Single shear	S. bolt	Rising head	Yes	1×2×3			
							Embedded head	No	3×2×3			
					Double shear	D. bolt				3×2×3		
		T2 (~3)	4	ETW	Single shear	S. bolt					3×2×3	
											RTD	1×2×3
											ETW	1×2×3
											RTD	1×2×3
											ETW	1×2×3
											RTD	1×2×3
		T3 (~2)	5	ETW	Single shear	S. bolt					1×2×3	
											RTD	1×2×3
											ETW	1×2×3
		T1 (~4)	4	RTD	Single shear	S. bolt					1×2×3	
											5	1×2×3
											6	1×2×3
40/50/10	40/50/10	T1 (~4)	4	RTD	Single shear	S. bolt			1×2×3			
									5	1×2×3		
									6	1×2×3		

Note In some cases, 3×2×3 specimens are used to establish the minimized B-base value and the derived decreasing coefficient can be used in other cases

5.2.4 Expression of Material Equivalence Evaluation and Mechanical Property Testing Data

In material applications, cases are frequently encountered in which verified material systems undergo changes to their constituents or manufacturing processes when used to make composite structures, while the original design and verification remains unchanged. For production of new parts, it is sometimes necessary to change the constituents and manufacturing processes of material systems, and perform a material equivalence evaluation to verify the equivalence of the new material system with the originally verified material system. Equivalence testing programs aim to guarantee that changes to a material and/or processing step do not reduced the material properties below those of the original verification. An alternate material system with major changes to its constituents and processing will require new verification. After passing verification, the structures manufactured by the new material systems will also require testing to verify the structural integrity.

5.2.4.1 Material Alternatives

Any case listed below is regarded as a material alternation.

- (a) A change in one or both of the basic constituents:
 - Resin;
 - Fiber (including size or surface treatment alone).
- (b) Same basic constituents with a change of the impregnation method.
 - Prepregging process (e.g., solvent bath to hot melt coating);
 - Tow size (3k, 6k, 12k) with the same fiber area weight;
 - Change of the prepregging machine at the same supplier or a supplier change for the same material (licensed supplier);
 - Others.
- (c) Same material but modification of the processing route (if the modification to the processing route governs the eventual composite mechanical properties):
 - Curing cycle;
 - Molds and tooling;
 - Layup method;
 - Environmental parameters of the laying room.

Case (a) (alternative material) should always be considered to be an important change; Case (b) and (c) are changes to an identical material system.

5.2.4.2 Scope of Material Equivalence

The principle of equivalence evaluation of alternate material system is that the alternate material system can meet the requirements of the material specification and processing specification, and has been verified, and proved to be equivalent to the original material system even if changes are involved including:

- (a) Alternate fiber;
- (b) Alternate resin;
- (c) Alternate fabric type;
- (d) Alternate fiber tow size;
- (e) Alternate sizing and coupling agent type.

The equivalence evaluation of the change in an identical material system is suitable for the particular alternation given below:

- (a) The material batch verification and acceptance should specify that the batch properties are equivalent to those available in a qualified data bank, e.g., this batch data can meet the acceptance standards of a certain material specification.
- (b) Suppliers change the raw material manufacturing processes.
- (c) The composite manufacturers uses another data bank for structural design, this manufacturer should certify the equivalence of the processing methods that can be used to obtain the equivalent material properties.
- (d) For composite components that already have property data bank, specification, and base values, manufacturers can change the production site and processing procedures without the need for rebuilding of the data bank.
- (e) Different manufacturers can use an identical processing method to that used previously to produce identical materials without the need for rebuilding of the data bank.

The above-mentioned alternations should satisfy the limitations given below:

- (a) All key prepreg constituents and/or their processing should be unchanged.
- (b) In the processing specification, all the key procedures for making initial and subsequent material systems should be equivalent. Any data that indicate the properties of replacement materials are lower than those of the qualified initial material systems are not allowed to be included in the subsequent material specifications.

In material equivalence evaluation, the initial data bank of the initial material system should be available.

Table 5.15 Material compatibility criteria

Worst	Best		←	→	Compatibility	
	1	2	3	4	5	6
Compatibility factor	1	2	3	4	5	6
Fiber type	Identical	Different	Identical	Different	Identical	Different
Sizing agent	Identical	Identical/ Different	Identical/ Different	Identical/ Different	Identical/ Different	Different
Fiber tow size	Identical	Identical/ Different	Identical/ Different	Identical/ Different	Identical/ Different	Different
Resin	Identical	Identical	Different	Identical	Different	Different
Resin supplier	Different	Identical	Identical	Different	Different	Different
Production line	Different	Identical	Identical	Different	Different	Different

Note 1. Identical—no changed in the alternate materials; Different—change of the alternate materials; 2. Column 1 denotes the change of a prepreg supplier and production line; 3. Column 2 denotes the changes of fiber type, supplier, and trade mark, the new qualified fiber types are equivalent to the originals; 4. Column 3 denotes a resin change; 5. Columns 4 and 5 reflect changes of the prepreg supplier, production line, and fiber/resin

5.2.4.3 Material Equivalence Evaluation Methods

(1) Essentials of Material Equivalence Evaluation

The essentials of material equivalence evaluation include:

- According to the structural importance, determine the key property parameter related to material equivalence, and give an explanation.
- Equivalence criteria include equivalence requirements for materials and other parameters closely related to structural manufacture and operation.
- Rationally establish the equivalence evaluation standards, considering that some parameters such as elastic modulus, density, fiber/resin content, and cured ply thickness should be controlled in a proper range, neither too low nor too high.
- For each parameter, decide the proper test items, measuring methods, and evaluation methods.
- Comprehensive evaluation, present equivalence conclusions.

(2) Material Compatibility

Material compatibility is determined by the criteria shown in Table 5.15. All the compatibility factors of the identical material system changes are defined as 1, the compatibility factors of the alternative material system change can be defined from 2 to 6 according to the nature of the change. In some cases, not included in this table, the evaluation should be based on the different compatible changes.

(3) Equivalence Testing Matrix

The recommended test matrices for unidirectional tapes and fabrics are given in Tables 5.16 and 5.17. In equivalence testing and inspection, identical testing

Table 5.16 Laminar level test requirements (unidirectional tape)

Laminar property	Batch number						Each batch number						Environmental conditions						Total					
	Compatibility factor						Compatibility factor						Compatibility factor						Compatibility factor					
	1	2	3	4	5	6	1	2	3	4	5	6	1	2	3	4	5	6	1	2	3	4	5	6
0°-tensile	2	3	3	3	3	3	4	4	4	4	4	5	2	2	2	2	2	2	16	24	24	24	30	36
90°-tensile	2	3	3	3	3	3	4	4	4	4	5	2	2	2	2	2	2	16	24	24	24	30	36	
0°-Compression	2	3	3	3	3	3	4	4	4	4	5	2	2	2	2	2	2	16	24	24	24	30	36	
90°-Compression	2	3	3	3	3	3	4	4	4	4	5	2	2	2	2	2	2	16	24	24	24	30	36	
L/T shear	2	3	3	3	3	3	4	4	4	4	5	2	2	2	2	2	2	16	24	24	24	30	36	
Total	-																		80 120 120 150 150 180					

Note Environmental conditions: RT/dry (RTD) and worst-case CTD or ETW

Table 5.17 Laminar level testing requirements (fabric)

Laminar property	Batch number						Each batch number						Environmental conditions						Total					
	Compatibility factor						Compatibility factor						Compatibility factor						Compatibility factor					
	1	2	3	4	5	6	1	2	3	4	5	6	1	2	3	4	5	6	1	2	3	4	5	6
L. tensile	2	3	3	3	3	3	4	4	4	4	5	6	2	2	2	2	2	2	16	24	24	24	30	36
T. tensile	2	3	3	3	3	3	4	4	4	4	5	6	2	2	2	2	2	2	16	24	24	24	30	36
L. Compression	2	3	3	3	3	3	4	4	4	4	5	6	2	2	2	2	2	2	16	24	24	24	30	36
T. Compression	2	3	3	3	3	3	4	4	4	4	5	6	2	2	2	2	2	2	16	24	24	24	30	36
In-plane shear	2	3	3	3	3	3	4	4	4	4	5	6	2	2	2	2	2	2	16	24	24	24	30	36
Total	-																		80 120 120 150 150 180					

Note Environmental conditions: RT/dry (RTD) and worst-case CTD or ETW

Table 5.18 Laminate test items

Material compatibility factor	Laminate testing items	Total	
		Uni. tape	Fabric
1	Unnotched laminates	20	20
2, 3, 4, 5	All static testing, two environmental conditions	70	70
6	All testing required	80	80

methods to those used for determination of the original material system B-basis values should be used and a statistical analysis performed to assess the test results and equivalence.

The alternate material system will require laminate mechanical testing to certify the property B-base values related to the key design parameters. A recommended test matrix is given in Table 5.18, and the specimen numbers are listed in Table 5.19. Fiber, resin, and prepreg alternation testing and specimen batches are given in Tables 5.20, 5.21 and 5.22. The left column in each Table reflects a description of the change indicating the recommended alteration. Detailed descriptions are given in Tables 5.23, 5.24, 5.25, 5.26 and 5.27.

5.2.5 Evaluation of Ability to Withstand Impact

One key issue of composite mechanical characteristics is their ability to withstand impact. Some studies have indicated:

- (a) In terms of the damage resistance and damage tolerance design of composite structures, the characteristics of composite behavior subjected to an impact are covered by damage resistance and damage tolerance.
- (b) Damage tolerance design requirements of composite structures necessitate that the structure can still bear the specified service loads even if barely visible impact damage (BVID) exists. In general, BVID means an indent depth (immediately measured after impact) greater than 1 mm, while the post compression strength is unchanged. Therefore, the compression failure strain (or strength) for an indent depth not smaller than 1.0 mm is recommended to characterize the damage tolerance of composites.
- (c) For determination of the impact behavior of composites, it is recommended that a representative quasi-isotropic laminate [45/0/-45/90]_{ns} be used to characterize damage resistance by quasi-static indentation (QSI) according to the ASTM D6264-07 test method. Referring to ASTM D7136-07 and ASTM D7137-07, an indent depth greater than 1 mm can be used to determine impact energy and the compression strength after impact (CAI) can be used to assess the damage tolerance behavior of composites [1-3].

Table 5.19 Laminate testing number

Structural properties	Loading		Laminate type/No.		Environmental conditions ^a		Specimen number ^b	Total specimens	
	Tensile	Compression	Uni. tape	Fabric	Uni.	Fabric		Uni. tape	Fabric
Static	•	•	1	1	2		5	20	20
	•	•	1	1	2		5	20	20
	–	•	1	1	2		5	10	10
	–	•	1	1	1		5	5	5
	•	–	1	1	2		5	10	10
	•	–	1	1	1		5	5	5
Total	–	–						70	70
Fatigue ^c	–	–	1	1	1		5	5	5
	–	–	1	1	1		5	5	5
	–	–							
Sum	–	–						10	10
Total	–	–						80	80

Note • Required testing items

^aTwo environmental conditions—RTD, worst-case—CTD or ETW, one environmental condition—RTD

^bOnly one batch material

^c $n = 1 \times 10^6$ residual strength testing required afterward

Table 5.20 Testing related to fiber alternation

Change	Test requirements—test batch numbers ^{a,b}						Laminate mechanical property					
	Constituent property ^c		Prepreg property				Laminate mechanical property					
	First change	Second change	Phys. property	Process. property	Mech. property verifying	Compres. (ETW)	In-plane shear (ETW)	Open-hole compres.	Open-hole tensile	CAI	Fracture toughness or interface bonding	
Table 22		Table 24	Table 25	Table 26								
New production line	3	3	2	–	1	1	1	–	–	–	–	
Precursor supplier change	3	3	3	–	3	3	3	2	2	–	2	
Sizing	3	3	3	1	3	3	3	2	2	–	2	
Fabric supplier	2	–	–	–	1	–	–	–	–	–	–	
Supplier change	2	–	–	–	1	–	–	–	–	–	–	
Main production equip.	2	By change content	–	–	1	1	1	–	–	–	–	
Processing	2	–	–	–	1	1	1	–	–	–	–	
Raw material	2	–	–	–	1	1	1	–	–	–	–	

^aIn prepreg testing, the most common resin system should be used

^bThree specimens for each physical and chemical test, five specimens for each mechanical test

^cFirst changes are minor changes; supplier completed additional testing beside normal acceptance testing, and verified no effects on the materials. Second changes are major changes; supplier completed adequate testing and verified that the material and the processing specifications need no changes

Table 5.21 Verifying testing related to resin formula change

Change	Test requirements—test batch numbers ^{a,b}										
	Constituent property ^c		Prepreg property			Laminate mechanical property					
	First change	Second change	Phys. property	Process. property	Mech. property verify	Compres. (ETW)	In-plane shear (ETW)	Open hole compres.	Open hole tensile	CAI	Fracture toughness or interface bonding
	Table 23		Table 24	Table 25	Table 26						
Constituent	3	3	2	1	2	2	2	2	–	1	1
Source	3	3	1	1	1	1	1	–	–	–	–
Processing	3	3	2	1	2	2	2	–	–	–	–
Equipment	3	3	2	1	2	2	2	–	–	–	–
Supplier change	2	–	1	–	1	1	1	–	–	–	–

^aIn prepreg testing, the most common resin system should be used

^bThree specimens for each physical and chemical test, five specimens for each mechanical test

^cFirst changes are minor changes; supplier completed additional testing beside normal acceptance testing, and verified no effects on the materials. Second changes are major changes; supplier completed adequate testing and verified that the material and the processing specifications need no changes

Table 5.22 Verification tests related top prepreg change

Change	Test requirements—test batch numbers ^{a,b}										
	Constituent property			Prepreg property			Laminate mechanical property				
	First change Table 23	Second change	Phys. property Table 24	Process. property Table 25	Mech. property verify Table 26	Compress. (ETW)	In-plane shear (ETW)	Open hole compress.	Open hole tensile	CAI	Fracture toughness or interface bonding
Processing/ equipment	3	1	2	2	2	2	2	–	2	3	1
New prod. line	3	1	2	2	2	2	2	–	2	3	1
Supplier change	2	1	1	1	1	–	–	–	–	2	1
New fiber/ resin	3	2	3	3	3	3	3	3	3	3	2

^aIn prepreg testing, the most common resin system should be used

^bThree specimens for each physical and chemical test, five specimens for each mechanical test

Table 5.23 Fiber testing matrix

Testing	First change	Second change
Tow tensile strength	•	–
Tow modulus	•	–
Density	•	–
Mass per unit length	•	–
Surface, such as ESCA/interface energy/microscopy	–	•

Note • Testing required

Table 5.24 Resin testing matrix

Testing	First change	Second change
High-pressure liquid chromatograph (HPLC)	•	–
Infrared spectrum (IR)	–	•
Differential scanning calorimeter (DSC)	–	•
Gel time	•	–
Bending modulus	–	•
T _g (dry and wet)	–	•
Viscosity	–	•
Water absorption	–	•

Note • Testing required

Table 5.25 Prepreg physical property testing

No.	Property
1	Resin content/fiber mass per unit area
2	Flow ability
3	T _g (dry and wet)
4	Water absorption

Table 5.26 Prepreg processing testing

No.	Property
1	Microcracking/cured laminate thermal cycling
2	Microcracking/cured laminate microstructure

Table 5.27 Mechanical property verification testing

Property	Room temperature	Elevated temp./dry
Tensile strength/modulus	•	–
Compression strength	•	•
Short-beam shear or in-plane shear	•	•

Note • Testing required

5.3 Characterization of Prepreg Performances

Prepregs are an intermediate material in a composite part or component fabrication. Prepregs are usually a semi-finished product with a resin system applied to reinforced fibers or fabrics, which is then subjected to some treatment and stored for later use. On the basis of the reinforcement type, prepregs can be categorized as prepreg tape, prepreg cloth, and unidirectional prepregs. The performances of prepregs will directly affect the composite performances. The characterization of prepreg performances is an important part of composite quality evaluation and control [4–8].

The characterization of prepreg performances involves three aspects: One is the characterization techniques used, which include thermal analysis (TA), infrared spectrometry (IR), gel penetration chromatography (GPC), high-pressure liquid chromatograph (HPLC), rheological analysis (RA), and dynamic dielectric analysis (DDA). The second aspect is the characterization of material characteristics, including the reinforcement of physical properties, resin content in the composites, fiber content, solvable resin content, solvent content, and the fiber mass per unit area. The third aspect is the prepreg processing performance. Composite processability includes issues such as the prepreg tack ability, resin flow ability, gel time, single layer thickness after curing, and the operation and shelf lives. Good control of prepreg processing performance is essential in composite processing.

5.3.1 *Advanced Techniques for Prepreg Characterization*

The application of modern scientific instruments has made a great contribution to composite prepreg quality control. In some international standards, IR and HPLC are used in composite prepreg quality control. In recent years, studies on glass fiber/epoxy resin prepreg quality control have also developed.

TA is a very important method for prepreg performance characterization and can effectively provide useful information about resin chemical composition and prepreg processability. IR spectroscopy and chromatographic methods can more precisely provide information about the resin chemical composition, relative molecular mass distribution, and cure degree of prepregs. These methods are easier to use and give rapid results in prepreg screening and quality control. RA and DDA are also often used to evaluate the resin viscosity characteristics related to the chemical structure changes during the cure process. These methods have been applied to quality control of the processing of thermosetting and thermoplastic resins. In the below, each of these characterization techniques will be discussed in more detail.

5.3.1.1 Thermal Analysis

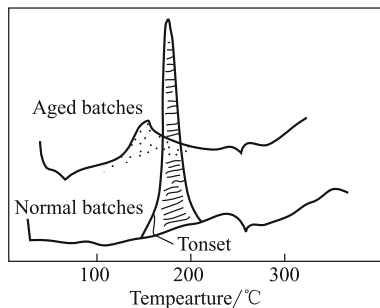
TA is a class of characterization techniques used to determine the correlation between a material's physical properties and its temperature, and includes a wide range of methods. In prepreg performance characterization, the most commonly used TA methods are differential scanning calorimetry (DSC), differential thermal analysis (DTA), thermogravimetry (TG), and dynamic mechanical analysis (DMA). These methods can provide useful information related to resin chemical composition and processing performance and are widely used in prepreg performance characterization.

(1) Differential scanning calorimetry (DSC)

When a prepreg is purchased and used by a customer, it is important to know the resin reaction state and the precured content for the later processing. The resin system in fresh prepreg will release a high reaction heat during its curing; however, for aged resins, the reaction heat will be smaller and the curing temperature will also be lower. On the basis of the standard material reaction behavior, it must be determined if an aged prepreg can still meet the operational requirements. Both DSC and DTA can be used to determine the resin cure reaction temperature and the reaction heat released during curing. Thus, these are effective methods for determining the degree of resin curing quantitatively. The major difference between these methods is that DTA measures the temperature difference between the sample and a reference material, while for DSC, the heat flow rate is determined. Both are quantitative methods, which are simple and effective, and have become widely used in characterization of prepreg performances.

DSC can characterize the precured degree of prepregs by determining the cure reaction heat. Because the cure reaction is generally exothermic, the quantity of heat produced by the reaction will depend on the resin functional group type and the number of groups taking part in the curing reaction, as well as the cure type and its ratio. For prepregs with a given matrix ratio, the cure reaction heat will be a certain value. Hence, the precure degree can be calculated by:

Fig. 5.11 Curing DSC curves of epoxy prepregs



$$\alpha = \frac{\Delta H_0 - \Delta H_R}{\Delta H_0} \times 100\% \tag{5.6}$$

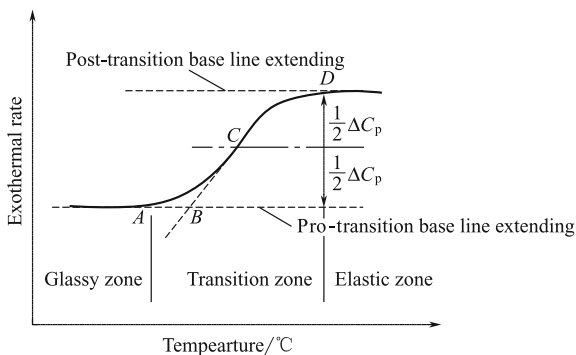
where α is the precure degree; ΔH_0 is the total reaction heat released from a fresh prepreg after full curing, (J/g); ΔH_R is the reaction heat released from the sample prepreg after full curing, (J/g).

Figure 5.11 presents DSC curves of epoxy prepregs from both normal batches and aged batches cured at 177 °C. The cure peak area of the aged prepreg is clearly smaller than that of the normal batches. The precured degree can be calculated by comparing the cure peak areas with that of fresh prepreg from the same batches. Thus, the precured degree of these two kinds of prepregs can be accurately determined. Furthermore, information can be derived from the shape and location of the cure peak. For example, aged prepregs have a wider cure temperature range and lower onset temperature than those of normal prepreg. On the basis of DSC measurements, the cure processing conditions can be established for different prepreg batches. For example, since the cure reaction onset point of aged prepregs occurs at lower temperatures the cure pressure should also be earlier applied. The cure temperature window will affect the pressure cycles applied during the prepreg curing.

In this way, DSC can be used to study prepreg shelf life. The prepreg is stored over different time periods under the same conditions, and samples are then subjected to DSC. With the use of Eq. (5.6), the precured degree of the stored prepregs can be calculated and correlation between the precured degree and different storage conditions can be obtained. Thus, the shelf life can be determined under different storage conditions.

In addition to characterization of cure reaction heat, both DSC and DTA can be also used to determine the glass transition temperature T_g of prepregs. The T_g of a matrix resin is an important performance parameter, which depends on the matrix resin chemical structure and is related to the prepreg precured degree. The presence of additives, and their type and ratio can also affect the T_g . Hence, the T_g can be used to characterize the prepreg cure state and its processing ability.

Fig. 5.12 DSC curve of glass transition



The determination of T_g by DSC is based on the increase in thermal capacity of a resin matrix at its glass transition. This change will appear as a base line shift to the endothermal direction on the DSC curve, as shown in Fig. 5.12. In this figure, point A is the onset shift point from the base line, extending the base line both before and after the transition. The distance between the two vertical lines to the baseline is defined as the thermal capacity difference ΔC_p before and after the transition. The point C at $\Delta C_p/2$ on the curve is found by marking a tangent line from point C, intersected with the extended baseline at point B. Generally, point B is defined as the glass transition temperature T_g . Because the determination of T_g varies depending on the methods used and the test conditions, the heating rate and other test conditions should be included with a measured T_g result.

In the determination of the T_g for thermosetting resin prepregs, DSC can also be used to determine the melting temperature of thermoplastic resin prepregs. The recommended methods for determination of T_g and T_m are given in ASTM standards D3417 and D3418.

(2) **Thermogravimetry (TG)**

TA in which a change of sample mass with temperature or time is measured under a given condition is classed as TG. This technique can provide information on the

Fig. 5.13 TG curve of glass-reinforced nylon prepreg

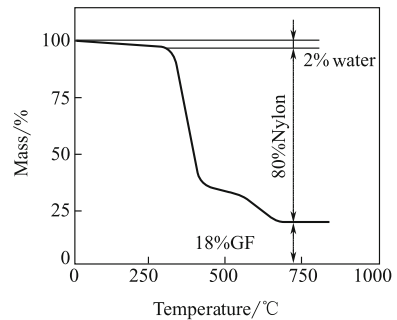


Fig. 5.14 TG curves with expanded vertical coordinate used to determine water content

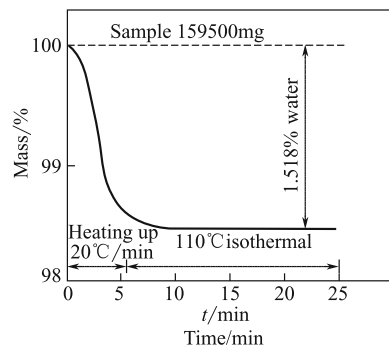


Fig. 5.15 Isothermal curing TG curves of phenolic resin

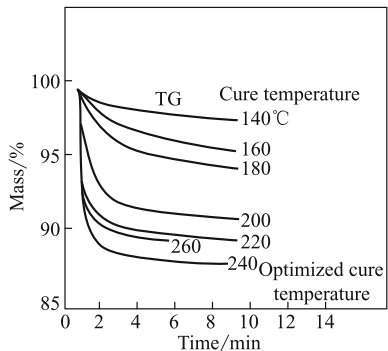
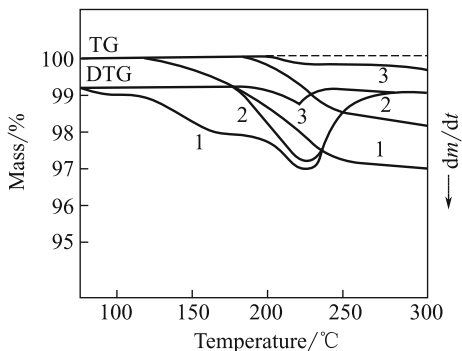


Fig. 5.16 TG and DTA curves of phenolic resin curing

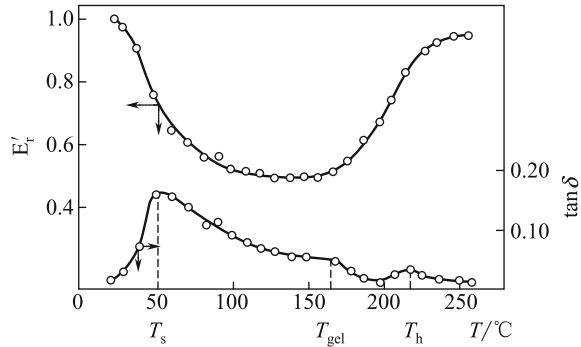


prepreg volatile content, resin, reinforcing fibers, and residual inorganic content. This method can also be used to characterize prepregs.

In the determination of volatile substance and fiber content by TG, both dynamic heating and static isothermal analyses can be used. In Fig. 5.13, the TG curve of water, nylon, and fiber content in glass fiber-reinforced nylon prepreg are presented, under a constant heating rate. One measurement can offer insight into the percentage contents of many constituent materials. If the water content in the prepreg is to be measured, static isothermal TG analysis can be used to ensure that water is fully evaporated avoiding overheating, which may cause resin matrix degradation. As shown in Fig. 5.14, the TG curve of water content in a prepreg measured at 110 °C is given, indicating that the water content of the sample is 1.52%.

The characterization of prepreg cure behavior by TG is based on the weight loss of volatile substances produced during resin matrix curing. For example, the curing of phenolic resin is a condensation reaction with water generated in the cure process. This kind of curing is an exothermal process that is accompanied by an endothermal process caused by water generation and vaporization. If DSC or DTA are used in these studies confusion can be caused in the analysis curves because the exothermal and endothermal peaks may overlap complicating the analysis. The use of TG can eliminate this problem. For example, its application to the phenolic resin dehydration

Fig. 5.17 DMA curves of prepregs cured at constant heating rate



and weight loss during curing reveals the maximum cure temperature to be 240 °C, as shown in Fig. 5.15.

A combination of TG-DTA methods can also be used to study the phenolic resin cure process. A fresh sample and precured samples with different curing degrees are subjected to TG-DTA testing under the same conditions. Three TG-DTA curves are obtained, as shown in Fig. 5.16. On the basis of the percentage weight loss of the TG curve, and the peak area of the DTA curve, the curing degree of phenolic resin can be directly determined.

(3) Dynamic mechanical analysis (DMA)

As for DSC, DMA can be also used to determine the glass transition temperature of prepreg resin and to characterize the prepreg cure processing behavior. In DMA analysis, one sample can be used to study and monitor the full curing process of prepregs without a decrease in sensitivity when the cure process enters the gel phase. Furthermore, DMA can reveal correlations between mechanical properties and chemical transitions, especially suitable for the selection of cure conditions.

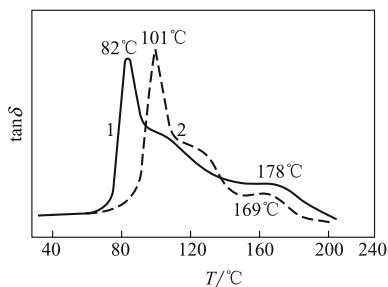
The uncured prepreg will soften during heating, which may cause difficulties for DMA analysis. Thus, the prepreg should be adhered to a stiff substrate to form a double-layer specimen (e.g., a vibration spring specimen), or by reducing the specimen aspect ratio (used in Du Pont 982 instrument) to increase the specimen stiffness. Figure 5.17 shows DMA curves obtained with a double-layer beam specimen under a constant heating rate. The vertical coordinate E'_r represents the ratio of the modulus E'_0 of the uncured specimen with the E'_r of a specimen cured at temperature T . This characteristic is known as the relative modulus. The figure shows that the modulus of the system decreases rapidly as temperature increases after a small initial decrease, which is caused by softening of the resin components with low relative molecular mass. At this moment, a camel peak will appear in the DMA damping curve, the corresponding temperature is known as the soften temperature T_s . After this point, the curve becomes flat and smooth, because while increased temperature can decrease the resin viscosity and modulus, molecular chain growth in the resins and branching occurs, which increases the modulus. When temperature increases to a certain level, the linear and branched molecules

begin to cross-link into network structures. At this point, insoluble gelled structures begin to grow to a large extent, causing the modulus curve to shift upward, and a shoulder peak appears in the damping curve. The temperature corresponding to this change is referred to as the gel temperature T_{gel} . If the temperature continuously increases and the cure reaction proceeds further the network molecules will begin to change into solid structures and the modulus will greatly increase. The rate of increase will show a maximum value at the second camel peak of the damping curve. This result indicates that the resin cross-linking reaction reaches a high level, and the resin can be said to have fully hardened. The corresponding temperature of this change is known as the hardening temperature T_h . Above T_h , as the cross-linking density increases, molecular movement will be increasingly suppressed. The uncured functional groups will become surrounded by cross-linked structures forming macromolecules, and their interactions will be greatly reduced. As the cure reaction proceeds, the number of active functional groups will gradually decrease. At temperatures higher than T_h , the system modulus will show less of an increase.

In Fig. 5.17, the positions of T_s , T_{gel} , and T_h are indicated on DMA curves and can be used as reference temperatures to determine the prepreg curing temperature. In general, the cure temperature is selected at T_{gel} ; however, to obtain full curing and increase the curing rate, cure temperatures slightly higher than T_{gel} can also be selected. The posttreatment temperature can be selected at T_h or higher. To increase the resin viscosity by inducing more molecular chain growth and branching, a temperature higher than T_s , and between T_s and T_{gel} can be selected as the isothermal precuring temperature. This temperature should be held for a certain time period during which pressure can be applied. If pressure is applied at a temperature lower than T_h , or higher than T_{gel} , it may be difficult to ensure sufficient pressure is applied because of hardening of the resin. This may result in void forming. If the pressure application temperature is selected at T_s , excessive resin out flow will result in resin starvation in the composites.

On the basis of these guide temperatures, an isothermal cure time can be determined that allows a prepreg to be fully cured. The curing period should be reduced for thick composites, because the consistency of the curing degree of the surface and inside layers should be considered. The cure speed should not be too fast to avoid the outer surface hardening, which might prevent the application of

Fig. 5.18 $\tan \delta$ - T curves of a prepreg



pressure to the inside. Time curves obtained by DMA scanning under isothermal temperature can be used to optimize cure processing conditions, and to screen the optimized cure temperature as well as the required cure time. The curing should aim for the prepreg modulus to stabilize over the process.

The processing ability of the same prepreg will vary because of different storage conditions and storage time. This is because chemical structures in the resins in prepregs, such as chain growth, branching, and partly gelation, will undergo changes. T_s will increase, T_{gel} will decrease, which will result in a narrower temperature zone between T_s and T_{gel} , degrading the prepreg processing ability. Therefore, to guarantee composite quality, prepregs should be carefully stored, and specifications should be established for each prepreg based on the T_s and T_{gel} from DMA curves. Any prepreg that cannot meet the specifications should be rejected. For example, prepregs should satisfy the solid $\tan \delta-T$ curve as shown in Fig. 5.18, that is T_s should be approximately 82 °C and T_{gel} should be approximately 178 °C. The dotted line is the $\tan \delta-T$ curve of a batch of rejected prepregs. If the $\tan \delta-T$ curve is regularly measured from the beginning of storage for a prepreg, the shelf life of prepreg can be easily determined based on the acceptance and rejection specifications.

As mentioned above, TG can give an indication of sample thermal degradation, and can also be used to estimate content of volatile substances, polymer and non-polymer additives, inorganic residuals. DSC and DTA are used to evaluate the cure behaviors of thermosetting resins to determine their glass transition temperature T_g , and to measure the crystal melting temperature T_m if polymers are semi-crystallized. Methods for determination of T_g and T_m can be found in the ASTM standards D3417 and D3418. TMA can be used to determine T_g as well as information about the thermal deflection temperature and thermal expansion coefficient. For grain or molded samples, the sample can be cut to size to fit the sample holder (thickness and diameter). If the sample materials are thin films or flakes with a thickness not greater than 0.04 mm, samples can be made into a small disk with a punch device.

Fig. 5.19 IR spectroscopy of resin in prepreg. 1—Fresh prepreg; 2—after storage for 42 d

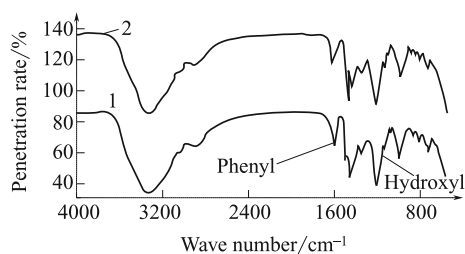


Fig. 5.20 Hydroxyl index versus storage time

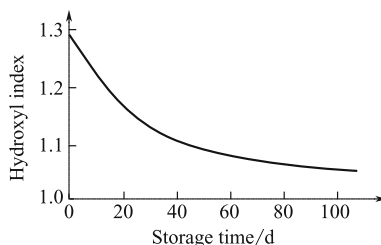
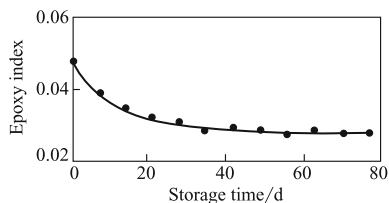


Fig. 5.21 Epoxy index versus storage time under room temperature



5.3.1.2 Infrared Spectroscopy

Compared with some other absorption or vibration spectroscopic methods IR spectroscopic analysis can offer more useful information about preregs, and is widely applied in their characterization. IR spectroscopy can qualitatively and quantitatively provide information about the chemical properties of polymer samples, such as structural repeat units, terminal groups and branch units, and additives and impurities. The absorption peaks of characteristic groups in the IR spectra can be used to identify the chemical composition of resin in preregs. Changes of the concentration of functional groups in the prepreg resin system can give information about the prepreg cure degree.

In Kejian's studies, IR was used to determine the chemical composition change of phenolic/glass fiber prepreg stored under conditions of 25 °C and RH 50%, by studying the relative content of active hydroxyl groups in the prepreg resin. The precured degree of the prepreg was quantitatively characterized. In Fig. 5.19, two IR spectra from fresh prepreg and prepreg stored for certain times are shown. The phenyl group showed no change while the hydroxyl groups gradually reduced. A comparison between the hydroxyl and phenyl peak areas can be used to define the cure degree of the prepreg. Figure 5.20 shows the change of the hydroxyl index (intensity ratio of the hydroxyl peak to phenyl peak) with storage time, based on the IR results. These results can give insight into the performance changes of a prepreg during storage.

Yinsheng et al. used IR spectroscopy to study the physical property changes of glass fiber/epoxy prepreg under different storage conditions, as shown in Fig. 5.21. The epoxy index (intensity ratio of the epoxy peak to phenyl peak) decreased with extended storage time.

Laser Raman spectroscopy is another complimentary technique to IR spectroscopy. If a sample is stable to high intensity laser light and does not contain any fluorescent components, no special sample preparation is needed. Solid samples simply require cutting to a size suitable to fit the sample holder. For transparent materials, the transmission spectrograms can be directly obtained by laser Raman analysis. For semi-transparent samples, a hole can be made for the incident light path and the transmission spectrograms can be derived by studying the scattering of vertical incident light. For non-transparent or highly scattering samples, the reflected light from the front surface can be used for analysis.

5.3.1.3 Gel Penetration Chromatography (GPC)

GPC, also known as steric exclusion chromatography or size exclusion chromatography, uses the retention properties of a gel to perform sample composition analysis. The relative molecular mass of constituents controls their retention time on the gel. The separation mechanism of GPC is similar to that of a molecular screen, but the gel hole diameter is much larger than that used of molecular screening, in the range of hundreds to thousands of Å ($1 \text{ \AA} = 10^{-8} \text{ cm}$). In GPC, the column is filled with gel having holes of certain sizes and an organic solvent is used as the mobile phase. When a sample flows into the column, molecules of different sizes will flow through the gel grain microstructure in the column. Molecules with large volumes cannot penetrate gel holes and will be excluded, or flushed out of the column more rapidly in the mobile phase. Molecules with intermediate size will be partially retained. Small-sized molecules will tend to penetrate the gel holes and be retained by the column for longer. Thus, the time a particular molecule spends on the column will vary according to the molecular size. This principle allows the components to be separated.

In prepreg resin systems, there are many constituents with different relative molecular masses, such as epoxy resin, curing agents and accelerators. The different constituents in a resin system can be separated by GPC according to their relative molecular masses to give information about the constituents of the resin system. When a prepreg is aged during storage, the resin system may undergo partial polymerization or cross-linking reactions, resulting in an increase in molecular

Fig. 5.22 GPC spectrograph of Narmco5208 prepregs

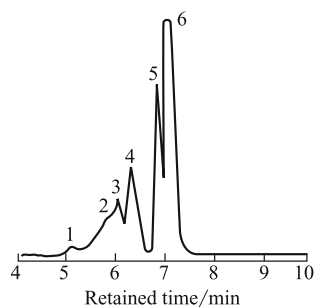
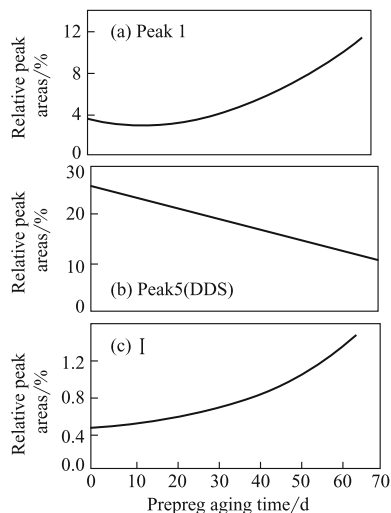


Fig. 5.23 Peak 1 (a), peak 5 (b) and polymerization content I (c) in GPC spectrograph versus prepregs aging time



chain lengths and molecular mass. The concentration of monomers with low molecular mass will decrease, while the concentration of monomers with high molecular mass will increase. In Fig. 5.22, the GPC results of a carbon fiber/epoxy prepreg are shown. Peaks 1–4 at shorter retention times are related to polymerized products with high molecular mass. Peaks 5 and 6 represent the small molecules including monomers, curing agents and accelerators.

In addition to identification of the chemical compositions of resin systems, GPC can be used to characterize the aging of prepregs. At extended aging times, the ratio of the reaction products with high molecular mass will gradually increase. The relative area of peak 1 will increase, as shown by the curve a in Fig. 5.23. The area of peak 5, representing molecules with relatively small molecular weight, will decrease, as shown by curve b in Fig. 5.23. The ratio of the sum of peak areas of high molecular weight products (peaks 1–4) and the sum of the monomer peak areas (peaks 5 and 6) can be used to represent the prepreg aging content. The value of this ratio will increase with extended storage time as indicated by curve c, in Fig. 5.23. Curve c can be used to characterize the aging behavior of a prepreg, and can also be used to evaluate the aging resistance of different prepregs by comparing curve shapes.

Thus, GPC is useful for inspection of resin chemical composition, characterization of prepreg aging behaviors, and determination of the contents of aged prepregs.

5.3.1.4 High-Pressure Liquid Chromatography

HPLC is an analytical separation technique used to determine chemical compositions and the concentration of polymer materials. In epoxy prepregs, unknown

Table 5.28 HPLC analysis of 5245C/graphite prepreg

Epoxy prepreg batch	Aging time at room temperature/d	Area/%			
		MDA-MBI	Bisphenol-A bi-cyanate	Main epoxy	Others
1006 mesh	0	8.98	17.8	31.5	41.6
1006 mesh	42	9.31	6.7	29.1	45.8
1006 mesh	140	9.8	10.4	24.6	55.2
1146 oriented fiber	7	13.6	24.4	43.4	18.6
1146 oriented fiber	47	6.3	20.6	32.8	31.3
1094 oriented fiber	3	13.6	20.4	46.0	20.0
1094 oriented fiber	56	14.6	17.9	47.2	20.3

reaction products may be generated, and it is difficult to characterize their composition. However, it is possible to determine the change in relative concentrations of known compositions. Scola et al. used HPLC to determine the changes of chemical composition in a graphite fiber/5245C epoxy prepreg, and the results are given in Table 5.28.

These data indicate clear differences in the chemical compositions of different prepreg batches. Thus, it is necessary to determine the monomer concentration of each prepreg before making composites.

For 1006 and 1146 prepreps, the concentrations of the main epoxy and bisphenol-A bi-cyanate decrease at extended aging times, while for other batches the concentrations of other constituents clearly increased. For 1094 prepreg, no obvious changes were observed at extended aging times.

5.3.1.5 Rheological Analysis

The processing abilities of thermoplastic and thermosetting resins depend on flow features, which can be characterized by RA. In RA analysis, viscometers and rheometers are used to measure temperature-dependent viscosity and obtain information about resin flow behaviors. The viscosity of thermosetting materials depends on the curing degree; hence, other methods can be used to characterize rheological performance such as DMA (discussed earlier) and torsion braid analysis (TBA). These mechanical methods can be used to measure the resin rheological response related to frequency, temperature, and curing degree.

Fig. 5.24 Phase correlation between I_x and E_x

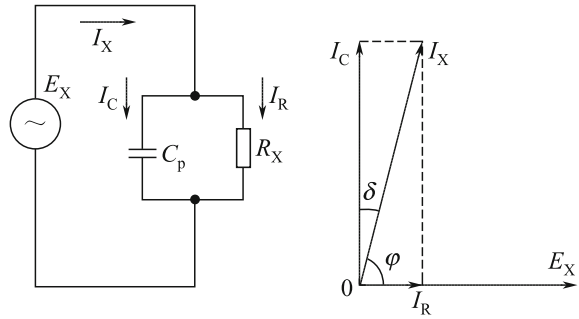
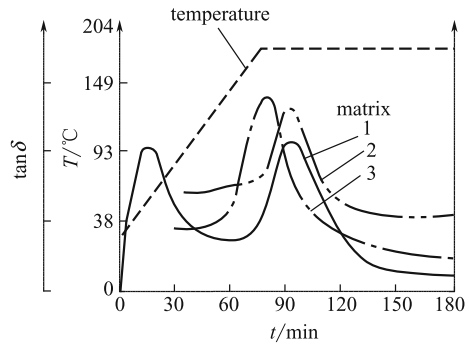


Fig. 5.25 DDA curve of TGMDA/DDS resin system



5.3.1.6 Dynamic Dielectric Analysis

DDA can monitor the change of dielectric constant, loss factor, capacity and/or conductivity related to electrical field frequency, time, and temperature. This method offers information about resin matrix rheological and curing behavior, and is often used to study and optimize prepreg processing parameters. The tangent of loss factor $\tan \delta$ will change more obviously during the resin curing process; thus, it is common practice to select $\tan \delta$ to characterize the prepreg performance and determine the cure processing conditions by DDA.

In testing, thermoplastic and thermosetting polymer matrices, glass fiber, and aromatic compounds have low dielectric loss. The prepreg to be tested and the test electrodes can be thought as a parallel equivalent circuit as shown in Fig. 5.24. For an ideal capacitor with a capacity C_p in the equivalent circuit, the current flowing through the capacitor is I_c , the loss resistance in the equivalent circuit is R , the current flowing through the resistor is I_R , and the total current I_x is the sum of I_c and I_R . The vector correlation of these variables is shown in Fig. 5.24. The phase difference angle between I_x and E_x is ϕ , its complementary angle is the loss angle δ . In testing, the phase difference angle ϕ between the total current I_x and total voltage E_x is determined from the phase monitoring circuit, which allows the value of δ and $\tan \delta$ to be determined.

Three epoxy resin matrices with similar flow features are taken as an example, and their DDA curves are as shown in Fig. 5.25. The third matrix contains one equivalent of curing promotor. Because they all have the same flow characteristics, only the flow curve section appears on the first matrix curve. It can be seen from this figure that these three matrices show two peaks in their dielectric loss curves: The first peak is dependent on the resin system melting and flow, and known as the “flow peak.” The second peak is related to the resin system curing, and is the so-called cure peak. The region between these two peaks is known as the “valley zone.” The transition point shown on the valley zone is the “gel transition point.” In general, the region from the gel transition point to the “cure peak” indicates the ideal conditions for application of pressure. In the figure, among the three matrices, the cure peak of the matrix containing a promotor appears earlier (corresponding to a lower curing temperature), indicating a more rapid curing reaction.

In general, the cure onset temperature determined by DDA is different from that obtained by DSC. These two analysis methods depend on the heating rate used as well as the electric field frequency used for DDA. On the basis of the DSC definition, the “gel point” is defined as the point when resin cross-linking approaches 40–60% of its potential, which correlates with the 50%-area enclosed in the DSC curve. This is usually located at the peak of the DSC curve, and its correspond temperature is the so-called gel point temperature, which is similar to the cure peak temperature on a DDA curve.

Table 5.29 Physical properties of preregs provided by Hercules

Reinforcing pattern	Designation	Fiber mass/unit area/g·m ⁻²	Width/mm	Resin content/%	Volatile content/%
Unidirectional	AS/3500-5A	150	305	35 ± 3 or 42 ± 3	<1
Unidirectional	AS4/3502	164	305	35 ± 3 or 42 ± 3	<1
Unidirectional	AS4/4502	145	305	35 ± 3 or 42 ± 3	<1
Unidirectional	AS4/1908	146	305	38 ± 3	<1.5
Unidirectional	AS4/1655	124	305	38 ± 3	<1
Unidirectional	HMS/3501-6	146	305	42 ± 3	<1
Fabric	A193-P/3501-5A	193	990	35 ± 3 or 42 ± 3	<1
Fabric	A370-8H/3501-6	370	990	35 ± 3 or 42 ± 3	<1.5

5.3.2 *Characterization of Prepreg Physical Properties*

The physical properties of prepregs include basic information parameters related to composite product quality such as reinforcement conditions, resin content, fiber content, and volatile content.

These parameters usually are provided by manufacturers for user selection according to their requirements. In Table 5.29, the carbon fiber prepregs produced by Hercules USA are given together with their physical properties.

Physical properties will change during prepreg delivery or storage, and it is necessary to characterize basic properties before application.

5.3.2.1 **Physical Description of Reinforcement**

The physical determination of composite reinforcement should be performed according to ASTM D3878 standard definitions in this section.

- (1) **Reinforcing pattern:** In terms of physical geometry, prepregs can be divided into two major types: unidirectional and fabric prepregs. In unidirectional prepregs, no weft yarns are used, and parallel fibers are bonded by resin matrices into sheets. The fibers can be used in laminate design according to the loading conditions. Thus, unidirectional prepregs can provide good mechanical performances. In fabric prepregs, fibers may be damaged to some extent, and warp and weft effects can occur during weaving, resulting in degraded mechanical performances. However, in terms of their usefulness in layering, or composite parts with angles, fabric prepregs have unique advantages and also can provide good mechanical performances in off-axis fabric applications.
- (2) **Straight-line alignment:** In unidirectional prepregs, fibers should be aligned on the longitudinal orientation. The error of the alignment angle should not be exceed 0.5° and there should be no fiber overlap, bubbles, twisting, wrinkles, or local buckling in prepregs cross section. In fabric prepregs, warp and weft yarns should be vertical to each other and parallel to the prepreg longitudinal and transverse directions. The parallel deviation in the full width should not exceed 50 mm and the deviation should not exceed 25.4 mm in any span 530 mm in length and width.
- (3) **Gaps:** Unidirectional prepregs may contain fiber gaps in the width direction caused by improper alignment. Too many gaps will degrade composite mechanical performance. The allowable gaps in long fibers or between long fibers should comply with certain specifications. For example, a gap in the width direction should not exceed 0.76 mm, the length of any gap should not exceed 0.61 mm in an average width of 0.76 mm. Gaps parallel to each other and separated by a space less than 25 mm should be considered as one gap, no matter how many of such gaps exist. Excessively wide or long gaps should be considered to be prepreg defects, which should be marked as a reference for prepreg changing.

- (4) **Width:** The allowable tolerance of prepreg width should be specified according to application requirements. In general, unidirectional prepregs should have a tolerance not greater than ± 1.27 mm, while for fabric prepregs, the tolerance is within ± 25.4 mm.
- (5) **Length:** Suppliers should give the length of each roll of prepregs. In addition, the weight and area of single roll prepregs can be discussed and decided between the supplier and user, to acquire prepregs more suitable for specific production requirements.
- (6) **Edges:** A wave-like deformation may occur on prepreg edges. This deformation may be more serious in larger width prepregs. The users should specify the acceptance of such deformations. In general, the straight edge line deviation should not exceed 1.5 mm over a 600-mm length, and edges with resin out flow should not exceed 1.5 mm.
- (7) **Splicing:** In terms of prepreg tapes, splicing is allowable if the fiber and resin batches are the same. However, the following requirements should be satisfied: The prepreg length needing splicing should not exceed 15 m; splicing should not occur more than three times in 50 m of each prepreg roll; the span between two instances of splicing should be greater than 30 mm; spliced prepreg should be recorded; and prepreg rolls with splicing should not exceed 20% of each batch of product.

5.3.2.2 Resin Content

Resin content is the sum of resin, curing agents and other additives in prepregs, indicated by percentages. To obtain proper resin content and good mechanical performance from composites, the resin contents in prepregs should be specified. Excessive resin content in prepregs can result in too much resin in the composites and degraded mechanical performance. Dislocation of fibers can occur during processing because of the large amount of resin out flow. Conversely, if resin content is too low, resin starvation can occur in the composites, leading to an increase in defects. Bubbles may become trapped in the prepreg prevented from release by the lack of resin out flow. The determination of resin content in prepregs involves the following three methods:

- (1) **Extraction:** The sample is put in Soxhlet extractor, and a solvent that can fully dissolve resin, but not the fibers, is used for extraction. The resin in the prepregs will fully dissolve the sample, and the mass change before and after extraction can be measured to calculate the resin content.

- (2) Dissolving: The sample is put into solvent and boiled for a period of time. The resin of the prepregs will fully dissolved. The sample mass change before and after testing is measured to calculate the resin content.
- (3) Burning: The sample is put in crucible and burned in a muffle furnace. The resin in the prepregs will burn off. The sample mass change before and after testing is measured to calculate the resin content.

In testing, the sample should be a single sheet with dimensions of 80 mm × 80 mm, and without any defects such as fluffiness, dried filaments, or non-uniformity color. The number of samples should satisfy the requirements of the specification. A sample number not be less than 3 should be used for each batch of prepregs.

Extraction and dissolving are not suitable for prepregs in which the resin may show large weight changes in solvent, or for high B-stage prepregs. Burning is generally suitable for glass fiber or its fabric-reinforced prepregs; however, for carbon and aromatic fiber prepregs, burning is not the first choice because of fiber oxidation and degradation during burning.

5.3.2.3 Fiber Content

Methods used to determine the resin content can also be used to determine the fiber content in prepregs. The sum of the resin and fiber contents should be 100% if void content is ignored. The fiber content in prepregs can be expressed in two ways: fiber mass content and fiber volume content. In testing, fiber mass content is typically measured. However, fiber volume content is used to calculate composite mechanical properties by mixing relationships. Thus, it is more convenient to work with the volume content and necessary to transform the mass content into volume content as follows:

$$V_f = \frac{\frac{w_f}{\rho_f}}{\frac{w_f}{\rho_f} + \frac{1-w_f}{\rho_r}} \times 100\% \quad (5.7)$$

where V_f is the fiber volume content; w_f is the fiber mass content; ρ_f is the fiber density; ρ_r is the resin density of the prepregs.

5.3.2.4 Dissolvable Resin Content

Dissolvable resin content is the percentage of dissolvable resin in the total resin mass. The method of its determination is to use three adhesive cloths with dimensions of 100 mm × 100 mm, which are weighed and recording as G (to precision of 0.01 g). The cloths are then dipped for 10 min in toluene and alcohol solution in a 1:1 ratio, and then removed to flush off the solvent, and placed in an oven (160 ± 2 °C) for 10 min. After cooling down and weighting G_1 is recorded. The cloth is then placed in a muffle furnace at 500–600 °C and burned until there is

no weight change, and then cooled to room temperature and weighed as G_0 . The dissolvable resin content can be calculated by:

$$\text{Dissolvable resin content (\%)} = \frac{G - G_1}{G - G_0} \times 100 \quad (5.8)$$

A greater dissolvable resin content will give better resin flow ability and adhering ability; however, resin flow-out and resin starvation will occur more easily. The cure time should be extended and the production rate will be lowered. It is important to control the dissolvable resin content.

5.3.2.5 Volatile Content

Volatile content is the percentage by mass of volatile substance in a prepreg. Volatiles in prepreps mainly come from low molecular weight substances in the resin, or solvent remaining from wet-impregnation. In composite quality control, a certain volatile content can improve the flow ability of a resin and give a more uniform resin distribution in the resulting composites. However, if the volatile content is too high, bubbles or residual volatiles may remain in the composite products, resulting in degraded electrical performance and mechanical properties.

Volatile content can be determined by placing the sample in an oven ($160 \pm 2^\circ \text{C}$) for 10 min then weighing the sample. TGA can also be used for volatile content measurements. In testing, the sample should not have any defects such as ruptured fibers, fluffiness, dried filaments, or non-uniform color. No less than three samples should be used.

5.3.2.6 Inorganic Filler and Additive Content

It is necessary to take care in quantitatively determining the inorganic filler and additive content in prepreg resins. If the organic resin can be fully dissolved in tetrahydrofuran (THF), while the inorganic fillers and additives remain insoluble, centrifugation can be used to separate the insoluble components. The deposits should be washed at least three times with solvent, then dried and weighted.

5.3.2.7 Fiber Mass Per Unit Area

The fiber mass per unit area refers to the fiber mass contained in a unit area of prepreg and is usually expressed in g/m^2 . The fiber mass of a prepreg sample, as determined in resin content tests, is divided by the sample area, and the fiber mass per unit area can be obtained. This parameter controls the thickness for different fiber volume contents and becomes a specification for composite structure design and processing quality control, different fiber mass per unit area will result in

different laminate thickness and fiber volume content. Usually this specification requires high accuracy with a strict tolerance range.

5.3.3 Characterization of Prepreg Processing Quality

5.3.3.1 Viscosity

Viscosity relates to the prepreg surface adherence ability, and the ease of peeling between layers after lamination. Prepregs with low viscosity provide poor tack and drape ability, and the interlaminar adherence will be poor. Prepreg viscosity depends on the resin type, volatile contents, curing degree in storage, and the ambient temperature. A test method for prepreg viscosity is given below: clean and dry a metal substrate and cool it to room temperature. Cut five or more prepreg samples with dimension of 75 mm × 25 mm. The first prepreg sample is bonded to a metal substrate and rolled by a rubber roller, the second sample is placed on top of the first sample and bonded. The samples are put on a test stand, the temperature is controlled between 20–25 °C and 30–70% RH. Acceptance requires no cracks or peeling after 30 min.

5.3.3.2 Resin Flow Ability

Resin flow ability refers to the prepreg resin flow ability measurement under a specified pressure and temperature. This is usually characterized by the quantity of resin out flow from the composite during the curing process. An excessively high resin flow ability will cause processing problems from severe resin loss, composite resin-starving, and non-uniformity of the fiber alignment. Low resin flow ability may cause poor adhesion between the fiber layers, or a non-uniform resin distribution. Proper resin flow ability can reduce void content, make the resin uniformly distributed, and increase the composite quality. Two methods can be used for determining resin flow ability: One is to cut cross-laminated samples and place these under a specified pressure and temperature for a time. The extruded resin mass is measured and recorded as the resin out flow quantity. Another method is to layup prepregs into a cross-laminate with 1 mm thickness, which is placed under a specified pressure and temperature for 2 min. The length-increase along the diagonal direction of the specimen (mm) is taken as the resin flow index.

Under the specified conditions, the resin flow ability is determined by the prepreg resin chemical composition, the reaction degree/stage as well as the resin content. In laminate processing, the processability and resin content of prepregs is controlled by the resin flow ability, while the selection of test conditions (temperature, pressure, prepreg ply number and bleed cloth layer number) will depend on the resin types and properties.

5.3.3.3 Gel Time

Gel time is an important processing parameter and the reference for pressure application. To determine the gel time a prepreg is cut into small square sheets and laminated. A PTFE film is placed on the top and bottom surfaces and the sample is placed between two metal or glass sheets preheated to a specified temperature. Pressure is applied through the sheets and a probe needle is used to test the resin change at the edge of metal sheets or glass sheets. The test is performed until no resin filament can be drawn out. This time point is defined as the prepreg gel time, which differs from the resin gel time because of the addition of fiber. The prepreg gel time can reflect the prepreg viscosity and degree of precuring, so it is an important specification for composite product processing parameters. The gel time is related to thermosetting prepreg resin compositions and the reaction degree. The testing temperature should be decided based on the resin type and the processability of prepreps will in turn depends on the resin gel time.

5.3.3.4 Cured Single Ply Thickness

A composite of single ply thickness is made under processing specifications. Currently, structural composites have a single ply thickness of 0.125 mm.

5.3.3.5 Operation Life

The operation time refers to the required time, over which the prepreg can meet the processing ability requirements and guarantee the composite quality under specified ambient conditions. Prepreps are taken out from low-temperature storage and placed in a clean room for cutting, laying-up into a half-finished product and packing. During this process, the resin viscosity should be maintained to meet processing requirements and ensure composite quality. Usually, prepreps are stored at low temperatures ($-18\text{ }^{\circ}\text{C}$), and the changes of the chemical compositions are very slow. When prepreps are placed in a clean room for an operation, chemical reactions will become faster. For large and complex parts with thick walls, the process may require an extended time of up to 2–3 weeks. Thus, prepreps should have a long room temperature operational life. Prepreps can be taken out from low-temperature storage from time to time according to the estimation of the processing period.

5.3.3.6 Shelf Life

The shelf life indicates the maximum time period a resin composite prepreg can be stored under specified conditions. For thermosetting resin prepreps, the shelf life will have a great effect on the composite processing performance. During storage,

low molecular weight substances will evaporate, and physical and chemical reactions will take place, resulting in decreased viscosity. The drape ability for ply laminating, the composite processing ability, and the product quality will be affected. If a prepreg is stored for too long, or stored and used under improper conditions, fiber rebound may occur at curved sections during laying-up. Fiber damage or resin cracking can also take place. The shelf life of prepregs should be determined under specific storage conditions according to resin composition. For example, QY8911 has a 12 months of shelf life under -18°C , and 30 days at room temperature. For 5222 prepregs, the shelf life is 6 months under -18°C , and 20 days at room temperature.

5.4 Laminate Performance Testing

Composite laminate performance testing is an important part of composite quality characterization and evaluation. Composite laminate performance testing covers many categories, and can be divided into laminate physical property testing, static mechanical property testing, fatigue resistant testing, and fracture toughness testing. In material studies, the main concerns are composite laminate tensile strength and modulus, compression strength and modulus, bending strength and modulus, interlaminar shear strength and impact strength. In structural design, much attention will be given to the composite compression and tensile strengths, moduli and Poisson's ratios, as well as the in-plane shear strength and modulus. In both material studies and structure design, special attention should be given to laminate properties that will correspond to structural performances, including: open-hole tensile (OHT) and compression (OHC), filled-hole tensile (FHT) and compression (FHC), model I interlaminar fracture toughness, damage resistance, CAI, model II interlaminar fracture toughness, mixed interlaminar fracture toughness, and damage tolerance. In this section, test methods and analysis of the above-mentioned characteristics will be introduced and discussed.

5.4.1 *Basic Physical Properties*

5.4.1.1 Density

Density is an important physical property of composites both as a material property and as a parameter in processing and property testing. In general, test methods used to measure the densities of typical solid materials can be adopted for composite materials. Density can be either directly measured, or indirectly calculated from separate test results of specimen volume and mass. For general test data, the density can be determined by directly measuring the specimen dimensions and calculating its volume. Common test methods for density measurements include: volume

measurements based on the Archimedean liquid level difference principle such as ASTM D792, GB/T 1463; density gradient methods and density meter direct measurement methods such as ASTM D1505. In this method, the specimen volume can be determined by measuring the pressure change of an inert gas in a tight pressure vessel. ASTM D4892 also adopts this method.

Of these three methods, the Archimedean method is most commonly used because of its simplicity, accuracy, and low cost. The principle of this method is that a comparison between the specimen weights in air and in a liquid (usually water), can be used to determine the density. When the specimen is immersed in liquid, surface bubbles should be removed. To avoid the effects of microbubbles, the use of steamed water is recommended. The specimen surface quality should also be taken into account.

In the Archimedean method, the density gradient method, and density meter method, the specimen must be soaked in water for testing. Thus, these methods are only suitable for materials, which will not change their mass or dimensions after water soaking.

The specimen dimensions may have some effects on the test results. In general, the larger the specimen size, the better the measured density results will be. If the specimen is too small in size, difficulty will be encountered in measuring its volume and weight, causing incorrect test results. To guarantee the reliability of data, a standard specimen size should be selected.

Furthermore, because of the strict requirements for ambient conditions, density testing should be performed under standard test conditions (23 ± 2 °C, $50 \pm 5\%$ RH). The specimen to be tested should be placed in the specified ambient condition for a long enough time to equilibrate.

5.4.1.2 Fiber Volume Content

Fiber volume content is an important composite parameter. As an alternative to direct microscope observations, methods based on separation of the matrix from the reinforcement can be used to measure fiber volume content, include etching-off and burning-off methods. Furthermore, the prepreg mass per unit area is often used to estimate fiber volume content.

In the etching-off method, a corrosive fluid is used to separate the matrix and reinforcement for measurement and calculation of the fiber volume content. In this method, care should be taken to ensure the fibers do not undergo any weight change and that the matrix does not contain any non-dissolvable additives. To ensure accuracy, the specimen should have a large enough size.

The burning-off method is suitable for composite systems in which the reinforcement will not show any weight change during the specimen combustion. In this method, specimen is placed in an oven until the matrix is completely decomposed. The weight of the clean unburned samples and that of the residual fibers after burning can be used to calculate the fiber weight content. The weight content can then be converted into the volume content. It is crucial that the fiber does not

change its weight during the testing, and that the matrix does not contain any inflammable fillers.

5.4.1.3 Cured Ply Thickness

In reviewing weight and dimensions, the thickness of composite parts is an important property. In general, the part thickness can be rationally estimated as the product of the mean cured ply thickness and number of plies. The cured ply thickness can be determined by measuring several laminate thicknesses (panels or parts) at different locations, taking the mean value, and then dividing by the number of plies. The laminate thickness can be measured either directly by calipers or indirectly by a supersonic instrument. Standard SRM 10R-94 is the only available standard for cured ply thickness measurement.

5.4.1.4 Void Content

Voids often exist in manufactured composites, and void content can affect composite mechanical properties. Composite structures of good quality can have a void content less than 1%. Similar to case of fiber volume content measurements, the void content can be determined by direct examination or by separating the fibers and matrix.

Direct examination by microscope observations of the specimen and calculation of the void content with image analysis software is one approach.

The separation method involves the use of an appropriate technique to separate the matrix and reinforcement, and then calculate the void content. This method has been adopted in some standards such as ASTM D2734.

In this method, the composite and its constituents should be identified with their density values, which can then be expressed as:

$$\rho_t = \frac{W_c}{\frac{W_r}{\rho_r} + \frac{W_f}{\rho_f}}, \quad (5.9)$$

where W_c is the specimen weight; W_r is the matrix weight in the specimen; W_f is the fiber weight in the specimen; ρ_t is the specimen density; ρ_r is the matrix density, ρ_f is the fiber density.

Void content (%) can be determined by:

$$V_c = \frac{\rho_t - \rho_c}{\rho_t} \times 100 \quad (5.10)$$

where V_c is the specimen void content; ρ_t is the specimen density; ρ_c is the composite density.

The test results will depend strongly on the measurement accuracy. The same concerns as those for fiber volume content measurements should be taken into account, and the relevance of the specimen should also be considered because of the low void content.

5.4.1.5 Glass Transition Temperature

Glass transition is a composite matrix transition process either from a glassy to an elastic state or from an elastic to a glassy state caused by a temperature change. The transition temperature will depend on molecular structures in the matrix and cross-linking levels, but can be affected by temperature increase/decrease rates of the test, or by the dynamic loading frequency (if dynamic analysis is used). In glass transition processes, material stiffness will change by 2–3 orders of magnitude. The glass transition temperature is commonly used to characterize this type transition, but this transition takes place over a broad temperature range, and a single temperature value cannot reflect this transition behavior accurately. Thus, in measurements of glass transition temperatures a proper calculation method should be selected and a standard test method used to specify the temperature change rate and the loading frequency for testing. In real applications, the glass transition temperature is often used to characterize material thermal resistance and hot–wet effects on material performances.

5.4.1.6 Moisture Absorption

Composites will absorb moisture, if exposed to a wet ambient environment, which can degrade performance. Thus, water absorption is a critical issue for most composite applications. It has been shown that moisture diffusion in composites follows Fickian diffusion. The composite moisture absorption can be assessed from the moisture diffusion rate and the balanced moisture absorbing content. These characteristics can be determined from weight scaled specimens (as in, for example, ASTM D5229 M, section A). The principles involved in composite moisture absorption include the following.

Moisture diffusion rate: a physical parameter to reflect the material moisture absorption rate, represented by an Arrhenius index plot versus reciprocal absolute temperature.

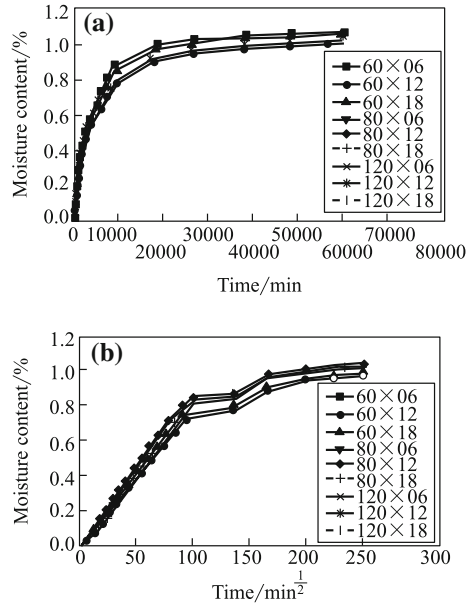
Moisture content: the total absorbed moisture as a percentage of the total weight of the whole specimen.

Balanced moisture content: the moisture content at an absorption equilibrium state, which is a function of ambient temperature and relative humidity.

Saturated moisture content: the balanced moisture content under 100% relative humidity.

In moisture content testing, the fully dried specimens are put in a wet ambient environment and their mass increase is recorded and plotted versus square root

Fig. 5.26 Composite moisture absorption



time. At the initial stage of the plot, the mass increment and time will show a linear correlation and the latter stage will feature a curved slope depending on the moisture content. As the specimen surface moisture absorption tends toward the equilibrium state the specimen mass will increase more slowly. The gradient of the curve will become smaller until the moisture absorption reaches the equilibrium state and no further mass increase occurs. The gradient of the curve will be almost parallel to the time axis at this stage and the specimen mass increase will reflect the balanced moisture content.

Figure 5.26(b) shows the relationship between the specimen mass increase versus square root time, and also shows the different moisture diffusion rates occurring at different temperatures.

From the moisture content curves, the balanced moisture content and moisture diffusion rate are determined as:

$$d = \pi \left(\frac{h}{4M_e} \right)^2 \times \left(\frac{M_2 - M_1}{\sqrt{t_2} - \sqrt{t_1}} \right) \tag{5.11}$$

where d is the moisture diffusion rate; h is the specimen thickness, mm; M_e is the equivalent balanced moisture content, g; $(M_2 - M_1)/(\sqrt{t_2} - \sqrt{t_1})$ is the initial gradient of the curve slope at, $\text{g}\cdot\text{s}^{-\frac{1}{2}}$.

The moisture diffusion rate is mainly related to temperature, and not strongly affected by relative humidity. It can be expressed by an Arrhenius equation as:

$$d = d_0 \exp\left(-\frac{E_d}{RT}\right) \quad (5.12)$$

where d is a constant; E_d is the activation energy; R is the universal gas constant; T is absolute temperature in dynamic calculation.

5.4.1.7 Dimensional Stability (Thermal and Water Absorption)

The dimensional changes of composites are functions of temperature and/or moisture content. Mechanical, optic and electronic sensors can be used to measure and record the length or volume changes of composite specimens as functions of temperature and time. The techniques used to measure dimensional changes of composites include dial gauge scales, calipers, telescopes, linear voltage differential transducers (LVDT), interferometers, and X-ray inspection.

(1) Dimensional stability (thermal)

The dimensions of most materials will change with temperature, expanding as temperature is increased. Isotropic materials including bulk metals, polymers, and ceramics, by definition will isothermally expand in all directions. Reinforcement of these bulk materials can be either isotropic or non-isotropic. For example, inorganic fibers such as glass, boron, and ceramic fibers are isotropic, while organic fibers such as carbon, aramid, polyethylene, and other materials are not isotropic.

Usually, thermal stability is defined by the coefficient of thermal expansion (CTE), and denoted by α which has the units of $10^{-6}/K$ or the microstrain per unit thermal dynamic temperature. In general, CTE is a function of temperature and will have different values for different materials depending on temperature.

Four ASTM standards are available for the determination of non-reinforced (pure) polymers and their composites. ASTM D696-03 is the most commonly used standard and can suit a narrow temperature range from -30 to 30 °C. ASTM E 228-95 uses similar testing equipment and can suit a specified temperature range of -180 to 900 °C; however, caution should be taken if the temperature exceeds 500 °C. ASTM E 831-00 is a standard for thermal mechanical analysis (TMA) to measure thermal expansion for an operational temperature range of -120 to 600 °C. It is possible to enlarge the testing temperature range for this standard depending on the instrument specifications and standard materials. ASTM E 289-04 is a standard for use with interferometers to measure CTE as small as $0.01/K$, within a temperature range of -150 to 700 °C. It is also possible to extend the temperature range depending on the instrument specifications and standard materials. Interferometry is a more complex method, which requires attention to be paid to the instrumentation.

(2) Dimensional stability (water absorption)

The dimensional change caused by water absorption is defined by the coefficient of moisture expansion (CME) denoted by β . Composites will show different CME

values in different directions, whereas unreinforced (pure) polymers will show the same expansion in all directions. The CME of unreinforced (pure) polymers is expressed by $10^{-3}/\%$ (mass fraction) M , and for reinforced polymers, the CME by $10^{-6}/\%$ (mass fraction) M , or $\text{ppm}/\Delta M$. Because the strains caused by temperature and moisture changes are proportional to $\alpha\Delta T$ and $\beta\Delta M$, respectively, moisture expansion has a more significance effect on dimensional stability than thermal expansion. To date, no standards are available for moisture absorption testing, although a referenced method is provided in Volume 1, of MIL-HDBK-17E.

5.4.1.8 Thermal Conductivity

The thermal conductivity of composites reflects their thermal response performance in general thermal flow situations. Test methods for stable and instantaneous thermal flow conditions are available. For stable thermal transfer, some ASTM testing methods are available and can be divided into two types: absolute (or primary) value measurements (C 177-04) and relative measurements (E 1225-04, C 518-04). The former standard thermal flow base is not general needed unless the test purpose is to calibrate accuracy or to establish a trace ability to certify a standard testing method. For the latter, the test results are compared with the thermal flow base.

5.4.1.9 Specific Thermal Capacity

The specific thermal capacity is defined as the energy change of a material per unit mass induced by a temperature change. The specific heat capacity c_p is a test value measured under normal pressure and normal enthalpy, which is denoted by an international standard unit $J/(\text{kg}\cdot\text{K})$. ASTM E 1269-95 is a standard test method to determine the specific heat capacity of polymer matrix composites based on differential scanning calorimeter (DSC). This method is suitable for thermal stable solid material testing with an operational temperature range of -100 to 600 °C. The test temperature range depends on the instrument and sample holder specifications.

5.4.1.10 Thermal Diffusion

Thermal diffusion is a material thermal response behavior under instantaneous heat flow conditions. If material density and specific thermal capacity are given, the thermal diffusivity α can be used to determine the material thermal conductive rate as:

$$\lambda = \rho c_p a$$

where λ is the thermal conductive rate, ρ is the density and c_p is the specific thermal capacity.

Standard testing method ASTM E 1461-01 is based on a flash method to determine the thermal diffusivity of homogeneous non-transparent solid materials. With the use of special shielding protection, this method can also be adapted to some transparent materials and composites.

5.4.1.11 Outgassing

Aerospace optical devices and components are exposed to a variety of particles and pollutants. It is necessary to analyze the pollution caused by material outgassing when selecting and specifying materials. Pollutants can cause the power output of solar cells to decrease and significantly affect optical device flowability. Two ASTM testing methods are available for the measurement of material outgassing characteristics and pollution. ASTM E 1559-03 is used to simulate outgassing and pollution data for optical system design. ASTM E 595-93(2003) is mainly used as a material screening technique to make a table of pollution classification for material screening.

5.4.1.12 Flame Retardant and Smoke Suppression Properties

For use of organic polymer matrix composites, special attention should be given to the fire (accidental or intentional) that might result in structural damage. A second problem of fire is the possibility of burning adhesive and composite surfaces causing flames to spread and the release of heat and toxic smoke.

(1) Flame spreading testing

For composites used in many residential applications, the possibility of fire spreading is a serious problem that should be addressed. It is necessary to determine the capacity of a material to inhibit fire spreading. Prevention measures include limiting the heat flow from fire to composite surfaces or inhibiting the inherent resin response to flame. The following test standards can be used for this purpose: ASTM E 84-05 “Standard test method for surface burning characteristics of building materials,” ASTM E 162-02a “Standard test method for surface flammability of materials using a radiant heat energy source,” ISO 9705 “Fire accident testing—Surface product testing for full size rooms,” and ASTM E 1321-97a (2002) “Standard test method for determining material ignition and flame spread properties.”

(2) **Smoke and toxicity test method**

Available test methods include: ASTM E 662 “Standard test method for specific optical density of smoke generated by solid materials,” NFPA 269 “The toxicity data development used for fire accident constructions.”

(3) **Heat release test method**

The heat release rate (HRR) is a main index to define the fire hazard in fire accident studies and flame dynamics. HRR can be used to analyze a fire accident under a given fuel load, geometrical configuration, and ventilation conditions. Fire analysis should include the material’s corresponding fire response parameters generated by small-scale HRR testing. Fire evaluation methods based on heat release measurements can be extended to composite applications. The HRR, in particular its peak, is the main behavior that determines the fire extent range, spread, and inhibition requirements. The following standards are available including: ASTM E 1354-04a “Standard test method for heat and visible smoke release rates for materials and products using an oxygen consumption calorimeter” and ASTM E 906-04 “Standard test method for heat and visible smoke release rates for materials and products.”

(4) **Fire test methods**

The potential of fire to spread and its retention time can be changed through selection of airplane cabin and structural members and assemblies that are properly designed accounting for potential fires. It is important to understand the fire resistance of both the structure and the materials. Fire resistance relates to the ability of a material to take part in a fire. The following standards are available including: ASTM E 119-00a “Standard test methods for fire tests of building construction and materials,” ASTM E 1529-00 “Standard test methods for determining effects of large hydrocarbon pool fires on structural members and assemblies,” and UL 1709 “Standard test methods for quickly igniting of structural steel protection materials.”

5.4.2 Basic Mechanical Properties

5.4.2.1 Tensile Property Testing

Tensile test methods are the most fundamental test methods for composites. The following unidirectional performances of composites can be determined: E_{1T} is the tensile modulus along the fiber axial direction, E_{2T} is the tensile modulus vertical to the fiber axial direction, X_{1T} is the tensile strength along the fiber axial direction, X_{2T} is the tensile strength vertical to the fiber axial direction, ν_{12} is the major Poisson’s ratio, ϵ_{1T} is the fracture strain along the fiber axial direction, ϵ_{2T} is the fracture strain vertical to the fiber axial direction.

Fig. 5.27 Straight-sided tensile testing specimen

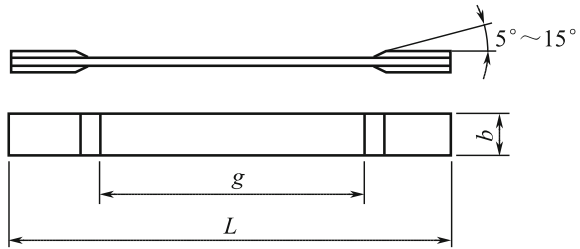


Table 5.30 Typical tensile specimen dimensions/mm

Laminating code	GB 3354		ASTM D3039	
	Specimen size	Tab length	Specimen size	Tab length
$[0]_{ns}$	230 × 15	50	250 × 15 (thick 1.0)	56
$[90]_{ns}$	170 × 25	50	175 × 25 (thick 2.0)	25
$[0/90]_{ns}$	230 × 25	50	250 × 25 (thick 2.5)	–
Symmetric laminates			250 × 25 (thick 2.5)	–
Random oriented short-fiber panel			250 × 25 (thick 2.5)	–

Currently, tensile test specimens mainly include three types: straight-sided, varied cross sections, and sandwich constructions.

(1) Straight-sided specimen

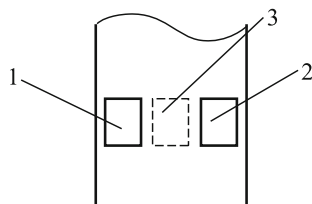
For high performance composites, straight-sided specimens are the most acceptable specimen configuration and used by most composite tensile testing standard methods (GB 3354-1999, ASTM D3039 M-00a). Straight-sided specimens have the following advantages: simple geometrical shape, ease of preparation, long gauge length, uniform stress distribution in the measuring gauge length, possibility to measure modulus, strength and fracture elongation simultaneously, and wide applicable range. This type specimen is suitable not only for unidirectional laminate testing, but also for multiple ply orientated laminates and fabric-reinforced composites. In the case of multiple ply orientated laminates and fabric-reinforced composite testing, the specimen width might need to be increased in some cases.

The geometrical shape of straight-sided specimens is shown in Fig. 5.27, and the dimensions are given in Table 5.30.

In this kind of test, the tensile stress is transferred to the specimen by the shear interface between the tab and specimen, and the strain is measured by an attached extensometer or strain gauges bonded to the specimen gauge length. In this way, the modulus can be measured.

To reduce the local stress concentration caused during loading, tabs are bonded on the clamping area of the specimen, which can protect the specimen surface from damage and transfer the loading to achieve a uniform stress distribution.

Fig. 5.28 Strain gauges on both sides of specimen. 1, 2—front side; 3—back side



However, technical problems exist in tab design. Improper tab design will cause the specimen failure to occur near to the tab, resulting in an unacceptable data ratio and a very low tensile strength. To guarantee the test result, tabs should be selected with good operational simplicity, low cost, and a 90°-ply orientation without a ramp. The latest studies have verified that successful tab design depends on the tab adhesive having adequate toughness rather than the ply orientation. Tabs without ramps bonded by tough adhesive are superior to currently adopted tabs bonded by adhesive of low toughness with cut ramps. Hence, the selection of adhesives used for tabbed specimens is critical.

Indeed, the best way to solve tab problems is to use untagged specimens. In some cases, it is possible to eliminate tabs, such as for some multi-ply orientated specimens. Specimens with 90°-plies layering can be untagged, but care should be taken to avoid damage to the specimen surface in clamping and testing.

Specimens with 0°- and 90°-plies are sensitive to the central alignment of loading. For a 0°-ply specimen, a small off-loading can have significant effects on the tensile strength. According to some studies, decreases in tensile strength up to 30% may be caused by a 1°-off-loading. For 90° specimens, poor alignment can have even more serious effects on test results. Although 0_m/90_n cross-ply specimens have been proposed to replace unidirectional specimen sin some studies, the current testing methods must still be used before the alternative is developed as a standard test method. Central misalignment should be minimized when clamping the specimen. The testing machine co-axial degree should be regularly calibrated and adjusted if necessary to ensure the testing machine has good co-axial alignment. A location pin can be used to guide the positioning of specimens. It is recommended to use strain gauges on both sides of specimen (Fig. 5.28) and to check the strain difference between the two sides according to Eqs. (5.13)–(5.15). The total value should be within 3–5% in 1000 με of the strain range.

$$B_y = \frac{\epsilon_{ave} - \epsilon_3}{\epsilon_{ave}} \times 100 \tag{5.13}$$

$$B_z = \frac{4/3(\epsilon_2 - \epsilon_1)}{\epsilon_{ave}} \times 100 \tag{5.14}$$

$$B_{total} = |B_y| + |B_z| \tag{5.15}$$

$$\epsilon_{ave} = (|\epsilon_1| + |\epsilon_2|)/2 + |\epsilon_3|/2$$

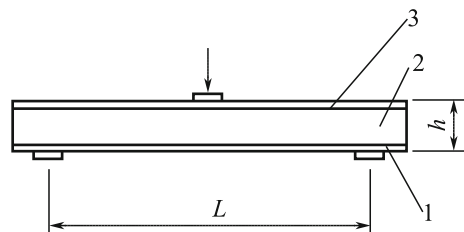
Preloading should be applied before testing, and should be performed repeatedly if necessary, to equalize the fiber deformation and to generate a good linear stress–strain curve. However, the preload should not be greater than 50% of the ultimate load, and should not cause any fiber rupturing.

(2) Varied cross-sectional specimen

In addition to straight-sided specimens, specimens with varied cross sections are used in some testing methods. In general, varied cross-sectional specimens are characterized as varied width and varied thickness specimens, and specimens with both varied width and thickness. Varied thickness and varied width and thickness specimens are typically represented by a thickness reduced RAE specimen and cross-sectional equal-stress designed streamlined specimens. Varied width specimens are usually used to test low strength materials. The materials to be tested are required to have adequate shear strength so that no shear failure will take place in the specimen width direction before tensile failure. Varied width specimens were first commonly used to test plastics and later were also used in composite testing. This kind of specimen, features a width that is shaped like a large circular arc as a transition connection zone, known as a dog-bone- or dumbbell-shaped specimen. For unidirectional composites, the width change will not have a significant effect on the test results. Machining of such specimen transition zones will cut out fibers; thus, in unidirectional fiber-reinforced composites, the applied load cannot be completely transferred from the clamped area of the specimen to the test section. Furthermore, owing to the variation of the width of the specimen, fiber splitting along the fiber longitudinal direction can occur, and no improvement in the stress distribution can be expected. The failure modes of this type of specimen are complicated, preventing its use for unidirectional composite in 0° -tensile testing. However, this type of specimen is suitable for testing of fabric fiber composites or non-unidirectional laminates, and has been adopted by some test standards. However, owing to the size limitations for this kind of specimen, the whole of a large woven pattern cannot be reproduced in a specimen when such fabrics are to be tested.

In terms of the machining, varied width specimens require high machining quality: The straight-side section and varied width section should have a smooth and perfect transition, otherwise fractures will easily occur in the transition area causing test failure. For this reason, straight-sided specimens are most widely used in composite tensile testing.

Fig. 5.29 Bending tensile testing on sandwich construction specimen. 1—Bottom surface of be tested; 2—core materials; 3—top surface



(3) Bending tensile test of sandwich construction specimen

Laminate tensile testing can be performed by bending a sandwich specimen (Fig. 5.29). When a sandwich specimen is subjected to a bending load, a tensile load and a compression load will be induced on the top and bottom surfaces of the laminates, respectively. Through control of the loading conditions, an expected tensile failure can be obtained on the laminated surface. This method is particularly suitable for 90° tensile testing of unidirectional composites.

To fulfill the expected tensile failure modes, the compressed surface of the laminate can be doubled in thickness with the same laminating code.

The main obstacles for this method are the specimen preparation and the testing costs.

Examination of the failure mode is very critical. The complexity of materials causes variations in their failure modes. If different failure modes are obtained for the same set of specimens, the results should be regarded as invalid and rejected. Thus, it is necessary to fully understand the testing principle and determine acceptable failure modes. In general, unidirectional laminates in longitudinal (0°) tensile failure will show fiber rupture as the dominant failure mode accompanied by other damage such as transverse and longitudinal matrix fracture and delamination. Transverse (90°) tensile failure is relatively simple, i.e., the specimen fractures along the fiber direction. The test record should include the failure load and strain, and the failure mode and location. If an unacceptable failure mode is encountered, the test result should be rejected. Examination of the failure mode may be useful for evaluating the test results and determining the source of abnormal data.

Table 5.31 Classification and features of composite compression tests

Classification	Loading condition	Technical features	Standard code
Based on loading condition	Shear loading	Load is transferred to specimen measuring section by shear force between tabs and specimen	ASTM D3410-08, GB/T3856-83
	End loading	Load is directly applied on the specimen ends, both composite panel and sandwich specimen can be used	ASTM D695-02a
	Mixed loading	Side-shear loading plus end loading	ASTM D6641, D6641 M-01
	Other loading	Using honeycomb sandwich construction bending to fulfill composite panel compression	ASTM D5467-97 (2004)
Based on specimen supporting	Short gauge length without side supporting	Short specimen gauge length with no buckling	GB/T3856-83
	Long gauge length with side supporting	Long gauge length and special anti-buckling tool required	ASTM D695-02a, GB/T5258-1995

Specimens prepared from different materials and processes will affect the consistency of test results. The test results will be strongly related to the different specimen materials and their preparation. In the worst-case, for a unidirectional specimen in the 0° direction, a 1° deviation of the fiber axis from specimen preparation or the testing procedure can result in a strength loss of up to 30%. A similar problem affects unidirectional specimens in the 90° direction. These kinds of specimen are very sensitive to loading conditions; thus, care should be taken during specimen preparation and testing. Specimen preparation can have marked effects on test results, especially for unidirectional specimens. Attention should be given to such issues including fiber alignment, machining surface quality, and machining damage during specimen preparation. To overcome these problems, some have tried to use [0/90] cross-laminates to replace unidirectional specimens. Specimens prepared with this type of laminating are insensitive to tab bonding, and may even not require tabs. Thus, highly reliable test results can be generated. The use of [0/90] cross-laminated specimens can reduce test costs and increase reliability.

5.4.2.2 Compression Testing

Composite compression testing has received much attention for many years. Many test methods have been proposed with different features of composites. In general, these methods can be classified based on the load conditions and specimen supports, as listed in Table 5.31.

These two classifications reflect the features of compression test methods from different sides and are complementary to each other. Their combination can more comprehensively describe the characteristics of composites. In fact, different test methods have different requirements on loading conditions, specimen configurations, and specimen crimping. In summary, there are three compression test

Fig. 5.30 Rectangular sleeve fixture for composite compression testing

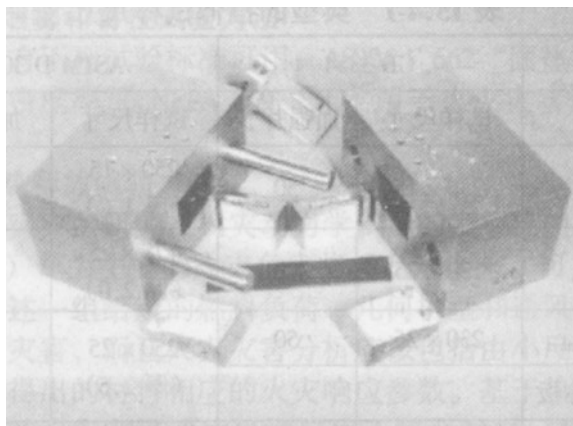


Fig. 5.31 Schematic of loading for composite compression test

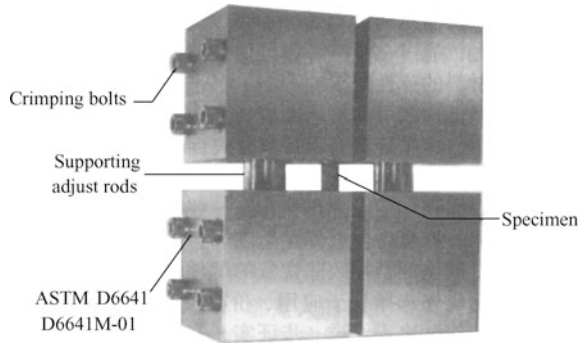
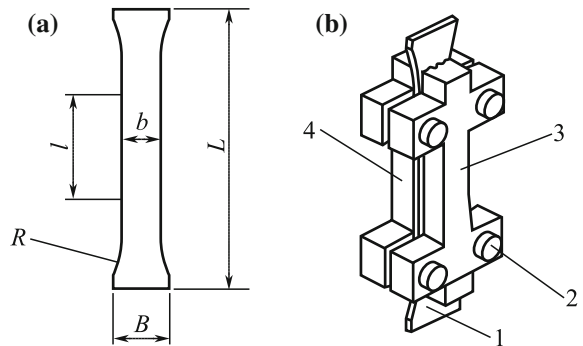


Fig. 5.32 Schematics of specimen and fixture for end loading compression testing (ASTM D695). 1—Specimen; 2—crimping bolts; 3, 4—lateral grooved plates



methods currently available: short gauge length specimens, long gauge length specimens, and honeycomb sandwich construction specimens.

(1) Test method for short gauge length specimen

Representative standards of this type of testing methods include ASTM D3410 and the China national standard GB/T 3856 (I category), the first version of the later was published in 1982, and is basically equivalent to ASTM D3410-750 with the only difference being a larger gauge length. This method is still in current use. In ASTM D3410/3410 M-03, a rectangular sleeve compression fixture is used, as shown in Fig. 5.30.

Application of shear loads will cause stress concentration on the front ends of tabs, and because of the short gauge length, the applied loads will be distributed over the gauge length area and generate a uniform stress distribution. However, this is not yet a regularly applied method. An important improvement to this method is to use blended shear and end loading. In 1980s, an aerospace industrial standard based on blended loading was established, by ASTM. A similar standard is also proposed as ASTM D6641-01, where the blended loading fixture is shown in Fig. 5.31.

The ASTM D6641/D6641 M-01 blended loading method can be used to measure the compression strength and modulus of laminated composites. The ratio of the specimen end load and the shear load can be controlled by adjusting the

clamping force of the crimping bolts. The standard specimen configuration is a straight-sided laminate without tabs. The specimen should be symmetrical and balanced, containing at least one layer in the 0° direction. The dimensions should be 140 mm in length, 12 mm in width, 12–25 mm gauge length and the thickness is not specified. Compared with ASTM D3410, this standard method uses a lighter fixture, which is lower in cost and can be effectively used under non-room temperature conditions. A limitation of this method is that untagged specimens can only be used for 50% 0° -plies, or equivalent laminates. For fiber direction-dependent composites, tabbed specimens should be used for strength measurements. For unidirectional composites (in the 0° layer direction), this method can be used to determine the modulus and Poisson's ratio but is not applicable for compression strength.

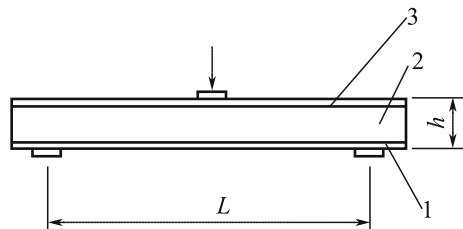
The main reason for recommending a blended loading approach is that sliding phenomenon, or the tear-off of the tabs can be avoided during the load application and more reliable test results can be ensured. The effectiveness in non-room temperature testing conditions is a secondary consideration.

(2) Test methods with long gauge length specimens

The most typical standard for this type method (II class) is ASTM D695-02a, which has been proposed for plastic plate compression testing, and later adapted for composites. In this method, a dumbbell-shaped specimen with a long gauge length is used. Two lateral grooved plates are mounted on both surfaces of the specimen to prevent buckling, a compression load is directly applied on the specimen ends, as shown in Fig. 5.32.

The load is applied to the specimen ends, where stress will also become concentrated. The effect of load application on the stress distribution of the gauge length area will decrease; however, because of the lateral grooved plates, an additional stress field will be introduced into the specimen gauge length area. Some unacceptable failure modes, such as end collapse, can be encountered because the end loading can result in low quality test data. As a test method for rigid plastic plates, this method is more applicable for compression testing of low strength materials, such as resin matrices. Although some problems exist, this method is still widely used in many applications. It is mainly recommended in processing quality control rather than for material design parameter testing.

Fig. 5.33 Schematics of compression test of sandwich structure specimen. 1—Bottom face; 2—Cores; 3—Measured face



To better suit composite compression testing, many improved methods have been developed. These methods retain many original features but are more applicable to composite material. For example, the Chinese national standard GB/T 5258-1995 is a method based on a long gauge specimen with grooved plates and the load is applied to the specimen ends.

(3) Test method for honeycomb sandwich construction specimens

This method tests sandwich structure specimens with composite faces. A four-point load or side load is applied to enable compression testing of the composite faces. A more commonly used method is the three-point bending test of sandwich structure specimens, as illustrated in Fig. 5.33. With proper design, the failure will take place on the compressed face of the specimen, and the compression strength and modulus of the composite face can be measured. ASTM D5467-00 (2005) is a standard compression testing method based on a sandwich bending specimen.

According to some reports, the compression strength measured by this method is approximately 10–15% higher than that obtained by ASTM D3410. Bending load application is most appropriate for unidirectional composite compression tests.

For this method, it is difficult to prepare and machine specimens, and the materials for the specimen are expensive. The test procedure is complicated by many potential failure modes, and the failure mode is the basis for determining whether the test result is reasonable or not. Thus, it is necessary for workers to have some experiences and knowledge to apply this method. For this reason, this method has not been widely accepted in composite testing.

(4) Evaluation and selection of test methods

The three test methods for composites mentioned above can be summarized and evaluated as following: In type I, specimens with a short gauge length are used, the compression load is applied by a specially designed fixture, and the load is transferred to the specimen by shearing through a crimped section of the specimen. The typical standards are ASTM D3410 in a cylindrical fixture and the IITRI method. In type II, usually a long gauge specimen is used. Grooved lateral plates are needed to avoid buckling. The standards available are ASTM D695 and GB/T 5258-1995 in China national standards. In type III, a sandwich structure specimen is used, and a bending load and side load are used to apply compression to the composite faces. Because of the complexity of the materials, specimen preparation, and test procedures, this method has been less widely adopted in composite testing.

Many test methods are available, and problems might arise in the comparison and selection of proper methods for composite testing. The first consideration for selecting a proper method is to evaluate the result reliability, correctness and consistency of failure modes, simplicity of the testing devices, and any additional factors affecting the testing results. Comparisons of different methods are available in many references. In this section, some typical test methods are evaluated based on the specimen material and preparation, and test procedures. This information is presented in Table 5.32.

Table 5.32 Evaluation and comparison of different compression test methods

Method and fixture	Material and processing			Testing procedures			Testing result				
	Materials	Process	Machining	Cost	Equipment	Fixture	Procedure	Strength	Modulus	Repeatability	Suitability
GB 3856	A	A	A	A	A	B	B	A	A	B	C
D6641	A	A	A	B	A	A	A	A	A	A	B
D695	A	A	B	B	A	B	B	B	D	B	B
D695-modified	A	A	A	A	A	A	A	A	B	A	B
Sandwich-specimen	C	B	C	C	A	C	C	A	A	B	C
GB5258	A	A	B	B	A	C	C	B	C	B	C

Note A—Excellent; B—good; C—fair; D—bad

The items listed in the table are limited and the comparison is not comprehensive because of other factors; however, this evaluation is a good reference for selecting a proper compression method for composites. If the quantitative index and weight number are given for each item, it is possible to provide the priority order for each method, which is useful for selecting a proper compression test method.

(5) **Improvement and advancement of test methods**

- (1) **Microsandwich specimen compression testing:** This method is considered to be the most effective and promising improvement to current compression methods. The specimen used in this method consists of top and bottom faces with a resin sandwich core between them. Because of the small dimensions compared with other sandwich specimens, it is known as a microsandwich specimen. This method can give test results with improved reliability. Some references indicate that a AS4/3501-6 unidirectional composite tested by this method showed compression strength as high as 2020 MPa. For other composites tested by this method, the compression strength will be considerably increased compared with that measured by other techniques. When this method is used to test 2D woven composites, similar compression results can be obtained compared with other testing methods.
- (2) **Cross-ply laminate conversion (orthogonal cross-ply laminating):** The use of orthogonal cross-ply or angle cross-ply laminates to determine unidirectional composite compression properties has been addressed in many studies. Some research has indicated that this method can give equivalent results to those obtained with a microsandwich specimen. The compression strength of composites measured by this method will be improved. Orthogonal cross-ply laminates are a particularly good choice for preparing specimens.
- (3) **Reduced thickness specimen:** Another effective improvement is to use reduced thickness specimens. A thick laminate is machined to the specified specimen thickness in the range of the gauge length, and the transition section features crossover by a circular arc. This kind of specimen can give improved test results.

5.4.2.3 In-Plane Shear Testing

The in-plane shear behavior is an important property of laminated composites and in-plane shear test methods have received considerable attention. To date, many testing methods have been developed including $\pm 45^\circ$ -longitudinal and transverse (L/T) shear, double V-slot shear, torsion of thin cylinder, 10° -off-axis tension, rail-shear, square plate diagonal tension, cross-beam bending, and plate torsion.

(1) **$\pm 45^\circ$ L/T shear**

On the basis of composite mechanics, composites under tension load will produce shear stress in the $\pm 45^\circ$ -off-axis direction. In this method, the tensile load is applied

to $[\pm 45^\circ]_{ns}$ cross-ply laminated specimens, and the in-plane shear strength and modulus of the unidirectional laminated composite is based on the measured tensile results. This method is easy and simple to apply. ASTM has featured this method as a standard (ASTM D3518-94 (2001)), and it is also used in an established national standard in China (GB/T 3355-1982). This method can be used to determine the in-plane shear performance of unidirectional composite laminates.

To measure shear modulus, it is necessary to determine the longitudinal and transverse strain, which can be measured with an L/T extensometer or bonding strain gauges placed at 0° and 90° in the central section of the specimen. The L/T shear modulus can be calculated by Eq. (5.16):

$$G_{12} = \frac{\Delta P}{2bh\Delta\varepsilon_x(1 - \Delta\varepsilon_y/\Delta\varepsilon_x)} \quad (5.16)$$

where G_{12} is the L/T shear modulus, MPa; b is the specimen width, mm; h is the specimen thickness, mm; ΔP is the load increment taken from the straight section on the strain–stress curve, N; $\Delta\varepsilon_x$ is strain increment correspond to ΔP ; $\Delta\varepsilon_y$ is the strain increment in the specimen vertical direction corresponding to ΔP .

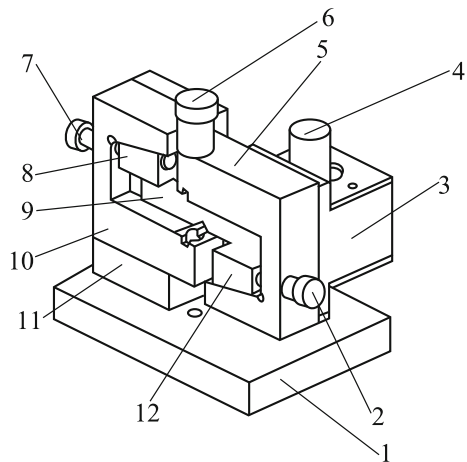
L/T shear strength can be calculated from Eq. (5.17):

$$S = \frac{P_b}{2bh}, \quad (5.17)$$

where S is the L/T shear strength, MPa; P_b is the maximum load at specimen failure, N; b is specimen width, mm; h is the specimen thickness, mm.

Advantages of the $\pm 45^\circ$ -off-axis tension method include the simple specimen preparation and loading conditions, and good reproducibility; however, a positive tensile stress equal to the shear stress and an edge interlaminar stress effect will be present during testing.

Fig. 5.34 V-notched specimen shear test apparatus. 1—Base; 2, 7—locking bolts; 3—guide axis out line; 4—guide axis; 5, 10—specimen hold slot; 6—loading head; 8, 12—specimen fixing adjust block; 9—specimen; 11—L support of base



(2) **Double V-notched specimen**

The shear test with double V-notched specimens was first proposed by Iosipescu for metal bar specimen. Arcan, Sleptetz, Walrath, and Adams have since applied the principles of this method to test composite shear properties. Several versions have been developed, including the Arcan disc shear, anti-symmetrical 4-points AFPB, and Iosipescu method. These methods can be successfully used to test composites with unidirectional, multiple-orientation laminates and can give very good result accuracy compared with that of thin cylinder torsion testing.

ASTM first included V-notched shear method as a standard (ASTM D5379-1993) which is applicable for in-plane shear testing of unidirectional, multi-ply ply laminates and 2D woven composites. The method can suit many different test requirements, and can be used for in-plane (1–2 direction), interlaminar (2–3 and 1–3 direction) shear testing. In China, an aviation industrial standard (HB 7237-1995) has also been established based on this method. The testing device is shown as in Fig. 5.34.

In testing, the specimen is placed into two slots and aligned with the load applying axis. The rest machine is run, and a load is applied to the top-half fixture block to generate a shear load.

To measure the G_{12} in-plane shear, $\pm 45^\circ$ strain gauges should be attached to the specimen central part, which is located in a $2 (0^\circ\text{-fiber direction}) \times 3 \text{ mm}$ zone. The sensor wire should be aligned along the $\pm 45^\circ$ direction. The gauge glue should not damage the tab adhesive layer or strain gauges, and should have no effect on the material properties. Automatic devices can be used to measure the shear modulus and strain–stress curve.

The in-plane shear modulus can be calculated from Eq. (5.18):

$$G_{12} = \frac{\Delta P}{Wh(\Delta\varepsilon_{45} - \Delta\varepsilon - 45)}, \tag{5.18}$$

where G_{12} is the L/T shear modulus, MPa; ΔP is the load increment taken from the straight section of the strain–stress curve, N; W is the distance between the bottom of the V-notches, mm; h is thickness, mm; $\Delta\varepsilon_{45}$ is the strain increment along the

Fig. 5.35 0° specimen shear testing curves (T300/5222)

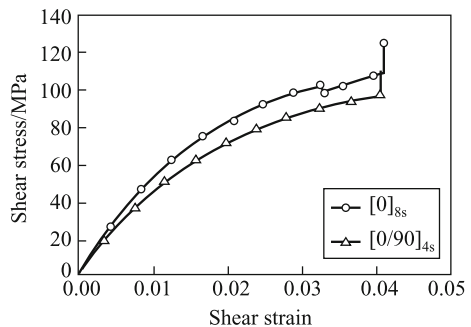


Table 5.33 Comparison of shear test between V-notched specimen and L/T shear (T300/5222)

Property	Double V-notched specimen				L/T shear	
	[0] _{8s}	[0/90] _{4s}	[±45°] _{4s}			
Average value	Strength/MPa 124	Modulus/GPa 5.47	Strength/MPa 114	Modulus/GPa 5.07	Strength/MPa 91.9	Modulus/GPa 4.97
Standard deviation	4.55	0.24	2.69	0.08		

45°-direction corresponding to ΔP ; $\Delta \varepsilon_{-45}$ is the strain increment along the -45°-direction correspond to ΔP .

The in-plane shear strength can be calculated from Eq. (5.19):

$$S = \frac{P_b}{Wh} \quad (5.19)$$

where S is the in-plane shear strength, MPa; P_b is the maximum load at specimen failure, N; W is the distance between the V-notch bottoms, mm; h is the specimen thickness, mm.

There is a small peak load in 0° tests (Fig. 5.35), and two adjacent small peaks in some tests. The corresponding failure is fracture along the horizontal direction, which is not located in specimen measuring zone. Further loading will cause shear failure in the measuring zone.

The V-notch in the specimen can produce a more uniform stress distribution than those without a V-notch. The uniformity of the stress distribution depends on the anisotropic properties of the specimen materials. Among all kinds of layer patterns, the $[0/90]_{4s}$ laminate has the most uniform stress distribution.

The initial failure is induced by stress concentration at the V-notch root. No initial failure peak will be generated in the $[0/90]_{4s}$ laminate, because no significant stress concentration will occur at the V-notch root. The shear strength of $[0]_{ns}$ measured in V-notch specimens will be clearly higher than that obtained in L/T shear testing, and also higher than that tested in $[0/90]_{4s}$ laminates (Table 5.33). The main reason is that excessive shear strain and deformation occur for this fiber direction. A higher bearing tensile load is produced, while a higher modulus results from strain concentration in the V-notch root. Thus, $[0/90]_{ns}$ laminates are a good selection for testing.

An excessive shear strain will present difficulties for the measurements and the mechanical principles used in the consideration. Furthermore, excessively large deformations will decrease the reliability of the results. In ASTM D5379, it is indicated that the shear strength should be defined as the shear stress at a specified deformation point. This definition is feasible and practical, because an excessively large deformation should not be allowed in practical engineering, which assures the structural stiffness integrity.

Owing to the small specimen dimensions, this method should not be used for coarse-textured braided composites. The small specimen measuring zone cannot assure a complete assessment of the braiding texture.

(3) Other shear testing methods

In addition to the two previously mentioned methods, several other methods are often used in composite tests. Some of their features and applications will be discussed as follows:

- (1) Thin-wall cylinder torsion: This method is the mostly accepted shear testing method, and can produce pure shear stress conditions. Results produced from

this method are often used as a basis for comparison between theoretical and test studies. In testing, torsion moments are applied to the cylinder ends and the specimen is placed under shearing stress. The shearing stresses will be distributed uniformly around circumference of the cylinder. The cylinder wall is thin, such that the stress gradient along the wall thickness can be ignored and accurate shear properties can be measured. However, the specimen preparation and machining, test fixtures, and procedures require complex test devices. More importantly, the differences of the processing techniques for composite cylinders and laminates can result in different properties, which cannot be ignored. Hence, this method is limited for use with composite materials.

- (2) Rail-shear testing: This method is recommended by ASTM as standard ASTM D4255 and was first proposed in 1983. A new version was published in 2001 based on modification of the original version. This is a simple test method for composite laminates and is widely used in aeronautical composite in-plane shear tests. On the basis of different test fixtures, the method can be divided into double-rail shearing and three-rail shearing. Three-rail shearing can provide a more uniform shear stress distribution but requires a larger specimen than that used in double-rail shearing. These methods can be used in shear modulus measurements; however, for shear strength measurements, the tests may not be accomplished because many other non-shear factors can cause specimen failure. Whitney evaluated these methods and suggested that the edge effect and the uniformity of the stress distribution along the specimen width depend on the length/width ratio (L/W) in the gauge length area of the specimen as well as the ratio of the material elastic constants (G_{xy}/E_y). Many studies have indicated that the edge effect can be ignored and uniform shear stress can be generated when $L/W \geq 10$. When the equivalent Poisson's ratio meets the conditions $\nu_{xy} = \nu_{yx} \approx -1$, the edge effect is unavoidable and the stress distribution will become irregular and cause unreliable test results for this kind of laminate. The modulus measured by rail-shear testing is insensitive to the L/W ratio, because the measurement is completed in the central area of the specimen where the stress distribution is more uniform. In practical testing, a uniform shear stress field in the specimen should be applied by the rails, but this is often accompanied by a large positive stress field depending on the rail stiffness. Furthermore, the large specimen dimensions can cause difficulties for specimen preparation.
- (3) 10° off-axis tension: This method can only be used for measurements of the shear performance of a unidirectional laminate. The off-axis angle can be set to another value; the optimized angle corresponds to the maximum relative shear strain $\gamma_{12}/\epsilon_{11}$, where the shear stress reaches the critical value. This angle is dependent on the anisotropic modulus and strength behavior of the measured materials. For composites materials, the optimum angle is in the range of 10° – 15° . Commonly, 10° is selected for off-axis tension measurements. Because the stress is sensitive to the off-axis angles, it is important to select the proper direction to cut the laminate for the specimen and also the use the correct loading direction and strain gauge measuring directions. To assure uniform stress distribution, long and narrow specimens should be used with an aspect

ratio (L/W) in the range of 14–16. Many studies have indicated that this method may generate higher modulus and lower shear strength and failure strain compared with results from the $\pm 45^\circ$ off-axis tension method.

- (4) Square plate diagonal tension and square torsion: A square plate can be used to measure the composite shear modulus by applying loads to the four points for torsion testing. This setup requires a complex testing device for shear testing. This method is suitable for the case of small deflections and can only produce reliable results when the ratio of the deflection and laminate thickness w_p/t is less than <0.5 . The initial linear part of the strain–stress curve should be used to calculate the shear modulus. This method has not been widely adopted because of the large specimen requires, high cost, and the complexity of the test device and procedures.

(4) Evaluation and selection of test methods

Although many test methods now are available, it remains difficult to select the optimal method, and is particularly difficult to obtain the ideal shear strength. For all shear testing methods, the common difficulties are handling of edge effects, specimen shape, nonlinearity of the materials, interfacial behavior, and stress distribution, these factors can often cause over-or under estimates of the shear strength. Existing positive stress is another factor, which may cause questionable shear strength results. In fact, there is no direct test method that can be used to determine the pure shear stress of materials to be tested. The measured shear strength will not be pure shear, and the failure mode will not be pure shear failure. Thus, the measured strength is not the real shear strength. The shear strength measured by currently available methods do not have a fully accepted comparative standard. Furthermore, the test principles are not applicable in the case of large specimen deformation. Thus, the use of shear stress under a specified deformation as the shear strength is more reasonable. In ASTM standards after 1994, the shear modulus was defined as the secant line through 2000 and 6000 microstrain points, and 5% shear deformation as a test termination point.

Thin-wall cylinder torsion, rail-shear, square plate diagonal tension, cross-beam bending, square plate torsion, and double V-notch specimen shear testing methods can be used for unidirectional and multidirectional laminated composites, and are also applicable for various fabric composites. The $\pm 45^\circ L/T$ shear method is suitable for unidirectional composite in-plane shear testing and can also be used for fabric-reinforced composites; however, because fabric materials have different fiber ratios warp- and filling-wise, difficulty can be expected determining the ideal stress field. Instead, a mixed field of positive stress and shear stress will be produced. Even for a fabric material with the same fiber ratio warp- and filling-wise, it is difficult to obtain ideal shear effects. Because of the fiber in curl state, the final failure is often a kind of tension fracture from which the shear modulus can be reasonably determined; however, the shear strength is not perfectly ideal.

Table 5.34 Failure modes of composite interlaminar shear (SBS) tests

No.	Failure mode	Remarks
1	Single shear	Shear failure takes place at a interlaminar layer
2	Multiple shear	Shear failure takes place in several layers
3	Mixed failure	Shear failure with local breakage
4	Bending fracture	No failure at interlaminar layer, specimen broken by bending
5	Bearing failure	No obvious interlaminar failure

A 10°-off-axis tension method is only suitable for unidirectional composite in-plane shear parameter measurements.

For these reasons, it is necessary to select a proper test method according to the materials to be tested.

5.4.2.4 Interlaminar Shear Testing

Interlaminar shear testing is a test method to evaluate the interlaminar properties of composites and can indicate the interfacial strength between the matrix and reinforcement. Currently available methods can only measure the interlaminar strength approximately; thus, for some methods, the interlaminar strength is referred to as the apparent shear strength.

SBS is the most commonly used method to determine the interlaminar shear strength of composites. In this method, three-point bending is used to apply a load to a composite short beam. When the ratio of the length to thickness (L/h) is small enough and shear stress is generated during the load application, interlaminar failure will take place in the specimen and the interlaminar shear strength can be obtained. In fact, the point of load application and the positive stress caused by bending can affect the shear strength. Some studies have indicated that the stress distribution in specimens was very different from that determined by classical theoretical analysis.

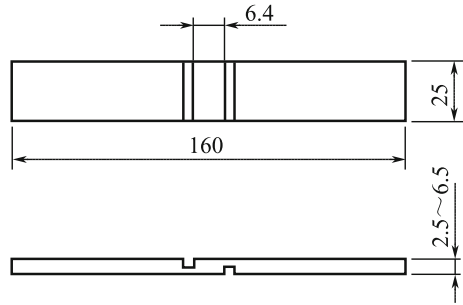
Theoretically, to assure shear failure rather than bending failure, the following conditions should be satisfied:

$$\frac{\sigma_f}{\tau} < \frac{\sigma_f^{\text{ult}}}{\tau_{\text{ult}}} \quad (5.20)$$

In general, for composites, the bending strength is about 15 times the interlaminar shear strength. Thus, this requires $L/h < 7$, and usually, $L/h = 4-5$.

Table 5.34 shows some typical failure modes occurring for SBS testing. The first failure mode usually takes place at the central layer or near the central layer of the specimen, which is relatively close to the maximum theoretical shear stress position. The second failure mode is multilayer cracking, which is also caused by shear stress. These two failure modes are the ideal shear failure modes. In a third case, it

Fig. 5.36 Specimen with slots on two faces used in interlaminar shear testing



might be difficult to identify the failure mode, while fourth and fifth modes are unacceptable failure modes. Bending fracture is mainly caused by fiber rupture taking place before interlaminar fracture owing to problems with the specimen or test conditions. Bearing failure might be induced by hot-wet conditions or high temperatures, which degrade the load-bearing ability of the specimen. Hence, there will be no obvious failure in the test procedures until bearing failure occurs in the span area between the two supporting points, indicating that no valid test results can be obtained.

Additionally, there is a shear testing method based on specimens with slots on two faces, which is adopted by ASTM as standard D3846-02. If the aforementioned SBS test methods cannot obtain valid results, this alternative method can be used; however, note that the shear stress distribution between the two slots is not uniform, such that the shear strength measured by this method is still an apparent shear strength.

The specimen used for this method is shown in Fig. 5.36.

5.4.2.5 Bending Property Testing

Bending testing is simple and widely used in composite processing control and quality inspection. Bending properties have become an essential parameter for property evaluation in composite systems.

On the basis of the load application method, bending testing methods can be divided into three-point and four-point bending methods. Three-point bending is the most commonly used bending testing method. The specimen used in bending testing is a unidirectional rectangle composite strip. The specimen is placed to span two support points at a distance L , which should be determined based on the ratio of the span to thickness (L/h). In three-point bending, the ratio of the span to thickness is determined according to the critical ratio $L/h = 1/2_b$ at which the tensile failure and interlaminar failure take place simultaneously. The bending failure will first take place in the surface fibers. For glass fiber and carbon fiber-reinforced plastics $L/h = 16 \pm 1$ and $L/h = 32 \pm 1$, respectively.

Fig. 5.37 Bending modulus as a ratio of span to thickness (M40J/5228)

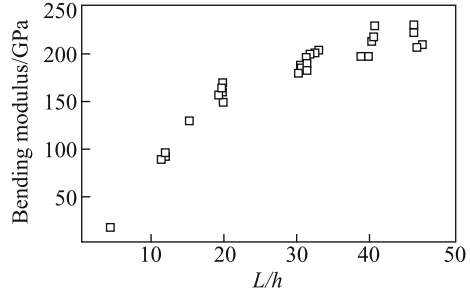
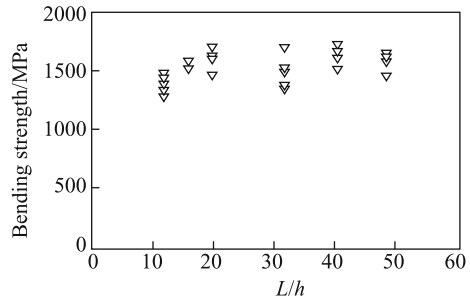


Fig. 5.38 Bending strength as a ratio of span to thickness (M40J/5228)



To reduce the effects of shear stress in bending modulus measurements, parameters of $L/h = 40$ are usually taken. The central deflection is measured and the load-deflection curve (P - f curve), the bending modulus can be calculated from Eq. (5.21):

$$E_f = \frac{\Delta PL^3}{4bh^3\Delta f}, \tag{5.21}$$

where E_f is the bending modulus, MPa; ΔP is the load increment corresponding to straight-line part on P - f curve, N; Δf is the central deflection of the specimen corresponding to ΔP , mm; L is the specimen supporting span, mm; b is specimen width, mm; and h is specimen thickness, mm.

The bending modulus measured from bending tests will often underestimate the modulus of materials. As the ratio of span to thickness increases, the test will show more pure bending, and the measured modulus will tend toward to the tensile modulus of the materials (Fig. 5.37).

In bending strength testing, the loading speed V is determined based on the relationship between the displacement speed at the loading point (the span central point) df/dt and the maximum strain rate of the tested materials d_{\max}/dt , such that $d_{\max}/dt = 1\%/min$. Usually, the loading speed is in the range of 2–5 mm/min.

Bending strength can be calculated from Eq. (5.22).

$$\sigma_f = \frac{3P_b L}{2bh^2} \quad (5.22)$$

where σ_f is the bending strength, MPa; P_b is the maximum load at the specimen failure, N; L is the specimen supporting span, mm; b is specimen width, mm; and h is specimen thickness, mm.

If the specimen is in bending failure and the ratio of the deflection to span $f/L > 10\%$, the effect of additional moment caused by supporting reactions should be accounted for in the calculation of bending strength. A modified equation is given below as:

$$\sigma_f = \frac{3P_b L}{2bh} \left[1 + 4(f/L)^2 \right] \quad (5.23)$$

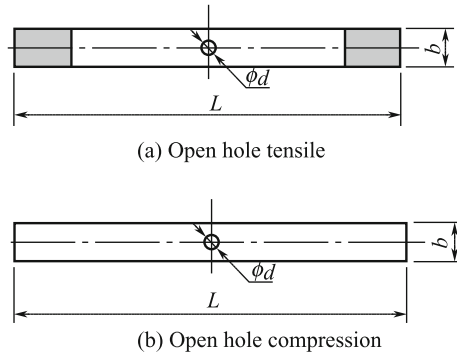
where f is the deflection at the center of the span when the specimen is in failure, mm.

Figure 5.38 shows the test results of bending strength under different spans. By reviewing the test results and failure modes together with the previous discussion, it is clear that when $L/h \leq 16$, mainly local failures occur in the interlaminar layer caused by interlaminar stress concentration. For $16 \leq L/h \leq 32$, the failure modes are in a state of transition. Although $L/h = 32$ is an internationally recommended condition, testing results indicate that specimen failure is often caused by local transverse stress concentration accompanied by interlaminar cracking, giving a wide data scatter. When $L/h = 40$ or even larger, a “brittle” failure mode can be expected. The specimen will break into two separate sections, based on observations of the fracture surface, it has been found that failure occurs mainly through longitudinal compression.

According to these test results, considering the data scatter, failure modes, and consistency of the results, the selection of a span-to-thickness ratio of $L/h = 40$ is more reasonable than the specified $L/h = 32$.

The effects of loading conditions and deformation are a source of some limitations in bending test results. The analysis of results depends on failure modes. In bending testing, possible failure modes include: local damage at loading points, outer surface tensile failure, internal longitudinal compression failure, bending breakage, brittle breakage, and combinations of several different failure modes. In the design of composite bending test methods, it is essential to determine the fiber tensile failure of the outer surface of the specimen. In ASTM D790-03, it is clearly specified that the method is not suitable for materials that show no fiber failure occurring on the outer surface. The purpose of this specification is to ensure the consistency of test result data. However, in many composite bending tests, failure is caused by microbuckling and occurs on the compressed surface. Also, some failures initially occur at loading points, which involve a mixture of failure mode caused by longitudinal compression and transverse shear local stress concentration. In this case, it is difficult to evaluate the real load-bearing ability of the materials. In many standards, it is clearly specified that bending testing cannot be used for design

Fig. 5.39 Specimen for open-hole tensile and open-hole compression



parameter testing, and only for material quality control. However, note that the more valuable results can be obtained from bending tests if data processing is performed properly.

5.4.3 Test Methods Related to Structural Performance

In this section, some test methods related to structural performances will be discussed, including open-hole tensile (OHT), open-hole compression (OHC), filled-hole compression (FHC), single pin bearing tensile edge delaminating, model I interlaminar fracture toughness, model II interlaminar fracture toughness, compression strength after impact (CAI), and quasi-static indentation.

5.4.3.1 Open-Hole Tensile and Compression

Open-hole tensile and compression are used to select materials and to evaluate the sensitivity of composite laminates to structural defects/damages (apart from impact damage). There are some ASTM standards available for open-hole tensile and compression (ASTM D5766-02 and ASTM D6484-04). In China, there are also some aeronautical standards available.

Specimens for open-hole tensile and compression are strips with dimensions $300 \text{ mm} \times 36 \text{ mm}$ with a hole with a 6-mm diameter in the center, as shown in Fig. 5.39. For open-hole tensile testing, ASTM D5766 M-02 requires specimen dimensions of length in 200–300 mm, width of 36 mm, hole diameter of 6 mm, nominal thickness of 2.5 mm, and a thickness range of 2–4 mm. For open-hole compression, ASTM D6484 M-04 uses modified specimen dimensions, specifically: length of 300 mm, width of 36 mm and hole diameter of 6 mm, nominal thickness of 4 mm, and a thickness range of 3–5 mm. The specimen materials are usually selected as $[45/0/-45/0]_{\text{ns}}$ prepreg tapes or $[45_i/0_j]_{\text{ns}}$ fabric laminates. The fiber layer content in each direction should be at least 5% in the four principal

directions. This is also applicable for other laminates used as specimens for these methods. The main difference between specimens for tensile and compression testing is that for tensile tests the specimen should be tabbed on ends.

Tensile specimens are directly mounted into top and bottom clampers of the fixture, and loaded at 1–2 mm/min.

In compression testing, a lateral buckling device is needed to protect against specimen buckling during application of a compression load, as shown in Fig. 5.43.

Open-hole tensile and compression strength can be calculated by Eq. (5.24):

$$\sigma_{t/c} = \frac{P}{bt} \quad (5.24)$$

where P is the maximum load at specimen failure, N; b is specimen width, mm; t is specimen thickness, mm.

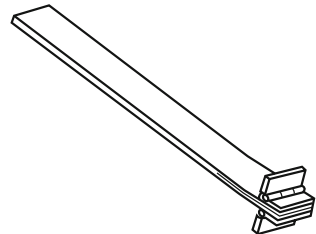
5.4.3.2 Filled-Hole Tensile and Compression Testing

This property is also used to select materials and to evaluate the sensitivity of composite laminates to structural defects/damages (other than impact damage). Standard ASTM D6742/D6742 M-02 can be followed to perform this test.

5.4.3.3 Single Pin Bearing Strength Testing

This property is used to evaluate the composite response to a single pin bearing. Standard ASTM D5961/D5961 M-01 can be followed to perform this test.

Fig. 5.40 Specimen for composite model I fracture toughness



5.4.3.4 Model I Interlaminar Fracture Toughness

This method is recommended in NASA RP1142 to characterize material toughness as a standard. The G_{IC} test method has become an ASTM standard and has been adopted by the China aviation industry.

Composite Model I fracture toughness (interlamination open type) G_{IC} testing uses a double-suspended beam specimen, as shown in Fig. 5.40. A PTFE film is inserted into one end at the central line of the specimen to introduce delamination. The thickness of PTFE film should be no greater than 0.05 mm.

A tensile load is applied to specimen in a displacement controlled manner, and the load-deformation curve is recorded. The load is removed when delamination expands to about 10 mm. The above procedures are repeated until the delamination length reaches approximately 100 mm, when loading is stopped. Equation (5.25) can be used to calculate the interlaminar fracture toughness G_{IC} at each time of load application-removal and the average value is taken. The loading speed should be 1–2 mm/min.

Model I interlaminar fracture toughness can be calculated by Eq. (5.25):

$$G_{IC} = \frac{mP\delta}{2ba} \times 10^3 \quad (5.25)$$

where G_{IC} is the interlaminar fracture toughness, J/m^2 ; m is the compliance fitting coefficient; P is the delamination expanding critical load, N; δ is the displacement at a loading point corresponding to applied load P , mm; b is the specimen width, mm; a is the delamination length, mm.

5.4.3.5 Mixed Interlaminar Fracture Toughness G_C

This method is recommended as a standard to characterize material toughness in NASA RP1142. The G_C testing method has now become an ASTM D6671/D6671 m-04 standard and has been adopted by the China aviation industry.

Composite interlaminar fracture toughness G_C uses a specimen with laminating code of $[\pm 30/\pm 30/90/90]_s$. A tensile load is applied to measure edge delamination and its growth. Test results of interlaminar fracture toughness of a material are obtained.

In this method, strip specimens with dimensions of 250 mm \times 30 mm and a clamp length of 40–50 mm are used. An extensometer is attached to the specimen center with a 100-mm gauge length. In testing, a tensile load is applied at 0.1–0.3 mm/min and the load vs deformation curve is recorded.

Edge delamination fracture toughness can be calculated with Eq. (5.26):

$$G_C = 0.16E_0\varepsilon_C^2h \times 10^{-6}, \quad (5.26)$$

Fig. 5.41 Test apparatus for quasi-static indentation

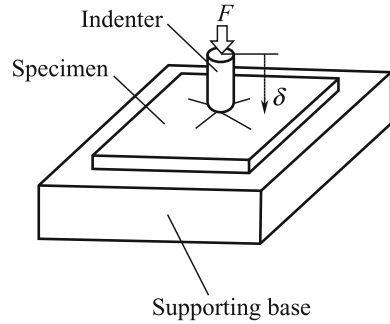
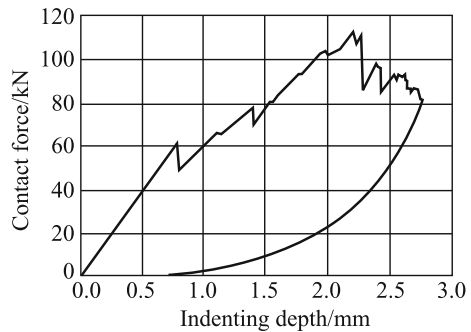


Fig. 5.42 Correlation between indention depth and contact force in quasi-static indentation testing



where G_C is the edge delamination fracture toughness, J/m^2 ; E_0 is the composite laminate modulus, GPa; ϵ_c is the initial strain of laminate delamination; h is the specimen thickness, mm.

5.4.3.6 Quasi-static Indentation

CAI has some deficiencies in terms of quantitative characterization of damage resistance. Quasi-static indentation is a supplementary method used to overcome the disadvantages of CAI. Quasi-static indentation can be used to quantitatively measure the damage resistant ability of composites under the action of a quasi-static transverse contact force. The load is applied in quasi-static conditions; thus, the whole load application process and damage process can be quantitatively measured on the specimen. This method is widely adopted as an effective method to evaluate the damage resistant ability of composites and is an ASTM standard [(D6264-98 (2004))].

The test apparatus is shown as in Fig. 5.41.

According to ASTM D6264-98, the specimen is a square plate with dimensions of $150 \text{ mm} \times 150 \text{ mm}$, the laminating code is $[45/0/-45/90]_{ns}$, the selection of n should satisfy a specimen thickness greater than 3.5 mm. This test uses a circular cylinder to support the specimen. The diameter of the circular cylinder is 127 mm.

For good data analysis, the specimen can be also placed on a steel back plate for comparison of test results.

In testing, the indentation load and indentation displacement are continuously recorded. The initial damage load and the ultimate damage load can be identified from the testing curve (Fig. 5.42). Some additional measures can be used for damage analysis if necessary.

After performing quasi-static indentation, the impact damage is equivalently generated. If compression after damage is needed, CAI tests can be performed.

5.4.3.7 Compression After Impact

Impact damage (in this section impact refers to low-speed impacts) involves the most sensitive delamination issues for composites. Damage caused by impacts is often not visibly inspectable and takes the form of internal damage, such as matrix cracking, fiber/matrix shearing, fiber rupture, and delamination. Although these damage types are not visibly inspectable, they can considerably decrease the structural load-bearing ability, in particular the compression-bearing ability. This poses a great potential danger to aircraft structures. In NASA RP1142, the compression strength after impact is recommended as a method to characterize the toughness of composites and is clearly specified as the standard test method for measurement of CAI and correlating requirements for material performances. This standard has become a critical guideline in aviation composite structure design and material selection. For easy testing, Boeing has modified this method by reducing the specimen dimension, and SCAMA has accepted Boeing's standard. CRAG in Europe proposed a similar standard and in China, an industrial aviation standard has been established. However, no ASTM standard has been established at this time. Owing to the high production costs of composites, the smaller specimen size of the SCAMA/Boeing CAI standards is commonly adopted. In Table 5.35, some technical specifications of commonly used CAI testing methods are listed. Of these methods, the most widely accepted is the method proposed by SCAMA/Boeing. The SCAMA/Boeing method is widely used in China, although a local aviation standard has been established.

Compression testing after impact is divided into two steps, involving the impact damage step of the composite laminates (usually by a half-ball steel impactor form dropped from a specified height to impact a specimen surface mounted on supports) and compression testing after damage.

A test method with size reduced specimen has now been introduced, although the results obtained from this method cannot be compared with those obtained from the SCAMA/Boeing method. However, these results are valuable as references for material screening in material research and development.

The impact test machine is composed of a specimen fixture, impactor and test control device, as shown in Fig. 5.43a. In testing, the specimen is mounted on a fixture, and an impactor will impact the central area of the specimen with a specified

Table 5.35 Impact and CAI test methods

Proposer/user	Specimen dimension/mm	Supporting/mm	Impactor		Energy/ (J/mm^{-1})	Laminating code
			Diameter/mm	Mass/kg		
NASA	300×175 cut into 300×125 after impact	125×125 square fixed support	$\phi 12.5$	5	4.45	[45/0/ -45/90] _{6s}
SCAMA/ Boeing	150×100	76×127 rectangle 4-point fixed support	$\phi 1$	5	6.67 4.45	[45/0/ -45/90] _{4s}
CRAG	Cut into 180×50 after impact	$\phi 100$ circular fixed support	$\phi 10$	According to needs		[45/0/ -45/90] _{2s}
QMW	89×55	$\phi 40$ square fixed support	$\phi 20$	4		[45/0/ -45/90] _{2s}

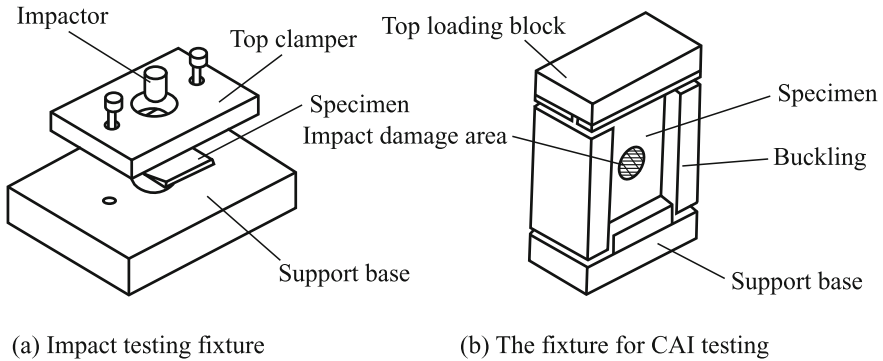


Fig. 5.43 Schematics of composite impact and CAI test machine

energy to create impact damage. The impact damage content is usually observable by visible or C-scan inspection.

It has been observed that a dent occurs on the damaged area of the front surface of the specimen when the load is applied at a certain level (Fig. 5.43a). A protruding spot will also appear on the back surface of the specimen (Fig. 5.43b), caused by delamination. It can be seen from the figures that the damage on the back surface has a larger size than that on front surface. When load is further increased, the delamination damage on back surface gradually expands along the transverse direction to the specimen edges. At this point, buckling begin to appear on the back surface and adjacent layers. The area of delamination in the specimen expands (Fig. 5.44d). In some specimens, no visible longitudinal damage expansion is observed. This phenomenon can be described by a sublayer model. When buckling occurs on sublayers, the back surface and its adjacent layers almost lose their load-bearing ability. However, the dent damage on the front surface only expands to the edge of the impact damage and expands no further. The front surface and the adjacent sublayers can continuously bear the load until total failure occurs (Fig. 5.44c).

The matrix cracking in layers and debonding between fiber and matrix are the initial damage modes to laminates subjected to low-speed impacts. The matrix cracks are mainly caused by the mismatch of matrix and fiber properties. Matrix cracks can be divided into shear cracks and bending cracks. The former are mainly created on impacted surfaces and the layers at the laminate central line, induced by transverse shear force. The later are mainly generated on the impacted back surface, induced by bending tensile stress.

Delamination is the most critical damage affecting laminate stiffness and strength. Only when the impact energy has reached a certain level will the matrix fracture, and delamination damage can take place. The matrix cracks in layers (or ply group) expand into the interlayers and will be restrained by layers in different

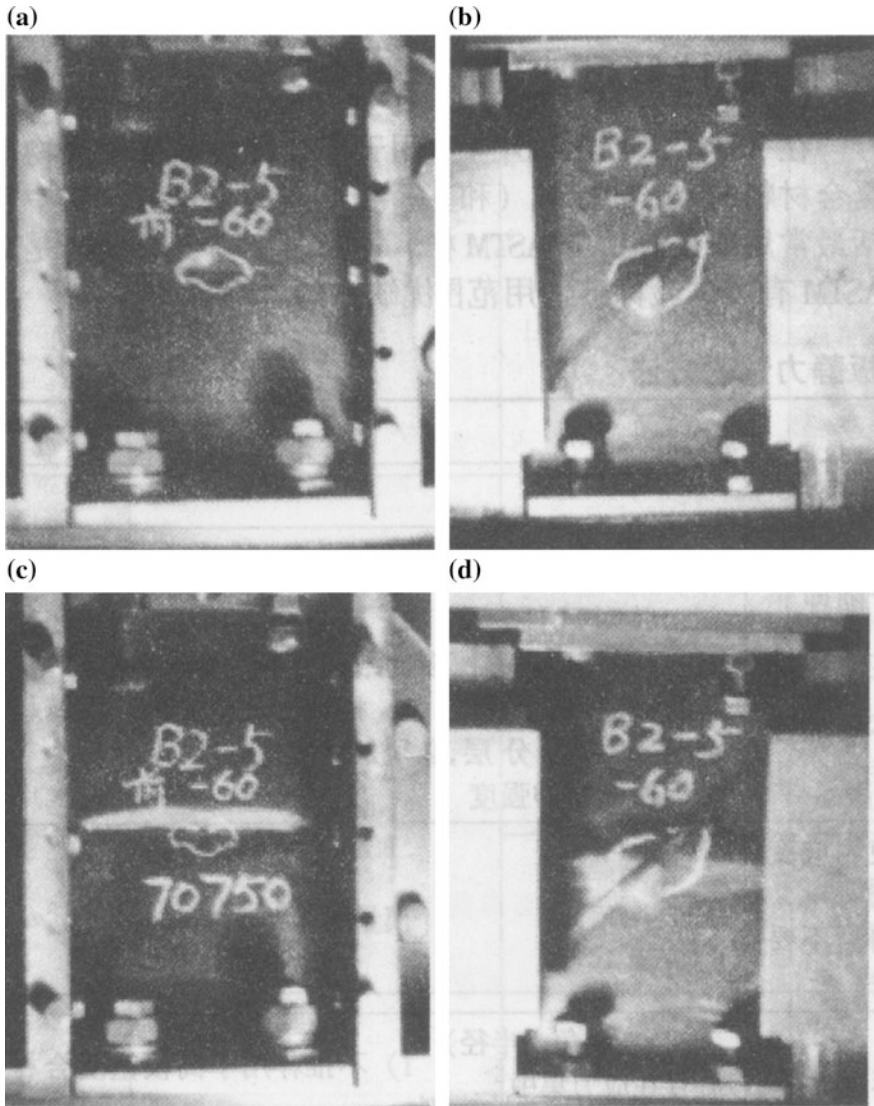


Fig. 5.44 Failure process of composite CAI test

directions and stop expanding. At this moment, a high positive stress and shear stress field will be produced near the matrix crack tips, resulting in delamination between layers. Delamination expansion is controlled by the longitudinal shear stress σ_{33} in the layers forming the interface, and the transverse positive in-plane stress σ_{22} , as well as the transverse shear stress σ_{23} of the aforementioned layers.

Fiber rapture is usually produced after matrix cracking and delamination damage, and is only limited to the impactor contact area, resulting from impactor

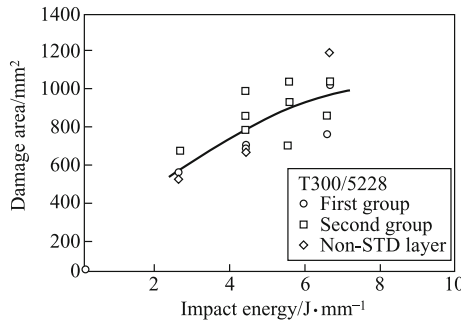
pressing stress and local indentation (mainly dominated by shear force). On the back surface, fiber rupture is mainly induced by bending stress.

After impact damage is introduced, CAI testing can be performed. In testing, a specimen with impact damage is mounted on the testing device for CAI testing, as shown in Fig. 5.43b, and a load is applied until specimen failure occurs. The failure process is observed and the failure load recorded, the CAI strength can be calculated by the equation below:

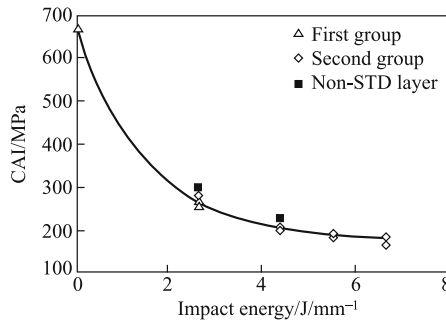
$$S_{CAI} = \frac{P}{bh} \tag{5.27}$$

where S_{CAI} is the compression strength after impact, MPa; P is the applied load at the specimen failure, N; b is specimen width, mm; h is the specimen length, mm.

The correlation between impact/CAI strength and impact energy is given in Fig. 5.45.



(a) The correlation between impact energy and damage area



(b) The correlation between impact energy and CAI strength

Fig. 5.45 Correlation between impact/CAI strength and impact energy

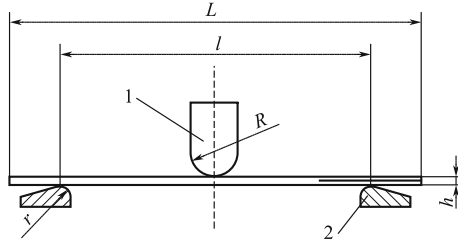


Fig. 5.46 Model II fracture toughness testing of composites. R —Top press head diameter; r —bottom support frame diameter; L —specimen length; l —span; h —specimen thickness; 1 —top press head; 2 —bottom support frame

5.4.3.8 Model II Interlaminar Fracture Toughness

Similar to model I interlaminar fracture toughness testing, model II interlaminar fracture toughness testing is recommended by NASA RP1142 as a property specification to characterize material toughness. No ASTM standard is currently available. In China, the relevant aviation industrial standard has been established.

Model II interlaminar fracture toughness (interlaminar shear) G_{IIC} testing uses a specimen with an end cut, and a 3-point or 4-point bending load is applied. In the standard HB7403-96, in China, 3-point bending is used as shown in Fig. 5.46.

In specimen preparation, one end is inserted into a PTFE film to induce delimitation. The film thickness should not be greater than 0.05 mm, and the predelamination length is approximately 40 mm.

The tensile load is applied in a displacement manner until specimen failure occurs, and the load vs deflection curve is recorded. G_{IIC} can be calculated by the equation below (assuming a loading speed of 1–2 mm/min):

$$G_{IIC} = \frac{9P\delta a^2}{2b(2L^3 + 3a^3)} \times 10^3 \quad (5.28)$$

where G_{IIC} is the model II interlaminar fracture toughness, J/m^2 ; P is the delamination expanding critical load, N; δ is the displacement at loading the point corresponding to the applied load P , mm; b is the specimen width, mm; a is the delamination length, mm; $2L$ is the span, mm.

5.4.4 Fabric-Reinforced Textile Composite Mechanical Property Testing

Fabric-reinforced textile composite mechanical property testing can refer to corresponding standards for fiber-reinforced composites; however, there are differences in the microstructures (or fiber textile patterns) of textile composites and

prepreg laminated composites. In textile composites, cross-woven yarns increase the non-uniformity of the laminate local displacement field. Because of the yarn size and the woven or braiding texture patterns, the non-uniformity in textile composites will be greater than that of traditional prepreg laminates. ASTM D6856-03 is a guideline for fabric textile composite testing standards, providing reference standards for testing textile composite mechanical properties, and instructions on the related standards.

5.4.5 Summary of Mechanical Property Test Methods

In ASTM D4672-04, a summary of ASTM standards (and other standards) applicable for continuous fiber-reinforced polymer matrix composites is presented, including the most commonly used ASTM standards, In Tables 5.36 and 5.37, the advantages and disadvantages of some ASTM standards are summarized.

5.4.6 Electrical Performance Testing

The electric characteristics of composites are very important in some applications. Those characteristics of interest include the dielectric constant, dielectric intensity, volume resistance coefficient, surface resistance coefficient, the resistance, dissipation, and loss factor. These values can be affected either by temperature and ambient conditions or by the curing agent types, fillers, and the fibers used in the composites. The following ASTM testing methods can be used to determine the electric performances of polymer matrix composite laminas and laminates.



ASTM D149-97a (2004) “Standard test method for dielectric breakdown voltage and dielectric strength of solid electrical insulating materials at commercial power frequencies” can be used to determine the dielectric properties of solid insulating materials.

ASTM D150-98 (2004) “Standard test method for A-C loss characteristics and permittivity (dielectric constant) of solid electrical insulation” can be used to determine the relative permittivity, dissipation factor, loss index, power factor, phase angle, and loss angle of specimens of solid electrical insulating materials when the standards used are lumped impedances.

ASTM D495-99 (2004) “Standard test method for high-voltage, low-current, dry arc resistance of solid electrical insulation” is used for material preliminary identification and generally should not be used in material specifications.

ASTM D2303-97 (2004) “Standard test method for liquid-contaminant, inclined-plane tracking and erosion of insulating materials” can be used to quantitatively assess an insulating material’s resistance to surface discharge of electricity. Such an electrical discharge can be likened to the problems occurring under the erosion effects of water condensation in air.

Table 5.36 Laminar and laminate static mechanical test methods

Test method	Specimen	Property measured	Advantages	Disadvantages	Remarks
In-plane tensile testing					
D3079		Tensile strength	<ol style="list-style-type: none"> (1) Straight-sided specimen (2) Suitable for both discontinuous and continuous fiber composites (3) Tabbed and untabbed configurations available 	<ol style="list-style-type: none"> (1) Tabbed configurations require careful adhesive selection and special specimen preparation (2) Prone to edge delamination which can affect tensile strength results 	<ol style="list-style-type: none"> (1) Preferred for most uses (2) Provides additional configurations, requirements, and guidance that are not found in D5083 (3) Limited to laminates that are balanced and symmetric with respect to the test direction
D638		Tensile modulus, Poisson's ratio, stress-strain response	<ol style="list-style-type: none"> (1) Requires use of strain or displacement transducers (2) Modulus measurements do not require use of tabs 		Modulus measurements typically robust
D5083		Tensile E strength/modulus	<ol style="list-style-type: none"> (1) "Dumbbell" shaped specimen (2) Easy test specimen preparation 	<ol style="list-style-type: none"> (1) Stress concentration at the radii (2) Unsuitable for highly oriented fiber composites 	<ol style="list-style-type: none"> (1) Not recommended for high-modulus composites (2) Technically equivalent to ISO 527-1
		Tensile strength/modulus	Straight-sided, untagged specimens only	Suitable for plastics and low-modulus composites	<ol style="list-style-type: none"> (1) A straight-sided alternative to D638 (2) Technically equivalent to ISO 527-4 except as noted below: <ol style="list-style-type: none"> 1. This test method does not include testing of Type I

(continued)

Table 5.36 (continued)

Test method	Specimen	Property measured	Advantages	Disadvantages	Remarks
					dog-bone-shaped specimens described in ISO 527-4. Testing of this type of specimen is primarily used for reinforced and unreinforced thermoplastic materials, as described in D638 2. The thickness of test specimens in this test method covers the 2–10 mm thickness range of ISO 527-4 and expands the allowable test thickness to 14 mm
In-plane tensile testing					
D5450		Transverse (90°) tensile strength	(1) Hoop-wound cylinder with all 90° (hoop) plies loaded in axial tension (2) Develops data for specialized process/form	(1) Limited to hoop-wound cylinders (2) Limited to transverse tensile properties (3) Must bond specimen to fixture	Must ensure adequate bonding to fixture
In-plane compression test methods					
D6641		Compressive strength	(1) Untabbed, straight-sided specimen loaded via a	(1) Might be necessary to tab highly oriented fiber	(1) Preferred method (continued)

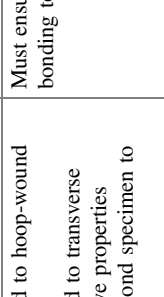
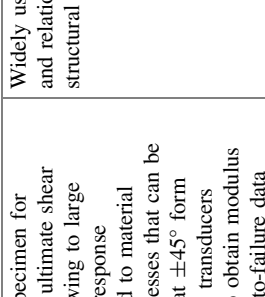
Table 5.36 (continued)

Test method	Specimen	Property measured	Advantages	Disadvantages	Remarks
		<p>combination of shear and end loading (2) Smaller lighter, less expensive fixture than that of D3410 (3) Good performance in non-ambient environments (4) Suitable for continuous fiber composites</p>	<p>composites or laminates with 0°-plies on the surface (2) Not recommended for determining compressive strength of unidirectional (0°-ply orientation) tape or tow laminates</p>	<p>(2) Thickness must be sufficient to prevent column buckling (3) Limited to laminates that are balanced and symmetric and contain at least one 0°-ply (4) For strength determination, the laminate is limited to a maximum of 50% 0°-plies, or equivalent</p>	
D695		<p>Compressive strength, Poisson's ratio, stress-strain response</p>	<p>Requires use of strain or displacement transducers</p>	<p>(1) Failure mode is often end crushing (2) Stress concentrations at radii (3) Specimen must be dog boned and ends must be accurately machined (4) No assessment of alignment</p>	<p>Unidirectional tape or tow composites can be tested to determine unidirectional modulus and Poisson's ratio</p>
		<p>Compressive strength/modulus</p>	<p>(1) "Dog bone"-shaped specimen with loading applied at the ends via a plate (2) Tabs are optional</p>	<p>(1) Not recommended for highly oriented or continuous fiber composites (2) Modified version of D695 released as SACMA SRM 1 test method is widely used in aerospace industry, but ASTM D30 and MIL-HDBK-17 prefer use of D6641 method</p>	<p>(continued)</p>

Table 5.36 (continued)

Test method	Specimen	Property measured	Advantages	Disadvantages	Remarks
D3410		Compressive strength	(1) Straight-sided specimen with load applied by shear via fixture grips (2) Suitable for random, discontinuous and continuous fiber composites (3) Tabbed and untabbed configurations available Requires use of strain or displacement transducers	(1) Strain gauges required to verify alignment (2) Poor for non-ambient testing owing to large fixtures	(1) Expensive and bulky fixtures (2) Thickness must be sufficient to prevent column buckling
In-plane compression test methods					
D5467		Compressive strength/modulus, stress-strain response	(1) Sandwich beam specimen loaded in 4-point bending (2) Intended result is a compression failure mode of the face sheet	(1) An expensive specimen that is not recommended unless the structure warrants its use (2) Strain gauges required to obtain modulus and strain-to-failure data	(1) Must take care to avoid core failure modes (2) Limited to high-modulus composites (3) Owing to the nature of the specimen construction and applied flexural loading these results may not be equivalent (continued)

Table 5.36 (continued)

Test method	Specimen	Property measured	Advantages	Disadvantages	Remarks
D5449		Transverse (90°) compressive strength	(3) Data are especially applicable to sandwich structures (4) Fixturing is simple compared with that of other compression tests	(3) Narrow specimen may not be suitable for materials with coarse features, such as fabrics with large filament count tows (12K or more) or certain braided materials	to a similar laminate tested by other compression methods such as D3410 or D6641
D3518		Shear strength/modulus, stress-strain response	(1) Tensile test of $[\pm 45]_{hs}$ layering (2) Simple test specimen and test method	(1) Limited to hoop-wound cylinders (2) Limited to transverse compressive properties (3) Must bond specimen to fixture	Must ensure adequate bonding to fixture
In-plane shear test methods					
D3518		Shear strength/modulus, stress-strain response	(1) Tensile test of $[\pm 45]_{hs}$ layering (2) Simple test specimen and test method	(1) Poor specimen for measuring ultimate shear strength owing to large nonlinear response (2) Limited to material forms/processes that can be made in flat $\pm 45^\circ$ form (3) Biaxial transducers required to obtain modulus and strain-to-failure data	Widely used for its low cost and relationship to actual structural laminates

(continued)

Table 5.36 (continued)

Test method	Specimen	Property measured	Advantages	Disadvantages	Remarks
In-plane shear test methods					
D3579		Shear strength/modulus, stress-strain response	<ul style="list-style-type: none"> (1) V-notched specimen loaded in special bending fixture (2) Provides the best shear response of the standardized methods (3) Provides shear modulus and strength (4) Can be used to test most composite types (5) Produces a relatively pure and uniform shear stress state 	<ul style="list-style-type: none"> (1) Might be necessary to tab the specimen (2) Specimen can be difficult to machine (3) Biaxial strain gauges required to obtain modulus and strain-to-failure data (4) Requires good strain gauge installation technique (5) In-plane tests not suitable for materials with coarse features, such as fabrics with large filament count tows (12 K or more) or certain braided materials (6) Unacceptable failure modes, especially with high-strength laminates, can occur due to localized failure of the specimen at the loading points 	<ul style="list-style-type: none"> (1) Recommended for quantitative data, or where shear modulus or stress/strain data are required (2) Enables correlation with out-of-plane properties (3) Must monitor strain data for specimen buckling (4) Limited to the following forms: <ul style="list-style-type: none"> ① Unidirectional tape or tow laminates with fibers parallel or perpendicular to loading axis ② Woven fabric laminates with the warp direction parallel or perpendicular to loading axis ③ Laminates with equal numbers of 0° - and 90° -plies with the 0°-plies parallel or perpendicular to loading axis ④ Short-fiber composites with majority of the fibers randomly distributed ⑤ Most accurate modulus measurements obtained from laminates of the [0/90] family

(continued)

Table 5.36 (continued)

Test method	Specimen	Property measured	Advantages	Disadvantages	Remarks
D4255		Shear strength/modulus, stress-strain response	(1) Rail-shear methods (2) Suitable for both random and continuous fiber composites	(1) Difficult test to run (2) Historically has had poor reproducibility (3) Stress concentrations at gripping areas (4) Strain gauges required to obtain modulus and strain-to-failure data	(1) Expensive specimen (2) Best reserved for testing of laminates
In-planes test methods					
D5448		Shear strength/modulus, stress-strain response	(1) Hoop-wound cylinder with all 90° (hoop) plies loaded in torsion (2) Develops data for specialized process/form	(1) Limited to hoop-wound cylinders (2) Limited to in-plane shear properties (3) Must bond specimen to fixture	Must ensure adequate bonding to fixture
Out-of-plane tensile test methods					
D6415		Curved laminate strength	(1) Right-angle curved laminate specimen loaded in 4-point bending (2) Suitable for continuous fiber composites	(1) A complex stress state is generated in the specimen that may cause an unintended complex failure mode (2) There is typically a large amount of scatter in the curved beam strength data (3) While the failure mode is largely out-of-plane, the result is generally considered	(1) Limited to composites with defined layers (no through-the-thickness reinforcement) (2) For structural comparison, the same manufacturing process should be used for both the test specimen and the structure

(continued)

Table 5.36 (continued)

Test method	Specimen	Property measured	Advantages	Disadvantages	Remarks
		Interlaminar tensile strength	(1) Right-angle curved laminate specimen loaded in 4-point bending (2) Suitable for continuous fiber composites	(1) A complex stress state is generated in the specimen that may cause an unintended complex failure mode (2) There is typically a large amount of scatter in the curved beam strength data (3) While the failure mode is largely out-of-plane, the result is generally considered a structural test of a curved beam rather than a material property	(3) Non-standard versions of the curved beam test yield a different stress state that may affect the strength and failure mode Tests for interlaminar tensile strength limited to unidirectional materials with fibers oriented continuously along the legs and around the bend
Out-of-plane tensile test methods					
D2344		Short-beam strength	(1) Short-rectangular beam specimen loaded in 3-point bending (2) Short-beam strength is a good indicator of resin dominated properties	(1) Short-beam strength may be related to interlaminar shear strength, but the stress state is quite mixed. Thus results are not recommended as an assessment of shear strength owing to the stress concentrations and high	Intended primarily for quality control, comparative data, and assessment of environmental effects

(continued)

Table 5.36 (continued)

Test method	Specimen	Property measured	Advantages	Disadvantages	Remarks
D5397		Interlaminar shear strength/modulus	(3) Simple, inexpensive specimen and test configuration (1) V-notched specimen loaded in special bending fixture (2) Provides the best shear response of the standardized methods (3) Provides shear modulus and strength (4) Can be used to test most composites (5) Produces a relatively pure and uniform shear stress state	secondary stresses at loading points (2) Shear modulus cannot be measured (1) May be necessary to tab the specimen (2) Specimen can be difficult to machine (3) Strain gauges required to obtain modulus and strain-to-failure data (4) Requires good strain gauge installation technique (5) Requires a very thick laminate, 20 mm (0.75 in.) for out-of-plane properties	(1) Recommended for quantitative data, or where shear modulus or stress/strain data are required (2) Enables correlation with in-plane properties (3) Must monitor strain data for specimen buckling
D3846		Shear strength	(1) Specimen with two machined notches loaded in compression (2) Suitable for randomly dispersed and continuous fiber-reinforced materials (3) May be preferable to D2344 for materials with randomly dispersed fiber orientations	(1) Failures may be sensitive to accuracy of notch machining (2) Stress concentrations at notches (3) Failure may be influenced by the applied compression stress (4) Requires postfailure measurement of shear area (5) Shear modulus cannot be measured	(1) Specimen loaded in compression using the D695 loading/stabilizing jig (2) Shear loading occurs in a plane between two machined notches (3) Often a problematic test (4) Note that this is an out-of-plane shear test (recognized terminology), despite the title that indicates in-plane shear loading

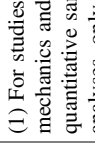
(continued)

Table 5.36 (continued)

Test method	Specimen	Property measured	Advantages	Disadvantages	Remarks
Out-of-plane tensile test methods					
C393		Core shear strength/modulus, sandwich flexural stiffness, face sheet compressive strength, face sheet tensile strength	(1) Sandwich beam specimen for sandwich constructions (2) Simple specimen construction and testing (3) Includes both 3-point and 4-point techniques, for different test objectives	(1) Method limited to 1D bending (2) Failures are often dominated by stress concentration and secondary stress at loading points, especially for specimens with low-density cores and thin face sheets (3) Care must be exercised when testing for core shear modulus to ensure that simple sandwich beam theory is valid (4) Specimen must be carefully designed to obtain the desired failure mode	(1) This method was developed for characterizing sandwich composite structures and the results apply to a beam that could be made up of both composite and non-composite components. Therefore, the failure may initiate in a non-composite element (core, adhesive) of the structure (2) Span-to-depth ratio >20:1 is recommended when testing for shear modulus (3) The ratio of face sheet thickness to core thickness (t/c) should be <0.10
D5476		Face sheet compressive strength, compressive modulus, stress-strain response	(1) Sandwich beam specimen loaded in 4-point bending (2) Intended result is a compression failure mode of the face sheet	(1) Limited to high-modulus composites (2) An expensive specimen that is not recommended unless the structure warrants its use	(1) Must take care to avoid core failure modes (2) Narrow specimen may not be suitable for materials with coarse features, such as fabrics with large filament count tows (12K or more) or certain braided materials

(continued)

Table 5.36 (continued)

Test method	Specimen	Property measured	Advantages	Disadvantages	Remarks
D6416	 <p>The diagram shows a rectangular specimen of thickness $2D$. It is supported at two points, one on each end. A single downward force is applied at the center of the specimen. The distance between the supports is indicated as being greater than $2D$.</p>	<p>Pressure deflection response, pressure-strain response, sandwich bending, and shear stiffness</p>	<p>(3) Data are especially applicable to sandwich structures (4) Fixturing is simple compared with that of other compression tests</p> <p>(1) Two-dimensional plate flexure induced by a well-defined distributed load (2) Apparatus, instrumentation ensure applied pressure distribution is known (3) Failures typically initiate away from edges (4) Specimens are relatively large, facilitating study of manufacturing defects and process variables</p>	<p>(3) Strain gauges required to obtain modulus and strain-to-failure data</p> <p>(1) For studies of failure mechanics and other quantitative sandwich analyses, only small panel deflections are allowed (2) The test fixture is elaborate and some calibration is required to verify the simply supported boundary conditions (3) Results highly dependent upon panel edge boundary conditions and pressure distribution (4) Relatively large specimen and support fixture geometry</p>	<p>(1) The same caveats that apply to C393 (above) also apply to D6416. However, this method is not limited to sandwich composites. D6416 can be used to evaluate the 2D flexural properties of any square plate (2) Distributed load is provided using a water-filled bladder (3) Ratio of support span to average sandwich specimen thickness should be between 10 and 30</p>
Laminate flexural test methods					
D790		<p>Flexural strength/modulus, flexural stress-strain response</p>	<p>(1) Flat rectangular specimen loaded in 3-point bending</p>	<p>(1) Stress concentrations and secondary stresses at loading points</p>	<p>Failure mode may be tension, compression, shear, or a combination</p>

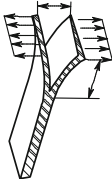
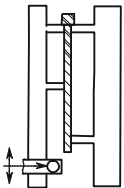
(continued)

Table 5.36 (continued)

Test method	Specimen	Property measured	Advantages	Disadvantages	Remarks
D6272		Flexural strength/modulus, flexural stress-strain response	<p>(2) Suitable for randomly dispersed and continuous fiber-reinforced materials</p> <p>(3) Simple test specimen preparation and testing</p> <p>(1) Flat rectangular specimen loaded in 4-point bending</p> <p>(2) Suitable for randomly dispersed and continuous fiber-reinforced materials</p> <p>(3) Simple test specimen preparation and testing</p> <p>(4) Choice of two procedures enable tension/compression/shear load distribution</p>	<p>(2) Results sensitive to specimen and loading geometry, strain rate</p> <p>(1) Center-point deflection requires secondary instrumentation</p> <p>(2) Results sensitive to specimen and loading geometry and strain rate</p> <p>(3) Span-to-depth ratio must increase for laminates with high tensile strength with respect to in-plane shear strength</p>	<p>(1) The quarter-span version is recommended for high-modulus composites</p> <p>(2) Failure mode may be tension, compression, shear, or a combination</p>
D6416		Pressure deflection response, pressure strain plate bending and shear stiffness	<p>(1) Two-dimensional plate flexure induced by a well-defined distributed load</p> <p>(2) Apparatus, instrumentation ensure applied pressure distribution is known</p> <p>(3) Failures typically initiate away from edges</p> <p>(4) Specimens are relatively large, facilitating</p>	<p>(1) For studies of failure mechanics and other quantitative sandwich analyses, only small panel deflections are allowed</p> <p>(2) The test fixture is elaborate, and some calibration is required to verify the simply supported boundary conditions</p> <p>(3) Results highly dependent upon panel edge boundary</p>	<p>(1) The same caveats applying to C393 (above) could apply to D6416. However, this method is not limited to sandwich composites, D6416 can be used to evaluate the 2-dimensional flexural properties of any square plate</p> <p>(2) Distributed load is provided by a water-filled bladder</p>

(continued)

Table 5.36 (continued)

Test method	Specimen	Property measured	Advantages	Disadvantages	Remarks
Fracture toughness test methods					
D5528		Mode I interlaminar fracture toughness, G_{IE}	(1) Flat rectangular specimen with delamination insert loaded in tension (2) Suitable for unidirectional tape or tow laminates (3) Relatively stable delamination growth	(1) Specimens must be hinged at the loading points (2) Crack growth not always well behaved	(1) Calculations assume linear elastic behavior (2) Crack growth should be observed from both sides of the specimen
D6671		Mixed mode I/III interlaminar fracture toughness, G_C	(1) Flat rectangular specimen with delamination insert loaded in bending (2) Suitable for unidirectional tape or tow laminates (3) Tests at most mode mixtures (4) Constant mode mixtures with crack growth	(1) Specimens must be hinged at the loading points (2) Crack growth not always well behaved (3) Complicated loading apparatus	(1) Good alignment is critical (2) Calculations assume linear elastic behavior

(continued)

Table 5.36 (continued)


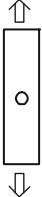



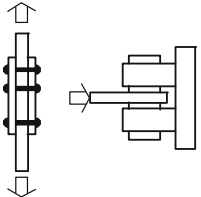
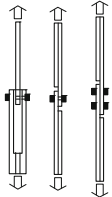
Test method	Specimen	Property measured	Advantages	Disadvantages	Remarks
E1922		Translaminar fracture toughness, K_{TL}	(5) Can obtain initiation and propagation toughness values (1) Flat rectangular specimen containing an edge notch loaded in tension (2) Simple test to perform	(1) Results are only valid for the particular laminate tested (2) Laminates producing large damage zones, which do not give valid values	

Table 5.37 Laminate/structural test methods

Test method	Specimen	Property measured	Advantages	Disadvantages	Remarks
Notched laminate tension test methods					
D5766		Open-hole tensile strength	(1) Straight-sided, untabbed, open-hole configuration (2) Procedure nearly equivalent to D3039	Limited to multidirectional laminates with balanced and symmetric stacking sequences Same as D5766	Provides requirements and guidance on specimen configuration and failure modes (1) Same as D5766 (2) Also provides guidance on hole tolerances, fastener torque/preload
D6742		Filled-hole tensile strength	(1) Straight-sided, untabbed, filled-hole configuration (2) Procedure and specimen nearly equivalent to D3039, D5766		
Notched laminate compression test methods					
D6484		Open-hole compressive strength	(1) Straight-sided, untabbed, open-hole configuration (2) Fixture can be loaded with either hydraulic grips or end plates	Limited to multidirectional laminates with balanced and symmetric stacking sequences Same as D6484	Provides requirements and guidance on specimen configuration and failure modes (1) Same as D6484 (2) Also provides guidance on hole tolerances, fastener torque/preload
D6742		Filled-hole compressive strength	(1) Straight-sided, untabbed, filled-hole configuration (2) Procedure, specimen, and apparatus nearly equivalent to D6484		

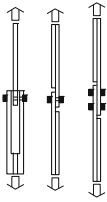
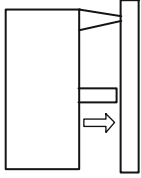
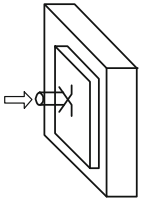
(continued)

Table 5.37 (continued)

Test method	Specimen	Property measured	Advantages	Disadvantages	Remarks
Bolted joint bearing test methods					
D953		Static pin bearing strength	(1) One fastener, double-shear pin bearing specimen (2) Two methods available: tensile and compressive pin bearing (3) Monitors global load versus deformation behavior	(1) Focus is plastics (2) Does not account for various fastener geometries, torque/preload levels (3) Deformation local to hole is not measured	(1) Some specimen geometric properties (for example, width/diameter ratio) vary from D5961 guidelines (2) Not recommended for continuous fiber composites
D5961		Static bearing strength	(1) One and two fasteners, double- and single-shear bearing specimens loaded in tension (2) Multiple specimen configurations provided to assess a variety of structural joint configurations (3) Procedures provided to monitor in-elastic deformation behavior at hole	(1) Limited to multidirectional laminates with balanced and symmetric stacking sequences (2) Response highly dependent upon specimen configuration and fastener torque/preload (3) Limited to bearing failure modes only (4) Some details of specimen configurations are not suitable for	Provides requirements and guidance on specimen configuration, type of loading, hole tolerances, fastener torque/preload and failure modes


(continued)

Table 5.37 (continued)

Test method	Specimen	Property measured	Advantages	Disadvantages	Remarks
D6873		Bearing stress-cycles (S-N) data	Specimen and apparatus equivalent to D5961, with cyclic loading procedures provided to monitor hole elongation for a variety of joint configurations and fatigue loading conditions	determining bypass failure strengths (1) Same as D5961 (2) Certain tests may require fastener removal or a variant quasi-static loading ratio to monitor hole elongation	(1) Same as D5961 (2) Also provides guidance on fatigue loading ratio effects
Static indentation test methods					
D2583		Indentation Hardness	(1) Provides a relative measure of hardness based upon load versus indentation depth response (2) Barcol impressor is portable and load is applied by hand	(1) Focus is plastics and low-modulus composites (2) Does not record force versus indentation depth response (3) Does not evaluate resulting damage state	Uses flat-tipped indenter
D6264		Force-indentation displacement response, dent depth, damage characteristics	(1) Flat rectangular laminated subject to a static point loading (2) Permits damage resistance testing of simply supported and rigidly backed plate specimens (3) Uses a conventional testing machine	(1) Limited to continuous fiber composites without through thickness reinforcement (2) Test method does not address dynamic indentation effects	(1) Uses 12.7 mm (0.50 in.) diameter hemispherical indenter (2) Often used to approximate the damage state caused by a dynamic impact

(continued)

Table 5.37 (continued)

Test method	Specimen	Property measured	Advantages	Disadvantages	Remarks
			(4) Contact force and indenter displacement data are obtained	(3) Narrow range of permissible specimen thicknesses	(3) Multidirectional fiber laminates with balanced and symmetric stacking sequences are usually used (4) The damage response is a function of the indenter geometry, support conditions, and specimen configuration
Translaminar fracture test methods					
E1922		Translaminar fracture toughness, K_{TL}	(1) Flat rectangular specimen containing an edge notch loaded in tension (2) Simple test to perform	(1) Results only valid for the particular laminate tested (2) Laminates producing large damage zones do not give valid values	

5.4.7 *Environmental Effects and Resistance Assessment*

Exposure to some types of environments and media will cause composite performance to decrease, and the evaluation of this performance degradation is particularly important for composite applications.

The most effective approach to assess the effects of environment and media on composite performances is to compare the performances before and after exposure and calculate the performance retention rate. The retention rate is referred to as the percentage of the residual property relative to its initial value.

The matrix dominated properties are generally most easily influenced by the environment and medium. The retention rates of these properties can be used to evaluate the material's resistance to an environment/medium. These properties include the glass transition temperature T_g , transverse tensile and compression, bending strength and modulus, in-plane and interlaminar shear, and open-hole tensile and compression. Among these, bending and interlaminar parameters are the most commonly used properties.

To evaluate the material properties under working conditions, material testing at high or low temperatures will often be performed to determine the material allowable values under application conditions. In addition, determining the ultimate working temperature is an important issue. For polymer matrix composites, high and low temperatures as well as wet ambient conditions are the most concerning problems.

Under a specified moisture absorption, when the temperature increases to a certain level, material properties will significantly decrease and irreversible changes will take place in the materials as the temperature is raised further. The characteristic temperature at which the properties decline rapidly is often used as a standard to define the material ultimate operational temperature. However, this ultimate operation temperature will be influenced by absorbed moisture content. For safety, generally, the highest possible moisture content will be selected as the baseline to determine the ultimate operation temperature.

In testing of composite hot-wet performance, it is necessary to adjust the specimen to a balanced moisture content; however, the balanced moisture content will change during testing because some moisture will be released. To reduce the moisture loss, a hot-wet ambient chamber can be used to keep the absorbed moisture in a specimen unchanged if the test temperature is lower than 100 °C. In the case of a temperature higher than 100 °C, this method is not effective. Another method to reduce moisture loss is to shorten the high-temperature exposure time during testing. Although some measures can be taken to reduce the moisture loss the specimen surface will definitely lose some moisture. Thus, the moisture content after testing and specimen failure should be measured and recorded.

To measure the moisture content after specimen failure, available methods include: use of a batch sample as a baseline to monitor the moisture content in the specimen. This batch sample should be of the same material, geometric shape and laminating pattern as the specimen, and be exposed to the same ambient conditions

for the same time. In testing, the batch sample is placed in an ambient chamber together with the testing specimen until the test is completed. The batch sample is taken out from the chamber and its moisture content measured. Alternatively, a small piece of the tested and failed specimen can be used to measure the moisture content.

The operation temperature is usually lower than material ultimate operation temperature. The material ultimate operation temperature is determined based on the possible highest moisture content-level encountered in practical applications. For aviation application, in MIL-HDBK-17, an 85% moisture content is specified as the most serious case. For testing temperature, the maximum testing temperature is determined based on the material performance and operation requirement. In aviation applications, the low testing temperature is commonly defined as $-55\text{ }^{\circ}\text{C}$.

The time required to reach thermal equilibrium will depend on the specimen materials and geometry. Thus, before testing, the specimen should be placed under the specified testing condition for 15–30 min.

One commonly used method to determine the ultimate operation temperature is the reduction of the glass transition temperature (T_g) to a specified temperature. For epoxy matrix composites, the reduced temperature is usually $30\text{ }^{\circ}\text{C}$. DMA is the most commonly used technique to measure T_g , there are also some other methods available. For example, the mechanical test data over a certain temperature range can be used. The matrix dominated composite properties will considerably change with temperature and represent a reliable measure for certifying the ultimate operation temperature. The currently used methods include SBS strength, in-place shear strength and modulus, and quasi-isotropic open-hole compression strength. These methods can accurately reflect the ultimate operational temperature. To show trends in the changes of these properties with temperature, 4–5 temperature levels are typically selected for testing.

DMA and mechanical test results can also be compared with each other. If the mechanical test results are consistent with the DMA results, the determined ultimate operation temperature is reliable. If the mechanical test results indicate that the DMA results are conservative, the ultimate operation temperature of the materials should be enhanced. If mechanical test results give a lower ultimate operation temperature than DMA, these values can be used as the material ultimate operation temperature.

Once the material's ultimate operation temperature and material properties at this temperature are determined, the material properties under a given operational condition can be calculated by interpolation. If necessary, limited verification tests can be performed to enable less conservative assessments of material performances.

5.5 Composite Quality Evaluation and Control

Composite quality evaluation and control are important issues in composite research and applications. These are also key factors in new material development, optimization of composite processing and composite performance as well as

production acceptance rates. For structural designers, quality control and evaluation are essential for rational design, to increase the material-structure conversion rate and structural effectiveness; for users and customers, quality control and evaluation are a guarantee of the composite property potential and effectiveness in a particular application. Quality evaluation can be considered to be a passive measure, while quality control is an active method. Owing to the variety of composite compositions and dimensional features of materials, structures, and material-structure processing, the combination of all the factors mentioned earlier can greatly complicate composite quality control and evaluation [9–13].

In this section, the complexity of composite quality evaluation is first analyzed. Then, two types of quality evaluation methods are briefly introduced, namely destructive evaluation and nondestructive evaluation. From this point of view, composite quality control is introduced, including several quality control methods.

5.5.1 Composite Quality Evaluation

5.5.1.1 Complexity of Quality Evaluation

To achieve composite quality control and to enhance composite performance, it is essential to perform comprehensive and objective evaluation of composites. Compared with metals and plastics, composite quality evaluation faces difficulties and complexities, caused by the characteristics of composites. The challenges are introduced in terms of the following three aspects.

(1) Variety of constituent materials

A composite system is composed from reinforcing materials and matrices. In terms of the reinforcing materials, beyond the differences in material types and classes, there are also many reinforcement forms such as fabrics, continuous fibers, chopped short fibers, whiskers, and particles. Combinations of two and more reinforcements can also exist. Matrices consist of resins, curing agents, toughening agents, and many other additives. Their contents and characteristic features can also greatly affect composite properties. Resins come in many types and categories with different synthetic raw material compositions and relative molecular weights and weight distributions that may cause differences in composite processing control. Furthermore, for a single selected reinforcement and resin, the relative contents and interfacial combining conditions may be greatly different and require different processing techniques. Thus, current quality evaluation of composites should consider the specific material types, constituents, and distribution, which adds to the difficulty of establishing general curing specifications.

(2) **Synchronism in material-structure processing**

In composites, especially resin matrix composites, material processing is often simultaneously integrated with formation of the structural products. The curing process features either resin chemical cross-linking reactions or physical reactions such as resin flow and fiber motion. These reactions are interrelated and make the mechanism analysis and processing control difficult. Moreover, each step in composite processing, such as resin system preparation, fiber preimpregnation, laying-up, packing and curing processes, can directly influence the composite product performances. Any deviation in any processing step can result in end product quality problems.

(3) **Designability of materials and structures**

The designability of composites is one of their important features, and is also a key factor in optimizing composite structures. For continuous fiber-reinforced composites, the structural characteristics and mechanical properties show anisotropic behaviors. Thus, based on the operational requirements and environmental conditions in which composite structures will be used, an optimized structure solution can be designed, and the optimized load-bearing state can be selected. To fulfill the optimized design and to enhance the service effectiveness of composite structures, it is important to know the appropriate design and analysis approaches before accumulating the data that are necessary for composite design.

5.5.1.2 Problems in Quality Evaluation

To increase the effectiveness of composite quality evaluation, it is essential to understand the problems that exist. At present, the main problems include:

(1) **Inadequate material knowledge**

To date, there is no comprehensive theory available that can be used to explain and predict composite behavior. In many cases, test measurement is the main empirical approach used in composite quality evaluation. This is because composites are an innovative material system, which is characteristically complex (multiple constituents and multiple phase non-homogeneity). Computational approaches play an important role in composite property prediction; however, a lack of fundamental data will limit the accuracy of such predictions. Because of the limited understanding of composite features, it is very difficult to theoretically evaluate composite reliability.

(2) **Scatter of material properties**

Inhomogeneity of raw material properties can result in scatter of composite performances. Because of the complexity of composite constituents, the non-uniform composite properties cannot be avoided in industrial production. Because composites are a blended material system, properties depend on both the constituents

and their processing conditions. In some cases, although identical constituents and processing techniques are used, the end composite products may show large differences in their performance.

(3) Irreproducibility of processing properties

Currently, composite manufacture cannot be performed on a large-scale with automatic production. Hand-laying-up processes are still used in many cases, resulting in poor reproducibility and scatter in composite performances.

(4) Imperfect test methods

Many proper characterization methods and standards are currently still lacking for inspection and testing certain properties of composites. For some established standard methods, the specimen test results cannot accurately reflect the real properties of the composite structures. A great amount of works is still required on correct evaluation of composite reliability by standardized nondestructive inspection methods.

(5) Data lack statistical power

Compared with traditional metal materials, statistical data on the properties of composites is lacking. Although many researchers have studied composite performances and a considerable amount of data has been collected by standard tests, these data are still insufficient. Most of these data reflect typical values; however, data that can meet composite reliability requirements are lacking. For composites used in real structural applications in particular, the load, environment, shape, and surface conditions are different, thus more data on these different features are required.

(6) Limited knowledge of time-dependent performance of composites

The material reliability refers to the potential of a material to adequately meet the requirement on design performance standards over the structure service life. Composite performance is time-dependent, especially resin matrix composites. Resin systems are very sensitive to time and temperature changes under certain ambient condition. Although this topic has been extensively studied, many mechanistic problems remain unsolved. Furthermore, the data accumulated on time-dependent performances under varied ambient conditions are limited. These limitations pose considerably difficulties for evaluating composite operational performances.

(7) Other problems

Additional issues include, for example: the revision of a real structure based on specimen testing; sensitivity of combined evaluations of material performance analysis; optimized application of materials; criteria for material failure, the availability of new material data.

5.5.1.3 Quality Evaluation Methods

Currently, there are two main methods used in composite quality evaluation: destructive tests and NDI evaluation (nondestructive inspection, NDI). Their application ranges are illustrated in Fig. 5.47.

(1) Destructive testing evaluation

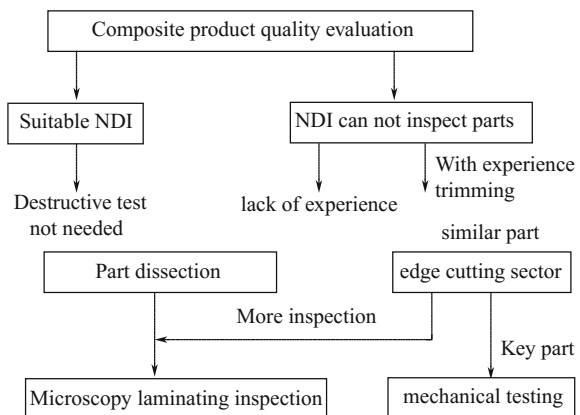
Destructive testing evaluation refers to quality evaluation either by taking a sample from composite or a structure or a batch of samples for performing quality inspection. The test specimens will depend on the design requirements. For structural composites, the main characteristics tested include tensile and compression shear strength and modulus, and the Poisson’s ratio. These fundamental mechanical tests can be used to directly evaluate composite quality variations. Currently, destructive tests used to evaluate damage resistance have received much attention in aerospace applications. Testing items include open-hole tensile (OHT), open-hole compression (OHC), CAI, G_{IC} , G_{IIC} , and G_C . These properties are particularly useful for composite quality evaluation.

When NDI cannot provide adequate detail of structural integrity, destructive testing should be adopted. Periodic dissection of the composite part to inspect the internal construction, from batch samples or the samples cut from the part, can be used for mechanical testing.

Dissection of a structural component is a type of destructive inspection, after which the part cannot be used anymore. Thus, this method can be used only after NDI has been performed and can give a detailed inspection of a part construction.

Component dissection can be used for the first part or one of the first batches in production inspection. This method can also be used for regular inspection of important part production. As production experience increases, the inspection cycles can also be extended. Component dissection is often performed in detailed sections with microstructural inspection and microscope imaging of the dissected areas. For example, to check the stacking sequence and fiber orientation of a

Fig. 5.47 Selection of quality inspection method for composite products



laminate, a small piece of the specimen is cut to reveal the layer structure. Alternatively, the sample may be ground to check the layer number and sequence of the cross section. For some defects such as fiber non-uniformity, layer wrinkles, and voids, it is necessary to inspect by microscope imaging. The inspected items and zones will include: the load path inside the part, the zones revealed by NDI inspection, the mold separated lines near the co-cured details, the layer loss area at slope sections, layer wrinkles, resin-starved and resin-rich areas, the round angle radius and co-cured details, filling between the core and surface, and the core in slope sections.

Compared with whole component dissection, batch sampling or specimen edge-cut piece inspection is a low-cost approach. It can be used to inspect the difference between microstructures, or for mechanical testing, which can ensure the structural load-bearing ability of the part and confirm the processing quality. Because of the low cost, this inspection method can be performed at regular time intervals. However, unlike whole component dissection, this kind of inspection cannot acquire all necessary data at every location because of the limited sampling. In practice, the samples should be taken from locations that can reflect the performance of the whole component. When edge-cut pieces are used as the specimen for mechanical testing, the tests should be performed by following the whole component failure modes or the failure modes that could take place at the location from which the edge-cut specimen is taken.

(2) **Nondestructive inspection (NDI)**

Some internal defects may be caused during composite part fabrication and machining, for which it may be difficult to evaluate the seriousness by visible inspection. In some cases, destructive testing cannot be performed either. Nondestructive evaluation can rapidly and accurately identify the shapes and locations of certain composite internal defects such as voids, delamination, impurities, and microcracks. Thus, nondestructive inspection has become more widely used in composite quality evaluation, and many techniques have been developed.

Currently used NDI methods in composite production include visible inspection, ultrasound, and X-ray inspection. Other methods such as infrared, laser holography, and acoustic emission have also been rapidly developed.

Visible inspection is a simple and easy NDI method, and can be used to check if the part can meet the requirements of the design schematics and for evaluation of the part appearance and surface smoothness. Visible inspection can be used to check certain defects such as voids, dents, external impurities, laminating abnormalities, surface roughness, and surface holes and wrinkles.

In Table 5.38, some NDI inspections are compared with their effectiveness on defect inspection.

Composites used as aircraft structures require high production quality, the quality requirements may differ depending on the location of the composites' use. For example, in the M-D Airplane company, the composite structures are divided into A, B, and C quality grades based on the application locations and the structure

Table 5.38 Comparison of NDI methods with their effectiveness on defect inspection

NDI method	Defect										
	Void	Delamination	Crack	Debonding	Resin-rich/starvation	Impurity	Fiber irregular	Loosen	Uneven thickness		
Ultrasound											
X-ray	○	○	○	○	○	○	○		○		
Acoustic emission	○	○	○				○	○			
Eddy			○				○	○			
Holography		○		○	○						
Optic fiber		○	○	○							
Infrared	○	○	○	○		○			○		
Pulse video/thermal imaging	○	○	○	○		○			○		

Table 5.39 z values in different quality levels

Quality level	z value/mm
A	9.5
B	12.5
C	19.05

Fig. 5.48 Signal defect evaluation

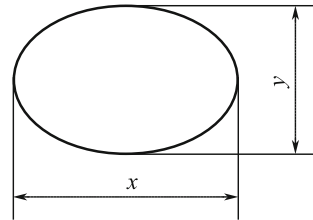


Fig. 5.49 Flake defect evaluation

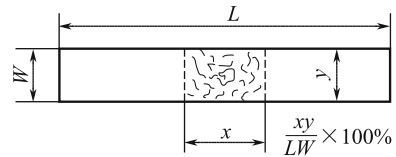


Table 5.40 z values in different quality levels

Quality level	Part aspect ratio $l/w > 10$ (the maximum defect area 64.5 m^2)	$l/w < 10$ (the maximum defect area 64.5 m^2)
A	10% or 6.45 cm^2	10% or 15.5 cm^2
B	15% or 9.67 cm^2	15% or 23.2 cm^2
C	25% or 16.125 cm^2	25% or 38.7 cm^2

Note The ratio of the defect area and the maximum defect area is $(xy/lw) \times 100\%$

types. Each grade has an allowable level of defects, as listed in Table 5.39, where $z = (x + y)/2$. A signal defect can be evaluated by the method shown in Fig. 5.48. For distributed flake defects, the evaluation is shown in Fig. 5.49 and Table 5.40.

The development of smart composites with fiber optic sensors will allow realization of quality evaluation and control of composite structures in service.

5.5.2 Composite Quality Control

Scatter of performance can directly influence the quality of composite products. In terms of mechanical properties, the performance scatter of composites is generally

much larger than that of metal materials. It is commonly regarded that the property data probability follows a two-parameter Weibull distribution:

$$f(x, \alpha, \beta) = \frac{\alpha}{\beta} \left(\frac{x}{\beta}\right)^{\alpha-1} e^{-(x/\beta)^\alpha} \quad (5.29)$$

where x is random variation; α is the shape parameter; β is a dimensional parameter (or characteristic value), while the distribution matrix average value μ , standard deviation σ and the coefficient of variation $C.V$ can be expressed in terms of α and β as:

$$\mu = \beta \Gamma\left(\frac{\alpha+1}{\alpha}\right), \quad (5.30)$$

$$\sigma = \beta \sqrt{\Gamma\left(\frac{\alpha+2}{\alpha}\right) - \Gamma^2\left(\frac{\alpha+1}{\alpha}\right)}, \quad (5.31)$$

$$C.V = \frac{\beta \sqrt{\Gamma\left(\frac{\alpha+2}{\alpha}\right) - \Gamma^2\left(\frac{\alpha+1}{\alpha}\right)}}{\Gamma\left(\frac{\alpha+1}{\alpha}\right)}, \quad (5.32)$$

$$\Gamma(x) = \int_0^{\infty} e^{-t} t^{(x-1)} dt$$

where $\Gamma(x)$ is a gamma function.

The shape parameter α reflects the scatter of the composite data distribution. The effects of constituents, composite processing, and test environment on the composite property scatter are also reflected in the value of α . A smaller α value, indicates greater scatter of data. Thus, the control of constituent scatter and processing quality control are key factors in composite production quality control. Constituent property characterization and control have been discussed in detail in other sections, and in this section, the stress will be focused on processing quality control and its relationship with quality stability of composite products.

5.5.3 Processing Quality Control

If constituent quality control is the essential to guarantee stable composite production quality, then processing quality control is key to ensuring composite quality stability. If the same constituent materials are used, the composite part quality will ultimately depend on the processing quality control. For resin matrix composites, processing quality control is particularly important. The curing of resin matrix composites is a complex process in which material processing and structure

fabrication are simultaneously performed. Changes of the chemical composition or construction of the resin matrix, and variation of the interfacial conditions between the matrix and reinforcement, can determine whether a part can fulfill its design specifications. The essence of processing control is to guarantee part quality and to shorten the process cycle. High quality means that the part is well compacted, homogeneously and properly cured, with minimum void content and residual stress. Furthermore, buckling and warpage should be avoided during production.

Composite processing quality does not depend only on material and equipment properties and conditions, which may be controlled. Quality is controlled by many factors such as the tools, temperature, pressure, ambient humidity, which contribute to the variation of composite properties and complicate precise control. In general, composite processing quality control involves two aspects: first, determining the optimized processing specifications in terms of temperature, pressure, and cure time. Second ensuring accurate implementation of the cure specification to guarantee the consistency between the real cure process and the cure specification. To achieve this goal, many process control methods are available including: theoretical cure modeling and computer simulation, in situ processing monitoring, statistical processing control (SPC), and empirical processing control.

5.5.3.1 Importance of Processing Quality Control

Defects may be caused if composite processing quality is not well controlled. These defects may contribute to weakness in products, which may lead to damage during service and then whole part failure. Moreover, the random distribution of defects is one of the main factors resulting in instable composite product quality. The causes of composite defects are complex and a single improperly controlled process can produce many different defects. Common defect types and their main causes in composite production are summarized as follows;

- (1) Voids: Void formation is a common defect in composites, and can generally can be categorized into single fiber holes (including holes in fiber bundles) and interlaminar holes. If the void content is less than 1.5%, the voids show spherical shapes with diameter in 5–20 μm . When the void content is greater than 1.5%, the voids show column shapes with larger diameters and orientation parallel to the fibers. Voids are typically caused by the three sources: ① Poor fiber impregnation, and failure to remove air bubbles during prepreg preparation and lamination. ② Volatilization of resin diluting agent or low molecular weight substances during composite fabrication. Some resins such as phenolic resin systems can release gases. ③ Improper processing conditions, for example, insufficient pressure, or late application of pressure during processing can cause trapped bubbles. Voids have a clear degrading effect on composite strength, modulus, fatigue resistance, and high-temperature properties. Some studies have indicated that void content higher than 20% can cause a static strength decreases of up to 40%. Void content and distribution are irregular,

making it difficult to account for these problems in composite processing quality control.

- (2) **Debonding:** Debonding refers to the resin matrix separating from the reinforcing fiber surface. This effect is caused by poor adhesion between the resin and fibers. The main causes of debonding include: ① Poor adhesion between resin and fibers. ② Poor resin impregnation of fibers. ③ Corroded fiber surfaces or poor fiber surface treatment.
- (3) **Delamination:** Delamination refers interlaminar separation between layers. Delamination is usually caused when prepregs beyond their shelf life are used resulting in degraded adherence and poor interlaminar bonding after the resin is cured. This type of defect may also be caused by improper part design, which produces excessively large stress in different directions with different thickness. For large size filament winding parts, large time intervals between adjacent winding of layers may also cause delamination, especially for cases in which the resin curing is insufficient. Debonding and delamination are serious defects in composite production and can have severe effects on composite performance.
- (4) **Impurities:** Impurities include external substances occasionally mixed into composites such as particles and coarse grains. Impurities may also be formed during the various processing steps with the main causes as follows: ① Small condensed resin lumps. ② Impurities in fillers. ③ External substances entering into the prepregs during drying and storage. When the composite is under loading, stress concentration or microcracking may be created at the sites of impurities, and composite mechanical properties can be influenced. In particular, these impurities can influence composite electrical performances.
- (5) **Deviations of the resin system:** Resin-rich, resin-starved regions, and non-uniform resin distribution can be caused by improper processing control. In general, improper design and non-uniform application of pressure can be result in resin deviation. Composite properties are dominated by the resin and fiber balance. Excessive deviation of the resin distribution will cause non-uniformity at different locations of composite parts and greatly influence the composite performance.
- (6) **Fiber deviation:** Fiber deviation relates to problems in the fiber stacking sequence in a lamination or curing process including misaligned stacking angle deviation and fiber buckling, which do not meet the design requirements. These random deviations can also change composite performance.
- (7) **Other defects:** Loosening, needle holes, non-uniform curing, poor interfacial bonding between the resin and fiber are additional common defects in composites, which can affect composite performance and should be accounted for in composite processing quality control.

Processing quality control can considerably reduce defects and improve the stability of composite quality. Currently, composite processing control methods include: theoretical cure models and computer simulation, in situ processing monitoring, statistic processing control, and empirical processing control.

5.5.3.2 Theoretical Curing Model and Computer Simulation

In theoretical curing models and computer simulation control of composite processing quality, so-called analog methods involve numerical models of curing behaviors based on the physical and chemical reaction mechanisms taking place during composite processing. The cure process is simulated and optimized by changing the processing parameters. In this method, some basic theories and concepts can be combined and applied to develop cure processes. The results provided can reflect essential characteristics, and guide cure processing schemes. Computational studies of cure processes can reduce the long testing period and high costs of empirical approaches. Reasonable curing parameters can be determined to give high-quality production with uniform curing and fewer defects. In the following section, applications of this method to composite autoclave curing and RTM processing will be presented.

(1) Simulation of autoclave curing

(1) Theoretical curing modeling: In composite manufacturing, it is necessary to understand the reactions occurring in resin curing processes regardless of the processing control method used. Thus, theoretical cure processing modeling has been developed. The applied temperature and pressure are combined with the cure state and void forming-consolidation behaviors to evaluate and optimize curing processes to produce high-quality composite parts. Currently, composite autoclave modeling mainly includes thermal-chemical modeling, resin flow modeling, void modeling, and residual stress modeling.

① Thermal-chemical modeling. In composite curing processes, temperature, curing degree, and viscosity changes exist in resin matrices. Thermal-chemical modeling involves equations for thermal transfer, reaction kinetics, and viscosity to analyze these changes in curing processes.

a. Thermal transfer equation. In composite curing, the cure uniformity of a composite part depends on the temperature distribution inside the part. The temperature distribution is related to the material heat transfer rate and the resin cure reaction heat generation rate.

Material heat transfer can be expressed by the Fourier equation:

$$\frac{\partial \rho c T}{\partial t} = \frac{\partial}{\partial Z} \left(K \frac{\partial T}{\partial Z} \right). \quad (5.33)$$

For thermosetting resins, the curing process is not only a heat transfer process, but the curing reaction also releases heat in the process. In the Springer and Loos model, the heat transfer of a cure process is

considered as a solid heat transfer equation with a heat source. The heat transfer can be expressed as:

$$\frac{\partial \rho c T}{\partial t} = \frac{\partial}{\partial Z} \left(K \frac{\partial T}{\partial Z} \right) + \rho H^{\&}, \quad (5.34)$$

where K is the composite heat conductivity; T is thermodynamic temperature; $\rho H^{\&}$ is the cure reaction thermal effect rate; $\partial T / \partial Z$ is the temperature gradient in the composite thickness direction; ρ is the composite density; c is the composite specific thermal capacity. On the basis of Springer and Loos's work, Blest et al. considered composite prepreg laminates with n layers as fiber layers with resin impregnation and pure resin layers, and developed the heat transfer equations:

$$\frac{\partial T_f}{\partial t} + u_f \frac{\partial T_f}{\partial x} + v_f \frac{\partial T_f}{\partial y} = K_f \left(\frac{\partial^2 T_f}{\partial x^2} + \frac{\partial^2 T_f}{\partial y^2} \right) + \frac{\varphi \rho_f H_R}{\rho_f c_f} \frac{\partial \alpha}{\partial t} \quad (5.35)$$

$$\frac{\partial T_r}{\partial t} + u_r \frac{\partial T_r}{\partial x} + v_r \frac{\partial T_r}{\partial y} = K_r \left(\frac{\partial^2 T_r}{\partial x^2} + \frac{\partial^2 T_r}{\partial y^2} \right) + \frac{H_R}{c_r} \frac{\partial \alpha}{\partial t}, \quad (5.36)$$

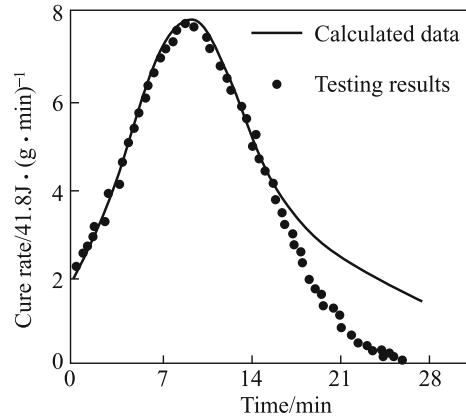
where K_i is heat conductivity, $K_i = k_i / c_i$, $i = r, f$, c_i is set as a constant in model; $\frac{\partial \alpha}{\partial t}$ is resin cure rate; $T_f(x, y, z)$ is the temperature function in the fiber layers; $T_r(x, y, z)$ is the temperature function in the resin layers; $\alpha_f(x, y, z)$ is resin cure degree; $u^i(x, y, z)$ and $v^i(x, y, z)$ are the resin flow sectors in x and y directions, respectively, when $i = r, f$.

If the relative parameters in the heat transfer equation are determined, and the initial and boundary conditions are input, the heat transfer equation can be solved. For example, K is the composite heat conductivity in the equation, which varies with temperature and curing conditions are changed in the cure process. Many empirical and theoretical equations for heat transfer have been used to predict the K value. If the cure rate in the equation needs to be determined, it is necessary to perform a reaction kinetics study.

- b. Reaction kinetics equation. The resin cure rate is usually expressed by the cure degree, while the cure degree can be expressed by the thermal heat $[H(t)]$ at the time when the cure reaction proceeds to a time t , and the total reaction heat $\{H_R\}$:

$$\alpha = \frac{H(t)}{H_R} \quad (5.37)$$

Fig. 5.50 Comparison between calculated data and test results



Souour and Kamal developed a kinetic reaction equation based on the curing mechanism of amine cured epoxy resin:

$$\frac{d\alpha}{dt} = (K_1 + K_2\alpha)(1 - \alpha)(B - \alpha), \quad (5.38)$$

where K_1 , K_2 are the reaction rate constants that can be determined from the Arrhenius equation, and B is the initial ratio of epoxy and curing agent.

Calculated data were compared with test results, as shown in Fig. 5.50. The calculated data were consistent with the test results at the initial cure stage; however, large differences were found at later stages of the curing process.

In testing, a large scatter existed in the kinetic parameters, making it difficult to express the cure degree accurately by a kinetic equation. As the curing proceeded, the cure degree changed causing the resin viscosity to change. Thus, the resin cure degree can be characterized by resin viscosity.

- c. Viscosity equation. In resin curing process, the viscosity of the resin system will change because of temperature and cross-linking reactions. Stolin et al. proposed a viscosity equation as:

$$\mu = \mu_\infty \exp(U/RT + K_v\alpha) \quad (5.39)$$

where ∞ , K_v , and U are constants, μ is viscosity, and can be determined from a rotating disk viscosity meter, to provide the viscosity-time correlation at a specific temperature.

The kinetic equation can be used to derive α , which can then be used in the above equation. The $\mu - \alpha$, $\mu_{\infty} \exp(U/RT) - 1/T$ curves can be fitted to determine the constants in equation, and the viscosity equation can be solved.

- ② Resin flow modeling: Resin flow model can be used to determine the cure time and the resin flow from laminate to bleed material. The parameters for this modeling include: resin viscosity, fiber volume fraction, resin pressure, laminate thickness, and the shape of the part and its dimensions. Currently available resin flow models include the Loos and Springer model, Gotowski model, Dave model, Master model, and Skordos parameter-free mathematical model. The Gotowski model and Dave model are independent with the same basic function. The Loos and Springer model and Gotowski model feature some differences, based on different considerations of the load distribution in the resin matrix and fiber. The Skordos parameter-free mathematical model is very different to the other models, and can simulate resin cure processes without the chemical reaction parameters. In these studies of Frank–Susich, Laananen, and Ruffener, DSC was used to determine the reaction heat characteristics. Parameters such as temperature, heat application time, autoclave pressure, cooling down and heating rates, reaction kinetic rate, viscosity, and void content were selected and used to study the cure process of thermosetting resins. A computer-aided cure model was established, as the Master Cure Model.

In the following section, the Loos and Springer model and Gotowski model will be introduced examining the differences of their heat/pressure assumption.

In the Loos and Springer model, the composite is assumed to be an incompressible void system, and the flow fields vertical and parallel to the laminate fiber direction are studied. In the vertical direction, an equation based on Darcy's law, for calculating the correlation between the resin flow-out mass ($M_r = \int_0^t \frac{dM_r}{dt} dt$), and laminate thickness ($h_c = n_s h_1$) is proposed. On the laminate flat surface, the resin flow vertical to fibers is ignored, only, the resin flow parallel to fibers is considered as a pipe flow movement.

The resin flow vertical to fiber during resin curing is considered to be a filtration process. According to Darcy's law, the resin flow rate at any time can be expressed as:

$$u_L = -\frac{S}{\eta} \left(\frac{dP_r}{dL} \right), \quad (5.40)$$

where u_L is the resin flow linear speed, S is the fiber network filtration rate, η is the resin viscosity, and dP_r/dL is the resin pressure gradient along flow direction.

The law of mass conservation can be used to set boundary conditions such that the resin out flow from the composite at any time is equal to the amount flowing into the bleeder layers. Thus, the mass change rate of the composite cure process can be determined.

Although the Loos and Springer model is the foundation of composite laminate processing modeling, the assumptions used in their model are overly simplistic, and do not consider differences in resin and fiber loading. Furthermore, the flow equations in vertical and horizontal directions are independently established, which produces some unreasonable factors in the model. For this reason, Gotowski developed 1D compact and 3D flow models based on consideration on the differences in resin and fiber loading, and the flow equations in the vertical and horizontal directions are coupled. The uncompact composite is treated as a porous nonlinear elastic medium fully impregnated with a viscous fluid. There are two important steps in continuous fiber composite compacting: (a) Resin passes through the porous medium and flows out; (b) Elastic fiber deformation occurs. In the early stage the fibers are not deformed, and all of the applied load will be transferred to the resin, in the form of resin out flow. As the fibers are compacted and their volume fraction increases, the fibers are gradually compacted and create an elastic force after compression and deformation. At this point some of the applied load will be taken by fibers and the pressure on the resin will decrease. As the laminate is continuously compacted, the proportion of load taken by the fiber will become greater, and the pressure in the resin will become smaller and eventually reduced to zero. Because the applied load is vertical to the plane of the laminate, the in-plane fibers of the laminate are restricted and cannot move. Thus, the composite laminate is cured and compacted only along the vertical direction and this is a 1D compaction process. The combination of the stress balance equation with 3D Darcy's law gives:

$$\frac{k_{xx}}{V_f} \frac{\partial^2 P_r}{\partial x^2} + \frac{k_{zz}}{V_f} \frac{\partial^2 P_r}{\partial y^2} + \frac{1}{V_0^2} \frac{\delta}{\delta z} \left(V_f k_{zz} \frac{\delta P_r}{\delta z} \right) = \mu \frac{\delta}{\delta t} \left(\frac{1 - V_f}{V_f} \right) \quad (5.41)$$

where V_f is the fiber volume fraction; V_0 is the initial fiber volume fraction; μ is the resin viscosity; P_r is the stress taken by the resin; k_{ii} is the fiber filtration rate in the i direction.

Gotowski's 1D compact and 3D flow model has become a classical model in simulating composite molding processes. Many further studies have since been performed on the basis of this model.

- ③ Void modeling. Voids are formed by entrapped air bubbles in laminates and volatile substances in resin. Void control is based on studies of bubble forming, growth, migration, and divisions of solid–liquid phases in composites. These problems are related to factors such as temperature, pressure, resin viscosity, and fiber density. Bubbles are formed by entrapped air and volatile substances (mainly water vapor). At equilibrium conditions:

$$P_v = P_r + 4\sigma/d, \quad (5.42)$$

where P_v is the pressure inside a bubble, which is the sum of the bubble air and water vapor pressure; P_r is the pressure around the resin; d is the bubble diameter; σ is the interfacial tension force between the bubble and the resin matrix.

If the resin pressure is changed, say, through a pressure decrease, the bubble will expand, the internal air and water vapor pressure will reduce. Water will diffuse into the bubble again, and finally the bubbles will reach a new equilibrium with different dimensions. If the temperature is changed, the water saturated vapor pressure will change. To reach a new water vapor saturated pressure, water vapor must diffuse along the interface. The temperature change will alter the air pressure inside the bubbles, which will in turn affect bubble expansion, contraction, and water diffusion. Finally, the bubble will reach a new equilibrium state under new dimensions. Water diffusion in resin follows Fick's diffusion law:

$$M = D \frac{dc}{dx}, \quad (5.43)$$

where M is the number of moles diffused per unit area, per unit time; dc/dx is the water concentration gradient in the resin; D is the diffusion coefficient.

With the use of Fick's diffusion law, based on mass conservation, the expression for water diffusion in resin around bubble is:

$$\frac{dc}{dt} = D \left(\frac{\partial^2 c}{\partial r^2} + \frac{2}{r} \frac{\partial c}{\partial r} \right), \quad (5.44)$$

where dc/dt is the rate of change of the water concentration with time; r is the radial coordinate of a spherical coordinate system centered at the center of the bubble gradient in the resin; D is the diffusion coefficient.

Before resin curing, water is uniformly distributed in the resin. The initial concentration is c_i . After curing is started, the water concentration in resin far from bubble remains at c_i , and water diffusion is under an

instant dynamic equilibrium. The water concentration is the saturated water vapor concentration of the bubbles c_m . The reason for this result is that the diffusion resistance of the resin is the main resistance, and c_m depends on the water pressure and temperature inside the bubbles.

Bubbles can migrate with the resin flow; hence, it is possible for a bubble to move out of the composite aided by resin flow. To force a bubble to move, the driving force from the resin flow should be greater than any resistance that blocks bubble movement, i.e., the pressure gradient along the resin flow direction should be greater than a certain critical value. If the resin is assumed to be a Newton fluid and the fibers do not deform, the approximate critical conditions causing bubble flow in resin can be derived as:

$$\left| \frac{dP_r}{dL} \right| > \left| \frac{dP_r}{dL} \right|_c = \frac{4\sigma \cos \theta}{d_c L_v}, \quad (5.45)$$

where dP_r/dL is the pressure gradient along the resin flow; σ is the interfacial tension force between bubble and fibers; θ is the surface contact angle between the bubble and fiber surface; d_c is the smallest diameter of flow path in the fiber network; L_v is the projected length of the bubble along the flow direction.

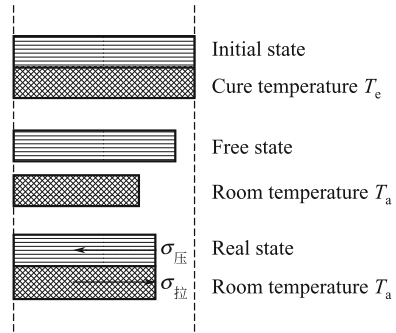
In practical processes, most bubbles are removed in pretreatment, but residual bubbles should be taken into account and must be removed in processing. On the basis of the above modeling if the distributed bubbles are controlled so that their dimensions are in a critical range, which can overcome the blocking by the fiber network and move with the resin flow, theoretically, all bubbles can be eliminated. The removal requires a combined treatment involving cure reaction heat, internal heat transfer, resin flow, and the elastic behavior of the fibers.

- ④ Residual stress modeling: When composite curing is terminated and the part is returned to room temperature there will be differences in shrinkage in the composite for different fiber orientations. Thus, internal strain and stress will be produced. This is known as residual stress and strain, as illustrated in Fig. 5.51. The existence of this strain and stress will decrease the composite mechanical performance, and damage may occur soon after production. Eliminating the effects of residual stress is an important issue in optimization of composite processing. Residual stress is discussed in the following section.

In Fig. 5.51, the $0^\circ/90^\circ$ cross-laminate is shown, the residual stress in one layer is:

$$\sigma = Q_{ij}(\epsilon_{0j} - \epsilon_j), \quad (5.46)$$

Fig. 5.51 Formation of residual stress



$$\varepsilon_j = a_j(T_e - T_a), \tag{5.47}$$

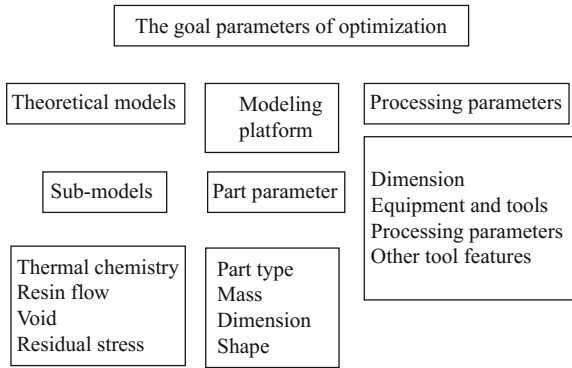
where Q_{ij} is the laminar modulus; σ_j is the real strain of the layers; ε_j is the free strain without layer restriction; T_e is the laminate temperature after curing; T_a is room temperature; a_j is the thermal expansion coefficient.

The physical parameters of the materials can be calculated by the mixing-law. On the basis of the equations above, the cure system and operating conditions can be used to calculate the residual stress and strain distribution in different layers. Testing has indicated that residual stresses depend on the fiber placement in different orientations and the maximum temperature of the material system during the cure process. Thus, residual stress can be eliminated by proper product design and processing quality control. However, elimination of existing residual stresses remains a problem for composite production.

The models discussed earlier for the composite curing process are not independent. For example, the temperature distribution depends on the reaction released heat and the thermal conduction inside and outside the system will control the viscosity distribution, and further influence the pressure application time, resin flow, and laminate shrinkage process. Temperature can also control the cure reaction rate and resin gel time, while the later in turn can affect the pressure application time, temperature, pressure, viscosity distribution, and resin flow as well as bubble activity and removal. The temperature applied in processes can also influence the residual stress in products. In real production, all these factors should be combined and considered.

- (2) Computer modeling optimization: On the basis of theoretical modeling of composite curing, computer simulations can be performed in composite processing, to optimize the processing parameters and control the processing quality. The goal of optimization should be specified, and the necessary theoretical models, and required processing parameters should be provided according to the structure and tool design. On the basis of the

Fig. 5.52 Schematic of composite hot/press processing simulation



simulation, a processing simulation and optimization can be performed. The simulated results can be compared with the optimization goals and a further optimization step can be performed, if necessary, until a satisfactory result is obtained. In Fig. 5.52, a schematic of a composite hot/press processing simulation is shown:

The aim of processing parameter optimization is to shorten the cure time, reduce cure costs, and obtain uniform curing.

To shorten the production cycle and reduce costs, it is necessary to use a faster cure rate. Thus, faster heating rates are preferred. However, rapid heating can cause a non-uniform temperature distribution inside thicker or complex shaped composite parts. The cure processes cannot be controlled properly and the resin will become brittle. Thus, typically conservative slow heating rates are used resulting in lower production output and higher costs. Processing control needs the cure cycle to be as short as possible under the circumstances that the composite quality can be guaranteed, which can be fulfilled by optimizing the heating rate based on a full understanding of the rules of cure reaction heat output and heat transfer.

Non-uniform curing can cause large residual stress in products. For larger and thicker laminates, it is impossible to eliminate the gradient of the cure degree, but cure advancement from the outer surface into the inner layers is useful to eliminate the effects of voids and impurities and can reduce residual stress. Early in the cure process, heat is transferred from air inside the autoclave to the laminate, causing the laminate surface temperature to increase first, as the curing reaction initiates. In the later stages of curing, the heat generated by exothermic curing reactions will change the temperature and the curing behavior inside the laminate. The cure process inside will become faster and exceed the surface curing speed. In the optimization, the curing rate should be controlled so that the temperature of the system is maintained below the gel point when the central layers and surface reach the same curing degree.

The following factors should also be considered: Extra resin should be removed before the gel point to obtain a proper fiber content with a uniform distribution. After curing, the void content in the material should be

minimized, with smaller void spaces and a uniform distribution. The residual stress inside layers should be as small as possible or totally eliminated. The temperature applied in cure process should be lower than the resin degradation temperature.

Tooling parameters include the dimensions, equipment, and tools used together with some adjustable processing parameters (temperature, pressure, and cure rate), and other equipment features. For example, in laminate production, if an autoclave is used, the vacuum bag is used to apply a constant static pressure, and to transfer the pressure onto the laminate top layer through a bleeder layer, which is placed on the mold. For mold press processing, the press plates are closed at a constant rate to a specified stage to pressure the laminate. Thus, the boundary conditions of the laminate top surface will change because of the different processing techniques used and the mathematical explanation of resin flow will also change.

Part parameters include: dimensions, shape, mass and part types (skin, stringer, wing beam). These factors are important for quality control. For example, in terms of dimensions it is easier to make a thick laminate 30 cm \times 30 cm with uniform thickness and no voids, because of the smaller length and width, which will help with resin flow allowing voids to be removed from the part. However, if the same material and processing are used to make a 90 cm \times 90 cm laminate with the same thickness, the part may feature many voids entrapped with non-uniform thickness. Voids in the center of such a part will be very difficult to remove.

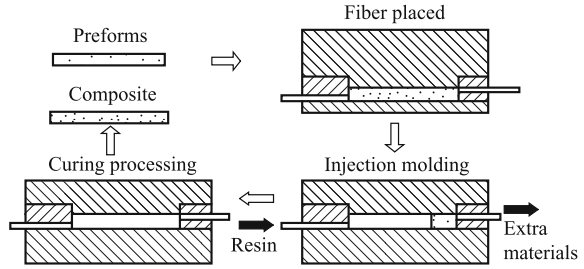
(2) Simulation in RTM processing

RTM is a liquid molding technique developed for low-cost composite production, which is suitable for making composite products with thin shells, complex outlines, and parts requiring good integration, smooth surfaces, and high precision dimensions. Thus, this method shows good prospects in many areas. In Fig. 5.53, a schematic of the RTM process is presented. In RTM, closed molds and injection process are used. The monitoring of curing with embedded sensors is practically difficult; hence, computer simulation and optimization are commonly used.

- (1) Parameter optimization goals: Optimization of RTM is performed with the aim of addressing the common problem of mold filling of resin.

In mold filling, the preform is initially in non-impregnated state. The macroscopic flow of resin injection and microscope movement of fiber impregnation take place simultaneously and control of these two competitive flows is the main problem of composite liquid molding. The main issues of resin injection include: mold not fully filled, poor fiber impregnation, preform deformation, and mold leakage. The goal of optimization is to fully impregnate the fiber networks so that no dry spots or bubbles are entrapped, to form a uniform resin distribution.

Fig. 5.53 RTM processing schematic



- (2) Theoretical modeling of RTM: To model mold filling, the following assumptions are made: no deformation occurs to the preform placed in the mold during resin injection; the inertial effect caused by resin injection can be ignored; the size of the mold cavity is much larger than that of any voids; and Darcy’s law can be used to express the resin flow equation. The speed vectors of a 3D flow Cartesian coordinate system consist of three components:

$$\begin{bmatrix} v_x \\ v_y \\ v_z \end{bmatrix} = -\frac{1}{\mu} \begin{bmatrix} S_{xx} & S_{xy} & S_{xz} \\ S_{yx} & S_{yy} & S_{yz} \\ S_{zx} & S_{zy} & S_{zz} \end{bmatrix} \begin{bmatrix} \frac{\partial P}{\partial x} \\ \frac{\partial P}{\partial y} \\ \frac{\partial P}{\partial z} \end{bmatrix}, \tag{5.48}$$

where S is the filtration tensor.

For an incompressible fluid, the linear continuous equation can be simplified as:

$$\frac{\partial v_x}{\partial x} + \frac{\partial v_y}{\partial y} + \frac{\partial v_z}{\partial z} = 0. \tag{5.49}$$

Because many composite liquid molding parts have a much smaller thickness than the dimensions of their plane, mold cavity filling can be simplified as a 2D flow. The simplified flow equation has the form:

$$\begin{bmatrix} S_{xx} & S_{xy} \\ S_{yx} & S_{yy} \end{bmatrix} \begin{bmatrix} \frac{\partial P(x,y)}{\partial x} \\ \frac{\partial P(x,y)}{\partial y} \end{bmatrix} dz = \begin{bmatrix} \bar{S}_{xx} & \bar{S}_{xy} \\ \bar{S}_{yx} & \bar{S}_{yy} \end{bmatrix} \begin{bmatrix} \frac{\partial P(x,y)}{\partial x} \\ \frac{\partial P(x,y)}{\partial y} \end{bmatrix}, \tag{5.50}$$

$$\begin{bmatrix} v_x(x,y,z) \\ v_y(x,y,z) \end{bmatrix} = \frac{1}{h_z} \int_0^{h_z} \frac{1}{\eta(x,y,z)},$$

where h_z is part thickness, S is the flow coefficient when viscosity and filtration rate take the average values along the thickness direction.

In RTM, the resin flow and mold filling are migration boundary processes, in which the boundary conditions in the resin flow field are different at any time. However, the resin flow field boundary condition at a specified time can be used as the defined boundary conditions, and can be solved by finite element analysis. Further iterations can be used to determine the entire flow field during the resin filling mold. The pressure distribution in the resin flow field can be simultaneously determined from the volume unit control method in fluid analysis. Hence, the leading edge of the resin flow field at any time can be determined. In Fig. 5.54, schematics of the finite element network and control volume unit in a RTM 2D flow field calculation are presented. In this figure Q_i is the amount of flow of the control volume unit at the N_{ij} node flowing into adjacent control volume units. The control volume unit is a closed volume formed by connected lines from one node to other nodes in the finite element analysis.

By calculating the filling coefficient F of the control volume unit, the flow leading edge is determined to be:

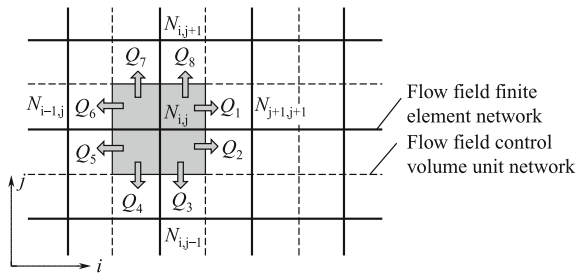
$$F = \frac{Q_r}{V}, \tag{5.51}$$

where Q_r is the resin volume in the N_{ij} control volume unit at time t ; V is the volume of the control volume unit in the N_{ij} -th control volume unit.

Hence,

- $F = 0$: no resin flow will occur into this node controlled volume unit. The node will be in an unfilled zone.
- $0 < F < 1$: resin flows into this node controlled volume unit. The node is in the flow leading edge.
- $F = 1$: resin has filled this node controlled volume unit. The node is in the filled zone.

Fig. 5.54 RTM flow field CV/FEM calculation concept



On the basis of the pressure field at each iteration, the flow leading edge location can be determined by calculating the F values at a specified time, and the entire process of resin flow filling mold in RTM can be calculated. If some dry spots are formed during the mold filling, the air pressure in dry spots will depend on the pressure in the impregnating area around the dry spots and the capillary tube pressure:

$$p_a = p_r + p_c \quad (5.52)$$

where p_a is the air pressure in the dry spot; p_r is the resin pressure in the impregnated area around the dry spot; and p_c is the capillary tube pressure. If the capillary tube pressure can be ignored, the air pressure in the dried spot can be estimated by the universal gas equation:

$$p_a = R \frac{m_a T}{(V_{\text{old}} - \Delta V_{\text{flow}})} \quad (5.53)$$

where R is gas constant; m_a is the air mass in the dry spot; T is the thermodynamic temperature; V_{old} is the final effective volume of the dry spot; ΔV_{flow} is the resin volume flow into dry spots from the surrounding impregnated area.

(3) Computer simulation

- ① Pressure distribution simulation: Resin is injected into molds to fill the mold cavity. If the pressure is too low the resin cannot penetrate the fiber bundle to impregnate the fibers and bubbles will be difficult to remove, extending the mold filling time. If an excessively high pressure is applied, the amount of resin flushing the fiber and mold will be greatly increased, resulting in fiber deformation and resin overflow. By simulating the liquid pressure distribution, the resin flow and mold filling can be predicted. Processing parameters such as the injection pressure can be optimized. The simulated results of the resin flow pressure field can also serve as a basis for predicting the flow advancement and resin/fiber impregnation effectiveness, and for optimization of the mold injection and resin overflow mouths, mold stiffness design, and force applied to the mold. In Fig. 5.55, a simulation of the pressure field distribution at an early injection stage and at the end stage is presented.
- ② Flow leading edge simulation: Computer simulation of the resin flow leading edge can predict the course of mold filling in RTM molding, revealing the flow leading edge location at any time, providing important information on the mold filling time, and the resin blending line. The simulation can also enable visual simulation of the whole process of resin flow and mold filling, as shown in Fig. 5.56. In this Figure, the different gray levels indicate the different resin flow leading

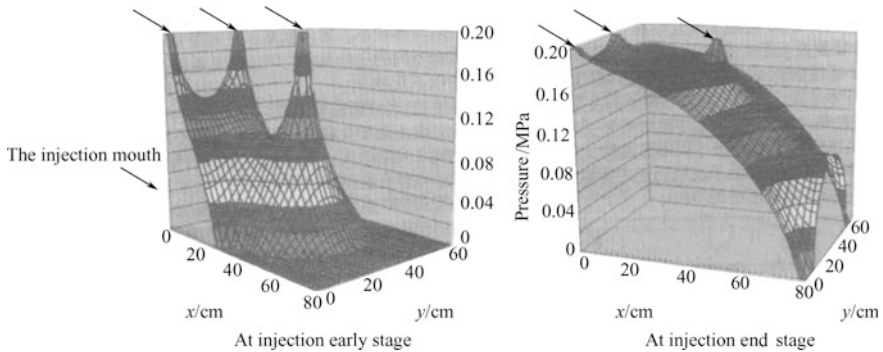


Fig. 5.55 Simulation of pressure field distribution

edges at any time. Furthermore, flow leading edge simulation can predict possible locations of dry spots as shown in Fig. 5.57. The numbers indicate the flow leading edge locations at specific times.

5.5.3.3 In Situ Process Monitoring

In situ processing monitoring refers to techniques that enable tracking of the cure process in situ in composite manufacturing. Such monitoring can enable optimized pressure application and curing temperature to guarantee the processing quality. The use of this technique can avoid some defects such as resin-rich and resin-starved regions, insufficient curing or over curing, and non-uniform curing can be avoided. In situ processing monitoring has become an important method to improve composite quality stability.

The basic principle of in situ processing monitoring is to place special sensors in the composite layers and determine the resin property changes during the cure process, such as temperature, viscosity, modulus, functional group concentration, and electrical performance. These property changes are recorded and input into a computer. Differences between the cure model and the input signals, allows the cure temperature and pressure to be regulated. This “smart” loop provides continuous automatic control of the cure process to ensure the composite quality.

On the basis of the different sensors used, composite in situ processing monitoring includes dielectric, fiber optic sensor, and thermal couple monitoring. Currently, dielectric monitoring is widely used; however, fiber optic sensor-based monitoring is rapidly advanced in composite processing.

(1) Dynamic dielectric monitoring

The principle of dynamic dielectric monitoring is to use special electrode sensors, placed at different positions on the composite to be cured. The sensors measure changes of dielectric properties caused by the resin matrix molecular structure and viscosity changes, which occur during the cure reaction. The

Fig. 5.56 Simulation of resin flow leading edge

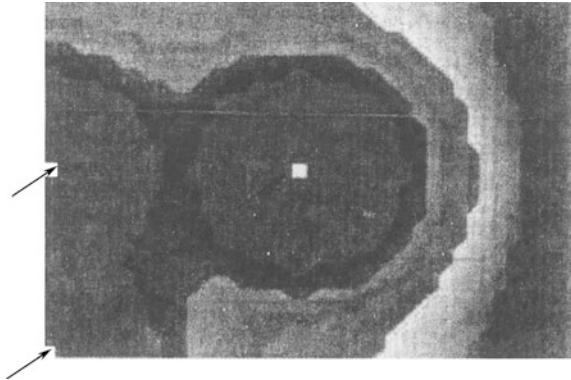
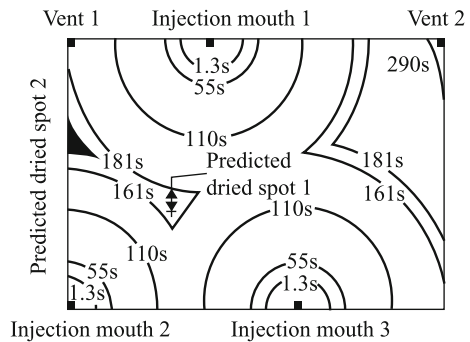


Fig. 5.57 Prediction of dried spots in unsymmetrical injection



measured electrical performance data are used to select an appropriate pressure application time, and adjust for control of the cure temperature.

Dielectric performance of a resin matrix reflects the ability to store and transmit electrical charge. These features are denoted as the dielectric constant and dielectric loss. The dielectric constant is a material parameter denoting the electrical energy stored when molecular polarization takes place in resin molecules. The dielectric loss is a material parameter denoting the electrical energy loss caused by conductive or orientation relaxation. The polarizations changes of these two parameters will be examined in the following section.

- (1) Induced polarization: Induced polarization includes electronic polarization and atomic polarization. Electronic polarization is electronic cloud migration against the atomic core under the action of an electric field, while atomic polarization refers to relative migration between two atomic cores. These two polarization contributions are small in a rapidly changing electric field. These polarizations are synchronous with the electrical field change; hence, induced polarization has a small contribution to both the dielectric constant and dielectric loss.

- (2) Orientation polarization: Orientation polarization relates to the orientation of polarized bonds with a permanent electric dipole moment under the action of electric field. This type of polarization dominates the dielectric behavior of glassy polymers. If no applied field exists, the orientation of the dipole moment of the polarized bonds will be randomly distributed. When a field is applied, the polarized bonds will rotate and orient along the field direction, i.e., orientation polarization takes place. Polarized bonds must overcome the forces acting between molecules to rotate in the electric field and reach a new equilibrium state. The time needed for this change is called the relaxation time τ , which depends on the polymer molecular structures. Generally, the relaxation time increases as the cure degree increases. Let the alternating field frequency be f . When $\tau \leq 1/f$, the dipole moment will take an orientation synchronous with the field because the stored energy in polymers in a charge-half cycle will be totally released in the discharge-half cycle. Although there is energy exchange between the polymer and the field, no energy loss will occur. The polymer will become highly polarized under such circumstances, giving a high dielectric constant without any dielectric loss. When $\tau \approx 1/f$ or $\tau > 1/f$, the orientation of the dipole moment is delayed with respect to the electric field change. The polymer polarization will gradually decrease resulting in a lower dielectric constant. Simultaneously, because the energy absorbed by polymers is less than the released energy, strong dielectric loss will occur. When $\tau \gg 1/f$, the orientation of the dipole moment cannot follow the field change and no polarization will occur. In this case, both the dielectric constant and loss tend to zero. Hence, resin cure information can be derived from the response of the dielectric constant and loss to a permanent electric field.
- (3) Ion migration: Ion migration refers to the movement of impurity ions in the resin under an applied electric field. This effect can give the resin a certain conductivity. Note that the material ion conductivity will be inversely proportion to viscosity over certain ion concentration and temperature ranges. Ion migration can only occur when resin is in a viscous state. This correlation can enable the resin viscosity during the curing process to be monitored by measuring ion conductivity.

In summary, if the dielectric constant of a resin matrix can be monitoring during the composite curing, information on resin viscosity and chemical structure changes can be obtained. For thermosetting resins that show a flow state at high temperature before gelling, the resin viscosity can be evaluated by analyzing the changes in ion conductivity. After gelling, the loss factor will mainly depend on the polarized orientation, which can be used to evaluate changes in the chemical structures. In Fig. 5.58, the resin ion viscosity change curve of the T300/QY8911 material system during curing is given, indicating the viscosity change mode of thermosetting resins at the early curing stage. Figure 5.59 is the loss factor change curve of this material system in the curing dwell time reflecting the increase in dielectric relaxation time caused by matrix resin cross-linking, which decreases the loss factor.

Dielectric monitoring can provide information on composite resin matrix viscosity and chemical structure changes occurring during curing process. This information is useful for performing curing processes under in situ monitoring; however, in practical applications, this technique is somewhat limited.

First, when resin is in the viscous-flow state, the ion conductivity will be subject to many influences, and the resin viscosity change can cause ion activity to increase, resulting in a different ion conductivity. However, other influences exist and there will not be a simple correlation between the ion viscosity based on the ion conductivity and the real resin viscosity or traditional shear viscosity. In practical monitoring, it can be assumed that the ion concentration and ion charges will remain unchanged in the same sample; hence, the conductivity change will be mainly caused by the viscosity change, and the ion change modes can reflect the real sample viscosity change modes. However, as mentioned earlier, the ion conductive behaviors of polymers are mainly caused by impurities in the materials. There will be a difference in the ion concentrations and as a result, the ion viscosity change curve derived from different monitoring methods cannot be used for quantitative comparison of the material's real viscosity.

Furthermore, it should be noted, in thermosetting resin matrix curing process, the ion viscosity value before the gel point can reflect the real viscosity change mode. After the gel point, the ion viscosity will no longer show a change and will rapidly tend to an infinitely large value and then gradually stabilize.

(2) Fiber optic sensor monitoring

Fiber optic sensor monitoring systems consist of an optic transmitter, sensor element, optic receiver, and signal processor. The basic principle is to use a special optic fiber as a sensor, which is embedded into to composite or structure to be cured. The optical system can then be monitored during the in situ cure process. Optic fiber sensors have the advantages of small size, high sensitivity,

Fig. 5.58 Logarithm ion viscosity change curve of T300/QY8911 during curing

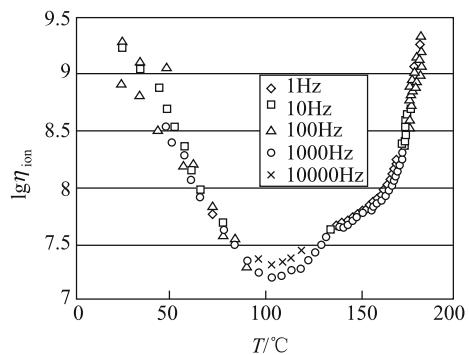
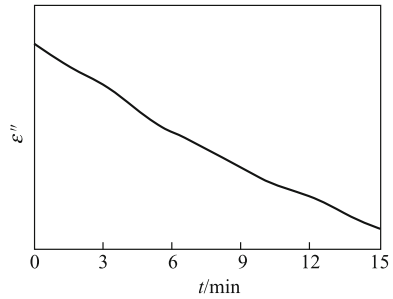


Fig. 5.59 Loss factor change curve of T300/QY8911 in curing dwell time



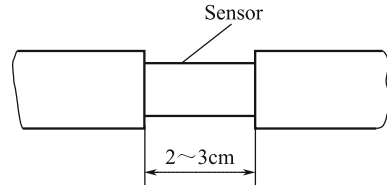
and good compatibility with resin matrices. On the basis of different monitoring mechanisms, fiber optic sensors can be divided into the following types.

- (1) Fiber optic refraction sensing: In composite resin matrix cure process, during the molecular cross-linking reaction, the ratios of different chemical bonds will change. Because each chemical covalent bond has different refraction coefficients, the changes in chemical bonding during curing will result in changes of the resin refraction. Thus, by monitoring changes of the resin refraction, information on the resin cure degree can be obtained. Fiber optic refraction sensors are designed based on this principle.

There are many types of fiber optic sensors available and a typical construction shown as in Fig. 5.60. The refractivity n_1 of the optic fiber core layer is slightly greater than that of the cladding layer n_2 . Total refraction will take place at the interface between the core layer and the cladding layer and light will be transmitted along the optic fiber core. If a section of the cladding layer (2–3 mm) is removed the exposed fiber core section will become the optical sensor in the composite curing monitoring technique. The fiber can be embedded into composites and light refraction will take place at the interface between the fiber core and resin, resulting in the loss of some light energy and light attenuation. Tracing of the optic energy change can give information on the resin cure degree.

An optic cure sensor system based on resin refraction measurements is simple in construction. Usually, a monochromatic light source is used. At the light measurement end, the change of the light energy is measured. Hence, this is an economical and practical approach to monitoring. However, in most cases, special optic fibers with a high refraction fiber core should be used, and can only qualitatively give information of cure reaction process. Furthermore, the refraction measurement range is limited. Another issue to consider is that resin refraction correlates with density, while density is largely dependent on the effects of temperature. Outside of ambient temperatures the measured resin refraction change will show the combined effects of cure degree and temperature. Thus, it is difficult to evaluate the cure degree change only from the refraction change. This

Fig. 5.60 Schematic of optical refraction sensor



monitoring approach is only suitable for measuring the cure degree during a dwell time in a curing process.

- (2) Infrared spectroscopic sensing: In infrared spectroscopic sensing, infrared light absorption by characteristic resin functional groups is used to determine the change of functional group content in the resin. The characteristic peak location and intensity relate to a specific functional group, and the peak intensity can be used to monitor its concentration change and determine the curing degree. For example, in an epoxy resin system, the cross-linking functional groups are epoxy groups. The characteristic peak change of the epoxy group can be analyzed to determine the cure degree of the composites. This information can be used to control the pressure application time and curing temperature. Infrared spectroscopic sensors include fiber optic infrared absorption sensors and evanescent wave sensors.

In fiber optic infrared absorption sensors, two optic fibers with an end distance of 0.5–1.5 mm are oriented in the same direction and embedded into prepregs. The two free ends of the fiber are connected with a monochromatic scanner and an infrared spectrometer. Once the cure reaction is initiated, the resin viscosity will increase and resin will flow into the gap between the two fiber ends. Infrared light will produce characteristic absorption peaks when passing through the resin layers. At the receiver end, the resin absorption spectrum can be analyzed. On the basis of the Beer–Lambert law, a series of resin infrared absorption spectra are collected at certain time intervals. Quantitative measurements of the epoxy, oxyhydrogen, and amine group concentration can allow the cure rate and degree to be determined.

Fiber optic evanescent wave sensors are another type of cure monitoring sensor based on analysis of infrared absorption spectra. The construction of this type of sensor is similar to that of the fiber optic refraction sensors shown in Fig. 5.60; however, the sensor section is longer than that of the evanescent wave sensor (approximately 20 cm). In cure monitoring, as the resin viscosity decreases, the optical evanescent wave will dissipate at the interface between the fiber core and resin. The absorption spectra measured at the light receiver can allow dynamic cure reaction information to be determined. In optic fiber evanescent wave sensors, a special optical fiber with a high core refractivity is required, which gives low sensitivity.

Fiber optic cure monitoring sensors based on infrared spectral analysis can quantitatively determine the cure degree; however, a wide band light source

and complicated spectrometer are needed together with complex data processing, which adds to the cost of this approach.

- (3) Fiber optic bend sensor: In applications of optic fibers, the fiber axis undergoes periodic bending on a micrometer scale caused by non-uniform pressure. Fiber optic bending can cause increased losses, resulting in energy dissipation during light transmission. The reason for this is that small periodic bending causes repeated coupling between the transmitting and radiation moduli, resulting in some light energy of the transmitting modulus radiating outside of the fiber core.

In composite prepregs, reinforced fibers have a defined density. The load on fibers will change at different times in the curing process. The pressure transmitted to the fiber sensor section will also change, which will change the degree of fiber microbending and the resulting minor bending loss. In composite autoclave processing, test results indicate that fiber bending sensors can be used to accurately determine the lowest viscosity point and completion of a curing process with good reproducibility. The sensitivity is related to the pressure field in the curing process.

In the use of fiber optic bending sensors to monitor composite cure process, it is important properly place the fiber based on the selected prepregs. This method has simple equipment requirements, is practical, and its results can be easily translated into production.

- (4) Bragg grating sensors: Bragg grating sensors have developed rapidly in recent years. In Bragg grating sensors, light wavelength coding is used for signal transmission, which can overcome fluctuations in the light energy output as well as losses of the fiber connectors and coupler. Wavelength multiplexing and quasi-distribution measurements can be performed in a single fiber.

The basic principle of a Bragg grating sensor is the Bragg wavelength measurement. The Bragg wavelength λ_B correlates with the fiber effective refraction n_{eff} and the period of a refraction grating A , as shown below:

$$\lambda_B = 2n_{\text{eff}}A. \quad (5.54)$$

When Bragg grating sensors are embedded in a composite resin matrix, the resin is strained and thus causes optical elastic effects, which can result in changes of n_{eff} and A . These effects produce a Bragg wavelength displacement. A modulator can be used to measure the Bragg wavelength displacement from which, the strain can be determined. Bragg grating sensors can be used to monitor composite autoclave processing. From a curve of the change of the Bragg wavelength vs time, the material changes can be tracked. Furthermore, the glass stage of the resin curing and some defects such as debonding and cracking in the measured zone can be identified.

Applications of Bragg grating sensors face a cross-sensitivity problem, i.e., the grating is sensitive to both stress and temperature. When the grating is used for measurements, it is difficult to determine whether a change of the

Bragg wavelength is caused by stress or temperature. In practical applications, it is necessary to take some measures to compensate or identify these differences.

Two in situ monitoring methods used in process are introduced above. Composite processing occurs under closed conditions. Knowledge of the processing parameters is the only way apply in situ monitoring. To properly select processing parameters, it is necessary to collect as much useful information as possible.

(3) **Data types in monitoring**

The first issue in in situ monitoring of composite processes to collect a large volume of curing information. Typically, three types of data on the process are collected: first condition parameters of the equipment; second, temperature and pressure data, which can indicate a material's curing conditions; third, information about the physical and chemical structure changes taking place in the materials during the curing process.

- (1) **Equipment condition:** The equipment condition is a very easily measured parameter. In most cases, the control of composite production is performed based on control of the equipment, such as the location of a filament winding head, winding speed, fiber tension, together with mandrel torsion moment, speed, and temperature. These parameters should remain consistent over different production cycles. Improper control will cause product quality problems.
- (2) **Temperature and pressure:** There are two types of temperature parameters, one is the directly controllable ambient temperature data, such as the heated air temperature in autoclave composite curing or the press molding plate temperature. The temperature conditions represented by these types of data will be directly controlled by a temperature control unit in the composite curing process. These values will be compared and maintained consistent with the preset control program. Another type of temperature data is indirectly controlled ambient temperature data, which reflects the actual temperature conditions. These depend on the controllable temperature, but are not direct controlled. It is difficult to maintain high consistency of these temperatures with a preset control program. For example, the mold temperature in composite autoclave curing is indirectly controlled by the air temperature inside the autoclave. However, it is very difficult to ensure accurate control of this temperature. In addition, the temperature inside the composite part can only be indirectly controlled by the external temperature control unit and is affected by the reaction heat generated during curing process. Hence, temperature is one of the more difficult parameters to control.

The pressure data reflect the pressure conditions induced on the composites during curing. The pressure conditions include the applied processing pressure, such as the air pressure in the autoclave, the plate pressure in press molding, and the actual pressure resin and fibers are subjected to.

Only the pressure induced to the resin can contribute to air bubble removal. In vacuum bag curing processes, the pressure data include both the applied positive pressure and the pressure produced by the applied vacuum.

- (3) Conditions of cured material include resin matrix cure degree, resin viscosity, fiber tension force, and fiber positions.

Ideal curing processes require that the cure reaction of the resin matrix be performed at the programmed speed, to avoid rapid curing, which might result in product quality problems, or excessively slow curing, which will increase the production costs. To achieve an optimal curing program in situ data of the cure degree related to the change of chemical structure of the resin matrix are collected during curing. To avoid mistakes in selection of the pressure application time, it is necessary to perform in situ monitoring of the resin viscosity change. Pressure applied when the resin viscosity is too low will cause resin out flow and the pressure will quickly decline and the resulting composite will not be well compacted, and may feature resin-starved regions. If pressure is applied too late, internal air bubbles cannot be removed completely contributing to void defects.

(4) **Creation of monitoring system**

Composite in situ processing monitoring systems can be built-up with different methods combined with a computer. On the basis of the collected data, in situ monitoring of processing parameters such as temperature and pressure can be performed to guarantee the product quality. A typical autoclave curing monitoring system is shown as Fig. 5.61, which is composed of three parts.

- (1) Data collection system in autoclave: This system can monitor the autoclave internal air temperature, pressure, part temperature, and material viscosity and chemical structure determined by dielectric or fiber optic sensors. These data are transferred to a computer processing system.
- (2) Computer decision system: The program module in the computer system can use the collected in situ processing monitoring data from the resin curing process. The temperature, cure degree, residual stress, and part deformation under curing of each layer can be analyzed and compared with available data and knowledge to obtain optimized processing parameters for further implementation. The analysis results can be displayed for evaluation and inspection.
- (3) Control system for curing parameters: This kind of system can use collected information from curing monitoring together with calculation results provided by an analysis module to drive the actuating unit in the controller cabinet and automatically adjust the processing parameters.

(5) **Problems in monitoring techniques**

Currently, some problems exist for in situ process monitoring of composite part production, including:

- (1) Measurability: no ideal sensors are available that can provide information on both the physical and chemical changes occurring during composite curing. Not all requirements for material conditions, such as prepreg status and

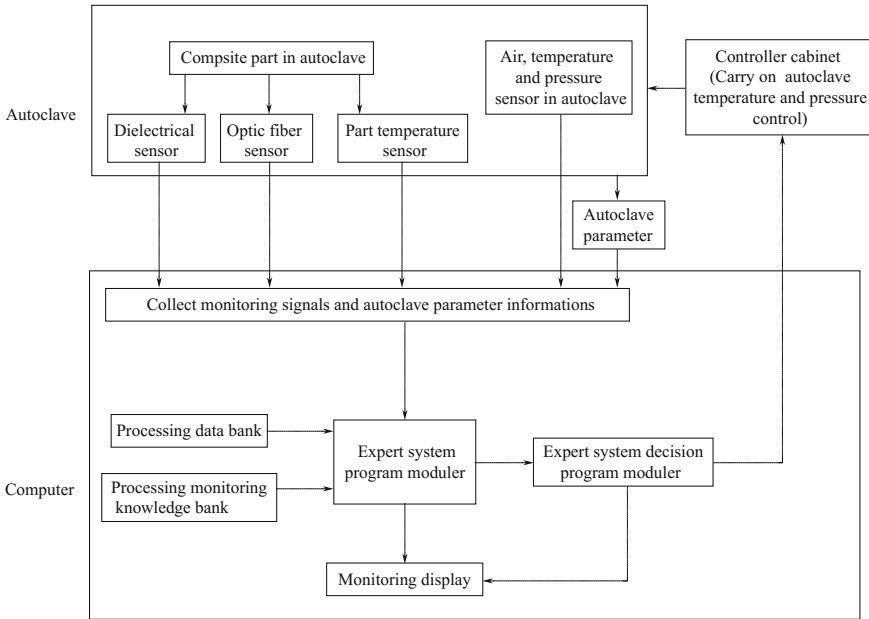


Fig. 5.61 Typical autoclave curing monitoring system

processing conditions (closed vacuum bag/autoclave conditions) can be determined during the composite part manufacture. Apart from traditional temperature and pressure sensors, all sensors used in part production monitoring can only provide information on trends of material viscosity and the curing reaction.

Temperature and pressure sensors can only give information at specified points in materials and full data on each section is difficult to acquire. To collect more curing parameter information from important areas, more sensors will need to be placed inside the composite parts.

Disturbances may cause some problems in data collection and the signal collection may vary over time. Hence, small fluctuations may lead to a discontinuous curve.

- (2) Feasibility refers to the ability to control the output of a specified value in a given time.

Measurement of output or process parameters with high spatial and temporal resolution is necessary but the control system should also have enough accuracy to enable control of parameters at different locations on a part. For example, one set of autoclave curing monitoring systems can inspect the distribution of the whole curing status inside a composite part. A computer analysis system can acquire the vector output of the processing parameters from the whole part. Common autoclave input control parameters are limited to temperature and pressure. Furthermore, only control of the air

temperature inside the autoclave can be achieved, which may not be consistent with each of the processing parameter and analyzed results. Owing to the large heat inertia of an autoclave, tools, and the part itself, the process control cannot be performed with high time resolution.

To achieve consistency between measurements and controls, the heating molds should have multiple independent temperature control zones, so that independent heat input can be applied to different sections of the composite and the spatial resolution can be improved.

- (3) **Low cost:** The use of sensors will increase the complexity of part packing before curing. In particular for fiber optic sensors, because of their brittleness, which requires special treatment before use. This will increase the work involved in packing and production costs. Sensors are mostly single-use elements; hence, the part cost should include the sensor cost. Thus, in situ processing monitoring system should be based on low-cost sensors that are easy to install.
- (4) **Compatibility:** The sensors are embedded into the composites, and many of them will remain inside the part for long time. The sensor materials should not influence the part curing behavior or produce additional defects in service. For materials and sensors to be used, it is necessary to inspect the effects of sensors on mechanical performance of the material to evaluate the compatibility between the sensors and material system.

5.5.3.4 Statistical Processing Control

Statistical processing control (SPC) is a kind of output control method, as shown in Fig. 5.62. In this control method, sampling, quality inspection, and statistical analysis of results are performed for composite products to determine and eliminate factors that cause quality problems. The feedback of this information forms a control loop, to realize the needs for quality control and quality improvement.

Fluctuations of composite properties and shape can be divided into normal and abnormal fluctuations. Normal fluctuation is generated from the unavoidable factors occasionally encountered during processing. These factors have less effect on the product quality and are technically or economically unfeasible to eliminate. Abnormal fluctuations are caused by system abnormalities and have a pronounced effect on product quality. These can be avoided and eliminated by proper counter measures. SPC involves the use of statistical analysis to identify random and abnormal fluctuations of product quality in production. This allows precautions to be taken for possible abnormalities in production.

(1) Statistical analysis methods

Statistical analysis is the basis of SPC, and includes many methods such as control charts, bar graphs, scatter diagrams, processing ability indices, and relative and regression analyses. Some of these methods will be discussed in the following:

Fig. 5.62 SPC control principle

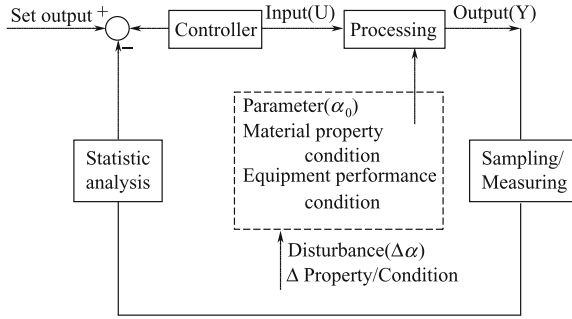
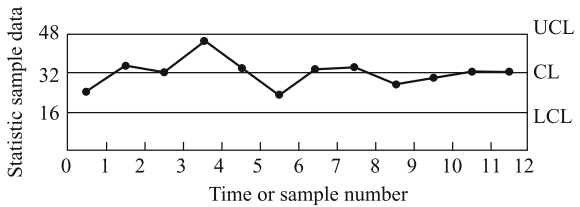


Fig. 5.63 Schematic control chart



(1) Control chart: A control chart is a kind of statistical graph used to monitor measure, diagnose, and improve processing conditions. A sample’s statistical results are ranked in a certain sequence, as shown in Fig. 5.63. In general, these results include an upper control limit (UCL), lower control limit (LCL), and a central line (CL). The central line typically represents the average sample value, while the upper and lower control limits depend on the quality stability requirements. In a regular inspection, if the sample value is higher than the UCL or lower than LCL, it can be concluded that abnormal conditions were present in production.

Current control charts include percentage control charts for rejected products, number control charts for rejected products, and defect ratio and defect number control charts.

- (2) Bar graph: Bar graphs show data distribution features, which can be used to directly display a data distribution.
- (3) Ranking graph: also known as Pareto figure, involves ranking the effects of each items from the most to the least important. It can be used to identify the primary, secondary, or common problems that affect product quality. The primary factors can be detected and quality improvements methods suggested.
- (4) Scatter diagram: the data point distribution is used to show the relationship between variation and to reveal and display the correlation between two sets of data or confirm and predict the correlation.

- (5) Relative analysis is used to study the relationships among variations and assumes that all variations change randomly at the same positions without separation from the primary and secondary ranks.

(2) **Data collection**

To acquire accurate and reliable statistical data, systematic sampling should be conducted. The sample selection should be continuously and randomly performed, where the randomness prevents unintentional selection of a sample. The samples should be representative of the materials. The sample data should be continuously accumulated so that the effects of factors that occur regularly can be determined. In this way, performance degradation in a production system can be recognized, serving as a reference for system optimization.

There may be many factors to inspect in one product and it is impossible to check and analyze all of them. Only key parameters that can give insight into the processing should be measured. Once the data are collected, the data should be processed into figures or curves based on statistical approaches. A table of the data alone is not sufficient to indicate changes in regularity, even in the case of only a few data points to be analyzed. In most cases, it is necessary to use the same data in different analyses to determine correlations among different factors, or time-dependent trends.

(3) **Implementation of SPC**

In practical applications, the implementation of SPC should be performed in two steps: first the analysis stage, second the control stage.

In the analysis stage, preparation for production should be performed, following certain standards, to ensure the raw materials, labor, equipment, and measurement systems are in place before production can be started. The production should be performed under conditions that minimize any abnormalities in analysis stage. Calculation of the control limits is based on the data collected in production, which is used to produce control graphs and bar charts. Process ability analysis can also be performed to check if the production is within a statistically stable state or not. If any single factor cannot be satisfied, the causes should be investigated and steps taken to improve the process before restarting the production preparation and analysis. If the requirements of the analysis stage are satisfied the analysis stage can be terminated allowing for advancement to the SPC control stage.

In the control stage, control graphs and other charts are used for monitoring production. In this stage, the control limits in control graphs are determined based on the analyzed results in the analysis stage. The data collected in production should be used in control graphs at the same time. The control graphs should be closely observed, and data fluctuation in control graphs will show whether the production is under control or not. If production is out of control, the causes should be identified and eliminated as quickly as possible.

In practical applications, each control item should proceed through the above stages, and the processes from analysis to monitoring should be repeated if necessary.

(4) **Advancement of SPC**

SPC is a new quality management system and not yet widely used in composite process control in China. However, SPC has been widely applied in other industries such as the electronic industry, and various types of computer software have been developed and applied to in situ process monitoring. SPC methods show good potential for overcoming the difficulty of composite processing control.

5.5.3.5 Experiential Control Methods

Experiential control method, also called trial-and-error methods, use experiences gathered over long-term production to decide the processing technique, or the use of simple specimens for testing and qualitative analysis of products. This method is only suitable for a narrow range of composites and is not applicable if the material and shape of the products changes. In these cases, repeat testing is necessary, resulting in a long production cycle and high costs. Hence, this method is not currently widely used in production.

5.5.3.6 Processing Quality Inspection

Whatever processing quality control method is used, it is necessary in quality assurance to inspect and track the processing quality. The quality assurance department is responsible for checking if production is performed under the specified specification. The work involved in processing quality inspection will be discussed in the following section:

(1) Raw material inspection

The following items should be included in raw material inspections.

- (1) Verify the raw material's name, grade, supplier and product series number, and perform tests on the key performance parameters to ensure quality.
- (2) Regularly inspect material storage and packages to avoid material degradation, damage, corrosion, and misidentification caused by storage problems or package breakage.
- (3) Recheck the contents in item (1) before using a material, verify that degradable materials, such as prepreg and adhesives are within the specified shelf life.
- (4) Check the records of the source, storage, and treatment of material that have already been used.

(2) Equipment and tools inspection

Equipment in good condition is essential to produce high-quality composite products. Before operation, all equipment, such as autoclaves, winding machines, and prepreg tape placing machines, should be carefully checked and calibrated. In production, use of the equipment should be recorded with their operating

conditions. Equipment should be regularly maintained to ensure good condition. Problems should be identified and repaired any in a timely manner.

Molds should be checked and verified according to specifications. The molds should be guaranteed to give products that can satisfy the design and the technical specification requirements based on the correct use of the materials processing techniques. The mold surface should be checked before use to guarantee a clean surface without any corrosion or damage.

(3) **Production condition inspection**

The inspection of composite production environment is also part of an inspection program. In a controlled environment, uncontrolled spray, exposing to dust, smoke, oil vapor, or any other chemical substances or grains that may affect processing, is prohibited. A clean laying-up room should be used with normal air filtering under positive pressure conditions.

(4) **Processing flow chart inspection**

In composite part laying-up and curing processes, certain key operation steps should be strictly controlled. These steps should be clearly indicated in the specification and guaranteed by inspection.

- (1) Check the release agent applied to the mold surface and its cured condition.
- (2) Check the prepreg laying-up to guarantee the correct layer number and orientation.
- (3) If core materials are used, check their correct splicing position.
- (4) Check the correct processing display and records.
- (5) Check the production records including:
 - ① Material supplier, data, series number, batch number, and the storage time in shelf life.
 - ② Processing parameters including applied pressure, temperature, heating-up rate, dwell time.
 - ③ Autoclave or heating chamber series number.
 - ④ Part or product series number.

(Translated by Jianmao Tang)

References

1. ASTM D6264-07 (2007) Standard test method for measuring damage resistance of fiber-reinforced polymer-matrix composite to concentrated quasi-static indentation force
2. ASTM D 7136-07 (2007) Standard test method for measuring the damage resistance of a fiber-reinforced polymer matrix composite to a drop-weight impact event
3. ASTM D7137-07 (2007) Standard test method for compressive residual strength properties of damaged polymer matrix composite plates
4. FAA AC 20-107B (2003) Composite aircraft structure (draft)

5. HB 7618-2009 (2009) Data presentation guidelines on mechanical properties for polymer matrix composite materials (Revised edition, in Chinese)
6. McCarvill W, Ward S, Bogucki G, Tomblin JS (2003) Guidelines and recommended criteria for the development of a material specification for carbon fiber/epoxy unidirectional prepregs. DOT/FAA/AR-02/109
7. MIL HDBK-17-1F (2002) Composite materials handbook Vol 1. Polymer matrix composites guidelines for characterization of structural materials
8. Shikhmanter L, Cina B, Eldror I (1991) Fractography of multidirectional CFRP composites tested statically. *Composites* 22(6):437–444
9. Shen Z, Chai YN, Yang SC et al (2006) The Outline of new specifications on strength of composite aircraft structures (In Chinese). *Acta Aeronaut Sinica* 27(5):784–788
10. Shen Z, Yang SC, Chen PH (2007) Behaviors of composite materials to withstand impact and structural compressive design allowables (in Chinese). *Acta Aeronaut Sinica* 28(3):561–566
11. Shen Z, Yang SC, Chen PH (2008) Experimental study on the behavior and characterization methods of composites to withstand impact (in Chinese). *Actamater Compos Sinica* 25 (5):125–133
12. Shen Z, Yang SC (2007) Property requirements of composite systems applicable to aircraft structures (In Chinese). *J Mater Eng China SAMPE* 248–252
13. Tomblin JS, Ng YC, Raju KS (2003) Material qualification and equivalency for polymer matrix composite material systems: Updated Procedure. DOT/FAA/AR-03/19